

Luciana Fenoglio-Marc

**Satellite geodesy
for sea level and climate change**

München 2015

Verlag der Bayerischen Akademie der Wissenschaften
in Kommission beim Verlag C. H. Beck

ISSN 0065-5325

ISBN 978-3-7696-5158-4

Diese Arbeit ist gleichzeitig veröffentlicht in:
Schriftenreihe Fachrichtung Geodäsie der Technischen Universität Darmstadt
ISBN 978-3-935631-32-7, Nr. 43, Darmstadt 2015



DGK Deutsche Geodätische Kommission
der Bayerischen Akademie der Wissenschaften

Reihe C

Dissertationen

Heft Nr. 746

Satellite geodesy for sea level and climate change

Vom Fachbereich Bau- und Umweltingenieurwissenschaften
der Technischen Universität Darmstadt
zur Erlangung der Venia Legendi im Fach
Physikalische Geodäsie und Satellitengeodäsie
genehmigte Habilitationsschrift

vorgelegt von

Dr.-Ing. Luciana Fenoglio-Marc

aus Mondovi, Italien

München 2015

Verlag der Bayerischen Akademie der Wissenschaften
in Kommission beim Verlag C. H. Beck

ISSN 0065-5325

ISBN 978-3-7696-5158-4

Diese Arbeit ist gleichzeitig veröffentlicht in:
Schriftenreihe der Fachrichtung Geodäsie der Technischen Universität Darmstadt
ISBN 978-3-935631-32-7, Nr. 43, Darmstadt 2015

Adresse der Deutschen Geodätischen Kommission:



Deutsche Geodätische Kommission

Alfons-Goppel-Straße 11 • D – 80 539 München
Telefon +49 – 89 – 23 031 1113 • Telefax +49 – 89 – 23 031 -1283 / - 1100
e-mail hornik@dgfi.badw.de • <http://www.dgk.badw.de>

Diese Publikation ist als pdf-Dokument veröffentlicht im Internet unter den Adressen /
This volume is published in the internet

<<http://dgk.badw.de>> / <<http://tuprints.ulb.tu-darmstadt.de/4412/>>

Gutachter: Dr. Anny Cazenave
Prof. Jürgen Kusche
Prof. Andreas Eichhorn
Prof. Matthias Becker

Tag der Einreichung: 15.01.2014

Tag des Vortrags und des wissenschaftlichen Gesprächs: 03.12.2014

© 2015 Deutsche Geodätische Kommission, München

Alle Rechte vorbehalten. Ohne Genehmigung der Herausgeber ist es auch nicht gestattet,
die Veröffentlichung oder Teile daraus auf photomechanischem Wege (Photokopie, Mikrokopie) zu vervielfältigen

ISSN 0065-5325

ISBN 978-3-7696-5158-4

Summary

This habilitation thesis presents the findings of the sea level change studies conducted at the Institute of Geodesy of the Technischen Universität Darmstadt between 2001 and 2013. Sea level is an important indicator of climate change. It has been traditionally measured by coastal tide gauges and by satellite altimetry since 1993. Tide gauge measurements indicate a coastal average sea level rise of 1-2 millimeters per year over the 20th century. Over the last two decades the average sea level rise increased to 3.3 ± 0.7 millimeters per year, consistently measured by tide gauges and satellite altimetry. The 2013 Intergovernmental Panel on Climate Change (IPCC AR5) predicts a global mean rise of 50 ± 20 cm by 2100 for a medium warming scenario for the interval 2081-2100.

Sea level rise is not uniform and some regions will be more affected than others. It can possibly exacerbate the effects of other factors, such as flooding and ground subsidence. Because of its potential impact on coastal regions, rising sea level is one of the major threats of climate warming. Changes in each component of the climate system, ocean, land and ice sheets, affects sea level. The two primary contributors of sea level rise, thermal expansion due to ocean warming and melting of continental glaciers and ice sheets, have been identified but large uncertainties remain. Locally non-climatic components, as subsidence, can cause relative sea level rise much larger than the global average mean sea level rise.

The global and highly accurate analysis of sea level variations is made possible by space-based techniques. Their main innovation is the use of the same accurate and global reference frame ensuring long-term, precise monitoring and integration in a Global Geodetic Observing System, which is crucial for many practical applications.

This thesis focuses on the use of geodetic techniques. Its aim is a comprehensive analysis of the regional sea level variability and of its causes with particular attention to the coastal zone. The three main scientific objectives are: improvement of multi-mission satellite altimetry records, quantification of global and regional sea level change and attribution of sea level rise.

Firstly the altimeter data from different missions are unified, improved in the coastal zone and validated with in-situ and model data. Secondly global and regional estimations of sea level variability from altimetry and tide gauge data are made. The third part of the work is dedicated to the analysis of the reason for sea level change. Here satellite altimetry and gravity missions data are combined with model data to detect the causes of this variation. The analysis includes the separation of mass and volume sea level change and the closing of the water budget.

This work shows the challenges of merging satellite data of different types for the understanding of physical processes in sea basins. It also deals with the challenges of new satellite altimetry missions in the coastal zone, where altimetry provides a consistent link to tide gauge stations co-located with Global Navigation Satellite System observations. It finally discusses the importance of highly accurate sea level variability and trends for modeling coastal processes and for long-term predictions.

Zusammenfassung

Diese Arbeit stellt eine Zusammenfassung der wesentlichen Ergebnisse meiner Untersuchungen zur Veränderung des Meeresspiegels dar. Die Veränderungen des Meeresspiegels sind ein wichtiger Indikator des Klimawandels. Traditionell wurde der Meeresspiegelanstieg durchweg mit Küstenpegel gemessen. Seit 1993 werden die Ozeanoberflächen durch die Messungen der Altimetersatelliten global bestimmt. Im 20. Jahrhundert wurde eine Änderung des globalen mittleren Mittelmeeresspiegels (MSL) von 20 cm festgestellt, was einer Rate von 1-2 mm/a mit einer deutlichen Beschleunigung in der letzten zwei Jahrzehnten entspricht. Die Vorhersagen vom 5. Report des International Panel von Climate Change (IPCC AR5 2013) sprechen von einem globalen MSL Anstieg von 50 +/- 20 cm bis Ende dieses Jahrhunderts unter der Annahme eines Szenarios mit mittleren Raten für die Erderwärmung. Der MSL Anstieg erfolgt nicht gleichmässig im gesamten Ozean, einige Regionen werden stärker als andere davon betroffen sein. Daraus können Überflutungen von Küstenregionen und steigende Grundwasserspiegel resultieren. Eine zunehmende Versalzung des Grundwassers steht zu befürchten.

Wegen der möglichen Effekte auf die Küstenregionen ist die Meeresspiegeländerung eine der größeren Gefahren von Klimawandel. Jede Änderung in einem der Bestandteile des Klimasystems -Ozean, Kontinent und Eiskappen - hat einen spürbaren Einfluss auf der MSL Anstieg. Großen Unsicherheiten bleiben, auch wenn zwei Hauptursachen des MSL Anstieges identifiziert werden konnten. Es sind primär die thermische Ausdehnung des Wassers durch die Erwärmung der Ozeane und das Abschmelzen der Gletscher und der polaren Eisdecken. Wesentliche Unsicherheitsfaktoren sind die Beiträge von Grönland und der westlichen Antarktis mit ihren großen Eisvorräten. Unsicher sind auch die regionalen Meeresspiegeländerungen und die Änderungen der kontinentalen Wasserspeicher. Darüber hinaus können anthropogene Effekte wie Landsenkungen Meeresspiegeländerungen relativ zur Küste verursachen, die mehr als viermal stärker als der weltweite Meeresspiegelanstieg sein können.

Diese weltweiten und sehr präzisen Analysen sind durch die Satellitenbeobachtungstechniken ermöglicht worden. Die Kombination der geodätischen Raumverfahren hat ein globales Bezugsreferenzsystem realisiert, das es erlaubt, präzise langjährige Beobachtungen in einem einheitlichen System zu beschreiben und signifikante Veränderungen zu erfassen.

Diese Arbeit basiert auf allen bisherigen Altimetersatellitenbeobachtungen in Verbindung mit Positionierungs- und Schwerefeldsatelliten. Das Ziel besteht in der Analyse der regionalen Meeresspiegelvariabilität und in dem Verstehen seiner Ursachen. Diese Arbeit beinhaltet auch Verbesserungen der Altimetrie im Küstennähe. Durch Re-tracking, d. h. neue Analyseverfahren der Radarechos, wurde der Einsatzbereich wesentlich erweitert. Für die grösste Herausforderung der Altimetrie, die Anbindung der Altimeterdaten an die Pegelmessungen, konnten dadurch deutliche Verbesserungen erzielt werden.

Damit eröffnet sich die Möglichkeit globale, regionale und lokale Effekte in einen Zusammenhang zu bringen. Historische Langzeitbeobachtungen können gemeinsam mit gegenwärtigen Meeresspiegelmessungen für Vorhersagen genutzt werden.

Contents

1	Introduction	7
2	Background	11
2.1	Improvement of multi-mission satellite altimetry records	11
2.2	Quantification of global and regional sea level change	14
2.3	Attribution of sea level rise	15
3	Synthesis of Publications	17
3.1	Improvement of multi-mission satellite altimetry records	17
3.2	Quantification of global and regional sea level change	20
3.3	Attribution of sea level rise	25
4	Outlook and future perspective: Observing our planet for a safer world	29
5	Publications	39
5.1	Included in this Habilitation	39
5.2	Other Publications	40
6	Improvement of multi-mission satellite altimetry records	45
6.1	Modelling the sea level variations for the unification of altimetry missions	46
6.2	An Assessment of satellite altimetry in proximity of the coastline	54
6.3	Coastal Sea Surface Heights from Improved Altimeter Data	62
6.4	A Study on the conformance of altimetry and in situ data near coast	71
6.5	Validation of CryoSat-2 data in SAR Mode in the German Bight Area	78
7	Quantification of global and regional sea level variability	91
7.1	Coastal and global sea level	92
7.2	Analysis and representation of regional sea level	107
7.3	Long-term sea level change in the Mediterranean Sea	130
7.4	Vertical land motion in the Mediterranean Sea	147
7.5	Sea level variability and trends in the Adriatic Sea	164
7.6	Sea level change and vertical land motion in the Indonesian region	185
8	Attribution of sea level rise	199
8.1	Mass variation in the Mediterranean Sea	200
8.2	Mass variation in the Mediterranean and Black Seas	211
8.3	Decadal variability of the net water flux at the Mediterranean Gibraltar strait	241
A	Glossary	267
	Bibliography	271

Chapter 1

Introduction

This compilation submitted for my Habilitation at the Fachbereich Bau- und Umweltingenieurwesen of the Darmstadt Technical University, comprises of 14 publications selected from 38 manuscripts which I have produced in the period 2001-2013. Of the the total 38 publications, 19 have appeared in international journals, 5 as book chapters and 14 in conference proceedings or in other journals.

The selected 14 manuscripts were all produced as a leading author. The support provided by the co-authors mainly consisted in sharing of data, contributions to discussions and participation in manuscript writing. Additional support is briefly described in Chapter 4.

I have been working on several projects related to sea level change, five of which have been funded by the German Research Foundation (DFG). The first project entitled "Modelling of the Variability of sea level from satellite observations at regional and global scales" signalled the beginning of my post-doc research work with a fellowship for habilitation (DFG FE534/1-2). This project supported investigations on regional temporal variation at seasonal and on interannual time scales.

The second project "European Sea Level Service Research Infrastructure (ESEAS-RI)" involving an international group funded by the European Union, supported investigations on both global and regional scales and included a larger database of in-situ data.

The third project "REgional COastal SEa LEvel change and sea surface Topography from altimetry, oceanography and tide gauge stations in Europe (RECOSETO)" and its continuation in the running project (Project 4) "COastal SEa LEvel" (COSELE), were dedicated to the reprocessing and improvement of altimetry data in selected coastal areas and to their validation against in-situ data.

The fifth and sixth projects "Spatial and Temporal Resolution Limits for Regional Mass Transport and Mass Distribution Parts 1-2" were part of DFG Priority Program SPP1257 Massentransport, which funded a national collaboration effort between disciplines. The supported investigation resulted in a comprehensive analysis of the regional mass transport and mass distribution in the Mediterranean and Black Sea catchments.

Finally, the DAAD project "Monitoring sea level variability in Indonesian coastal waters using satellite altimetry" and the European Union (EU) Project "GEO2TECDI" were also applicable to this work. All investigations have substantially benefited from the excellent and constructive collaborations within the projects.

The general aim of this work is a comprehensive analysis of the regional sea level variability and of its causes with particular attention to the coastal zone. The three main scientific objectives are:

1. **Improvement of multi-mission satellite altimetry records**
2. **Quantification of global and regional sea level change**
3. **Attribution of sea level rise**

The innovative aspects consist of:

- (a) **unification of approximately 20 years of multi-satellite data.** For a very accurate estimation of global and local sea level change long-time series of high accurate sea level heights are mandatory. Time series longer than each satellite lifetime are obtained by combining the data from different missions and need intensive calibration and validation activities to homogenisation the data and the environmental corrections applied.
- (b) **improvement of data quality in coastal area and validation with in-situ and model data.** A challenging aspect is actually the extension of satellite altimetry analysis to the coastal zone, which has been neglected during the first ten years of satellite altimetry due to the too noisy measurements.
- (c) **separation of mass and volume sea level change.** Gravity missions directly measure the mass change, while the total (volume) change is directly measured by satellite altimetry. Contemporaneous observations allow the detection of the relative importance of those two terms.
- (d) **closing of budget and accuracy estimates based on empirical comparisons.** The application of the water budget equation to a closed basin (or globally for the complete Earth) is based on observational estimates and allows the derivation of one part of the budget, with the case of the Mediterranean Sea considered in this instance.

Chapter 2 provides a general introduction to the topic. In Chapter 3 the results of the various publications are summarized and grouped into three parts corresponding to the main objectives 1-3 given above. Chapter 4 provides an outlook. Chapter 5 lists all my papers; the most significant of which are included in Chapters 6, 7 or 8 following the grouping defined above.

Chapter 6 (five papers) is dedicated to both the validation and the analysis of the altimetric measurements with particular attention to the coastal zone. The first paper deal with the single- and multi-mission data unification in open sea, while the next three papers present an assessment in coastal regions of both standard and newly re-tracked altimetry data in pulse-limited mode. The last paper describes the regional validation of data in Synthetic Aperture Radar (SAR) mode from the CryoSat-2 altimeter mission.

Chapter 7 (six papers) presents global and regional estimations of sea level variability from altimetry and tide gauge data. It includes a study on global coastal sea level as well as regional studies in Europe and in regions characterized by high sea level rise rates, in the western Tropical Pacific.

Chapter 8 (three papers) is dedicated to the analysis of the reason for sea level change. In the first two papers, space-based data and models are combined to separate volume from

mass change in the Mediterranean-Black Sea region and to evaluate the corresponding errors. Finally the last paper provides an estimation of the Gibraltar net flow over 40 years by closing the water budget and combining multiple observational data and regional model simulations.

Chapter 2

Background

2.1 Improvement of multi-mission satellite altimetry records

Satellite altimeters are nadir-pointing active microwave instruments measuring the two-way travel time of short pulses reflected from the Earth's surface. The shape of the reflected signal, known as the waveform, represents the time evolution of the reflected power as the radar pulse hits the surface.

Since the beginning of the Topex/Poseidon (T/P) mission in 1992, satellite altimetry has provided near-global maps of sea level change with high spatial and temporal resolution for oceanography and geodesy goals, e.g. establishing a multi-mission climate record, monitoring of the circulation mesoscale in near real time, determination of mean sea surface, bathymetry etc.

In total ten satellite altimetry missions have been flown from 1992 to 2013 (T/P, ERS-1, ERS-2, Jason-1, Envisat, GFO, Jason-2, CryoSat-2, HY-2A, SARAL/AltiKa). All of them, with exception of CryoSat-2, use a low resolution mode (LRM) and provide pulse-limited altimeter products [Chelton *et al.*, 1989], Jason-3 is the follow-on to Jason-2 and will inherit its main features, including orbit, instruments and measurement accuracy. Cryosat signaled the start of a new type of altimeter based on Synthetic Aperture Radar (SAR) [Wingham *et al.*, 2004] [Wingham *et al.*, 2006], which is also planned on Sentinel-3 and Jason-CS. Figure 2.1 shows past and new missions for the period 1992-2015.

The wide-swath altimetry technology of the Surface Water Ocean Topography (SWOT) mission is expected to allow an almost full coverage of the world's oceans and freshwater bodies. Discussion now focuses on the importance of high-rate waveform sampling for improved waveform re-tracking. The optimal utilisation of end-of-life missions for both geodetic and mesoscale applications is also a critical issue.

For long-term sea level studies, the continuity and the unification of the altimetry missions is critical and therefore a priority. The accuracy on the derived range is in the order of centimetres and varies between satellites. Errors are mainly due to inaccuracies in the orbit and in the corrections applied. The sea level relative to a geocentric reference frame is estimated with accuracy between 3 and 5 centimetres (total root mean square (RMS) error at 1Hz along track sampling). On open sea, Topex/Poseidon and Jason-1 and 2 missions claim accuracy of 4 cm for 1-sec measurements while lower orbit satellites, e.g. Envisat, have a lower single measurement accuracy of 6 cm. The claimed accuracy for global mean sea level, averaged

over a 10-day orbital cycle, is 2-4 mm, which translates into a 0.05-0.1 mm/yr uncertainty for global mean sea level changes. Nevertheless, differences of up to 0.5 mm/yr in altimetry-based rates of sea level rise are common [Ablain *et al.*, 2009]. Instrumental factors, time-gaps between the missions, unknown bias in the altimeter range and residual errors in corrections still affect the estimated sea level change [Dorandeu *et al.*, 2004]. Corrections for Sea State Bias (SSB) (Labroue *et al.*, 2004), wet tropospheric delay (from the satellite microwave radiometer (MWR)), [Scharroo *et al.*, 2004] and atmospheric pressure effects (IB, *Le Traon and Gauzelin* [1997],) have been improved.

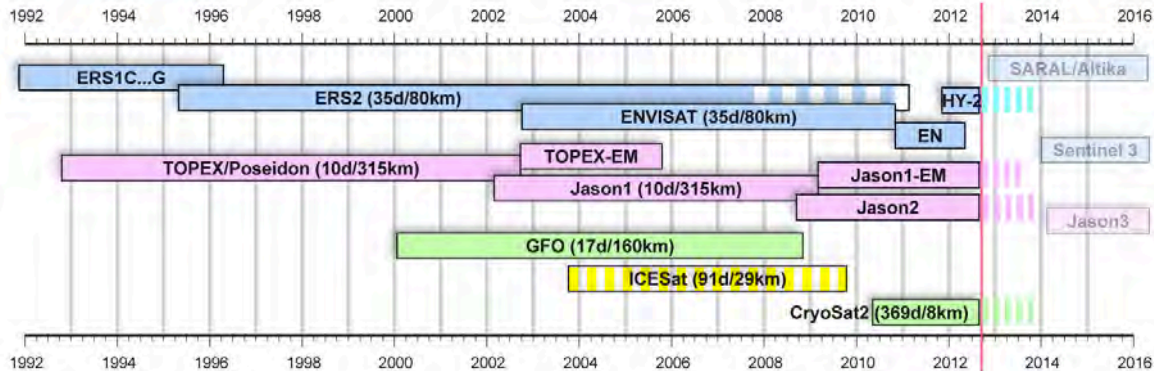


Figure 2.1: Past and future altimeter missions. The ESA missions ERS-1, -2 and ENVISAT (blue) have a repeat cycle of 35 days and a 80 km track separation at equator, The CNES/NASA missions T/P, Jason-1, 2 (red) have a repeat cycle of 10 days and 315 km at equator. CyoSat-2 has a repeat cycle of more than 300 days. SARAL/AltiKa has the same ground-track of ENVISAT. Sentinel-3 and Jason-3 are the next missions (from *Kusche et al.* [2013]).

While standard Geophysical Data Records (GDR) 1-Hz data have been successfully used in open ocean applications, coastal applications require dedicated processing to get close to the shore [Dufau *et al.*, 2011]. Many technical improvements have been made over the last few years in recovering data from the coastal zone and improving the error budget. One of the main areas of improvement is re-tracking; wet tropospheric and ocean tide corrections have also developed. Shallow-water tides have been taken into account for developing dedicated regional tidal corrections in coastal regions.

A major limitation for altimetry is the contamination of the radar signal close to the coast when the reflection of the radar pulse is partly due to both the ocean surface and to land. Standard altimetry data, under the usual processing schemes, have been proven to be unreliable at distances closer than 40 km to the coast.

The satellite radar altimeters emit pulses of electromagnetic waves and record waveforms associated with the reflection from the surface of the Earth within the instrument footprint area. The on-board tracking system ties the half-power point on the leading edge of the waveform to a specific location in the time domain corresponding to the echo from the nadir surface. The on-board tracker keeps the reflected signal from the Earth surface within the altimeter analysis window and predicts the likely position of the next echo based on information derived from the echoes the receiver has just recorded. To improve the accuracy on range measurements, today altimeters downlink the waveforms to Earth and the final retrieval of geophysical parameters from the waveforms is performed on the ground. This is called waveform re-tracking. We distinguish between empirical (e) and physically-based retrackerers (p), the last are derived from theoretical knowledge of microwave scattering at nadir. The empirical retrackerers are divided again in two categories: the one based on statistical properties of the waveforms (e1) and the other based on empirical function forms (e2). In (e2) and in (p) a

functional model is fitted to the waveforms. The functional model is either purely empirical (e) or based on physics (p). Figure 2.2 (left) gives the parameters extracted by the empirical β_5 retracker: thermal noise level (β_1), return signal amplitude (β_2), mid point on the leading edge (β_3), waveform rise time (β_4), slope of the trailing edge (β_5). Figure 2.2 (right) gives the geophysical parameters retrieved by a Maximum Likelihood Estimator (MLE) fit to the Brown ocean model [Brown, 1977]: MLE-3 retrieves the three parameters range, SWH and σ_0 , MLE-4 retrieves in addition the antenna mispointing angle.

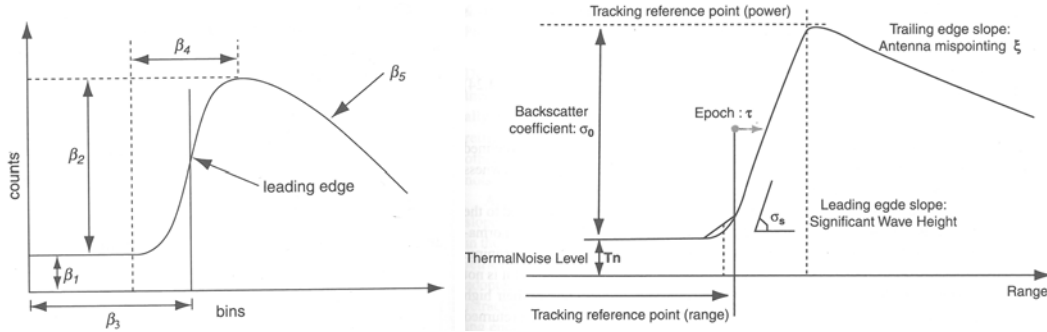


Figure 2.2: Schematic diagram of β_5 (left) and Brown (right) retracker [Gommenginger et al., 2011]

Recently a number of improved re-trackers have been identified as performing better close to the coast. Bright target returns in the coastal zone can be mitigated by re-tracking over a truncated version of the waveforms. Modified re-tracking models combine the Brown model with models including one or more spurious peaks (e.g. Halimi et al. [2011], Halimi et al. [2013]). Another approach is to clean the waveform of the peaks with some filtering scheme before re-tracking (Thibaut et al. [2010], Idris and Deng [2012]). Finally innovative re-tracking schemes use information in adjacent waveforms; examples are the de-noised estimations with Singular Value Decomposition, the geometric approaches to waveform cleaning near the coast, and the Bayes Linear re-tracker [Amarouche et al., 2004].

The SAR mode allows a higher resolution and improved altimeter derived parameters, which is of particular interest in the coastal zone. The CryoSat-2 SAR mode offers two types of products for the same Full Bit Rate (FBR) acquisition. The standard procedure consists in the transformation of FBR data, also called L1a data, in multi-looked Delay-Doppler (aka SAR) processed waveform data (L1b data). The L1b waveforms are subsequently retracked, analogously to pulse-limited altimetry, in order to derive the geophysical products (L2 data). Alternatively, FBR data can be still processed without exploiting the synthetic aperture concept and in this case they are referred as Pseudo Low Resolution Mode (PLRM). The SAR mode of CryoSat-2 is expected to provide Sea Surface Height (SSH) and Significant Wave Height (SWH) with improved accuracy and resolution compared to the pulse-limited altimeter product (LRM). Figure 2.3 shows the two principles.

The re-tracking results can be evaluated by comparison of the altimetric-derived sea level heights, waves and winds with in-situ data. Tide gauges and synthetic heights derived from coastal radars [Roesler et al., 2013] and geoid heights [Hwang, 1997], have been used to validate altimeter SSH data in the coastal zone. Moored acoustic Doppler current profilers were used to validate near surface geostrophic velocity, wave-rider buoys to validate SWH (Gomez-Enri et al. [2010], Caballero et al. [2013]) and in-situ and model outputs to validate the wind speed [Abdalla et al., 2011].

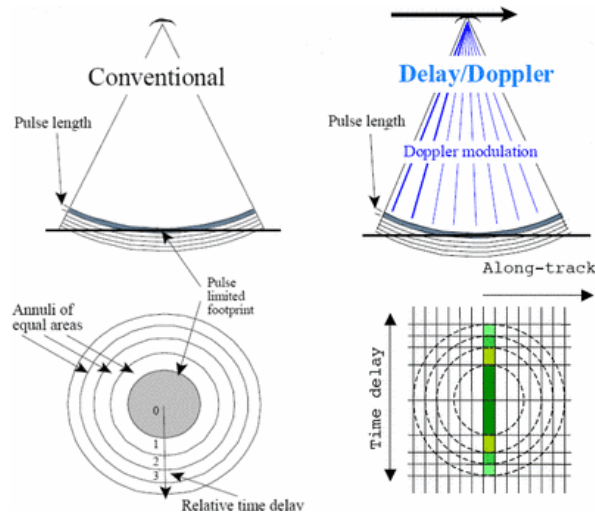


Figure 2.3: Conventional Low Resolution Mode (LRM, left) and Synthetic Aperture Radar (SAR, right) principles [CLS, 2013]

2.2 Quantification of global and regional sea level change

The analysis of sea level change based on tide gauges alone reflects the local sea level change relative to land, while the sea level change based on altimeter data is relative to the Earth’s centre, more precisely to a reference ellipsoid, and is global.

Sea level change has therefore in altimetry its global primary source of information. Satellite altimetry has shown that sea level varies on seasonal, interannual, decadal and long-term time scales and that these variations are not globally uniform. At least 50-years of records are needed to separate secular, decadal and interannual variations [Douglas, 2001]. However, there are only a few tide gauges along the world coastlines available for the analysis which cover such a lengthy period [Church *et al.*, 2008], [Church *et al.*, 2011]. The spatial distribution of tide gauges as well as the existence of interannual and low frequency signals affect the recovery of secular trends in short records. Thus it is important to develop techniques for the estimation of sea level trends cleaned from decadal variability.

Over the past century, the coastal global average sea level rise derived from tide gauge data is in the range of 1-2 mm/yr (Cazenave and Nerem [2004], Holgate and Woodworth [2007], Church and White [2006], Domingues *et al.* [2008]). Jevrejeva *et al.* [2006] assign an error of 1 mm/yr to the global sea level change derived from tide gauges, due to the non-uniform data distribution.

In comparison, estimates for the global sea level rise derived from altimetry without accounting for the Glacial Isostatic Adjustment are around 2.8 ± 0.4 mm/yr between 1993-2003 (Bindoff *et al.* [2007], Lombard *et al.* [2005]) 3.1 ± 0.4 in 1993-2006 [Beckley *et al.*, 2007] and 3.1 ± 0.1 mm/yr between 1993-2007 [Prandi *et al.*, 2008]. In addition to the uncertainty of the rate due to the fitting procedure, measurement errors and omission error are involved. The altimeter calibration using co-located altimetry and tide gauge stations gives an error of 0.4 mm/yr [Mitchum, 2000], [Leuliette and Nerem, 2004]. Estimates of sea level rise obtained by different research groups over the same period 1993-2012, provided the same results, a 3.2 mm/yr trend with a 0.4 mm/yr uncertainty [Masters *et al.*, 2012]. Departures result from differences in the data processing and in the geophysical corrections used. Understanding and

reducing the differences between the time-series and the uncertainty in the global mean sea level time series is important for improving confidence in the climate record for monitoring climate change.

”Is the rise of sea level uniform?” is the fundamental question. *Holgate and Woodworth* [2004] report a coastal sea level trend of 4 mm/yr between 1993-2002 and, comparing this value to the lower global rate of 3.1 ± 0.4 ask : ”Is the rise of coastal and global sea level different?”. It is now accepted that the difference between the rates from global altimetry and coastal tide gauges is due to the different sampling [*White et al.*, 2004] and to the interannual variability [*Prandi et al.*, 2008].

Geographical patterns of sea level change are far from being uniform, as revealed by altimeter satellites [*Cazenave and Llovel*, 2010]. When considering coastal security issues, especially regional and local sea level (relative to the coast line) are important, while the global mean is less relevant. Regionally, the global sea level rise (SLR) in response to ocean warming and ice melting [*Nicholls and Cazenave*, 2010] has important implications, such as beach erosion, inundation of land, increasing salination of coastal aquifers, increasing flood, storm damage, and loss of the coastal ecosystem. The climate-related sea level rise may be reinforced by land subsidence due to natural (e.g. tectonics and volcanism) and anthropogenic (e.g. ground water extraction) causes.

In the presence of decadal variability it is difficult to detect accelerations in the sea-level rise. Those decadal variations are mainly related to changes in heat content and circulation and caused by climate patterns such as El Nino Southern Oscillation (ENSO) and the North Atlantic Oscillation (NAO) [*Cazenave et al.*, 2012]. Thus it is necessary to separate the different physical components causing the decadal variability and understand the reason for the observed variations. The attempts to reconstruct past-decade sea levels, combining sparse and long tide gauge records with sea level time series of limited temporal coverage, have shown that the results are very sensitive to the input of spatial information (e.g. *Church and White* [2011], *Meyssignac et al.* [2012b] for global scale and *Meyssignac et al.* [2011], *Calafat and Gomis* [2009] for regional scale). The ultimate goal of those reconstructions is to constrain coupled climate models used by the IPCC, to predict SLR over the 21st century.

2.3 Attribution of sea level rise

Understanding ongoing and predicting future sea level changes requires an understanding of the contributing processes at regional and local levels.

The sum of the observed contribution to sea-level rise has been compared on a global scale to the observed rise over multi-decadal period and recent results show an improved closure of the sea-level global budget both in trends and in mean trend variability. (e.g. *Cazenave and Llovel* [2010], *Moore et al.* [2011], *Church et al.* [2011]).

We distinguish between five components of sea level change, namely the mass-, steric-, meteorological-, circulation- and the climate/anthropological components, the last one being a forcing factor of the first four. As an example, the anthropologic forcing causes, by increasing CO_2 , a warming of the atmosphere. This effect causes changes both in the mass component (through ice melting) and in the steric component (through the coupling of the warmer atmosphere with the ocean). When dealing with slow processes, the major factors for global sea level are water mass addition/removal from the oceans due to the melting/growing of continental ice, referred to as the mass component [*Henry et al.*, 2012], [*Becker et al.*,

2012] and changes in the volume of the water column, mainly attributed to thermal expansion/contraction and referred to as the steric component [Levitus *et al.*, 2000]. The salinity changes on a global level are considered of less importance, although such statements are based on the unverified assumption that the total salt content of the oceans remains constant. On a regional scale, however, and in the Mediterranean Sea in particular, salinity plays an important role as it affects both the mass component and the density of the sea water and hence its volume. The thermosteric spatial patterns are not stationary but fluctuate in time and space in response to driving mechanisms such as ENSO, NAO the Pacific Decadal Oscillation (PDO) [Lombard, 2005] and result from the redistribution of heat and fresh water through air sea fluxes and changes.

The effect of atmospheric pressure and wind, referred to as the meteorological component of sea level, and changes in the circulation also contributes to regional long term sea level variability and to its mass change. Surface wind stress has been identified as the driving mechanism of circulation-based heat and salt redistribution over the past few decades [Timmermann *et al.*, 2010].

Although progress has been made in quantifying the two primary contributors to sea-level rise, namely, thermal expansion due to ocean warming and melting glaciers and ice sheets, large uncertainties remain regarding the effect of changes in continental water storage [Döll *et al.*, 2003]. Present day regional sea level changes appear to be primarily caused by natural climate variability [Meyssignac *et al.*, 2012a]. However, the imprint of anthropogenic effects on regional sea level will grow with time as climate change progresses. Toward the end of the 21st century regional sea level patterns will be a superposition of climate variability modes and of natural and anthropogenically-induced static sea level patterns, with the anthropogenic contributions becoming more prominent.

Interdisciplinary studies are necessary to interpret the observations and analyse the causes of the sea level observations in view of climate change. According to [Kohl and Stammer, 2008] surface fluxes and buoyancy fluxes may have played an increasing role over the past two decades. It is common thought that, by altering the composition of the atmosphere and affecting a variety of other climate factors, human beings have driven the Earth out of radiative balance. In response, the Earth is absorbing excess heat. The World oceans have by far the largest heat capacity of any component of the Earth's climate system and as it warms, the majority of this heat is absorbed by the oceans. Global ocean heat content may therefore provide a proxy for measuring the Earth's energy balance. Furthermore, it has been suggested that the large thermal inertia of the oceans will result in a lag between the radiative forcing that causes climate change and the response of Earth's surface temperature. As such, any climate change caused by changes in the Earth's radiative balance must depend critically on the uptake, storage and transport of heat by the oceans [Solomon *et al.*, 2007].

The advanced remote sensing capabilities provide unprecedented opportunities for monitoring, studying, and forecasting the ocean environment. Altimetry provides the total sea level variability; it does not distinguish between volume (steric) and mass (non-steric) sea level change. To separate between mass and volume change, measurement of mass change and volume change estimated from changes of temperature and salinity of water are necessary. The first comes from GRACE observations, the second from observations and oceanographic models. The GRACE-derived and the altimetry-derived ocean mass change have been shown to be in agreement on both global (e.g. Willis *et al.* [2008b]) and regional scales. GRACE data have been used to separate altimetrically observed sea level variations into the mass and steric components (e.g. Rietbroek *et al.* [2012]). Integration of altimetry, GRACE and ARGO data may also allow for quantification of steric contributions within the deep ocean.

Chapter 3

Synthesis of Publications

In the following chapters recently published results are presented in a total of 14 publications. The manuscripts are arranged into three thematic chapters as follows:

3.1 Improvement of multi-mission satellite altimetry records

This chapter includes analysis of validation, calibration and improvement of multi-mission satellite altimetry data in open ocean and coastal zones.

F-01: Modelling the sea level variation for the unification of altimetric mission, in Chapter 6.1.

A careful merging of altimetry data from different missions is mandatory to increase both the time-series length and the spatial resolution of the data. The time-series need to be harmonized in absolute bias and corrections. A cross-validation and calibration of contemporaneous altimetric mission data is performed in a dual crossover analysis to estimate the relative biases between the missions data. The early ESA missions (ERS-1, -2) data have the higher errors. The higher quality of T/P is confirmed by the better agreement with in-situ tide gauge data observations (F-06), where the spurious negative trend in ERS-2 shown by the cross-over differences are corrected by fitting ERS-2 to the T/P data. Today the errors of altimetry data are well below those of the last decade and are small for all the satellite missions.

The continuity of the altimetry missions is of high concern in F-01 and an attempt is made to compare non-simultaneous missions using proxy data. Due to the strong correlation between the sea level and sea surface temperature in the Mediterranean Sea, the sea surface temperature is successfully used as predictor to construct an extrapolated model of sea level variability. Empirical statistical models are obtained by applying the Principal Component Analysis (PCA) and Canonical Correlation Analysis (CCA) methods.

The results show that the monitoring of dual crossover (DXO) differences of Sea Surface Heights (SSH) data corrected by an Sea Level Variability (SLV) predicted model is promising to cross-calibrate present and past altimetric missions. However the correlation between sea level and sea-surface temperature change is made more complex by atmospheric pressure change, wind effects, circulation and water transfer with the Atlantic, which are related to the NAO and ENSO climatic indices.

F-02: An assessment of satellite altimetry in proximity of the Mediterranean coastline, in Chapter 6.2.

A major limitation for altimetry is the contamination of the radar signal near the coast where the reflection of the radar pulse is partially due to the ocean surface and partially to land. Various satellite altimeter databases are investigated to determine the minimum distance from the land at which they remain usable. The standard Level 2 products (GDR) and the corresponding re-tracked Topex/Poseidon data sets (R-GDR) are considered, as well as the data obtained from ERS-2. Cross-comparison of the altimeter data and in-situ validation at tide gauge stations show a better performance of the re-tracked data. Standard altimetry data is considered less reliable at distances closer than 40 km to the coast. Here more usable R-GDR than GDR data starting from 25 km from the coast is found.

F-03: Coastal sea surface heights from improved altimeter data in the Mediterranean Sea, in Chapter 6.3.

This paper shows that the usual open ocean validity checks are too restrictive near the coast and that improved data screening strategies retain a larger number of valuable Envisat data. The selected test area is the Mediterranean Sea and a validation with in-situ data is included. The selection criteria analysis shows that the microwave radiometer wet tropospheric correction and the standard deviation of the 18 Hz re-tracked ranges are the most frequent causes for data rejection. Envisat has better skills than Topex/Poseidon in coastal regions and that sea-land transition is preferable over land-sea transition. The analysis is pursued in *Bouffard et al.* [2011], where a similar conclusion for the X-TRACK altimetric dataset is found (CTOH/LEGOS), which is based on an improved data screening only, without re-tracking of the original waveforms.

Conversely, in F-03, the Envisat waveforms are re-tracked in the coastal zone to improve the estimation of SSH near land. Also it is analyzed which characteristics of the land and ocean transition (e.g. flight from sea to land or from land to sea (Fig. 3.1) and sea state conditions) affect the waveforms and therefore the quality of the measured altimeter range. The empirical re-tracking methods used are based either on the statistical properties of the waveform data (threshold and improved threshold re-tracking algorithms), or consists of fitting empirical functional forms (as the β_5 re-tracker). A detailed description of the empirical methods is provided in *Gommenginger et al.* [2011]. The quality of the SSH data is quantified by the standard deviation of differences between SSHs and geoid heights using the Improvement Percentage (IMP) factor. The improvement obtained by re-tracking, is quantified by comparing the standard deviations defined above for both standard and re-tracked data. The most significant improvements are achieved with the (β_5) and the Improved Threshold re-tracker methods. It is observed that at that distance of 5 to 10 Kilometer from the coast the waveforms start to differ significantly from the normal ocean-like Brown form. The data rejection is however related to both the signal and the re-tracking method used. In our case, when both the improved selection criteria and the empirical re-tracking are applied, the altimeter data are usable for a sea-land transition at 3 km from the coast, and for land-sea transitions at 5 Km from coast. It can be concluded that the applied strategy avoids systematic rejections and the recovered sea level anomalies still exhibit a physical significance.

F-04: A Study on the conformance of altimetry and in situ surface data near coast in Chapter 6.4

The paper describes a validation exercise of altimetry-derived sea level heights against in-situ data. This is the first paper using the German Bight as validation area. The satellite mission is Jason-2. The paper shows that the German Bight is a suitable area for in-situ validation, due to its network of tide gauges, offshore platforms, GNSS stations. High frequency in-situ measurements of wave height, wind and sea level above the reference ellipsoid are here available. In particular, this last (sea level at tide gauge with GNSS) is directly comparable to

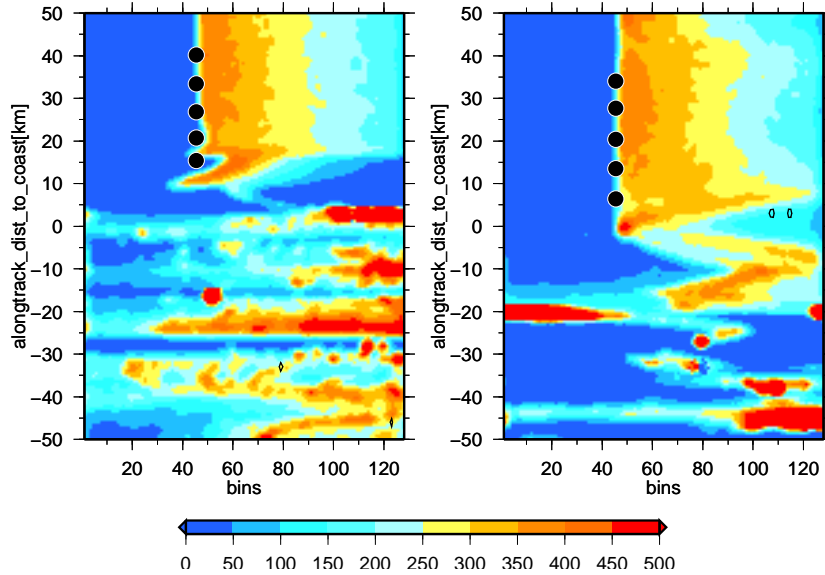


Figure 3.1: Perturbation due to sea-land and land-sea transition: Envisat waveforms at a sea-land (Genova, left) and a land-sea (Imperia, right) transition and Envisat 1 Hz NP (circles). Scale is waveform amplitude in FFT filter units

sea level measured by satellite altimetry. Since 2000, the Bundesanstalt für Gewässerkunde (BfG) is building up a set of 28 tide gauges with continuous Global Navigation Satellite System measurements (GNSS) and carefully quality checked one minute sea level values, made available in real time by the Wasser- und Schifffahrtsverwaltung des Bundes (WSV). In this paper we validate both the standard products (GDR) of the RADS database at 1Hz and the coastal products of the PISTACH database at 20 Hz.

The results show that at off-shore locations tide gauge and standard altimetry give comparable sea level heights; however at coastal stations the agreement is lower. The PISTACH data give a significant improvement in SSH between 5 and 10 km from the coast, but at less than 4 kilometers from coast also the PISTACH data are too noisy. The second author, R. Weiss, significantly contributed as part of his PhD Thesis [Weiss, 2013]. The validation of sea wave heights is performed in the same region in Passaro *et al.* [2015] and shows an improved accuracy in the wave heights derived from the ALES retracker [Passaro *et al.*, 2014], which is dedicated to the coastal zone.

F-05: Validation of CryoSat-2 altimetry in SAR Mode in the German Bight Area in Chapter 6.5

The Synthetic Aperture Radar (SAR) altimetry is expected to provide improved precision and along-track resolution compared to the conventional low-resolution mode (LRM) radar altimetry. CryoSat-2 enables a quantitative comparison of SAR and Pseudo-LRM (PLRM) data derived respectively from a coherent and an incoherent processing of the same SAR echoes. In this paper we perform their cross-validation and validation against in-situ and model data to derive precision and accuracy at 1 Hz in open ocean, at distances larger than 10 kilometers from the coast. All three altimetry-derived parameters are considered: sea wave heights (SWH), wind speed at 10 meters height (U10) and sea level height. In addition to the network of in-situ data, ocean, wave and weather-models data are used here, made available for example by the Bundesamt für Seeschifffahrt und Hydrographie (BSH). To derive the geophysical parameters from the SAR waveforms, the power return is modeled by the SAMOSA fully analytical model truncated at the zero-order term (Eq. 43 in Ray *et al.*

[2015], known as SAMOSA3). The SAR processing includes a Look Up Table to correct for approximations of the Point Target Response (PTR) applied in the retracking procedure. Both the PLRM and the SAR processing scheme include identical environmental and geophysical corrections.

The results show that coherent (SAR) and incoherent (PLRM) processing of SAR altimetry give consistent unbiased results. The Look-up table significantly benefit SWH retrieval during SAR altimeter processing. Sea level and wave height from SAR are twice as precise as Pseudo Pulse Limited data. The second author, S. Dinardo, significantly contributed to this analysis. See details of the analysis and updates in *Fenoglio-Marc et al.* [2015].

3.2 Quantification of global and regional sea level change

This chapter includes analysis of regional and global analysis of sea level variability.

F-06: Coastal and global sea level in Chapter 7.1.

A global analysis of sea level change has been performed during the period 1993-2008. Four types of averaged sea level have been compared; (1, GSLA) global averaged sea level from altimetry; (2, CGSLAT) global averaged sea level from altimetry at selected tide gauges locations; (3, CGSLA) coastal sea level from altimetry; and, (4, CGSLT) coastal sea level from tide gauges at selected locations.

Comparable results have been found for (2) and (4) using 267 tide gauges: the mean coastal sea level from tide gauge and co-located altimetry (CGSLT and CGSLAT) have correlation 0.97 and RMS 3.7mm. Regionally, there is also a similarity between coastal and open-ocean sea level variability from altimeter data, and trends are positive in the main world basins. Over 10 years, from January 1993 to December 2004 both (1), (2) and (3) rise by about 3.0 ± 0.5 mm/year. However over shorter periods the coastal sea level rises faster and over longer periods slower than the global mean. Figure 3.2 shows the trends and trend errors estimated using intervals of different lengths starting in 1993.

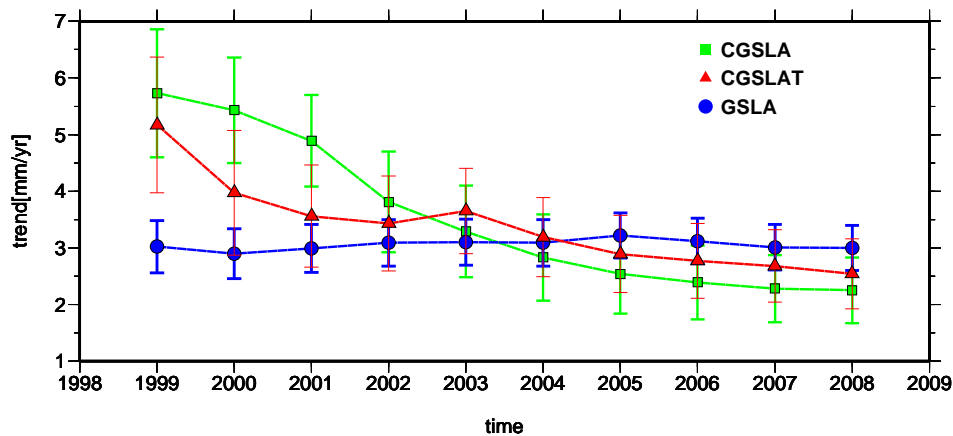


Figure 3.2: Trends and error bars of global sea level (circle), coastal sea level within 150 km from coast (square) and coastal sea level at the 267 altimeter locations co-located to the tide gauge stations (triangle). Time intervals start in 1993.

It is shown that the interannual variability is regionally dependent. In particular, the difference of coastal and global trends is due to the higher interannual variability of coastal sea level. The sea level regional variability is averaged out when computing the global mean.

The regional interannual variability causes also the differences between coastal sea level rise observed at a selected set of 267 stations of the Permanent Service for Mean Sea Level and coastal sea level rise computed from satellite altimetry in a distance of 150 km from the coast. Also the sea level drop in the Eastern Pacific and the sea level rise in Western Tropical Pacific is due to the regional interannual variability.

It is shown that the interannual variability is highly correlated with the El Niño Southern Oscillation (ENSO) and the North Atlantic Oscillation (NAO) climatic indices over both the altimeter period and the period 1950-2001. Due to the large scale of those signals, a small number of stations with good spatial coverage are needed.

It is attempted to reconstruct the interannual variability using the spatial pattern from altimetry and the temporal patterns from tide gauges correlated to NAO and SOI. This reconstruction restitutes about 50% of the observed interannual variability from 1993-2001. Over the longer period 1950-2001, the correlation between the SOI and NAO climatic indices and the temporal patterns of the interannual and interdecadal models holds; however, the number and location of the available tide gauge stations significantly affect the correlation. The variability of the trends is therefore related to the time-scales of the NAO and SOI indices.

This analysis contributes to answer to the question: "Is the rise of sea level uniform?", and also to the slightly different question: "Is the rise of coastal and global sea level different?" posed by Holgate [Holgate and Woodworth, 2004]. Agreement is reached with Prandi *et al.* [2008] that the different rates between coastal and global mean sea level noticed between 1993-2002 by Holgate and Woodworth [2007] do not arise from a coastal mean sea level rising faster than the global mean, but from the interannual variability of coastal sea level.

F-07 Analysis and representation of regional sea-level variability from altimetry and atmospheric-oceanic data in Chapter 7.2

The regional sea level change in the three main European basins, the Mediterranean Sea, North Sea and Baltic Sea, is performed for the period 1993-2000. The aim is to characterize the differences in the sea level variability and in the relationship between this parameter and other climate parameters, namely the sea surface temperature and atmospheric pressure. Statistical analysis is performed. Spectral and multi-variate analysis of the three parameters is made. The analysis method allows the identification of the dominant characteristics of the variability of each field with spectral analysis and principal component analysis. Finally a linear regression analysis and a canonical correlation analysis are used to study the coupled variability between pairs of the fields.

The strongest annual and semi-annual signals are in the Mediterranean Sea, whereas in the other two seas, especially the Baltic Sea, the dominant spectral components have comparable power. The highest positive trends are observed in the eastern Mediterranean Sea; here trends are interpreted as interannual variability due to the shortness of the investigated time period. The coupled-fields study shows a high correlation between the sea-level height and the sea-surface temperature in the Mediterranean Sea and between the sea-level height and the wind speed in both the North and Baltic Seas. In the Mediterranean Sea only four modes of variability are sufficient to explain more than 90% of the variance of the sea level.

The single-mission sea-level variability models constructed, taking the first few relevant modes, are seen here as a first step towards the construction of a multi-mission sea-level model. The Mediterranean Sea was chosen as test area to check the accuracy of the models as well as the ability of the canonical correlation method to predict the sea-level variability. The model accuracy is assessed from the dual crossover height differences between the Topex/Poseidon

and ERS-1 and ERS-2 sea-surface heights corrected using the variability models. Both the single- and the coupled-fields models are found to be a good representation of the sea-level variability in the Mediterranean Sea, whereas the extrapolated canonical correlation model, derived using the sea-surface temperature as a predictor, is less accurate, but still acceptable. Relative bias and drift between the Topex/Poseidon and ERS data result from the analysis and reflect a non homogeneous pre-processing of the altimetry data.

F-08: Long-term sea level change in the Mediterranean Sea from multi-mission satellite altimetry and tide gauges in Chapter 7.3

The regional analysis in F-07 is pursued in F-08 for the Mediterranean Sea for the period 1993-2000. A basin average sea level rise of 2.2 mm/year is estimated, however the rise is not geographically uniform on the basin. Indeed, the positive trend was lower in the western sub-basin (0.4 mm/year), higher in the eastern sub-basin (9.3 mm/year) and a negative trend is found in the Ionian sub-basin (-11.9 mm/year). Single- and coupled-field analysis of the variability of sea level, sea surface temperature, wind and pressure are made by applying different statistical methods (Principal Component Analysis, Canonical Correlation Analysis, spectral analysis and Multi-taper analysis technique). It is noticed that, while at seasonal scales the observed sea level change is of thermal origin primarily, at lower frequencies the atmospheric pressure and wind field variations play an important role. In particular, the correlation analysis between the fields shows that SSH and sea surface temperature fields are strongly correlated at seasonal scales in the entire Mediterranean Sea, while the correlation at low frequencies is significant (more than 0.6) only in the Eastern Mediterranean Sea.

The Western Mediterranean sea level variability is dominated by the seasonal cycle and the interannual variability is lower than in the eastern Mediterranean. Very interesting is the negative trend in the Ionian Sea, observed from altimetry and confirmed by tide gauge data available only in the last decade. The negative sea surface temperature change observed in the sea surface temperature field in that region supports a sea level drop, resulting in a cooling at the sea surface and at a depth associated to a sea level drop. The significant correlation between the low-pass filtered sea level height and atmospheric pressure fields also suggested an atmospheric reason for the negative sea level change. Climatic variations in atmospheric forces can drive substantial changes in the basin-wide large scale currents (see F-12). A negative sea level trend in the circulation of the Ionian Sea is modelled on an oceanographic model run with interannual daily atmospheric forces [*Pinardi and Masetti, 2000*]. There is a strong correlation between cooling in sea surface temperature (and therefore negative sea surface anomaly changes due to the steric components), positive NAO index in successive winters and an increase in the anticyclonic circulation.

F-09: Vertical Land Motion in the Mediterranean Sea from altimetry and tide gauge stations in Chapter 7.4

In this paper vertical land motion has been derived from combined altimeter and tide gauge station sea level measurements. (Fig. 3.3). Hourly data from the Italian tide gauge network has been quality-checked and pre-processed to produce monthly data. In addition monthly data available from the PSMSL dataset are available. Differences of near-simultaneous, monthly and deseasoned monthly sea level height time-series have been considered.

Two datasets have been used: (1) the MED PSMSL dataset that contains 49 stations with monthly time-series extracted from the PSMSL dataset; and (2) the MED LOCAL dataset of 41 stations with hourly data, including 25 stations that are not part of the MED PSMSL dataset.

The PSMSL dataset in the Mediterranean region has been found to be of good quality by comparing monthly data of the stations available in both sets. Jumps in the summer of 1998 in the reference level of all the Italian stations of MED LOCAL are estimated from the monthly differences of altimetry and tide gauge data with an uncertainty less than 2 centimetres. Selection criteria for the tide gauge stations have been applied based on five parameters: (1) the distance (*dist*) between altimeter and tide gauge locations, (2) the correlation between the time-series, (3) the formal error rate of the linear fit to the sea level height differences, (4) the standard deviation of the sea level height differences, and (5) the number of time samples N_m available. Tide gauge stations are selected that satisfy the conditions: (1) *dist* smaller than 110 kilometers, (2) r_{at} higher than 0.60, (3) σ_{at} smaller than 5 mm/yr, (4) std_{at} smaller than 8 centimeters, and (5) N_m bigger than 50. Monthly data, deseasoned monthly data, and near-simultaneous data lead to similar values for the estimated trends. The mean uncertainty of the estimated linear-term is 1.9 ± 0.5 mm/yr for monthly and 1.6 ± 0.4 mm/yr for deseasoned monthly time-series, it increases to 2.3 ± 0.8 mm/yr when accounting for the dependence of the measurements. Results for various stations are in agreement with estimates of vertical land motion from geodetic methods. Comparison with vertical motion estimated by GPS at four locations shows a mean difference of -0.04 ± 1.8 mm/yr, however the length of the GPS time-series and the number of locations are too small to draw general conclusions.

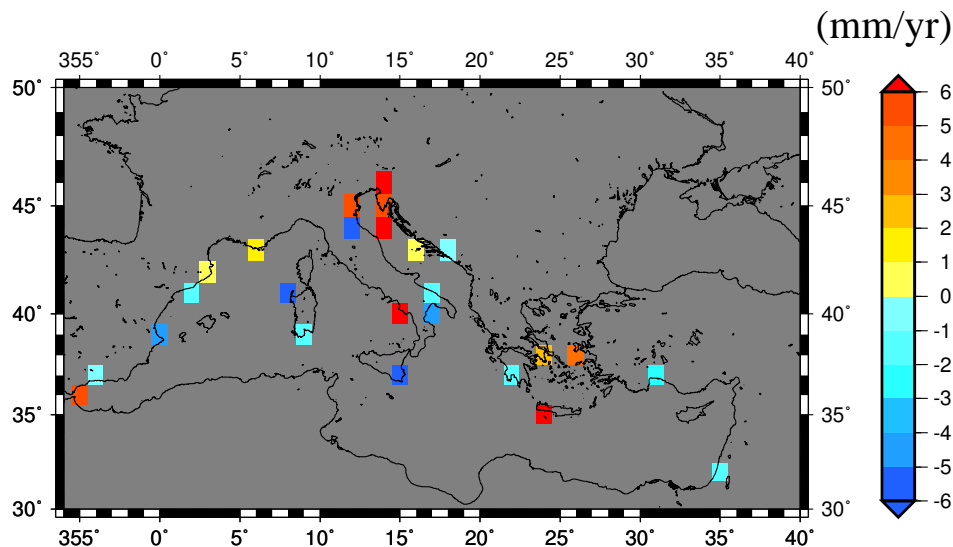


Figure 3.3: Vertical Land Motion estimated from de-seasoned monthly differences of sea level heights from altimetry and tide gauge data.

A similar analysis was applied in *Fenoglio-Marc et al.* [2005] to the complete Iberian Peninsula to investigate, over the period 1993-2001, the interannual to decadal sea level changes.

F-10: Sea level variability and trends in the Adriatic Sea in 1993-2008 from tide gauges and satellite altimetry in Chapter 7.5

The paper gives a consistent view of the low frequency sea level variability in the Adriatic Sea from both satellite altimetry and tide gauge records. 16 years of sea level observations from multi-satellite altimetry and tide gauge records in the time period 1993-2008 have been analysed. First, the impact of the corrections applied to the altimetry-derived sea level variations and the consistency of the altimetric and the tide gauge sea level observations are evaluated. Both observations are then used to characterize sea level trends, interannual variability and land vertical motion in the Adriatic region. Eight tide gauges along the coast show very coherent interannual sea level variations, with an increase in sea level before 2001 and a decrease afterwards. The average of the eight de-seasoned time-series corresponds with the

basin average of the altimeter data, with correlation coefficient 0.84 and root mean square difference 12 mm.

It is found that the linear change is higher for altimetry than for tide gauges and strongly depends on the length of the time-interval, being 3.2 ± 0.3 mm/yr and 1.9 ± 0.3 mm/yr over the period 1993-2008.

The steric contribution to sea level change correlates with the sea level suggesting that the low frequency variability is likely related to oceanic and climatic processes and mainly due to temperature and salinity variations. The decadal sea level variability is correlated in Adriatic and Eastern Mediterranean and anti-correlated in Adriatic and Ionian Sea.

At a given location, the trend of the differences of sea level observations by tide gauges and co-located satellite altimetry gives the vertical land motion, if it is assumed that the sea level signals are truly common. Statistically significant trends are found at the 90% confidence level at two locations, that indicates land uplift along the eastern coast in Rovinj (3.0 ± 1.2 mm/yr) and land subsidence in Marina di Ravenna (-1.5 ± 1.1 mm/yr), while at other locations, e.g. in Trieste (1.3 ± 1.1 mm/yr) the significance is lower. The resulting rate agrees in general in sign with GPS derived rates, but not in magnitude, like in Marina di Ravenna, where the strong subsidence measured by GPS is related to the local anthropogenic subsidence. The differences in trends are partially explained by the spatial distance between the tide gauge and the co-located altimeter.

In the related study [*Tsimplis et al.*, 2011] it is possible to conclude that despite the coherency of the Adriatic in terms of sea level variability, atmospheric trend differences are found locally and the coherency of the northern basin partially breaks up at higher frequencies.

F-11: Sea Level Change and Vertical Motion from Satellite Altimetry, Tide Gauges and GPS in the Indonesian Region in Chapter 7.6

Unlike in the semi-closed Mediterranean Sea, the eustatic sea level rise in Asia has a higher rate than the rate of the global average. The sea level rise in Indonesia was investigated during the period 1993-2011 using satellite altimetry and tide gauge data. Satellite altimetry indicates a positive sea level rise with mean of 4 ± 0.5 mm/yr, which is higher than the global averaged mean sea level rise. The difference of the sea level trends from tide gauge and co-located satellite altimetry is in many cases greater than 3 mm/yr and is in agreement with land subsidence estimated by GPS at Enggano and Tanjung Lesung. Land subsidence is also found in Jakarta, Surabaya and Benoa.

Similarly in *Trisirisatayawong et al.* [2011] high vertical motion and high rates of sea level are found in the Gulf of Thailand. As tide gauge data are available over a longer period of time, the sea level change relative to land is corrected for land motion detected from repeated precise GPS campaign measurements yielding absolute long-term trends. The co-located altimetric sea level rates are between 3 and 6 mm/yr over the past 20 years. Throughout the rest of the Gulf the trend is positive with rising rates in the range of 3 to 5.5 mm/yr. It can be concluded that the fast rising sea level combined with high rates of post-seismic downward crustal motions makes coastal areas and river estuaries along the Gulf of Thailand, and particularly the low-lying megacity of Bangkok, highly vulnerable to flooding (see also [*Fenoglio-Marc and Groten*, 2010]).

3.3 Attribution of sea level rise

In this chapter sea level and mass changes are investigated regionally in an attempt to identify the origin of sea level change. The test area is the Mediterranean and Black Sea region.

F-12: Mass variation in the Mediterranean Sea from GRACE and its validation by altimetry, steric and hydrologic fields in Chapter 8.1

The seasonal component is investigated in this first attempt to assess the ability of GRACE to recover the seawater mass variation in semi-closed basins. Two additional corrections to GRACE data have been identified, which are needed in the type of basins and which were generally not applied in global analysis. They are: (1) the correction for the leakage of hydrology due to the smoothing and to the basin shape and (2) the scaling of the amplitude because of the higher smoothing radius. For the first correction model data is used. For this second correction it has been suggested to derive the scaling factor from another estimation of mass derived from altimetry and steric data or model. The mass change is estimated in the Mediterranean Sea between April 2002 and July 2004 from GRACE and altimetry data and from hydrologic and oceanographic models. A smoothed spatial averaging kernel has been applied in order to obtain a comparable basin average monthly time-series. The smoothing is done in the spectral domain for the GRACE SH fields and in the spatial domain for the regional gridded data to avoid their SH expansion. It was found that the GRACE seawater mass corrected for the leakage of continental hydrology and the filtered steric-corrected altimeter sea level have similar annual amplitude and phase. The correlation between hydrology-corrected GRACE and filtered steric-corrected altimetry is found when using SLR degree-2 annual coefficients and LaD hydrology, the largest departure when GRACE degree-2 terms are included. The estimated scaled mass signal has an annual amplitude of 52 ± 17 mm peaking in November. An attempt to estimate the seasonal component of net flow at the Strait of Gibraltar from the combination of seawater mass variation with the Mediterranean freshwater deficit was made.

In *Fenoglio-Marc et al.* [2007], in a comparison of the accuracies of GRACE-based versus altimetry-based water mass variation in the Mediterranean Sea at the seasonal scale, it is shown that the error of the GRACE estimate is still larger than the error of the estimate derived from the steric-corrected altimeter data. However, an examination of additional temperature and salinity data results in an even closer agreement between GRACE estimates and altimetry measurements than reported in the first study.

F-13: Water mass variation in the Mediterranean and Black Sea in Chapter 8.2

In this paper the analysis is further extended to space and time including the Black Sea domain and longer time-series from August 2002 to July 2008. The analysis of both seasonal and interannual time scales has been introduced. The corrections are improved using more realistic model results. The basin average series agree in terms of annual and inter-annual signals, which is in line with earlier works, although the different model corrections influence the consistency in terms of seasonal signal and trend. The closure of the water budget in both the Mediterranean and Black Sea deriving the strait flows at Gibraltar and through the Bosphorus from the water budget has also been introduced. In this comparison, a variety of auxiliary data have been considered. Continental hydrological models have been used to estimate the leakage correction to the GRACE observations and oceanographic models and data to derive the steric correction to the altimetric sea level observations. The closure of the water budget additionally requires evaporation, precipitation and river runoff estimates.

The comparison between the steric-corrected altimetry and the hydrology-corrected GRACE is good in the Mediterranean Sea, with a comparable accuracy of both series. It is therefore suggested that the missing full agreement of the annual signal is due to an underestimation of one of the two corrections (the steric or the hydrological correction) applied. Fig. 3.4 (top) graphically shows annual amplitudes and phases of the observed and inferred parameters (mass, steric- and continental hydrological leakage correction), for a variety of hydrological models (WaterGAP2, LAD, GLDAS) and steric corrections (MFSTEP, ECCO, Ishii). From the possible combinations, the mass estimates corresponding to MFSTEP and WaterGAP2 corrections have the best agreement over the complete interval.

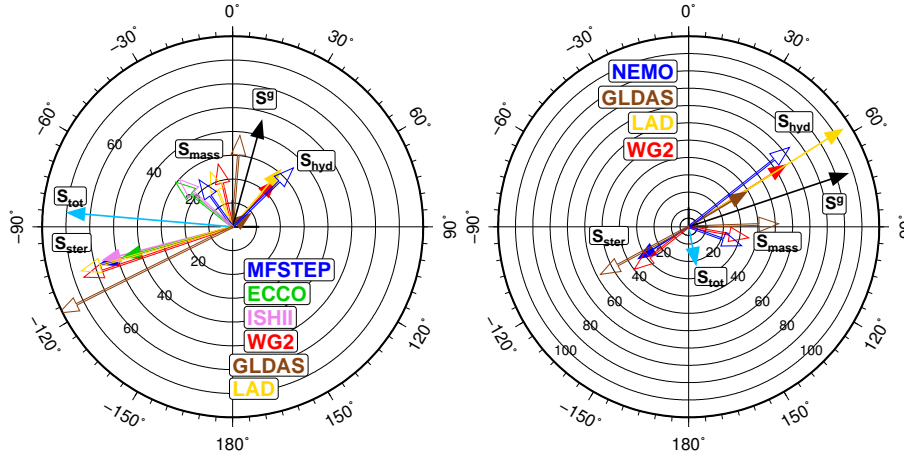


Figure 3.4: Annual amplitude and phase in Mediterranean Sea (top) and in Black Sea (bottom) of mass-induced sea level change (S_{mass}) and of observed and inferred estimates of steric correction (S_{ster}) and continental hydrological leakage (S_{hyd}) for selected land hydrology and ocean models. The parameters derived from GRACE- and altimetric sea level observations (S^g and S_{tot}) are kept fixed. Three land hydrology models are used in each basins. Three ocean models in the Mediterranean Sea and one in the Black Sea are used. Full/empty markers indicate observed/inferred quantities.

Also introduced in this paper is the analysis of the trend in mass variability, which strongly depends on the choice of the corrections. Finally, although resolution and accuracy of the mass-induced sea level estimates have been improved by using the latest GRACE models and the improved filtering methods, results are still dependent on the accuracy of the auxiliary data and models used to compute the corrections. The cross validation performed in this study is a viable tool to asses those errors and improve them for future studies.

In the related study [Aus der Beek *et al.*, 2012] we used an improved regional hydrology model, incorporating anthropogenic water use models, to estimate the hydrological water leakage in GRACE data. The first results did not show any evident improvements in the accuracy of the estimated mass change variation in the Mediterranean and Black Sea basins.

F-14: Decadal variability of the net water flux at the Mediterranean Gibraltar Strait in Chapter 8.3

This paper explores the long-term variability of the net water flux into the Mediterranean Sea at the Gibraltar Strait over the period 1960-2009. It is based on an approach combining multiple observational datasets and results from a regional climate model simulation. The approach includes deriving Gibraltar net inflow from the application of the Mediterranean Sea water budget equation using observationally based estimates of mass variation, evaporation, precipitation and simulated river discharge and Bosphorus Strait water fluxes. This derivation is compared with results from a simulation using the PROTHEUS regional ocean-atmosphere coupled model considering both individual water cycle terms and overall Gibraltar water flux.

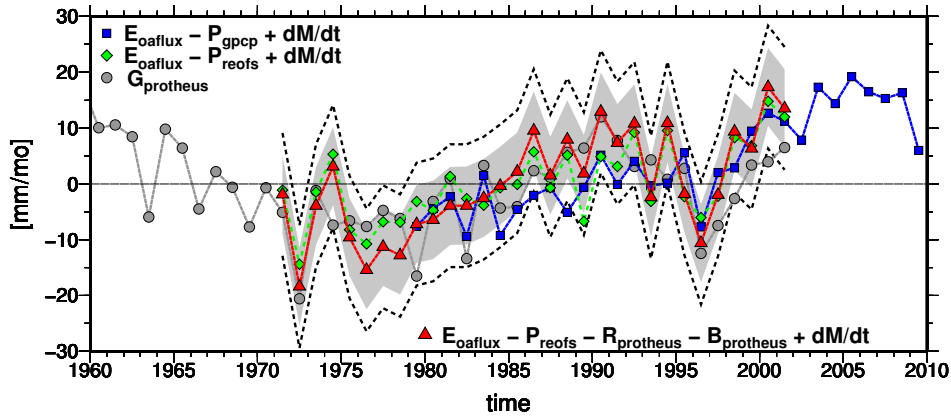


Figure 3.5: Estimates of Gibraltar water flux anomalies during the period 1960-2010 (reference period is 1979-2001). Shown are yearly values from the PROTHEUS model simulation (circle) and from the water budget equation using observational estimates of E, P, dM/dt and simulated R and B (triangle), and similar estimates neglecting R+B (square, diamond). E is from OAFLUX, P is from the REOFS and from GPCP, dM/dt is from the steric corrected sea-level reconstruction using Ishii data.

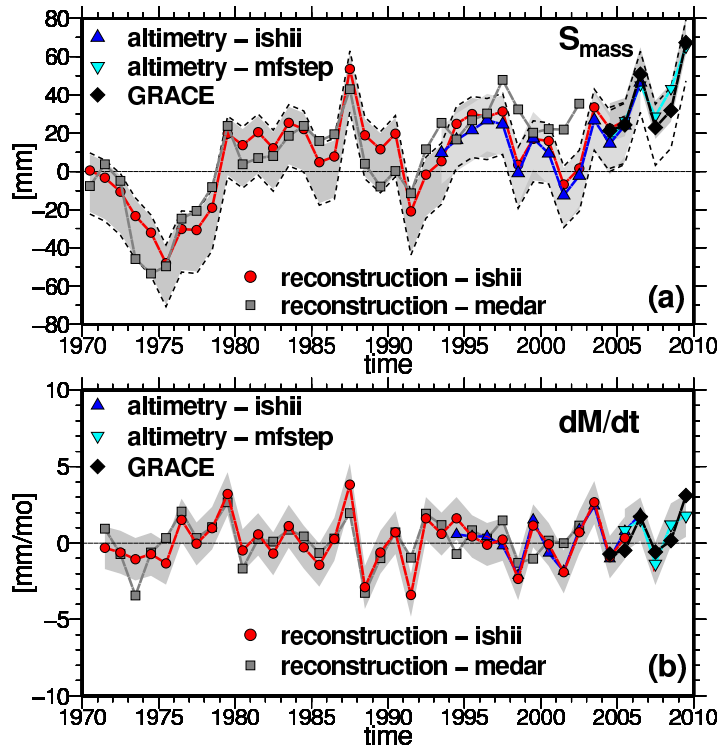


Figure 3.6: Yearly mass-induced sea level anomaly in Mediterranean Sea (a) and its time derivative (b) over the period 1970-2009. Shown are estimates based on the steric-corrected sea-level reconstruction using two different steric corrections (squares for Medar/Medatlas and circles for Ishii), on the steric-corrected sea-level altimetry using two different steric corrections (inverted triangles from MFSTEP and triangles from Ishii) and on GRACE-based mass retrievals (diamonds).

Results from both methodologies point to an increase in net water flux at Gibraltar over the period 1970-2009 (0.8 ± 0.2 mm/mo per year based on the observational approach). Simulated Gibraltar net water flux shows decadal variability during 1960-2009 including a net Gibraltar water flux decrease during 1960-1970 before the 1970-2009 increase (Fig. 3.5).

Decadal variations in net evaporation at the sea-surface, such as the increase during 1970-2009, appear to drive the changes in net inflow at Gibraltar, while river runoff and net inflow at the Bosphorus Strait have a modulating effect. Mediterranean Sea mass changes are seen to be relatively small compared to water mass fluxes at the sea surface and do not show a long-term trend over 1970-2009 (Fig. 3.6 bottom). The Atlantic Multi-decadal Oscillation (AMO) and the North Atlantic Oscillation (NAO) are relevant indirect influences on net water flux at Gibraltar via the influence they bear on regional evaporation, precipitation and runoff.

Collaboration in *Tsimplis et al.* [2013] confirms previous results obtained in *Fenoglio-Marc et al.* [2012] and *Fenoglio-Marc et al.* [2013b], namely that: (1) the sea level change trend of $3.0 \text{ mm/yr} \pm 0.5 \text{ mm/y}$ is dominated by the increase in the oceanic mass in the basin (Fig. 3.6 top), (2) this increase does not take place linearly but over two 2-3 year periods each contributing 2-3 cm of sea level, (3) the variability in the basin sea level and its mass component is dominated by the winter North Atlantic Oscillation (NAO). It further shows that the NAO influence on sea level is primarily linked with atmospheric pressure changes and local wind field changes. However neither the inverse pressure correction nor a barotropic sea level model forced by atmospheric pressure and wind can fully remove the NAO influence on the basin sea level. Thus a third contributing mechanism linked with the NAO is suggested. See in *Tsimplis et al.* [2007] and *Gomis et al.* [2012] a contribution to a review within MEDCLIVAR.

Chapter 4

Outlook and future perspective: Observing our planet for a safer world

This study shows the importance of geodetic observation in monitoring sea level and in analysing the processes that contribute to its rise. It also contributes to answering some of the questions, and opens new perspectives and topics for investigation.

Today both the importance of sea level in climate change studies and the relevance of the satellite observations for sea level monitoring are well recognized. The Intergovernmental Panel on Climate Change (IPCC) [*Church et al.*, 2013], identifies sea level rise as one of the major consequences of climate change and coastal vulnerability and social impacts as two important aspects to be accounted for.

Looking at the future, it is necessary to analyse what is needed to better cope with the sea level rising and its consequences. The three goals presented in this work, i.e. **Improve the measurements**, **Quantify the changes** and **Understand the causes** still hold.

From the observational side, various missions and initiatives have been planned and are in realization. The Earth Explorer missions (e.g. CryoSat-2, GOCE, SMOS, SWARM) form the science and research element of ESA's Living Planet Programme and focus on the atmosphere, biosphere, hydrosphere, cryosphere and Earth's interior. In the larger context of the European Earth Observation Program Copernicus, previously Global Monitoring for Environment and Security (GMES), the objectives for a series of satellites encompass the commitment to consistent, long-term collection of remotely sensed marine and land data, of uniform quality, for operational ocean state analysis, forecasting and service provision. Copernicus (e.g. Sentinel-3) is the most ambitious Earth Observation Programme to date. It will provide accurate, timely and easily accessible information to improve the management of the environment, understand and mitigate the effects of climate change and ensure civil security. Specifically, the environmental data gained as part of the Program Copernicus (e.g. Sentinel-3) as well as the gravity data provided by GOCE/GRACE/GRACE Follow-On and the ESA's Earth Explorers (CryoSat-2, GOCE, SMOS, SWARM) are expected to provide improved data quality, cover and revisiting time, and increase the value of Earth Observation data for scientific work and future emerging applications. They should address upcoming socially important challenges such as the need for climate action, efficiency in resource use and options for sustainable agriculture.

From the analysis/quantification side, on the other hand, the Global Climate Observing System (GCOS), in support of the United Nations Framework Convention on Climate Change (UNFCCC), has identified a set of requirements for satellite data to meet the needs of the climate change community. These are given for key parameters of the Earth's system, called the 'Essential Climate Variables' (ECVs), which are analysed, for example, in the Climate Change Initiative (CCI) Program, set up by the European Space Agency (ESA) to respond to this need for climate-quality satellite data. The specifications given by GCOS for each ECV data product are designed to provide information to characterise the state of the global climate system and enable long-term climate monitoring. The uncertainties of the climatic simulations, which predict the evolution of sea level for the next decades, are essentially large. Long and consistent time-series of measurements are needed to improve the accuracy of the model simulations, either by assimilation in the models or by validation of the results. At the same time, a better understanding of the causes of sea level variability in space and time is necessary to improve the model accuracy. Sea level is one of the parameters to be monitored.

In line with the above considerations, my study also contributes to answering some of the questions, and opens new perspectives and topics for investigation..

The first outcome of my work is the **quantification of the improvement (data accuracy)** of sea level coastal altimeter data, obtained thanks to the use of new technologies. Implicit is the suggestion of using the **improved geodetic measurements as validation data**.

While until recently the altimeter observations located at distances less than 10 Kilometres from the coast were disregarded as noisy, it is now possible to use observations at less than five Kilometres from the coast. The improvements have been achieved by applying improved environmental corrections and improved re-tracking methods to the low-resolution single-pulse mode (LRM) radar altimeter data. Additionally, it has been shown that the new generation of satellite altimeter data, the Synthetic Aperture Radar (SAR) Altimetry, also called Delay-doppler (DD), has significantly smaller measurement errors than the classical LRM. The SAR mode has in flight direction a higher resolution than the LRM data. Its footprint, i.e. the surface that reflects most of the signal, has along the flight direction a resolution of 250 m, which is approximately 10 times smaller than the footprint of the LRM data.

The future perspective goes towards an application of the SAR technique on both ocean and land and ice. The SAR Altimetry technology, which was first applied in the CryoSat-2 mission for both the conventional SAR and the interferometric SARIn modes, is now foreseen for the SRAL instrument on Sentinel-3, Jason-CS etc. In coastal regions and on land waters, where the radar echoes are distorted due to the presence of land in the footprint and therefore the spatial resolution of the data is very important, the SRAL technology offers a new set of data whose advantages are to be investigated. The development of dedicated retracking for pulse-limited altimeter data is still very important in coastal regions. See Fig. 4.1, which shows the distortion of the waveforms in extreme sea state conditions during a storm surge in the German Bight at 4 Kilometers from the coast. The perturbation of the waveform changes clearly in time.

A careful validation of altimetry data using in-situ data and at the same time a validation of models with in-situ and altimetry data is needed. The German Bight is a suitable calibration and validation area thanks to the existing infrastructure which provides high quality in-situ data and model simulations (Fig. 4.2). Here the comparison with in-situ data is done in an absolute sense, above the ellipsoid, thanks to the GNSS data. Based on our first validation with CryoSat-2, the plans for the upcoming altimeter missions look quite promising. The

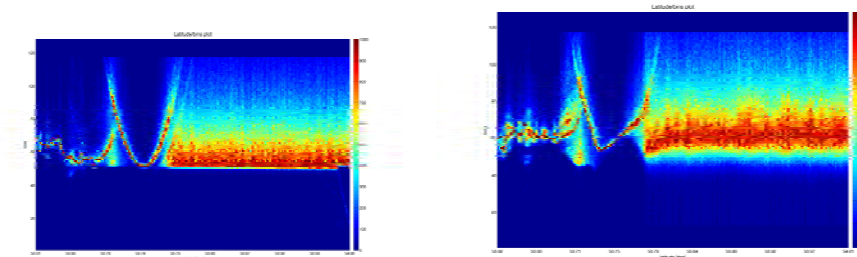


Figure 4.1: Perturbation due to sea state condition: SARAL/AltiKa waveforms in the German Bight along pass 269 cycle 1 (left) and cycle 8 (right) during the storm surge of the 8th December 2013

development of tools and the analysis is also expected to bring new information on the SAR technique, to be used in the planning of new missions.

Another prospective goes towards the assimilation of altimetric data in models. The planned assimilation of altimetric SWH in a regional model wave is expected to improve the prediction of wave models in ocean and coastal zones. The same is expected for an assimilation of altimetric sea level (SSH) in an ocean model.

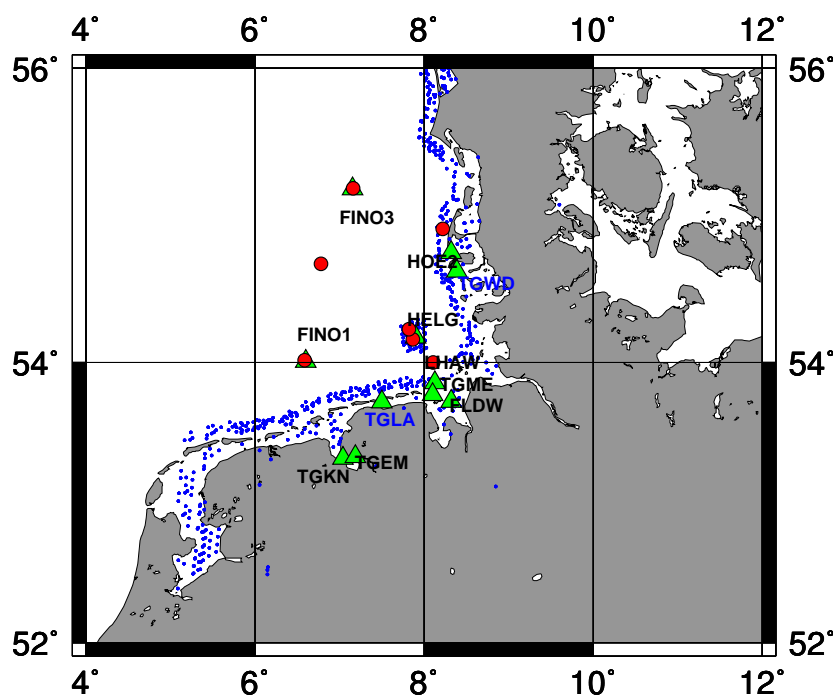


Figure 4.2: Validation area for open sea and coastal data in the German Bight.

The second outcome of my work is a **quantification of sea level change by using geodetic measurements**. The global sea level analysis shows that the spatial patterns of sea level change are variable in time and that the global average of sea level is increasing. The global mean sea level time-series (GMSL) does not show an acceleration over the altimeter interval, mainly because of the large interannual and decadal sea level variability and the short altimeter sea level time series. The trend of the global averaged sea level in Fig. 4.3 is 3.1 ± 0.4 mm/yr over the time period 1993-2012 in agreement with the results obtained by other research groups. Of course differences in global sea level trends derived at various institutes

are due to the different processing methodologies adopted, e.g. gridded versus non-gridded sea surface heights anomalies [Masters *et al.*, 2012].

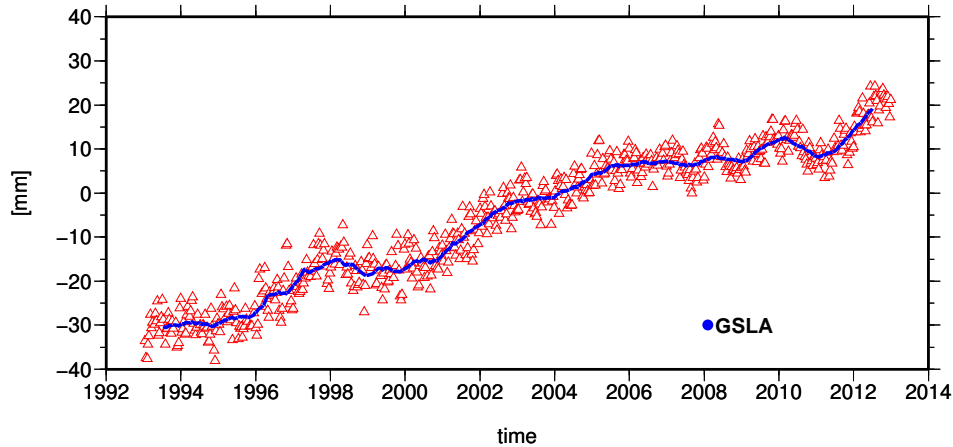


Figure 4.3: Global sea level change over 1993-2013 from Topex/Poseidon, Jason-1 and Jason-2 altimeter data. Annual variability has been eliminated and running average applied.

At regional and local scale the dynamics of the coastal region is of great interest for the development of our society. For the security of our coastal region, climate change need to be considered. Measurements and model predictions are the basis for future concepts of planning. Satellite altimetry, with its quasi-global coverage and short revisit time, allows a sea level change analysis which is complementary to the analysis made using tide gauge data. A good example of the synergy of altimeter and tide gauge data for NRT applications is shown in Fig. 4.4 for the storm surge of 6th December 2013 [Scharroo and Fenoglio, 2013]. The sea level change, wind speed and significant wave height derived from the altimeter measurements are shown to be consistent with the in-situ measurements. The BSH model was able to predict the storm surge with a good accuracy along the satellite track (bottom of Fig. 4.5). Model and data intercomparison are very useful to validate both model and data. In this case, the departures between the DWD and the altimeter wind speed (top of Fig. 4.5) need to be investigated.

Clearly there are also differences between the two ways of measuring sea level, which are also seen from the figure. The first difference is in the time/location sampling. While tide gauges measure sea level constantly at a single location, an altimeter captures the variation along its ground track. Thus the altimeter can display the shape of the storm surge as a function of the distance to the coast while the tide gauge cannot. On the other hand, the tide gauge provides repeated measurements at that location, showing the full history, while the altimeter revisits the same location only over longer intervals, in this case 35 days. This is known as the trade-off of time and space sampling that is the subject of the planning of every altimeter mission. With a constellation of different missions the space-time sampling can be further improved. In this context satellite altimetry is expected to become more and more operational.

The second difference is in the reference used for the measurements. This reference is a well defined reference ellipsoid for satellite altimetry and a point on land for the tide gauges. Part of the difference in the measurements is therefore due to the land vertical motion. In agreement with the goals of Copernicus, the combination of altimetry with other space techniques, such as GPS and INSAR, allows an analysis of the vertical land motion and therefore the determination of sea level change relative to the coast.

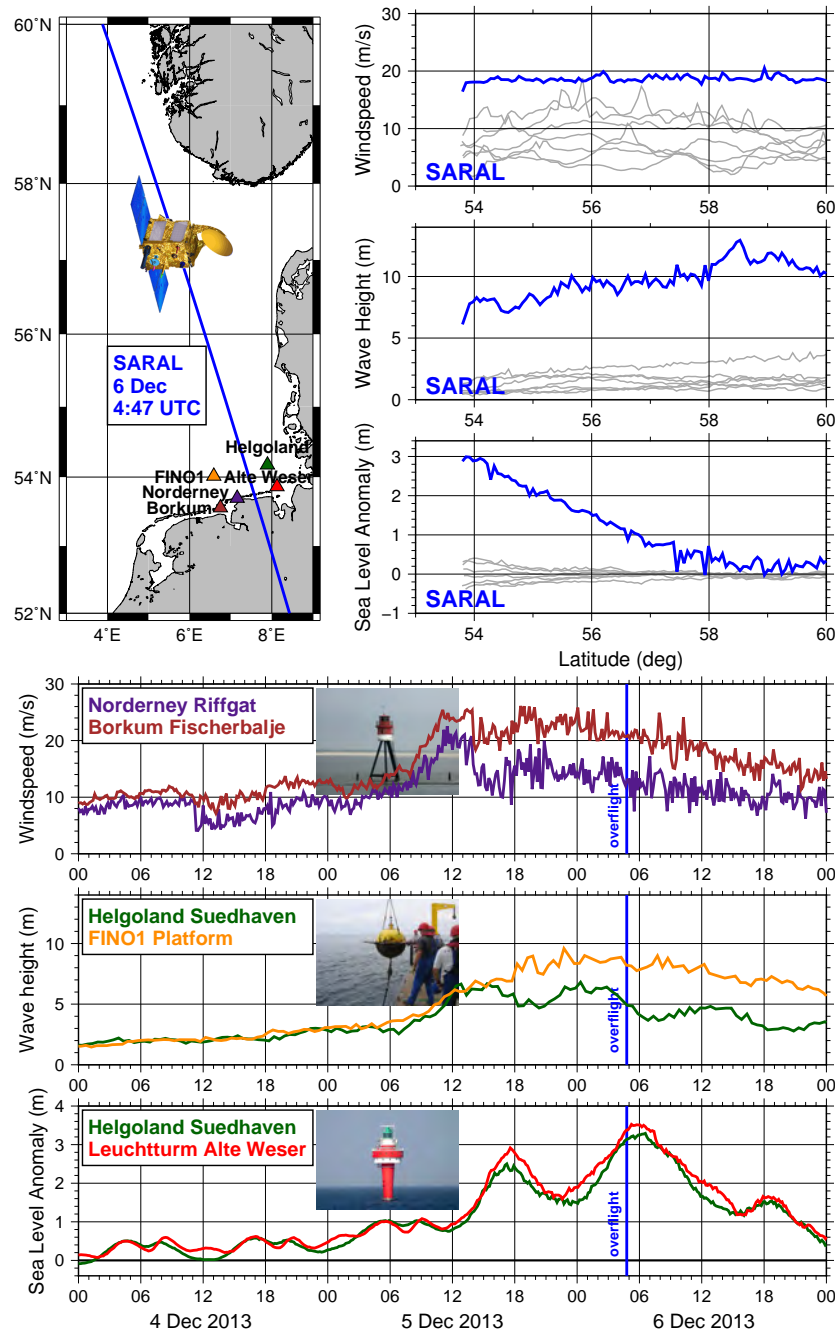


Figure 4.4: Detection of Storm Surge by satellite altimetry and in-situ data. Top: SARAL overflight of the German Bight at around 4:47 UTC on 6 December 2013. The pass runs from south to north. Locations of in-situ measurements are indicated by triangles, whose colours correspond to the time series in the bottom figure. Right, from top to bottom: profiles of wind speed, significant wave height, and sea level anomaly during the overflight (in blue). Measurements during 8 previous passes are shown in grey. Bottom: In-situ measurements of conditions during 4-6 December 2013. From top to bottom: wind speed measured by anemometers at Norderney Riffgat (purple) and Borkum Fischerbalje (brown, inset); Significant wave height at Helgoland (green) and the wave rider at the FINO1 platform (orange, inset) Sea level anomaly at Helgoland (green) and Leuchtturm Alte Weser (red, inset).

The third outcome of this work is **the identification of the causes of sea level change in the analysed areas**. In combination with gravity measurements and or in-situ temperature and salinity data, mass and volume changes in sea water have been separated.

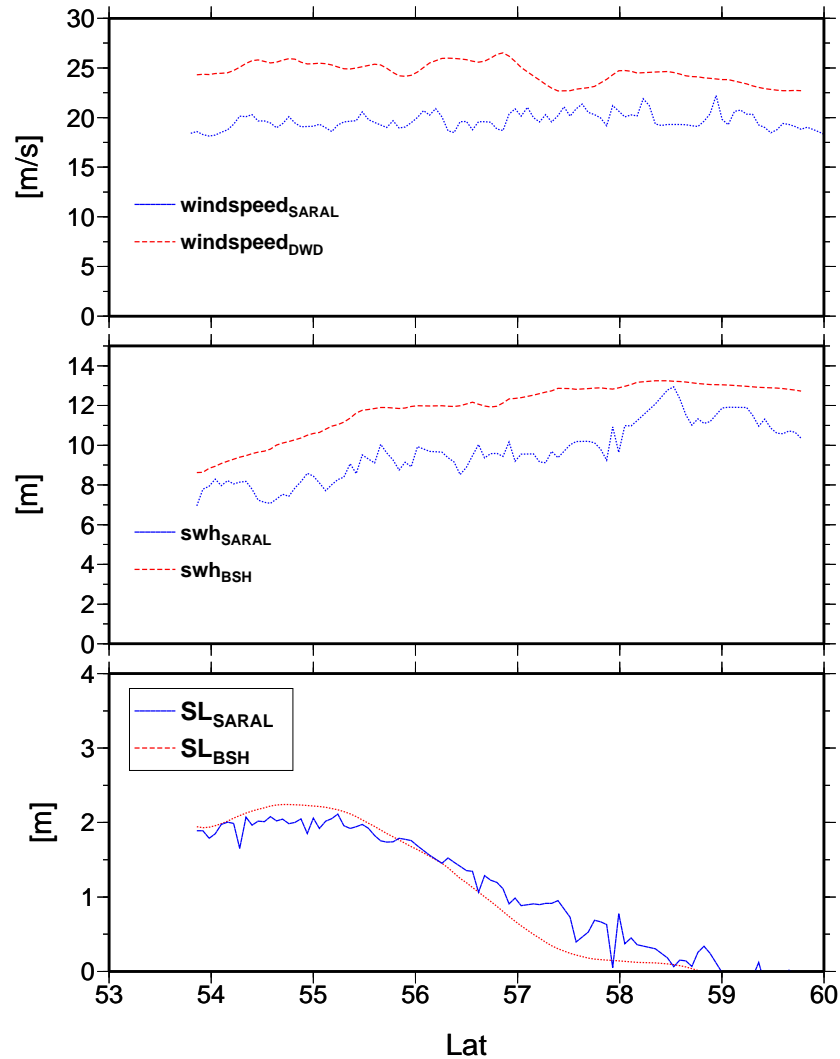


Figure 4.5: Prediction of Storm Surge by the BSH model along the SARAL/AltiKa overflight of the German Bight at around 4:47 UTC on 6 December 2013. The geographical location is shown in Fig. 4.4. From top to bottom: profiles of wind speed, significant wave height, and sea level anomaly during the overflight. The BSH model uses the wind of the Deutscher Wetterdienst (DWD).

It was shown that, differently than in the world ocean, in the Mediterranean Sea the sea level change is driven at decadal scales from mass change and not from steric sea level changes. Moreover it was shown that the closure of the budget in small semi-closed basins, as the Mediterranean-Black Sea basin, gives potentially a way to check the accuracy of data and model estimations.

From the analysis in the Indonesian region we concluded that, even if the regional sea level change is still primarily caused by natural climate variability, the imprint of anthropogenic effects on regional sea level is locally strong. In details, we have shown that sea level change is closely linked to the ENSO mode of variability and is spatially homogeneous at both inter-annual and decadal scales. The rates of absolute eustatic sea level rise derived from satellite altimetry through a 20-year long precise altimeter observation are in average higher than the global mean rate. However several tide gauge records indicate an even higher sea level rise relative to land because of the land vertical movement. Subsidence has been found in Jakarta and in three other tide gauge stations (Fig. 4.6). The method combines tide gauges

and co-located altimetric measurements and represents an interesting alternative to the use of collocated GPS at the tide gauge stations when GPS is not available.

Clearly sea level rise represents a major threat for low-lying highly populated coastal regions worldwide. It is expected that the regional sea level rise will strongly affect particular regions with direct impacts including submergence of coastal zones, rising water tables and salt intrusion into groundwater. It can possibly also exacerbate other factors as flooding, associated to storms and hurricanes, as well as ground subsidence of anthropogenic nature. Needed are interdisciplinary studies in selected regions where the sea level rise is particularly critical.

In summary the author's work has shown that the interdisciplinary studies are mandatory to interpret the observations and analyse the causes of the sea level observations in view of climate change. An integrated approach of merging remote sensing data with in situ measurements and ocean and hydrological models is therefore highly desirable, both for oceanography and for marine gravity and geodesy on the regional, basin and global scales.

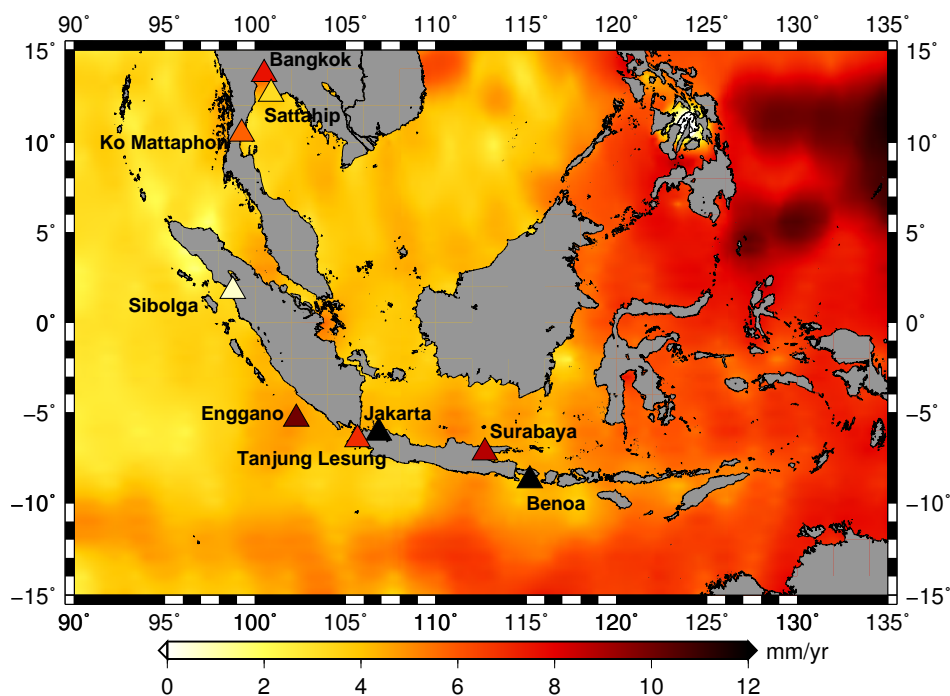


Figure 4.6: Sea Level Rise (SLR) from satellite altimetry in 1993-2011 and corresponding Relative Sea Level Rise (RSLR) from tide gauge stations (triangle) in the Indonesia-Thailand region.

The current analysis on ocean and coastal regions can be extended to study other global change issues, e.g. related to inland waters. A preliminary analysis in the Mekong region [Buchhaupt *et al.*, Poster, Living Symposium Edinburgh, ESA, 2013] shows a similar seasonal variability of Envisat and SARAL/AltiKa water level data with better resolution for the second, thanks to the 40Hz-data and to the smaller footprint. The altimeter observations correlate well in time and space with the mass change observed by GRACE and with the inundation maps [Prigent *et al.*, 2007]; a nice seasonal peaking occurs in October. Infact the observations from space, when used in conjunction with in situ observations and hydrological modelling, have the potential to significantly improve our understanding also of hydrological processes affecting large river basins in response to climate variability. A promising application for satellite-gravity and remote sensing techniques is therefore the monitoring and prediction of water balance of large river basins on time scales ranging from weeks to months. The

total water mass change on land measured by GRACE and surface waters height change measured by satellite altimetry (rivers, wetlands and floodplains) provide very useful data for the estimate and prediction of spatio-temporal variations of terrestrial water storage in soil (soil wetness and groundwater) and in surface water reservoirs.

Another important global change issue is direct alteration of the continental water cycle for irrigation, hydroelectricity, and other human needs. Stabilization of water supply has always been a fundamental preoccupation of human society and is a key security concern for most nations. Reducing flood hazard, enhancing food security, and redirecting runoff from water-rich to water-poor areas continue to provide a major challenge to our engineering infrastructure.

Following the three main goals already identified, relevant topics for future research are here listed:

Improvement of multi-mission satellite altimetry

The processing of low level SAR data is today an important research topic. The step from Full Bit Rate (FBR Level-1a) to Level-1 data is the real challenge in the use of the new SAR technology. This step is different from the corresponding pulse-limited processing.

Moreover improved re-tracking methods for both pulse-limited and SAR altimetry will give more usable data in coastal, in-land water and ice zones. Improved classification and re-tracking need to be based on simulated waveforms and validated with in-situ data. A first study on this topic is the Bachelor thesis by *Buchhaupt* [2013]. A Graphic User Interface was developed, which allows selection of the altimeter data, re-tracking and validation in an interactive and friendly way. Its use is planned for research and for teaching purposes. The continuation of the work on CryoSat-2, alongside the preparation for Sentinel-3 data analysis, as part of S-3 altimetry validation team, is a promising and interesting task.

Quantification of regional sea level change

A regional study validating the products against reliable in-situ data is necessary to verify if the expected quality of the data is reached.

A main source of error in computing the global and the regional Mean Sea Level (MSL) trends is the uncertainty to link together all the altimetry missions in order to provide a continuous MSL time series from 1993 onwards. The uncertainty in MSL due to this global bias is now close to 0.2 mm/yr, which is not negligible for MSL studies. Concerning the regional MSL bias at basin scales, systematic geographical biases between altimetry missions could impact directly the regional estimation of the MSL trends with a potential effect locally higher than 1 mm/yr. These are systematic differences due e.g. to the wet troposphere correction in coastal areas, sea state bias, orbit errors etc.

We have identified the German Bight as a suitable area for the validation, thanks to high quality in-situ observations. The availability of sea level data referred to a geodetic reference system allows an absolute comparison of altimeter and tide gauge sea level data. A follow up study of the work by *Weiss* [2013], for pulse-limited altimetry, and of the study by *Fenoglio-Marc et al.* [2013a], for CryoSat-2 in SAR mode, is expected to be a useful validation effort. The interdisciplinary collaboration between Geodesy, Coastal Engineering and Oceanography needs to be a central part in this analysis to allow simulation and interpretation of the results at a larger scale.

Attribution of sea level rise: Regional and local sea level is directly or indirectly affected by many if not all components of the climate system, including the ocean, cryosphere, solid Earth and terrestrial hydrology, local vertical movement of the sea floor, biological processes (e.g., coral growth) and human activities (e.g., ground-water extraction) [Stammer *et al.*, 2013], [Nicholls and Cazenave, 2010]. To date, we have not yet been able to quantify the role each process played in the past, nor can we quantify their relative contribution to future sea level changes as a function of timescale. Only interdisciplinary scientific programs can identify and quantify processes and provide comprehensive information on societal responses in the past, societal resilience capacities, and preparedness for undertaking adaptation measures. Such programs provide the scientific basis for a well-founded investigation of adaptation strategies to sea level change. Both geographical and societal aspects are different regionally, e.g. in the North Sea and in the Tropical Pacific (Thailand/Mekong/Indonesian region), and need to be accounted for.

To conclude, the consequences of a warming climate are far-reaching, potentially affecting fresh water resources, global food production and sea level. Threatening impacts on the natural environment and life on Earth for generations to come, climate change is high on political, strategic and economic agendas worldwide.

Observations from space provide the unique information that greatly assist in the successful understanding and management of climate change. The global coverage and continuous measurements that satellites can provide already give researchers vital information about the climate system. In the context of sustainable development and coastal resilience of societies, understanding and predicting changes at regional and local scale is extremely important, and still more relevant than at global scale.

Chapter 5

Publications

The compilation for the Habilitation comprises of 14 publications ¹ selected from 38 manuscripts ² which I have produced in the period 2001-2013.

5.1 Included in this Habilitation

1. **F-01:** Fenoglio-Marc L. and Groten E., Modelling the sea level variation for the unification of altimetric missions, *Adv. Space Res.*, 30, 11, 2357-2362, 2002.
2. **F-02:** Fenoglio-Marc L., S. Vignudelli, A. Humbert, P. Cipollini, M. Fehlau, M. Becker, An assessment of satellite altimetry in proximity of the Mediterranean coastline, in 3rd ENVISAT Symposium Proceedings, SP-636, ESA Publications Division, 2007.
3. **F-03:** Fenoglio-Marc L., M. Fehlau, L. Ferri, M. Becker , Y. Gao, S. Vignudelli, Coastal sea surface heights from improved altimeter data in the Mediterranean Sea, in IAG Symposia N. 135, Gravity, Geoid and Earth Observation, Mertikas S.P. (eds), Springer Verlag, 253-262, 2008.
4. **F-04:** Fenoglio-Marc L. , R. Weiss, S. Dinardo, M. Becker, A.Sudau, A Study on the conformance of altimetry and in situ surface data near coast, In Proceedings of the 20 Years of progress in radar altimetry symposium, ESA SP-710, ESA/ESTEC, 2012
5. **F-05:** Fenoglio-Marc L., Dinardo, S., Scharroo R., Roland A., Lucas B., Weiss R., Detour Sikiric M., Becker M., Benveniste J., Validation of CryoSat-2 Observations in SAR Mode in the German Bight, Proceedings Living Planet Symposium Edinburgh, SP-ESA, ESA Publications Division, 2013
6. **F-06:** Fenoglio-Marc L., E. Tel, Coastal and global sea level, *Journal of Geodynamics* 49, 151-160, 2010.
7. **F-07:** Fenoglio-Marc L., Analysis and representation of regional sea level variability from altimetry and atmospheric data, *Geophysical Journal International*, Vol. 145, 1, 1-18, 2001

¹12 Peer-reviewed articles, 2 Proceedings articles

²24 Peer-reviewed (19 in journals, 5 in books) articles, 14 Proceedings articles

8. **F-08:** Fenoglio-Marc L., Long-term sea level change in the Mediterranean Sea from multi-mission satellite altimetry and tide gauges, *Physics and Chemistry of the Earth*, Vol. 27, pp. 1419-1431, 2002.
9. **F-09:** Fenoglio-Marc L., E. Groten and C. Dietz, Vertical Land Motion in the Mediterranean Sea from altimetry and tide gauge stations, *Marine Geodesy* 27, 3-4, 683-701, 2004.
10. **F-10:** Fenoglio-Marc L. C. Braitenberg and L. Tunini, Sea level variability and trends in the Adriatic Sea in 1993-2008 from tide gauges and satellite altimetry, *Physics and Chemistry of the Earth*, doi:10.1016/j.pce.2011.05.014, 2011.
11. **F-11:** Fenoglio-Marc L., T. Schöne , J. Illigner , M. Becker , P. Manurug, Khafid, Sea Level Change and Vertical Motion from Satellite Altimetry, Tide Gauges and GPS in the Indonesian Region, *Marine Geodesy*, 35:sup1, 137-150T, 2012.
12. **F-12:** Fenoglio-Marc L., J. Kusche, M. Becker, M., Mass variation in the Mediterranean Sea from GRACE and its validation by altimetry, steric and hydrology fields, *Geoph. Res. Lett.*, 33, L19606, 2006.
13. **F-13:** Fenoglio-Marc L., M. Becker, R. Rietbroeck, J. Kusche, S. Grayek and E. Stanev, Water mass variation in Mediterranean and Black Sea, *J. of Geodynamics*, 59-60, 168-182, 2012.
14. **F-14:** Fenoglio-Marc L., A. Mariotti, G. Sannino, B. Meyssignac, A. Carillo, M.V. Struglia, Decadal variability of the net water flux at the Mediterranean Gibraltar Strait , *Global and Planetary Change* 100, 1-10, 2013.

5.2 Other Publications

Peer-reviewed

1. Aus der Beek T., L. Menzel, Fenoglio-Marc L., S. Grayek, R. Rietbroeck, M. Becker, J. Kusche, and E. Stanev Modelling water resources of the Black and Mediterranean Sea river basins and their impacts on regional mass changes, *J. of Geodynamics*, 59-60, 157-167, 2012.
2. Bouffard J. , L. Roblou, F. Birol, A. Pascual, L. Fenoglio-Marc, M. Cancet, R. Morrow and Y. Ménard , Assessment of improved coastal altimetry strategies over the north western Mediterranean Sea, in Vignudelli (eds), *Coastal altimetry*, Springer Verlag, 297-330, 2011.
3. Fenoglio-Marc L. and Groten E., Time Varying Mean Sea Level in Freedom, M.Z. Nashed, T. Sonar (Eds.), *Handbook of Geomathematics*, Springer Verlag, 2010.
4. Fenoglio L. and E. Groten, Mean Sea Level Determination in small ocean basins using ERS-1 Altimetry in a combined approach, *Manuscripta Geodaetica* 20:394-407, 1995.
5. Fenoglio-Marc L., J. Kusche, M. Becker and I. Fukumori, Comments on "On the steric and mass-induced contributions to the annual sea level variations in the Mediterranean Sea" by D. Garcia et al., *J. of Geophysical Res.*, Vol. 112, C12018, 2007.
6. Fenoglio-Marc L., E. Tel, M.J. Garcia and N. Kjaer, Interannual to decadal sea level change in south-western Europe from satellite altimetry and in-situ measurements, in *Gravity, Geoid and Space Missions*, IAG Symposia 129, 242-247, Springer Verlag, 2005.
7. Gomis D., Tsimplis M., Marcos, M., Fenoglio-Marc L., B. Perez, F. Raicich, I. Vilibic, G. Wöppelmann, S. Monserrat, *Mediterranean Sea Level Variability and trends in Lionello P. (eds.) The Climate of the Mediterranean Region from the past to the future*, Elsevier, 257-299, 2012.

8. Gommenginger C., P. Thibaut, L. Fenoglio-Marc, X. Deng, J. Gomez-Enri, Y. Gao, Retracking altimeter waveforms near the coasts, in Vignudelli (eds), Coastal altimetry, Springer Verlag, 61-101, 2011.
9. Groten E., L. Fenoglio, T. Mueller, A comparison between classical crossover techniques and a Stochastic Deterministic Approach, *Adv. Space Res.* 14, 5, 1994
10. Trisirisatayawong I., Naeije M., Simons W. and Fenoglio-Marc L., Sea level change in the Gulf of Thailand from GPS-corrected tide gauge data and multi-satellite altimetry, *Global and Planetary Change* 76, 137-151, 2011.
11. Tsimplis M., F. Calafat , M. Marcos , G. Jordá, D. Gomis , L. Fenoglio-Marc , M. V. Struglia , S. Josey. The effect of the NAO on sea level and on mass changes in the Mediterranean Sea, *J. of Geophysical Research*, 118, 944-952, doi:10.1002/jgrc.20078, 2013.
12. Tsimplis M., F. Raicich, L. Fenoglio-Marc, A.G.P. Shaw, M. Marcos , S. Somot, A. Bergamasco. Recent developments in understanding sea level rise at the Adriatic coasts, *Physics and Chemistry of the Earth*, 2011.
13. Tsimplis M.N., E.Alvarez-Fanjul, D.Gomis, L.Fenoglio-Marc, B.Perez, Mediterranean Sea level trends: atmospheric pressure and wind contribution, *Geoph. Res. Lett.*, 32, 20, L20602, 2005.
14. Tsimplis M.N., A.G.P.S. Shaw, A. Pascual, M. Marcos, M. Pasaric, L. Fenoglio-Marc, Can we reconstruct the 20th century sea level variability in the Mediterranean Sea on the basis of recent altimetric measurements? In *Remote Sensing of the European Sea*, in Barale A. and Gade M., Springer Science, 2007.

Proceedings and newsletters

1. Fenoglio-Marc L., Dinardo, S., Scharroo R., Roland A., Lucas B., Weiss R., Detour Sikiric M., Becker M., Benveniste J., A Validation Exercise for CryoSat-2 in SAR Mode in the German Bight Area, *Proceedings Cryosat 3rd User Workshop*, Dresden, SP-ESA SP-717, ESA Publications Division, 2013
2. Fenoglio-Marc L., M. Becker, J. Kusche, R. Rietbroek, Leakage of Continental Hydrology in seawater mass change estimations from Space in the Mediterranean and Black Sea, in *Proceedings of the 2nd Space for Hydrology Symposium*, WPP-280, ESA Publications Division, 2007a.
3. Fenoglio-Marc L., J. Kusche, M. Becker, Estimation of mass variation and mean dynamic topography in the Mediterranean Sea from altimetry and GRACE/GOCE geoids, in *3rd GOCE Users Symposium Proceedings*, SP-627, ESA Publications Division, 2007b.
4. Fenoglio-Marc L., M. Becker, Modeling the sea level variability in the last decade, *Proceedings of the Symposium on 15 Years of Progress in Radar Altimetry*, ESA SP-614, 2006.
5. Fenoglio-Marc L., E. Groten, Long-term sea level variability from multi-satellite altimetry in the European Seas, *Proc. Envisat Symposium*, Salzburg, ESA SP-572, 2004.
6. Fenoglio-Marc L., E. Groten and C. Dietz, Sea level change and cross calibration of satellite altimetry missions using tide gauge data, in *Proceeding for Prof. Moritz 60 Birthday*, Graz, pp.93-109, Institut für Geodäsie, Technische Universität Graz, 2003.
7. Fenoglio-Marc L., Cross-calibration of the Envisat altimeter range in the Mediterranean Sea using multi-satellite altimetry and tide gauge data, in *Proceedings of the Envisat RA2/MWR Cross-calibration and Validation Activities*, ESA Editions, 2003.
8. Fenoglio-Marc L. and E. Groten, Local improvement of the marine geoid using altimetry data, *Cahiers du Centre de Geodynamique et de Seismologie*, 20, 113-117, 2003.
9. Fenoglio-Marc L. and E. Groten, On the variability of mean sea level, *Allgemeine Vermessung Nachrichten* 2/2003, Wichmann, 55-59, 2003.

10. Fenoglio-Marc L., Altimetry data improvement by dual crossover method in European Seas and along-track stationary sea surface topography, *Allgemeine Vermessungs-Nachrichten* 10/1997, 354-359, Wichmann, 1997.
11. Fenoglio-Marc L. and M. Martinez-Garcia, Sea level trends in the Mediterranean Sea from satellite altimetry and tide gauge stations, in *Proceedings of Final Workshop of Cost Action 40. Sea level in Europe: Observation, Interpretation and Exploitation*, pp. 114-117, Hydrographic Institute of the Republic of Croatia, Split, 2001.
12. Fenoglio-Marc L., Multi-mission altimetry data analysis and unification in the Mediterranean Sea, in *ERS-ENVISAT Symposium Proceedings*, ESA SP-461, 2001b.
13. Fenoglio-Marc L., Y. Wang and E. Groten, Investigation at regional scales of sea level variability at low and medium frequencies, in *AVISO Newsletter N.7*, 40-43 CNES, 2000.
14. Fenoglio-Marc L., E. Groten E., Geodetic aspects of long term sea level variations in european seas rom altimetry and tide gauge data, *Proceedings of the Third ERS Symposium*, ESA SP-414, 3, 1103-1108, 1997.
15. Fenoglio L., E. Groten, A Stochastic Deterministic Approach as an alternative to crossover techniques in small ocean basins, *Proceedings of the First ERS-1 Symposium*, ESA SP-359, 1, 407-411, 1992.
16. Groten E., Fenoglio-Marc L., Wang L., El Nino 1997 - main characteristics and interannual earth rotation variability, *Allgemeine Vermessungs-Nachrichten* 4/2000, Wichmann, 140-146, 2000.
17. Nurmaulia S., Fenoglio-Marc L. and M. Becker, Long-term sea level change from satellite altimetry and tide gauges in the Indonesian region, in *Proceedings of the Living Planet Symposium Bergen*, ESA Publications Division, 2010.

Reports

1. Fenoglio-Marc L., A software tool for altimeter data pre-processing, IPGD-2010-02, Schriftenreihe des Instituts für Physikalische Geodäsie der TU Darmstadt, 2010.
2. Bachmann S., Fenoglio-Marc L., A software tool for tide gauge data pre-processing, IPGD-2010-01, Schriftenreihe des Instituts für Physikalische Geodäsie der TU Darmstadt, 2010.
3. Tsimplis M., A. Shaw, O. Andersen, L. Fenoglio-Marc, N. Kjaer, P. Knudsen, M. Pasaric, F. Raicich and K. Suselj, Report on secular trends de-contaminated for decadal sea level variability, ESEAS-RI WP3 Task 3.4, 2005.
4. Kjaer N., O. Andersen, P. Knudsen and L. Fenoglio-Marc, Report on sea level variations for the European Seas and the North Atlantic Ocean using satellite altimetry and tide gauges, ESEAS-RI WP3 Task 3.1 Final Report, 2004.
5. L. Fenoglio-Marc, Kjaer N., O. Andersen, P. Knudsen, M.J. Garcia and E. Tel, Report on interannual to decadal sea level variations from satellite altimetry and tide gauge data, ESEAS-RI WP3 Task 3.2 Final Report, 2004.
6. Fenoglio-Marc L. and K. Suselj, Report on interdecadal model for the Mediterranean Sea, ESEAS-RI WP3 Task 3.3 Final Report, 2004.
7. Fenoglio-Marc L., PO-TN-ESR-RA-102 Comparison of altimetry and tide gauge data of the SIMN italian dataset, ESA Editions, 2003.
8. Fenoglio-Marc L., Tropical Pacific 1992-1999: analysis and representation of sea level variability from altimetry and climate data, TUD/IPG/Altimetry Report N.2, 2002.
9. Fenoglio-Marc L., Long-term sea level change in the Ionian Sea, TUD/IPG/Altimetry Report N.3, 2002.
10. Fenoglio L., M. Belikov, Geoid determination in Mediterranean Sea by inclusion of inverted altimetry data, *Reports of the Finnish Geodetic Institute*, 95:7, Latest developments in the computation of regional geoids, pp. 43-51, 1995.

11. Fenoglio L., Evaluation of the geopotential for application in Baltic Sea, in Studies of the Baltic Sea, Subcommission IAG SSC 8.1, Riga Latvia, 34-43, 1996.

PhD and M.Sc. Thesis

1. Fenoglio-Marc L., Sea Surface Determination with Respect to European Vertical Datums, PhD Thesis, Deutsche Geodätische Kommission, Heft Nr. 464, München, 1996.
2. Fenoglio L., Ipotesi di cattura nella formazione del Sistema Solare, Università degli Studi di Torino. Corso di Laurea in Matematica, Torino, 1982.

Chapter 6

Improvement of multi-mission satellite altimetry records

6.1 Modelling the sea level variations for the unification of altimetry missions

F-01: Fenoglio-Marc L. and Groten E., Modelling the sea level variation for the unification of altimetric missions, *Adv. Space Res.*, 30, 11, 2357-2362, 2002.

Abstract Regional single-mission models for the interannual and medium-term sea level variability are constructed in the Mediterranean Sea from altimetry data using statistical methods. Their estimated accuracy is a few centimetres at spatial scales of 50 Kilometres and at monthly time scales. The single-mission model is used to check bias and drifts between multi-mission sea surface height data. The extrapolated model constructed from sea-surface height and sea-surface temperature using the sea-surface temperature as predictor allows a comparison of non-simultaneous multi-mission data.

Keywords: sea level change, altimetry, tide gauge

1. Introduction

An altimetric mission of high accuracy and long duration is ideal to study the long-term sea level variability. In reality several altimetric missions have been flown and the corresponding sea-surface heights (SSH) present an increasing accuracy thanks to the improved orbital and geophysical corrections applied to the measured data. Different data pre-processings, residual altimeter bias, offsets in the reference frames make the data of different missions not homogeneous. The discrepancies have to be taken into account in merging the altimetric multi-mission data. Global long-term monitoring analyses have been performed to quantify the discrepancies by examining the variation over time of the dual crossover (DXO) mean differences of the SSHs of two satellites with a difference in time of less than a few days, to be able to neglect the sea level variability (Stum et al., 1999). This method is restricted to simultaneous missions. Statistical methods that account for the correlation between sea level and atmospheric-oceanic parameters have been used to build regional single-satellite sea level variability (SLV) models and an extrapolated model has been constructed in the Mediterranean Sea from the SSH anomaly (SLA) and the sea-surface temperature anomaly (STA) fields (Fenoglio-Marc, 2001). The extrapolated SLV model can be used to unify non overlapping altimeter missions. The method and the accuracy of the models are investigated here from 1992 to 1999.

2.2 Multi-mission data analysis

Altimetric SSHs from both the Topex/Poseidon (T/P) and the ERS missions and sea-surface temperature data are considered in the Mediterranean Sea in the interval of 7 years between October 1992 and September 1999. The T/P data are derived from the T/P Geophysical Data Records (GDR) (Aviso, 1996), the ERS data from the ERS-GDR (CERSAT, 1996), the sea-surface temperature from the weekly AVHRR/NOAA data (Nasa, 1999). Errors in the 1/sec altimetric SSHs are mainly due to the radial orbit error (Scharroo and Visser, 1998) and to systematic errors, as errors in the instrumental bias and in the geophysical corrections. Due to the higher accuracy of the T/P orbit, T/P and ERS data are generally merged in a DXO adjustment to improve the ERS data (Fenoglio, 1997). On the other hand the long-term discrepancies between the two satellites are analysed here computing the aver-

Table F-01-1: Relative bias of ERS-1, ERS-2 and T/P in the Mediterranean Sea

missions	interval (cm)	rel. bias (ERS-GDR) (cm)	rel. bias (ERS-DEOS) (cm)
ERS-1 phase c / TP	1993 - 1994	2	5
ERS-1 phases e,f / TP	1995 - 1996	6	6
ERS-2 / TP	1995 - 1999	8	8
ERS-1 phases e,f / ERS-2	1995 - 1996	2	2

aged differences of the original ERS and T/P SSH data at DXO points in the Mediterranean Sea with a time-difference of less than 10 days. This quantity mainly reflects the systematic errors mentioned above as well as coordinate frame offsets and gravity-induced errors in the ERS orbit, assuming that T/P gravity-induced errors are much smaller. The DXO differences are averaged over each ERS-1 and ERS-2 35-day cycle and over each 37-day subcycle of the ERS-1 168-day cycle. Fig. F-01-1 shows a relative drift between ERS-1 and T/P from 1992 to 1996: the relative bias between ERS-1 and T/P is almost zero in 1993 and about 6 centimetres in 1996. In the ERS-2 phase the bias is constant with an averaged DXO difference of around 8 centimetres. The geographical dependence of the gravity-induced orbit error explains the difference between this result and the global values (Stum et al, 1999). The relative bias between ERS-1 and ERS-2 is about 2 centimetres during the Tandem Mission phase. Fig. F-01-2 is equivalent to Fig. F-01-1 and it is obtained using ERS data pre-processed by DEOS by applying consistent geophysical corrections during all the ERS phases and re-calibration algorithms (Scharroo et al., 2000). The reduced drift indicates that the drift observed in Fig. F-01-1 is mainly due to the inconsistency between the corrections applied in the ERS-GDR. Moreover the similar results obtained for ERS-2 show that CERSAT and DEOS use similar geophysical corrections in the pre-processing of ERS-2 data. Tab. F-01-1 summarises the relative bias obtained by using the ERS data pre-processed from the ERS-GDR and by using the ERS data pre-processed by DEOS. The DXO method with the 10-day time-constraint is applicable only to simultaneous data, while the sea level variability has to be accounted for considering not simultaneous missions. The time-constraint can be neglected computing SSH differences at the DXO points if the SSH observations are corrected for the sea level variability. The construction of a simple and accurate model for the sea level variability is here investigated.

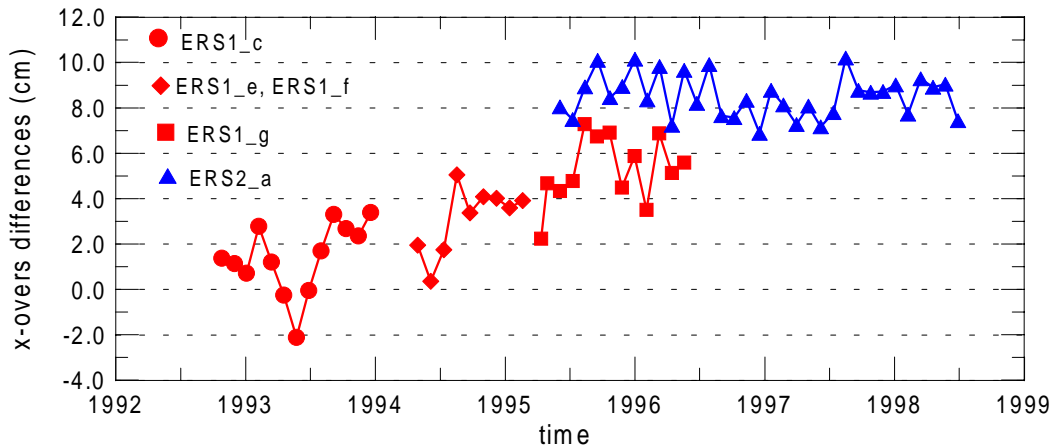


Figure F-01-1: Average over each ERS 35-day cycle (ERS-1 phases c,g and ERS-2 phase a) and over each 37-day sub-cycle of the ERS 168-day cycles (ERS-1 phases e,f) of sea-surface height differences at DXO points between ERS and T/P with epoch differences of less than 10 days. Data are pre-processed as from the User Manuals

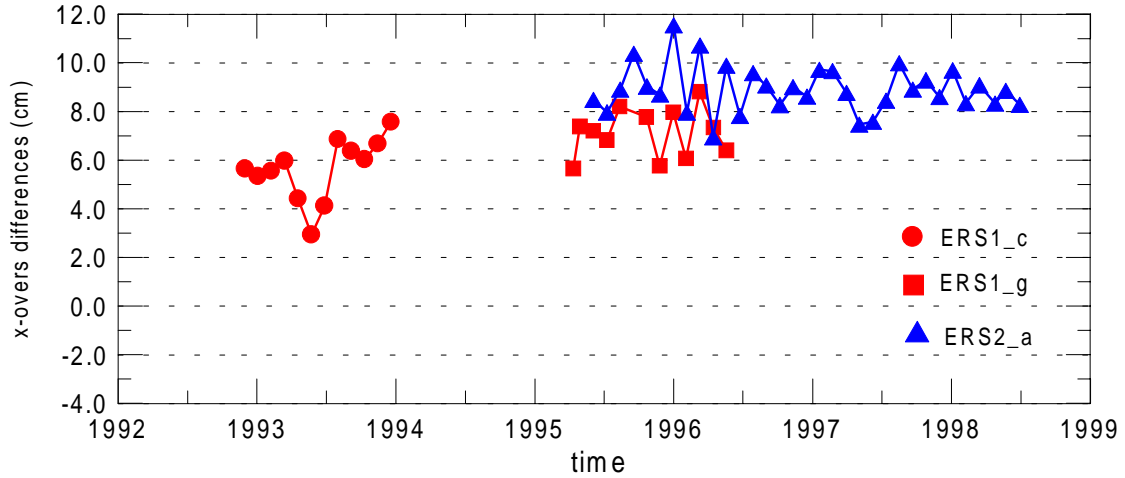


Figure F-01-2: Average over each ERS 35-day cycle (ERS-1 phases c,g and ERS-2 phase a) of sea-surface height differences at DXO points between ERS and T/P with epoch differences of less than 10 days. Data are pre-processed with homogenised corrections by DEOS

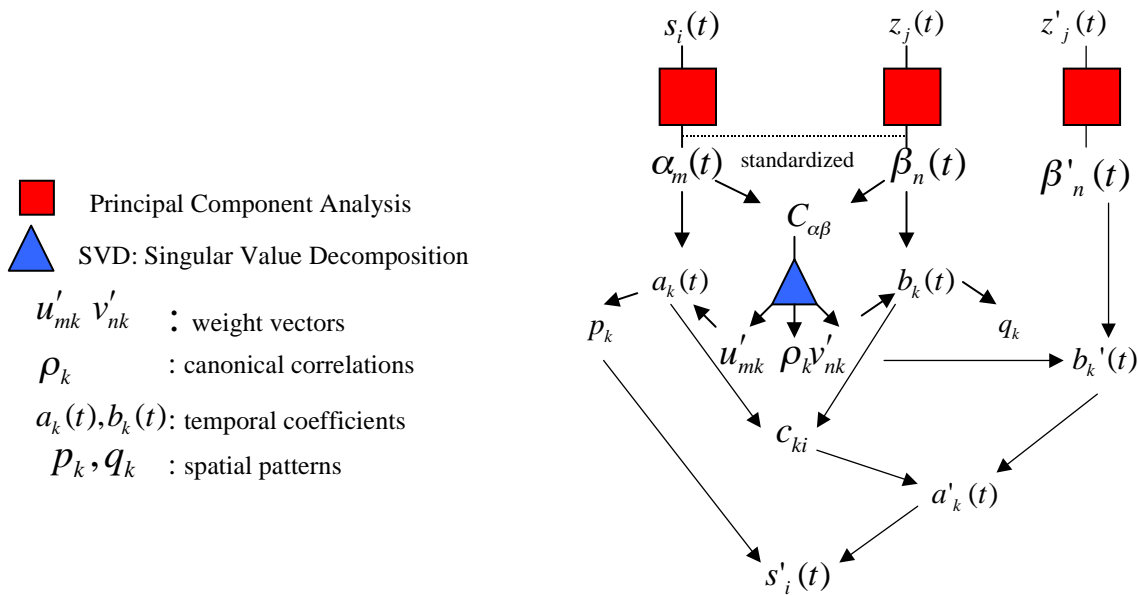


Figure F-01-3: Scheme of the predicted PCA-CCA analysis

3. Results

3.1 Single-mission models for the sea level variability

The altimetric SSH and the sea-surface temperature data are gridded in time and space with a monthly time-interval and a spatial grid spacing of 0.5 degrees in latitude and longitude. To avoid discrepancies between the missions due to not homogeneous data pre-processing or to residual bias and drifts, only altimetric data of the T/P mission are used. The monthly and spatial average acts as a low-pass filter to the data. Subtracting the mean at each node, an anomalous time-series field $s(p,n)$ is obtained, where p is the space index and n is the time index. The grid points in the Mediterranean Sea are about 1000. Three SLV models are

constructed using statistical methods applied to the gridded data. The Principal Component Analysis (PCA)(Jolliffe, 1986), the Canonical Correlation Analysis in PCA basis (PCA-CCA) (Bretherton et al., 1992) and the predicted PCA-CCA analysis (PPCA-CCA), which is an extension of the PCA-CCA method, are used. Fig. F-01-3 gives the scheme of the PPCA-CCA method. Let us consider two anomalous time-series fields \mathbf{s} and \mathbf{z} , overlapping over a given time-interval, but not necessarily defined on the same spatial points, with the time-interval of the second field longer than the time-interval of the first field. The first field has to be extrapolated over the non-overlapping time-interval. The first step consists in applying the PCA-CCA method to the overlapping temporal interval of the two fields. Each field is pre-filtered by a PCA decomposition. The singular value decomposition (SVD) of the covariance matrix of the standardized PCA temporal coefficients of each single field α and β gives the weight vectors \mathbf{u} and \mathbf{v} and the canonical correlations ρ . The temporal coefficients \mathbf{a} and \mathbf{b} and the spatial patterns \mathbf{p} and \mathbf{q} of the two fields are given by the analysis formula and by the canonical correlation maps:

$$\begin{cases} \mathbf{a} = \mathbf{u}^T \alpha \\ \mathbf{b} = \mathbf{v}^T \beta \\ \mathbf{r}[\mathbf{s}(t), a_k(t)] = p_k \\ \mathbf{r}[\mathbf{z}(t), b_k(t)] = q_k \end{cases} \quad (\text{F-01-1})$$

The complete dataset \mathbf{z} is pre-filtered by a PCA decomposition obtaining standardized temporal coefficients β' . Temporal coefficients \mathbf{b}' for the field \mathbf{z} are:

$$\mathbf{b}' = \mathbf{v}^T \beta' \quad (\text{F-01-2})$$

The temporal coefficients \mathbf{a}' of the field \mathbf{s} over the complete interval of \mathbf{z} are:

$$a'_k = \sum_{j=0}^J c_{kj} b'^j_k \quad (\text{F-01-3})$$

where c_{kj} are the regression coefficients of the temporal coefficients \mathbf{a} and \mathbf{b} . The PPCA-CCA model corresponding to the field \mathbf{s} is given by the synthesis formula:

$$\tilde{\mathbf{s}} = \mathbf{p} \mathbf{a}' \quad (\text{F-01-4})$$

The STA field is used as second field (the predictor) in the PPCA-CCA method, as in the Mediterranean Sea the STA and the SLA fields are highly correlated (Fenoglio-Marc 2001). Five years (from 1992.9 to 1997.8) of the SLA field and the complete STA field are used to extrapolate the SLA field over the following two years (from 1997.9 to 1999.8). A PCA and a PCA-CCA models are built using the complete SLA and STA datasets (from 1992.9 to 1999.9). The first four components of the PCA, PCA-CCA and PPCA-CCA decompositions are retained to form the models. The first four modes of each decomposition accounts together for about 90% of the variance of the SLA field. The first mode of the PCA decomposition accounts for 80% of the variance, whereas the first mode of the PCA-CCA decomposition accounts for about 60% of it. The high correlation between the SLA and the STA fields is expressed in the PCA-CCA model by the first canonical coefficients, near to unit, and by the high cumulative fraction of the total variance (CVF) of the first four modes of both the SLA and STA PCA-CCA models (0.9). The models formed by the first components of the decompositions are therefore a good representation of the SLA field.

Table F-01-2: Regional accuracy of the SLV models comparing observations and models

SLV model	o-c RMSE (cm)	o-c MAE (cm)	o-c ME (cm)
PCA (1992.9-1999.8)-D	1.84	2.48	1.d-3
PCA-CCA (1992.9-1997.8)-D	1.79	1.21	1.d-4
PCA-CCA (1992.9-1999.8)-D	2.23	1.41	1.d-3
PPCA-CCA (1992.9-1999.8)-D	3.68	2.48	0.2

3.2 Accuracy of the Models

The accuracy of the SLV models is analysed by comparing the averaged anomalous field, formed by the monthly gridded values, and the results of the SLV models. Fig. F-01-4 shows in one geographical point the SLA field and the SLA computed from the PCA (a), PCA-CCA (b) and PPCA-CCA (c) models together with their differences. The squared mean differences are 1.16, 1.92 and 3.19 for the PCA, PCA-CCA and PPCA-CCA SLV models. The PCA and PCA-CCA models have therefore the highest accuracy, but also the PPCA-CCA model is able to reproduce the averaged observations over the complete interval with an acceptable accuracy (F-01-4.c). Fig. F-01-4.d shows the observed SLA and STA patterns and their phase-lag. As the phase-lag is not found in the results of the PPCA-CCA model the goodness of the prediction is confirmed. Two scalar measures of accuracy are the root-mean-square error (RMSE) and the mean absolute error (MAE). The first is the average square difference between the observation and model forecast pairs, the second is the average of the absolute differences between observation and model. The mean error (ME) is the averaged difference between observed and model values. The accuracy of the SLV models is estimated considering the anomaly field and the models in each node of the grid in the Mediterranean Sea. Tab. F-01-2 corresponds to ERS-DEOS data, the RMSE values show that the regional accuracy is about 2 centimetres for both the PCA and the PCA-CCA models and 4 centimetres for the PPCA-CCA model.

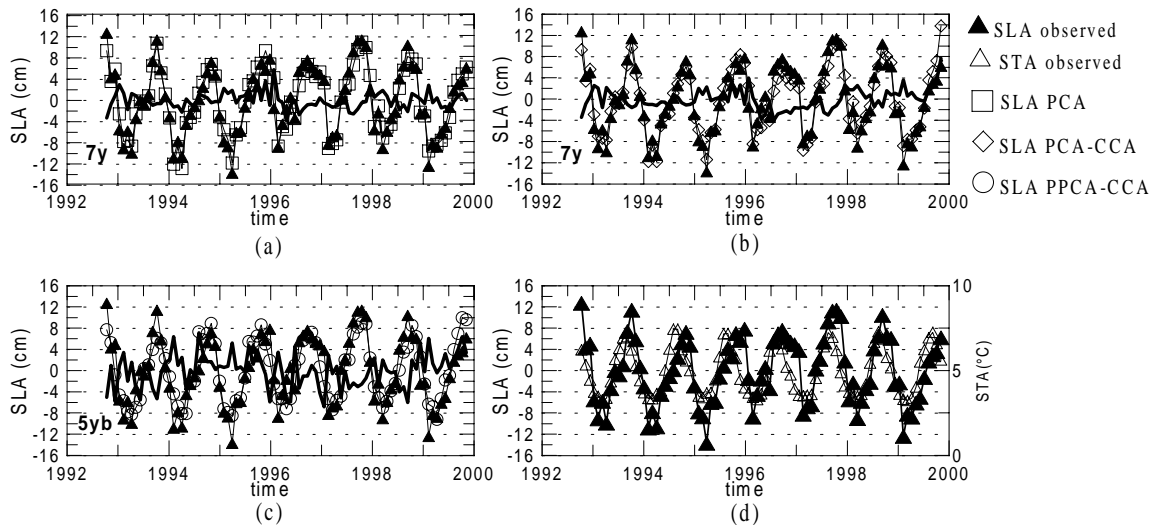


Figure F-01-4: Monthly averages of SLA and their differences (dark tick line) at one location (lat=40 deg, lon=10 deg) as observed from T/P and computed from the PCA (a), PCA-CCA (b) and PPCA-CCA (c) models. Monthly means of the observed SLA and sea-surface temperature anomalies (STA) are shown in (d).

3.3 Application to Multi-mission Analysis

Another way to estimate the accuracy of the SLV model is to apply the model to the instantaneous sea surface height (SSH) data and to compute the DXO differences without the time constraint. If the model is accurate enough, the sea level variability has been eliminated and therefore does not show up in the DXO differences. The DXO differences are computed between the complete set of ERS data and the T/P data corresponding to the first ERS-2 repeat cycle (T/P cycles from 97 to 102).

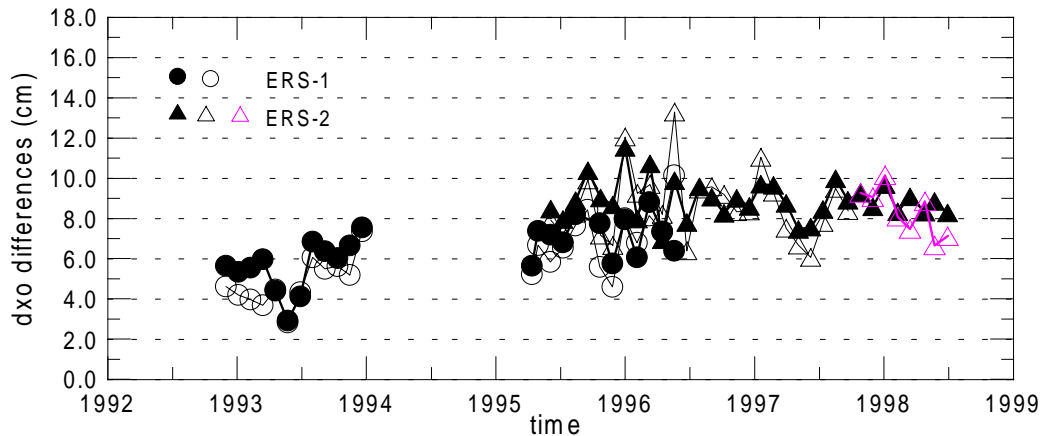


Figure F-01-5: Average over each ERS-35 day cycle of sea-surface height differences at DXOs between ERS and TP with a 10-day time constraint (full symbol black) and between ERS and T/P cycles 97-102 corrected using the PCA-CCA (empty symbol) and the PPCA-CCA (full symbol grey) models

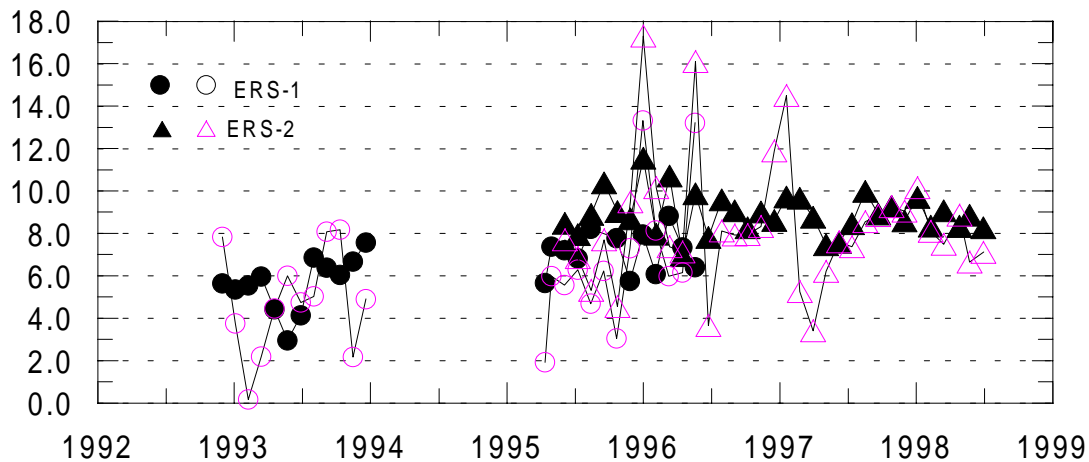


Figure F-01-6: Average over each ERS-35 day cycle of sea-surface height differences at DXOs between ERS and TP with a 10-day time constraint (full symbol black) and between ERS and T/P cycles 97-102 corrected using the predicted PCA-CCA model (empty symbol)

Fig. F-01-5 shows sea level height differences at DXOs averaged over each ERS cycle. Both DXOs corresponding to the 10-day constraint (as in Fig. F-01-2 and DXOs without the time-constraint and computed using two SLV variability models have been considered. The PCA-CCA model obtained from the five years of data is applied between 1992.9 and 1997.8 and the PPCA-CCA model is applied between 1997.9 and 1999.8. As measure of accuracy we

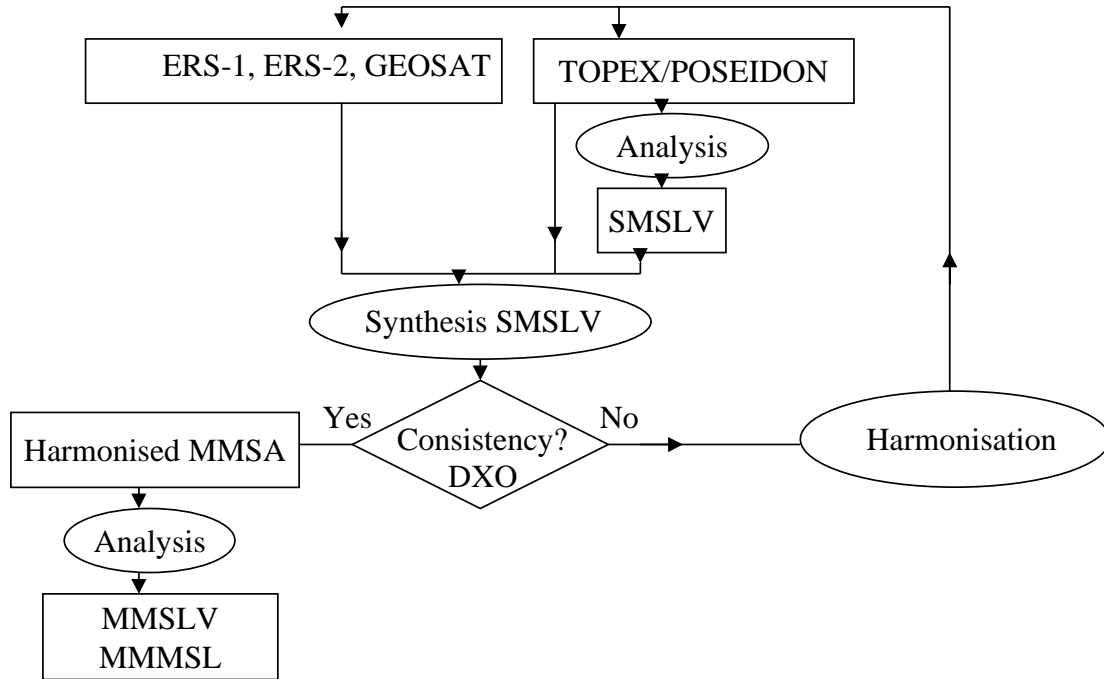


Figure F-01-7: Multi-mission analysis scheme

use the root-mean-square difference between the mean DXOs obtained with and without the 10-day constraint as well as the mean absolute difference and the mean difference. Tab. F-01-3 corresponds to ERS-DEOS data except for the PCA results. The estimated accuracy is higher than 2 centimetres for both the PCA and the PCA-CCA SLV models and of 3 centimetres for the PPCA-CCA model. The PPCA-CCA model performs quite well over the extrapolated time-interval, while the performance over the overlapping time-interval is worst than for the PCA-CCA model.

Table F-01-3: Regional accuracy of the SLV models derived from comparison of DXO (10-day constraint) and models

SLV model	DXO RMSE (cm)	DXO MAE (cm)	DXO ME (cm)
PCA (1992.7-1997.7)-G	0.86	0.68	0.16
PCA-CCA (1992.9-1998.5)-D	1.25	0.98	-0.28
PPCA-CCA (1992.9-1998.5)-D	2.94	2.32	-0.55
PPCA-CCA (1997.5-1998.5)-D	1.08	0.84	-0.58

4. Discussion and conclusions

The use of multi-mission altimetric data requires an effort to reduce the discrepancies between the datasets, which are mainly due to not homogeneous geophysical corrections and to instrumental bias and drift. The method is an attempt to cross-calibrate the time series in the Mediterranean Sea in a regional long-term monitoring analysis. First step is the estimation of a single-satellite sea level variability model from the T/P data using statistical methods. Not simultaneous missions require a predicted model. The strong correlation between the SLA and the STA fields in the Mediterranean Sea allows to build a predicted SLV model from the

STA data. The accuracy of the PCA and PCA-CCA models is higher than 2 centimetres, that of the predicted PCA-CCA is about 3 or 4 centimeters. A similar accuracy is estimated by two different methods and give confidence to the value and to the SLV models. The lower accuracy obtained for the PPCA-CCA model is explained by the complex relationship between SLA and STA. There are interannual effects, like the NAO and ENSO effects, linked to atmospheric pressure change, wind effects, mass transfer with the Atlantic which make complex the correlation between sea level and sea-surface temperature change. The results obtained show that the monitoring of DXO differences of SSH data corrected by a SLV predicted model is promising to cross-calibrate present and past altimetric missions.

Acknowledgements

The authors acknowledge R.Scharroo (DEOS) for the pre-processed ERS altimetry data, ESA for the ERS altimetry, AVISO for the Topex/Poseidon altimetry and NOAA for the sea-surface temperature data.

References

- AVISO, User Handbook, Merged Topex/Poseidon products, avi-nt-02-101-cn, Aviso, Toulouse, France, 1996
- Bretherton C., Smith C., Wallace J., An intercomparison of methods for finding coupled patterns in climate data change, *J. of Climate*, **5**, 541-560, 1992
- Cersat, Altimeter and Microwave radiometer ERS products User Manual, C2-MUT-A-01-IF, Cersat, Toulouse, France, 1996
- Fenoglio-Marc L., Altimetry data improvement by dual crossover method in European Seas and along-track stationary sea surface topography, *AVN*, **10**, 354-359, 1997
- Fenoglio-Marc L., Analysis and representation of regional sea level variability from altimetry and atmospheric data, *Geoph. J. Int.*, , in press
- Jolliffe I., Principal Component Analysis, Springer Series in Statistics, 272 pp., Springer, New York, 1986
- Scharroo R. and Visser P., Precise orbit determination and gravity field improvement for the ERS satellites, *J. geophys. Res.*, **102**, **C4**, 8113-8127, 1998
- Scharroo R., Schrama E., Naeije M., Benveniste J., A recipe for upgrading ERS altimeter data, Proceedings of the ERS-ENVISAT Symposium Gothenborg, ESA, 2000
- Stum J., Ogor F. and Dorandeu J., A comparison stud of Topex/Poseidon, ERS-1 and ERS-2 altimeter and radiometer data, Report of Task 4 of Ifremer contract N. 99/2.210 765, CLS/DOS/NT/00.233 Report 1-13, CLS, Ramonville, France, 1999

6.2 An Assessment of satellite altimetry in proximity of the coastline

F-02:Fenoglio-Marc L., S. Vignudelli, A. Humbert, P. Cipollini, M. Fehlau, M. Becker, An assessment of satellite altimetry in proximity of the Mediterranean coastline, in 3rd ENVISAT Symposium Proceedings, SP-636, ESA Publications Division, 2007.

Abstract Altimeter data from various satellite missions are investigated in the coastal zone to determine the minimum distance from the land at which they remain usable. The data used here are the standard Level 2 products and corresponding re-tracked data sets, when available. An attempt is made to determine to what extent the land and ocean characteristics might affect the altimeter data in coastal regions. The different datasets are inter-compared and the satellite-derived sea level variability is compared with that measured from tide gauges at selected sites.

Keywords: coastal altimetry, validation with in-situ data

1. Introduction

Satellite radar altimeters measure the sea surface height as an average value over the altimeter footprint. The height accuracy is essentially determined by knowledge of the satellite orbit, the altimetric range, the environmental range corrections and the characteristics of the sea surface.

While over open ocean waters there is a long history of research into quantifying uncertainty in altimeter data, in coastal regions the quality of the measurements has been less investigated so far (Vignudelli et al., 2005, 2006). The situation in these areas is more problematic, due to the inadequacy of some corrections in shallow waters and to the land contamination in the footprints very close to the coast.

Satellite altimetry has an observational record of almost 15 years from a series of missions (ERS-1 and -2, TOPEX/Poseidon, Geosat Follow-On, Envisat, Jason-1). This huge volume of data needs to be re-analyzed and possibly exploited in the coastal region, in order to provide valuable new information about many hitherto under-sampled sections of the world's coasts. In the last few years new tracker models for the raw altimeter data have been developed to increase the number of usable footprints (Deng et al., 2002; Hwang et al. 2005). Some re-tracked products already exist (Callahan and Rodriguez, 2004), whose suitability to investigate the coastal regions needs to be assessed. Selection criteria specific to coastal regions and the best suitable environmental corrections need to be investigated as well (Carrère and Lyard, 2003).

In this paper we re-analyse the widely distributed 1 Hz data and some recently available higher rate re-tracked data in proximity of selected coastlines in the Mediterranean Sea. Our main purpose is to establish to what extent altimeters are applicable close to the coast. Results from the different missions are inter-compared and then tested with corroborative in situ measurements, such as sea level variability measured from tide gauges at selected sites.

2. Data

The region chosen as test zone for this work is the northernmost portion of the Western Mediterranean Sea, which extends between the Italian regions of Liguria and Tuscany (north

and east) and the French island of Corsica (south) (Fig. F-02-1). The time period of the investigation is that of the available re-tracked product, specifically from July 2000 to August 2002. We use altimeter data from TOPEX/Poseidon, ERS-2 and ERS-1 missions. The corrections and the selection criteria used are shown in Tables F-02-1 and F-02-2, respectively. The GEBCO bathymetry data are used to compute depth and distance to the coast.

The Level 2 Geophysical Data Records (GDR) of the Topex/Poseidon and ERS-2 altimeter missions are extracted from the Radar Altimeter Database System (RADS) (Naejie et al., 2002). They are 1 Hz data. The Retracked Geophysical Data Records (R-GDR) from the Topex/Poseidon mission are provided by NASA-JPL Physical Oceanography Distributed Active Archive Center (PODAAC, P. Callahan, release 2.1). The temporal coverage is from July 28, 2000 to August 11, 2002, corresponding to cycles 290 to 364 (without 362). The last 21 cycles cover the TOPEX-Jason collinear period. Two types of retracking data are available, corresponding to two different algorithms (least squares and maximum a posteriori). Both 1 Hz and 10 Hz data are available. Retracked data from the ERS-1 geodetic mission (ERS-1 GM) are kindly provided by De Montfort University and the Danish National Space Center (P. Berry and O. Andersen). A 2-parameter retracked product is available, which is based on eleven different retrackers. The data are available with a frequency of 18 Hz. Range and geophysical corrections were already applied (Andersen et al., 2000, 2005).

Sea level is routinely measured at selected sites in the study region by acoustic tide gauges operated by the National Mareographic Service of the Agency for Environmental Protection and Technical Services (APAT). Data are available as quality controlled hourly values of sea surface elevation, the reference being a benchmark connected to the national datum. We select the tide gauges located in Imperia, Genova, Livorno, Porto Torres and Macinaggio, whose data are available in the time interval chosen.

As we compare sea level heights from altimetry with tide gauge observations, we do not correct the altimeter measurements for the ocean tide, the pole tide and the barometer effect (Fenoglio-Marc et al., 2004). We apply the standard corrections to the altimeter measurements as summarised in Table F-02-1. These include corrections for environmental (path delay in troposphere and ionosphere, response to pressure), geophysical (solid earth tide and load tide) and sea state bias corrections. Sea level height anomalies are computed using as reference the CLS01 mean sea surface. We select the data that satisfy the criteria listed in Table F-02-2.

The differences between the handling of Topex and ERS-2 from the RADS database are the choice of the type of ionosphere correction applied (no dual frequency available in ERS-2) (Tab. F-02-1) and the check of the radiometer flag in Topex, but not in ERS-2 (Table F-02-2). The reason for this last difference is the elimination of a huge amount of ERS-2 data, not only near to the coast, when the check of the radiometer instrumental flag is included in selection criteria for ERS-2.

The handling of Topex GDR and RGDR data should in principle be the same, however differences can arise from the unavailability of some of the corrections as directly applicable by the user (e.g. the sea state bias) or from checking of flags that have slightly different names in the RADS database.

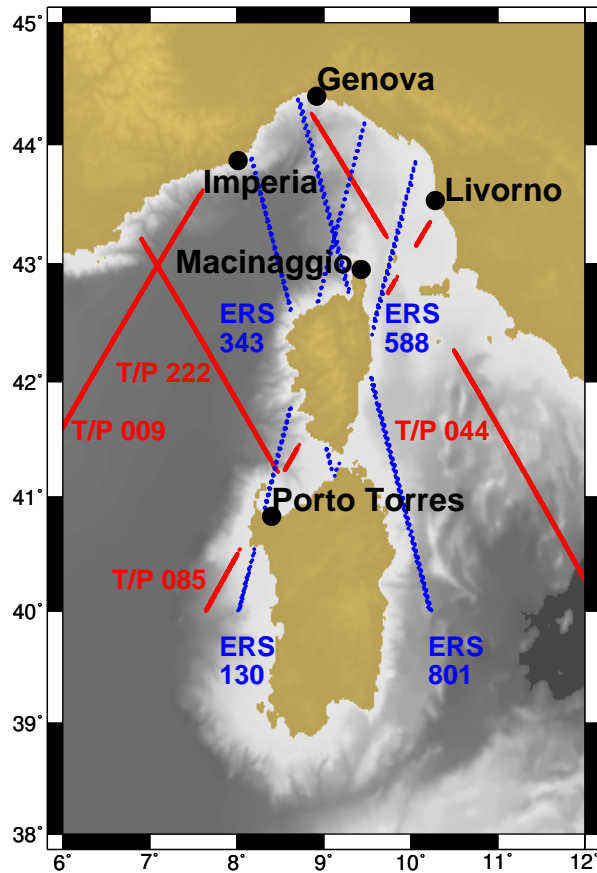


Figure F-02-1: Study area showing some T/P ground tracks and the position of ERS tracks

3. Results

3.1 Along-track Comparison

Fig. F-02-2 displays the sea level anomaly for GDR, R-GDR (from both retracers) versus the latitude for cycle 328 and pass 44 (see position in Fig. F-02-1). The bathymetry is shown as a blue line and points are colour-coded depending on the distance to the coast. The closest distance to the coast near Genova for the selected cycle and track is 17.2 km with retracked data, whereas it is 27.3 km for GDR. There is a bias of a few cm between the GDR and the R-GDR sea level anomalies. Fig. F-02-3 displays the sea level anomaly versus the latitude for ERS-2 cycle 55 and pass 801 near Genova. The bathymetry is shown as a blue line. The closest distance to the coast for the selected cycle and pass is 5 km. The left panel of Fig. F-02-4 displays the tracks of the retracked data from the ERS-1 geodetic mission. Track 16916 is highlighted and shown in the right panel. It is located in the same region as tracks in Figs. F-02-2, F-02-3. Retracker No. 9 performs normal Brown waveform retracking and occurs most often. Values corresponding to retracker No. 8, which does a "fat patch" waveform retracking, are shown as triangles. Their color gives the distance to the coast. The 1 Hz data, in grey, are obtained by filtering the 18 Hz data. The closest usable point to coast is at a distance of 1.6 km. The along-track sea level anomaly has a behaviour comparable to the along-track sea level anomaly shown in Figs. F-02-2, F-02-3 for the Topex and ERS-2 passes near to Genova.

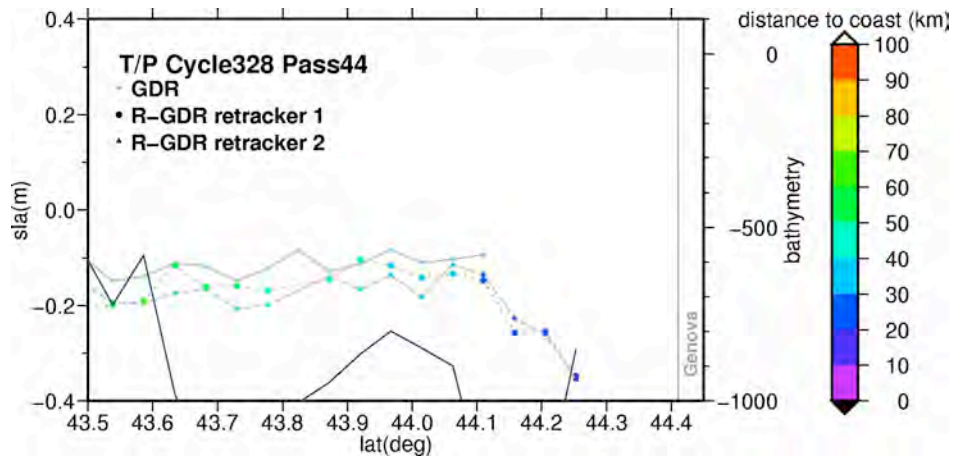


Figure F-02-2: Sea level anomaly relative to the CLS01 mean sea surface along Topex cycle 328, pass 44 in the Ligurian Sea from GDR and RGDR retracker 1 and 2. The bathymetry is given by the blue continuous line

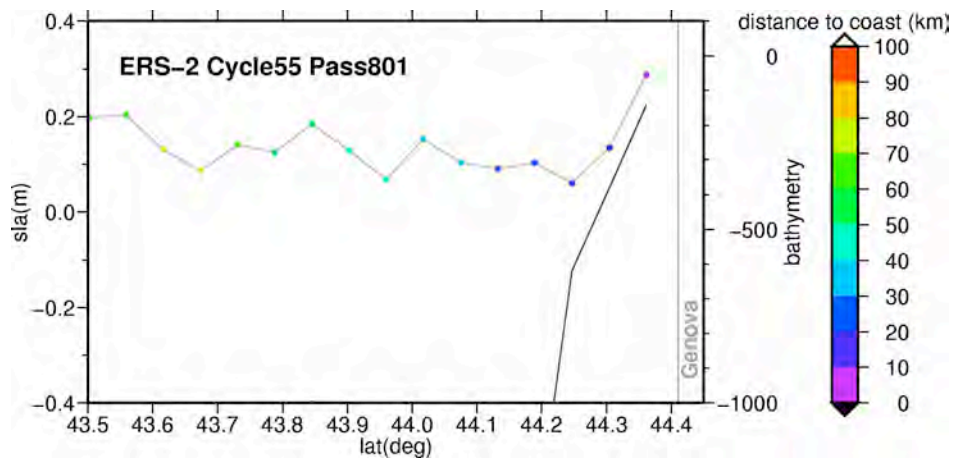


Figure F-02-3: Sea level anomaly relative to the CLS01 mean sea surface along ERS-2 cycle 55, pass 801 in the Ligurian Sea (from the GDR). The bathymetry is given by the blue continuous line

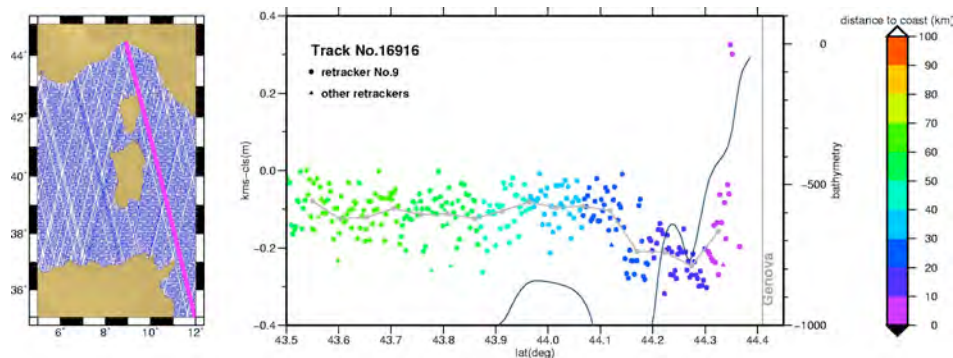


Figure F-02-4: Sea level anomaly relative to the CLS01 mean sea surface from the retracked ERS-1 GM data at 18Hz (dots) and at 1 Hz (after smoothing with a 19-point Hanning window and resampling) along pass N. 16916 in the Ligurian Sea. The bathymetry is given by the blue continuous line.

3.2 Comparison at normal points

We compute time series at normal points (NPs) along the tracks . We define the normal points on the basis of the equator passing time of the track; we do not account for cross-track

Table F-02-1: Environmental and Instrumental corrections applied to Topex GDR and R-GDR and to ERS-2 GDR (NA=not applied)

missions	TP GDR	ERS-2 GDR	TP R-GDR
wet troposphere	radiometer	radiomete	radiometer
dry troposphere	ECMWF	ECMWF	ECMWF
response to atm. pressure	NA	NA	NA
ionophere	dual frequency	IRI95 model	dual frequency
ocean tide	NA	NA	NA
solid earth tide	FES2004	FES2004	FES2004
load tide	FES2004	FES2004	FES2004
pole tide	NA	NA	NA
sea state bias	BM3/BM4 model	BM3/BM4 model	BM3/BM4 model

and along-track departure of the point from its mean position over the considered interval. The six NPs nearest to the coast are investigated analysing their following properties: number of time points, distance to coast, depth, standard deviation of the differences between altimeter and tide gauge sea level (Table F-02-3).

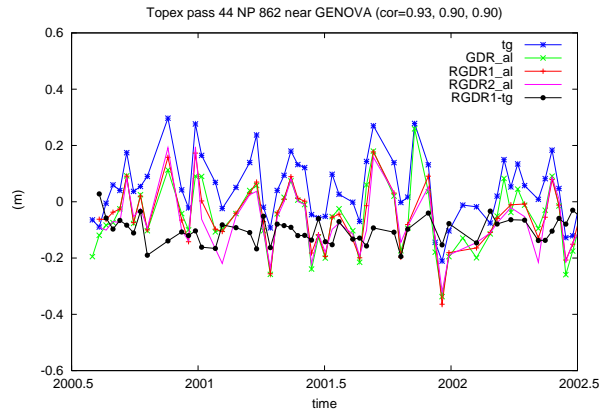


Figure F-02-5: Sea level anomaly time-series at a normal point near Genova (pass 44, normal point 862) from Topex GDR (green), RGDR1 (red) and RGDR2 (violet). The blue and black curves are interpolated heights from the tide gauge and their differences w.r.t. RGDR1, respectively

Using the retracked dataset more time samples are retained at each normal point and we approach more to the coast. The correlation of the altimeter and tide gauge time series is lower. Only values within 3σ from the mean are considered.

Sea level anomalies from the Topex retracked data are significantly smaller than those from the Topex GDRs. This is seen in Figs. F-02-2, F-02-3. The distances to the coast of the nearest points depends on the different morphological coastal conditions in the areas. There is a slight evidence of larger differences between R-GDR and GDR towards larger distances from coast.

The average difference between the retracker 1 and 2 is small. In pass 044 of cycle 328 the difference between the retracker varies from -0.13 to 0.062m. The largest variations in this pass over all cycles go from -0.395 to 2.031m. The differences between the retracker are represented by a gaussian-like distribution with peak near to zero.

Table F-02-2: Selection criteria applied to the GDR (Topex/Poseidon and ERS-2) and R-GDR

Filters	TP and ERS-2 RADS GDR	TP R-GDR
N. obs	$8.5 \leq \text{val} \leq 10.5$	≤ 10
Sigma range	$0. < \text{val} < 0.5 \text{ m}$	$0. < \text{val} < 0.5 \text{ m}$
Dry troposphere	$-2.4 < \text{val} < -2.1 \text{ m}$	$-2.5 < \text{val} < -1.9$
Wet troposphere (radiometer)	$-0.6 < \text{val} < -0.0001 \text{ m}$	$-0.5 < \text{val} < -0.0001 \text{ m}$
Ionosphere (dual frequency)	$-0.40 < \text{val} < -0.04 \text{ m}$	$-0.40 < \text{val} < -0.04 \text{ m}$
solid earth tide	$-1.0 < \text{val} < 1.0 \text{ m}$	$-1.0 < \text{val} < 1.0 \text{ m}$
load tide	$-0.5 < \text{val} < 0.5 \text{ m}$	$-0.5 < \text{val} < 0.5 \text{ m}$
sea state biase	$-1.0 < \text{val} < 1.0 \text{ m}$	NaN
SWH	$0 < \text{val} < 8.0 \text{ m}$	$-1.0 < \text{val} < 11.0 \text{ m}$
sigma SWH	$0 < \text{val} < 0.9 \text{ m}$	$0 < \text{val} < 0.9 \text{ m}$
backscatter sigma	$6 < \text{val} < 27 \text{ dB}$	$7 < \text{val} < 30 \text{ dB}$
wind speed	$0 < \text{val} < 30 \text{ m/s}$	$0 < \text{val} < 30 \text{ m/s}$
off nadir angle	$-1d20 < \text{val} < 1d20$	NA
AGC RMS K	NA	$\text{val} < 100$
AGC Pts Avg K	NA	$\text{val} > 10$
Flag ocean	checked	checked GeoBad1 bit1
Flag iono	checked	checked IonoBad
Flag land	checked	checked GeoBad1 bit2
Flag no rain	checked	checked GeoBad2 bit0
Flag no ice	checked	checked GeoBad1 bit3
Flag TRM bad	checked	checked TRMbad

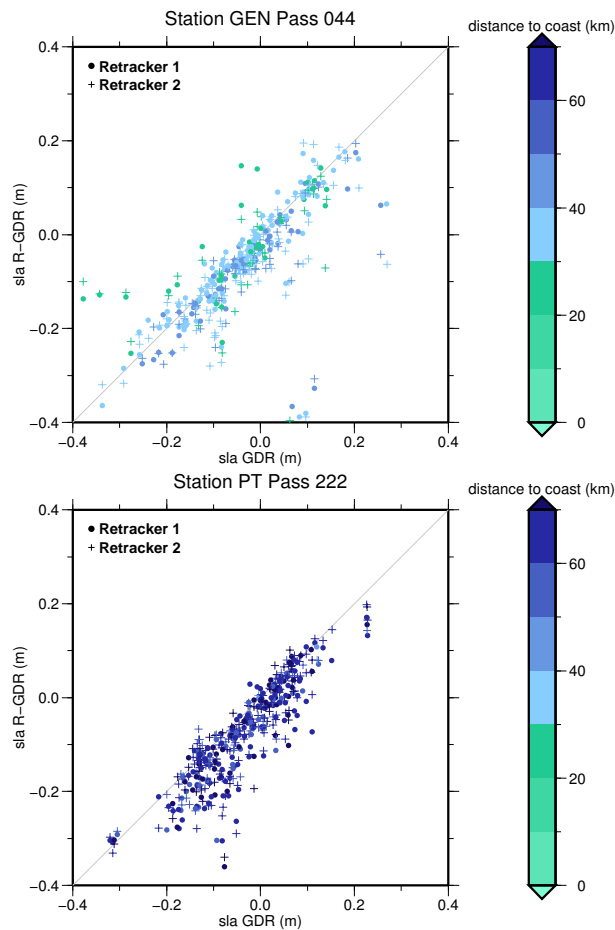


Figure F-02-6: Scatterplots of sea level heights near Genova (left) and Porto Torres (right) from Topex GDR and RGDR data.

Table F-02-3: Statistics at Normal points near Genova (pass 44) from GDR, RGDR1 and RGDR2: number of times, correlation and standard deviation (mm)

NP	Depth (km) (km)	Dcoast (km) (km)	Nt GDR	Cor GDR	Std GDR (mm)	Nt R-1	Cor R-1	Std R-1 (mm)	Nt R-2	Cor R-2	Std R-2 (mm)
865	-1114	21				23	0.87	48	23	0.87	45
864	-1425	25	9	0.92	121	29	0.84	48	28	0.80	62
863	-1271	27	45	0.70	92	44	0.81	48	45	0.60	85
862	-929	30	59	0.93	44	53	0.90	48	53	0.89	50
861	-848	34	58	0.92	44	58	0.68	48	57	0.75	80
860	-8024	38	61	0.94	40	57	0.72	48	56	0.80	73

4. Conclusions

The along-track comparison of retracked 18 Hz ERS-1 data of the geodetic mission and of the GDR and RGDR missions show a similar behaviour of the sea level height anomaly in the same area. The analysis of sea level height variability from the Topex exact repeat mission shows that starting from 25 kilometres from the coast we could extract time-series at the normal points with more than 50% of the available data from the 1 Hz GDR data. Using the same criteria for the retracked Topex data, we obtain more data at distances smaller than 25 Kilometres from the coast and a comparable number of data at bigger distances. The use of the retracked data is therefore promising for coastal investigations. At present, for our example of tide gauge stations, the correlation between the retracked and the tide gauge data is lower than that of the GDR data. This holds independently from the number of points in the time-series. This may be due to points not yet eliminated by the selection criteria or to other reasons presently under investigation.

Acknowledgements

We kindly acknowledge ESA, CNES, JPL and the Montfort University for the altimetry data, APAT for the tide gauge data.

References

- Andersen, O. B., S. Dreyer, P. Knudsen, P. A. M. Berry, E. L. Mathers, R. Trimmer, S. Kenyon, Deriving 2hz ERSs-1 Geodetic Mission Altimetry for gravity and marine geoid purposes, ESA-special publication SP572, 2005.
- Andersen, O. B. and P. Knudsen, The role of Satellite Altimetry in Gravity Field modeling in Coastal Areas, *Phys. Chem. Earth*, 25 (1), 17-24, 2000.
- Callahan P.S. and E. Rodriguez, 2004. Retracking of Jason-1 data, *Mar. Geod.* 27: 391-407
- Carrère L. and F. Lyard (2003). Modeling the barotropic response of the global ocean to atmospheric wind and pressure forcing - comparisons with observations, *Geophys. Res. Lett.*, 30(6), 1275, doi:10.1029/2002GL016473
- Deng X., W. Featherstone, C. Hwang and P.A.M. Berry, 2002. Estimation of contamination of ERS-2 and Poseidon satellite radar altimetry close to the coasts of Australia, *Marine Geodesy*, 25: 249-271

- Fenoglio-Marc L., Groten E. and Dietz C., 2004. Vertical Land Motion in the Mediterranean Sea from altimetry and tide gauge stations, *Marine Geodesy* **27**, C3-4, 683-7018.
- Hwang C., J. Guo, Y. Liu and X. Deng, 2006. Coastal gravity anomaly from retracked Geosat/GM altimetry: improvement, limitation and role of airborne gravity data, *J. of Geod.*, 80, 204-216.
- Naeije M., E. Doornbos, L. Mathers, R. Scharroo, E. Schrama and P. Visser (2002), Radar Altimeter Database System: Exploitation and Extension, Final Rep. NUSP-2 02-06, Space Res. Organ. Neth., Utrecht, Netherlands
- Vignudelli S., Snaith H. M., Lyard F., Cipollini P., F. Venuti, Birol F., Bouffard J., Roblou L.: Satellite radar altimetry from open ocean to coasts: challenges and perspectives, United States Society of Photo-Optical Instrumentation Engineers (SPIE), Vol. 6406, 64060L 1-12, doi: 10.1117/12.694024, 2006.
- Vignudelli S., Cipollini P., Roblou L., Lyard F., Gasparini G. P., Manzella G. M. R., and Astraldi M., Improved satellite altimetry in coastal systems: Case study of the Corsica Channel (Mediterranean Sea), *Geophys. Res. Lett.*, 32, L07608, doi:1029/2005GL22602, 2005.

6.3 Coastal Sea Surface Heights from Improved Altimeter Data

F-03: Fenoglio-Marc L., M. Fehlaue, L. Ferri, M. Becker, Y. Gao, S. Vignudelli, Coastal sea surface heights from improved altimeter data in the Mediterranean Sea, in IAG Symposia N. 135, Gravity, Geoid and Earth Observation, Mertikas S.P. (eds), Springer Verlag, 253-262, 2008.

Abstract Standard and newly re-tracked altimeter data of the Topex/Poseidon and Envisat missions are analysed in the Mediterranean Sea in the proximity of selected coastlines. Over-conservative selection criteria in standard level 2 products cause rejection of many data in coastal regions. Among the standard criteria, most critical for the data rejection are the checks on microwave radiometer wet tropospheric correction and on standard deviation of the 18 Hz ranges. Using a model tropospheric correction, Envisat performs better than Topex and is approaching the coast up to 5 Kilometres at sea-land transitions. A further improvement in quality of coastal data is obtained using off-line retracked Topex-RGDR and Envisat data, these latter ones retracked with the β_5 and Improved Threshold empirical methods.

Keywords: coastal altimetry, re-tracking

1. Introduction

There has been considerable interest recently in addressing the retrieval of altimeter data in coastal regions to monitor more accurately sea level change. Data distributed by operational centers are not targeted to coastal areas. Standard altimeter products are therefore usually flagged as bad and removed. Moreover the signal to noise ratio is rapidly degraded as altimeter and radiometer are disturbed at 10 and 50 km to the coast respectively. In particular, due to the contamination of land surface in the measurements of brightness temperature made by the on-board microwave radiometer (MWR), the MWR derived wet tropospheric correction cannot be used at distances smaller than 50 km to the coast (Desportes et al. 2007). New post-processing techniques recover additional coastal data and allow to detect smaller ocean dynamical processes (Roblou et al. 2007, Bouffard et al., 2008). In-situ sea level data at selected sites are used to assess the quality of the altimeter data (Fenoglio-Marc et al. 2007, Vignudelli et al. 2005). New pre-processing of the altimeter waveforms, using non-standard waveform models in the attempt to recover the ocean surface parameters, improves the accuracy of altimeter ranges (Anzenhofer et al. 1999, Deng et al. 2002, Deng and Featherstone 2006). Purpose of this paper is to establish to what extent (1) standard criteria are applicable close to coast to both standard products and off-line re-tracked altimeter data, (2) non-uniform local conditions affect the altimeter retrievals on sea-land and land-sea along-track direction, (3) retracking methods improve the quality of data near coast. In section 2 we describe data and methods. Results are presented in section 3, conclusions in section 4.

2. Data and Methods

The Mediterranean Sea region is analyzed using Topex and Envisat data. Both standard products and newly retracked data are used. For Topex, standard Level 2 Geophysical Data Records (GDR) at 1 Hz are extracted from the Radar Altimeter Database System (RADS) (Naeije et al. 2002). RADS data are provided at 1 Hz. Topex retracked data are

the off-line retracked Geophysical Data Records (R-GDR) provided by the NASA-JPL Physical Oceanography Distributed Active Archive Center (PODAAC, P. Callahan, release 2.1). Two retracking products, corresponding to the least squares (RGDR1) and the maximum a posteriori estimation (RGDR2) algorithms, exist. Data at 1 Hz and 10 Hz are available for about two years, between July 2000 and August 2002 (cycles 290 to 364 without 362). For Envisat, standard Level 2 data are extracted from the RADS database. In addition, the standard SGDR products (CLS, 2006) are used, with data at both 1 and 18 Hz. Envisat data are analysed over one year, between February 2006 and July 2007 (cycles 44-45, 47, 50, 52-59). First the standard selection criteria (CLS 2006, AVISO 2006) are applied. Based on the data rejection analysis, criteria are slightly modified to compute sea level anomalies (SLA) (Section 3.2). For the comparison with tide gauges in Section 3.3 the altimetric SLA are computed without ocean and pole tide corrections and without accounting for the effect of atmospheric pressure on sea level (Fenoglio-Marc et al. 2004). We assess the data quality of : (1) standard Envisat, (2) standard Topex products and (3) retracked Topex products by comparing the sea level variability measured from altimetry and tide gauges at the sites of Genova and Imperia. Hourly sea level measurements at the tide gauges are made available by the National Mareographic Service of the Agency for Environmental Protection and Technical Service (APAT). Bathymetry data available from the Italian navy and from the General Bathymetry Chart of the Ocean (GEBCO) (<http://www.bodc.ac.uk>). We finally retrack the Envisat waveforms contained in the SGDR Level 2 products using four empirical retracking methods: the β_5 retracker (Martin et al., 1983), the Off-Center Of Gravity retracker (OCOG) (Wingham et al., 1986), the Threshold (Davis, 1995) and the Improved Threshold (Hwang et al., 2006). The quality of the retracked sea surface heights (SSHs) is evaluated from the improvement percentage (IMP) (Anzenhofer et al. 1999), defined by:

$$IMP = \frac{\delta_{raw} - \delta_{retr}}{\delta_{raw}} 100 \quad (\text{F-03-1})$$

where δ_{raw} and δ_{retr} are the standard deviations of the differences between raw SSHs and retracked SSHs and geoid heights (EGM2008), respectively.

3. Results

3.1 Distance analysis

Four types of distances to the coast are considered: (1) distance to tide gauge, (2) distance to coast, (3) along-track distance at sea-land transition (sl) and (4) along-track distance at land-sea transition (ls). The minimum sampling of the last two is about 7 kilometers for 1 Hz data and 400 meters for the Envisat 18 Hz data, 700 meters for the Topex 10 Hz data. The histogram in Fig. F-03-1 (top) shows that almost all passes have a minimum distance to coast smaller than 10 kilometers. Nearly 50% of Envisat and 45% of Topex passes have a minimum along-track distance in sea-land direction smaller than 7 kilometers (Fig. F-03-1, bottom). In land-sea direction only 15% of Envisat passes and none Topex pass have a minimum along-track distance smaller than 7 Kilometers (Fig. F-03-1, middle). The sea-land coastline crossing direction provides therefore more advantageous measurements conditions.

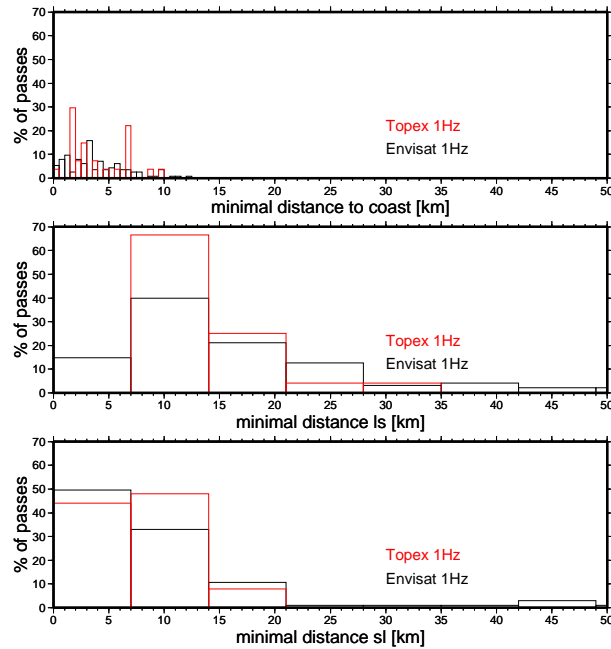


Figure F-03-1: Sea level anomaly relative to the CLS01 mean sea surface from GDR and RGDR retracers 1 and 2 from GDR and RGDR retracers 1 and 2 along Topex cycle 328, pass 44 (left) and only from GRD along ERS-2 cycle 55, pass 801 (right). The bathymetry is given by the blue continuous line

3.2 Analysis of data rejections

Standard selection criteria, including checks on the MWR land and the rain flags are used (Tab. F-03-1). The wet tropospheric radiometer correction and the standard deviation of the 18 Hz ranges are the main causes of rejection, with 8% and 4% of data rejection (Fig. F-03-2). The model wet tropospheric correction from ECMWF is used in Section 3.3. Outliers are eliminated by a 3σ criteria, instead of spline fitting, with 3σ standard deviation of the data

3.3 Sea level comparison at tide gauges

Altimetric and tide gauge sea level heights are compared near Genova and Imperia, in the N-W Mediterranean Sea. The differences between the local and GEBCO bathymetry are in the range of ± 200 metres, there is a strong gradient in land and sea bottom topography (Figs. F-03-3, F-03-4).

The altimeter data are interpolated at fixed locations, called Normal Points (NP) along the altimeter tracks. The relevant distances: (1) distance to tide gauge, (2) distance to coast and (3) along-track distance, as well as the type of transition, are shown for the first few NPs near to coast in Tab. F-03-2. Envisat has in Genova a sea-land transition, the first NP is at 6 Kilometres from coast for both RADS and SGDR data. The distance to the tide gauge is 18 Kilometres. Topex has in Genova a land-sea transition with the first NP at 15 and 24 Kilometres for the R-GDR and RADS data. The distances to tide gauge are 18 and 29 Kilometres. Envisat has in Imperia a land-sea transition. The first NP of Envisat is at 8 Kilometres from coast for both RADS and SGDR data. The corresponding distance to the tide gauge is 29 Kilometres. Topex has in Imperia a sea-land transition with first NP at 6 and

Table F-03-1: Selection criteria for Topex (T) and Envisat (N1)

Criteria	Envisat	Topex
N. obs	10	10
std range	0. < val < 0.25 m	0. < val < 0.15 m
Dry troposphere	-2.5 < val < -1.9 m	-2.4 < val < -2.1
Wet troposphere (radiometer)	-0.5 < val < -0.001 m	-0.6 < val < -0.001 m
Ionosphere (dual frequency)	-0.40 < val < -0.04 m	-0.40 < val < -0.04 m
solid earth tide	-1.0 < val < 1.0 m	-1.0 < val < 1.0 m
inverse barometer	-2.0 < val < 2.0 m	-2.0 < val < 2.0 m
load tide	-0.5 < val < 0.5 m	-0.5 < val < 0.5 m
sea state bias	-0.5 < val < 0.0 m	NaN
SWH	0 < val < 11.0 m	0 < val < 11.0 m
backscatter	7 < val < 30 dB	7 < val < 30 dB
wind speed	0 < val < 30 m/s	0 < val < 30 m/s
off nadir angle	-0.2 < val < 0.16	NA
MWR Land Flag	checked	checked GeoBad1 bit2
Flag no rain	checked	checked GeoBad2 bit0

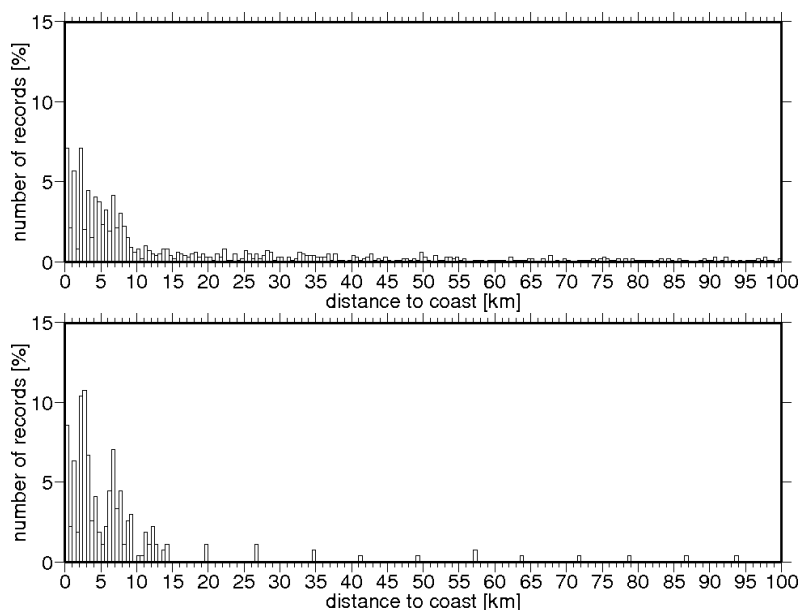


Figure F-03-2: Histogram of Envisat records rejected for the MWR wet tropospheric correction (top) and for the standard deviation of ranges (bottom)

22 Kilometres with R-GDR and RADS data respectively. The corresponding distances to the tide gauge are 31 and 53 Kilometres.

The time-series at each NP is compared to tide gauge sea level heights by analysing a set of parameters: (1) number of usable time-points, (2) correlation and Root Mean Square (RMS) difference of altimeter and tide gauge time series. The three parameters are shown in Fig. F-03-4 (y-axis) for the first NPs against the distance from the tide gauge (x-axis). The total Topex cycles are 72, the Envisat cycles are 11. As the location approaches the coast, the number of observations at each Topex NP decreases quicker for RADS than for RGDR data. In Genova the Topex data reduction reaches 85% and 60% of the 72 observations at 24 km to the coast for RADS and RGDR data (Fig. F-03-5). The RGDR data show the best agreement, with correlation higher than 0.8 and RMS differences lower than 60 mm at all the NPs. Similar results are found with RGDR1,-2 retracked data. For Envisat, as the NP location approaches the coast, the decrease in the number of observations is slower. Both RADS and SGDR data agree with tide gauge data, correlation is higher than 0.9 and RMS differences smaller than 40 mm. Near Genova the correlation has a minimum at a distance

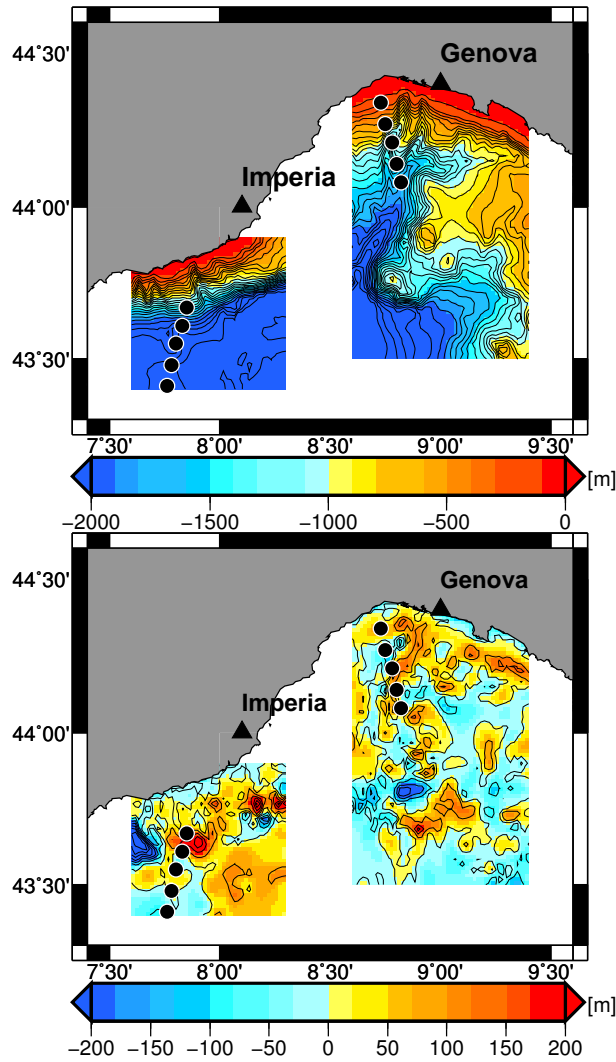


Figure F-03-3: Locations of Envisat (circle) and Topex (diamond) NPs near Genova and Imperia with local bathymetry (left) and difference between local and GEBCO (right)

of about 40 km from the tide gauge station. In Imperia the Topex data reduction is smaller than in Genova, 50% and 20% of the observations for RGDR and RADS at 22 km from the coast (Fig. F-03-6). The lower agreement between Topex and tide gauge is partially explained by the relative position of tracks and stations. Correlations are lower than 0.8 and standard deviation higher than 60 mm. Envisat has a better agreement (correlation bigger than 0.8, RMS smaller than 50 mm). The agreement is higher for Envisat than for Topex, results are similar for Envisat RADS and SGDR. Topex retracked data are more near to coast than standard Level 2 products. The sea-land transition is the most advantageous.

3.3 Re-tracking

Figure F-03-5 shows two examples of land contamination from the Envisat RA-2 altimeter. Plotted are along-track distance to coast (x-axis), gate number (y-axis) and waveform amplitude in FFT filter units (scale). Brown-like ocean waveforms are more near to land (5 km) in the sea-land transition (Genova) than in the land-sea transition (Imperia).

Table F-03-2: Minimum distance to coast for Genova and Imperia for Envisat (N1) and Topex/Poseidon (TP) at sea-land (s-l) and land-sea (l-s) transitions

Sat	Product	TG	Dcoast (km)	DistTG (km)	DistTRACK (km)	Type
N1	SGDR	GEN	6.4	17.9	6.1	s-l
N1	RADS	GEN	6.2	18.2	5.9	s-l
N1	SGDR	IMP	8.9	28.7	10.1	l-s
N1	RADS	IMP	20.3	33.6	24.2	l-s
TP	RGDR	GEN	15.5	17.7	18.2	l-s
TP	RADS	GEN	24.2	28.8	32.2	l-s
TP	RGDR	IMP	6.0	30.8	6.9	s-l
TP	RADS	IMP	22.4	53.4	30.7	s-l

The Envisat waveform data are retracked using the four retracker methods: OCOG, β_5 , Threshold and Improved Threshold retracker. The performance of the retracked data is assessed by analyzing: (1) the two standard deviations of the differences between SSHs calculated from both raw and retracked ranges and geoid heights, (2) the improvement percentages (IMP). A negative improvement factor indicates that retracking deteriorates the SSHs. Table F-03-2 gives the statistics of the performance of the four retrackers for latitudes between 43.3 and 44.3 degrees of cycle 59 track 801 near Genova, The total number of waveforms is 307. The statistics for SSHs obtained from the SGDR ocean-1 range is given for comparison. The noise of the raw data is generally reduced in the retracked data. The β_5 and Improved Threshold methods produce retracked SSHs with less noise than the ocean-1 SGDR data. The success rate, i.e. the percentage of waveforms that could be retracked, is 87% for the β_5 method and 100% for the other methods.

Using the retracked dataset more time samples are retained at each normal point and we approach more to the coast. The correlation of the altimeter and tide gauge time series is lower. Only values within 3σ from the mean are considered. Sea level anomalies from the Topex retracked data are significantly smaller than those from the Topex GDRs. This is seen in Fig. F-03-2 and in Fig. F-03-6. The distances to the coast of the nearest points depends on the different morphological coastal conditions in the areas. There is a slight evidence of larger differences between R-GDR and GDR towards larger distances from coast. The average difference between the retrackers 1 and 2 is small. In pass 044 of cycle 328 the difference between the retrackers varies from -0.13 to 0.062m. The largest variations in this pass over all cycles go from -0.395 to 2.031m. The differences between the retrackers are represented by a gaussian-like distribution with peak near to zero.

4. Conclusions

Most of the Envisat data elimination near to the coast is due to the checks on the wet tropospheric correction (8%) and on the standard deviation of the 18 Hz retracked ranges (4%). We therefore use the wet tropospheric model corrections from ECMWF to reduce the data rejection near coast. Applying standard selection criteria to both satellites, Envisat data perform better in coastal regions with up to 15% more 1 Hz data available in the last 5 km. Envisat provides more usable data near to the coast independently from the crossing-land direction. In general, sea-land transitions perform better than land-sea transitions, with both satellites providing usable data closer than 15 km to the coastline for 90% of all passes in the Mediterranean Sea. In land-sea direction, Envisat provides data for the last 7 km offshore, while no Topex data are available in that distance range. The agreement between corrected altimetry and in-situ sea level is higher for Envisat than for Topex data in both correlation

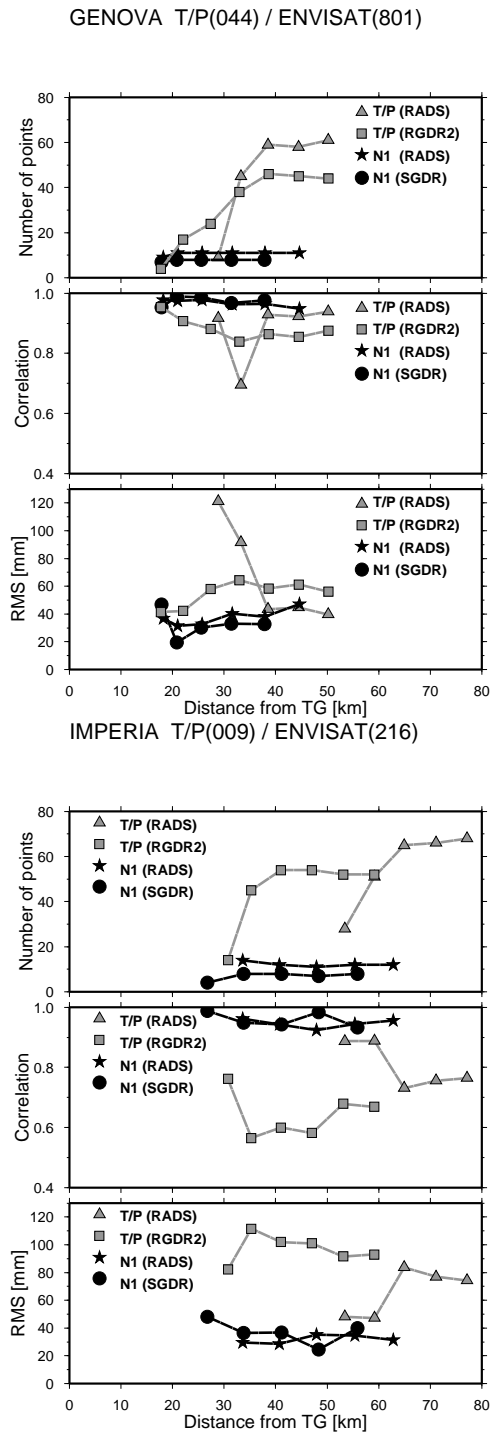


Figure F-03-4: Statistics of normal points near Genova (left) and Imperia (right).

and RMS differences. The noise of the 18 Hz ranges is reduced by retracking the Envisat data with empirical retracker methods. The improved threshold and the β_5 retracker are giving the best results.

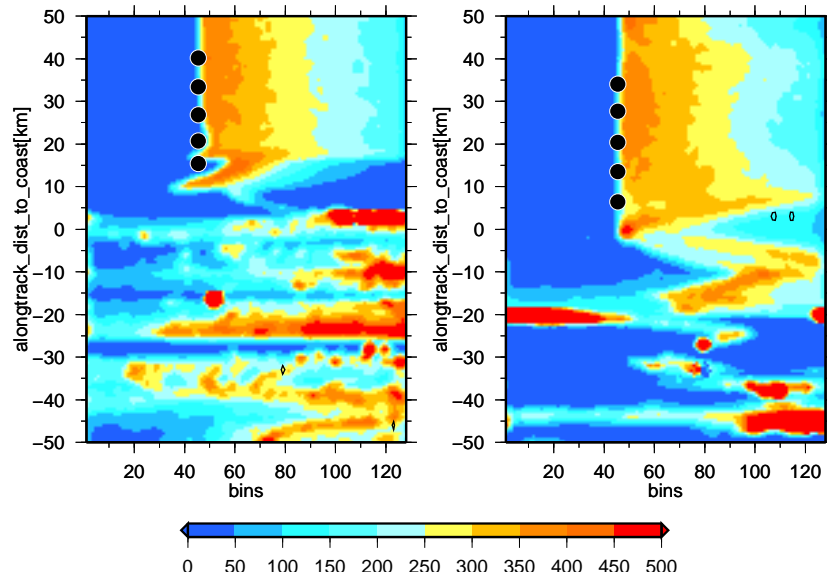


Figure F-03-5: Envisat waveforms at a sea-land (Genova, left) and a land-sea (Imperia, right) transition and Envisat 1 Hz NP (circles). Scale is waveform amplitude in FFT filter units

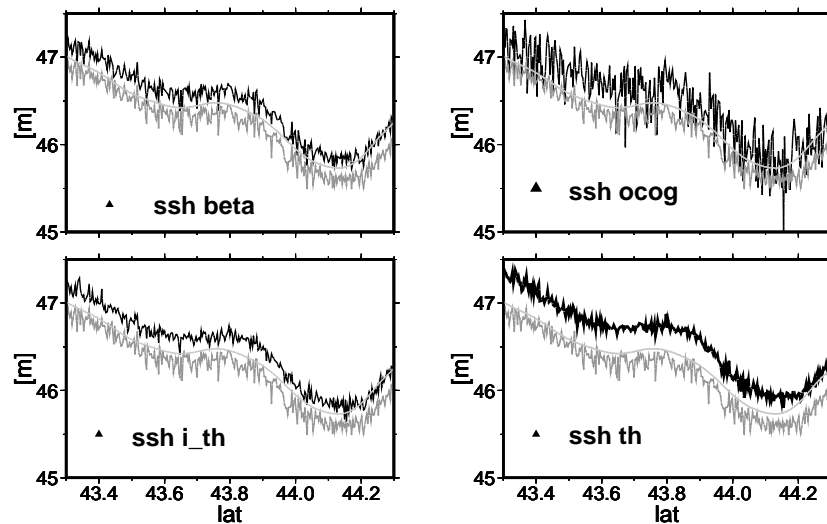


Figure F-03-6: SSH from beta-5, OCOG, Improved Threshold and Threshold retracker (dark) compared to GDR ocean (grey) SSH and EGM2008 (light grey) for Envisat cycle 59, pass 801 near Genova

References

- Anzenhofer, M, Shum C. K., Rentsh, M. (1999): Coastal altimetry and applications. In: Technical Report N. 464, Geodetic Science and Surveying, The Ohio State University Columbus, USA, pp. 1-40
- AVISO (2006). AVISO and PODAAC User Handbook, IGDR and GDR Jason Products, SMM-MU-M5-OP-13184-CN, 3.0, CNES
- Bouffard, J., S. Vignudelli, P. Cipollini, and Y. Menard (2008), Exploiting the potential of an improved multimission altimetric data set over the coastal ocean., *Geophys. Res. Lett.*, 35, L10601, doi:10.1029/2008GL033488
- CLS (2006). Envisat RA-2 /MWR Level 2 User Manual, Issue 1.2, ESA

- Davis, CH. (1995), Growth of the Greenland Ice Sheet: A Performance Assessment of Altimeter Retracking Algorithms. In: IEEE Transactions on Geoscience and Remote Sensing 33(5), pp. 1108-1116, 1995
- Deng, X., W. Featherstone, C. Hwang,, P.A.M Berry, (2002), Estimation of contamination of ERS-2 and Poseidon satellite radar altimetry close to the coasts of Australia. In: Marine Geodesy, 25, pp. 249-27,
- Deng., X., W. Featherstone (2006), A coastal retracking system for satellite radar altimeter waveforms: application of ERS-2 around Australia. Journal of Geophysical Research, 111
- Desportes, C., E. Obligis, L. Eymard, (2007), On the Wet Tropospheric Correction for Altimetry in Coastal Regions. In: IEEE Transactions on Geoscience and Remote Sensing
- Fenoglio-Marc, L., Groten E., Dietz C. (2004), Vertical Land Motion in the Mediterranean Sea from altimetry and tide gauge stations. Marine geodesy, 27, pp. 683701
- Fenoglio-Marc, L., S. Vignudelli, A. Humbert, P. Cipollini, M. Fehlau, M. Becker (2007), An assessment of satellite altimetry in proximity of the Mediterranean coastline. In: 3rd ENVISAT Symposium Proceedings, SP-636, ESA Publications Division, 2007
- Hwang, C., Guo JY, Deng XL, Hsu HY, Liu YT (2006), Coastal gravity anomalies from retracked Geosat/GM altimetry: improvement, limitation and the role of airborne gravity data. Journal of Geodesy, 80, pp. 204-216
- Martin, T. V., Zwally, H. J., Brenner, A. C., et al. (1983): Analysis and retracking of continental ice sheet radar altimeter waveforms,. J. Geophys. Res., 88, 1608-1616.
- Naejie M., E. Doornbos, L. Mathers, R. Scharroo, E. Schrama and P. Visser (2002), Radar Altimeter Database System: Exploitation and Extension, Final Rep. NUSP-2 02-06, Space Res. Organ. Neth., Utrecht, Netherlands
- Roblou, L., F. Lyard, M. Le Henaff, C. Maraldi (2007), X-track, a new processing tool for altimetry in coastal ocean. In:3rd ENVISAT Symposium Proceedings, SP-636, ESA Publications Division
- Vignudelli, S., P. Cipollini, L. Roblou, F. Lyard, G.P. Gasparini, G. Manzella, M. Astraldi, (2005), Improved satellite altimetry in coastal systems: case study of the Corsica Channel (Mediterranean Sea), Geophysical Research Letters, 32
- Wingham, D. J., Rapley, C.G., Griffiths H. (1986): New techniques in satellite tracking system. In Proceedings of IGARSS88 symposium, Zurich, 1339-1344.

6.4 A Study on the conformance of altimetry and in situ data near coast

F-04: Fenoglio-Marc L. , R. Weiss, S. Dinardo, M. Becker, A.Sudau, A Study on the conformance of altimetry and in situ surface data near coast, In Proceedings of the 20 Years of progress in radar altimetry symposium, ESA SP-710, ESA/ESTEC, 2012

Abstract The aim of this paper is the validation of sea surface heights and sea wave heights derived from altimeter data. A network of in-situ data from tide gauges, GNSS stations and offshore platforms in the German Bight is used. The altimeter sea surface heights from standard altimetry products (GDR) and from tide gauges show a good agreement at offshore locations, whereas the agreement is lower for coastal stations. The PISTACH coastal product data represent a significant improvement of the standard sea surface heights between 5 and 10 km from the coast. However, at less than 4 kilometers from the coast also the PISTACH data are too noisy. The comparison with in-situ wave heights with significant wave heights derived from CRYOSAT data in SAR mode using the SAMOSA SAR Echo Mode shows a good agreement for sea wave heights higher than 1 meter.

Keywords: coastal altimetry, in-situ validation

1. Introduction

Satellite altimetry in the coastal zone has the potential to yield a large amount of unique information for coastal management and long-term monitoring of coastal dynamics and sea level change. However, coastal areas are one of the major challenges for satellite altimetry due to deterioration of altimeter signals by land contamination. The improvement of altimeter data close to the coastline is a non-standard procedure that requires the use of dedicated re-tracking algorithms to process high rate waveform data and additional information on environmental corrections and coastline bathymetry. The goal is to provide improved coastal altimeter data for a better estimation of sea level variability. In the last years there has been considerable interest in addressing some of the long-term technical difficulties associated with retrieving valid measurements from satellite altimeters in coastal areas (Gommenginger et al., 2011). Developments of altimeter waveform retracking techniques, together with the now-established practice of giving users access to altimeter waveform data, has led to rapid progress in our understanding of the challenges posed by waveform shapes in the vicinity of land. A number of new and alternative methods of raw waveform retracking have been developed. The retracked data have been made available to the coastal altimeter community by the project PISTACH (CNES, 2010), (<http://www.pistach.fr>).

In this paper we validate sea level heights and significant wave heights from altimetry missions in the German Bight. In Section 2 we describe the data used. In Section 3 the validation of the altimetric products is made by comparison to in-situ data. In Section 4 we discuss our results and provide an outlook for future investigations.

2. Data and Methods

The network consists of two platforms offshore (FINO1 and FINO3, <http://www.fino3.de>) and of tide gauge (TG) stations on lighthouses, islands and on the continent (Figure F-04-1).

Several stations are equipped with continuously operating Global Navigation Satellite System (GNSS) receivers. Additional instruments measure sea waves and currents.

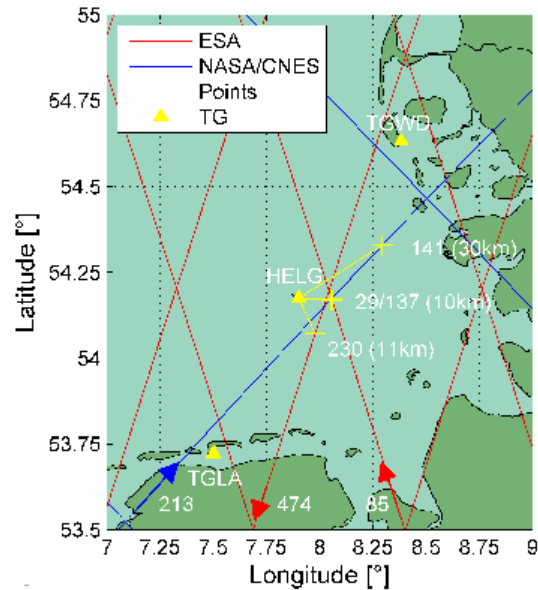


Figure F-04-1: The Jason-1 altimeter track 213 and the three tide gauge stations (yellow triangles) used in this study

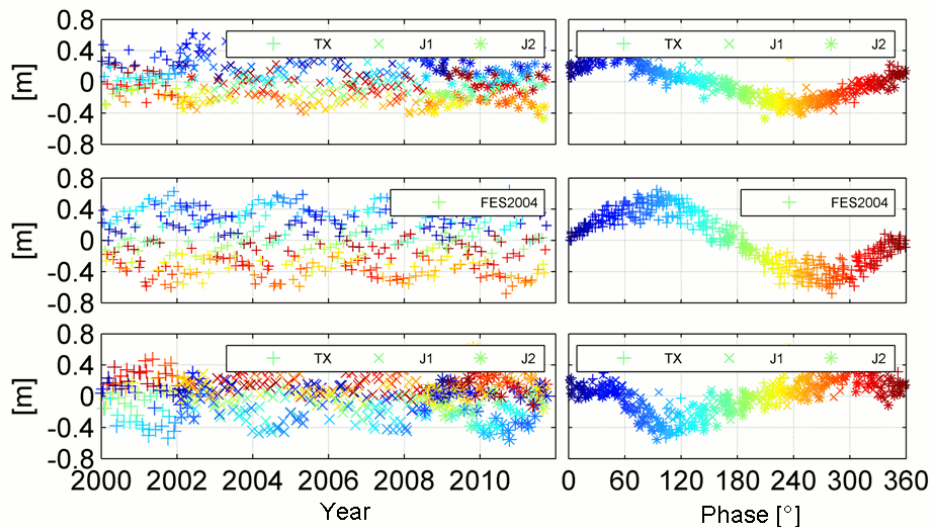


Figure F-04-2: Instantaneous SSH differences (altimetric minus tide gauge) at location 141 along J1 altimeter track 213 (top), difference of FES2004 ocean tide model at both locations (middle) and SSH differences with the FES2004 ocean tide correction applied (bottom)

We perform instantaneous comparisons of altimetric and tide gauge station sea level (Fenoglio-Marc et al., 2004) at the off-shore and coastal locations indicated in Figure F-04-1. The Helgoland tide gauge (HELG) is an off-shore location, the tide gauges of Langeoog (TGLA) and Wittdün (TGWD) are coastal locations. All the three sites are located within 10 kilometers from Pass 213 of the Jason-2 mission. Moreover the two stations of Hörnum (HOE2, Pass 94) and Pellworm (TGPE, Pass 213) have been considered (not shown here). High frequency tide gauge values (1 per minute) are made available by the Waterway and Shipping Administration (WSV) (Goffinet et al., 2011). The GNSS-stations HELG and HOE2

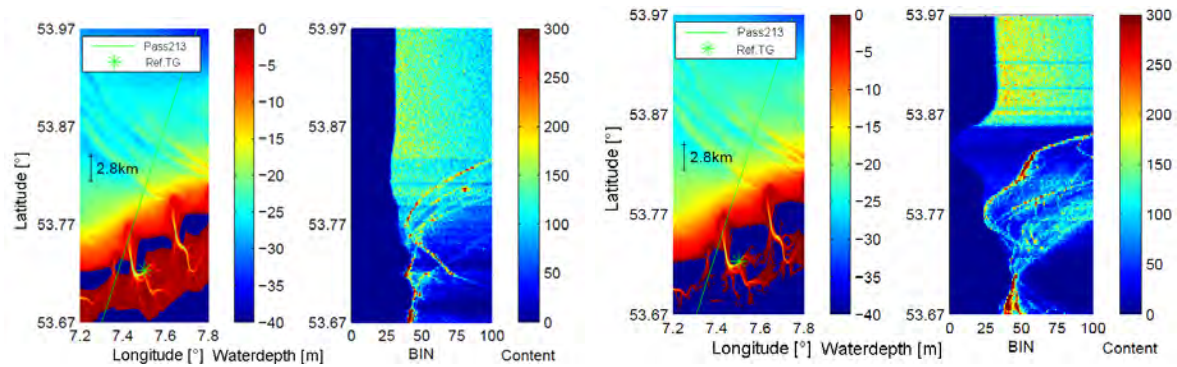


Figure F-04-3: Land/water coverage (left) and waveforms (right) at the Langeoog in-situ tide gauge during high water (cycle 40, left) and low water (cycle 50, right)

are EUREF-stations of BKG. The gauge datum height values were derived by GNSS and the mean value over 2010 is used. The processing includes 30 GNSS-sites and 10 IGS Frame sites as fiducial stations for IGS05 and ITRF2005 solutions. The tide gauge stations of TGWD and TGLA are not equipped with continuous GNSS.

For the comparison at the offshore location we consider multi-mission altimetry data of Envisat (2002-2012), Topex/Poseidon (1993-2005), Jason-1, -2 (2002-2009, 2008-2012) at 1Hz available via the Radar Altimetry Database System (RADS) (Naeije et al., 2008).

For the comparison at the coastal locations we use altimetry data of the Jason-2 data at 20 Hz from both the Geophysical Data Records (GRD) and the PISTACH database. The standard geophysical corrections have been applied to altimetry. For consistency with the tide gauge records the pole and ocean tide correction are not applied and the effect of atmospheric pressure is not accounted for. Environmental (wet and dry tropospheric from the ECMWF model, ionospheric from IRI2007, sea state bias) and geophysical corrections (solid earth and load tides) have been applied. To retain more data near the coast the correction from model has been chosen and most of the conservative flags were ignored, thus allowing the inclusion of data closer to land. The real water depth values result from a combination of bathymetry and water level observations of the nearest tide gauge. Bathymetry and water levels are related to the German datum network (NHN). We assume that the water level change is representative for an area around the tide gauge station.

Finally we also perform the instantaneous comparison of significant sea wave heights (SWH) derived from CRYOSAT measurements in SAR mode and measured by Acoustic Wave and Current Profiler (AWAC) instruments at the offshore platform FINO3.

3. Results

3.1 Validation of offshore sea surface heights

In open sea, for standard products (RADS, GDR) the comparison of instantaneous 1-Hz multi-mission altimetric and TG SSHs shows a good agreement. Interference from land is absent for passes near Helgoland, where the minimum spatial distance between the tide gauge and the Topex/Jason track 213 is around 10 kilometers. At that location (Point 137, Figure F-04-1) the comparison of SSHs gives a correlation higher than 0.9 and a standard deviation (STD) of 8.6 cm over the 2000-2011 period, the absolute SSHs difference is 5.7 centimeters

(Table F-04-1). Similar values for the statistics of the SSH differences are obtained for near-simultaneous comparison along the nearest ERS-2/Envisat track.

The SSH difference increases with the distance between the tide gauge and the altimetric location. As an example, along track 213 the STD increases to 20.3 cm for a distance of 30 kilometers from the Helgoland tide gauge (Table F-04-1). For a given altimeter location the SSH differences depend on the phase of the tide counted from its minimum (Figure F-04-2). The application of an ocean tide correction derived from a global ocean model does not reduce significantly the SSH difference (Table F-04-1, Figure F-04-2). The highest reduction is obtained with the tide model DUT2010. We derive an empirical correction.

3.2 Validation of coastal sea surface heights

The consistency between the altimeter and the tide gauge SSHs is lower at the coast. Here the correlation decreases and the STD of the differences increases. Moreover fewer altimetry data are available approaching the coast. In the PISTACH coastal data four retracers, called ICE1, ICE3, RED3, OC3, are applied simultaneously on each waveform. Distorsion in the waveforms are usual in the trailing edge when approaching the shorelines. In addition the amplitude of the tides are here large and as a consequence, the waveforms differ from cycle to cycle at a same location (Fig. F-04-3). The altimeter footprint is computed using the mean SWH over the pass. We expect the ICE3 and the RED3 retracers to perform better than the other two in coastal areas, because both ICE3 and RED3 retracers work selecting an analysis window centered on the main leading edge of the waveform and retracking parameters in this reduced window. Finally the RED3 applies a Maximum Likelihood Estimator to solve for 3 parameters (MLE3): range, amplitude and Sigma composite. An MLE3 retracking algorithm is also applied in the OCE3 algorithm on waveforms already filtered by Singular Value Decomposition Filtering (SVD). This should allow to reduce the multiplicative speckle noise on the waveform and thus to reduce the estimation noise for each parameter. However our results show that this retracker does not work correctly near coast.

The statistics of the comparison (correlation, standard deviation, number of points) between the station TGLA (land-sea) and the altimeter locations along Pass 213(20 Hz data) is given in Fig. F-04-4), where the three parameters are shown as function of the distance from land. Within 10 kilometers from coast the performance of the retracker differs. The OCE3 retracker performs poorly below 10 kilometers. The RED3 retracker provides SSHs that are in agreement with the SSH from tide gauge between 10 and 4 kilometers and its performance degrades for a distance to coast lower than 4 kilometers. The same conclusions are obtained considering a point along track at 10.5 Km from the Langeoog tide gauge station (Fig. F-04-5). OCE3 SSH are missing near coast. RED3 retracker gives the better agreement with in-situ tide gauge SSHs, see statistics in Figure F-04-4 and Table F-04-2).

3.3 Validation of Cryosat significant sea wave heights

Significant Wave Heights (SWH) at 20 Hz have been derived from CRYOSAT data in SAR mode using the SAMOSA SAR Echo Model (SAMOSA, 2013). Passes within 50 kilometers from the FINO3 platform have been considered. The nearest in time SWH measurement made at the FINO3 platform by the AWAC sensor has been compared to the CRYOSAT SWHs, if the difference in time is smaller than 30 minutes. Fig. F-04-7 shows both the SWHs at 20Hz and at 1Hz along the CRYOSAT pass and the corresponding FINO3 SWH, for an

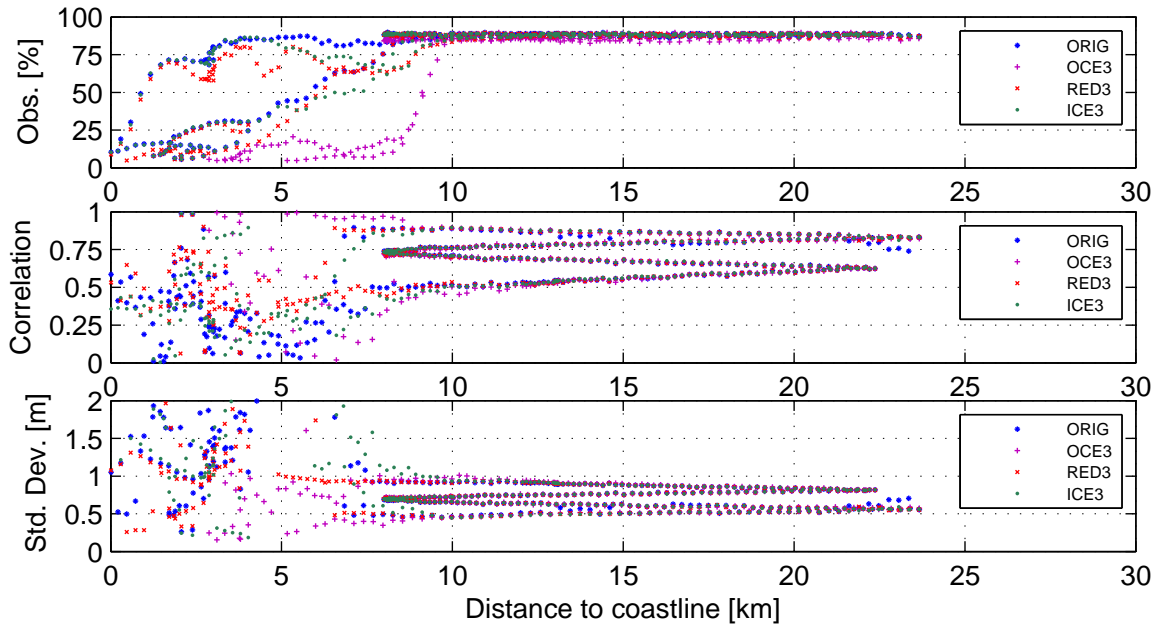


Figure F-04-4: Number of valid observations, correlation and standard deviation of SSH differences between tide gauge Langeoog and locations along Pass 213

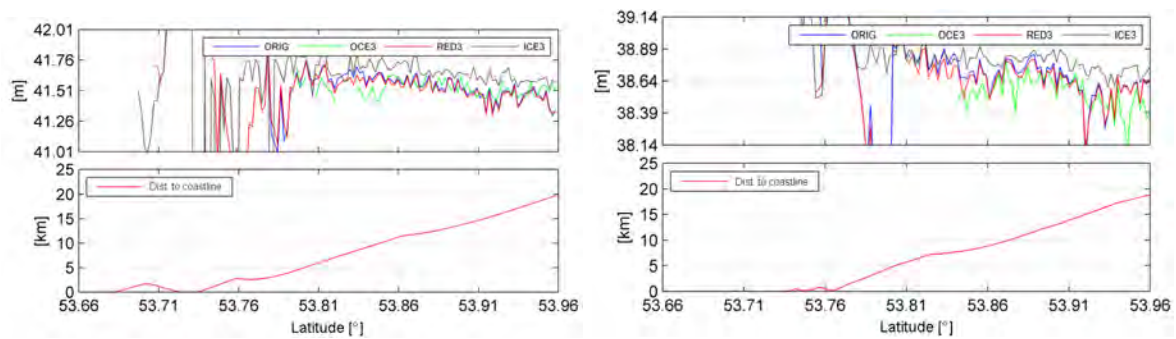


Figure F-04-5: SSH along pass 213 at high water (cycle 40, left) and low water (right)

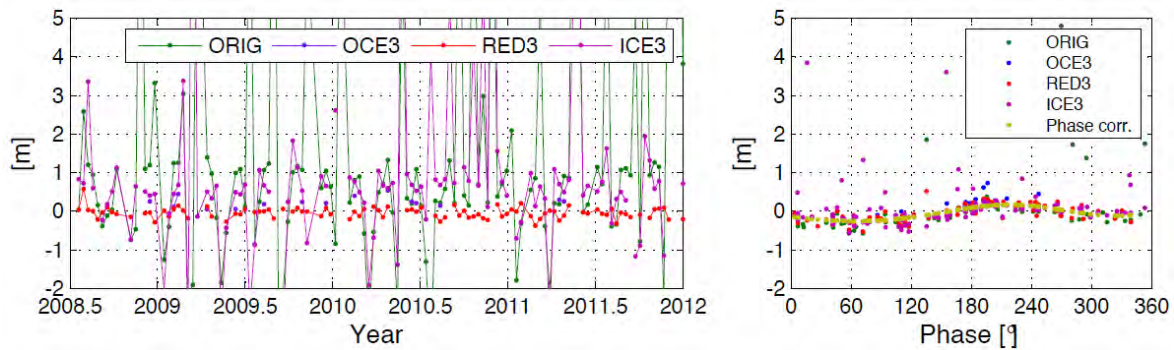


Figure F-04-6: SSH differences between altimeter point P355 of Pass 213 (J2) and TGLA

event in August, with differences of 2 minutes and 9 kilometers respectively between the SWHs measurements. A total of 21 passes between March and September 2011 are analysed. The correlation and the STD of the differences between the CryoSat 20 Hz SWH and the AWAC data are 0.82 and 0.42 m respectively (Table F-04-3). Differences between observed

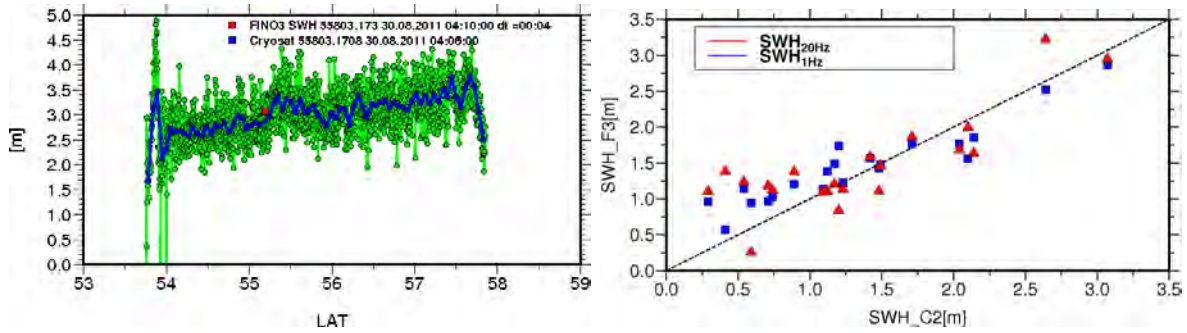


Figure F-04-7: in-situ validation of SWH: SWH from CryoSat-2 and from AWAC in August 2011 (left) and scatterplot of SWH from CryoSat-2 (SWH-C2) against AWAC (SWH-F3)

Table F-04-1: Statistics of ellipsoidal sea surface heights differences (al-tg) at tide gauge Helgoland and altimeter

Point	Corr	Dist	Mean	Std	Obs/max	Type
137	0.9974	10.0	0.057	0.086	409/430	s-l
141	0.9981	30.9	-0.099	0.203	389/430	s-l
132	0.9920	24.0	-0.136	0.178	382/430	l-s
137F04	0.9767	10.0	0.054	0.086	409/430	l-s
137D10	0.9841	10.0	0.059	0.069	409/430	l-s
137E11A	0.9711	10.0	0.054	0.094	409/430	l-s

Table F-04-2: In-situ validation at TGLA station: differences between tide gauge and and PISTACH SSH at Jason-2 point 355 (distance 10.5 km)

Point	Corr	Std	Obs/max
	(m)	(m)	(m)
GDR	0.49	3.54	106/118
OCE3	0.79	0.23	15/118
ICE3	0.53	1.90	96/118
RED3	0.97	0.19	85/118

Table F-04-3: In-situ validation at FINO-3 platform: differences between AWAC and CryoSat-2 SAR SWH (20 Hz)

	Mean	Std	RMS
	(m)	(m)	(m)
SWH-C2	1.45	0.66	1.59
SWH-FINO3	1.34	0.73	1.52
DIFF	0.12	0.42	0.43

(in-situ) and derived from Cryosat SWHs are higher for SWH smaller than 1 meter (Fig. F-04-7), suggesting a possible CryoSat's inadequacy to measure in SAR mode low SWHs. This inadequacy might be due to the current operated multi-looking scheme that averages always almost all possible looks whereas over quasi-flat/specular surfaces it would be more sensible to limit the multi-looking average only to the near nadir looks.

4. Conclusions

Our approach allows the absolute comparison of ellipsoidal sea surface heights from tide gauge and altimetry data. At offshore locations the comparison of SSHs shows a good agreement (correlation higher than 0.9, standard deviation of 8.6 cm over the 2000-2011 period) with standard altimeter data. The absolute SSHs difference is 5.7 centimeters. The consistency between the altimeter and the tide gauge SSHs decreases significantly at the coast. In coastal regions the retracker RED3 available in the PISTACH coastal product gives the best agreement with tide gauge sea level in terms of correlation, standard deviation of the differences and retained observations. For a point at 10 km from coast we obtain correlation 0.97, standard deviation 19 cm and 85% of the data are used. The Pistach data are a significant improvement of the level 2 GDR between 5 and 10 km from the coast. At less than 4 kilometers from the coast also PISTACH data are too noisy.

The comparison with in-situ wave heights with significant wave heights derived from CRYOSAT data in SAR mode using the SAMOSA SAR Echo Mode shows a good agreement for sea wave heights higher than 1 meter. The standard deviation of the difference is 0.4 metres.

References

- CNES (2010). Coastal and Hydrology Altimetry product (PISTACH), CLS-DOS-NT-10-246, SALP-MU-P-OP-16031-CN 01/00
- Fenoglio-Marc L., E. Groten and C. Dietz (2004). Vertical Land Motion in the Mediterranean Sea from altimetry and tide gauge stations, *Marine Geodesy* 27 (3-4), pp.683-701
- Goffinet P., J. Blasi, A. Sudau, and G. Liebsch (2011). National Report of Germany. GLOSS-Report, p.1
- Gommenginger C., P. Thibaut, L. Fenoglio-Marc, X. Deng and J. Gomez-Enri, Y. Gao. (2011). Retracking altimeter waveforms near the coasts, in *Book Coastal altimetry*, Eds S. Vignudelli, A. Kostianoy. P. Cipollini, J. Benveniste, Springer Verlag
- Naejie, M., Scharroo, R., Doornbos, E. and Schrama, E. (2008). GLOBal Altimetry Sea-level Service: GLASS, Final Report. NIVR/DEOS publ., NUSP-2 report GO 52320 DEO.
- SAMOSA (2013) Development of CryoSat SAR mode studies and applications over ocean, Coastal zones and Inland water(SAMOSA), <http://www.satoc.eu/projects/samosa>

6.5 Validation of CryoSat-2 data in SAR Mode in the German Bight Area

F-05: Fenoglio-Marc L., Dinardo, S., Scharroo R., Roland A., Lucas B., Weiss R., Detour Sikiric M., Becker M., Benveniste J., Validation of CryoSat-2 Observations in SAR Mode in the German Bight, In Proceedings of the Living Planet Symposium Edinburgh, SP-ESA, ESA Publications Division, 2013

Abstract

The scope of this study is a regional analysis and inter-calibration exercise of the CryoSat-2 SAR altimeter observations against in-situ data and model results. Open sea altimeter data, located at distances larger than 10 kilometres from the coast are considered. Data in SAR mode are processed to produce both pseudo pulse-limited (PLRM) and Delay-Doppler processed SAR waveform data. The first are provided via the RADS database, the second by the EOP-SER Altimetry Team at ESRIN, which re-tracks the Delay-Doppler processed SAR waveform data using the SAMOSA re-tracker. The validated parameters are the sea surface height above the ellipsoid (SSH), the significant sea wave height (SWH) and the wind speed. The time interval spans the two years 2011-2012.

The in-situ SSH, SWH and wind data are from a network of tide gauge stations, GNSS stations and offshore platforms in the German Bight. Two regional wave models are used: the Wave Watch III model run in the North-Eastern Atlantic (*WW3-ATNE*) and the local LSM wave model of the Deutsche Wetterdienst (DWD), which is operationally run at the Federal Maritime and Hydrographic Agency (BSH). The two corresponding wind models ECMWF and COSMO-EU are considered.

The cross-validation analysis shows the consistency of PLRM and the SAR data, without significant bias neither in sea surface or sea wave heights or wind speed. The SAR data are more precise and have less noise than the PLRM values, as expected.

The in-situ comparison at the stations FINO-3 and Helgoland show a good consistency with no bias of SSH and SWH and a higher agreement with SAR than with PLRM data.

The wind forecast product of ECMWF agrees better than the COSMO-EU wind fields to the altimeter product. Conversely, the SWH of the wave model WW3-ATNE is less consistent than the LSM wave model.

Keywords: sea level change, altimetry, tide gauge

1. Introduction

Unlike previous altimetric missions CryoSat-2 has a Synthetic Aperture Radar (SAR) mode which should allow a higher resolution and improved altimeter derived parameters in the coastal zone. The SAR mode of CryoSat-2 is expected to provide Sea Surface Height (SSH), Significant Wave Height (SWH) and wind speed at 10 meter height (U10) with improved precision and resolution compared to the conventional pulse-limited altimeter product (LRM). The SAR technique is however rather new, therefore validation with in-situ data and cross-calibration with standard altimeter data is necessary for the new data. A comparison with high-resolution regional models is also needed to understand limits of models and new challenges for altimetry.

The CryoSat-2 SAR mode offers two types of products for the same Full Bit Rate (FBR) acquisition. The standard procedure consists in the transformation of FBR data, also called L1a data, in multi-looked Delay-Doppler (aka SAR) processed waveform data (L1b data). The L1b waveforms are subsequently retracked, analogously to pulse-limited altimetry, in order to derive the geophysical products (L2 data). Alternatively, FBR data can be still processed without exploiting the synthetic aperture concept and in this case they are referred as Pseudo Low Resolution Mode (PLRM). The SAR mode of CryoSat-2 is expected to provide Sea Surface Height (SSH) and Significant Wave Height (SWH) with improved accuracy and resolution compared to the pulse-limited altimeter product (LRM).

In the North Sea acquisition are performed in SAR mode. In this paper we validate in the German Bight in open sea the derived SSH and SWH. In Section 2 we describe the data used. In Section 3 the validation of the altimetric products is made by comparison to in-situ and to model data. In Section 4 we discuss our results and provide an outlook for future investigations.

2. Data and method overview

The following approach is adopted. Pseudo pulse-limited (PLRM) altimetric observations (PLRM SSH, SWH, U10), processed as from CryoSat-2 FBR (Full Bit Rate, L1a) data provided via the RADS database, are cross-compared against the altimetric observations (SAR SSH, SWH, U10) derived after re-tracking the CryoSat-2 SAR Echo Waveforms to estimate possible biases occurring in SAR mode with respect to the PLRM Mode and tune up the SAR re-tracking scheme. We perform also an absolute in-situ calibration/validation of the altimetry range by direct over-flight at two dedicated GNSS sites located offshore: Helgoland and FINO-3. The absolute range bias is derived in this case from the differences of the sea level heights recorded at the tide gauge/GNSS station and the CryoSat-2 SSH. We also perform the in-situ instantaneous comparison of SWH as derived from CryoSat-2 measurements and as measured by Acoustic Wave and Current Profiler (AWAC) instruments at the offshore platform FINO3.

The ESRIN EOP-SER Altimetry Team (Dinardo et al., 2013) has provided the L1b Delay-Doppler (SAR) Processing and the L2 SAR Re-tracking. The data have been Delay-Doppler (SAR) processed as from the Full Bit Rate (FBR) Level until the L1b level and subsequently re-tracked by using the SAMOSA3's SAR (<http://www.satoc.eu/projects/samosa>) Echo Model (Maquardt, 1963) and a fitting scheme based on the bounded Levenberg-Marquardt Least-Squares Estimation Algorithm (LEVMAR-LSE) (Lourakis, 2004). The SSH, SWH, U10 values at 20 and 1 Hz have been computed. Instead, the CryoSat-2 PLRM altimeter data at 1-Hz, derived again from CryoSat-2 FBR SAR data (Scharroo, 2013), have been provided via the Radar Altimetry Database System (RADS).

The SWHs provided from ESRIN have been computed using a Range PTR dimensionless width value of 0.513 (same value used in RADS for PLRM PTR dimensionless width). Errors in the SWH related to the analytical, and not numerical, modelisation of the echo, as done by ESA/ESRIN, are corrected a posteriori using a calibration table.

The SWH in SAR mode having a 1 Hz standard deviation σ_{SWH} larger than 40 cm have been filtered out. As in the case of SSH, we assume those outliers as due to ships, offshore platforms, rain events, etc.

In order to derive the wind speed in SAR mode, at L1b stage the SAR received waveforms have been calibrated in power for automatic gain correction (AGC) values, AGC setting value and PTR power drift. Wind speed has been derived from retracked received power parameter (Pu) by performing the following steps: - inverting the SAR radar equation (the radar equation encompassing now the SAR footprint and not more the pulse-limited footprint) to revert Pu in sigma nought. - aligning the CryoSat-2 sigma nought to Envisat sigma nought, applying a -3.45 dB bias (sigma nought mission inter-calibration) - using the Envisat wind speed model (Abdalla, 2007) to revert sigma nought in wind speed at 10 meter height. SAR Wind Speed measurements are available at both 1 and 20 Hz. PLRM Wind Speed measurements are determined in a similar way and are available at 1-Hz only.

The in-situ network consists of two platforms offshore (FINO1 and FINO3, <http://www.fino3.de>) and of tide gauge (TG) stations on lighthouses, islands and on the continent. Several stations are equipped with continuously operating Global Navigation Satellite System (GNSS) receivers. Additional instruments measure sea waves and currents. Here the validation is carried out at the offshore platform FINO3 and at GNSS site Helgoland (Figure 1). The Waterway and Shipping Administration (WSV) makes high frequency tide gauge values (1 per minute) available (Goffinet et al., 2011). The gauge datum height values were derived by GNSS and the mean value over 2010 is used. The processing includes 30 GNSS-sites and 10 IGS Frame sites as fiducial stations for IGS05 and ITRF2005 solutions. Significant wave height is measured by an Acoustic Wave and Current Profiler (AWAC) instrument at the FINO3 platform and made available by the Federal Maritime and Hydrographic Agency (BSH) with hourly sampling.

For the comparison between PLRM and SAR sea level data, the uncorrected sea level has been defined for both datasets as: orbit minus range measurement plus a bias (0.247 m in PLRM and 0.715 m in SAR), to refer the data to the TOPEX/Poseidon reference level. To analyse open ocean data only, we select the SAR points with distance from coast larger than 10 km (Figure 1) and the corresponding PLRM points with time difference within 0.45 seconds. SSH data in SAR mode with 1 Hz standard deviation σ_{SSH} larger than 4 cm have been filtered out. As in the case of SWH we assume that those high values are caused by disturbance to the measurement caused by ships, offshore platforms, rain events, etc. Sea Level Anomalies (SLA) above the reference mean sea level surface have been computed in both datasets by applying to the uncorrected sea level height the corrections available in the SAR products and same Mean Sea Surface Model (MSS). In this way we use the same corrections for PLRM and SAR sea level measurements.

We perform SWH instantaneous in-situ comparison at FINO3, where wave heights are measured by an Acoustic Wave and Current Profiler (AWAC) instrument and SSH instantaneous in-situ comparison at the Helgoland tide gauge station. To analyse the consistency of instantaneous sea level heights with the tide gauge records, the ocean part of the pole tide and the ocean tide corrections have not been applied, the effect of atmospheric pressure has not been accounted for (Fenoglio-Marc et al., 2004, 2012). The sea state bias has not been considered either for both cases since it is not available for CryoSat-2 SAR data at this stage. Environmental (wet and dry tropospheric from the ECMWF model, ionospheric from IRI2007) and geophysical corrections (solid earth, load tides and the earth part of pole tide) have been applied. To retain more data near the coast most of the conservative flags were ignored in RADS, thus allowing the inclusion of data closer to land. As the solid earth tide correction does not include the zero frequency term, i.e. the permanent tide, the resulting altimeter heights are referred to a mean tide system. We convert the in-situ ellipsoidal height from the tide-free to the mean-tide system by adding:

Table F-05-1: Characteristics of models used for Regional Validation of SWH in open ocean

	WAM-DWD	WW3-IOWAGA
Wave Model Name	LSM	WW3-ATNE
Wind in wave model	COSMO-EU	ECMWF
Spatial resolution	0.1 x 0.17	0.1 x 0.17
Spectral res. (frequencies, directions)	25, 25	31, 24
Forecast range (h)	78	144
Numerics	WAM	WW3
nesting global model	in GSM	NO
2-way coupling with global	NO	YES, WW3
Assimilation of altimetric SWH in wave model	sea state GSM	NO
Assimilation of altimetric U10 in wind model	NO	NO

$$\Delta h_{\text{mean}} = 0.099 h_2 (1 - 3 \sin^2 \varphi) \quad [\text{m}] \quad (\text{F-05-1})$$

with φ latitude and h_2 (0.61) Love number describing the vertical displacement of the crust relative to the ellipsoid.

The validation of the SWH derived from SAR and PLRM is made by using two regional wave model datasets. The first dataset is the Wave Watch III (Tolman, 1991) third generation wave model for the North-Eastern Atlantic (WW3-ATNE, <http://wwz.ifremer.fr/iowaga>), the second is the Local Wave Model (LSM) of the German Weather Office (Deutscher Wetterdienst, DWD) for the North Sea and Baltic Sea, which is operationally run at the Federal Maritime and Hydrographic Agency (BSH). The resolution of the LSM is 0.1 x 0.17 deg, whereas the WW3-ATNE nested grid has resolution 0.17 deg. Beside the numeric the main difference in the wave models is the physical description of the wind input, which is COSMO-EU for DWD and ECMWF for WW3-ATNE, and dissipation. Table F-05-1 gives the main characteristics of the two models. The 1st wave model dataset (hereafter WW3-ATNE) is generated within the IOWAGA project (e.g. Rasclé et al., 2012, <http://wwz.ifremer.fr/iowaga>) and uses the WW3 model, which was setup for the whole globe and use a two way nesting techniques (Tolman, 2010) to focus on the north east Atlantic with resolution of 1/6 deg. The numerical grid of this regional hindcast spans from -30 deg to 30 deg in longitude and 25 to 70 in latitude. It is driven by ECMWF winds. The 2nd wave model dataset (hereafter LSM) is the regional sea wave model LSM (Behrens and Schrader, 1994) for the North Sea and Baltic Sea. It is part of the numerical weather prediction system of DWD and is used by BSH. It predicts the significant wave height, frequency and direction of the wind sea and swell. It is driven by the COSMO-EU winds and by the global model GSM at the open boundaries of the LSM model, which are the English channel and the Northern and Western boundaries off the North Sea. Since 2008 near-real time SWH altimetry data from ERS-2, Jason-1,2 and Envisat are assimilated in the GSM model. This additional data, even if sparse, is expected to improve the first guess of the model (Bruns personal communication). The numerical scheme is based on the WAM Model (Günther et al. 1999). Both forcing wind fields do not assimilate altimeter data. Both models solve the Wave Action Equation (e.g. Komen et al., 1994) using different numerical technique. WW3 utilizes higher order propagation schemes, e.g. Ultimate Quickest (Leonard et al., 1991) whereas the WAM uses 1st order schemes. The physical representation of the sources and sinks differs as well, especially with respect to the representation of the wave breaking dissipation function that has a nonlinear term based on spectral saturation term (e.g. Ardhuin et al. 2009). It was shown by Ardhuin et al. (2010) that based on the newly defined spectral balance the wave model results could be improved globally in contrast to the coming physics as e.g. used in the WAM model.

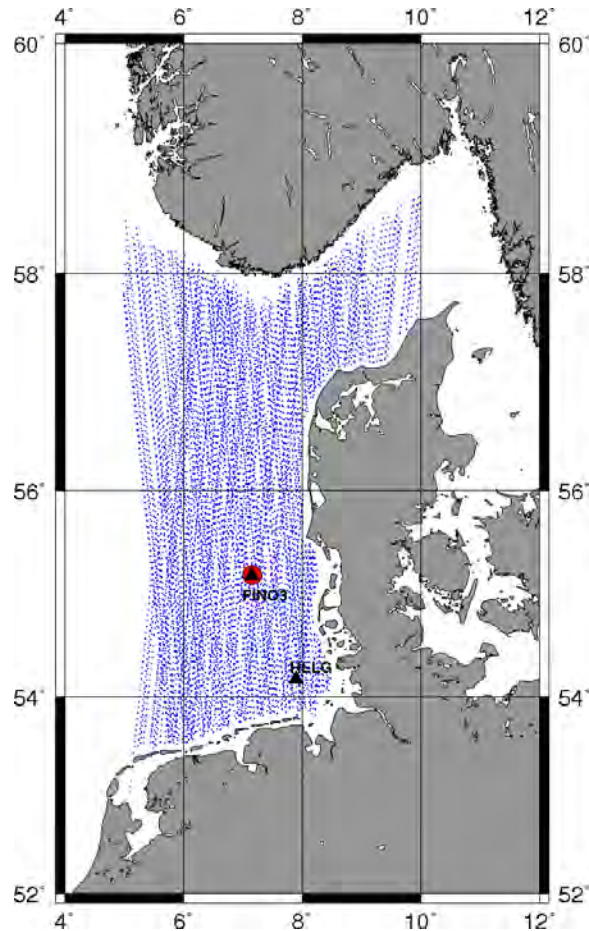


Figure F-05-1: Precision of 1 Hz Sea Surface Height (left) and SWH (right) from open sea SAR and PLRM in the German Bight

3 RESULTS

3.1 Cross-Validation of SAR and PLRM CryoSat-2 SSH, SWH and wind speed U10

Fig. F-05-2.a shows the performance curves of 1 Hz SSH (1 Hz SSH standard deviation vs. SWH). The SAR measurements have a higher precision than PLRM. At a SWH of 2 meters, the precision is 0.89 cm in SAR and 2.3 cm in PLRM. Similarly, Fig. F-05-2.b shows the performance curve of 1 Hz SWH (1 Hz SWH standard deviation vs. SWH). At a SWH of 2 meters, the precision of 1 Hz SWH is 6.8 cm in SAR and 16.9 cm in PLRM. For sigma nought at a SWH of 2 meters, the precision of 1 Hz sigma nought is 0.07 dB in SAR and 0.31 dB in PLRM (Fig. F-05-3.a). For wind speed at a SWH of 2 meters, the precision of SAR 1 Hz wind speed is 7 cm/s and 25 cm/sec in PLRM (Fig. F-05-3.b).

The statistical parameters used for the comparison of SSH, SLA and SWH are mean and standard deviation (std) (of model, observation data and of their differences), the correlation (cor), the slope of the regression line through the origin and the scatter index (SI, defined as the standard deviation of the data with respect to the best-fit line, divided by the mean observed value). We focus on the slope, which indicates the presence of biases and the scatter index that gives indications about typical scatter around this bias.

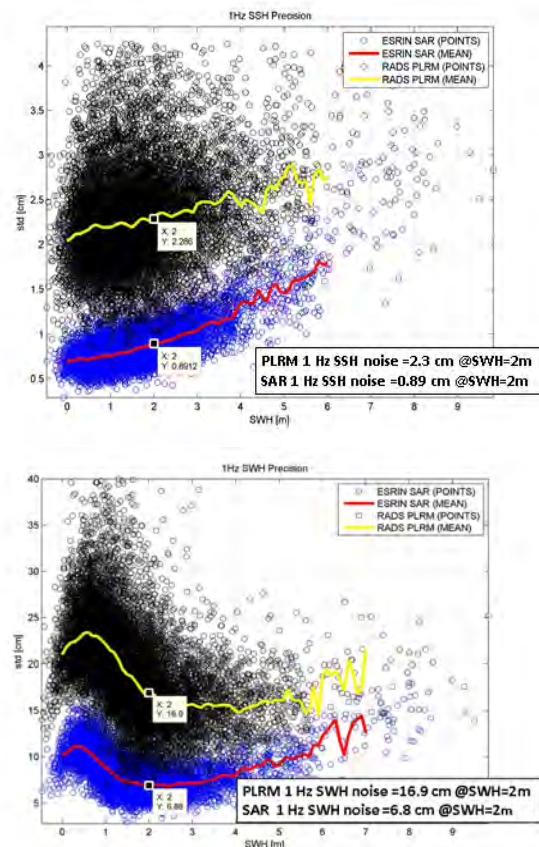


Figure F-05-2: Precision of 1 Hz Sea Surface Height (left) and SWH (right) from open sea SAR and PLRM in the German Bight

The SAR and PLRM SWH have a mean difference of 7 cm and standard deviation of the differences of 30 cm (Fig. F-05-4). Their general agreement is good (correlation coefficient and slope 0.97, SI 0.18, Tab. F-05-2). The agreement between the PLRM and the SAR uncorrected SSH is very good over the region (correlation coefficient 0.99, slope 1.003, SI 0.001, standard deviation of differences 6 cm, Tab. F-05-3). Similarly, PLRM SLA and SAR SLAs obtained from the uncorrected SSHs as described in Section 2 are in good agreement (correlation 0.96, slope 0.93, SI 0.7, mean and standard deviation of differences 1 and 4 cm respectively, Tab. F-05-3). The SAR and PLRM wind speed U10 have a mean difference of 4 cm/s and standard deviation of the differences of 0.37 m/s (Fig. F-05-4, Tab. F-05-4). Their general agreement is good (correlation coefficient and slope 0.99, SI 0.05). Tab. F-05-1 shows the regional statistics for the comparison with modeled SWH data. The SWHs of the WW3-ATNE model have the lowest average and standard deviation values. The slopes in Fig. F-05-6 indicates an underestimation of the model with respect to altimetry, especially SWH above 4.5 meters are overestimated in SAR. The general agreement between observations and model is lower than the agreement between SAR and PLRM, as discussed previously. There is a slightly better agreement of LSM with SAR (standard deviation of differences 0.32, SI 0.20) than with PLRM (standard deviation of differences 0.35, SI 0.22).

3.2 Validation of SAR and PLRM CryoSat-2 SWH and U10 against models

Tab. F-05-2 shows the regional statistics of the SWH data and of their differences with the modeled SWH data. Both PLRM and SAR altimeter data are in better agreement with LSM

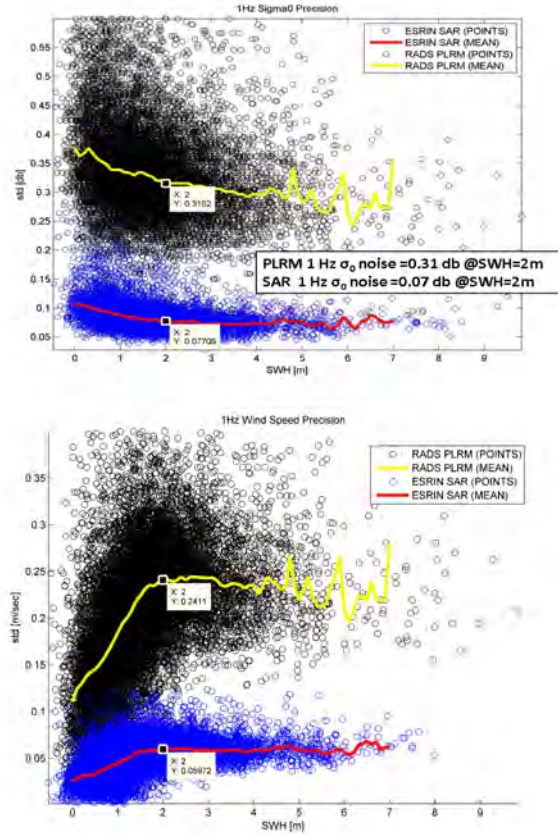


Figure F-05-3: Precision of 1 Hz sigma nought (left) and wind speed (right) from open sea SAR and PLRM in the German Bight

than with WW3-ATNE wave heights (Fig. F-05-6) The SWHs of the WW3-ATNE model have the lowest average and standard deviation. The slopes indicate an underestimation of the model WW3-ATNE with respect to both the LSM model and to altimetry. Especially SWH above 4.5 meters are overestimated in SAR. The general agreement between observations and model is lower than the agreement between SAR and PLRM, as discussed previously. The agreement between SAR and LSM is higher (standard deviation of differences 0.32, SI 0.20) than between SAR and PLRM (standard deviation of differences 0.35, SI 0.22). Both PLRM and SAR altimeter data are in better agreement with ECMWF than with COSMO-EU wind speed (Tab. F-05-4, Fig. F-05-7) The ECMWF wind speed model data over-estimate the COSMO-EU wind speed for high wind speeds and under-estimate them for low wind speed (Fig. F-05-5.b).

Table F-05-2: Statistics of 1Hz open sea SWHs (m)

	mean	std	rms	cor	slope	SI
WW3-ATNE	1.50	0.96	1.78			
LSM	1.60	1.06	1.92			
PLRM	1.69	1.12	1.82			
SAR	1.73	1.11	2.06			
PLRM - LSM	0.07	0.35	0.36	0.947	0.98	0.22
PLRM - WW3	0.11	0.39	0.40	0.938	0.81	0.20
SAR - LSM	0.13	0.32	0.35	0.957	1.01	0.20
SAR - WW3	0.17	0.37	0.41	0.948	0.80	0.17
SAR - PLRM	0.07	0.29	0.29	0.969	0.97	0.17

Table F-05-3: Statistics of 1Hz open sea uncorrected SSH and fully-corrected SLA (m)

	mean	std	rms	cor	slope	SI
SSH PLRM	37.9	0.95	37.9			
SSH SAR	37.9	0.95	37.9			
SSH SAR-PLRM	0.01	0.06	0.06	0.998	1.004	0.002
SLA PLRM	-0.078	0.21	0.22			
SLA SAR	-0.068	0.20	0.21			
SLA SAR-PLRM	0.01	0.06	0.06	0.96	0.93	-0.7

Table F-05-4: Statistics of 1Hz open sea U10 (m/s)

	mean	std	rms	cor	slope	SI
PLRM	7.61	3.49	8.37			
SAR	7.70	3.45	8.43			
COSMOEU	8.11	4.07	9.07			
ECMWF	7.28	3.54	8.09			
COSMO-EU - PLRM	0.50	1.6	1.7	0.92	0.79	0.17
ECMWF-PLRM	0.55	1.26	1.37	0.94	0.94	0.16
COSMO-EU-SAR	0.47	1.61	1.67	0.92	0.79	0.17
ECMWF-SAR	0.55	1.26	1.38	0.93	0.93	0.16
COSMO-EU-ECMWF	0.11	1.59	1.59	0.93	1.08	0.20
PLRM-SAR	0.04	0.37	0.37	0.99	0.99	0.05

Table F-05-5: SWH in-situ validation at FINO3 : CryoSat-2 and in-situ AWAC measurements (53 pt)

	mean	std	rms	cor	slope	SI
PLRM	1.55	1.01	1.85			
SAR	1.62	0.98	1.89			
FINO3	1.57	0.89	1.80			
PLRM-FIN3	0.02	0.34	0.33	0.945	1.07	0.21
SAR-FIN3	0.005	0.26	0.26	0.966	1.06	0.16
SAR-PLRM	0.07	0.25	0.26	0.970	0.94	0.16

Table F-05-6: SSH In-situ validation in Helgoland: Cryosat-2 and tide gauge and GPS, comparison in mean tide system

	mean	std	rms	cor	slope	SI
PLRM	39.24	0.87	39.25			
SAR	39.24	0.93	39.25			
HELG	39.25	0.95	39.26			
PLRM-HELG	0.002	0.21	0.21	0.98	0.95	0.005
SAR-HELG	-0.023	0.20	0.20	0.98	0.97	0.005

3.3 Validation of altimetry-derived SWH and SSH with in-situ data

Only passes within 50 km (lag distance) from the FINO3 platform have been considered. The nearest in time SWH AWAC measurement at the FINO3 platform is compared to the CryoSat-2 SWHs if the difference in time is smaller than 30 minutes (lag time). This results in a total of 53 passes between March 2011 and December 2012. The SWH differences are analysed. The scatterplot in Fig. F-05-8) shows altimeter versus the FINO3 AWAC SWH in-situ measurements. The PLRM and SAR SWH are consistent (bias 7 cm, standard deviation of differences 25 cm, correlation 0.97, Tab. F-05-5). The best agreement with in-situ data is realized by the SAR data (bias 0.5 cm, std 26 cm, correlation 0.97). The altimeter-derived SWHs overestimate the FINO3 in-situ measurements. With respect to previous results (Fenoglio-Marc et al. 2013) the agreement for SWH smaller than 1 meter has improved.

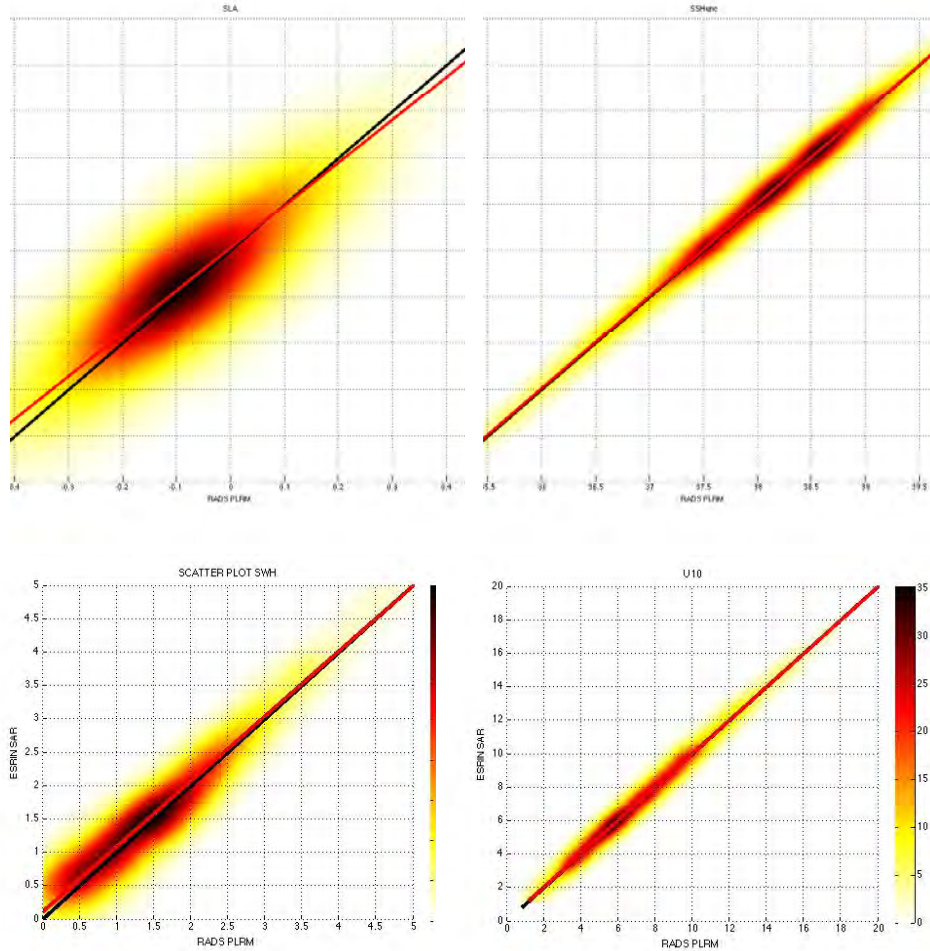


Figure F-05-4: Cross-validation of altimeter data: Scatterplot of sea level anomaly (SLA), SSH (m), SWH (m) and wind-speed from open sea altimeter data

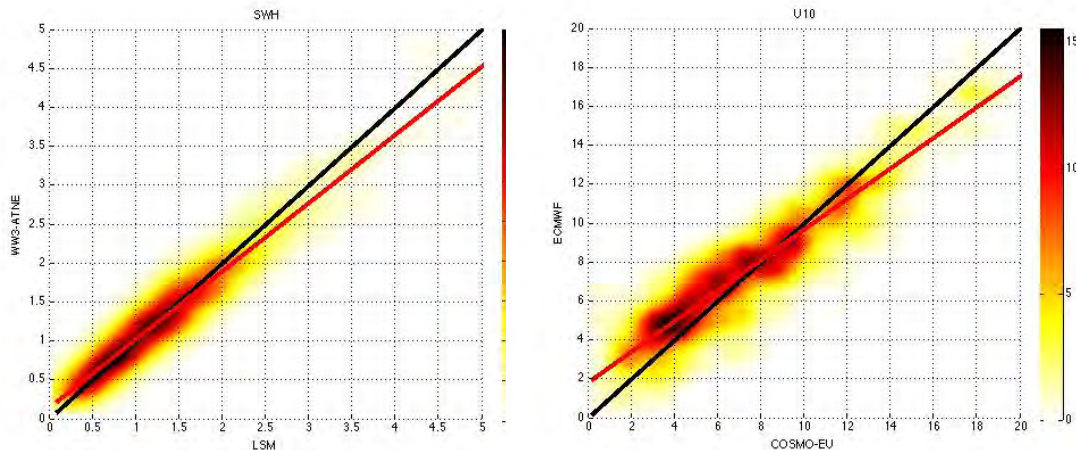


Figure F-05-5: Cross-validation of model data: Scatterplot of SWH from LSM versus WW3-ATNE (left) and of U10 from the COSMO-EU versus ECMWF (right)

The scatterplot in Fig. F-05-9) shows altimeter versus the Helgoland SSH in-situ measurements. The PLRM and SAR 1Hz SSH are consistent. The agreement between the 1Hz instantaneous SAR SSH and the SSH obtained from tide gauge and GPS data is good (mean bias 2 cm and std of the differences 20 cm, correlation 0.98, Tab. F-05-6). The best agreement

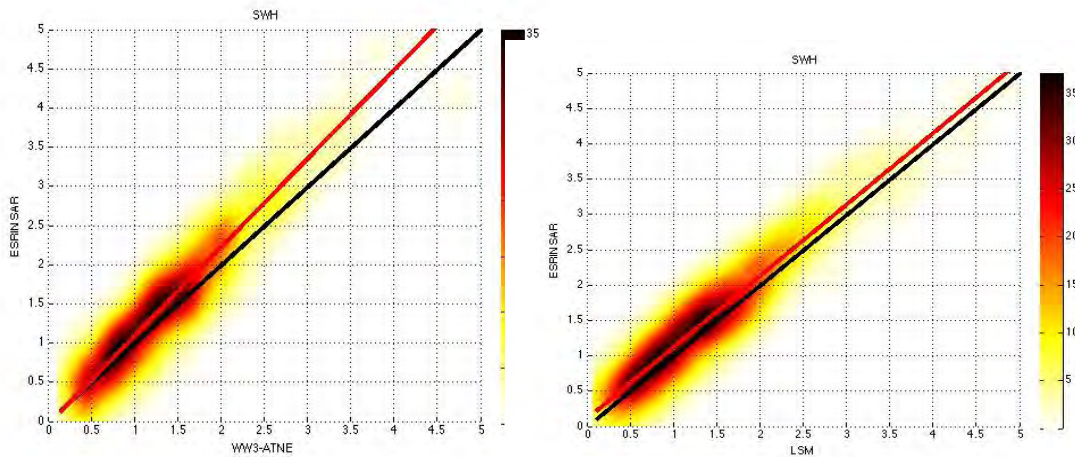


Figure F-05-6: Cross-validation of altimeter and model data : Scatterplot of SWH from altimeter data versus WW3-ATNE model (top) and LSM (bottom). Colour bars give data density.

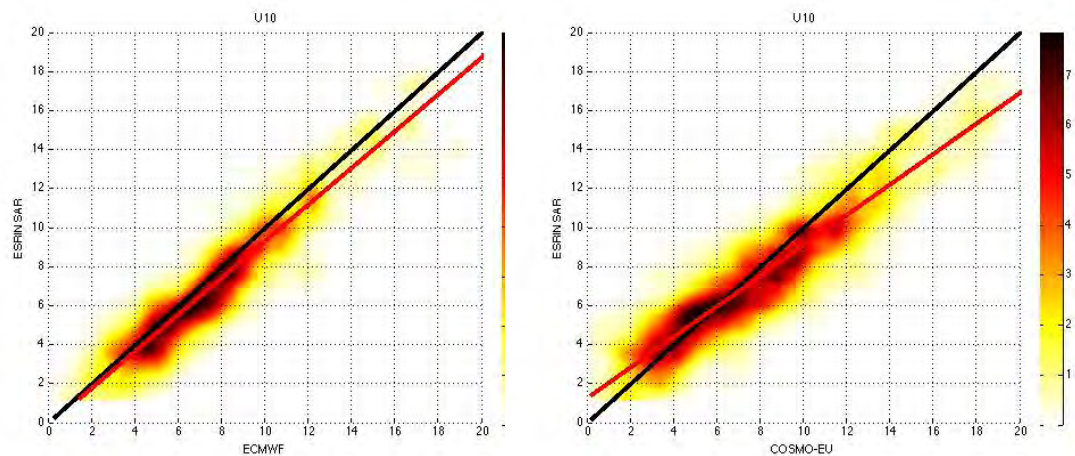


Figure F-05-7: Scatterplot of U10 from SAR versus COSMO-EU (middle) and ECMWF (bottom). Colour bars give data density

corresponds to SAR data in FINO3. Application of the sea state bias correction is expected to reduce the differences between tide gauge and altimetric results.

Altimeter and in-situ instantaneous sea surface height above the reference ellipsoid measured at the FINO3 platform do not have a significant bias. Figure F-05-10 shows the along-track SSH. The outliers present in the SAR/SSH measurement, and not in the PLRM/SSH, could be due a cargo ships, frequently sailing in the German Bight, which are detectable in the High Resolution SAR mode but undetectable in Pulse-Limited Low Resolution Mode. Figure F-05-11 shows a stack of L2 SAR echoes for the pass in June 2011, ordered in a time sequence, forming a so-called radar-chronogram. In the radar image a scattering point is clearly recognizable around 10 meter above the sea surface, likely associated with a cargo ship passing under the satellite track. This scattering point causes the observed outlier in SAR SSH at 56.5 deg North.

4. CONCLUSION

The regional validation in open sea in the German Bight shows the consistency of PLRM and the SAR data. There is no significant bias in the SSHs, SWH and winds derived from

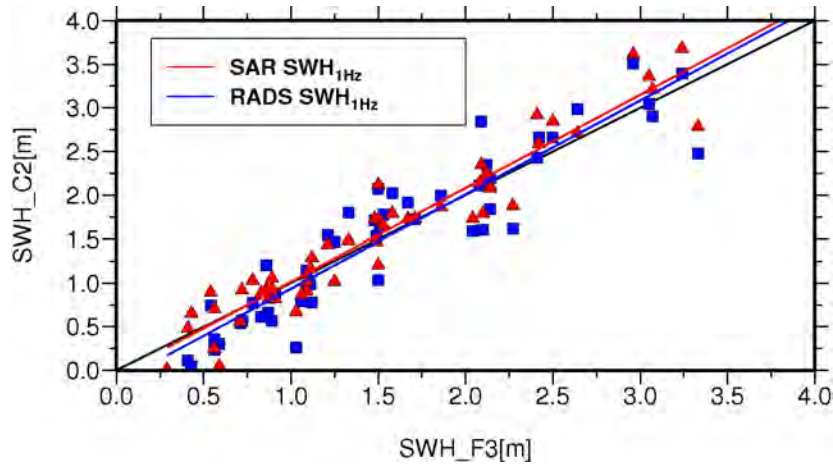


Figure F-05-8: SWH from CryoSat-2 (SWH_{C2}) and from in-situ AWAC data in FINO3 (SWH_{F3})

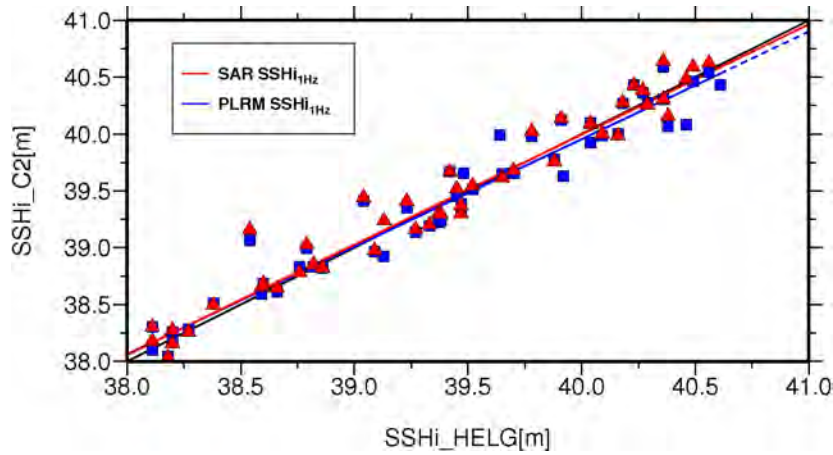


Figure F-05-9: SSH from C-2 and from in-situ tide gauge and GNSS station in Helgoland

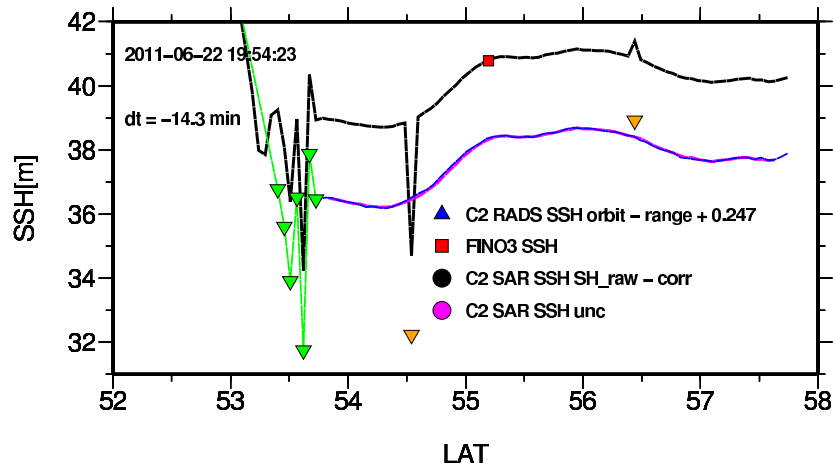


Figure F-05-10: Instantaneous 1Hz SSH corrected (black) and uncorrected (pink, violet) and in-situ SSH (red)

both techniques. The SAR data are more precise and have less noise than the PLRM values, as expected.

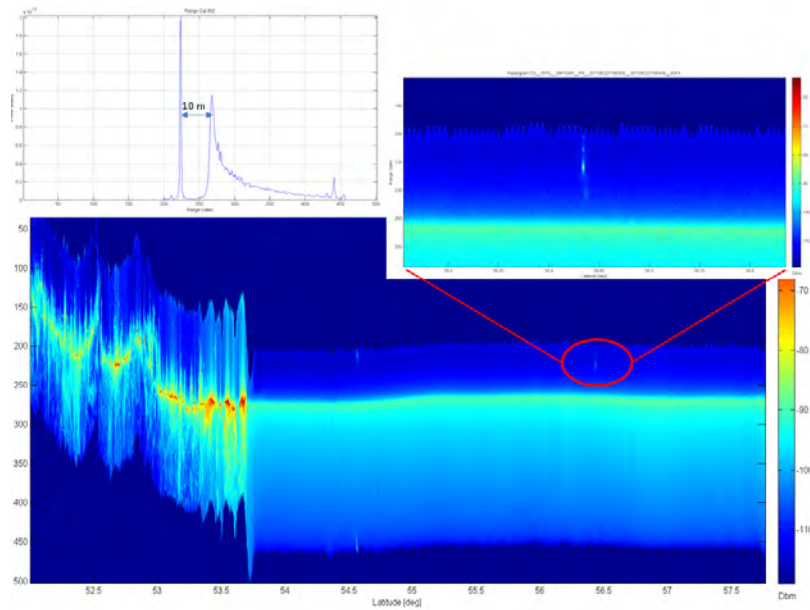


Figure F-05-11: Radargram (dBm) for the CryoSat-2 Pass in June 2011 with a zoom on the point scatterer location (around 10 meters above the sea surface), units of the range-cut waveform are in watt

In-situ and the altimeter-derived SWH are also consistent, as shown in the in-situ analysis at the FINO3 platform in 2011-2012. The best results correspond to SAR altimetry (bias 0.5 cm, standard deviation of differences 26 cm, correlation 0.97). SAR and PLRM SWHs are more consistent to each other (correlation 0.95, slope 0.97, SI 0.19, standard deviation of differences 29 cm) than with model data. The WW3 SWH model underestimate the SWHs, a better agreement is achieved with the LSM model.

The SSH in-situ analysis shows a good consistency between the PLRM and the SAR uncorrected SSH (bias 2 mm, standard deviation of differences 4 cm, correlation 0.999) and between SAR/PLM SSH against Helgoland GNSS elevations.

Finally, also the wind speed in SAR and PLRM mode are consistent. The scatterplot against PLRM wind speed points out the very good correlation between the two datasets (bias 4 cm, standard deviation 30 cm, correlation and slope 0.99). The regional comparison shows a better agreement with the ECMWF wind fields than with the COSMO-EU fields that overestimate the altimeter winds

In the latest version of WW3 is an option of unstructured grids based on the WWMII model (e.g. Roland et al. 2012), which was also implemented in the ECWAM model recently (Roland, 2012). Future application could benefit from a higher resolution of the numerical model since the resolution of the two datasets did not cover all valid locations provided by the flying sensors.

References

Ardhuin, F., Rogers, E., Babanin, A., Filipot, J-F., Magne, R., Roland, A., Van Der Westhuysen, A., Queffelec, P., Lefevre, J-M., Aouf, L, and Collard, F. (2010). Semi-empirical dissipation source functions

- for ocean waves: Part I, definition, calibration and validation,. *J. Phys. Oceanogr.*, 40, 1917-1941. Doi: 10.1175/2010JPO4324.1
- Behrens A., Schrader, D. (1994). The wave forecast system of the Deutscher Wetterdienst and the Bundesamt für Seeschifffahrt und Hydrographie: A verification using ERS-1 altimeter and scatterometer data, *Deutsche Hydrografische Zeitschrift*, 46, 2, 131-149, doi: 10.1007-BF02225836
- Dinardo S., Lucas B., Benveniste J., (2013). A Toolkit for CryoSat Investigations by the ESRIN EOP-SER Altimetry Team, Proceedings Third CryoSat-2 User Workshop, Dresden, Germany, ESA SP-717
- Fenoglio-Marc L., R. Weiss, S. Dinardo, M. Becker, A. Sudau (2012). A Study on the conformance of altimetry and in situ surface data near coast, in Proceedings of the 20 Years of Progress in Radar Altimetry Symposium, Venice, Italy, 24-29 September 2012, Benveniste, J. and Morrow, R., Eds., ESA Special Publication SP-710, 2012.
- Fenoglio-Marc L., E. Groten and C. Dietz (2004). Vertical Land Motion in the Mediterranean Sea from altimetry and tide gauge stations, *Marine Geodesy* 27, 3-4, pp.683-701
- Goffinet P., J. Blasi, A. Sudau, and G. Liebsch (2011). National Report of Germany. GLOSS-Report 1.
- Günther, H., Hasselmann, S. and Janssen, P.A.E.M., 1992. The WAM model Cycle 4. *Deutsch. Klim. Rechenzentrum*, Techn. Rep. No. 4, Hamburg, Germany.
- Lourakis M.I.A. (2004). LEVMAR: Levenberg Marquardt non linear least squares algorithms in C/C++, <http://www.ics.forth.gr/lourakis/levmar/>
- Janssen, S. Abdalla1, L. Aouf, J.-R. Bidlot, P. Challenor, D. Hauser, H. Hersbach, J.M. Lefevre (2008) 15 Years using Altimeter sea state products, ECMWF Technical Memorandum
- Komen G.J., L. Cavaleri, M. Donelan, K. Hasselmann S. Hasselmann P. A. E. M. Janssen (1994), Dynamics and Modelling of Ocean Waves, Cambridge: Cambridge University Press, ISBN 0-521-47047-1.
- Magne, R., Ardhuin, F., Roland, A. (2010) Waves forecast and hindcast from global ocean to the beach, *European Journal of Environmental and Civil Engineering*, 4, 149-162, doi: 10.3166/EJECE.14.149-162
- Marquardt, D. (1963). An Algorithm for Least-Squares Estimation of Nonlinear Parameters. *SIAM J. Appl. Math.* 11, 431-441, 1963.
- Rasche N. and Ardhuin F. (2013). A global wave parameter database for geophysical applications. Part 2: Model validation with improved source term parameterization, *Ocean Modelling*, 70, 174-188, ISSN 1463-5003, <http://dx.doi.org/10.1016/j.ocemod.2012.12.001>.
- Ray C. SAR Altimeter Backscattered Waveform Model, C.Ray et al, TGRS (to be submitted)
- Roland, A., Zhang, Y.J., Wang H. Y., Meng, Y., Teng, Y.C, Maderich, V., Brovchenko, I, Dutour-Sikiric, M and Zanke, U. (2012). A fully coupled 3D wave-current interaction model on unstructured grids, *JGR Oceans*
- Tolman H.L (1991). A 3rd Generation model for wind-waves on slowly varying, unsteady, and inhomogeneous depths and currents, *J. of Physical Oceanography*, 21, 6, 782-797
- SAMOS Team (2013) Detailed Processing Model (DPM) of the Sentinel-3 SAR Altimeter Ocean Waveform Retracker v2.2
- Scharroo R, Smith W F, Leuliette E W, Lillibridge J L. (2013). The performance of CryoSat as an ocean altimeter. Proceedings Third CryoSat-2 User Workshop, Dresden, Germany, ESA SP-717

Chapter 7

Quantification of global and regional sea level variability

7.1 Coastal and global sea level

F-06: Fenoglio-Marc L., E. Tel, Coastal and global sea level, *Journal of Geodynamics* 49, 151-160, 2010.

Abstract Both coastal and global mean sea level rise by about 3.0 ± 0.5 mm/yr from January 1993 to December 2004. Over shorter intervals the coastal sea level rises faster and over longer intervals slowly than the global mean, which trend is almost constant for each interval and is equal to 2.9 ± 0.5 mm/yr in 1993-2008. The different trends are due to the higher inter-annual variability of coastal sea level, caused by the sea level regional variability, that is further averaged out when computing the global mean.

Coastal sea level rise is well represented by a selected set of 267 stations of the Permanent Service for Mean Sea Level and by the corresponding co-located altimeter points. Its departure from coastal sea level computed from satellite altimetry in a 150 Kilometer distance from coast, dominated by a large rise in the Eastern Pacific, is due to the regional inter-annual variability.

Regionally the trends of the coastal and open-ocean sea level variability are in good agreement and the main world basins have a positive averaged trend. The inter-annual variability is highly correlated with the El Nino Southern Oscillation (SO) and the North Atlantic Oscillation (NAO) climatic indices over both the altimeter period and the interval 1950-2001. Being the signal of large scale a small number of stations with good spatial coverage is needed. The reconstruction of the inter-annual variability using the spatial pattern from altimetry and the temporal patterns from tide gauges correlated to NAO and SOI restitutes about 50% of the observed inter-annual variability over 1993-2001.

Keywords: sea level, altimetry, tide gauge, global and regional change

1. Introduction

Sea level rise is an important aspect of climate change and at least 50-year records are needed to separate secular, decadal and interannual variations (Douglas 2001). Over this long time interval only few tide gauges along the world coastlines are available for the analysis (Church, 2008). The spatial distribution of tide gauges as well as the existence of interannual and low frequency signals affect the recovery of secular trends in short records. Thus, it is important to develop techniques for the estimation of sea level trends cleaned from decadal variability.

The analysis based on tide gauge alone reflect however only the coastal sea level, while the global sea level change is derived from altimeter data, that are available over the past 15 years. A coastal global averaged sea level (CGSL) rise over the past century has been observed from tide gauge data in the range of 1-2 mm/yr (Cazenave and Nerem, 2004), with 1.8 ± 0.3 mm/yr for the period 1950-2000 (Church and al., 2004, Church and White, 2006). Over the last decade, both altimetry and tide gauges have been used to estimate global coastal and open sea changes. Estimates for the rate of the global sea level (GSL) estimated by altimetry are: 2.8 ± 0.4 mm/yr over 1993-2003 (Cazenave and Nerem, 2004, Lombard et al. 2005), 3.1 ± 0.4 mm/yr in 1993-2006 (Beckley et al., 2006), 3.1 ± 0.1 mm/yr in 1993-2007 (Prandi et al., 2009). Jevrejeva et al.(2006) report a coastal global sea level trend of 2.4 ± 1.0 mm/yr from 1993 to 2000 obtained from tide gauges only and estimate its error from the difference between sea level trends in sub-regions. Holgate and Woodworth (2004) give in 1993-2002 a rate of

Table F-06-1: Number of tide gauge stations satisfying selected constraints

	Available 90% gaps < 2 years	Near TG < 2	altimetry	no gaps filled	gaps filled
1900-2008	24	15	15	15	15
1950-2008	126	99	99	30	77
1950-2008	126	99	99	80	86
1993-2008	427	406	267	197	197

4 mm/yr and suggest that the coastal sea level is rising faster than the global mean, while White et al. (2005) conclude that the observed difference between the rate from altimetry and tide gauges is due to the sampling. Prandi et al. (2009) show that considering 15 years of data the rates of both coastal and global means from altimetry as well as the mean from a set of tide gauges are similar, the differences are an artifact due to the interannual variability.

In addition to the uncertainty of the rate due to the fitting procedure, measurement errors and omission error are involved. The calibration of altimeter data using co-located altimetry and tide gauge stations give an error of 0.4 mm/yr for the altimetric sea level change (Mitchum 2000, Leuliette et al., 2004). Jevrejeva et al. (2006) assign an error of 1 mm/yr to the global sea level change derived from tide gauges, due to the non-uniform data distribution. The number of tide gauge stations used in previous studies are different, from more than 1000 stations in (Jevrejeva et al., 2006) to 91 stations in Prandi et al. (2009), while the selection criteria and the filling of the incomplete time series also reduce the effective number of stations.

In this study we investigate if the coastal sea level observed by tide gauges conveniently represent the global sea level using both altimetry and tide gauge stations. Our study differs from the global analysis of Prandi et al. (2009) in the selection of tide gauge stations, and in the analysis of three different types of sea level averages globally and in sub-regions. We expect a slight dependence of the reported resulting rate on the number of tide gauge stations used. We distinguish between (a) global sea level change derived from altimetry (GSLA), (b) coastal sea level change derived from altimetry (CGSLA) and (c) coastal sea level change derived from tide gauge stations (CGSLT) and (d) from the co-located altimetry (CGSLAT). First we consider the time average of these four global sea level estimates on the entire globe and on sub-regions. Then we analyse the main component of the interannual and interdecadal variability of the detrended time-series and their dependence on the climatic indices.

2. Data and Methodology

Tide gauge data from the PSMSL (Permanent Service for Mean Sea Level - <http://www.pol.ac.uk/psmsl/>) database are used. We study the distribution and time length of the time-series and apply a selection criteria based on the data gaps. The number of stations available in each of the three intervals 1900-2008, 1950-2008 and 1993-2008 is 1155, 1109 and 761 respectively. A station is used if it is available over 90% of the interval with gaps shorter than 2 years (availability criteria). The number of stations fulfilling these criteria is 24, 126 and 427 respectively (Tab. F-06-1) and are mostly located in the northern hemisphere along the European and North-American coasts (Fig. F-06-1).

Standard corrections are applied to the Topex/Poseidon, Jason-1 and Envisat altimetry data from January 1993 to December 2008 available via the RADS database (Naeije et al., 2002). A Gaussian weighted average method (half-weight equal to 1 and search radius equal to 150 kilometers) is used to compute monthly altimetric time-series in a 1x1 degree grid. The MOG2D correction for the effect of atmospheric pressure (Carrere and Lyard, 2003) is applied to altimetry.

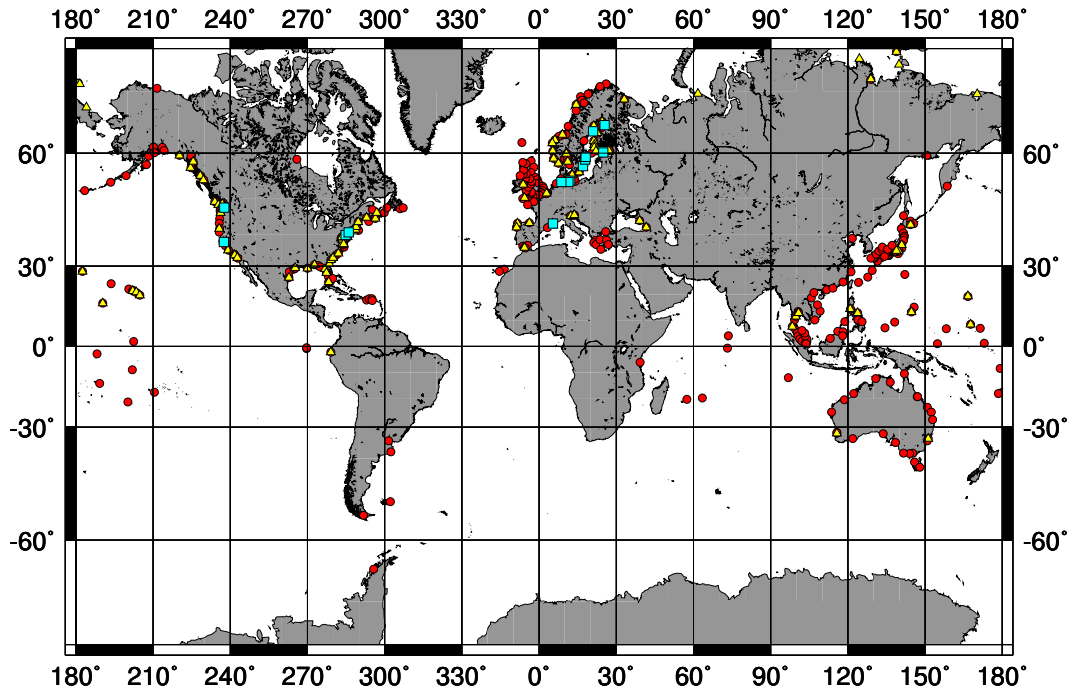


Figure F-06-1: Tide gauge stations of the PSMSL dataset satisfying availability criteria. Numbers of stations are 447 in 1993-2008 (circle), 117 in 1950-2008 (triangle) and 15 in 1900-2008 (square).

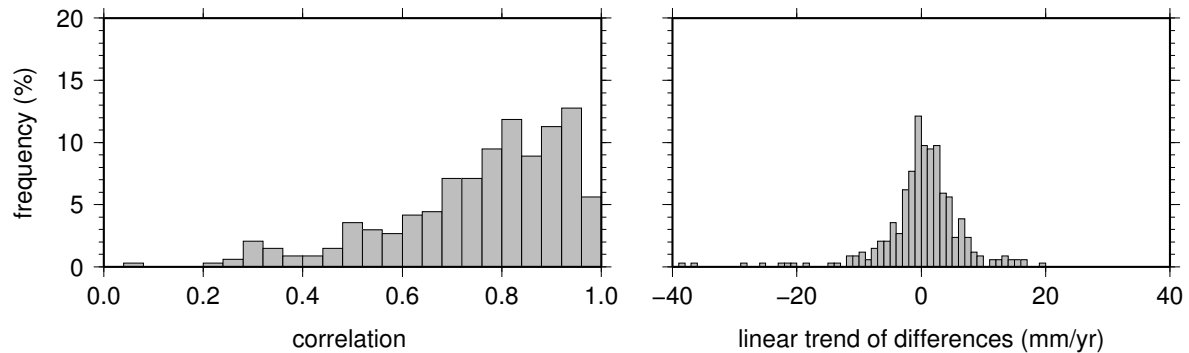


Figure F-06-2: Histograms of correlation (left) and linear trend of differences between altimetry and tide gauges (right) over 1993-2008.

To correct the sea level at the tide gauge station for Glacial Isostasy we use the SELEN software (Spada and Stocchi, 2007) forced with the ICE5-G glaciation history and a visco-elastic Maxwell Earth derived from VM2 (Paulson et al., 2007). Tide gauge stations suitable for large-scale sea level change analysis are selected by comparison with satellite altimetry in 1993-2008. The chosen stations represent the large-scale open sea level variability, therefore stations describing the local sea level variability are eliminated. The sea level change derived from the altimeter is corrected for the GIA effect and this correction increases the satellite estimates of global sea surface rates by 0.3 mm/yr (Peltier, 2004).

The mean seasonal cycle is removed from the monthly time-series and the trend is evaluated by linear regression. The probable uncertainty of the linear term of the regression is estimated accounting for the temporal auto-correlation of the residuals. The effective degree of freedom n_1 (EDOF) and the probably uncertainty of the linear term are computed as:

Table F-06-2: Mean sea level trends between January 1993 and End of Year (column 1) of global altimetry (GSLA), coastal altimetry (CGSLA) and co-located altimetry at the 267 stations (CGSLAT). Error σ_{adj} is computed accounting for Degree of Freedom (dof) for interannual variability and standard error σ_{st} . Total error σ_{tot} is also given.

	GSLA dof	CGSLA dof	CGSLAT dof	GSLA b, σ_{st} , σ_{adj} , σ_{tot}	CGSLA b, σ_{st} , σ_{adj} , σ_{tot}	CGSLAT σ_{adj} , σ_{tot}
1999	46	19	35	3.02 ± 0.17 (0.22/0.46)	5.73 ± 0.51 (1.06/1.13)	5.17 ± 0.7 (1.1, 1.20)
2000	49	22	38	2.90 ± 0.13 (0.18/0.44)	5.43 ± 0.40 (0.83/0.93)	3.97 ± 0.63 (0.98/1.1)
2001	76	25	43	2.99 ± 0.11 (0.13/0.42)	4.89 ± 0.47 (0.70/0.81)	3.56 ± 0.52 (0.81/1.9)
1999	46	19	35	3.02 ± 0.17 (0.22/0.46)	5.73 ± 0.51 (1.06/1.13)	5.17 ± 0.7 (1.1/1.20)
2002	85	20	48	3.09 ± 0.10 (0.11/0.41)	3.81 ± 0.32 (0.79/0.89)	3.43 ± 0.43 (0.68/0.84)
2003	93	20	57	3.10 ± 0.08 (0.09/0.41)	3.29 ± 0.28 (0.72/0.81)	3.65 ± 0.37 (0.56/0.75)
2004	103	21	61	3.09 ± 0.07 (0.08/0.41)	2.83 ± 0.25 (0.65/0.76)	3.19 ± 0.32 (0.50/0.70)
2005	108	23	63	3.22 ± 0.06 (0.07/0.40)	2.54 ± 0.22 (0.57/0.70)	2.89 ± 0.30 (0.46/0.68)
2006	116	25	63	3.12 ± 0.05 (0.06/0.40)	2.39 ± 0.19 (0.50/0.65)	2.77 ± 0.27 (0.44/0.66)
2007	104	27	68	3.01 ± 0.05 (0.06/0.40)	2.28 ± 0.17 (0.44/0.59)	2.68 ± 0.25 (0.40/0.64)
2008	100	28	70	2.9 ± 0.05 (0.06/0.40)	2.25 ± 0.15 (0.43/0.57)	2.54 ± 0.23 (0.40/0.63)

$$n^1 = n \frac{1 - r^1}{1 + r^1}, \quad (\text{F-06-1})$$

$$\sigma^1 = \sigma \left(\frac{1 + r^1}{1 - r^1} \right)^{1/2} \quad (\text{F-06-2})$$

with n the number of samples, r^1 the lag-1 autocorrelation of the detrended average time-series, σ the standard error obtained from the linear regression (Wilks 1995, Fenoglio-Marc et al., 2004). The selection of the tide gauges is based on proximity and agreement criteria with satellite altimetry (Fenoglio-Marc et al., 2004). A station is eliminated if the minimum distance from a point of the altimeter grid is greater than 150 Kilometers. For each tide gauge station we consider the nearest node of the altimeter grid within this distance and four parameters: (1) correlation, (2) trend of the difference, (3) standard error of the trend of the difference, (4) standard deviation of the difference are used as indicators of the agreement between altimetry and tide gauge data. The criteria are: correlation > 0.5, trend and standard error of the trend < 5 mm/yr and standard deviation of the differences < 80 mm. Not fulfillment of the selection criteria can arise from a jump in the record or to local variability (location in an harbor or near to an estuary). In this last case, the station, also if correctly recording, will not be used for sea level change analysis.

The selected time-series present gaps. The number of stations is further reduced as we use only complete time-series to estimate the empirical representation of sea level derived by Principal Component Analysis (PCA), called here further empirical models. To increase the number of tide gauge stations, the gaps in the records are filled by linear regression with the highest correlated time-series. For each of the time-series of anomalies trend and seasonal signal are subtracted and the correlation matrix of the residuals computed. Gaps in the time-series are filled by linear regression of the residuals with the complete time-series that realizes the highest correlation. The process is repeated until all the gaps are filled. The filling is not done for a time-series if the correlation coefficient with any of the complete tide gauges is lower than 0.5. The time-series are then reconstructed by adding trends and seasonal cycles. Four standardized climatic indices are used: the El Nino Southern Oscillation (SO) index, defined as the difference of standardized pressure at Tahiti and Darwin (Trenberth et al., 1984) (<http://www.cgd.ucar.edu/cas/catalog/climind>), the Northern Atlantic Oscillation (NAO) index, defined as the normalized pressure difference between Reykjavik and Ponta Delgada (<http://www.cru.uea.ac.uk>), The Pacific Decadal Oscillation (PDO), defined as the

Table F-06-3: Mean sea level trends between January 1993 and December 2008 of global altimetry (GSLA), coastal altimetry (CGSLA) and co-located altimetry at the 267 stations (CGSLAT) for the world and for 4 sub-regions

	GSLA	CGSLA	CGSLAT	TG
Globe	3.0 +/- 0.05	2.3 +/- .17	2.7 +/- 0.25	267
Atlantic Ocean (30S-66N, 70W-30E) (10N-66N, 110W-30E)	2.0 +/- 0.07	3.4 +/- 0.4	2.8 +/- 0.20	122
Indian Ocean (30S-30N, 30E-110E)	3.3 +/- 1.4	2.7 +/- 0.2	3.1 +/- 0.2	25
Tropical Pacific (30S-30N, 110E-100W) (30S-10N, 100W-70 W)	2.9 +/- 0.05	3.8 +/- 0.3	3.4 +/- 0.42	54
Northern Pacific (30N-66N, 110E-90W)	1.6 +/- 0.7	0.7 +/- 0.2	-0.6 +/- 0.3	56

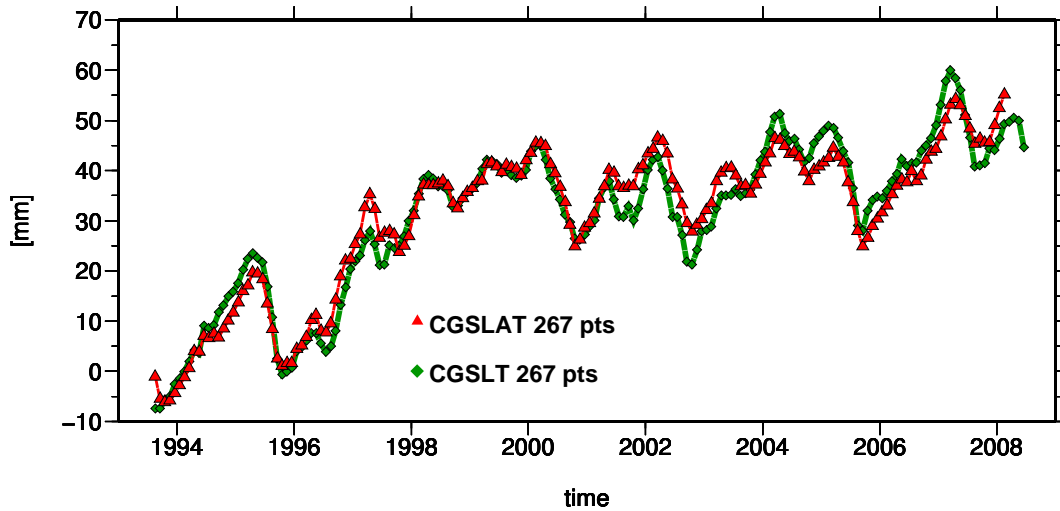


Figure F-06-3: Averaged coastal sea level from the 267 tide gauge stations (diamond) and from the altimeter nearest grid points (triangle). A 12-month running average is applied

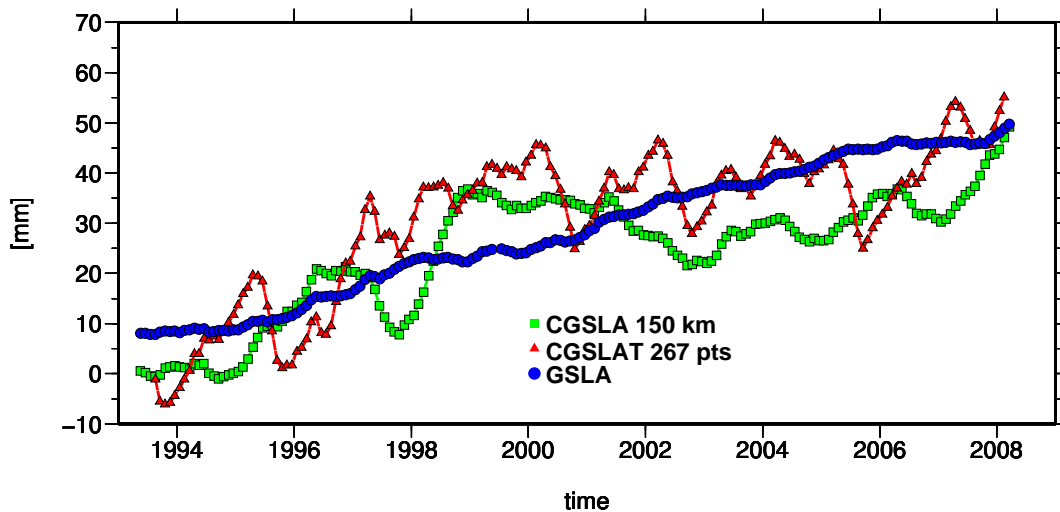


Figure F-06-4: Mean sea level from altimetry: averaged global sea level (circle), coastal sea level within 150km from the coast (square) and sea level in grid points corresponding to the 267 tide gauge stations (triangle). A 12-month running average is applied.

leading Principal Component of monthly Sea Surface Temperature in the North Pacific Ocean (<http://www.atmos.washington.edu>) and the North Pacific (NP) index, the area-weighted sea

Table F-06-4: Percentage of variance and correlation between dominant modes of PCA-CCA decomposition in 1993-2001 of inter-annual sea level heights from altimetry (a) and tide gauges (b) and of interannual climatic indices

Mode	%(a)	NAO(a)	SO(a)	PDO(a)	NP(a)	%(b)	NAO(b)	SO(b)	PDO(b)	NP(b)
1	25.0	0.45	0.62	-0.41	0.38	24.1	0.45	0.63	-0.41	0.38
2	15.5	-0.39	-0.21	0.46	-0.1	17.4	-0.39	-0.22	0.45	-0.08
3	12.5	0.67	-0.08	-0.34	-0.08	8.0	0.68	-0.09	-0.31	0.47
4	12.1	-0.30	-0.35	0.12	-0.35	13.4	-0.24	-0.37	0.21	-0.63

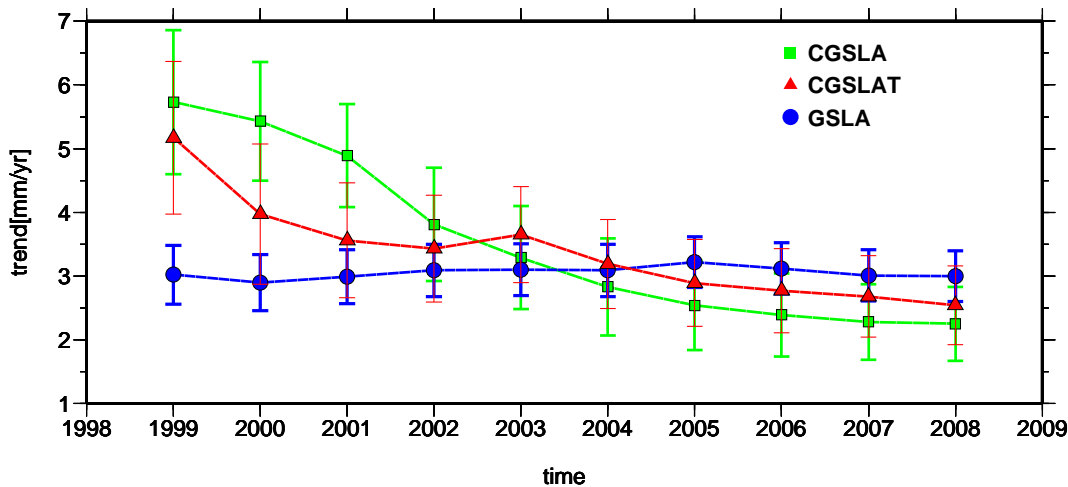


Figure F-06-5: Trends and error bars of global sea level (circle), coastal sea level within 150km from coast (square) and coastal sea level at the 267 altimeter locations co-located to the tide gauge stations (triangle). Time intervals start in 1993.

level pressure over the region 30N-65N and 160-140W (<http://www.cgd.ucar.edu/cas/jhurrel>) (Trenberth and Hurrel, 1994).

For the analysis of the long-term trends over the complete globe and over few selected basins we compute spatial averages of the de-seasoned time-series. A moving averaged with a window of 12 months is further applied for plotting purposes.

For the analysis of both interannual and interdecadal signals, for each time-series a linear trend and mean seasonal cycle are removed, finally the residuals time-series are low-pass filtered. The filtering consist, for the interannual analysis, in computing running means of the monthly data over 1-yr interval with 0.5-yr time step, for the inter-decadal analysis it consists in computing running means of the monthly data over 5-yr interval with 2.5-yr time step.

The statistical method of PCA (Preisendorfer, 1988) is applied to the interannual and interdecadal anomaly fields to detect the principal modes of variability. We apply a significance test based on a Monte Carlo technique (Overland and Preisendorfer, 1982) to find the number k of principal components to be retained. The eigenvalues for which the signal is above the level of noise are found by comparing the normalised eigenvalue statistics corresponding to the real data and to random data. Independent sequences of independent gaussian variables of zero mean and unit variance are generated and the eigenvalues of the correlation matrix computed. The procedure is repeated 100 times. The principal components with eigenvalues greater than the value 95 in the sequence, the so called Rule N are considered as significant. The rule is applied to the temporal and spatial effective sizes n^1 and p^1 . The temporal effective size n^1 is estimated as in Equation F-06-1. The PCA method is first applied separately to the standardized anomaly fields of altimetry and of tide gauges. We select the modes of the decompositions that have the temporal coefficients correlated to the same climatic indices

Table F-06-5: Percentage of variance and correlation between PCA modes of interannual sea level from altimetry and interannual climatic indices in 1993-2001

Mode	%	NAO	SO	PDO	NP
1	26.2	0.25	0.63	0.49	-0.47
2	15.4	-0.43	-0.37	0.30	-0.42
3	12.6	0.80	0.24	0.33	-0.27
4	9.9	0.11	0.13	0.09	0.33

and we build an empirical model of the sea level variability using the corresponding spatial patterns from altimetry and the temporal coefficients from tide gauges. We also investigate the coupled variability of altimetric and tide gauge data using the Canonical Correlation Analysis in the PCA basis (PCA-CCA), a method which decomposes the sea level variability maximising the correlation between the temporal patterns (Bretherton et al., 1992).

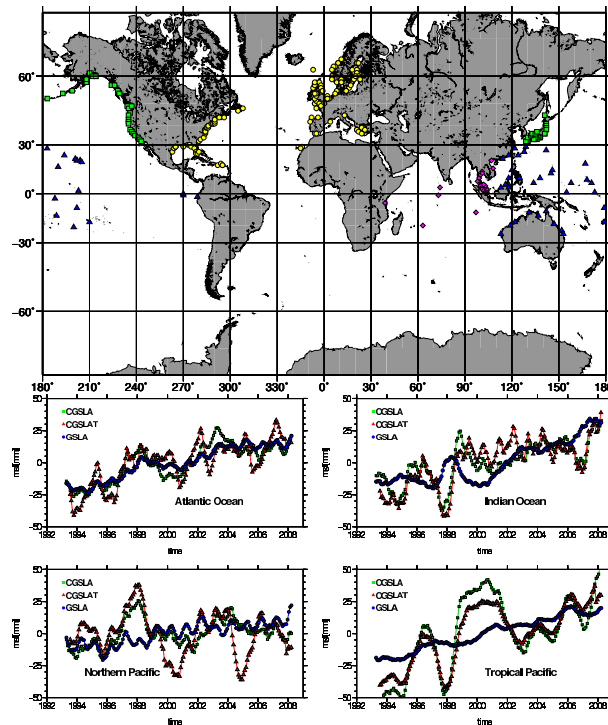


Figure F-06-6: Top: PSMSL tide gauge stations in the four sub-region: Atlantic Ocean (circle), Indian Ocean (diamond), Northern Pacific (square) and Tropical Pacific (triangle). Bottom: Basin averaged sea level over the four sub-regions obtained from altimetry in the open-ocean (circle), within 150km from coast (square) and at the co-located locations; a 12-month running average is applied.

3. Results

3.1 Spatial average

Co-located altimeter monthly time-series can be computed for 406 of the 427 stations in 1993-2008. Histograms of correlation and linear trend of differences between altimetry and tide gauges are given in Fig. F-06-2. The selection criteria described in Section 3 are satisfied by 267 stations, their averaged time-series and the average of the nearest corresponding point in the altimetry grids, called hereafter co-located altimeter point, have correlation 0.9 and Root Mean Error (RMS) 10.7 mm. Once smoothed by a 12 month moving average the two time-series have correlation 0.97 and RMS of 3.7 mm (Fig. F-06-3). Uncorrected and MOG2D-

Table F-06-6: Percentage of variance and correlation between dominant modes of interannual sea level from 197 tide gauges and interannual climatic indices in 1993-2001 with 197 (a) and 30 (b) stations respectively

Mode	%(a)	NAO(a)	SO(a)	PDO(a)	NP(a)	%(b)	NAO(b)	SO(b)	PDO(b)	NP(b)
1	31.4	0.80	-0.35	-0.24	0.05	36.2	0.64	0.03	-0.54	0.04
2	25.1	-0.13	0.60	0.67	-0.58	16.1	-0.02	0.46	0.51	-0.46
3	11.3	-0.27	0.54	-0.26	-0.04	10.8	-0.21	0.75	0.70	-0.60
4	8.3	-0.40	-0.34	0.17	0.32	6.9	-0.01	0.49	-0.34	0.07

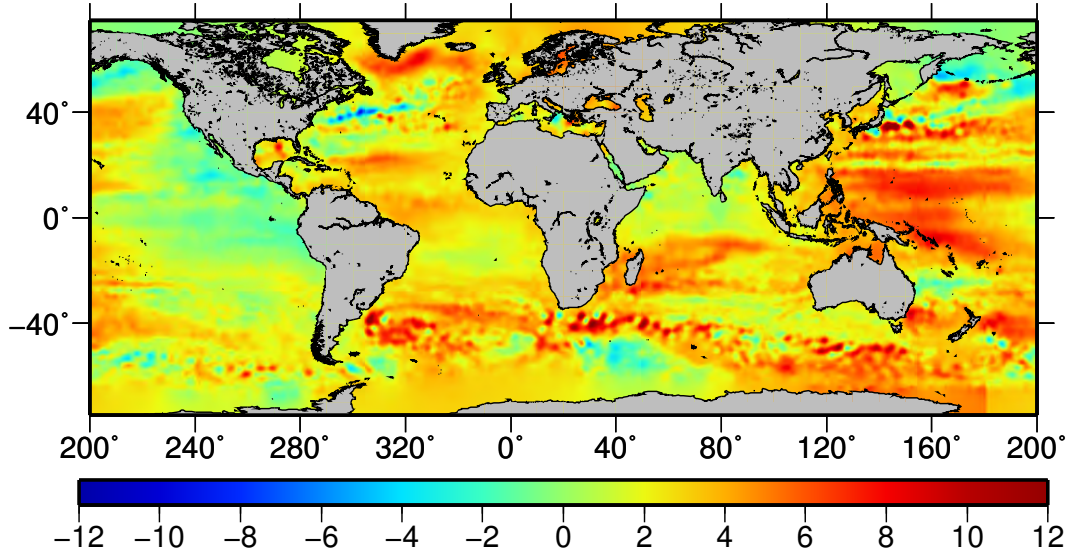


Figure F-06-7: Trend of sea level over 1993-2008 derived from T/P and Jason-1 data

corrected smoothed altimeter time-series are also in good agreement, with RMS differences of 4.8 mm and correlation 0.92.

We further use altimeter data corrected for the effect of pressure by MOG2D to represent sea level at the tide gauge location and to study the effect of the spatial distribution of the locations. We compare the average time-series of GSLA, CGSLA and CSLAT, the time-series smoothed by a moving average are shown in Fig. F-06-4. The trends are computed by linear regression of the de-seasoned monthly time-series. A realistic uncertainty for the total error of the trend σ_{tot} accounts for the effect of the serial correlation in the time-series σ_{adj} and for two additional errors: the measurement errors σ_{meas} and the omission error σ_{miss} due to incomplete coastal coverage of the tide gauge stations. The adjusted error σ_{adj} is evaluated from Equation F-06-2 using the effective degree of freedom of the de-trended residuals and the standard error σ_{st} (Tab. F-06-2). The CGSLA has in general a smaller adjusted standard errors than the CGSLAT, being the degree of freedom of the time-series smaller. The omission error, σ_{miss} is derived from the difference in trend between CGSLA and CGSLAT and is estimated to be 0.3 mm/yr. We consider a measurement error of the altimeter σ_{meas} of 0.4 mm/yr (Mitchum, 2000).

The trends are evaluated over intervals starting from January 1993. The GSLA has an almost constant trend, that is 2.9 ± 0.4 mm/yr for 1993-2008, the trend of CGSLA is monotonic decreasing, 2.27 ± 0.59 mm/yr in 1993-2008. The trend of CGSLAT is more variable, 2.54 ± 0.64 mm/yr in 1993-2008. The best agreement between all trends is in 1993-2004 (Tab. F-06-2). The σ_{tot} are small for GSLA trends (0.42 mm/yr in mean), higher for CGSLA (from 0.59 to 1.13 mm/yr) and CGSLAT trends (from 0.64 to 1.2 mm/yr) (Tab. F-06-2). The differences in the trends with GSLA are significant for most of the intervals. Over the sub-interval

Table F-06-7: Percentage of variance and correlation between dominant modes of interannual sea level from 197 tide gauges and interannual climatic indices in 1993-2001 with 197 (a) and 30 (b) stations respectively

Mode	%(a)	NAO(a)	SO(a)	PDO(a)	NP(a)	%(b)	NAO(b)	SO(b)	PDO(b)	NP(b)
1	36.2	0.49	0.18	-0.18	0.24	26.8	0.50	-0.19	0.03	0.27
2	16.1	0.21	0.35	0.26	-0.28	16.7	0.35	-0.02	0.03	-0.10
3	10.8	-0.06	0.36	0.44	-0.39	16.0	0.06	0.68	0.43	-0.50
4	6.9	0.32	0.28	-0.18	0.08	11.5	0.53	-0.45	0.40	-0.34

2003-2008, the GSLA trends obtained from Envisat and Jason-1 (1.2 ± 0.5 mm/yr and 1.6 ± 0.4 mm/yr respectively) are lower than the GSLA trends estimated over the complete interval 1993-2008.

The error due to the incomplete coastal coverage of the tide gauge stations (σ_{miss}) is 0.3 mm/yr and is obtained from the difference in trends between coastal altimetry and altimetry at the 267 co-located locations. The uncertainty of the trend is smaller for GSLA (around 0.42 mm/yr) and higher for CGSLA (from 0.59 to 1.13 mm/yr) and CGSLAT (from 0.64 to 1.2 mm/yr). The trend differences are mainly caused by the different number of locations used to compute the three averaged time-series. Starting from the 1993-2002 the differences between the CGSLA and CGSLAT trends are within the error bars (about 0.5 mm/yr). The differences between the GSLA and CGSLA trends are significant in most of the intervals, are not significant in 1993-2003 and 1993-2004 and increase for longer intervals again (Fig. F-06-5).

We compute the averages of GSLA, CGSLA and CGSLAT over the four sub-regions: Atlantic Ocean, Tropical Pacific, Indian Ocean and Northern Pacific, with respectively 122, 25, 54 and 56 of the selected 267 tide gauge stations (Figs. F-06-6 and Tab. F-06-3). The trends are all positives in the Atlantic, in the Indian and Tropical Pacific and the inter-annual variability is regionally dependent. In the Tropical Pacific the averaged coastal sea level from altimetry and from the few tide gauge stations has the highest correlation and the best agreement with the CGSL world coastal sea level (Fig. F-06-4), the Tropical Pacific clearly dominates the global coastal variability. The difference between Prandi et al. (2009)'s average of the coastal sea level obtained from 91 tide gauge stations and our CGSLT and CGSLAT at 267 tide gauge stations (Fig. F-06-4) is clearly due to the location of the stations, being most of the UHSLC stations in Tropical Pacific while most of the PSMSL stations are in North-Atlantic. In Northern Pacific the regional average sea level from tide gauges has a negative trend, as most stations are located along the North-American coast where sea level is falling, as shown in Fig. F-06-7.

3.2 Spatial variability

The empirical models are constructed from the tide gauge time-series without gaps, that are 197 for the interannual model in 1993-2001, 30 for the interannual model in 1950-2002 and from 80 for the interdecadal model in 1950-2002. To increase the number of tide gauge stations, the gaps in the records are filled by linear regression with the highest correlated time-series. Alternatively, over 1950-2001, 80% of the gaps of the original monthly matrix have been filled, 61% of the original gaps is filled using a time-series with correlation coefficient bigger than 0.7. After filling of the gaps, the number of stations with complete interannual and interdecadal time-series in 1950-2001 increases from 30 to 77 and from 80 to 86 stations respectively. The decompositions by PCA of both the filled and unfilled time-series give however very similar results, as the additional stations do not add more information.

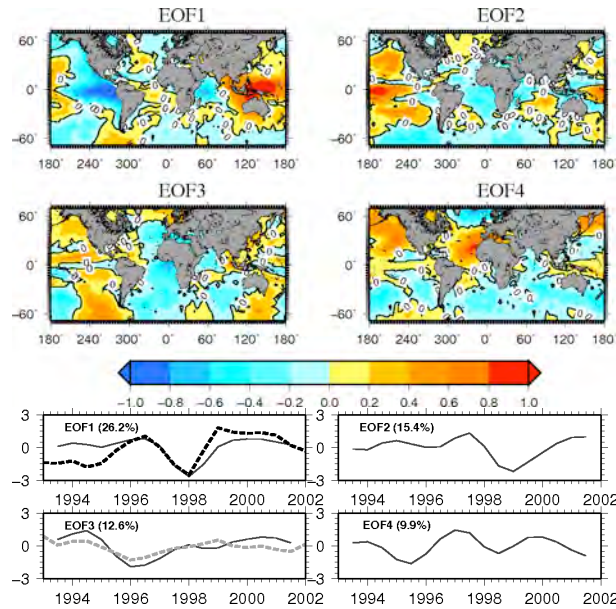


Figure F-06-8: Dominant spatial patterns (top), temporal PCA coefficients and cumulative percentage of variance (centre) from altimetric standardized interannual variability 1993-2002. Interannual component of SO (dashed black) and NAO (dashed grey) indices plotted with the temporal coefficients having the highest correlation

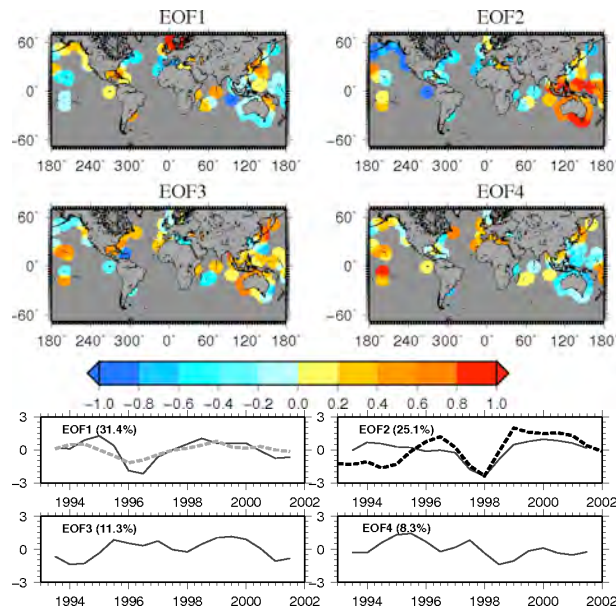


Figure F-06-9: Dominant spatial patterns (top) and temporal PCA coefficients of interannual variability from 197 tide gauge stations in 1993-2001. Interannual component of SO (dashed black) and NAO (dashed grey) are plotted with the temporal coefficients having the highest correlation.

The spatial scale of the interannual variability is of about 300-400 km. The interannual time series of size 17 have a temporal effective size of 15 (95% and 99% confidence level with correlation 0.48 and 0.60). For modes 1-4 of the PCA decomposition the ratio of the normalized eigenvalue statistics (percentage of variance explained) of the data and of the random variables (U95) is greater than 1.5, they are statistically significant and explain more than 75% of the interannual variability. Also the first four modes of the PCA-CCA

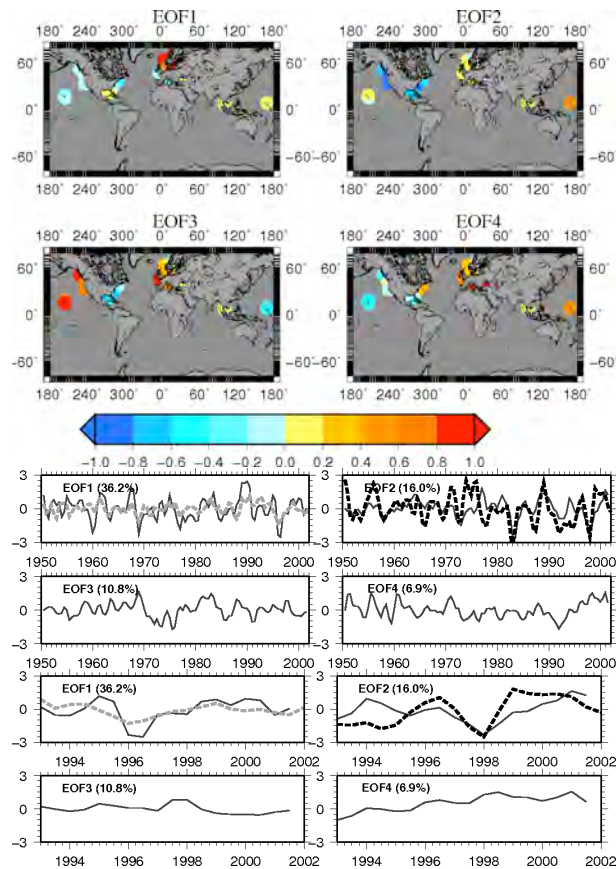


Figure F-06-10: Dominant spatial patterns (top) and temporal PCA coefficients of interannual variability from 30 tide gauge stations in 1950-2002 (centre) with sub-interval 1993-2001 (bottom). Inter-annual part of SO (dashed black) and NAO (dashed grey) are plotted with the temporal coefficients having the highest correlation.

decomposition of the altimetry and tide gauge fields explain more than 70% of the common variability and more than 60% of the variability of each single field. The correlations of the first mode with SO (0.62) and of the third mode with NAO (0.67) are both above the 99% confidence level (Tab. F-06-4).

Some of the spatial and temporal modes of the PCA decomposition of the interannual variability are highly correlated to the climatic indices. Over 1993-2001 the PCA decomposition of the interannual altimeter sea level has the first mode correlated with SO (0.63) and the third mode with NAO (0.80) (Fig. F-06-8, Tab. F-06-5), both correlations are above the 99% confidence level. The correlation of the second mode with NAO and NP is above the 90% confidence level. Similar correlations are found for the first two modes of the model derived from the tide gauge data (Fig. F-06-9): the first mode with NAO (0.80) and the second with SO (0.60). The second mode is also correlated with PDO (0.67) and the third mode with SO (0.54) above the 95% confidence level (Tab. F-06-6.a). The order of the modes is not the same as most of the stations are concentrated in the North Atlantic. The value of the correlation depends on the spatial distribution of the stations, as shown when using over 1993-2001 the subset of 30 tide gauge stations available in 1950-2001. In this case the correlation is 0.64 between the first mode and NAO and only 0.46 between the second mode and SO. (Tab. F-06-7.b).

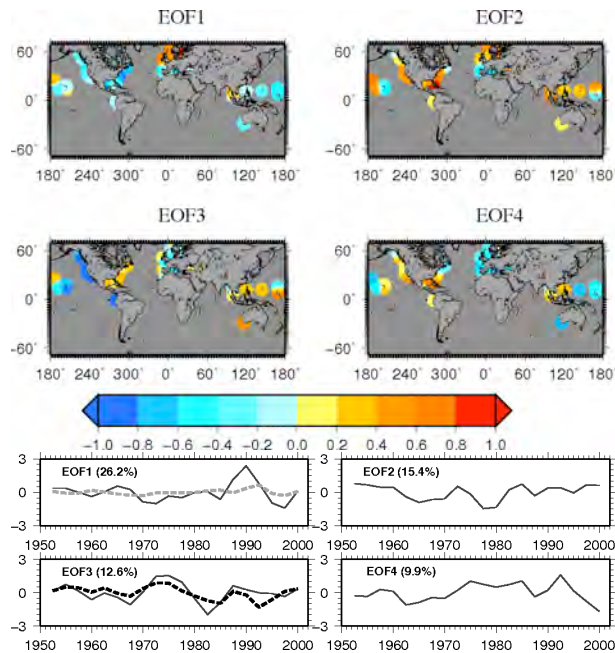


Figure F-06-11: Dominant spatial patterns (top) and temporal PCA coefficients (bottom) of inter-decadal variability from tide gauge stations in 1950-2002.

Over 1950-2001 the interannual empirical model derived from the 30 tide gauges (Fig. F-06-10) has the first mode correlated with NAO (0.49) and both the second and third mode correlated with SO (0.35 and 0.36), both correlations are above the 99% confidence level (0.25). The correlation of the third mode with PDO is higher than with SO (0.44) (Tab. F-06-7.a). For the smoother inter-decadal model the correlation with the indices is higher with the first mode correlated to NAO (0.50, above the 95% confidence level) and the third mode to SO (0.68, above the 99% confidence level) (Tab. F-06-7.b) (Fig. F-06-12).

We reconstruct the sea level variability in 1993-2001 (Fig. F-06-13) using the spatial patterns of the PCA altimeter model and the corresponding temporal coefficients of the tide gauge model that are correlated above the 99% confidence level with the same climatic index. The corresponding components are (1) the spatial pattern of the 1st mode from altimetry and the temporal coefficients of the 2nd mode from tide gauges, which are correlated to SO, and (2) the spatial pattern of the 3rd mode from altimetry and the temporal coefficients of the 1st mode from tide gauges, which are correlated to NAO.

The accuracy of the reconstructed model in Fig. F-06-13 is derived from the root-mean-square error (RMSE), defined as the root of the average squared difference between the observations and the model, and from the root-mean-square (RMS) of the differences between the global average of the model and of the data. The RMSE is 2.8 mm and the RMS differences are 2.6 mm. A similar RMS (2.3 mm) is obtained over 1993-2001 when using temporal coefficients estimated from tide gauges over 1950-2001. The global averages of the interannual altimeter field and of the interannual model corresponding to the first four PCA components have an RMS difference of 0.9 mm.

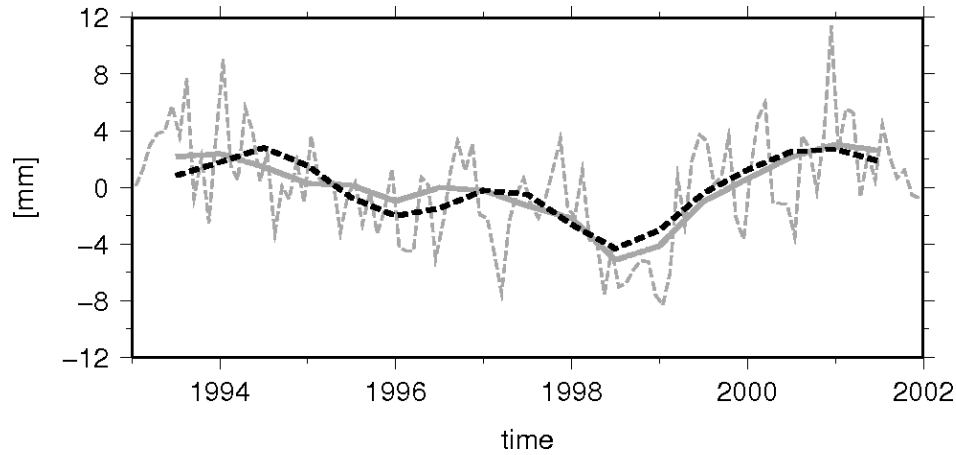


Figure F-06-12: Global mean of de-trended and de-seasonalised monthly sea level (grey dashed) and interannual (grey solid) sea variability from altimetry in 1993-2001, global average of model made by first four dominant modes of interannual altimeter variability (black dashed).

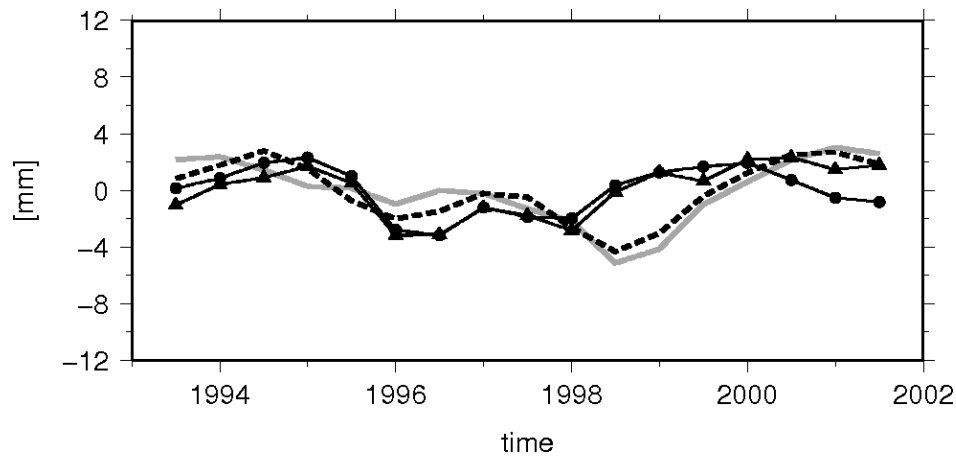


Figure F-06-13: Global mean of interannual model made by spatial patterns from altimetry and temporal coefficients from tide gauges, that mostly correlated to SO and NAO. Temporal coefficients are from 1993 to 2001 (circle) and from 1950 to 2001 (triangle). Global mean of observed interannual variability (solid grey) and interannual model from first four PCA modes (black dashed).

4. Conclusions

Global mean sea level observed by satellite altimetry has a trend of 2.9 ± 0.4 mm/year between January 1993 and December 2008. Over the same interval the coastal mean sea level derived from an set of 267 tide gauge PSMSL stations and from satellite altimetry along the world coasts, has slightly smaller trends of 2.4 ± 0.6 and 2.3 mm/yr ± 0.5 mm/yr respectively.

The differences in the trends are due to the interannual variability of the both coastal mean sea level estimates, due to the regional variability of sea level that is further smoothed out when the considering the global average. We therefore agree with Prandi et al. (2009) that the different rate between coastal and global mean sea level noticed in 1993-2002 by Holgate and Woodworth (2004) does not arise from a coastal mean sea level rising faster than the global mean, but from the interannual variability of coastal sea level. Over 1993-2002 we found a trend of CGSLA of 3.8 ± 0.93 mm/yr. We use a different set of tide gauge stations as Prandi et al. (2009) and this explains the slightly different trends obtained.

Tide gauges conveniently represent global sea level over the long time intervals, however over short intervals interannual and low frequency signal affects the recovery of the secular trends. Several decades are then needed to separate secular, decadal and interannual variations and over this long time interval only few tide gauges along the world coastlines are available for the analysis. Both the spatial distribution of tide gauges as well as the existence of interannual and low frequency signals affect therefore the recovery of secular trends.

Satellite altimetry provides since 1993 thigh-precision, high resolution measurements of sea surface height with global coverage and temporal sampling a few weeks at a same location. There is a good agreement between the mean coastal sea level from tide gauge and co-located altimetry, with correlation of 0.97 and RMS of 3.7 mm for CGSLT and CGSLAT at 267 tide gauges. Also regionally there is a good agreement between coastal and open-ocean sea level variability from altimeter data, and trends are positive in the main world basins.

There is a strong correlation between the climatic indices and the patterns of interannual variability. We have selected the interval 1993-2001 and shown that the SO and the NAO climatic indices are significantly correlated to the dominant modes of the sea level variability. The empirical representation of sea level based on those modes reproduces about 50

As sea level rise is a very important component of climate change, the estimated sea level trends should be cleaned from the decadal and interannual variability.

5. References

- Beckley, B. D., F. G. Lemoine, S. B. Luthcke, R. D. Ray, and N. P. Zelensky (2007), A reassessment of global and regional mean sea level trends from TOPEX and Jason-1 altimetry based on revised reference frame and orbits, *Geophys. Res. Lett.*, 34, L14608, doi:10.1029/2007GL030002.
- Bretherton C., Smith C. and Wallace J. (1992). An intercomparison of methods for finding coupled patterns in climate data change, *Journal of Climate*, 5, 541-560
- Cazenave A. and Nerem R.S. Present-day sea level change (2004). Observations and causes, *Rev. of Geoph.*, 42, RG3001, doi:101029/2003RG000139
- Carrere L. and F. Lyard (2003). Modeling the barotropic response of the global ocean to atmospheric wind and pressure forcing, comparison to observations, *Geoph. Res. Lett.* 30, 8-1, 2003
- Church J.A., N.J. White, R. Coleman, K. Lambeck, J.X. Mitrovica (2004). Estimates of the regional distribution of sea level rise over the 1950-2000 Period, *Journal of Climate*, 2609-2625
- Church J.A. and N.J. White (2006). A 20th century acceleration in global sea-level rise, *Geophys. Res. Lett.*, 33, L01602, doi: 10.1029/2005GL024826
- Church J., N.J. White, T. Arrup, W.S. Wilson, P.L. Woodworth, C.M. Domingues, J. R. Hunter, K. Lambeck (2008) Understanding global sea levels: past, present and future, *Sustain Sci.* 3:9-22, doi:/10.1007/s11625-008-0042-4
- Douglas B.C. (2001). Sea level change in the era of the recording tide gauge, in *Sea Level Rise, history and consequences*, International Geophysics Series Volume 75, Academic Press
- Fenoglio-Marc L., Groten E. and Dietz C. (2004). Vertical Land Motion in the Mediterranean Sea from altimetry and tide gauge stations, *Mar. Geod.* 27, 3-4, 683-701
- Holgate S.J. and P.L. Woodworth (2004). Evidence for enhanced coastal sea level rise during the 1990s, , *Geophys. Res. Lett.*, 31, L07305, doi:10.1029/2004GL019626
- Jevrejeva S., A. Grinsted, J.C. Moore and S. Holgate (2006). Non linear trends and multiyear cycles in ea level records, *J. of Geophysical Research*, vol. 111, C09012, doi:10.1029/2005JC003299

- Leuliette E., R.S. Nerem and G. Mitchum (2004). Calibration of Topex/Poseidon and Jason altimeter data to construct a continuous record of mean sea level change, *Mar. Geod.*, 23 (I), doi:10.1080/01490410490465193.
- Lombard A., A. Cazenave, P.-Y. Le Traon and M. Ishii (2005). Contribution of thermal expansion to present-day sea level change revisited, *Global and Planetary Change*, 47, 11-16
- Mitchum G. (2000). An improved calibration of satellite altimetric heights using tide gauge sea level with adjustment for land motion, *Mar. Geod.*, 23, 145-166.
- Naeije M., E. Doornbos, L. Mathers, R. Scharroo, E. Schrama and P. Visser (2002); RADAR altimeter Database System: Exploitation and extension (RADSxx), Final rep. NUSP-2, 02-06, space Res. Organ. Utrecht, Netherlands
- Overland J.E. and R.W. Preisendorfer, (1982). A significance test for principal components applied to cyclone climatology, *Monthly Weather Review*, Vol.110, N.1, pp. 1-4.
- Paulson A., S. Zhong and J. Wahr (2007). Inference of mantle viscosity from GRACE and relative sea level data, *Geophysical Journal International*, 171, 497-508, doi:10.1111/j.1365-246X.2007.03556.x
- Peltier, W.R. (2004). Global Glacial Isostasy and the Surface of the Ice-Age Earth: the ICE-5G (VM2) model and GRACE, *Ann. Rev. Earth and Planet Sci.*, 2004, 32, 111-149
- Prandi, P., A. Cazenave, and M. Becker (2009), Is coastal mean sea level rising faster than the global mean? A comparison between tide gauges and satellite altimetry over 1993-2007, *Geophys. Res. Lett.*, doi:10.1029/2008GL036564
- Preisendorfer R.W. (1988). *Principal Component Analysis in Meteorology and Oceanography*, n. 17 in *Developments in Atmospheric Science*, Elsevier, Amsterdam
- Spada G. and P. Stocchi, (2007): Selen: a fortran 90 program for solving the sea-level equation, *Computer and Geosciences*, 33, 538-562
- Trenberth K.E. (1984). Signal versus noise in the Southern Oscillation, *Monthly Weather Review* 112: 326-332
- Trenberth K.E. and J.W. Hurrell (1994). Decadal atmosphere-ocean variations in the Pacific, *Climate Dyn.* 9, 303-319
- White N.J., J. A. Church and J.M. Gregory J.M. (2005). Coastal and global averaged sea level rise for 1950 to 2000, *Geoph. Res. Lett.*, 32, L01601, doi:10.1029/2004GL021391
- Wilks D. (1995). *Statistical methods in the Atmospheric Sciences*, Academic Press

7.2 Analysis and representation of regional sea level

F-07: Fenoglio-Marc L., Analysis and representation of regional sea level variability from altimetry and atmospheric data, *Geophysical Journal International*, Vol. 145, 1, 1-18, 2001

Keywords: regional sea level change, altimetry, tide gauge

Abstract A simple representation for the sea level variability at low and medium time frequencies and at large and medium spatial scales is investigated accounting for the correlation between the sea level heights and other atmospheric and oceanic parameters. The selected fields are sea level height, sea surface temperature, wind speed and sea surface atmospheric pressure, they are considered in the interval between 1992 and 1997. The sea level height data correspond to a single space-altimetry mission (Topex/Poseidon) and provide an homogeneous dataset. The dominant characteristics of the variability of each field and the coupled variability between two fields are analysed in the European seas using the spectral analysis method and the statistical methods of principal component analysis and of canonical correlation analysis. In the single-field study, both the spectral and the principal component analysis show in the three seas different characteristics for the sea level height variability. The strongest annual and semiannual signals are in the Mediterranean Sea, whereas in the other two seas, especially in the Baltic Sea, the dominant spectral components have comparable power. The trends are interpreted as interannual variability due to the shortness of the investigated time interval, the highest positive trends are observed in the eastern Mediterranean Sea. In the coupled-fields study, both the linear regression analysis and the canonical correlation analysis show a high correlation between the sea level height and the sea surface temperature in the Mediterranean Sea and between the sea level height and the wind speed in the North Sea and the Baltic Sea. The Mediterranean Sea is particularly suitable for building sea level height models from the statistical methods, as the first four modes of both the single- and the coupled-fields models account for about 90% of the variance of the sea level height field. It is therefore chosen as test area to check the accuracy of the models and the ability of the canonical correlation method to predict the sea level variability. The accuracy of the statistical models is assessed computing dual crossover height differences between the Topex/Poseidon and ERS-1 and ERS-2 sea surface heights corrected using the variability models. Both the single- and the coupled-fields models are found to be a good representation of the sea level variability in the Mediterranean Sea, whereas the extrapolated canonical correlation model, derived using the sea surface temperature as predictor, is less accurate, but still acceptable. Relative bias and drift between the Topex/Poseidon and the ERS data result from the analysis and reflect a non-homogeneous pre-processing of the altimetry data. The single-mission sea level variability models are a first step towards the construction of a multi-mission sea level model from unified multi-mission altimetry data.

sea level change, spectral analysis, principal component analysis, canonical correlation analysis.

1. Introduction

The sea level variability is for many applications of altimetry in oceanography and geodesy the signal to be recovered, for other applications it has to be eliminated to recover the geophysical quantities of interest. In geoid and mean sea level determination a sea level variability model is useful when the number of altimetric repeat cycles is too small to compute a significant mean (Rapp and Yi, 1997). In long-term sea level change studies, the sea level variability

is the investigated parameter as well as a noise in the unification of data from different missions. In global studies, its temporal variation has been modelled in the frequency domain considering annual and semi-annual components, bias and bias rate, which are solved in a least-squares adjustment alone or together with other parameters (Knudsen 1994, Yi 1995, Wangi and Rapp 1994, Nerem et al. 1994, Koblinsky et al. :1992). The sea level temporal variation has been neglected in non-simultaneous mission studies assuming a constant monthly variability and considering dual-crossovers for the same months (Wagner et al. 1997). The space and time spectra of the variability have been estimated globally (Wunsch 1991, Wunsch and Stammer 1995) and regionally (LeTraon et al. 1994). Empirical analysis shows correlations between sea level height and atmospheric-oceanic parameters. Sea level trends and a high coherence between some parameters of the global ocean-atmosphere system have been identified at global scale using satellite remote sensing data (Anzenhofer and Grueber 1998). Regional studies are based on data collected at tide gauge stations (Cui et al. 1995, Heyen et al. 1996) and on remote sensing fields (Jones et al. 1998, Wunsch 1991). The satellite remote sensing techniques acquire data with a global coverage, a dense spatial sampling and a temporal sampling adequate for low and medium frequency analysis. The utility of satellite altimetry for studying the sea level variability, as well as the accuracy and internal consistency of the altimetric sea level heights have been demonstrated (Cheney et al. 1994). The aim of this study is to estimate regional changes in the sea level heights and in a set of atmospheric-oceanic parameters, as well as their correlation at regional scales, using global coverage datasets and to test simple models for the sea level variability. Consistent data are particularly important for long-term variability analysis (Wagner and Cheney, 1992). For this reason, only data from the Topex/Poseidon (T/P) mission are considered here, to avoid errors due to the relative bias and drift between the satellites and to differences in the data pre-processing, as the different geophysical corrections used in the T/P and in the various ERS mission phases (Stum et al. 1998, Scharroo et al. 2000). The construction of a multi-satellite altimetry model with incorporation of ERS and Geosat data is of interest because it extends the interval of analysis and improves the time and spatial resolution of the model. It requires an homogeneous data pre-processing and a careful analysis. The single-mission variability model resulting from the study is a first step towards the construction of a multi-satellite altimetry model.

The investigated areas are the Mediterranean Sea, the North Sea and the Baltic Sea, whose characteristics are quite different, both in the meteorological conditions and in the basin structure. In a previous study (Fenoglio-Marc and Groten, 1997) based on altimetric sea level height data and on atmospheric data at tide gauge stations, it was shown that the spectral characteristics of the sea level anomalies and of the atmospheric pressure anomalies are different in these three seas, whereas those of the air-temperature anomalies are similar. Here, the analysis is extended to global coverage data for all the parameters. The spectral analysis and the principal component analysis (Jolliffe 1986) are used to identify the main components of the variability of each field, linear regression and canonical correlation analysis (Bretherthon et al., 1992) to study the coupled variability of the fields. In Section 2 the choice of the investigated parameters, the data used and the common pre-processing step are discussed. Sections 3 and 4 present methods and results of the single field and of the coupled variability analysis. The accuracy of the models constructed from the first components of the statistical methods to represent and to predict the sea level variability in the Mediterranean Sea is assessed in Section 5.

2. Parameters and data

2.1 Parameters selection

The sea surface height is a depth-integrated quantity that depends on the temperature and salinity structure of the water column, the baroclinic contribution, and on the external atmospheric forcing, the depth-independent barotropic contribution. For the selection of the atmospheric-oceanic parameters, the physical factors affecting the sea level at low and medium frequencies and the regional characteristics of each sea are considered. The sea level changes in the Mediterranean Sea are mainly due to evaporation, thermal expansion and inflow from and outflow to the Atlantic Ocean. Relevant variations in North Sea are wind-induced, the tidal motion is a dominant feature in its southern part, which is a shallow water region (Otto et al., 1990). Changes in sea level of the Baltic basin are primarily due to the river inflow in the north-eastern part of the basin and to the inflow from and outflow to the North Sea, the wind stress is the most important forcing process (Ekman 1998). The Mediterranean Sea and the Baltic Sea are semi-closed seas, whereas the North Sea is more open to the Ocean.

The sea surface temperature, the atmospheric air-pressure and the wind speed are the parameters investigated here together with the sea surface height. Their fields contribute to the ocean-atmosphere interaction and are directly and indirectly related to each other. Some of these parameters are used in the computation of the geophysical corrections to the altimetric sea surface heights: the wind speed for the sea state bias, the atmospheric pressure for the dry tropospheric and for the inverted barometer corrections. Of course, if the correction made is not perfect, one may be introducing into the measurements a wrong dependence upon one of the fields. In the case of the inverted barometer correction, for example, one assumes an isostatic response to pressure loading, i.e. a static and instantaneous response of the sea level to an atmospheric pressure variation. Usual geophysical environmental corrections, as the inverted barometer and the ocean tide corrections, have to be applied in the selected areas with caution, the first due to the quasi-lake condition of Mediterranean Sea and Baltic Sea (LeTraon and Gauzelin, 1997), the second due to the presence of shallow water regions, as in the south-eastern part of the North Sea (Andersen 1999). For this reason, the SLA fields with and without application of the inverted barometer correction are analysed in the Mediterranean Sea and in the Baltic Sea.

2.2 Data description

Three of the parameters under investigation are measured directly from remote sensing, they are the sea surface height, the sea surface temperature and the wind speed. A period of five years, from October 1992 to September 1997, is investigated. Sea surface heights w.r.t. the T/P reference ellipsoid (AVISO GDR-MS, 1996) are obtained at 1/sec sampling from the first 183 cycles of the T/P Geophysical Data Records (GDR). The corresponding wind speed is contained in the GDR, the atmospheric air-pressure value is computed from the dry-tropospheric correction contained in the GDR using the relationship:

$$P_{atm} = \frac{Dry_{corr}}{-2.277[1. + 0.0026 \cos(2\phi)]} \quad (\text{F-07-1})$$

where ϕ is the latitude of the sub-satellite point. Eq. (F-07-1) reconstructs the pressure data value used to compute Dry_{corr} , which was determined from numerical model outputs computed every six hours from the European Centre for Medium Range Weather Forecasting (ECMWF). Thus, the atmospheric air-pressure is available at the same spatial and temporal

sampling of sea surface height and wind speed data (1/sec sampling), the real sampling depending on the ECMWF pressure data. Monthly sea surface temperatures are available from July 1991 to March 1996 in 0.5 x 0.5 degrees grids computed from ATSR ERS data (Murray 1995). The overlapping of the sea surface temperature with the other three fields occurs during the period from October 1992 to March 1996.

2.3 Data pre-processing

The altimeter measurements are corrected for the dry and wet tropospheric, ionospheric, inverted barometer, sea state bias, solid tide, loading tide, polar tide and ocean tide effects. The global ocean tidal model FES95.2.1 (LeProvost et al, 1994) performs quite well in the Mediterranean Sea, but it is not defined in the Baltic Sea and it does not contain shallow water constituents, which are relevant in the southern part of the North Sea. A reference surface, the mean-tide geoid corresponding to the geopotential model EGM96 (Lemoine et al 1997) is subtracted from the corrected sea level heights, its choice does not influence the sea level variability results as it is constant in time. The height difference is called sea surface dynamic topography (SSDT) height.

The spectral and the statistical analysis are applied to data gridded in time and space with a monthly interval and a grid spacing of 0.5 degrees. The monthly and spatial average acts as a low-pass filter to the data. The sea level height, the air-pressure and the wind-speed data corresponding to each month are interpolated to the nodes of the grid by a Gaussian weighted average method (Nerem et al. 1994). The half weight parameter is chosen to be equal to 1 and the search radius equal to 3 degrees, to ensure that a pair of ascending and descending T/P arcs contributes to each node value. The node is considered if the data time-series has no interruption. Subtracting the mean at each node, we obtain an anomaly time-series field $s(p, n)$, where p is the space index and n is the time index, for each of the parameters: sea level anomaly (SLA), sea surface temperature anomaly (STA), air-pressure anomaly (APA) and wind speed anomaly (WSA). The number of grid points is about 1000 in the Mediterranean Sea, 400 in the North Sea and 200 in the Baltic Sea. The root mean square (rms) of the SLA gridded data gives an estimation for the magnitude of the sea level variability at medium time scales. It is between 5 and 10 centimetres in the Mediterranean Sea, with maximum in the eastern basin, between 4 and 22 centimetres in the North Sea, with maximum in the southern part, between 11 and 18 centimetres in the Baltic Sea, with maximum in the central and eastern parts.

The single field analysis is performed for the SLA, WSA and APA fields from October 1992 to September 1997, for the STA field from July 1991 to March 1996. The correlation of STA with the other fields is investigated over three years, from April 1993 to March 1996.

3. Single field analysis

The variability of the fields is due to the interaction of components of different spatial scales and temporal frequencies, which are superposed to a noise component and exhibit stationarity or non-stationarity in their statistics. The identification of the main components of the variability, the analysis step, consists in finding the coefficients corresponding to a given set of basis functions. We consider two methods: the spectral analysis and the principal component analysis. In the first, the basis functions of the model are chosen a priori, whereas the second uses a data-adaptive basis set.

3.1 Spectral Analysis

A one-dimension spectral analysis is performed both on the SLA, STA, APA and WSA fields averaged over each sea and on each retained grid node of the SLA field. The analysis of the averaged fields gives the principal spectral characteristics of the four fields, the grid analysis gives the regional distribution of the sea level variability. The analysis is performed in two steps. At first, the frequencies of the dominant constituents, i.e. of the components which have the higher spectral power, are determined in a least-squares spectral analysis method through the computation of the Lomb periodogram spectral estimate (Lomb 1976, Press et al. 1992). Once determined the frequencies corresponding to the first four peaks having the highest power, their amplitudes and phases are evaluated, together with a linear term, in a least-squares harmonic fit. In the analysis of monthly data over five years, the number N of time points is 60, the lowest independent frequency f_{min} is 0.2 cycles per year (cpy), f_{max} is 6 cpy. The Lomb periodogram of the four spatially averaged monthly fields is shown in Fig. F-07-1.

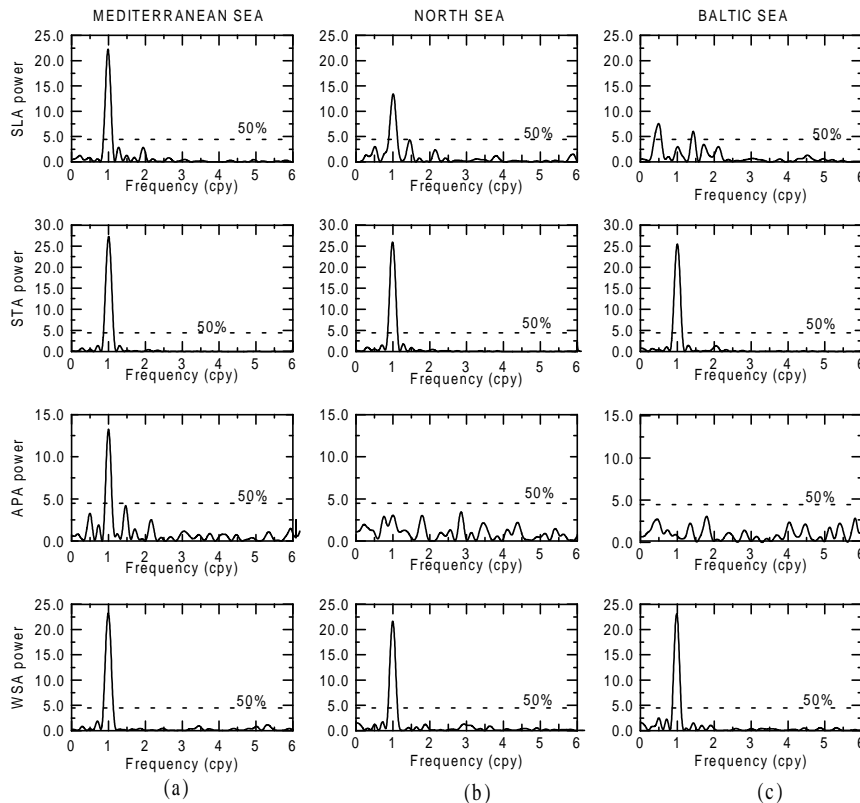


Figure F-07-1: Lomb normalized periodogram and 50% significance of SLA, STA, APA WSA fields in Mediterranean Sea (a), North Sea (b) and Baltic Sea (c)

The parameters STA and WSA have a dominant annual period, while the spectral characteristics of the SLA and APA fields are different in the three seas. For SLA, in both the Mediterranean and in the North Sea, the power of the annual signal is dominant and above the 99% confidence level, while in the Baltic Sea the dominant peak has a two year period and all peaks have a low confidence level. For APA, the annual signal is dominant in the Mediterranean, while in the North Sea and in the Baltic Sea the spectrum presents several peaks, all below the 50% confidence.

Tab. F-07-1 gives amplitudes, periods, phases and linear drifts. The SLA estimated trend is positive in the Mediterranean Sea and in the North Sea and negative in the Baltic Sea. The

Table F-07-1: Period, amplitude and phase of the first four spectral components and linear trend of the SLA, STA, APA and WSA fields averaged over each sea.

	P_1	A_1	φ_1	P_2	A_2	φ_2	P_3	A_3	φ_3	P_4	A_4	φ_4	Trend
SLA	(y)	(mm)	(deg)	(mm/y)									
Med	1.01	74.1	0.74	0.78	9.4	0.65	0.52	22.4	0.34	0.67	8.1	0.44	7.9 ± 2.0
Nse	0.99	61.8	0.84	0.68	31.7	0.05	1.97	27.2	0.11	0.47	23.7	0.02	3.5 ± 3.0
Bal	2.02	94.5	0.10	0.70	74.4	0.70	0.58	56.1	0.57	0.47	58.0	0.05	-10.0 ± 7.6
STA		(C°)		(C°/y)									
Med	0.99	5.7	0.64	1.41	0.1	0.13	0.77	0.1	0.15	3.60	0.4	0.62	0.1 ± 0.05
Nse	1.01	4.4	0.63	0.78	0.2	0.42	1.42	0.2	0.38	3.33	0.7	0.32	0.01 ± 0.07
Bal	1.00	7.4	0.61	0.77	0.3	0.29	0.49	1.6	0.1	1.40	0.2	0.40	-0.22 ± 0.11
APA		(mb)			(mb)			(mb)			(mb)		(mb/y)
Med	1.00	2.6	0.01	0.68	1.3	0.03	2.02	1.1	0.08	0.46	1.1	0.03	-0.08 ± 0.16
Nse	0.35	2.9	0.10	1.00	2.7	0.51	0.56	2.7	0.20	1.32	2.7	0.28	0.5 ± 0.4
Bal	0.56	2.3	0.23	2.20	2.1	0.87	0.25	2.0	0.12	0.74	1.8	0.17	0.59 ± 0.38
WSA		(m/s)			(m/s)			(m/s)			(m/s)		(m/s/y)
Med	1.01	1.4	0.00	1.43	0.07	0.16	0.29	0.3	0.20	3.51	0.1	0.14	0.02 ± 0.05
Nse	1.00	2.7	0.01	1.39	0.3	0.91	0.34	0.7	0.03	1.99	0.3	0.9	-0.17 ± 0.09
Bal	1.01	2.3	0.96	2.00	0.5	0.10	1.4	0.2	0.01	0.70	0.4	0.02	-0.13 ± 0.06

estimated accuracy of the trend is generally higher in the Mediterranean Sea than in the other seas. Due to the relatively short time period of the input data, the trend is interpreted as interannual variability. In the Mediterranean Sea, STA has a positive trend, while the trends of APA and WSA are not significant. In the North Sea, STA has no significant trend, APA a slightly significant positive trend and WSA a negative one. In the Baltic Sea, STA has a negative trend, APA a positive trend and WSA a negative trend.

The one-dimensional spectral analysis of the SLA grid nodes gives the geographical dependence of the SLA field. Fig. F-07-2 shows the period, the amplitude of the dominant spectral component and the trend.

The amplitude of the periodic component is geographically dependent. In the Mediterranean Sea the first dominant component has an annual period everywhere, the second and the third dominant components have periods of 280 and 180 days in the western and southern basins, while in the eastern and northern basins the opposite occurs. The amplitude of the annual component, quite larger than the amplitude of the other components, is generally smaller than 8 centimetres in the Western basin and larger in the central and eastern basins, with a maximum of 12 centimetres south-east of Crete. This location corresponds to the Irapetra anticyclonic gyre, which is a high energetic gyre with a strong annual cycle (Larnicol et al. 1995). In the North Sea the dominant component has an annual period except in the south-eastern part, where the period is about two years. As this is a shallow water region, the use of a regional ocean tide model could improve the results. In the Baltic Sea the dominant spectral component of SLA has a two year period, the maximum amplitude of 12 centimetres is reached in the eastern part of the sea. The uncertainty of the estimated trend is low in the Mediterranean Sea and quite large in the Baltic Sea. The largest range for the trend occurs in the Mediterranean Sea, where the trend is mostly positive with higher values in the eastern than in the western part of the basin. The largest positive trend (28 mm/year) occurs at the Irapetra Gyre and the largest negative trend west of Greece (-15 mm/year), another relatively high negative trend (-5 mm/year) is found in the Balearic basin. In the North Sea, the drift is lower, between ± 5 mm/year in most of the area, and of the order of its uncertainty. In the Baltic Sea the drift is highly negative, up to -15 mm/year, in the northern central part and positive, up to 5 mm/year, in the southern part. As in the averaged study, the trend in SLA is interpreted as interannual sea level change.

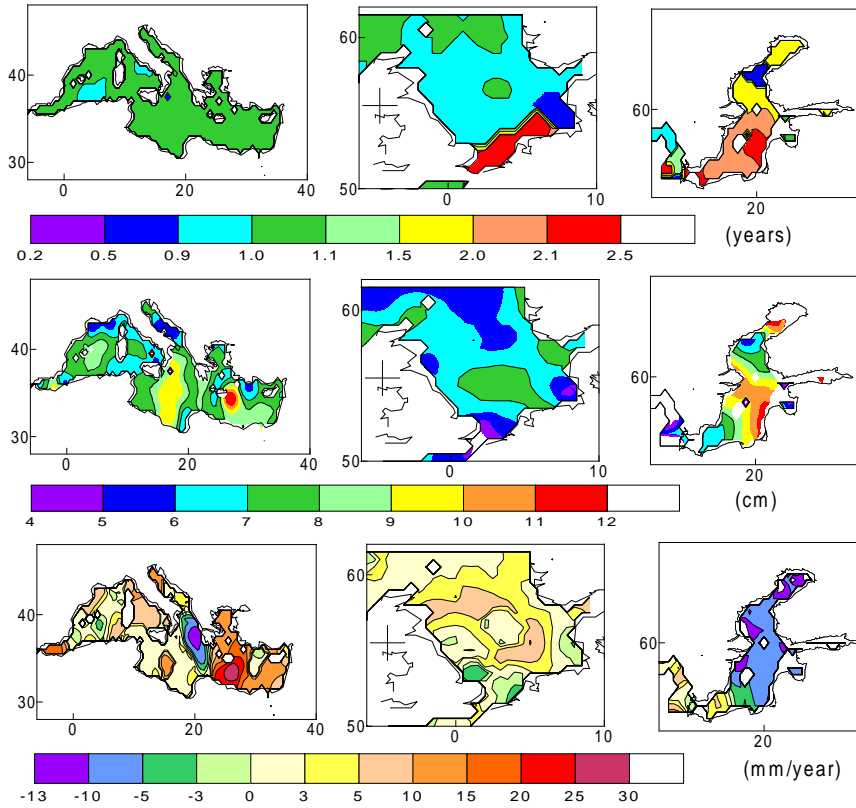


Figure F-07-2: Dominant periods (years), dominant amplitude (centimetres) and trend (millimeter/year) of the T/P SLA field estimated by spectral analysis in the interval 1992-1997.

3.2 Principal Component Analysis

The Principal Component Analysis (PCA) method (Preisendorfer 1988) expands the signal in terms of basis functions that concentrate most of the variance into a small number of components. The dataset $s(p, n)$ is separated into a set of orthonormal spatial patterns \mathbf{e}_k , which define the spatial structure, and the corresponding orthogonal temporal coefficients $a_k(t)$, which define the temporal evolution. The relationship between data, spatial and temporal patterns are given by the synthesis and analysis formulas that, restricted to the first K Empirical Orthogonal Functions (EOF) modes, are

$$\begin{cases} \mathbf{s} = \mathbf{e}\mathbf{a}, \\ \mathbf{a} = \mathbf{e}^T \mathbf{s} \end{cases} \quad (\text{F-07-2})$$

where $\tilde{\mathbf{s}}$ is the $P \times N$ matrix of the synthetic data reconstructed using the K modes, \mathbf{a} a $K \times N$ matrix and \mathbf{e} a $P \times K$ matrix. In our application the number of space samples P is bigger than the number of time samples N .

A method with minimum operation counts and subroutines of the *Lapack* mathematical library (Lapack 1995) are used. The PCA decomposition is obtained by the Singular Value Decomposition (SVD) of the data matrix s

$$\mathbf{s} = \mathbf{l}\mathbf{\Lambda}\mathbf{r}^T \quad (\text{F-07-3})$$

the left singular vectors \mathbf{l} give the spatial patterns and $\mathbf{r}^T \mathbf{\Lambda}$ gives the temporal coefficients a (Kelly 1988). To make the choice of the spatial eigenvector \mathbf{e}_k unique for each mode k , its biggest component for that mode is chosen to be positive. The input data are normalized to

standardized anomalies, by dividing each point time-series by its standard deviation, and the output spatial vectors are normalized to the maximum value for each mode k . The normalisation of the data to standardized anomalies ensures that regions with high variance do not dominate the SVD and focuses the analysis towards large-scale coherent patterns, rather than local high amplitude variability. The normalisation of each spatial vector to the maximum value for each mode k is preferred for the graphical representation.

The cumulative fraction of total anomaly variance (CVF) indicates how successful the PCA method is in representing the observed variance using a small number K of dominant modes

$$CVF_K = \frac{\sum_{k=1}^K \lambda_k}{\sum_{k=1}^{K_r} \lambda_k} = \frac{\sum_{i=1}^P \sum_{l=1}^N \tilde{s}(i, l)^2}{\sum_{i=1}^P \sum_{l=1}^N s(i, l)^2} \quad (\text{F-07-4})$$

where $K_r = \min(P, N - 1)$ is the maximum number of modes, which coincides with the rank of the variance-covariance matrix ss^T . The CVF accounted for by the first six modes of the four fields is shown in Fig. F-07-3.

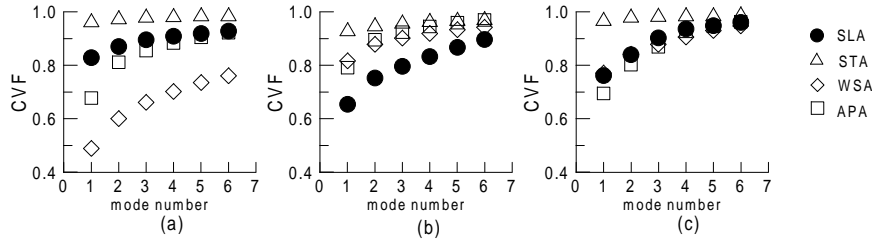


Figure F-07-3: Cumulative Variance Fraction (CVF) accounted by the first six modes of the SLA, STA, WSA and APA single field PCA decomposition in the Mediterranean Sea (a), North Sea (b) and Baltic Sea (c).

The convergence of the eigenfunctions is rapid, the quicker convergence occurs for STA. The first four modes account for more than 85% of the total variance in all cases, with exception of SLA in the North Sea and of WSA in the Mediterranean Sea. The CVF of the first EOF is more than 75% almost everywhere, therefore a strong relationship between the time variability of the first temporal coefficients and that of the original data is expected. The temporal coefficients and the spatial patterns of the first three EOFs of the SLA, STA and WSA fields are given in Figs F-07-4, F-07-5, F-07-6 respectively for the Mediterranean Sea, North Sea and Baltic Sea.

Fig. F-07-7 shows the EOFs of the APA fields. The first mode of each field correspond to a variability mode with all points in phase. The other modes show small scale phenomena with points out of phase.

In the Mediterranean Sea, the first eigenvector of SLA, which account for 83.6% of the variance of the data, primarily represents the annual cycle. On the corresponding time series, peaks occur in Fall. The temporal pattern of the second eigenvector of SLA (4.1% of the variance) has almost an annual period with maximum in late Summer and much smaller amplitude that for the first EOF. The relevant spatial feature of the second EOF occurs in the Western Mediterranean Sea, south of the Balearic Islands. The third mode (2.5% of the variance) has a negative temporal trend in the eastern Ionian basin near Greece. The first mode of STA accounts for almost all the variance of the data (95.8% of the variance) and has an annual period with the maximum in August. The second mode (1.4% of the variance) has an annual period with the maximum in late Summer and indicates a different phase in the north-western and in the south-eastern parts of the basin. The first mode of WSA accounts for only 48.9% of the variance, has an annual period with the maximum in Winter, its spatial

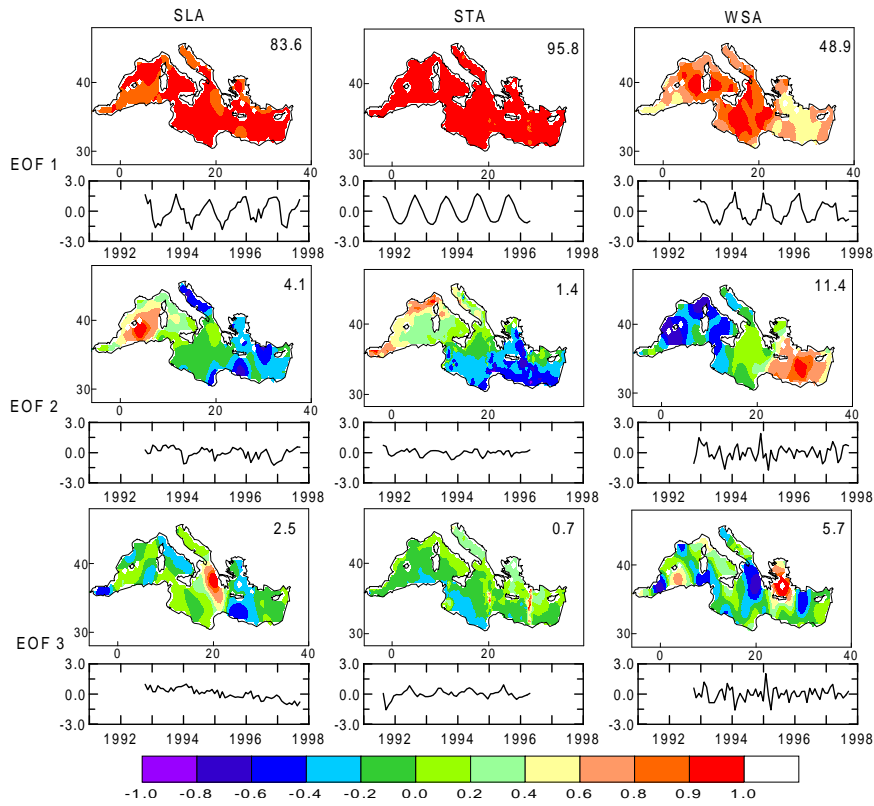


Figure F-07-4: First three spatial and temporal PCA patterns of SLA, STA and WSA in the Mediterranean Sea with fraction of the total variance. Anomalies are standardized and patterns normalized to the maximum absolute value for each mode

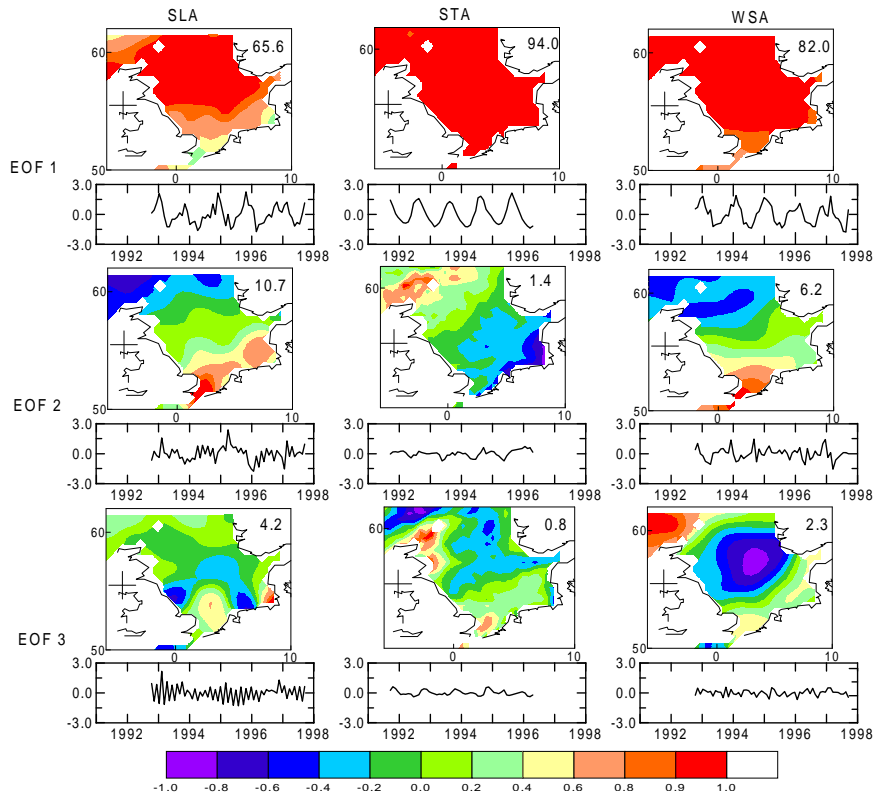


Figure F-07-5: as in Fig. F-07-4 for the North Sea

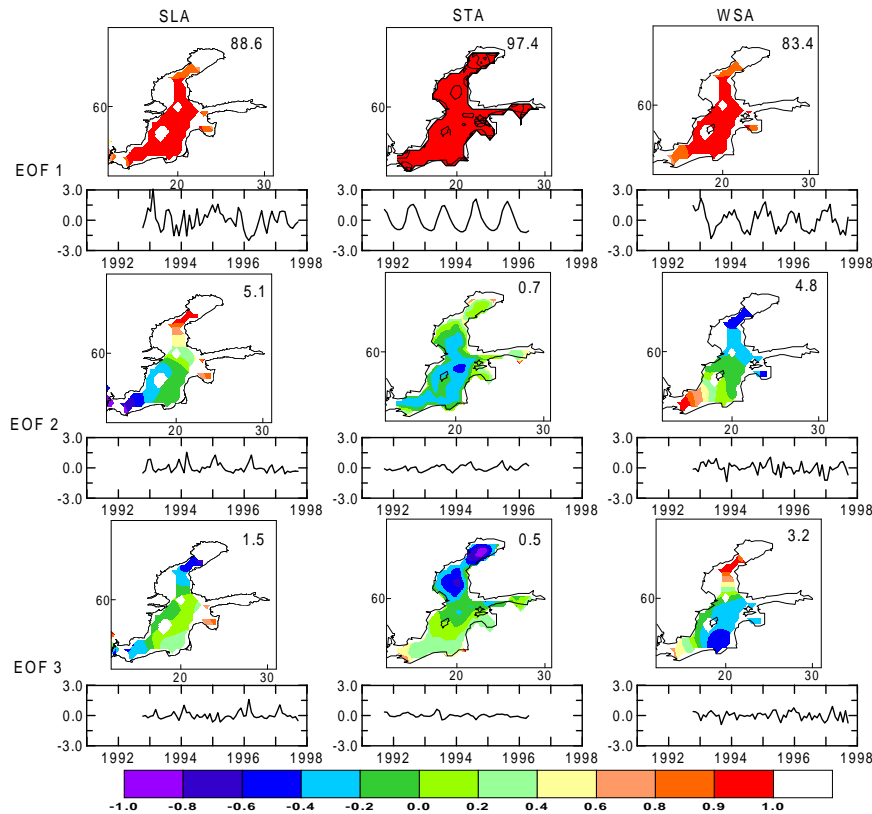


Figure F-07-6: as in Fig. F-07-4 for the Baltic Sea

maxima occur in the Gulf of Lion and in the Ionian Sea. The second mode accounts for 11.4% of the variance and shows a high frequency signal and a phase difference between the western and eastern basins. The third mode (5.7%) has a high frequency signal in the Egean Sea and south of the Balearis Islands. The first and second mode of APA (67.8% and 13.6% of the variance, cf. Fig. F-07-7) have an annual period with the maximum in Winter. In the second, the western and the eastern basins have an opposite phase. The third mode (4.4% of the variance) shows higher frequency and a spatial maximum in the Ionian Sea.

In the North Sea, the SLA spatial eigenvectors show a different variability in the southern and northern parts of the sea. The first eigenvector (65.6% of the variance) represents, as in the Mediterranean Sea, primarily the annual cycle and shows the smallest amplitudes in the southern part of the sea. The second mode accounts for a considerable part of the variance (10.7% of the variance) and presents an annual signal with superposed higher frequency components, the corresponding spatial pattern shows an opposite phase in the southern and northern basins. The temporal pattern of the third mode (4.2% of the variance) has an higher frequency. We attribute part of the signal in the southern North Sea to the tidal model used, which does not account for the shallow water tidal constituents. As in the Mediterranean Sea, the first mode of STA, accounts for almost all the variance of the data (94.0%), it has an annual period with the maximum in August. The second and the third mode (1.4% and 0.8% of the variance) have annual periods with the maximum in late Summer and indicate a difference in the phase of the southern and northern parts of the basin. The first mode of WSA (82% of the variance) has an annual period with the maximum in Winter, the spatial minimum is in the southern part of the Sea. The second mode (6.2%) shows a high frequency signal and a phase difference between the northern and southern basins. The third mode (2.3%) shows a higher frequency signal and a phase difference between the central part of the

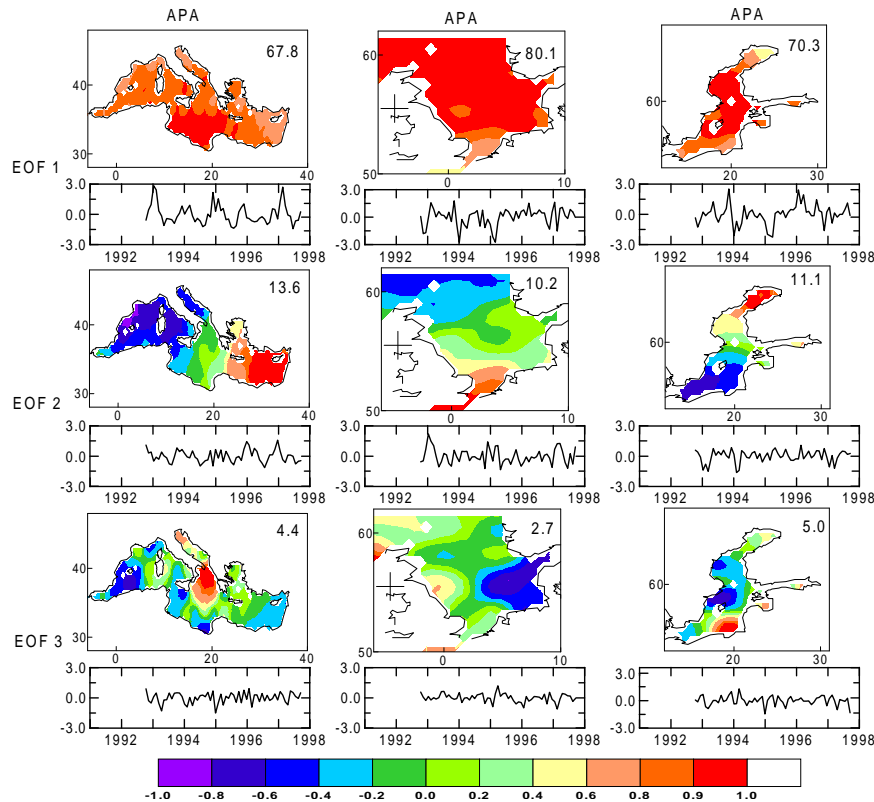


Figure F-07-7: First three spatial and temporal PCA patterns of APA in Mediterranean Sea, North Sea and Baltic Sea with fraction of the total variance. Anomalies are standardized and patterns normalized to the maximum absolute value for each mode

North Sea and the ocean. The first and second eigenvector of APA (80.1% and 10.2% of the variance) have irregular temporal patterns. An opposite phase appears in the southern and northern basins in the second mode. The third mode (2.7% of the variance) shows a spatial maximum in the eastern coast.

In the Baltic Sea, the first mode of SLA (88.6% of the total variance) does not have a clear annual cycle, as in the previous two regions. The maximum variability occurs in the central-eastern part of the sea. The second mode (5.1% of the variance) shows an opposite phase in the northern and southern parts, with an almost annual period with extreme in Winter. Higher order patterns are more complex. The first mode of STA (97.4% of the variance) has an annual period with the maximum in August. The second mode explains 0.7% of the variance. The first mode of WSA (83.4% of the variance) has an annual period with the maximum in Winter. The second mode (4.8%) shows a high frequency signal and a phase difference between the northern and southern basins. The first and the second mode of APA (70.3% and 11.1% of the variance) have irregular temporal patterns. In the second mode an opposite phase appears in the southern and the northern basins. For the SLA field comparable results have been obtained by Wroblewski (Wroblewski 1992) using tide gauge stations observation from 1891 until 1970 and by Heyen (Heyen *et al.* 1996) using observations at 23 tide gauge stations from 1899 to 1987.

4. Correlation between parameters

The coupled variability of two datasets $\mathbf{s}(p, n)$ and $\mathbf{z}(p, n)$ is investigated by analysing the temporal correlation of the time-series at the same spatial points and by applying statistical

techniques to identify the coupled pairs of spatial patterns and temporal coefficients that best explain the coupled variability of the two fields. The coupled variability of the SLA field and APA and WSA fields is investigated over five years, between October 1992 and September 1997, whereas the coupled variability of the SLA and STA fields is investigated over three years, between April 1993 and March 1996.

Simple correlation

The Pearson correlation coefficient r_c is computed at each grid point P between two time-series $s_P(t)$ and $z_P(t)$ to obtain the Pearson correlation map

$$\mathbf{hc} = \mathbf{r}_c [\mathbf{s}(t), \mathbf{z}(t)] = \frac{\langle \mathbf{s}(t), \mathbf{z}(t) \rangle}{\langle \mathbf{s}^2(t) \rangle^{1/2} \langle \mathbf{z}^2(t) \rangle^{1/2}} \quad (\text{F-07-5})$$

where the angular brackets $\langle \cdot, \cdot \rangle$ denote the inner product and the spatial index is omitted in indicating the analysed time dependency. Fig. F-07-8 shows the Pearson correlation maps corresponding to sea level heights corrected for the inverted barometer effect. In the Mediterranean Sea the SLA and STA fields are positive correlated, the correlation between the SLA and WSA fields is not significant and a negative correlation is observed between SLA and APA in the western part of the basin. In the North Sea the SLA and WSA fields are positive correlated in the north-western part of the basin, while both the correlations between SLA and STA and between SLA and APA are low. In the Baltic Sea the SLA and WSA fields are positive correlated in the eastern part of the basin, SLA and APA are negative correlated, while the correlation between the SLA and STA fields is not significant. The correlation between SLA and APA is of course higher if the inverted barometer correction is not applied to the sea level heights (not shown). In case of a perfect isostatic response, the residual correlation between APA and SLA corrected for the inverted barometer effect is low. The significant negative correlation observed in Fig. F-07-8 between SLA and APA in the Western Mediterranean Sea and in the Baltic Sea confirms that the response of the sea level overshoots a simple inverted barometer at subsynoptic frequencies in semi-closed basins (LeTraon and Gauzelin, 1997), (Pasarić and Orlic, 1992). Fig. F-07-8 is compared in the next section to the correlation maps obtained from the statistical methods (Fig. F-07-9).

Statistical Analysis of two fields

The statistical methods identify sequential pairs of patterns \mathbf{p}_k and \mathbf{q}_k in the two fields \mathbf{s} and \mathbf{z} , which fulfill an optimality criterion. While in the PCA the patterns are orthogonal and therefore appear in both the synthesis and in the analysis formula, in the methods involving more than one dataset the spatial vectors \mathbf{u} of the analysis equation, called weight vectors, do not necessarily coincide with the spatial patterns \mathbf{p} of the synthesis equation. It is :

$$\begin{cases} \tilde{\mathbf{s}} = \mathbf{p}\mathbf{a} \\ \mathbf{a} = \mathbf{u}^T \mathbf{s} \end{cases} \quad (\text{F-07-6})$$

which corresponds to eq. (F-07-2).

Two types of correlation maps, the homogeneous and the heterogeneous correlation maps \mathbf{ho}_k and \mathbf{he}_k (eqs. (F-07-7) and (F-07-8)), are generated from the spatial and the temporal patterns of the first (\mathbf{p}_k, a_k) and of the second (\mathbf{q}_k, b_k) fields. They are the vectors of correlations between one field and the k-th temporal coefficients of the same field (homogeneous

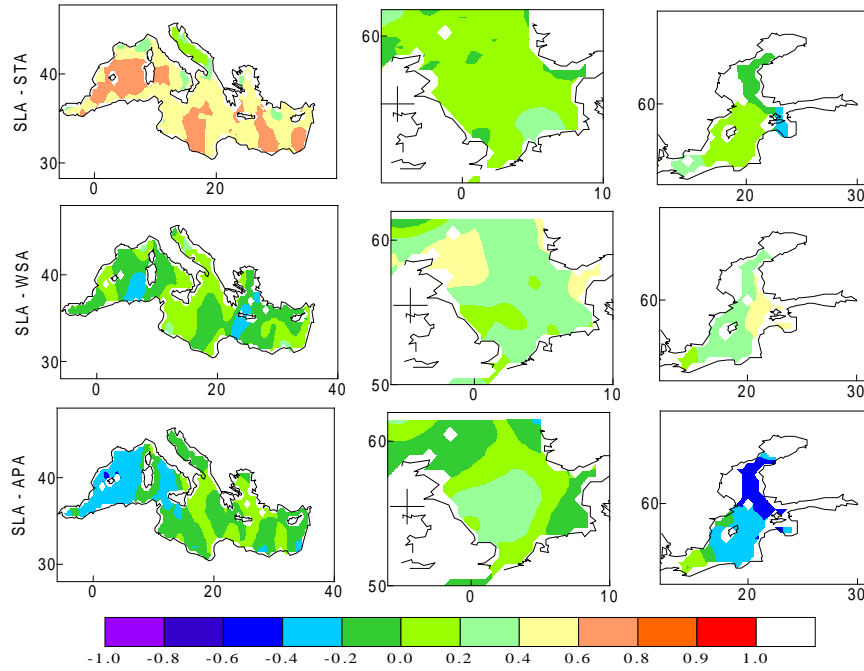


Figure F-07-8: Pearson correlation maps of SLA-STA, SLA-WSA and SLA-APA

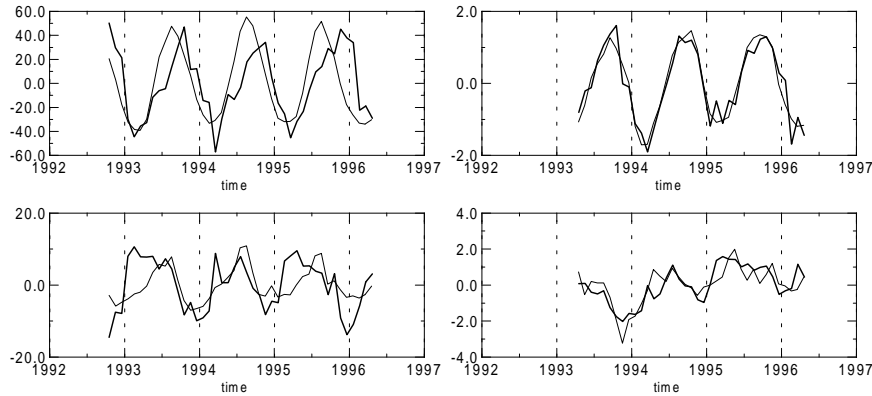


Figure F-07-9: First (above) and second (below) expansion coefficients pairs of SLA (dark) and STA in the Mediterranean Sea corresponding to the SVD (left) and PCA-CCA (right) decomposition

maps) and of the other field (heterogeneous maps).

$$\mathbf{h}\mathbf{o}_{\mathbf{k}} = \mathbf{r}_{\mathbf{k}} [\mathbf{s}(t), a_k(t)] = \frac{\langle \mathbf{s}(t), a_k(t) \rangle}{\langle \mathbf{s}^2(t) \rangle^{1/2} \langle a_k^2(t) \rangle^{1/2}} \quad (\text{F-07-7})$$

$$\mathbf{h}\mathbf{e}_{\mathbf{k}} = \mathbf{r}_{\mathbf{k}} [\mathbf{s}(t), b_k(t)] = \frac{\langle \mathbf{s}(t), b_k(t) \rangle}{\langle \mathbf{s}^2(t) \rangle^{1/2} \langle b_k^2(t) \rangle^{1/2}} \quad (\text{F-07-8})$$

Two methods are considered here, they differ in the choice of the representational basis. In the first method, the pairs of temporal coefficients explain as much as possible of the mean-squared temporal covariance between the two fields, in the second method they have the maximum correlation coefficient. The first method, called here Singular Value Decomposition (SVD), is similar to the PCA of one single field and consists in computing the SVD of the covariance matrix C_{sz} between the two fields to obtain left and right singular vectors \mathbf{l}, \mathbf{r} and the matrix Θ of singular values θ_k

$$\mathbf{C}_{sz} = \mathbf{l}\Theta\mathbf{r}^T \quad (\text{F-07-9})$$

The squares of the singular values θ_k gives the total covariance explained by the pair of patterns of index k , the right and the left vectors are the spatial patterns, and, as they are orthogonal, patterns and weight vectors coincide. The temporal coefficients are obtained by projecting the data onto the spatial patterns, the heterogeneous correlation maps are proportional to the spatial patterns. The relevant relationships are:

$$\begin{cases} \mathbf{p}_k = \mathbf{u}_k = \mathbf{l}_k, \\ \mathbf{q}_k = \mathbf{v}_k = \mathbf{r}_k, \\ \mathbf{r}[\mathbf{s}(t), a_k(t)] = \frac{C_{ss}}{\langle a_k^2(t) \rangle} \mathbf{p}_k, \\ \mathbf{r}[\mathbf{s}(t), b_k(t)] = \frac{\lambda_k}{\langle b_k^2(t) \rangle} \mathbf{p}_k \end{cases} \quad (\text{F-07-10})$$

where C_{ss} is the variance matrix of the first field. In the second method, called Canonical Correlation in PCA basis method (PCA-CCA) (Bretherton et al. 1992), the data are first prefiltered by projection onto a leading subset of EOFs before application of the classical CCA method (Nicholls 1987). The preliminary temporal coefficients are computed by SVD of the single fields and then standardized obtaining α_k and β_k , where k is the index for the modes of the single field decomposition. Here, the first six modes are considered. The weight vectors \mathbf{u} , \mathbf{v} and the CCA canonical correlations ρ are computed by the SVD of the covariance matrix of α and β

$$\mathbf{C}_{\alpha\beta} = \mathbf{u}\Theta\mathbf{v}^T \quad (\text{F-07-11})$$

where Θ is the matrix of singular values ρ . In this case, the homogeneous correlation maps coincide with the patterns, while the heterogeneous correlation maps are proportional to the patterns. The relevant relationships are:

$$\begin{cases} \mathbf{a} = \mathbf{u}^T \alpha, \\ \mathbf{b} = \mathbf{v}^T \beta, \\ \mathbf{r}[\mathbf{s}(t), a_k(t)] = \mathbf{p}_k, \\ \mathbf{r}[\mathbf{s}(t), b_k(t)] = \rho_k \mathbf{p}_k \end{cases} \quad (\text{F-07-12})$$

The goal is to assess whether the paired patterns (\mathbf{p}, a) and (\mathbf{q}, b) are highly coupled and how well they explain the coupled variability of the two fields. For this scope, the significant parameters in the SVD method are the the cumulative variance fraction (CVF) and the cumulative squared covariance fraction (CSCF). The first (eq. (F-07-4)) quantifies the total amount of variance explained by the first K modes of each single field, the second quantifies the success of each mode in explaining the observed covariance matrix between the fields. The CSCF parameter is given by:

$$CSCF_K = \frac{\sum_{k=1}^K \theta_k^2}{\sum_{k=1}^{K_r} \theta_k^2} \quad (\text{F-07-13})$$

where θ_k are the singular values of the matrix C_{sz} (eq. (F-07-9)) and K_r is the maximum number of modes. The relevant parameters in the PCA-CCA method are the cumulative variance fraction (CVF) and the canonical correlation coefficients $r_k(a, b)$ between the canonical temporal coefficients a and b for a same mode k . The PCA-CCA canonical temporal coefficients for a given mode have the maximum correlation at zero-lag and their correlation coefficient is decreasing by definition, whereas the SVD temporal coefficients have the maximum correlation at different lags, as shown in Fig. F-07-10 for the coupled SLA and STA fields in the Mediterranean Sea. The fields are highly correlated if, for the first modes, the canonical

correlation coefficients, the CVF and the CSCF are near to 1. Fig. F-07-11 shows the relevant parameters for each of the two methods.

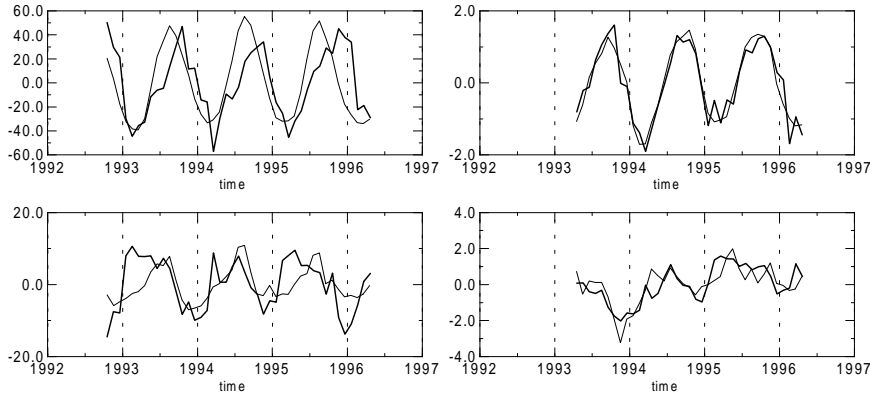


Figure F-07-10: Relevant parameters for the statistical analysis of coupled fields using SVD and PCA-CCA in the Mediterranean Sea (a), North Sea (b) and Baltic Sea (c). Parameters for the SVD are the Cumulative Variance Fraction (CVF) of each field and the Cumulative Squared Covariance Fraction (CSCF), parameters for the PCA-CCA are the CVF of each field and the correlation of the canonical temporal coefficients.

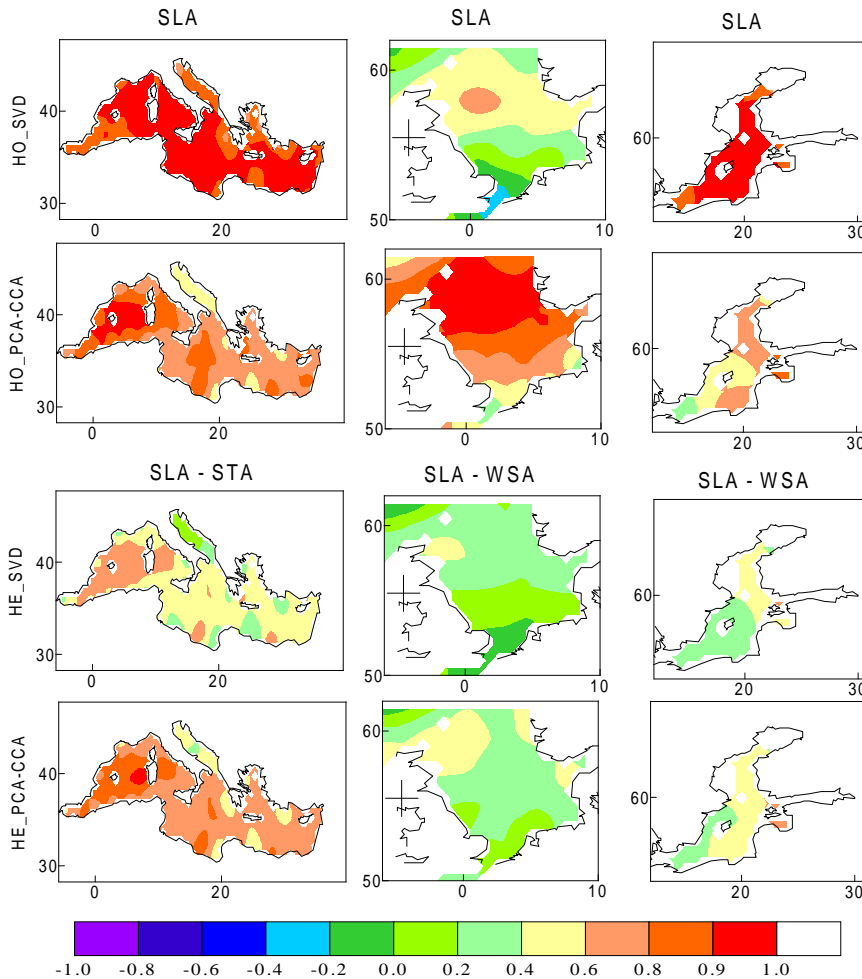


Figure F-07-11: First homogeneous correlation maps of the SLA field and its heterogeneous correlation maps with the 1st temporal coefficients of SLA in Mediterranean Sea and of WSA in North Sea and Baltic Sea, obtained by the SVD method and by the PCA-CCA method

The highest correlation is between the SLA and the STA fields in the Mediterranean Sea and between the SLA and the WSA fields in the North Sea and Baltic Sea. The results of the SVD SLA-STA analysis indicate a strong correlation between the fields in the Mediterranean Sea, as the first CVF of both SLA and STA fields is more than 0.8 and the corresponding CSCF is almost 1. The correlation between SLA and WSA is low in the Mediterranean Sea, as the first CSCF is 0.5 and the first CVF of both fields are low. The SVD SLA-WSA analysis shows a correlation of the SLA and of the WSA fields both in the North Sea and in the Baltic Sea, with a first CSCF near to 1 and values of the first CVF of both fields above 0.6, the first CVF of SLA is higher in the Baltic Sea (0.7) than in the North Sea (0.6). Also the PCA-CCA part shows a high correlation between the SLA and the STA fields in the Mediterranean Sea, with the correlation of the first canonical coefficients near to 1 and the CVF of the first modes above 0.6. The PCA-CCA analysis of the coupled SLA and WSA fields in the North and Baltic Seas indicates a lower correlation, with a correlation coefficient between the first canonical temporal coefficients of 0.6 in the North Sea and 0.75 in the Baltic Sea and a relatively low CVF for SLA (15% in the North Sea and 30% in the Baltic Sea). Fig. F-07-11 corresponds to sea level heights corrected for the inverted barometer effect. The correlation between APA and SLA is higher if the inverted barometer correction is not applied.

In the Mediterranean Sea, for example, the first canonical correlation coefficient given by the PCA-CCA analysis is 0.8 with the correction applied (top of Fig. F-07-11 and 0.9 without the correction (not shown)). Fig. F-07-9 gives the first heterogeneous and homogeneous correlation maps between the SLA field and the STA temporal coefficients in the Mediterranean Sea and between the SLA field and the WSA temporal coefficients in North Sea and in Baltic Sea. The PCA-CCA homogeneous correlation maps have values higher than the corresponding SVD maps only in the North Sea, whereas the PCA-CCA heterogeneous maps have values higher than the SVD maps for all the considered cases. The similarity between the first heterogeneous correlation map and the corresponding Pearson maps, indicates the ability of the first mode of the second field to represent the part of the variability of the second field which is coupled with the first field. The SVD method gives the most similar maps in the Mediterranean Sea and in the Baltic Sea, the PCA-CCA method in the North Sea.

5. Application in the Mediterranean Sea

The statistical methods described in Sections 3 and 4 are suitable to build a simple model for the sea level variability in the spatial and time intervals of the data, the two statistical methods described in Section 4 are also suitable to extrapolate the model outside the time interval. The Mediterranean Sea is chosen as test area because in this region the models constructed using the SLA field and the combined SLA and STA fields converge rapidly, i.e. the first few modes explain most of the variability. The first four modes of each model account for about 90% of the variance of the SLA field (Fig. F-07-3 and F-07-11). The first mode of both the PCA and the SVD models accounts for 80% of the variance, whereas the first mode of the PCA-CCA model accounts for 60% of it.

5.1 Data reconstruction

After the PCA, the SVD and the PCA-CCA decompositions, the SLA model is available in a simple form: as a linear combination of two-dimensional spatial grids in latitude and longitude and of temporal functions up to a given mode, as for the synthesis formula (eq. F-07-6). The sea level variability is reconstructed at any given location and time, within the

Table F-07-2: Accuracy of the sea level variability models.

Model	<i>RMSE</i> (cm)	<i>MAE</i> (cm)	<i>ME</i> (cm)
PCA (1992.7 - 1997.7)	1.85	1.38	1.d-5
PCA-CCA (1993.3 - 1995.8)	1.65	1.24	1.d-5
predicted PCA-CCA (1992.7 - 1996.3)	3.98	2.60	0.112

spatial and temporal period, by bi-linear spline interpolation of the spatial grids and simple interpolation of the temporal coefficients. As the input data have been centered and standardized, the mean spatial grids \mathbf{m} and the standard deviation spatial grids σ are accounted for to reconstruct the original data

$$\tilde{\mathbf{s}} = \mathbf{e}\mathbf{a}\sigma + \mathbf{m} \quad (\text{F-07-14})$$

and the sea level variability around its mean

$$\tilde{\mathbf{s}}_{\mathbf{v}} = \mathbf{e}\mathbf{a}\sigma \quad (\text{F-07-15})$$

The quality of the restituted model depends on the spatial and temporal spacing of the gridded data and on the number of modes considered. The standardized input field s_{st} is represented as a sum of the contribution from the considered k principal components and of a residual part \mathbf{R} .

$$\mathbf{s}_{st} = \mathbf{e}\mathbf{a} + \mathbf{R} \quad (\text{F-07-16})$$

If most of the variance of the data is explained by the first modes, few modes are sufficient to build a model for the variability. The accuracy of the SLA models is assessed by computing sea level height differences at dual crossovers between ERS and T/P and averaging the results over each ERS 35-day repeat cycle and over each 37-days sub-cycle of the ERS-1 geodetic phase. It is assumed that the sea level variability can be neglected when the difference between the crossover passes is less than 10 days. Two different kinds of crossover differences are considered: those corresponding to DXOs with this time-constraint (10 days) and those corresponding to DXOs without time-constraint and obtained from altimeter heights corrected by a SLA model. In the second case, DXOs between the complete set of ERS data and the T/P data corresponding to the first ERS-2 repeat-cycle (T/P cycles from 97 to 102) are considered. Fig. F-07-12 gives the averaged sea level height differences at DXOs both for the first case (full symbol) and for the second case with the SLA model formed by the first four modes of the PCA decomposition (empty symbol). The circles correspond to DXOs between ERS-1 and T/P, the triangles to DXOs between ERS-2 and T/P. Fig. F-07-13 represents the averaged sea level height differences at DXOs obtained in the first case (full symbol) and in the second case with the SLA model formed by the first four modes of the PCA-CCA decomposition (triangle). As the agreement between the mean DXO differences is within 2 centimetres, both the PCA and the PCA-CCA models represent the sea level variability in the Mediterranean Sea with a good accuracy. An alternative estimation for the model accuracy is obtained by comparing the original gridded observations and the corresponding model values. Two scalar measure of accuracy are the root mean square error (RMSE) and the mean absolute error (MAE). The first is the average squared difference between the model values and the observables, the second is the average of the absolute differences between the model values and the observables. The mean error (ME), which is the average difference between the model values and the observables, expresses the bias of the model (Wilks 1995). Tab. F-07-2 shows that both the PCA and the PCA-CCA models have an accuracy of around 2 centimetres, in agreement with the previous results. The time mean of the DXO differences provides an estimate of the relative bias between the two missions and its change in time an estimate of

the drift. Fig. F-07-12 shows a drift in the DXO differences between October 1992 and April 1995 and a relative bias both between ERS and T/P and between ERS-1 and ERS-2.

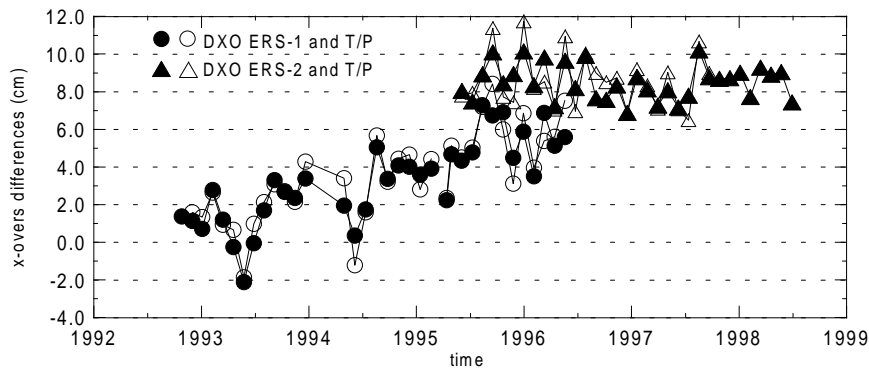


Figure F-07-12: Average over each ERS cycle (ERS-1 phases C and G, ERS-2) and sub-cycle (ERS-1 phases E and F) of sea level height differences at dual crossovers between ERS-1 and T/P and between ERS-2 and T/P with 10-day time difference constraint (full symbol) and with correction by the PCA sea level variability model (empty symbol)

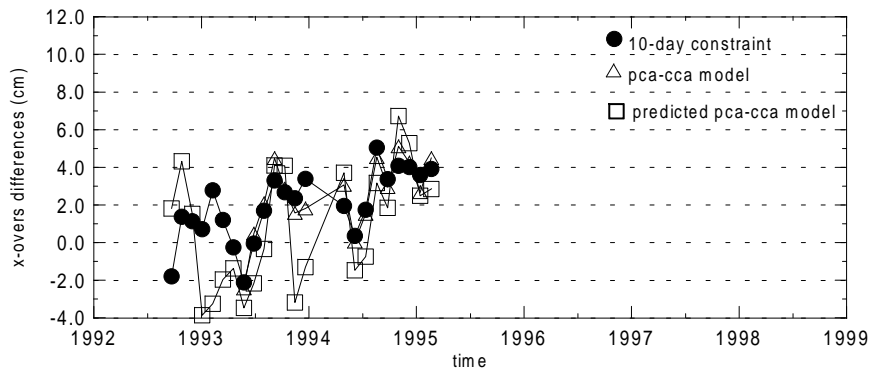


Figure F-07-13: Average over each ERS-1 cycle (phase C) and sub-cycle (phases E and F) of sea level height differences at dual crossovers between ERS-1 and T/P with 10-day time difference constraint (disk), with correction by the PCA-CCA sea level variability (SLV) model (triangle) and with correction by the PCA-CCA extrapolated SLV model (square)

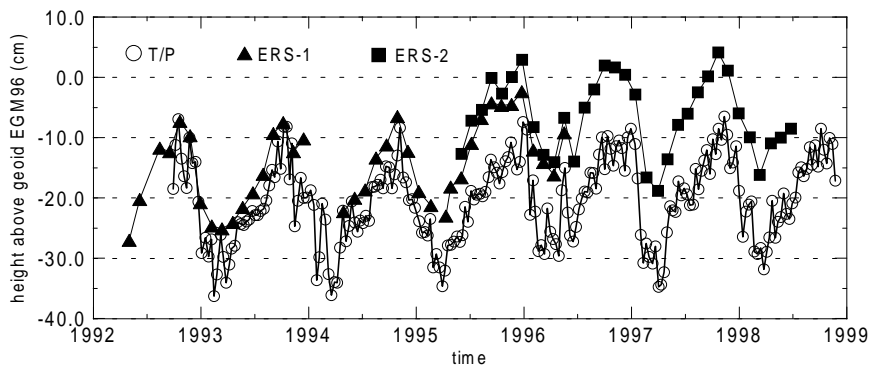


Figure F-07-14: Average over each ERS cycle (ERS-1 phase C and G, ERS-2) and subcycle (ERS-1 phase E and F) of sea level heights above the geoid EGM96 in the Mediterranean Sea

The relative bias between ERS-1 and ERS-2 amounts to about 2 centimetres in the Tandem mission phase (from Mai 1995 to April 1996), the relative bias between ERS and T/P is below 4 centimetres in 1993 and around 8 centimetres during the ERS-2 mission. To investigate the bias and drift behaviour, the average over each cycle of the sea level heights w.r.t. the geoid EGM96 is computed in the Mediterranean Sea for T/P, ERS-1 and ERS-2 independently. The patterns of the three satellites agree fairly well as far as the variability is concerned

and a relative bias and its change in time are evident (Fig. F-07-14). The observed drift is due to a change in the ERS data pre-processing in the estimation of the geophysical corrections, as discussed by Scharroo (Scharroo et al 2000). The averaged DXO differences between T/P and ERS in the Mediterranean Sea is estimated here to be about 8 centimetres during the ERS-2 mission. This quantity reflects, in addition to a relative bias, gravity-induced errors in the ERS orbit, assuming that T/P errors are much smaller, and coordinate frame offsets (Scharroo and Visser, 1998). The geographical dependence of the gravity-induced orbit errors explains the difference between the DXO average values obtained in the Mediterranean Sea and the global values (Stum et al, 1999). The relative bias observed between ERS-1 and ERS-2 is in agreement with the global analysis and may be due to differences in the instrumental characteristics.

5.2 Data prediction

A model to predict the SLA field using the STA field as the predictor is build from a modification of the PCA-CCA method. The PCA-CCA method is preferred to the SVD method, as the properties of the CCA temporal patterns, i.e. maximum correlation for the same mode and uncorrelation otherwise, simplify the computation of the predicted temporal patterns. Fig. F-01-3 shows the scheme of the predicted PCA-CCA method. The PCA-CCA coupled analysis over the overlapping period of the two fields identifies the spatial patterns \mathbf{p} and \mathbf{q} , their temporal coefficients a and b and the weight vectors \mathbf{u} and \mathbf{v} (eq. (F-07-12)). Given the STA field over a time interval longer than the interval of the SLA field, the extrapolated PCA-CCA model for the SLA field is build using the same spatial patterns of the PCA-CCA decomposition and the recomputed and extrapolated temporal patterns. For each mode k , the linear regression coefficients c_{kj} between the canonical temporal coefficients a_k and b_k are estimated fitting a polynomial of degree J in b_k to the a_k values:

$$a_k(t) = \sum_{j=0}^J c_{kj} b_k^j(t) \quad (\text{F-07-17})$$

The PCA single-field analysis of the complete STA field gives the new PCA temporal patterns β' . New canonical temporal coefficients b'_k for the complete STA field are estimated from the PCA-CCA weight vectors \mathbf{v} and from the PCA temporal coefficients β'

$$b' = v^T \beta' \quad (\text{F-07-18})$$

The new canonical temporal coefficients of the SLA field are obtained as:

$$a'_k(t) = \sum_{j=0}^J c_{kj} b_k^j(t) \quad (\text{F-07-19})$$

The SLA data are then predicted by the synthesis equation (see eq. (F-07-6)) using the new canonical coefficients a' and the previously determined spatial patterns \mathbf{p}

$$\tilde{s}' = \mathbf{p} a' \quad (\text{F-07-20})$$

The SLA and STA fields have an overlapping period of three years, from April 1993 to March 1996. As the complete STA field is available from July 1991 to March 1996, the PCA-CCA method is used to predict SLA data between July 1991 and March 1993. The first two modes are chosen to form the extrapolated PCA-CCA model. To assess the quality of the model,

two kinds of sea level differences at DXOs are computed between January 1993 and August 1994, averaged and compared as described in the previous session. The agreement between the averaged DXOs obtained with the 10-day time constraint and with the application of the PCA-CCA extrapolated model is within 4 centimetres (Fig. F-07-13). Tab. F-07-2 gives a similar value for the accuracy estimated as the square root of the average squared differences between the model and the observation pairs. The extrapolated PCA-CCA model is less accurate than the other two models, the PCA and the PCA-CCA models, but still acceptable. Its lower ability to represent the sea level variability is also seen in the rms of the DXO differences over each ERS cycle. The mean value of the rms is about 8.5 centimetres without model (case one), 10 centimetres with both the PCA and the PCA-CCA model (case two) and 12 centimetres with the extrapolated PCA-CCA model (case three).

6. Discussion and conclusions

Simple models for the sea level variability are constructed in the European seas using altimetry data and accounting for the correlation between sea level height and other oceanic and atmospheric parameters. They are single-mission models, as only altimetric sea level height data from the Topex/Poseidon mission are used. The ERS data are not included to avoid effects due to differences in the data pre-processing. The single- and coupled-fields analysis and synthesis are the main intermediate steps in this study. In the single-field analysis, both the spectral and the PCA statistical decompositions give the dominant components of the sea level height signal. The PCA decomposition is selected due to the simplicity of the resulting model, but also the spectral decomposition and the related trend estimation are of interest. The trend is interpreted as interannual variability, due to the relatively short interval of time analysed. Its estimated accuracy is low in the North Sea and in the Baltic Sea, higher in the Mediterranean Sea, where the highest trends coincide with persistent oceanic features and confirm the interpretation given above for the trend. Interesting is the comparison of the sea level variability of the three seas in terms of their spectral components: characteristic of the Mediterranean Sea is a dominant annual signal, with a same phase for all the points, whereas in the North Sea and the Baltic Sea the first spectral components have a similar power. Comparing the results from the two methods of analysis, a basic agreement is found. The greatest similarity is seen in the Mediterranean Sea, where both methods identify the main oceanographic features in agreement with numerical simulations of the interannual variability of the Mediterranean Sea upper ocean circulation (Pinardi et al. 1997). The main similarities are here shortly summarized. The energetic gyro southeast of Crete appears both in the trend analysis with a high trend (28 mm/year) and in the first PCA spatial pattern of the SLA not standardized data. A gyro south of the Balearic Islands appears in the trend analysis with a lower trend (5 mm/year) and in the second PCA spatial pattern of SLA. A structure in the eastern Ionian basin, along the Peloponnisos coast, appears in the trend analysis and in the third PCA spatial pattern of SLA, it could coincide with the anticyclonic Pelops gyro (Larnicol et al. 1995). In the North Sea and the Baltic Sea, the trends and the PCA spatial patterns do not correspond to oceanographic features, but to a different global behaviour in the northern and southern parts of the sea. In the coupled-fields analysis, significant correlations are identified by both the simple correlation and the SVD and PCA-CCA statistical methods. The Pearson, the first homogeneous and heterogeneous correlation maps are used in addition to the more usual indicators, i.e. the cumulative variance fraction, the cumulative squares covariance fraction and the correlation of the canonical temporal coefficients. The first homogeneous correlation map indicates how well the first mode of the model agrees with the data, the first heterogeneous correlation map indicates the correlation between the fields.

In the case of highly coupled fields, all maps approach the unity and the Pearson and the first heterogeneous maps are similar. Results from the SVD and the PCA-CCA method agree with each other. The strongest correlation occurs between SLA and STA in the Mediterranean Sea, significant correlations are observed between SLA and WSA in both the North Sea and the Baltic Sea. The statistical decompositions are selected to build a single-mission model and reconstruct the sea level variability in the Mediterranean Sea. Only the first few statistical modes need to be considered because they account for most of the variability. In the single-field case, the advantage of the PCA representation over the spectral one comes from the easier implementation and the smaller computational effort required. The model is formed by spatial grids and time series that are interpolated to the required space and time position respectively to compute the value for the model. The models constructed from the statistical analysis of the coupled fields have a similar structure. No direct physical relationship necessarily exists between the statistical modes identified in the two fields, however the SVD method is more suitable to produce decompositions with physically correlated components because the PCA-CCA canonical temporal patterns have a zero-lag, constraint which is often not realistic. For example, the 1-month lag between the first temporal patterns of the SVD decomposition of the SLA and STA fields has a physical interpretation. For the construction of the model, however, the physical relationship between the modes is not a priority and the PCA-CCA method is chosen for the extrapolation of the model because the zero-lag condition simplifies the computations. The accuracy of each SLA model in representing the sea level variability in the Mediterranean Sea is assessed comparing sea level height differences at DXOs having a 10-day constraint with DXOs obtained from data corrected using that model. It is assumed that the sea level variability can be neglected in case of the 10-day constraint. Both the PCA model, made from five years of sea level height data, and the PCA-CCA model, made from three years of sea level height and sea surface temperature data, have an accuracy of about two centimetres. The accuracy of the extrapolated PCA-CCA model, constructed from three years of sea level height data and from five years of sea surface temperature data using the sea surface temperature as the predictor, is lower, of about four centimetres, and still acceptable. It is concluded that the three SLA models are a good representation of the sea level variability in the Mediterranean Sea at wavelengths longer than 50 kilometres and periods greater than 30 days. An additional reason for the interest on this test of accuracy, is that the DXO differences provide an estimate of the relative bias and drift between the two satellites, if the sea level variability can be neglected or eliminated by a single-mission variability model. The observed drift in the DXO differences and their mean different from zero are interpreted as a relative bias and drift between ERS and T/P. The drift is due to a non homogeneous pre-processing of the ERS data, whereas the relative bias is related to ERS gravity induced orbit errors and has a geographical distribution. An interesting application of the extrapolated PCA-CCA model is the estimation of bias and drift between multi-mission data from not overlapping mission, as the usual method, based on DXO differences with a few days time difference constraint, is in that case not applicable. The single-mission sea level height variability models are a first step towards the construction of multi-mission models, build from harmonised multi-mission sea level height data to cover a longer time interval with increased spatial and temporal resolution.

Acknowledgments

The author kindly acknowledge AVISO, for providing the Topex/Poseidon altimetry data, ESA for the ERS altimetry, sea surface temperature ATSR data and the mean wind fields.

Comments and suggestions by the anonymous reviewers improved the manuscript. The Max-Planck Society is acknowledged for the general support to the working group at our Institute.

References

- Bretherton, C., Smith, C. & Wallace, J., 1992. An intercomparison of methods for finding coupled patterns in climate data change, *J. of Climate*, **5**, 541-560
- Cheney, R., Miller, L., Agreen, R., Doyle, N. & Lillibrige, J., 1994. Topex/Poseidon: the 2-cm solution *J. geophys. Res.*, **99**, **C12**, 24555-24564
- Cui, M., von Storch H. & Zorita E., 1995. Coastal sea level and the large-scale climate state: a downscaling exercise for the Japanese islands, *Tellus*, **47 A**, 132-144
- Ekman, M., 1998. Long-term changes of interannual sea level variability in the Baltic Sea and related changes of winter climate. Small publications in Historical Geophysics, Ekman
- Fenoglio-Marc, L. and Groten, E., 1997. Geodetic aspects of long term sea level variations in European seas from altimetry and tide gauge data, in *Proceedings of the 3rd ERS Symposium on Space at the service of our Environment, ESA SP-414*, **2**, 1103-1108
- Heyen, H., Zorita & E. von Storch H., 1996. Statistical downscaling of monthly mean North Atlantic air-pressure and sea level anomalies in the Baltic Sea, *Tellus*, **48 A**, 312-323
- Jolliffe I., 1986. Principal Component Analysis. Springer series in statistics, Springer Verlag
- Jones, M.S., Allen, M., Guymer, T. & Saunders, M., 1998. Correlations between altimetric sea surface heights and radiometric sea surface temperature in the South Atlantic, *J. geophys. Res.*, **103**, **C4**, 8073-8087
- Kelly, K., 1988. Comments on "Empirical Orthogonal Functions analysis of advanced very high resolution radiometer surface temperature patterns in Santa Barbara Channel", *J. geophys. Res.*, **102**, **C12**, 15753-15754
- Knudsen, P., 1994. Global low harmonic degree models of the seasonal variability and residual ocean tide from Topex/Poseidon data, *J. geophys. Res.*, **99**, **C12**, 24643-24656
- Koblinsky, C.J., Nerem, R.S., Williamson, R., Klosko, S., 1992. Global scale variations in sea surface topography determined from satellite altimetry, In *Sea Level Change Determination and effects, AGU, Geophysical Monograph 69*, 155-165
- Larnicol, G., LeTraon, P.Y. Ayoub, N., & De Mey, P.D., 1995. Mean sea level and surface circulation variability of the Mediterranean Sea from two years of Topex/Poseidon altimetry, *J. geophys. Res.*, **100**, **C12**, 25163-25177
- Lemoine, F.G., Smith, D.E., Kunz, L., Smith, R. & Pavlis, E.C., 1997. The Development of the NASA GSFC and NIMA Joint Geopotential Model, Proceedings of the International Symposium on Gravity Geoid and Marine Geodesy, Springer Verlag, New York
- LeProvost, C., Genco, M., Lyard, F., Vincent, P. & Canceil, P., 1994. Spectroscopy of the world ocean tides from a finite element hydrodynamic model *J. geophys. Res.*, **99**, **C12**, 24777-24798
- LeTraon, P.Y. & Gauzelin, P., 1997. Response of the Mediterranean mean sea level to atmospheric pressure forcing, *J. geophys. Res.*, **102**, **C1**, 973-984
- LeTraon, P.Y., Stum, J., Dorandeu, J. & Gaspar, P., 1994. Statistical Analysis of Topex and Poseidon data, *J. geophys. Res.*, **99**, **C12**, 24619-24631
- Lomb N., 1976. Least-squares frequency analysis of unequally spaced data, *Astrophys. Space Sci.*, **39**, 447-462
- Murray, J., 1995. Sea-surface temperatures from ATSR. Space Science Department Rutherford Appleton Laboratory, <http://www.atsr.rl.ac.uk>
- Nerem, R.S., Schrama, E.J., Koblinsky C. & Beckley, B., 1994. A preliminary evaluation of ocean topography from the Topex/Poseidon mission, *J. geophys. Res.*, **99**, **C12**, 24565-24583

- Nicholls, N., 1987. The use of canonical correlations to study teleconnections, *Mon. Weather Rev.*, **115**, 393-399
- Otto, L., Zimmermann, J., Furnes, G. Mork, M. , Saertre, R. & Becker, G., 1990. Review of the physical oceanography of the North Sea, *Netherlands Journal of Sea Research*, 161-238
- Pasaric, M. & Orlic, M., 1992. Response of the Adriatic sea level to the planetary-scale atmospheric forcing, In *Sea Level Chang Determination and effects*, AGU, *Geophysical Monograph 69*, 29-39
- Pinardi, N., Korres, G., Lascaratos, A., Roussenov, V. & Stanev, E., 1997. Numerical simulation of the annual variability of the Mediterranean Sea upper ocean circulation, *grl*, **24**, **4**, 425-428
- Preisendorfer, R.W., 1988. *Principal Component Analysis in Meteorology and Oceanography. Developments in Atmospheric Science, Nr. 17* , Elsevier, Amsterdam
- Press, W.H., Flannery, B.P., & Teukolsky, S.A., 1992. *Numerical Recipes, the Art of Scientific Computing*, 2nd edn, Cambridge University Press
- Yi, Y., 1995. Determination of gridded mean sea surface from Topex, ERS-1 and Geosat altimeter data, *Report 434*, Department of Geodetic Science and Surveying, The Ohio State University Columbus
- Rapp, R.H. & Yi, Y., 1997. Role of oceanic variability and dynamic ocean topography in the recovery of the mean sea surface and gravity anomalies from satellite altimetry data, *J. of Geodesy*, **71**, 617-629
- Scharroo, R., & Visser, P., 1998. Precise orbit determination and gravity field improvement for the ERS satellites, *J. geophys. Res.*, **103**, **C4**, 8113-8127
- Scharroo, R., Schrama E., Naeije, M. & Benveniste, J., 2000. A recipe for upgrading ERS altimeter data. In Proceedings of the ERS-ENVISAT Symposium, Gothenburg
- Stum, J., Ogor, F., & Dorandeu J., 1999. A comparison study of Topex/Poseidon, ERS-1 and ERS-2 altimeter and radiometer data. Report of Task 4 of Ifremer contract N. 99/2.210 765, CLS/DOS/NT/00.233.
- Stum, J., Ogor, F., Dorandeu J., Gaspar, P., & Dumont, J.P., 1998. An internal calibration study of Topex-Poseidon, ERS-1 and ERS-2 altimetric missions. Final Report of Ifremer contract N. 97/2 426086/C, CLS/DOS/NT/98.070.
- Wagner, C.A., & Cheney, R., 1992. Global sea level change from satellite altimetry, *J. geophys. Res.*, **97**, **C10**, 15607-15615
- Wagner, C.A., Klokochnik J., & Cheney, R., 1997. Making the connection between Geosat and Topex/Poseidon, *J. of Geodesy*, **71**, 273-281
- Wang, Y.M. & Rapp, R.H., 1994. Estimation of sea surface topography, ocean tides and secular changes from Topex altimeter data, *Report 430*, Department of Geodetic Science and Surveying, The Ohio State University Columbus 617-629
- Wilks, D.S., 1995. Statistical methods in the atmospheric sciences. International Geophysics Series, 59. Academic Press
- Wroblewski, A., 1992. The application of EOF in determining basin mean sea level using computations for the Baltic Sea as an example, In *Sea Level Chang Determination and effects*, AGU *Geophysical Monograph 69*, 23-28
- Wunsch, C.A., 1991a. Global-scale sea surface variability from combined altimetric and tide gauge measurements, *J. geophys. Res.*, **96**, **C8**, 15053-15082
- Wunsch, C.A., 1991b. Large-scale response of the ocean to atmospheric forcing at low frequencies, *J. geophys. Res.*, **96**, **C8**, 15083-15092
- Wunsch, C.A., Stammer, D. 1995. The global frequency-wave number spectrum of oceanic variability estimated from Topex/Poseidon, *J. geophys. Res.*, **100**, **C12**, 24895-24910

7.3 Long-term sea level change in the Mediterranean Sea

F-08:Fenoglio-Marc L., Long-term sea level change in the Mediterranean Sea from multi-mission satellite altimetry and tide gauges, *Physics and Chemistry of the Earth*, Vol. 27, pp. 1419-1431, 2002.

Abstract The long-term sea level change during 1992-2000 is investigated in the Mediterranean Sea from satellite altimetry data of the Topex-Poseidon, ERS-1 and ERS-2 missions and from tide gauge data. Tide gauge data observations during 1996-2000 agree better with Topex-Poseidon than with ERS-2 data. A relative sea level change (trend) between Topex/Poseidon and ERS-2 data is observed and reduced by fitting the ERS-2 data to the Topex/Poseidon data. During the first eight years of the Topex/Poseidon mission the average linear sea level change over the entire Mediterranean Sea is 2.2 mm/yr, in the western Mediterranean Sea the change is small (0.4 mm/yr), while it is higher in the eastern Mediterranean and in the Ionian Sea, 9.3 mm/yr and -11.9 mm/yr respectively. The high correlation of sea level height and sea surface temperature variations indicates the observed sea level change is of thermal origin primarily at seasonal scales. At low frequencies the atmospheric pressure and wind field variations play also a role.

Keywords: sea level change, altimetry, tide gauge

1. Introduction

Long-term sea level change analysis requires time series of sea level heights over several years, for sea level rise at least 50-year records are needed (Douglas, 2000), long records are necessary to separate secular, decadal and interannual variations. Records over the last century are available at several tide gauge stations and provide sea level variation relative to land and not homogeneously distributed around the world. For climate change, being the parameter of interest the sea level change in a fixed reference frame, also the vertical crustal movement at the tide gauge site has to be accounted for. In the Mediterranean Sea the tide gauge stations with long records are located along the northern coast. Absolute sea level variations were studied in Zerbini et al. (1996), a sea level drop was observed over the last four decades from tide gauge records (Tsimplis and Baker, 2000; Tsimplis and Josey, 2001). Climate changes in the Mediterranean Sea have been discussed by several authors (Theocharis et al., 1999; Ross et al., 2000; Ribera et al., 2000).

Global coverage and sea level measurements in a fixed reference frame are the characteristics that distinguish altimetry from tide gauge measurements. The altimeter sampling is denser in space but less dense in time at a given location, the data-span is shorter than the tide gauge data-span. The Topex/Poseidon (T/P) and ERS altimetry missions provide measurements since 1992, making the altimetric sea level records considerably shorter than the tide gauge records are. The time and spatial sampling of the altimeter depend on the mission characteristics and range from the 10-day time sampling and 300 kilometres track-spacing at equator of the Topex-Poseidon (T/P) mission to the 168-day time sampling and 8 kilometres spacing at equator of the ERS-1 geodetic phase. In the Mediterranean Sea the spacing between the tracks amounts to 230, 60 and 12 kilometres respectively for T/P, the ERS-1 and ERS-2 35-day repeat cycles and the ERS-1 168-day cycles. The multi-mission altimetry extends the data span above the duration of a single mission. Long-term sea level changes have been mainly investigated using T/P data (Nerem and Mitchum, 2001), but also using ERS data (Anzenhofer and Gruber, 1998; Cazenave et al., 1998; Fenoglio-Marc and Groten, 2001). The stability of the

altimeter instrument is fundamental in long-term studies, as a drift in the satellite instrument can be interpreted as a change in sea level. While tide gauge sea level measurements can show apparent sea level trends due to bias and drift in the instrument as well to a change in the reference point and land motion (Cazenave et al., 1999), satellite altimetry can show spurious sea level change due to instability in the instrument (Mitchum, 2000) and not homogeneity of the geophysical corrections (Scharroo et al. 2000). Relative biases between T/P, ERS-1 and ERS-2 data exists (Scharroo et al. 2000; Moore 2001; Fenoglio-Marc and Groten, 2001).

The T/P altimeter data have been analysed in the Mediterranean Sea during 1992-1997 (Fenoglio-Marc, 2001) together with sea surface temperature, wind speed and atmospheric pressure data detecting an high correlation between the sea level height and sea surface temperature fields. Here long-term sea level changes in the Mediterranean Sea are studied using tide gauge data, ERS and T/P altimeter data from September 1992 to August 2000 and sub-intervals formed by an integer number of years to include the complete annual cycle.

2. Absolute and relative sea level change

2.1 Multi-mission altimetry

Topex/Poseidon altimetry data (AVISO, 1996) are analysed in the Mediterranean Sea from September 1992 to August 2000 (cycles 1-300). ERS-1 data (CERSAT, 1996) are considered from April 1992 to March 1996 (phases c,e,f,g) and ERS-2 data from May 1995 to April 2000 (cycles 1-54). For T/P the altimetric heights, geophysical corrections and orbital heights are taken from the AVISO CD ROMs version C. For ERS the altimetric range and geophysical corrections are taken from the precise ocean products (OPR), the ESA/ESRIN corrections for ultra stable oscillator (USO) bias drift and for ERS bias jumps as characterised by the single point target response (SPTR) are applied using the recent tables, the orbital heights corresponding to the DGM-E04 orbits (Scharroo and Visser, 1998) released by DEOS, Delft University of Technology, are used. The local inverse barometer correction is applied, that accounts for the inverted barometer sea level response to atmospheric loading. For each of the satellite missions the average over each cycle and over the entire Mediterranean Sea of the corrected sea surface heights (SSH) above the mean sea surface model MSSH95 (Yi, 1995) is computed and a simple regression model is fitted to the results (Fig. F-08-1). High positive values for the regression are observed for the ERS-1 data, as they are now under reprocessing (CERSAT communication) they will not be analysed here in details. The linear sea level change is computed for T/P and ERS-2 in a least squares analysis together with the four main spectral components (Tab. F-08-2). Three time-spans are chosen for the analysis, they are: the first eight years of the T/P mission (1992.8-2000.8), the first five (1995.4-2000.4) and the first three (1995.4-1998.4) years of the ERS-2 mission. For a given mission, the linear sea level change slightly depends on the time-span, while the estimated accuracy increases with long-time series. T/P data give a linear sea level change of 2.2 ± 0.8 mm/yr during the eight-year time-span, of -3.3 ± 1.6 mm/yr during the five-years time-span. For a given time-span, the linear changes obtained from ERS-2 and from T/P differ for more than their formal uncertainty. During the five-year time-span 1995.4-2000.4, mission overlapping, the linear sea level change amounts to -3.3 ± 1.6 mm/yr as estimated by T/P and to -12.6 ± 2.7 mm/yr as estimated by ERS-2. The formal uncertainty of the linear change is too small, as the assumption made in the linear regression model that the signal consists in a trend with added normally distributed random noise is not satisfied. The residuals about the trend are serially correlated, moreover the relative drift between ERS-2 and T/P is inconsistent

with the assumption of stationarity and is responsible for a large part of the linear change observed.

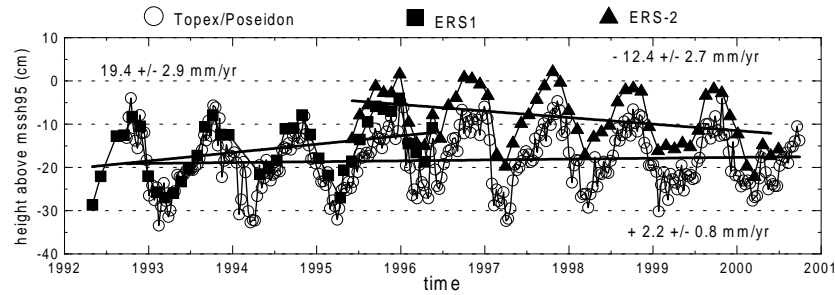


Figure F-08-1: Average over each cycle and over the Mediterranean Sea of sea level heights above the mean sea surface MSSH95

Relative bias and linear drift between the altimeter missions are investigated computing averages over each ERS cycle and over the entire Mediterranean Sea of the SSH differences at dual crossover (DXO) points between T/P and ERS with a time difference at the DXO of less of 10 days. A simple regression model is fitted to the averaged DXO residuals ((Fig. F-08-2). High positive values for the regression are observed for the ERS-1 data, as in Fig. F-08-1. ERS-2 and T/P have a relative negative drift of -3.7 ± 1.4 mm/yr between May 1995 and Summer 1998 (cycles 1-34) and of -10 ± 5.8 mm/yr afterwards, an annual component appears in the differences after Summer 1998. The application to the ERS-2 data of different SPTR correction tables, an additional instrumental correction still under investigation, does not remove the large drift in the differences.

Table F-08-1: Period and amplitude of the main spectral components and linear sea level change (trend) of sea level derived from heights averaged over the Mediterranean basin and over each altimeter repeat cycle

Mission-time-cycles	P1 (yr)	A1 (mm)	P2 (yr)	A2 (mm)	P3 (yr)	A3 (mm)	P4 (yr)	A4 (mm)	Trend (mm/yr)
TP 92.8-00.8 001-300	1.0	76.3	1.2	5.1	0.8	15.0	0.5	5.1	2.2 ± 0.8
TP 95.4-00.4 099-283	1.0	78.5	0.5	24.1	0.6	7.9	1.4	3.4	-3.3 ± 1.6
TP 95.4-98.4 099-210	1.0	76.7	0.5	24.9	0.4	16.7	0.2	13.5	1.3 ± 3.6
E2 95.4-00.4 001-054	1.0	79.3	1.4	2.1	2.8	2.0	1.8	5.1	-12.6 ± 2.7
E2 95.4-98.4 001-034	1.0	78.4	0.5	7.6	0.4	12.0	1.8	3.5	-5.8 ± 4.8
E2 98.4-00.4 035-054	1.0	76.8	0.5	23.0	0.2	11.4	0.4	13.8	-20.4 ± 4.5
E2 95.4-98.4 001-34cor	1.0	76.2	0.5	10.8	0.4	14.0	0.2	12.6	-3.3 ± 4.1
E2 95.4-00.4 001-054	1.0	79.3	1.4	3.2	0.5	20.9	0.4	15.0	-5.5 ± 1.8

Amplitudes and periods of the main spectral components are also given in Tab. F-08-2 for the ERS-2 and T/P SSH averaged time-series. Except for the annual component, the spectral characteristics of the dominant components over the entire overlapping time-span (1995.4-2000.4) are different for the two missions. This difference is partly due to the relative drift in the satellite data starting from Summer 1998, as observed in Fig. F-08-2. During the first three years of the ERS-2 mission (until cycle 34 for ERS-2 and cycle 213 for T/P) a better agreement exist. Considering separately both sub-intervals (cycles 1-34 and cycles 35-54) more realistic spectral characteristics are obtained for the ERS-2 data. It is assumed

that the DXO differences between ERS-2 and T/P are due to errors in the ERS-2 SSHs and the time-series of averaged ERS-2 sea level heights (pro-cycle and over the entire sea) are corrected subtracting the averaged DXO difference per ERS-2 cycle. After this correction both the spectral characteristics and the linear change are in better agreement: using ERS-2 corrected data the linear sea level change during the first five years of the ERS-2 mission is reduced from -12.6 mm/yr to -5.5 mm/yr, which is near to the -3.3 mm/yr obtained using T/P data over the same time-span.

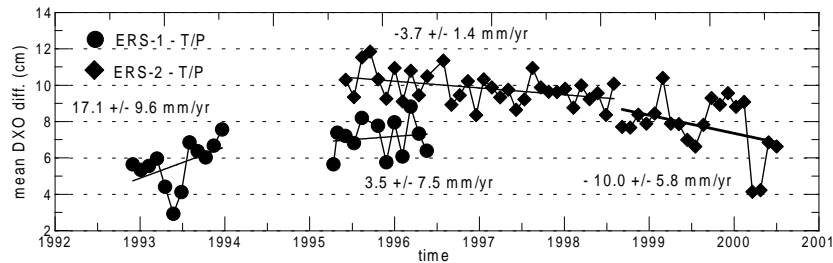


Figure F-08-2: Average over each ERS cycle and over the Mediterranean Sea of sea level height differences at DXO between ERS-1 and T/P and at DXO between ERS-2 and T/P with 10-day DXO time difference constraint.

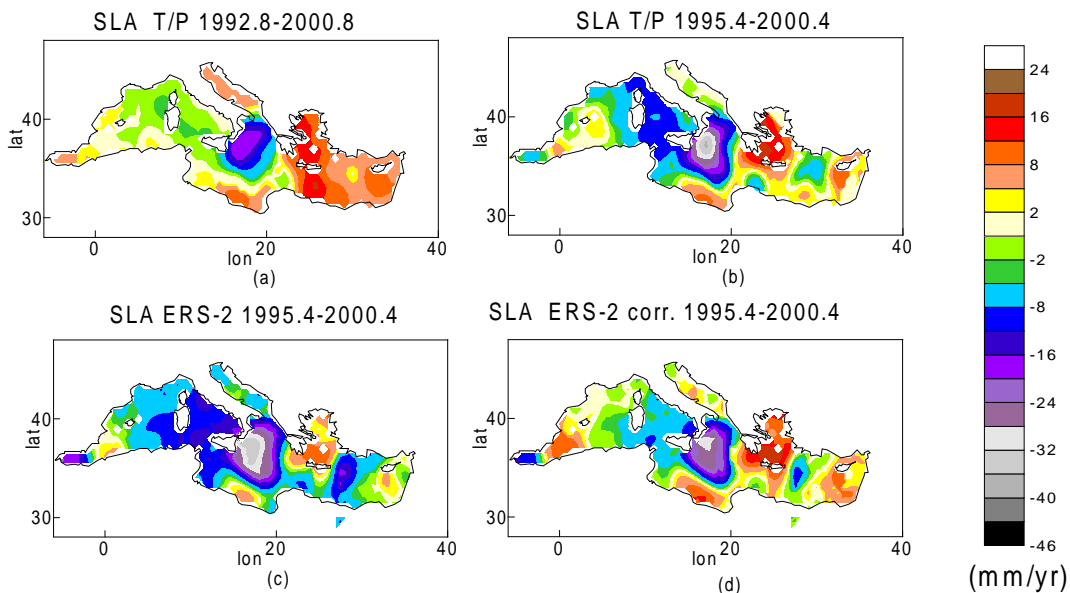


Figure F-08-3: Linear sea level change from monthly averages of sea level heights: from T/P during 1992.8-2000.8 (a), from T/P during 1995.4-2000.4 (b), from ERS-2 during 1995.4-2000.4 without correction (c) and after correction using T/P (d). Grid spacing is $0.5^\circ \times 0.5^\circ$

For a 2-dimensional study, each altimetry data set is gridded with a monthly interval and a grid spacing of 0.5 degrees using a Gaussian weighted average method. The half-weight parameter is chosen to be equal to 1 and the search radius equal to 3° to ensure that a pair of ascending and descending T/P arcs contributes to each node value. At each node the time-series is analysed by spectral analysis and both the dominant four main spectral components and the linear sea level change are determined. For a given mission, the linear sea level change is also here slightly dependent on the chosen time-span and the formal uncertainty decreases with long-time series. The linear sea level changes per year estimated by T/P over the eight-year time-span and over the five-year time-span are compared in Fig. F-08-3.a, Fig. F-08-3.b. During the longer time-span it is in the range $-/+4$ mm/yr in the western Mediterranean Sea,

it is negative with an extreme at -20 mm/yr in the Ionian Sea, it is positive with a maximum of 16 mm/yr south of Crete in the eastern Mediterranean Sea. The formal uncertainty for the linear term is lower than 1.5 mm/y in most of the Sea and lower than 3 mm/yr in the regions corresponding to the higher trends. During the five-years time-span the linear sea level change is generally more negative, the main difference occurs in the eastern Mediterranean Sea where the sea level change, that was positive everywhere in the longer interval, is negative near to the Rhodos insland. The main difference with respect to results obtained over the first five years of the T/P mission (Fenoglio-Marc, 2001) is the displacement of the location of the maximum negative trend from the eastern to the western part of the Ionian Sea. The spatial behaviours of the linear sea level change estimated during the first five years of ERS-2 from T/P (Fig. F-08-3.b) from ERS-2 (Fig. F-08-3.c) data are similar. The relative drift observed in Fig. F-08-2 between ERS-2 and T/P data shows up in the estimated trends, the agreement increases after the adjustment of the ERS-2 data as described above (Fig. F-08-3.d).

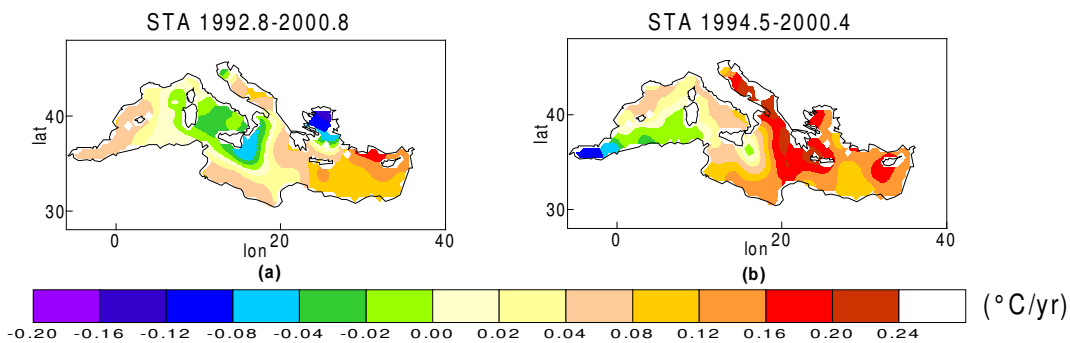


Figure F-08-4: Linear sea surface temperature change from monthly averages of AVHRR sea surface temperature during 1992.8-2000.8 (a) and during 1994.5-2000.4 (b). Grid spacing is $0.5^{\circ} \times 0.5^{\circ}$.

2.2 Tide gauge station

Tide gauge stations data in the Mediterranean Sea are analysed to evaluate the dependency of the results on the chosen interval and to determine sea level trends corresponding to the altimetry data. Monthly values of sea level heights at the tide gauge stations are available from the Permanent Service of the Mean Sea Level (Spencer and Woodworth, 1991). The distribution of the stations is not uniform and the reliable stations are concentrated in the northern part of the Mediterranean Sea. Few stations have data over several decades, as Marseille since 1886, Venezia and Trieste since 1900, Dubrovnik since 1965. More stations have data since 1970, as Alicante, Kalamai, Soudhas. In general the data are available until end of 1999. The PSMSL dataset does not include tide gauge station in the Ionian Sea, the data at Crotone, made available by the Servizio Idrografico e Mareografico Nazionale (SIMN, Italy) and checked against altimetry, are used starting from 1995 and corrected for a change in the reference level in Summer 1998. A few tide gauge stations are selected for their location and for the relatively small data gaps (full circles in Fig. F-08-5), a running average has been computed with a 1-yr window to remove high-frequency signals (Fig. F-08-6) ordered from west to east). Linear sea level change per year and four main spectral components are estimated from the monthly averages as described in Section 2.1 for the altimetry data. To investigate the effect of the length of the time interval, intervals of different lengths are considered keeping fix the end of the time interval and shortening the interval of 0.2 years at each computation step. Relevant differences in linear change in sea level are observed with intervals of less than 20 years (Fig. F-08-7). Results for the intervals 1970-1999 and 1993-1999

(first and second columns in Tab. F-08-3 show a bigger sea level change in the last seven years than in the longer time-span. To investigate if an acceleration in the sea level change is observed on recent data, intervals of constant lengths for 10 and 20 years are analysed. The procedure corresponds to a smoothing of the original series. Results from the long data records of Marseille and Trieste show a positive sea level rate of change since 1990. High values have been reached also in the past, for example in Trieste at the end of 1970s and are observed also at other stations (Fig. F-08-8).

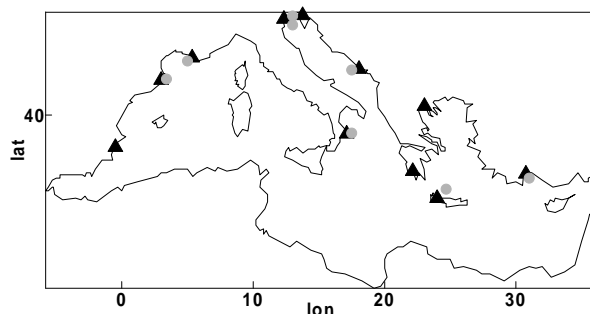


Figure F-08-5: Location of selected tide gauge stations (triangle) and of the corresponding nearest altimeter grid node (circle)

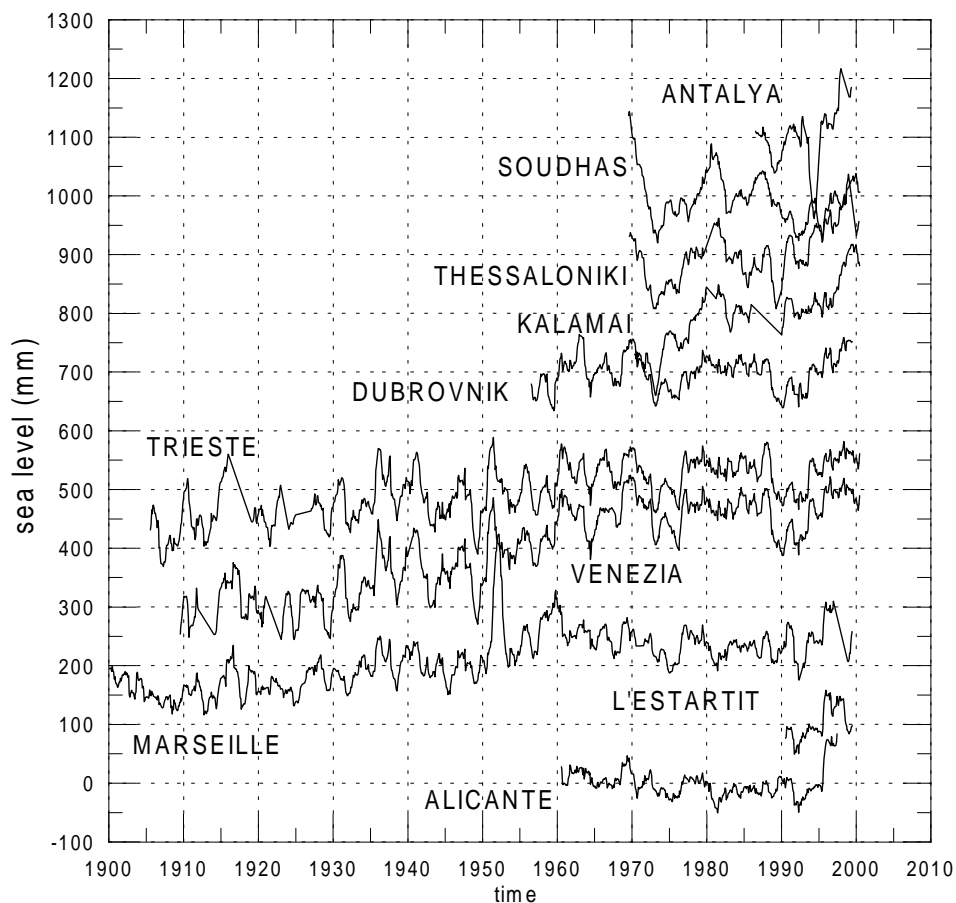


Figure F-08-6: Sea level anomaly time-series at tide gauge stations. Data shown are one-year running averages

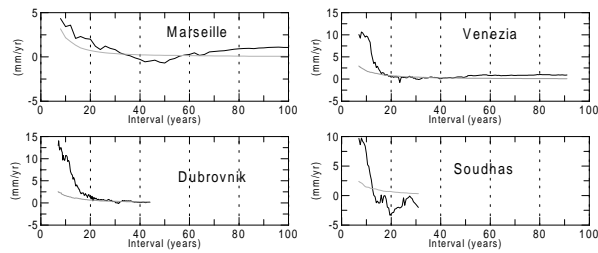


Figure F-08-7: Linear sea level change (mm/year) from monthly tide gauge sea level data for increasing length of the data interval. Drawn is the linear sea level change computed over the last n years before year 2000

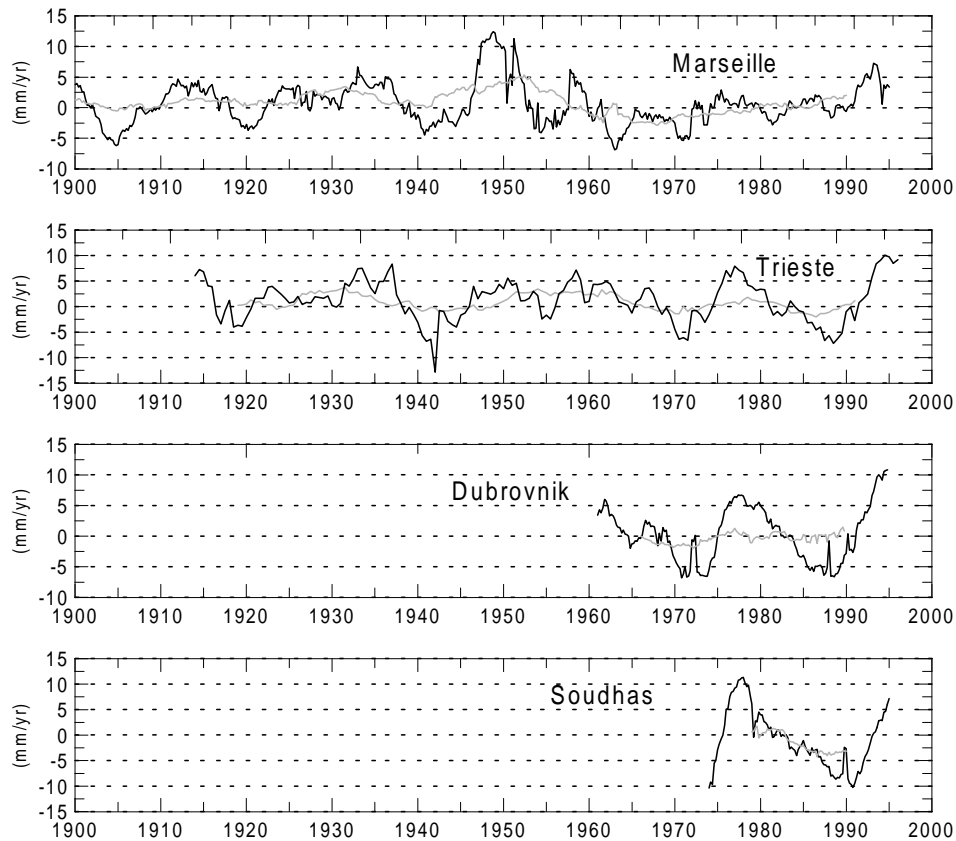


Figure F-08-8: Linear sea level change (mm/year) from monthly tide gauge sea level data estimated over intervals of 10 years (black) and 20 years (grey)

2.3 Comparison between altimetry and tide gauge station

Monthly sea level variability grids are computed as described in Section 2.1 from T/P and ERS-2 altimetry data. Monthly time series at a few tide gauge stations and at the nearest node (Fig. F-08-5) of both the T/P and the ERS-2 altimeter fields are selected and the corresponding linear sea level changes compared during the five-year overlapping time-span (Tab. F-08-2). The inverse barometric correction is not applied to the altimeter data as it is not applied to tide gauge data either. The agreement between the tide gauge and T/P altimetry is quite good at Soudhas, Estartit and Crotone. In general, the tide gauge station results agree better with T/P than with ERS-2 results. After correction of the ERS-2 data

Table F-08-2: Linear sea level change during 1995.4-2000.4, first five years of the ERS-2 mission, from sea level height monthly averages at a few tide gauge stations and at the corresponding locations on sea from T/P and ERS-2 altimetry. The inverse barometric correction is not applied

Station	TG monthly 1995.4-2000.4	T/P monthly 1995.4-2000.4	ERS-2 monthly 1995.4-2000.4	ERS-2 monthly corrected 1995.4-2000.4
Estartit	-8.4 ± 3.7	-10.5 ± 3.9	-9.2 ± 4.2	-2.3 ± 4.2
Trieste	1.5 ± 3.9	-5.6 ± 5.9	-12.5 ± 5.6	-5.3 ± 5.5
Dubrovnik	9.4 ± 4.2	0.3 ± 3.4	-12.4 ± 4.5	-6.3 ± 4.3
Soudhas	12.4 ± 3.6	14.7 ± 3.3	7.9 ± 3.5	14.7 ± 3.5
Crotone	-19.8 ± 3.6	-26.7 ± 3.9	-28.1 ± 4.4	-21.3 ± 3.8

for the relative drift, the agreement between ERS-2 and tide gauge results improves. The application of the inverse barometric correction has a minor effect, as shown in Tab. F-08-3.

The longest time-span of contemporaneous altimetry and tide gauge data occurs for most of the stations during 1993-1999. During this seven years, sea level time-series at the tide gauge station and at the nearest node of the T/P field are compared by estimating their correlation and the linear sea level changes (Tab. F-08-3). The linear sea level changes from altimetry with and without the inverse barometric correction are similar and have a lower formal error with the correction applied. The correlation between the monthly averages is higher without the inverse barometric correction applied to the altimeter data, as it is not applied to the tide gauge data either. The agreement between the linear changes is within the estimated error for stations in western and central Mediterranean (first five stations in Tab. F-08-3, it is slightly worse for the stations in the eastern Mediterranean where the magnitude of sea level change increases. In case of an altimeter grid node several kilometers away from the tide gauge station, the compared sea level time-series can show a different behaviour in a region of high variability. During 1993-1999 the sea level changes are positive at every chosen location with exception for the station in the Ionian Sea, the highest value of sea level change is obtained in the eastern Mediterranean Sea. The linear sea level change estimated from the tide gauge smoothed data in Fig. F-08-6 (third column of Tab. F-08-3 agrees with the not-smoothed tide gauge monthly data and has a smaller formal uncertainty as the number of effective degrees of freedom is smaller in the smoothed time-series. The departure from the results obtained in Tab. F-08-2 and Fig. F-08-3 confirms the dependency of the linear sea level change on the analysed time-interval.

3. Analysis of the single fields

The T/P altimeter data are analysed over the first eight years of the mission. Three regions are selected for the analysis of the SLA field: the western Mediterranean, the Ionian Sea and the eastern Mediterranean. The spatial averaged time series are spectral analysed using the Lomb method and a confidence level of 95% is obtained for the trend in the Ionian Sea and in the eastern Mediterranean (Fig. F-08-9). Tab. F-08-4 summarises the results for the spectral and trend analysis of sea level heights in each of the three region, while the results for the entire Mediterranean Sea is given in Tab. F-08-1. Seasonal (annual and semiannual) signals

Table F-08-3: Linear sea level change from sea level height monthly averages at a few tide gauge stations and at the corresponding locations on sea from T/P altimetry. Correlation of the time-series with (r1) and without (r2) inverse barometric correction applied to T/P data during 1993-1999, the first seven years of T/P mission

Station	TG 1970-1999	TG 1993-1999	TG smooth 1993-1999	TP (ibc) 1993-1999	r1	TP (no-ibc) 1993-1999	r2
Estartit		4.2 ± 2.9	5.3 ± 1.1	5.3 ± 1.6	0.79	6.1 ± 2.7	0.9
Marseille	0.8 ± 0.4	5.6 ± 2.9	4.2 ± 1.6	5.2 ± 0.4	0.55	5.5 ± 2.6	0.58
Venezia	-0.2 ± 0.4	10.9 ± 2.9	9.6 ± 0.7	10.7 ± 2.5	0.79	11.6 ± 3.6	0.81
Trieste	-0.1 ± 0.5	10.8 ± 2.9	7.8 ± 0.7	10.6 ± 3.3	0.69	11.9 ± 4.2	0.73
Dubrovnik	0.1 ± 0.4	12.9 ± 2.5	10.5 ± 0.5	8.1 ± 1.7	0.81	8.7 ± 2.3	0.84
Soudhas	1.6 ± 0.5	9.7 ± 2.4	8.5 ± 0.6	16.0 ± 1.9	0.79	16.2 ± 2.5	0.86
Anthalia		17.9 ± 5.0	28.9 ± 0.9	10.1 ± 2.1	0.57	10.2 ± 2.5	0.59

are dominant except in the the Ionian Sea where the second dominant component corresponds to interannual fluctuations (4-5 years).

The Multitaper analysis technique (Mann and Park, 1994) is used as alternative method for the identification of significant spatial-temporal signals. The MTM-SVD performs a local frequency-domain decomposition of statistically independent spectral estimates. It isolates statistically significant narrowband oscillations that are correlated among a sufficient large number of normalized independent series as to represent a significant fraction of the data variance. As in the Lomb spectral method, the interannual and long-term frequencies reach a confidence level of at least 90% in the Ionian and in the eastern Mediterranean in the Local Fractional Variance (LFV) spectrum (Fig. F-08-10).

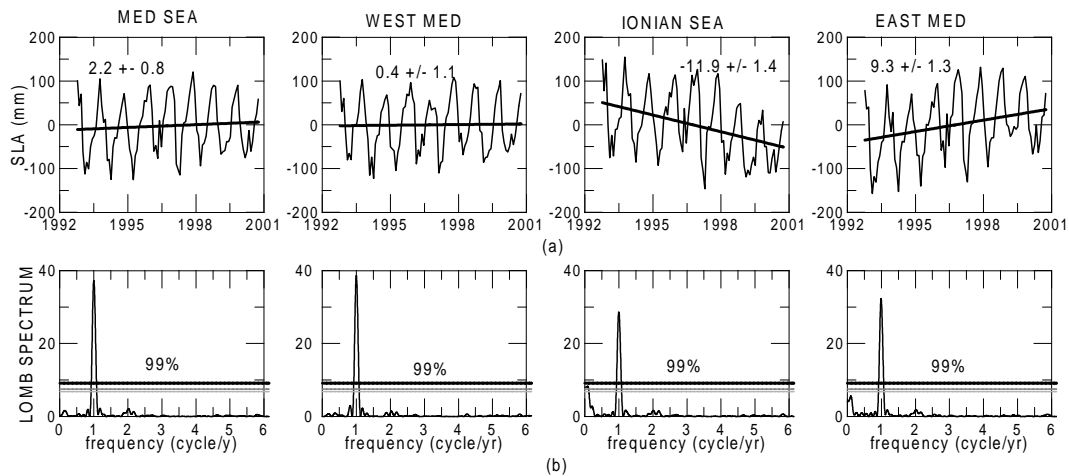


Figure F-08-9: Values and linear regression line (a), Lomb spectrum and 99%, 95%, 90% confidence levels (b) of monthly spatial averages of T/P sea level heights over the entire Mediterranean Sea, western Mediterranean, Ionian Sea and eastern Mediterranean during 1992.8-2000.8.

Sea surface temperature, wind speed and atmospheric pressure anomaly fields, called STA, WSA and APA fields hereafter, are analysed over the same time interval of the sea level height anomalies (SLA). The sea surface temperature field is obtained from the weekly AVHRR/NOAA data (Nasa, 1999). Wind speed and atmospheric pressure data are available

Table F-08-4: Linear sea level change (trend), period and amplitudes of main spectral components evaluated during 1992.8-2000.8 from T/P sea level heights monthly averages over three sub-regions of the Mediterranean Sea

Basin	P1 (y)	A1 (mm)	P2 (y)	A2 (mm)	P3 (y)	A3 (mm)	P4 (y)	A4 (mm)	Trend (mm/y)
Western basin	1.0	75.0	1.2	7.2	0.8	10.2	0.5	13.1	0.4 ± 1.3
Ionian basin	1.0	79.3	4.7	20.3	0.8	17.1	0.5	16.9	-11.9 ± 1.4
Eastern basin	1.0	82.7	0.5	19.7	0.8	16.6	1.2	2.1	9.3 ± 1.3

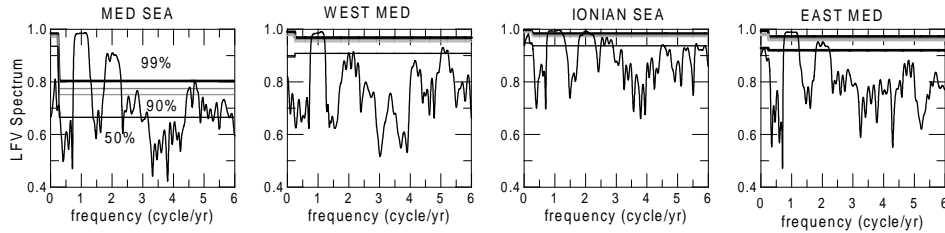


Figure F-08-10: LFV spectrum and 99%, 95%, 90% confidence levels of monthly spatial averages of T/P sea level heights over the entire Mediterranean Sea, western Mediterranean, Ionian Sea and eastern Mediterranean during 1992.8-2000.8

from the GDR (AVISO, 1996) and derived from the dry-tropospheric correction contained in the GDR in correspondence to each altimeter observation, they have therefore the same spatial and temporal sampling of the T/P sea surface heights. The fields are gridded in time and space and analysed as described above for the altimeter data. The geographical distribution of the linear sea surface temperature change per year over the first eight years of the T/P mission is similar to the geographical distribution observed in Fig. F-08-3 for the linear sea level change. A positive value up to $0.12 \text{ }^\circ\text{C/yr}$ is obtained in the eastern Mediterranean, a negative trend in the central Mediterranean with the highest negative trend in the western Ionian ($-0.06 \text{ }^\circ\text{C/yr}$). The uncertainties associated with the computed trends do not exceed $0.03 \text{ }^\circ\text{C/yr}$. The results obtained during the first eight years of T/P and during the first five years of ERS-2 are compared in Figs. F-08-4.a and b. In both cases the change is small (less than $0.08 \text{ }^\circ\text{C/yr}$) or negative in the western Mediterranean and in the Ionian Sea and positive in the eastern Mediterranean. In the shorter interval the positive values in the eastern Mediterranean are higher (up to $0.2 \text{ }^\circ\text{C/yr}$). The estimated error of the change is higher in the shorter interval (below $0.08 \text{ }^\circ\text{C/yr}$). The linear changes computed from the atmospheric pressure and the wind speed fields are not significant, as their uncertainties are higher than the changes themselves.

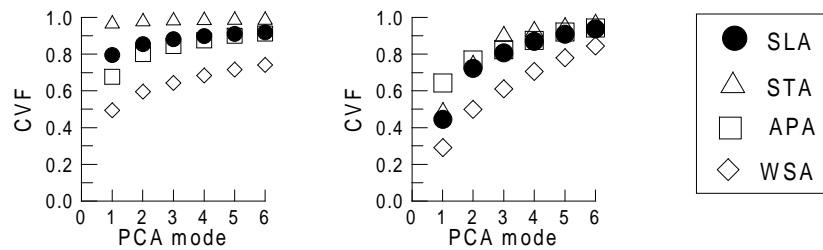


Figure F-08-11: Average over each cycle and over the Mediterranean Sea of sea level heights above the mean sea surface MSSH95

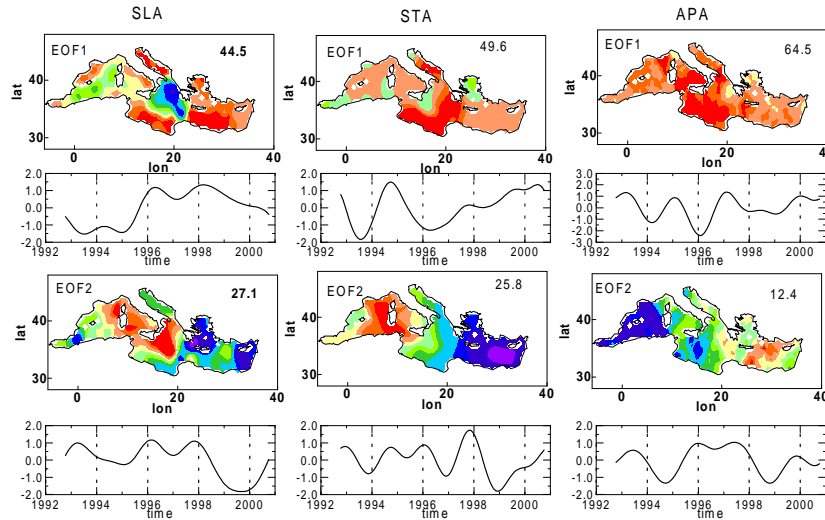


Figure F-08-12: Average over each cycle and over the Mediterranean Sea of sea level heights above the mean sea surface MSSH95

The high frequency part of each field is filtered out by a Butterforth low-pass filter with a cut frequency of 18 months and order 8. The last nine months are excluded to avoid edge effects.

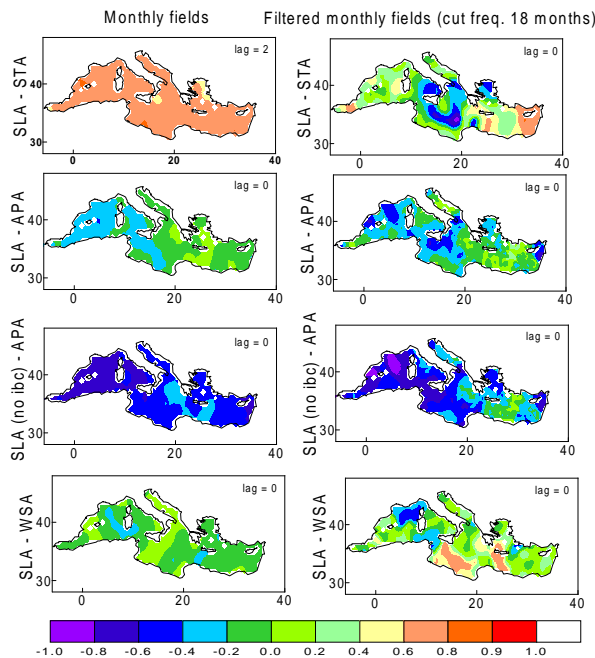


Figure F-08-13: Average over each cycle and over the Mediterranean Sea of sea level heights above the mean sea surface MSSH95

The Principal Component Analysis (PCA) (Preisendorfer, 1988) is applied to both the complete and the low-pass filtered anomaly fields after standardisation, i.e. each time-series is de-meaned and divided by the standard deviation to avoid that a point with high variability dominates the analysis. The highest variability of both SLA fields are observed in the Ionian Sea and in the eastern Mediterranean. Fig. F-08-11 shows the Cumulative Variance Fraction (CVF) accounted for by the first six modes of the PCA decomposition of the complete (a) and of the low-pass filtered (b) fields. With exception of the APA field, the first modes of

the filtered fields account for a smaller fraction of the total variance than the first modes of the decomposition of the complete fields. In the complete SLA field the dominant mode of the sea level variability is the annual component (80% of the total variability), the second (5.9%) corresponds to the trend in the eastern Mediterranean Sea and in the Ionian Sea, the third mode (2.7%) to a signal in the Balearic Islands. Similar results have been shown for the interval 1992-1995 (Fenoglio-Marc, 2001), where the second and third mode were exchanged. The first mode of the SLA filtered field, which account for 44.5% of the total variability of the low-pass filtered field, represents the negative trend in the Ionian Sea and the positive trend in the eastern Mediterranean Sea (Fig. F-08-12). The second mode of the low-pass filtered SLA field (27.1% of the variance) has an opposite phase in the eastern and in central Mediterranean, the temporal patterns show a signal with a strong minimum in 1999. The third mode (20% of the variance) corresponds to a signal near to the Balearic Islands (not shown). The first principal mode of the STA filtered field explains 49.6% of the variance and is an in-phase oscillation of almost the entire basin corresponding to the trend in the sea surface height observed in Fig. F-08-3. The temporal pattern has maximum in 1995. The second mode explains 25.8% of the variance, has opposite phases in the eastern and western Mediterranean and minimum in 1999. The first mode of the APA filtered field, which account for 64.5% of the total variability, corresponds to a signal with opposite phase in the eastern and western Mediterranean.

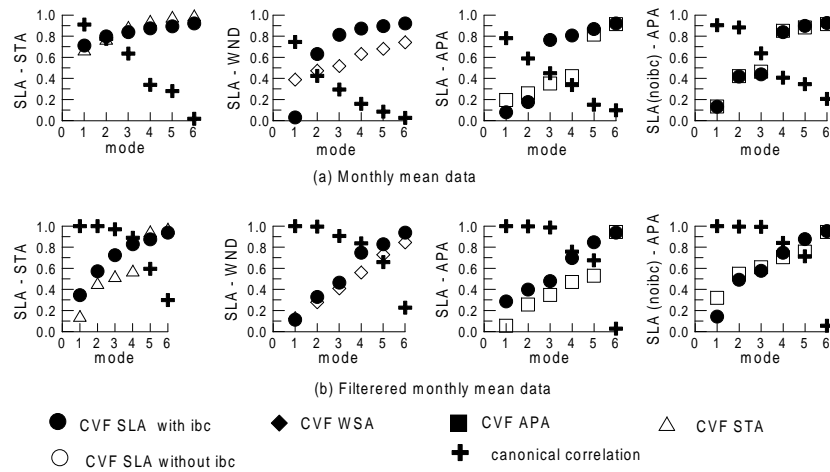


Figure F-08-14: Average over each cycle and over the Mediterranean Sea of sea level heights above the mean sea surface MSSH95

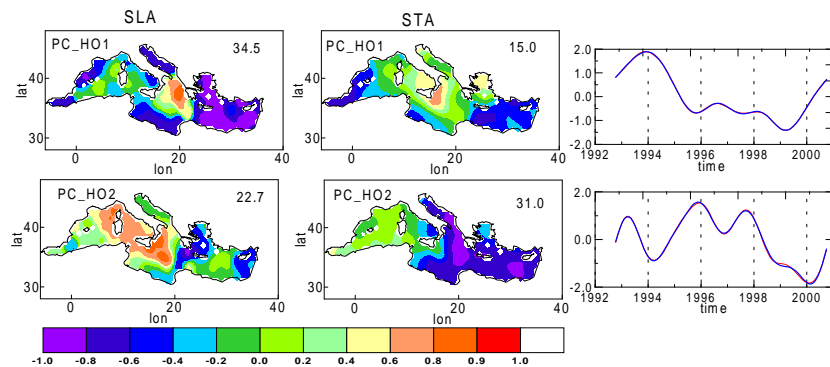


Figure F-08-15: Average over each cycle and over the Mediterranean Sea of sea level heights above the mean sea surface MSSH95

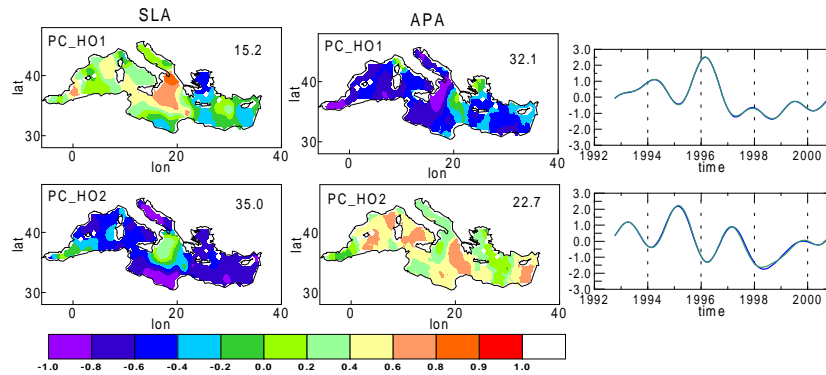


Figure F-08-16: Average over each cycle and over the Mediterranean Sea of sea level heights above the mean sea surface MSSH95

4. Correlation between the fields

The coupled variability of the fields is investigated using two methods: by computing the simple Pearson correlation of the time-series at the same spatial points and by applying the Canonical Correlation Analysis in PCA basis method (PCA-CCA) (Bretherton et al., 1992). Sea level heights with and without application of the inverse barometric correction are considered in the correlation with the APA field.

The Pearson correlation corresponding to different time-lags is evaluated. The SLA and STA complete fields show the highest correlation in the western Mediterranean Sea (0.85) at the lag of one month, on the entire sea a coefficient bigger than 0.6 is obtained with a lag of two months. The SLA and STA low-pass filtered fields have only in the eastern Mediterranean Sea a significant positive high correlation (Fig. F-08-13). The SLA field without application of the inverse barometric correction and the APA complete fields are negatively correlated (coefficient lower than -0.4) at zero lag, as expected for the isostatic response to pressure loading. The corresponding low-pass filtered fields have a higher correlation in the Ionian and in the western Mediterranean Sea than in the eastern Mediterranean Sea. The residual significant negative correlation in the western Mediterranean Sea between the APA field and the SLA field corrected for the inverse barometric correction confirms that the response of the sea level overshoots a simple inverse barometric in semiclosed basins. With one and two months lags between the complete fields the correlation in the eastern Mediterranean is slightly higher. The correlation of the filtered monthly fields does not change significantly with the lag, as expected. The correlation of the SLA and the WSA complete fields is not significant, an higher correlation is obtained for the filtered fields.

The second method gives the coupled pairs of spatial patterns and temporal coefficients that best explain the coupled variability of the two fields. In the PCA-CCA analysis, the fields are highly correlated if, for the first modes, the canonical correlation coefficients and the Cumulative Variance Fraction (CVF) are near to 1. Figure F-08-14 gives the parameters for both the complete and the low-pass filtered fields. The results for the complete fields are equivalent to the results over 5-years (Fenoglio-Marc, 2001). The filtered fields have higher canonical correlation coefficients, lower CVFs in the SLA-STA analysis and higher CVFs in the SLA-APA analysis. The first PCA-CCA mode of the STA and STA analysis corresponds to the rise of both sea level and sea surface temperature in the eastern Mediterranean and to their drop in the Ionian Sea. It represents 34% of the variability of the SLA and 15% of the STA field (Fig. F-08-15). The first two PCA-CCA modes of the STA and APA analysis

(both with and without inverse barometric correction) show in the spatial patterns a strong signature in the Ionian Sea. The temporal pattern of the first mode has an oscillation with maximum in 1996 (Fig. F-08-16).

Results from both methods show that the correlation between the low-pass filtered SLA and STA fields is lower than the correlation between the complete corresponding fields, while the correlation between the low-pass filtered SLA and APA fields is higher than the correlation between the corresponding complete fields.

5. Conclusions

The merging of multi-mission altimetry data increases the time series lengths and the spatial resolution of the data. The first advantage is important for long-term sea level change, as the altimeter satellite lifetime is too short for long-term, decadal and interannual studies. In this study altimetry data from different missions have been used over the same decade. The contemporaneous missions of Topex/Poseidon, ERS-1 and ERS-2 allows to check the departure between the data, the comparison of the data shows how different sensors agree in their measurements and gives an estimate of errors. Topex/Poseidon and ERS-2, simultaneously operating since April 1995, have different orbit accuracy, different spatial and temporal coverage. Due to the different coverage, differences are expected in the spectral characteristics of the signal, but not in the linear sea level change.

The linear sea level change depends on the time-interval selected due to the short altimetry time-series available. The spatial distributions of the linear sea level change during 1995.4-2000.4 corresponding to each satellite are similar, but the magnitude of the linear sea level change is different due to a relative drift between the ERS-2 and T/P data. The reliability of the linear sea level change estimated by the altimetry data is checked by comparing sea level monthly averages estimated from tide gauge stations and from altimetry over the same time interval. A good agreement is found between the tide gauge station data and the T/P altimetry, that is than used as reference altimeter dataset. The average over each ERS-2 cycle of the sea level height differences at the dual-crossover (DXO) points between T/P and ERS-2 is used as correction for the ERS-2 monthly sea level height data, the differences in the magnitude of the estimated trends is reduced. The results can be improved by using a finer modelling of the correction, like a smaller interval for the computation of the correction table and a spatial dependency of the correction.

T/P data alone have been used in the single-field analysis as the first part of the study has shown that they are the most reliable, moreover they are the longest altimeter data set available. Both the spectral and the PCA statistical decompositions of the complete and the low-pass filtered sea level fields give the dominant components of the sea level variability. Due to the relatively short altimetry time-series available, the linear sea level change is function of the time-interval selected. The average linear sea level change over the entire Mediterranean Sea in the interval between August 1992 and September 2000 is 2.2 mm/yr. In the western Mediterranean Sea the change is small, 0.4 mm/yr in average, while a strong positive change (9.3 mm/yr in average) is observed in the eastern Mediterranean Sea and a strong negative change (-11.9 mm/yr in average) in the Ionian Sea. A confidence level of more that 90% is reached for the linear sea level change in the Ionian and in the eastern Mediterranean Sea, that confirms that in those parts of the Sea a change at low frequencies occurs.

Also most of the tide gauge station data give a positive sea level change in the time-span 1993-2000. The tide gauge analysis shows in the time-span 1990-2000 an increase in sea level rise with respect to the previous decade. Sea level rise of almost similar strength are observed in the past from the longer tide gauge records indicating that the rise observed today by altimetry can have interannual or decadal frequencies. A general sea level drop starting from 1960 (Tsimplis and Baker, 2000) has not been observed here neither from tide gauge data nor from altimetry.

A high positive linear sea surface temperature change occurs in the eastern Mediterranean, i.e. in the same region where the high positive sea level change occurs. It is therefore of interest to analyse the correlation between the sea surface temperature and sea level height variations. In the coupled-field analysis significant correlations are identified by both the simple correlation and the PCA-CCA statistical method. The correlation analysis between the fields shows that sea surface height and sea surface temperature fields are strongly correlated at seasonal scales in the entire Mediterranean Sea, while the correlation at low frequencies is significant (more than 0.6) only in the eastern Mediterranean Sea. Previous studies have already shown that the interannual variability is higher in the eastern than in the western Mediterranean, where the seasonal cycle dominates (Fenoglio-Marc, 2001). A negative sea level change is observed from both altimeters in the Ionian Sea and confirmed by tide gauge data available only in the last decade. The negative sea surface temperature change observed in the sea surface temperature field in that region supports a sea level drop, being a cooling at the sea surface and at depth associated to a sea level drop. Also an increase in the salinity, documented in other parts of the Mediterranean Sea in the last decade (Roether et al., 1996) causes a negative sea level change, but this parameter has not been investigated here. The significant correlation between the low-pass filtered sea level height and atmospheric pressure fields suggests an atmospheric reason for the negative sea level change. Climatic variations in atmospheric forces can drive substantial changes in the basin-wide large scale currents (Vignudelli et al., 1999). A negative sea level trend in the Ionian Sea was obtained by Pinardi e Masetti (2000) modelling the interannual circulation of the Mediterranean Sea by a model run with interannual daily atmospheric forces. An increase in the anticyclonic circulation during a positive NAO in successive winters could then produce negative sea surface temperature and negative sea surface anomaly changes. Further analysis with new data types and longer time series are needed.

Acknowledgements

This study was supported by the Deutsche Forschungsgemeinschaft (DFG). Comments and suggestions by one of the reviewer, C.K. Shum, improved the manuscript. Aviso, ESA, Nasa, DEOS, PSMSL and the Servizio Idrografico e Mareografico Nazionale (SIMN, Italy) are acknowledged for providing the data.

References

- Anzhofer M. and Gruber T., Fully reprocessed ERS-1 altimeter data from 192 to 1995: feasibility of the detection of long-term sea level change, *J. Geophys. Res.*, 103, 8089-8112, 1998
- AVISO, Use Handbook, Merged Topex/Poseidon Products, avi-nt-02-cn edn, 1996
- Bretherton C., Smith C. and Wallace J., An intercomparison of methods for finding coupled patterns in climate data change, *Journal of Climate*, 5, 541-560, 1992

- Cazenave A., Deminh K., Gennero M., and Ferret B., Global mean sea level change observed by Topex-Poseidon and ERS-1, *Phys. Chem. Earth*, 29, 1069-1075, 1998
- Cazenave A., Deminh K., Ponchaut F., Soudarin L., Cretaux J. and Prevost C.L., Sea level change from Topex-Poseidon altimetry and tide gauges, and vertical crustal motion from Doris, *Geophys. Res. Lett.*, 26, 2077-2080, 1999
- Cersat, Altimeter and Microwave Altimeter ERS Product User Manual, c2-mut-a-01-if, 2.2 edn. 1996
- Douglas B.C., Sea level change in the era of the recording tide gauge, in *Sea Level Rise, history and consequences*, International Geophysics Series Volume 75, Academic Press, 2001
- Fenoglio-Marc L., Analysis and representation of regional sea level variability from altimetry and atmospheric oceanic data, *Geophys. J. Int.*, 145, 1-18, 2001
- Fenoglio-Marc L. and Groten E., Modelling the sea level variations for the unification of altimetry missions, *Advances in Space Research*, in press, 2001
- Lemoine F.G., Smith D.E., Kunz L., Smith R., Pavlis E. C., *Proc. Int. Symp. On Gravity Geoid and Marine Geodesy*, Springer Verlag, New York, 1997.
- Mann M. and Park J., Global-scale modes of surface temperature variability on interannual to century timescales, *J. Geophys. Res.*, 99, 25819-25833, 1994
- Moore P., The ERS-2 altimetric bias and gravity field enhancement using dual crossovers between ERS and Topex/Poseidon, *Journal of Geodesy*, Vol.75, N. 5-6, 2001
- Michum G., An improved calibration of satellite altimetric heights using tide gauge sea levels with adjustment for land motion, *Marine Geodesy*, 23, 145-166, 2000
- Nasa, AVHRR Weekly Global Gridded MCSST, JPL.PODAAC Product 016, 1999
- Nerem S. and Mitchum G., Sea level change, in *Satellite altimetry and Earth sciences*, Academic Press, San Diego, 2001
- Pinardi N. and Masetti E., Variability of the large scale general circulation of the Mediterranean Sea from observations and modelling: a review, *Paleo*, 153-174, 2000
- Preisendorfer R.W., Principal Component Analysis in Meteorology and Oceanography, n. 17 in *Developments in Atmospheric Science*, Elsevier, Amsterdam, 1988
- Ribera P., Garcia R., Diaz H.F., Gimmeno L. and Hernandez E., Trends and interannual oscillations in the main sea-level surface pressure patterns over the Mediterranean, 1955-1990, *Geophys. Res. Letters*. Vol.27, N. 8, 1143-1146, 2000
- Ross Tetjana, Garrett C. and Le Traon P.Y., Western Mediterranean sea-level rise : changing exchange flow through the Strait of Gibraltar, *Geophys. Res. Letters*. Vol.27, N. 18, 2949-2952, 2000
- Roether W., Manca B., Klein B. : Recent changes in the Eastern Mediterranean Deep Waters, *Science* 271, 333-335, 1996
- Scharroo R., Naeije M, Schrama E. and Benveniste J., A recipe for upgrading ERS altimeter data, in *ERS-ENVISAT Symposium CD*, SP-461, ESA Publications Division, 2000
- Spencer N.E. and Woordorth P.L., Data Holding of the Permanent Service for Mean Sea Level, Bidston Observatory, UK, 1991
- Theocharis A., Nittis K., Kontoyiannis H., Papageorgiou E. and Balopoulos E., *Geophys. Res. Letters*. Vol.26, N. 11, 1617-1620, 1999
- Tsimplis M.N. and Baker T.F., Sea level drop in the Mediterranean Sea : an indicator of deep water salinity and temperature changes?, *Geophys. Res. Letters*. Vol.27, N. 12, pp. 1735-1738, 2000

- Tsimplis M.N. and Josey S.A., Forcing of the Mediterranean Sea by atmospheric oscillations over the North Atlantic, *Geophys. Res. Letters*. Vol.28, pp. 803-806, 2001
- Vignudelli S., Astraldi M., Schiano M., A possible influence of the North Atlantic Oscillation on the circulation of the western Mediterranean Sea, *Geophys. Res. Letters*, 26, 623-626, 1999
- Yi Y., Determination of gridded mean sea surface from Topex, ERS-1 and Geosat altimeter data, Report N. 434, Department of Geodetic Science and Surveying, The Ohio State University, Columbus, Ohio, 1995
- Zerbini S., Plag H.-P., Baker T., Becker M. et al., Sea level in the Mediterranean: a first step towards separating crustal movements and absolute sea-level variations, in *Global and Planetary Change* 14, pp.1-48, 1996

7.4 Vertical land motion in the Mediterranean Sea

F-09: Fenoglio-Marc L., E. Groten and C. Dietz, Vertical Land Motion in the Mediterranean Sea from altimetry and tide gauge stations, *Marine Geodesy* 27, 3-4, 683-701, 2004.

Abstract We have computed estimates of the rate of vertical land motion in the Mediterranean Sea from differences of sea level heights measured by the Topex/Poseidon radar altimeter and by a set of tide gauge stations. The comparison of data at 16 tide gauges using both hourly data from local datasets and monthly data from the PSMSL dataset shows a general agreement, significant differences are found at only one location. Differences of near-simultaneous, monthly and de-seasoned monthly sea level height time-series have been considered in order to reduce the error in the estimated linear-term. In a subset of 23 tide gauge stations the mean accuracy of the estimated vertical rates is mm/yr. Results for various stations are in agreement with estimates of vertical land motion from geodetic methods. A comparison with vertical motion estimated by GPS at 4 locations shows a mean difference of mm/yr, however the length of the GPS time-series and the number of locations are too small to draw general conclusions. Both coastal and global mean sea level rise by about 3.0 ± 0.5 mm/yr from January 1993 to December 2004. Over shorter intervals the coastal sea level rises faster and over longer intervals slowly than the global mean, which trend is almost constant for each interval and is equal to 2.9 ± 0.5 mm/yr in 1993-2008. The different trends are due to the higher inter-annual variability of coastal sea level, caused by the sea level regional variability, that is further averaged out when computing the global mean.

Keywords: sea level, altimetry, tide gauge, vertical land motion

1. Introduction

The vertical land motion of the Earth crust relative to the geocentre has several causes including glacial isostatic adjustment (Peltier, 2002), volcanicity and tectonic activity (Melini et al., 2004) and subsidence due to natural and anthropogenic causes (Zerbini et al., 2002). Tide gauge stations measure sea level change relative to the Earth's crust, their measurement is therefore affected by vertical land motion. Assuming no long-term change in sea level, the vertical land motion was estimated in the past by computing trends of the sea level measured by the tide gauge stations (Emery and Aubry, 1991). It is also obtained by precise geodetic measurements like continuous GPS data (Zerbini et al. 1996), Satellite Laser Ranging (SLR), Very Long Baseline Interferometry (VLBI) and Doris (Soudarin et al., 1999).

Satellite altimetry gives an alternative and independent method to estimate the vertical land motion, as shown in previous studies (Cazenave et al. 1999, Nerem and Mitchum 2002, Kuo et al, 2004). The sea level measured by altimetry is relative to the geocentre and is therefore independent from vertical land motion, while the sea level measured by a tide gauge station is relative to the Earth's crust. For this reason the vertical land motion is contained in the long-term component of the difference between satellite altimetry and tide gauge sea level height measurements (here indicated as ALT-TG). The Topex/Poseidon (T/P) altimeter measurements are given in the Earth-centered terrestrial reference of the T/P orbit (CSR95L01/95D02) (Fu et al., 1994), our results are therefore valid in this frame. Today the global reference frame can be realised with an accuracy in the position of about 1 cm (Schuh et al., 2003) and the accuracy of the absolute positioning with respect to the Earth's center of mass is of the same order of magnitude (Tapley et al., 1994). The present analysis ignores the motion of the geocentre in this crust-fixed reference frame and systematic trends

in the reference frames (Nerem et al., 2000). The Topex data used have been corrected for the instrumental drift estimated at dedicated sites (Christensen et al. 1994, Menard et al. 1994) and by global analysis using a large set of tide gauge stations (Mitchum 1998) and accounting for vertical land motion (Mitchum 2000). The remaining error in the drift is 0.4-0.5 mm/yr for the global tide gauge calibration and is partly due to the average residual crustal motion of the tide gauge stations used (Mitchum, 2000). Thus the vertical crustal motion rates given here are relative to the mean crustal motion of those stations (Nerem and Mitchum, 2002).

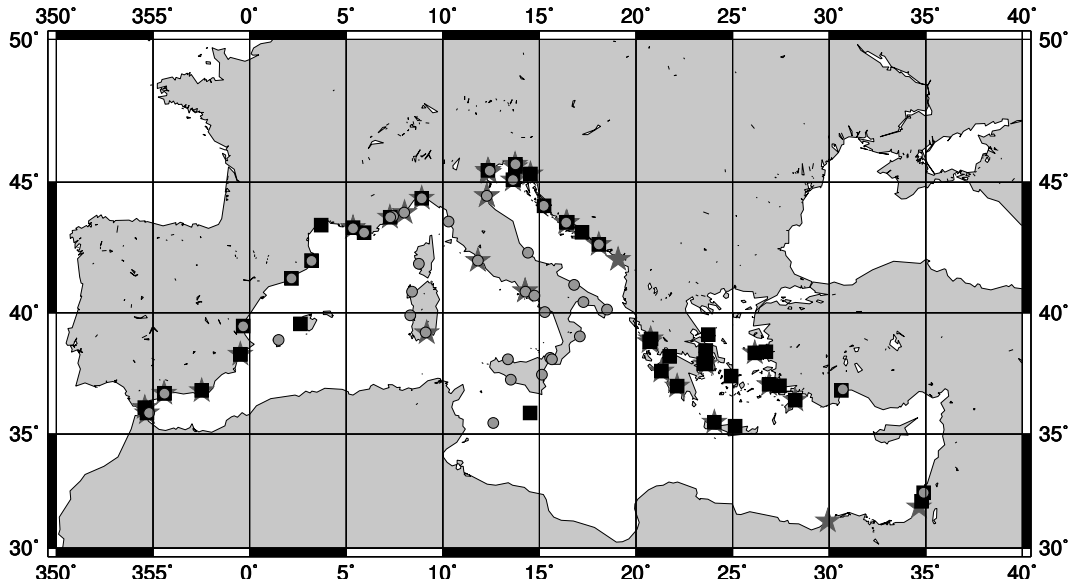


Figure F-09-1: Location of tide gauge stations with monthly averages available in the MED-PSMSL data set before 1993 (stars) and after 1993 (squares) and with hourly data available from local organisations after 1993 in the MED-LOCAL data set (circles)

Residuals errors in the altimeter environmental corrections, that are particularly critical in coastal regions, are neglected. Circulation, meteorological effects are present in the long-term differences and represent noise in our analysis. The Mediterranean Sea is interesting for this study for its small ocean tides and ocean circulation. Previous studies (Zerbini et al. 1996, Fenoglio-Marc 2001, Fenoglio-Marc 2002, Mangiarotti 2002) have shown that seasonal and longer term sea level variability from tide gauge and altimetry are in good agreement. The interval of analysis starts in 1993, with the availability of Topex/Poseidon data. Tide gauge stations with hourly data are used to allow both a quality-check of the sea level data and the use of near-simultaneous observations. In Section 2 a dataset is constructed that contains the hourly data collected from the local organisations after inspecting the differences with respect to the monthly PSMSL data. In Section 3 near-simultaneous measurements, monthly averages and de-seasoned monthly averages are used to estimate the trend of the differences ALT-TG as well as their accuracy. The accuracy of the trend is further discussed in Section 4. In Section 5 the results are compared to land motion rates estimated by GPS only, as data from SLR, VLBI and DORIS were not available in the analysed region.

2. Data Analysis

In this study Topex data from the JPL Pathfinder Project (PODAAC) Version 2 in the interval between January 1993 and December 2001 are used. The altimeter data are provided as time-series at fixed locations called normal points (Brenner et al., 1991). The

Table F-09-1: Statistics of altimetric and tide gauge sea level heights and of their differences at l'Estartit in 1993-1999 for application or not application of inverse barometric and ocean tide corrections

Time spacing	IBC	Ocean Tide (mm)	Δ_{at} (mm)	$\frac{\Delta_a}{\Delta_t}$	N_m	r_{at}	$b_{at} \pm \sigma_{at}$
Near-simultaneous	not applied	not applied	44	133 / 130	166	0.95	0.9 ± 2.0
Near-simultaneous	applied	not applied	45	93 / 97	166	0.90	0.5 ± 2.0
Near-simultaneous	not applied	applied	44	117 / 124	166	0.93	-1.2 ± 2.0
Monthly average	not applied	applied	31	78 / 79	84	0.92	1.4 ± 1.7
Monthly average	applied	applied at altimeter	29	58 / 60	84	0.88	2.0 ± 1.6
Monthly average	not applied	not applied	105	112 / 79	84	0.44	5.0 ± 5.6

following environmental corrections are applied to the altimeter data: dry tropospheric, wet tropospheric, ionospheric, sea state bias, electromagnetic bias, solid earth tide, load tide. The effects of the inverted barometer and of the ocean tidal corrections have been analysed at the station of l'Estartit in terms of standard deviation and correlation of the series and of standard deviation of their differences (Tab. F-09-1). The application of the corrections reduces the standard deviation of each time-series and of their differences both with monthly (see also Fenoglio-Marc 2002, Fenoglio-Marc 2003) and with near-simultaneous values, also the correlation of the time-series is reduced. In general homogeneous corrections applied at the tide gauge and at the altimeter data produce small standard deviation of the differences and a similar standard deviation of each time-series. There is an exception, as the agreement between the monthly averages obtained from altimeter data corrected for ocean tide and the monthly averages obtained from tide gauge data not corrected for the ocean tide is higher than the agreement between the monthly averages obtained from data both corrected for the ocean tide. This is due to the fact that the short-period (diurnal, semi-diurnal) ocean tides average to zero at a given location if tide gauge hourly data are averaged over one month but do not if the three T/P altimeter in each month are averaged. The same does not happen for the inverse barometer correction, as this correction does not average to zero at a given location over one month using high frequency observations.

The application of the ocean tide correction to the altimeter data reduces the standard deviations of both the monthly time-series and of their differences. Its application to the near simultaneous altimetry and tide gauge data reduces the standard deviations of the time-series, while the standard deviation of their differences is only slightly reduced due to the low spatial resolution and inaccuracy of the ocean tide models (FES2001) that does not account for shallow tide components. Therefore, we apply the ocean tide correction neither to altimeter nor to tide gauge data when near-simultaneous measurements are compared and we do apply the ocean tide correction to the altimetry data to evaluate gridded sea level monthly averages. Due to the unavailability of pressure data for most of the tide gauges we have considered, we apply the inverted barometric correction neither to altimeter nor to tide gauge data. The sea level anomalies are averaged in monthly grids with spacing in latitude and longitude of 1x1 degrees using a Gaussian weighted average method with the half-weight parameter equal to 1 and the search radius equal to 1.5 degrees (Fenoglio-Marc 2001).

The tide gauge stations in the Mediterranean Sea are mostly concentrated along the northern coast. The MED-LOCAL dataset contains hourly data of 41 tide gauge stations obtained from local organisations in Spain (Puertos del Estado and Universidad Politecnica de Catalonia), France (Système de l'Observation du Niveau des Eaux Littorales SONEL), Italy (Agenzia per la Protezione dell'Ambiente e Servizi Tecnici - APAT), Croatia (Hydrographic Institute of the Republic of Croatia), Israel (Israel Oceanographic and Limnological Research) and Turkey (General Command of Mapping). The tide gauge data frequency is every two hours at Estartit and hourly at the other stations. A MED-PSMSL dataset contains monthly data

Table F-09-2: Statistics of altimetric and tide gauge sea level heights and of their differences at l'Estartit in 1993-1999 for application or not application of inverse barometric and ocean tide corrections

Time spacing	IBC	Ocean Tide (mm)	Δ_{at} (mm)	$\frac{\Delta_a}{\Delta_t}$	N_m	r_{at}	$b_{at} \pm \sigma_{at}$
Near-simultaneous	not applied	not applied	44	133 / 130	166	0.95	0.9 ± 2.0
Near-simultaneous	applied	not applied	45	93 / 97	166	0.90	$0.5 \pm 2.0i$
Near-simultaneous	not applied	applied	44	117 / 124	166	0.93	-1.2 ± 2.0
Monthly average	not applied	applied	31	78 / 79	84	0.92	1.4 ± 1.7
Monthly average	applied	applied at altimeter	29	58 / 60	84	0.88	2.0 ± 1.6
Monthly average	not applied	not applied	105	112 / 79	84	0.44	5.0 ± 5.6

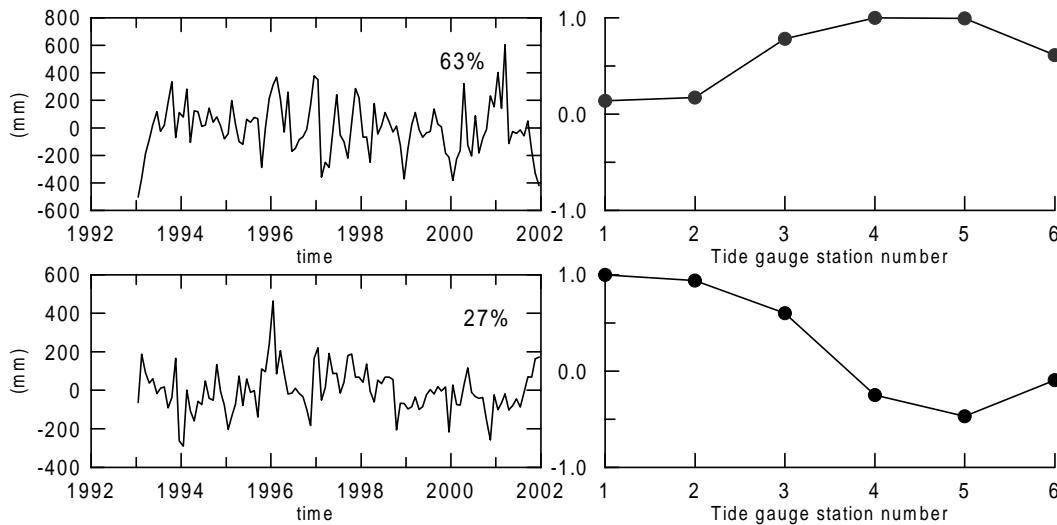


Figure F-09-2: First and second EOFs obtained by the decomposition of sea level heights from six tide gauge stations of the PSMSL database in the interval 1993-2001 (Algeciras, Malaga, l'Estartit, Trieste, Koper, Khalkis North)

of 49 tide gauge stations in the Mediterranean Sea available from the Permanent Sea Level Service (PSMSL) of the Proudman Oceanographic Laboratory in the Revised Local Reference (RLR). The quality of the monthly PSMSL data is low in the eastern Mediterranean (Tsimplis and Spencer, 1997). The two datasets MED-PSMSL and MED-LOCAL do not contain the same stations and the interval of availability is generally shorter in the PSMSL dataset. Fig. F-09-1 shows the geographical distribution of the tide gauge data available in the MED-LOCAL dataset starting from 1993 and in the MED-PSMSL dataset before and after 1993. The MED-PSMSL dataset includes only 16 out of the 41 stations made available by the local organisations; of the 25 Italian stations of the hourly dataset only 3 (Genova, Venezia and Trieste) are part of the 49 MED-PSMSL stations. The MED-PSMSL database ends in 2001, whilst the local database ends in 2002.

The MED-PSMSL data are checked against the monthly averages computed from the hourly data of the MED-LOCAL dataset. The differences between the monthly values are mainly small, with significant differences only for the station of Antalya. For the other stations the differences in the estimated vertical land motion computed from monthly averages (see Section 3) over the same period are lower than 0.5 mm/yr. Higher differences arise with a too short period of analysis.

Most of the organisations provided hourly data of high accuracy over the complete decade, however, as a high quality control of the benchmark is not always done, the rate observed could reflect in some cases not only crustal motion but also motion of the pier relative to the

Table F-09-3: Statistics of altimetric and tide gauge sea level heights and of their differences at l'Estartit in 1993-1999 for application or not application of inverse barometric and ocean tide corrections

	PSMSL Mon	PSMSL De-seas	MEDlocal Mon	MEDlocal De-seas	Final mon	Final de-seas mon
Original/ selected TG	49/24	49/15	41/23	41/19	35	24
AL-TG (km)	63/26	63/26	67/24	67/24		
	60/27	60/27	62/26	62/26	62/27	60/25
Correlation	0.77/0.12	0.64/0.19	0.70/0.24	0.62/0.22		
	0.76/0.08	0.71/0.10	0.81/0.09	0.77/0.08	0.78/0.1	0.75/0.08
Trend formal error (mm/yr)	3.6/3.0	3.3/2.9	4.9/11.6	3.4/3.4		
	2.2/0.7	1.9/0.7	1.8/0.5	1.5/0.4	1.9/0.5	1.6/0.4
Std of difference (mm)	56/24	51/23	65/42	62/41		
	55/12	44/10	48/12	40/9	52/12	42/19
Sample in time-serie	80/26	80/26	78/22	78/22		
	93/17	93/17	91/17	91/17	93/15	96/14

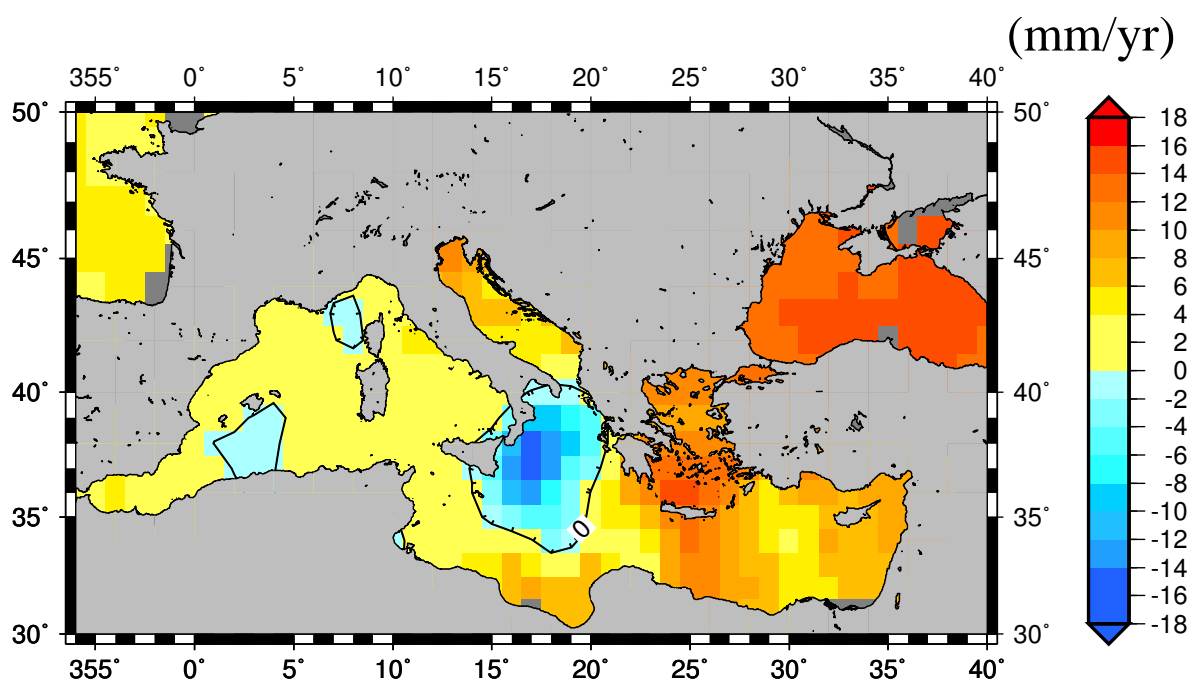


Figure F-09-3: Rate of geocentric sea level change (mm/yr) in the Mediterranean Sea in 1993-2002 from altimetry data averaged in monthly grids of 1 x 1 degrees

benchmark. Least reliable are the tide gauge data in Italy that all present a vertical offset in Summer 1998 due to a change from a floating tide gauge to a radar tide gauge instrument. As the vertical displacement of the reference point is not available, we have for each of the 25 Italian APAT stations a time-series of sea level heights with an unknown step function included. We estimate this datum shift using the Topex altimeter data. We compute monthly differences of altimeter and tide gauge sea level heights and we model each of the two series, before and after the switchover point, with a linear model. The difference between the constant terms of the two models gives an estimation of the vertical datum shift for each station. The uncertainty of the vertical offset obtained by this method is estimated by using the monthly tide gauge data of high quality of the MED-LOCAL set, it is below 2 centimetres when at least three years of data before and after the switchover point are used. As an error of 2 centimetres in the vertical offset introduces an error of 2 mm/yr in the trend of a 10-year long time-series, tide gauge stations data having unknown vertical offsets have to be considered

Table F-09-4: Comparison of de-seasoned monthly T/P altimetry and tide gauge sea level heights at 24 tide gauge stations from starting year (column 2) to end of 2001

Station	Start year	d (km)	Δ_{at} (mm)	$\frac{\Delta_a}{\Delta t}$ (mm)	N	r_{at}	$b_a \pm \sigma_a$ (mm/yr)	$b_t \pm \sigma_t$ (mm/yr)	$b_{at} \pm \sigma_{at}$ (mm/yr)	σ_{at} (mm/yr)
Ceuta	1993	21	37	55/43	107	0.74	3.6 ± 2.0	-1.3 ± 1.7	5.0 ± 1.3	1.4
Malaga	1993	87	50	64/52	108	0.64	4.1 ± 2.4	5.0 ± 1.9	-0.9 ± 1.9	2.1
Valencia	1993	58	48	55/56	107	0.62	0.8 ± 2.1	5.4 ± 2.1	-4.6 ± 1.8	3.6
Barcelona	1993	41	36	56/57	106	0.80	1.9 ± 2.1	3.5 ± 2.1	-1.5 ± 1.3	2.1
Estartit	1993	66	23	56/58	108	0.92	3.0 ± 2.1	2.4 ± 2.2	0.5 ± 0.9	1.0
Toulon	1993	15	29	50/54	106	0.85	1.9 ± 1.9	0.1 ± 2.1	1.8 ± 1.1	1.5
Venezia	1993	65	50	85/64	96	0.75	14.1 ± 3.0	8.5 ± 2.7	5.6 ± 2.1	2.5
Trieste	1993	93	53	85/70	108	0.78	15.0 ± 2.8	8.5 ± 2.5	6.5 ± 1.9	1.9
Rovinj	1993	50	50	85/67	108	0.81	15.0 ± 2.8	9.2 ± 2.4	5.7 ± 1.8	1.9
Split	1993	63	40	67/64	108	0.81	9.2 ± 2.4	8.8 ± 2.3	0.3 ± 1.5	1.7
Dubrovnik	1993	73	30	58/59	108	0.87	7.7 ± 2.0	8.6 ± 2.1	-0.9 ± 1.1	1.5
Antalya	1993	101	42	50/56	95	0.69	9.4 ± 1.7	12.4 ± 1.7	-3.0 ± 1.6	2.1
Kalamai	1993	12	44	56/58	100	0.71	12.4 ± 2.0	14.0 ± 2.0	-1.6 ± 1.8	3.0
Pyraeus	1993	109	60	64/71	67	0.63	13.6 ± 2.1	15.2 ± 2.2	-1.6 ± 2.4	4.6
Khalkis N.	1993	69	50	60/51	107	0.64	12.5 ± 2.0	6.8 ± 1.8	5.7 ± 1.7	3.6
Khios	1993	45	51	62/63	99	0.67	12.0 ± 2.2	7.6 ± 2.4	4.4 ± 1.2	2.4
Soudhas	1993	56	44	64/52	103	0.72	15.1 ± 1.8	6.8 ± 1.8	6.3 ± 1.5	2.2
Hadera	1994	60	42	50/49	88	0.65	15.1 ± 1.7	12.4 ± 1.7	-3.0 ± 1.6	4.5
Catania	1995	95	37	71/59	96	0.87	$-16. \pm 2.3$	-8.3 ± 2.1	-7.9 ± 1.2	2.0
Taranto	1995	53	40	55/57	94	0.76	-0.4 ± 2.3	4.3 ± 2.2	-4.7 ± 1.5	2.2
Bari	1995	101	29	55/51	84	0.85	1.6 ± 2.6	2.9 ± 2.4	-1.2 ± 1.4	2.1
Cagliari	1995	79	34	49/55	77	0.79	1.2 ± 2.0	3.2 ± 2.2	-2.0 ± 1.4	1.6
Porto Torres	1995	38	32	49/54	52	0.80	-0.5 ± 3.6	4.6 ± 3.1	-5.1 ± 2.0	2.7
Ravenna	1996	80	114	85/100	63	0.56	10.6 ± 6.3	18.7 ± 6.0	-8.1 ± 6.0	13.0

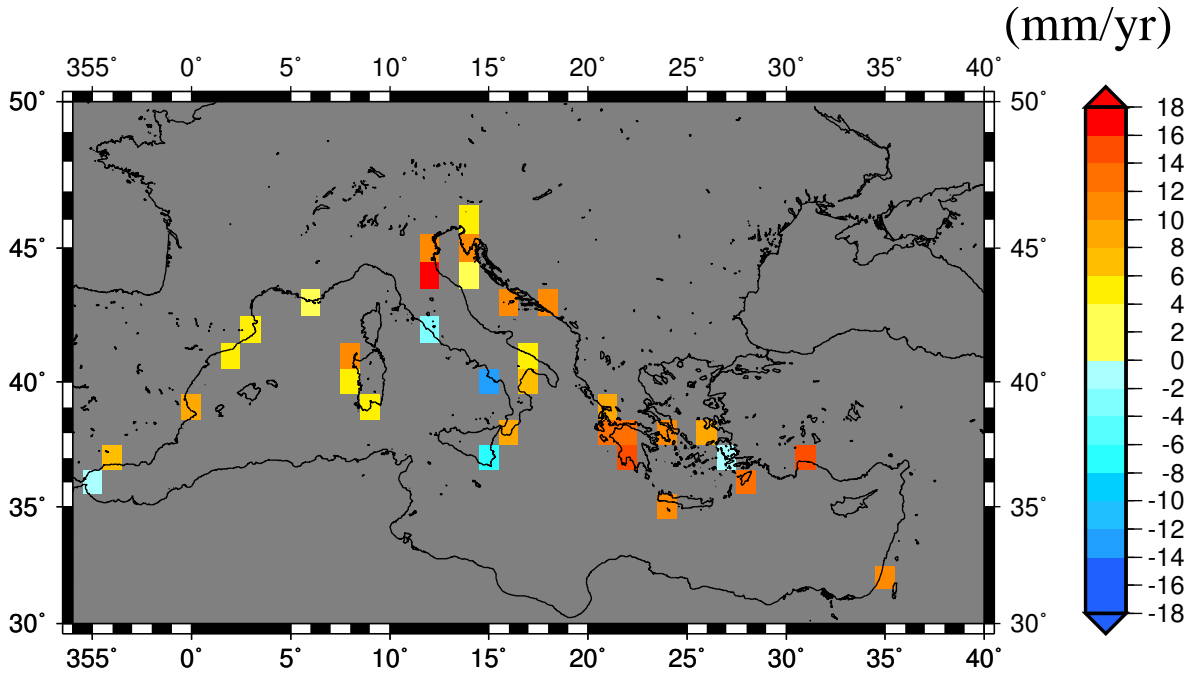


Figure F-09-4: Rate of geocentric sea level change (mm/yr) in the Mediterranean Sea in 1993-2002 from monthly averages of tide gauge data

with care. We have included in our further analysis the six APAT stations of Catania, Taranto, Bari, Cagliari, Porto Torres and Ravenna as their time-series are long enough.

Of the 41 stations with hourly values, only 13 stations have reliable hourly data over the complete interval 1993-2001. The series that are too short or present too many gaps have

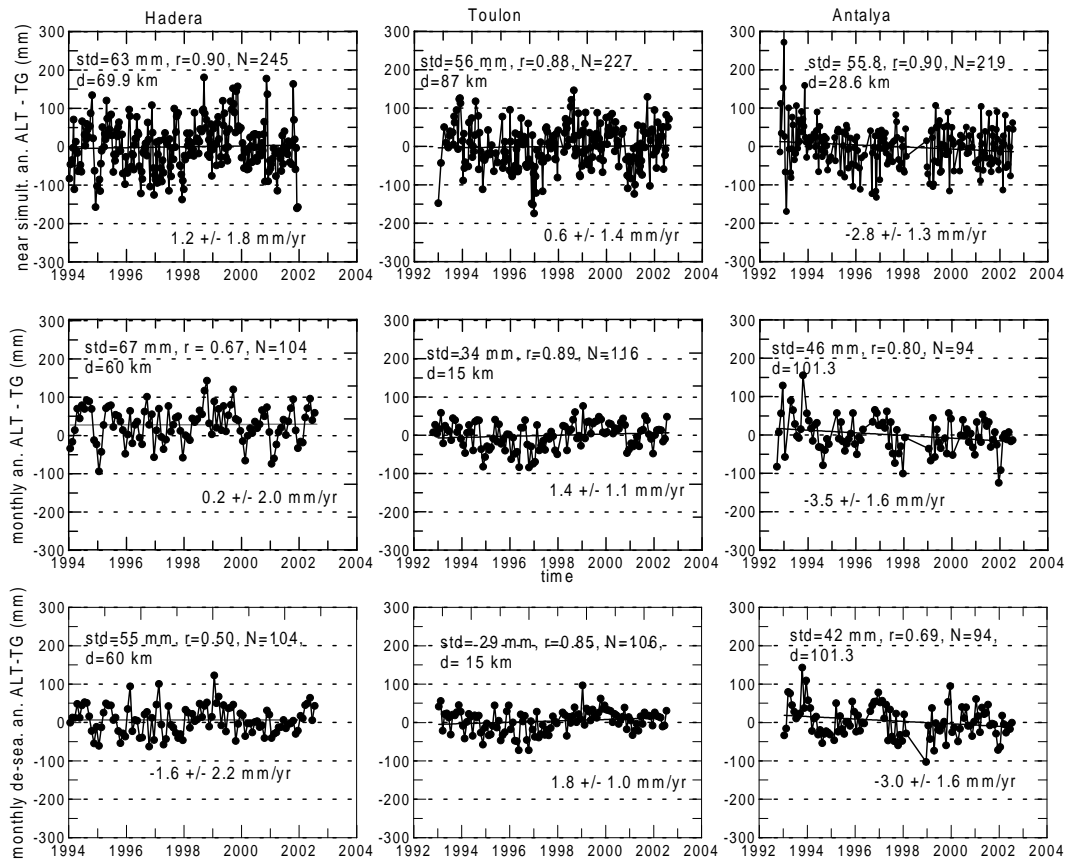


Figure F-09-5: Anomalies of sea level height differences of Topex altimetry and tide gauge data at the stations of Hadera, Toulon and Antalya corresponding to near-simultaneous measurements (top), monthly averages (middle) and de-seasoned monthly averages (bottom)

been excluded. As hourly data from Greece were not available, monthly data from the MED-PSMSL are used in this region. The seasonal component is evaluated and subtracted from the monthly value to obtain de-seasoned monthly anomalies. The consistency of nearby records is checked by differencing the records, by estimating the correlation between the time-series and by performing an Empirical Orthogonal Functions (EOF) analysis both on the monthly and on the de-seasoned monthly anomalies. Differences are identified between the regional basins, as shown by the spatial coefficients of the EOF decomposition of six tide gauge stations of the PSMSL database in the interval 1993-2001 (Fig. F-09-2). Non-standardized anomalies are considered and the spatial vectors are normalised to the maximum value for each mode. The first and second EOFs explain respectively 63% and 27% of the total variability. The remaining EOFs fail a significant test based on a Monte Carlo technique (Overland and Preisendorfer 1982, Preisendorfer 1988) that selects principal components for which the signal is greater than the level of noise. The first EOF correspond to an oscillation in phase for all the six stations, whilst the second EOF corresponds to an oscillation out of phase between the stations located in the eastern and in the western basins, in agreement with results from altimetry data alone (Kjaer et al., 2003). Correlation in time with the nearest altimeter grid point time-series is used in the next session as additional check on the quality of the tide gauge data.

3. Sea level change and vertical motion

The geocentric vertical motion is related to the rate of vertical sea level change relative to the Earth crust measured by the tide gauge and to the rate of geocentric sea level change measured by altimetry through the relationship:

$$\dot{u}(P) = \dot{g}(P) - \dot{s}(P) \quad (\text{F-09-1})$$

The geocentric vertical motion is determined directly at each tide gauge station from the differences of altimetric and tide gauges time-series in Eq. F-09-1 (Nerem and Mitchum, 2002). Kuo (Kuo et al, 2004) uses additional conditions to link the relative vertical land motion between all the stations.

The rate of geocentric sea level change \dot{g} measured by altimetry in the period 1993-2001 is evaluated in each point of the grid through a least squares procedure by solving for the linear-term of the time-series of monthly averaged altimetric sea level heights. The resulting \dot{g} is mostly positive in the European region and lower than 6 mm/yr except in the Ionian part of the Mediterranean Sea (up to 14 mm/yr) and in the eastern Atlantic Ocean at the location of the Gulf Stream. Higher values are observed in the eastern Mediterranean Sea (up to 10 mm/yr) and in the Black Sea (up to 14 mm/yr). The standard error of the linear-term of sea level change is smaller than 3 mm/yr almost everywhere, it is higher than 4 mm/yr in the regions of high variability. The rate of geocentric sea level change is dependent on the period analysed. Fig. F-09-3 shows the values in the Mediterranean Sea. The rate of vertical sea level change relative to the Earth crust \dot{s} is evaluated over the same time interval 1993-2001 from monthly averages of tide gauge data at a set of stations in the Mediterranean Sea. The resulting \dot{s} is in general agreement with the altimetric results, with the positive highest values in the eastern Mediterranean and negative values along the southern Italian coasts (Fig. F-09-4). Because of the different spatial and temporal sampling of altimetry and tide gauge data, care must be taken to match the hourly sea level measurements made at the tide gauge stations with the 10-day sea level measurements from Topex. In Nerem (Nerem and Mitchum, 2002) daily-averages at the tide gauge stations and up to eight passes of the altimeter were used, temporal and spatial lags were allowed before differencing the series and the altimetric height data were smoothed in the along track direction (Mitchum, 2002). Due to the local characteristics of sea level variability and circulation in the semi-closed Mediterranean Sea, we use the absolute sea level heights measured by satellite altimetry in the vicinity of each tide gauge station. For de-seasoned monthly and monthly averages the geocentric altimetric sea level heights at the closed grid-point are used, while for near-simultaneous measurements the geocentric altimetric sea level heights interpolated along-track to the nearest normal point are used. In this last case the differences in ocean tide and ocean circulation between the location of the tide gauge station and the altimeter point are neglected due to the small ocean tides and ocean circulation in the Mediterranean Sea. Five parameters are identified for the comparison between altimetry and tide gauge sea level heights. They are: (1) the distance d_{at} between altimeter and tide gauge locations, (2) the correlation r_{at} between the time-series, (3) the formal error σ_{at} of the linear fit to the sea level height differences, (4) the standard deviation Δ_{at} of the sea level height differences, (5) the number of months N_m available. Tab.F-09-2 gives in bold (upper lines) the mean and the standard deviation of the five parameters for both the MED-PSMSL and the MED-LOCAL datasets. Both the correlation r_{at} and the standard deviation Δ_{at} as well as the formal error σ_{at} decrease using de-seasoned monthly data. The mean difference of the seasonal components of the altimeter and of the tide gauge is 25 millimetres, the elimination of the seasonal components reduces the variability in the

time-series themselves and in the time-series of the differences. The higher standard deviation of the parameters are observed in the original MED-LOCAL dataset, as it correspond to APAT data uncorrected for the vertical datum shift. Selection criteria are defined for each of the parameters 2-5 choosing values close to the minimum value of the average for r_{at} and N_m and to the maximum for σ_{at} and Δ_{at} . Distances up to 110 kilometres are allowed between the altimetry and the tide gauge locations.

Tide gauge stations are selected that satisfy the conditions: (1) d_{at} smaller than 110 kilometres, (2) r_{at} higher than 0.60, (3) σ_{at} smaller than 5 mm/yr, (4) Δ_{at} smaller than 8 centimetres, (5) N_m bigger than 50. Tab.F-09-2 shows in the lower lines the statistics of the parameters for both the MED-LOCAL and the MED-PSMSL datasets after application of the selection criteria. With de-seasonal data, 19 stations out of the 41 stations of the MED-LOCAL dataset satisfy the conditions, whilst with monthly data 23 stations satisfy the conditions. Of the 49 stations of the MED-PSMSL dataset 15 stations satisfy the conditions with de-seasoned data, 24 stations with monthly data. The statistics of parameters 2-5 for the selected stations is given in the last two columns of Tab.F-09-2 for the monthly and for the de-seasoned monthly time-series. The mean correlation is 0.78 and 0.75, the mean formal error of the trend is 1.9 mm/yr and 1.6 mm/yr, the mean standard deviation of the differences is 52 mm and 42 mm respectively for monthly and de-seasoned monthly time-series. Most of the spanish and french stations of the MED-LOCAL dataset satisfy the selection criteria. To cover the other geographical regions, six stations of the MED-PSMSL dataset in Greece are included, as well as five stations in southern Italy that are available over an interval shorter than the base interval 1993-2001. The station of Ravenna does not satisfy the criteria, but is selected to be compared with GPS results.

Tab.F-09-3 shows the 24 stations selected from the de-seasoned monthly time-series. The linear sea level changes estimated independently from altimetry and from tide gauge data (column 7 and 8) are in good agreement, as already shown in Figs. F-09-3 and F-09-4 for the monthly time-series, the linear-term of the differences is in general small and within the standard error. When accounting for the departure of the residuals from a Gaussian random noise, the error of the linear-term increases. The good agreement between altimetry and tide gauge time-series is shown by a small standard deviation Δ_{at} of the height differences (column 3), a similar standard deviation Δ_a and Δ_t of each of the time-series (column 4) and their high correlation r_{at} (column 6). The best agreement is generally achieved with a large number of time-points and a short distance to the grid node, because the differences in sea level changes increase generally with the distance. The parameter distance d_{at} plays a bigger role when instantaneous data are used due to the averaging at each grid point. The accuracy of the estimated linear-term of the differences depends on the standard deviation of the residuals along the trend line (Equation F-09-2) and therefore also on the standard deviation of the differences between altimeter and tide gauges. With additional corrections and improved models the standard deviation decreases (Mangiarotti, 2003). The linear term of each time-series depends on the interval considered, whilst the linear term of the differences is less dependent on the interval chosen. Tab. F-09-4 shows the corresponding parameters for monthly time-series in a sub-set of the stations. The results are in agreement with the values computed from the de-seasoned monthly averages.

The comparison between near-simultaneous altimetric and tide gauge sea surface heights has been used for the calibration of the altimeters and for the monitoring of the altimeter drift (Mitchum 1998, Xiaojun et al. 2002, Liebsch et al. 2002, Bosch 2002), here they are used in the same way as the monthly averages to evaluate the change in the parameters 2-5 (r_{at} , σ_{at} , Δ_{at} and N_m). No corrections have been applied to the hourly tide gauge data. Time-series

Table F-09-5: Comparison of monthly Topex altimetry and tide gauge sea level heights in a subset of Tab.F-09-3 from starting year (column 2) to end of 2001

Station	Start year	d (km)	Δ_{at} (mm)	$\frac{\Delta_a}{\Delta t}$ (mm)	N	r_{at} (mm/yr)	$b_a \pm \sigma_a$ (mm/yr)	$b_t \pm \sigma_t$ (mm/yr)	$b_{at} \pm \sigma_{at}$ (mm/yr)
Malaga	1993	87	55	83/69	108	0.76	5.7 ± 3.0	6.7 ± 2.5	-1.0 ± 2.0
Barcelona	1993	41	41	88/83	106	0.89	4.3 ± 3.3	5.6 ± 3.0	-1.3 ± 1.5
Estartit	1993	66	29	78/77	108	0.94	4.8 ± 2.8	4.4 ± 2.8	0.4 ± 1.0
Toulon	1993	15	35	71/75	106	0.89	3.6 ± 2.6	1.9 ± 2.7	1.6 ± 1.2
Antalya	1993	101	45	69/79	83	0.82	8.9 ± 2.6	11.9 ± 2.9	-3.0 ± 1.7
Hadera	1994	60	46	85/67	96	0.85	8.0 ± 3.7	8.5 ± 2.8	-0.5 ± 2.0

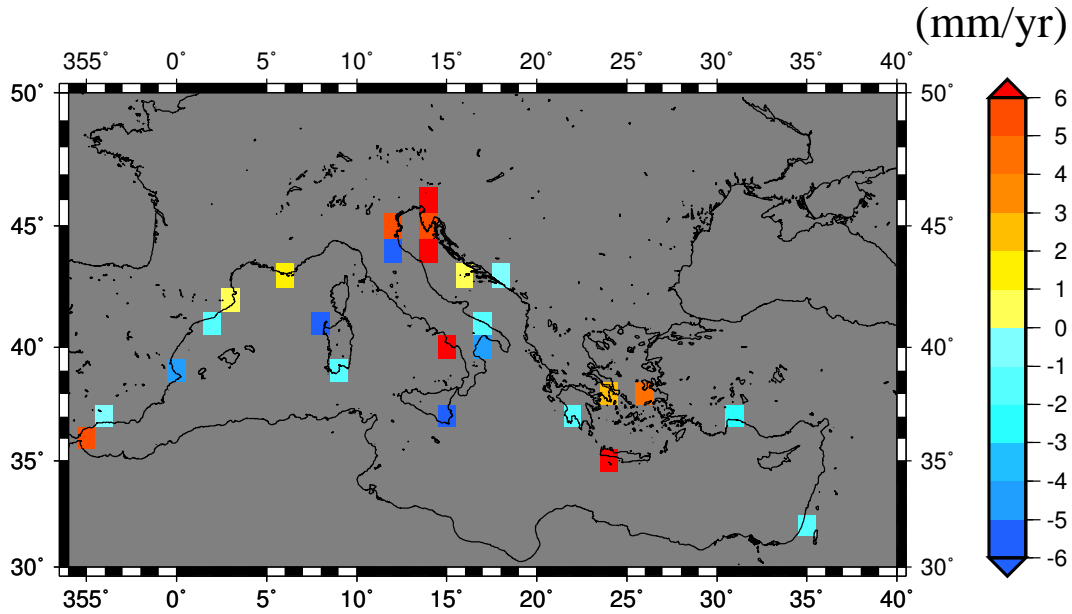


Figure F-09-6: Vertical Land Motion estimated from de-seasoned monthly differences of sea level heights from altimetry and tide gauge data.

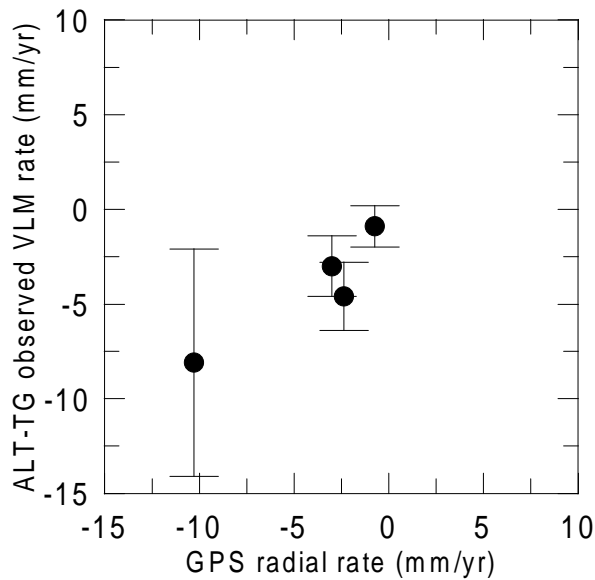


Figure F-09-7: Comparison of 4 vertical motions derived from the combination of altimetry and tide gauge data with GPS rates. Rate differences greater than 10 mm/yr have been excluded from this comparison.

Table F-09-6: Comparison of instantaneous sea level heights from tide gauge and from Topex altimetry from starting year (column 2) to end of 2001

Station	Start year	d (km)	Δ_{at} (mm)	$\frac{\Delta_a}{\Delta t}$ (mm)	N	r_{at} (mm/yr)	$b_a \pm \sigma_a$ (mm/yr)	$b_t \pm \sigma_t$ (mm/yr)	$b_{at} \pm \sigma_{at}$ (mm/yr)
Malaga	1993	89	85	218/185	195	0.92	2.5 ± 6.0	8.8 ± 5.1	-6.3 ± 2.3
Barcelona	1993	50	64	125/115	230	0.86	-2.7 ± 3.1	1.7 ± 2.9	-4.4 ± 1.6
Estartit	1993	21	41	124/126	255	0.95	3.1 ± 3.0	2.2 ± 3.0	0.8 ± 1.0
Toulon	1993	87	56	112 /115	208	0.88	-1.6 ± 3.3	-2.7 ± 3.2	-1.0 ± 1.6
Antalya	1993	28	51	126 /123	199	0.92	12.0 ± 3.2	13.7 ± 3.0	-1.6 ± 1.3
Hadera	1994	70	63	145 /129	245	0.90	10.7 ± 4.0	9.5 ± 3.5	1.1 ± 1.8
LesSables D'Olonne	1993	48	110	1166./1176.	197	0.99	$-0.8 \pm 31.$	$1.1 \pm 31.$	-9.9 ± 2.8

of the tide gauge data are constructed at the time of the altimeter pass near to the station. The not perfect alignment of the ground-tracks of the repeat-track satellites does not allow to assume that the variations in height among the repeat tracks is only due to the sea surface variability. In regions of steep geoid gradients in the cross-track direction, the orbit misalignment can cause significant geoid-induced height variability. The cross-track geoid gradients are accounted for the computation of normal points in the Pathfinder dataset. Tab.F-09-5 shows the relevant parameters obtained from the near-simultaneous time-series. The results are in general agreement with the values computed from the de-seasoned monthly averages. The standard deviation of the differences increases as well as the correlation. Comparison with a tide gauge in the Atlantic Ocean shows a higher standard deviation of the differences in the Atlantic Ocean than in the Mediterranean Sea, due to the higher sea level variations in the ocean. Also, the correlation coefficient between the tide gauge data and the selected altimeter normal-point is higher in the Atlantic Ocean than in the Mediterranean Sea, this higher correlation is also confirmed by the analysis of normal-points along the same altimeter track: in the Atlantic Ocean the correlation is higher than 0.91 for a distance between points smaller than 40 kilometres for all the considered tracks, while in the Mediterranean Sea this holds only for 62% of the tracks. To reduce the standard deviation of the differences at the overflight, we have applied the ocean model GOT002 estimated at the altimeter and at the tide gauge location. The effect of this differential correction on the sea level height differences is almost zero in the Mediterranean Sea and in the Atlantic Ocean is small, as the standard deviation of the differences is reduced by less than one millimetre near Toulon (Mediterranean Sea) and by 12 millimetres near Les Sables d'Olonne (Atlantic Ocean). As the global model does not contain the shallow water constituents, those components remain in the ALT-TG residuals. Fig. F-09-5 shows the ALT-TG differences obtained using near-simultaneous, monthly and de-seasoned monthly data at the three stations of Hadera, Toulon and Antalya. The standard deviation of the differences is higher for near-simultaneous values, part of the differences is due to the differential variability at the station and at the altimeter point. Fig. F-09-6 gives the vertical land motion estimated by de-seasoned monthly time-series. The smallest values are obtained at stations in the north-western Mediterranean.

4. Accuracy of vertical motion

Linear regression has been used to estimate a linear trend in the sea level heights and in the differences of altimetric and tide gauge station sea level heights. The linear regression model assumes that the signal consists of a trend with Gaussian random noise, that is that the residuals are independent random variables with zero mean and constant variance. The probable uncertainty of the linear term of the regression is

Table F-09-7: Accuracy of the linear-term in Ceuta computed from lag-1 autocorrelation , corresponding Effective Degree of Freedom (EDOF) and inflation factor compared to the formal error and degree of freedom DOF for monthly and de-seasoned sea level heights of altimetry and tide gauge data and for their differences. DOF is equal to 105.

Time-series	r^1	EDOF	F_l	σ (mm/yr)	σ^1 (mm/yr)
Monthly ALT	0.50	34	1.74	2.7	4.8
Monthly TG	0.51	34	1.75	2.1	3.7
Monthly ALT-TG	0.20	70	1.23	1.5	1.9
De-seasoned monthly ALT	0.31	55	1.38	2.1	2.8
De-Seasoned monthly TG	0.33	53	1.42	1.6	2.3
De-Seasoned monthly ALT-TG	0.06	94	1.06	1.3	1.4

$$\sigma = \frac{s_e}{[\sum_{i=1}^n (t - \bar{t})^2]^{1/2}} \quad (\text{F-09-2})$$

where s_e is the standard deviation of the residuals around the trend line (i.e. the root of the sum of the squares of the residuals divided by the number of observations n minus 2) and the summation is over all values of the time t (Wilks, 1995). In case of uncorrelated measurements σ is a good estimation of the error in the linear part, but deviation from this hypothesis limits its reliability. Fig. F-08-5 shows that there is a serial correlation of the residuals about the trend line. The lag-1 autocorrelation of the de-trended sea level time-series values r^1 , also called serial correlation coefficient, is a measure of the independence of the measurements (Maul and Martin 1993). With a lag-1 correlation r^1 the effective sample size is reduced from n to

$$n^1 = n \frac{1 - r^1}{1 + r^1} \quad (\text{F-09-3})$$

and the probable uncertainty of the linear-term is

$$\sigma^1 = \sigma F_l = \sigma \sqrt{\frac{1 + r^1}{1 - r^1}} \quad (\text{F-09-4})$$

where F_l is the inflation factor.

With a lag-1 correlation coefficient of 0.33, the effective degree of freedom (EDOF) is one-half the number of observations and the estimated error increases by about 40%. Tab.F-09-6 gives the lag-1 correlation r^1 , the EDOF, the standard error σ and the error σ^1 of the linear-term for the monthly and de-seasoned monthly altimetric and tide gauge time-series as well as for the corresponding differences between altimetric and tide gauge time-series at the station of Ceuta. The lag-1 correlation is higher for the monthly than for the de-seasoned monthly time-series and is higher for the time-series than for their differences. For both monthly and de-seasoned monthly time-series the EDOF is one-half the number of observations or smaller, it is bigger for the time-series of the differences. Accounting for the dependence of the measurements, the mean of the errors of the trend of the differences between altimetry and tide gauge for the 24 stations of the final de-seasoned monthly dataset (Tab.F-09-2) increases from a σ of 1.6 ± 0.4 mm/yr to a σ^1 of 2.3 ± 0.8 mm/yr.

5. Discussion of results

The agreement between the linear changes in nearby stations is within the standard error for most of the stations along the north-western coast of the Mediterranean Sea. As we

Table F-09-8: Comparison of instantaneous sea level heights from tide gauge and from Topex altimetry from starting year (column 2) to end of 2001

Station	Interval GPS year	$b \pm \sigma$ (mm/yr)	Interval ALT-TG	$b_{at} \pm \sigma_{at}$ (mm/yr)
Ceuta	2000.6-2002.9	-6.3 ± 4.6	1993-2001	5.0 ± 1.3
Dubrovnik	2000.7-2002.9	-0.7 ± 0.8	1993-2001	-0.9 ± 1.1
Valencia	2001.0-2002.9	-2.4 ± 0.9	1993-2001	-4.6 ± 1.8
Antalya	1992-2002	-2.4 ± 0.9	1993-2001	-3.0 ± 1.6
Ravenna	1996-1999.5	-2.4 ± 0.9	1993-2001	-8.2 ± 6.0

represent ALT-TG , a positive value of the trend corresponds to a land uplift. The linear component of the ALT-TG values indicates smaller VLM along the north-western coast of the Mediterranean sea and higher VLM in the Italian peninsula and in the eastern part of the Mediterranean coasts.

Vertical land motion in the Mediterranean Sea region is not dominated by glacial isostatic adjustment (GIA). The mean of the vertical land rates derived from 63 tide gauge stations in the Mediterranean area using the ICE-4G (VM2) model (Peltier, 2002) is -0.07 ± 0.17 mm/yr, with extreme values smaller than 0.5 mm/yr. The observed VLM is therefore due to volcanicity and tectonic activity and subsidence due to natural and anthropogenic causes. The results are compared with results from previous studies on VLM.

In the Carpatho-Balcanic region (CBR, Adriatic eastern coast) a relatively small vertical land motion ranging from 4 to 6 mm/yr has been recorded by geodetic levelling (Joo et al., 1981) with uplift in the northern part and subsidence in the southern part of the coast. This is in quite good agreement with the small negative subsidence and uplift estimated respectively in Dubronik (-0.9 mm/yr) and in Split (0.3 mm/yr) and with the higher uplift estimated in Rovinj (5.7 mm/yr). Similar rates are found in (Di Donato et al., 1999) modelled by the combined effects of GIA and active tectonics and in Zerbini et al.(1996).

In Spain the vertical rate of height change is small with a higher uplift in southern Spain (Becker et al., 2002), in agreement with the small values registered in Barcelona and in L'Estartit (-1.5 ± 1.3 mm/yr and 0.5 ± 0.9 mm/yr, respectively) and higher values in the southern part that is the most tectonically active.

Small land uplift along the ligurian coasts from Nice to Genova are in agreement with other works were altimetry data have not been used in the investigation (Zerbini et al. 1996, Woodworth 2003, Lama and Corsini 2003). A strong land subsidence of -10.3 ± 0.1 mm/yr due to anthropogenic reasons has been measured in Ravenna by continous GPS measurements over 4.5 years starting from 1996 (Becker et al. 2002, Zerbini et al. 2002) and is in agreement with the land subsidence (-8.1 ± 6.0 mm/yr) derived during the same period from altimeter and tide gauge differences (Tab.F-09-3 and Tab.F-09-7). The accuracy of the vertical land motion we estimate is low, due to the low quality of the tide gauge data in Ravenna, while the high estimated uncertainty given by Becker (Becker et al., 2002) correspond to the formal error only.

In Greece a general tendency for land subsidence was detected in most of the stations except in Piraeus by the SELF project using two epoch GPS campains (Becker et al. 2002). Here we have found both subsidence (Piraeus and Kalamai) and uplift (Khalkis North, Khios and Soudhas).

In Turkey the subsidence in Antalya (-3.0 ± 1.6 mm/yr) is in agreement with the subsidence of the primary tide gauge benchmark of Antalya (-5.3 ± 1.8 mm/yr) estimated by episodic GPS campains in the interval 1992-2002 (Yildiz et al., 2003). The subsidence value obtained

using the monthly averaged hourly data is by a factor of 10 smaller than the value computed using the monthly means available in the PSMSL dataset, that are clearly not correct.

The up-component of the GPS measurements monitors the land vertical motion. The time-series provided by EUREF (<http://www.epncb.oma.be/dataproducts/timeseries/index.html>) and by SONEL (<http://www.sonel.org>) are still too short for a significant estimation of their trend. The rates of VLM are evaluated from the GPS measurements by computing the trend of the up-components of about two years of weekly GPS solutions of the SONEL database (left in Tab.F-09-7). The rates computed in Dubrovnik (-0.7 ± 0.8 mm/yr) and in Valencia (-2.4 ± 0.9 mm/yr) are in agreement with the trend of sea level differences, while the rate computed in Ceuta are in disagreement (-6.3 ± 4.6 mm/yr). Considering the four stations in Tab.F-09-7 with rate differences lower than 10 mm/yr, the mean the mean difference between the vertical rates estimated from GPS and from altimetric and sea level tide gauge differences is -0.04 ± 1.8 mm/yr. Fig. F-09-7 displays a comparison between the T/P-tide gauge vertical crustal motion estimates and the GPS VLM rate estimates.

6. Conclusions

We have estimated absolute vertical land motion in the Mediterranean Sea relative to the geocentre by computing the linear-term of the differences of altimetric and tide gauges sea level height time-series. Two datasets have been used: (1) the MED-PSMSL dataset that contains 49 stations with monthly time-series extracted from the PSMSL dataset, (2) the MED-LOCAL dataset of 41 stations with hourly data including 25 stations that are not part dataset. By comparing monthly data of the stations available in both sets, significant differences are found in only one of the stations, showing a general good quality of the PSMSL dataset in the Mediterranean region. An unknown change in the reference level in the Italian stations of MED-LOCAL in Summer 1998 is estimated from monthly differences of altimetry and tide gauge data, a check using stations with high quality data shows that the vertical offset can be estimated with an uncertainty of less than 2 centimetres if the time-series is sufficiently long at both sides of the switchover point.

The agreement between monthly time-series of altimeter and tide gauge data is used to define selection criteria for the tide gauge stations. The criteria are based on the mean values of four parameters and are applied to both the monthly and de-seasoned monthly differences. More stations satisfy the criteria when monthly data are used than when de-seasoned monthly data are used. Whilst most of the stations of both the MED-PSMSL and the MED-LOCAL datasets satisfy the criteria, the criteria are not satisfied in a few italian stations with time-series too short or several not documented vertical offsets for the same record. Monthly data, de-seasoned monthly data and near-simultaneous data lead to similar values for the estimated trends. The use of an ocean tide model does not reduce significantly the standard deviation of the near-simultaneous differences both in the Mediterranean Sea and in the North Atlantic Ocean as it does not account for the shallow water components. A reduction using spectral analysis of the time-series themselves would be more appropriate, however the improvement is expected to be small in the Mediterranean Sea, as the ocean tide is here small. The mean of the uncertainty of the estimated linear-term of the monthly differences is reduced from 1.9 ± 0.5 mm/yr to 1.6 ± 0.4 mm/yr with de-seasoned monthly time-series. Accounting for the dependence of the measurements, it increases to 2.3 ± 0.8 mm/yr for the subset of 24 stations with de-seasoned monthly time-series.

Comparing the estimated vertical crustal motion to independent estimates from satellite geodetic measurements and classical techniques, we observe that the T/P-tide gauge trends identify subsidence and uplift phenomena in agreement with the geophysical properties of the region. In particular, a realistic small linear-term of the differences is obtained at several stations along the north-western Mediterranean coast, with the smallest value at L'Estartit. Higher values of the linear-term observed in the Italian peninsula and in the eastern Mediterranean Sea are probably related to vertical land motion, but also to instrumental errors in the Italian data, as the quality of those data is sometimes poor.

Comparison with the trend of the vertical component of GPS measurements at four stations yields a difference of mm/yr, however the length of the GPS time-series and the number of locations are too small to draw general conclusions. This preliminary study shows that some correlation exists between the geodetic solution for vertical positions and our results, but that longer GPS time-series are necessary for the comparison. Extension of the altimeter data span and of the hourly tide gauge set would also improve the accuracy of the absolute vertical motion estimated.

Acknowledgments

The authors acknowledge NASA for the Pathfinder Topex-Poseidon data and the local organisations providing the hourly tide gauge data (Puerto del Estado, Universitat de Catalunya in Barcelona, Système de l'Observation du Niveau des Eaux Littorales, Agenzia per la Protezione dell'Ambiente e dei Servizi tecnici, the Israel National Institute of Oceanography and the Turkish Mapping Authority). Comments and suggestions of the two reviewers improved the quality of the paper. Financial support to the first author was provided by the Deutsche Forschungsgemeinschaft and by the European Sea Level Service Research Infrastructure (ESEAS-RI) Project of the European Union.

5. References

- Becker M., Zerbini S., Baker T., Bürki B., Galanis J., Garate J., Georgiev I., Kahle H., Kotzev V., Lobazov V., Marson I., Negusini M., Richter B., Veis G., Yuzefovich P., 2002. Assessment of height variations by GPS at Mediterranean and Black Sea coast tide gauges from the SELF projects, *Global and Planetary Change* 34, 1-30
- Bosch W. 2001. Correlation between multi-mission altimeter time-series and tide gauge registration in the Caribbean Sea, In Drewes H., Dodson A., Souto Fortes L.P., Sanchez L. and Sandoval P. editors, *IAG Symposium 124: Vertical Reference Systems*, pp. 231-237, Springer Verlag, Berlin, Heidelberg, New York
- Brenner C.A., Koblinsky C.J. and Beckley B.D., 1990. A preliminary estimate of geoid-induced variations in repeat orbit satellite altimeter observations, *J. Geophys. Res.* 95 (C3):3033-3040
- Cazenave A. et al., 1999. Sea level change from Topex-Poseidon altimetry and tide gauge and vertical crustal motions from DORIS, *Geoph. Res. Lett.* 26 (14):2077-2080
- Christensen E.J., Haines B.J., Keihm S.J., Morris C.S., Noran R.A., Purcell G.H., Williams B.G., Wilson B.D., Born G.H., Parke M.E., Gill S.K., Shum C.K., Tapley B.D., Kolenkiewicz R., Nerem R.S. 1994. Calibration of Topex/Poseidon at Platform Harvest, *J. Geophys. Res.* 99 (C1):24465-24485
- Di Donato G., Negredo A.M., Sabadini R. and Vermeersen L.L.A., 1999. Multiple processes causing sea-level rise in the Central Mediterranean, *Geoph. Res. Lett.* 26 (12):1769-1772
- Emery K.O. and Emery D.G.; 1991: *Sea levels, land levels and tide gauges*, Springer-Verlag 237 pages
- Fenoglio-Marc L., 2002. Long-term sea level change in the Mediterranean Sea from multi-mission satellite altimetry and tide gauge stations, *Physics and Chemistry of the Earth*, 27:1419-1431

- Fenoglio-Marc L., Groten E., 2002. On the variability of mean sea level, *Allgemeine Vermessungs-Nachrichten*, 27:1419-1431
- Fenoglio-Marc L. and Groten E., 2003. Cross-calibration of the Envisat range using multi-mission altimetry and tide gauges in the Mediterranean Sea, in publication, *Envisat Calibration Report*, ESA
- Fenoglio-Marc L., 2003. Comparison of altimetry and tide gauge data of the SIMN italian dataset, PO-TN-ESR-RA-102, in publication, *Envisat Calibration Report*, ESA
- Joo E. et al., 1981. Recent vertical crustal movements of the Carpatho-Balkan Region, *Tectonophysics*, 71:41-52
- Kjaer N., Andersen O., Knudsen P. and Fenoglio-Marc L., 2003. Report on sea level variations for the European Seas and the North Atlantic Ocean using altimetry and tide gauge data, ESEAS-RI WP3.1 annual report.
- Kuo C.Y., Shum C.K., Braun A. and Mitrovica J.X., 2004. Vertical crustal motion determined by satellite altimetry and tide gauge data in Fennoscandia, *Geoph. Res. Lett.* 31 (1), 10.1029/2003GL019106, L01608
- Liebsch G., Novotny K., Dietrich R. and Shum C.K., 2002. Comparison of multimission altimetric sea-surface heights with tide gauge observations in the Southern Baltic Sea, *Marine Geodesy*, 25:213-234
- Mangiarotti, 2003. Les variations basse fréquence du niveau de la mer Méditerranée au cours de la deuxième moitié du XX siècle par altimétrie spatiale et maregraphie, Université Paul Sabatier Toulouse, PhD Thesis, 178 pages
- Maul G.A., Martin D.M., 1993. Sea level rise at key west Florida, 1846-1992: America's longest instrument records?, *Geoph. Res. Lett.* 20 (18):1955-1958
- Melini D. and Piersanti A., Spada G., Soldati G., Casarotti E. and Boschi E., 2004. Earthquakes and relative sea level changes, *Geoph. Res. Lett.* 31 (9), 10.1029/2003GL019347, L09601
- Menard Y., Jeansou E. and P. Vincent, 1994. Calibration of the Topex Poseidon altimeters at Lampedusa : Additional results at Harvest, *J. Geophys. Res.* 99 (C12):24487-24504
- Mitchum G., 1998. Monitoring the stability of satellite altimeters with tide gauge stations, *J. of the Atmospheric and Oceanic Technology*, 15 (3):721-730.
- Mitchum G., 2000. An Improved calibration of satellite altimetric heights using tide gauge sea levels with adjustment for land motion, *Marine Geodesy*, 23: 145-166.
- Nerem R.S. and Mitchum G., 2002. Estimates of vertical crustal motion derived from differences of Topex/Poseidon and tide gauge sea level measurement, *Geoph. Res. Lett.* 29 (19) 10.1029/2002GL015037, 1934
- Nerem R.S., Eanes R.J., Ries C. and Mitchum G.T., 2000. The Use of a precise reference frame in sea level change studies, in *Towards an Integrated Global Geodetic Observing System (IGGOS)*, Rummel R., Drewes H., Bosch W. and Hornik H. editors, Springer Verlag, Proceedings IAG Symposia 120:8-12.
- Overland J.E. and Preisendorfer R.W., 1982. A Significance test for Principal Components applied to a Cyclone Climatology, *Monthly Weather Review* 110 (1), 1-4.
- Peltier W., 200. Global glacial isostatic adjustment: Paleogeodetic and space-geodetic tests of the ICE-4G (VM2) model. *J. Quaternary Science*, 17, 5-6, 491-510
- Preisendorfer R.W., 1988. *Principal Component Analysis in Meteorology and Oceanography*, Elsevier, 425 pages.
- Lama R. and Corsini S., 2003: *La rete mareografica italiana, analisi delle serie storiche*, Published by Agenzia per la Protezione dell'Ambiente e Serviz Tecnici, Istituto Poligrafico e Zecca dello Stato, Roma
- Schuh A., Dill R., Greiner-Mai H., Kutterer H., Müller J., Nothnagel A., Richter B., Rothagel M., Schreiber U. and Soffel M., *Erdrotation und globale dynamische Prozesse*, 2003. *Mitteilungen des Bundesamtes für Kartographie und Geodäsie*, Band 32, Verlag des Bundesamtes für Kartographie und Geodäsie, Frankfurt am Main

- Soudarin L., Cretaux J.F. and Cazenave A., 1999. Vertical crustal motions from the Doris space-geodesy system, *Geoph. Res. Lett.* 26 (9):1207-1210
- Tapley B.D., Ries J.C., Davis G.W., Eanes R.J., Schutz B.E., Shum C.K., Watkins M.M., Marshall J.A., Nerem R.S., Putney B.H., Klosko S.M., Luthcke S.B., Pavlis D., Williamson R.G. and Zelensky, 1994, Precision orbit determination for Topex/Poseidon, *J. Geophys. Res.* 99 (C12): 24383-24404
- Tsimplis M.N. and Spencer N.E. 1997: Collection and analysis of monthly mean sea level data in the Mediterranean and Black Sea, *J. of Coastal Research* 13 (2), 534-544
- Tsimplis M.N. and Josey S.A. 2001: Forcing of the Mediterranean Sea by atmospheric circulation over the North Atlantic, *Geoph. Res. Lett.* 28 (5): 803-806
- Woodworth P., 2003. Some comments on the long sea level records from the northern Mediterranean, *J. of Coastal Research* 19:212-217.
- Xiaojun D., Woodworth P., Moore P. and Bingley R., 2002. Absolute calibration of the Topex/Poseidon altimeters using UK tide gauges, GPS and precise local geoid differences, *Marine Geodesy* 25:189-204
- Yildiz H. and Demir C., Mean Sea level changes and vertical crustal movements at Turkish tide gauges for the period of 1984-2001, *Workshop of Vertical Crustal Motion and sea level change, Toulouse 2002*
- Yildiz H., Demir C., Gürdal M.A., Akabali O.A., Demirko I., Ayhan M.E., 2003. Analysis of sea level and geodetic measurements of Antalya-II, Bodrum-II, Erdek and Mentesh tide gauges in the period of 1984-2002, *Harita Dergisi, Special Issue*, 17-75 (in Turkish)
- Wilks, D.S., 1995. *Statistical Methods in the Atmospheric Sciences*, Volume 59 in International Geophysics Series, Academic Press, 467 pages
- Zerbini S., Plag H.-P., Baker T. Becker M. et al., 1996: Sea level in the Mediterranean Sea: a first step towards separating crustal movements and absolute sea-level variations, *Global and Planetary Change*, 14:1-18.
- Zerbini S., Negusini M., Romagnoli C., Domenichini F., Richter B. and Simon D., 2002. Multi-parameter continuous observations to detect ground deformation and to study environmental variability impacts, *Global and Planetary Change*, 34:37-58

7.5 Sea level variability and trends in the Adriatic Sea

F-10: Fenoglio-Marc L. C. Braitenberg and L. Tunini, Sea level variability and trends in the Adriatic Sea in 1993-2008 from tide gauges and satellite altimetry, *Physics and Chemistry of the Earth*, doi:10.1016/j.pce.2011.05.014, 2011.

Keywords: regional sea level change, altimetry, tide gauge

Abstract The scope of this paper is to give a consistent view of the low frequency sea level variability in the Adriatic Sea from both satellite altimetry and tide gauge records. We analyze sixteen years of sea level observations from multi-satellite altimetry and tide gauge records in the time interval 1993-2008. First, the impact of the corrections applied to the altimetry-derived sea level variations and the consistency of the altimetric and the tide gauge sea level observations are evaluated. Both observations are then used to characterize sea level trends, interannual variability and land vertical motion in the Adriatic region.

Eight tide gauges along the coast show very coherent interannual sea level variations, with an increase in sea level before 2001 and decrease afterwards. The average of the eight deseasoned time-series agrees with the basin average of the altimeter data, with correlation coefficient 0.84 and root mean square difference being 12 mm. The linear change is higher for altimetry than for tide gauges and strongly depends on the length of the time-interval, being 3.2 ± 0.3 mm/yr and 1.9 ± 0.3 mm/yr respectively in the interval 1993-2008. The steric contribution to sea level change correlates well with the sea level suggesting that the low frequency variability is likely related to oceanic and climatic processes and mainly due to temperature and salinity variations.

At a given location, the trend of the differences of sea level observations by tide gauges and co-located satellite altimetry gives the vertical land motion, if we assume that the sea level signals are truly common. We find trends statistically significant at the 90% confidence level at two locations, that indicate land uplift along the eastern coast in Rovinj (3.0 ± 1.2 mm/yr) and land subsidence in Marina di Ravenna (-1.5 ± 1.1 mm/yr), while at other locations, e.g. in Trieste (1.3 ± 1.1 mm/yr) the significance is lower. The results agree in general in sign with GPS derived rates, but not in magnitude, like in Marina di Ravenna, where the strong subsidence measured by GPS is related to the local anthropogenic subsidence. The differences are partly explained by the spatial distance between the tide gauge and the co-located altimeter locations.

Keywords: sea level, altimetry, tide gauge, regional sea level change

1. Introduction

Sea level rise is an important environmental parameter and indicator of climate change (Bindoff et al., 2007). Its impact is particularly important in selected coastal zones. The Northern Adriatic Sea is one of those vulnerable areas presenting a great sensitivity to climate change and a low adaptability. The Adriatic sea is an elongated semi-closed basin communicating with the Mediterranean Sea through the narrow and shallow Otranto Strait. The eastern Po plain, from Ravenna to the Venice region, is part of a subsiding sedimentary basin. Over the last millennia, changes in the ground elevation with respect to the Adriatic Sea level have caused modifications in the features of the region. Nowadays, the relative sea level rise (RSLR), resulting from the combination of land vertical motion due to natural and anthro-

pogenic causes and of the eustatic sea level rise, represents a threat for the region (Carbognin et al. 2009, Lionello et al., 2005).

Various authors (Orlic and Pasaric 2000, Wöppelmann et al. 2006, Zerbini et al., 2007, Antonioli et al., 2009) have reported on land subsidence in the Northern Adriatic, with a weak or even positive (uplift) rate in Trieste, small negative rate in Venice and larger negative rate in Marina di Ravenna, partly related to human effects. Some post-glacial isostatic response models predict subsidence of 0.3-0.5 mm/yr (Lambeck and Johnston 1995, Stocchi and Spada 2009), whereas others predict uplift of 0.2-0.3 mm/yr (Tushingham and Peltier 1989). For the last decades an integrated monitoring system based on earth observation techniques has confirmed a land subsidence along the coasts of the lagoon (Tosi et al., 2009).

It is generally agreed that at least 50-year-long tide gauge records are needed to separate secular, decadal and interannual variations (Douglas 2001) because interannual and low frequency signals affect the recovery of secular trends in short records. Tide gauge records give for the 20th century a global mean positive RSLR rate of 1.7 mm/yr (e.g., Church et al., 2008; Holgate, 2007, Domingues et al., 2008), that is higher than the corresponding regional mean RSLR rate over the Adriatic. In the Adriatic Sea, the long-term RSLR trend derived from tide gauge records over the last century varies between 0.5 ± 0.2 and 1.2 ± 0.1 mm/yr (Marcos and Tsimplis 2008, Raicich 2007), except for the higher trend in Venice (2.5 ± 0.1 mm/yr). The latter is due to anthropogenic subsidence ascribed to water extraction, which ceased in 1970 (Pirazzoli, 1991; Tiezzi and Marchettini, 1997; Woodworth, 2003). For the period 1960 to 2000 small rates between -0.4 ± 0.4 mm/yr and 0.3 ± 0.4 mm/yr have been found, higher rates correspond to the last decade of the twentieth century. Sea level trend exhibits large interdecadal variability with good coherence between the tide gauge records (Marcos and Tsimplis 2008, Klein and Lichter 2008, Pirazzoli and Tomasin 2008). The tide gauges in the Adriatic are particularly important for sea level change studies, as the records of Trieste and Venice are two of the longest in the world.

Since early 1993, sea level variations are also accurately measured by satellite altimetry. The total measurement accuracy for the altimetry based sea surface height is about 80 mm (95% error) for a single measurement based on one-second along-track, the 95% error is due to its global coverage, altimetry reveals considerable regional variability in the rates of sea level change and is therefore particularly suited to determine global mean sea level change and low frequency processes of annual and interannual variability. One of its main problems is still the aliasing of short-period signals that cannot be resolved due to the coarse temporal sampling of the satellites. Another difference between the tide gauge and altimetric measurements is their different reference frame. While satellite altimetry measures sea level in a geocentric reference frame, the tide gauge observes the sea level with respect to a reference point on land which can move vertically relative to the geocenter due to geodynamic effects, as tectonics, volcanism, post-glacial isostatic adjustment or due to anthropogenic causes. At present, vertical land motions at tide gauges can be measured to a high accuracy by means of space techniques such as Satellite Laser Ranging (SLR), Very Long Baseline Interferometry (VLBI), Global Positioning System (GPS) and Doppler Orbitography and Radiopositioning Integrated by Satellite (DORIS) (Blewitt et al., 2010). Several studies have estimated vertical land motion from the difference between satellite altimetry and tide gauge sea level height measurements at selected locations (Braitenberg et al. 2010, Cazenave et al. 1999, Dong et al. 2002, Mitchum 2000, Nerem and Mitchum 2002, Fenoglio-Marc et al. 2004, Kuo et al. 2004, Ray et al. 2010). A positive difference corresponds to land uplift and a negative difference to land subsidence, therefore, in case of land subsidence the tide gauge measures an higher sea level rise than satellite altimetry. Care is needed to match up the two types of sea level measurements, and

the method is not applicable everywhere, since the tide gauges are not always located near to the satellite groundtracks and the altimetry measurements have lower accuracy near coast than on open sea.

Various authors have analysed the sea level change in the Mediterranean Sea derived from altimetry data and have reported for the Adriatic Sea on a positive sea level rate between 1993 and 2002 and a negative rate after 2002 (Cazenave et al. 2001, Fenoglio-Marc 2001, 2002, Vigo et al. 2005). In this study, we estimate the low frequency sea level variability from multi-satellite altimetry and eight tide gauges in the Adriatic Sea over a 16-year long time interval. The analysis aims at clarifying the following issues, namely the description of (1) the long-term difference between eustatic sea level rise observed by altimetry and sea level rise relative to land observed by tide gauge records and of (2) the main spatial and temporal characteristics of sea level change over the Adriatic basin. The first issue opens the discussion on the interpretation of differential trends as land motion at the coast. The multi-satellite missions enhance temporal and spatial resolutions with respect to a single satellite analysis. The coherency in the variability of the tide gauge and co-located satellite altimetry indicates how representative the altimetry data are for the coastal sea level variability. The comparison of sea level trends observed by tide gauges and altimetry allows in principle to derive vertical crustal movements. We discuss here whether for a basin like the Adriatic this method is usable, taking into account the location of the tide gauges relative to the position of the satellite tracks and the presently available time interval.

Data and method of analysis are presented in Section 2. In Section 3 we describe the results. The differences observed and the possible geophysical interpretations are further discussed in Section 4.

2. Data and method of analysis

2.1 Altimetry data

We use altimetric sea level height data from the satellites Topex/Poseidon, Jason-1, Jason-2 and Envisat. The 16-year long altimetric time series allows an analysis of interannual and long term variability of sea level at regional scales relative to a geodetic reference frame.

Using Topex/Poseidon and Jason missions alone, the coverage is poor and ground-track is 161 is the nearest track to most of the tide gauge stations. By including Envisat data the coverage is improved, we do not include data of the ERS-1 and ERS-2 missions because of their lower accuracy. First, the impact of the corrections applied to the altimetry-derived sea level variations and the consistency of altimetric and tide gauge sea level observations are evaluated and a suitable procedure is identified. Special attention has been paid to the consistency of the corrections applied to altimeter and tide gauge data. We perform two types of comparisons, that we call **monthly** and **daily** comparison methods. In the first multi-mission gridded altimeter data are compared to monthly tide gauge records, in the second along-track altimeter data are compared to tide gauge records, corrected for the ocean tide effect, at the point of nearest approach (diamond in Fig. F-10-1). Both comparison methods require the same corrections to be applied to the altimeter data to compute sea level height anomalies above a reference surface. We use the Radar Altimeter Database System (RADS) database, that provides an harmonized, validated and cross-calibrated set of altimeter data (Naeije et al., 2008). To merge data from different satellites we apply the reference frame biases that reflect the differences in the orbits as well as some other geographical differences in the

altimeter dependent models. For the small area we are considering, these modelled biases amount to an almost constant value (Trisirisatayawong et al., 2011). Detailed inspection and special care is needed because we are analysing data close to the coast.

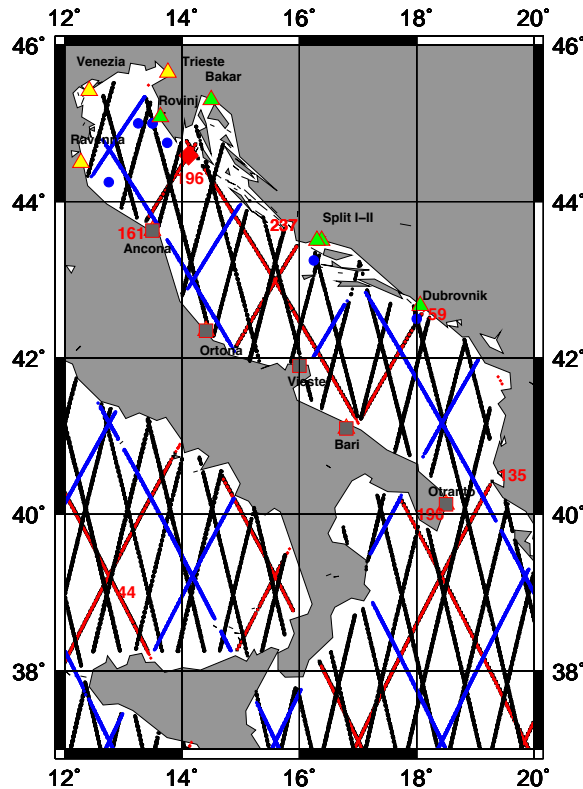


Figure F-10-1: Location of the eight tide gauge (triangle) and co-located altimeter time-series used in monthly (blue dots) and daily (red diamond) comparisons. Ground-tracks are from Envisat (black), Topex/Poseidon phase b (blue), Jason-1 and Topex/Poseidon phase a (red with track number). Additional tide gauge stations available over a shorter interval are shown (squares)

The impact of the altimeter corrections on sea level variations has been evaluated through comparing the standard deviation of sea level anomalies for different choices of a given correction, we select the choice giving the smallest standard deviation.

Tab. F-10-1 presents a summary of the chosen models and corrections to infer sea level anomalies from the altimeter record, that coincide in most of the cases with the default corrections of the RADS database. The pole tide correction is not applied for consistency with the tide gauge records. We apply environmental (wet and dry tropospheric, ionospheric, sea state bias) and geophysical corrections (solid earth, ocean and load tides). To retain more data near coast we choose the wet tropospheric correction derived from the European Centre for Medium-range Weather Forecasts (ECMWF) model and ignore most of the conservative flags, thus allowing inclusion of data closer to land. The response to atmospheric pressure forcing is here accounted for by applying the Dynamic Atmospheric Corrections (DAC), which consists at low frequencies of the Inverse Barometer (IB) response and at high frequencies of the barotropic model MOG2D-G (Carrère and Lyard, 2003). This correction is particularly suitable for the Adriatic Sea, as here the response is far from an inverse barometer (Pascual et al. 2008). The DAC Corrections are produced by CLS Space Oceanography Division using the Mog2D model from Legos and distributed by Aviso, with support from Cnes (<http://www.aviso.oceanobs.com/>) with temporal resolution of 6 hours and spatial resolution

Table F-10-1: Corrections applied to the altimeter data, changes to RADS defaults are indicated by (*)

Correction/model	Edit criteria (m) Min/Max	Description
Orbit		EIGEN GL04C
Dry troposphere	-2.4 -2.1	ECMWF
Wet troposphere(*)	-0.6 0.0	ECMWF
Ionosphere	-0.4 0.04	All sats: altimeter dual frequency, smoothed
Dynamic atmosphere	-1.0 1.0	MOG2D model
Ocean tide	-5.0 5.0	GOT4.7 model
Load tide	-0.5 0.5	GOT4.7 model
Solid earth tide	-1.0 1.0	Elastic response to tidal potential (Cartwright)
Sea state bias	-1.0 1.0	TOPEX/JASON/ENVISAT: CLS non parametric
Reference	-1.0 1.0	DNSC08 mean sea surface (Andersen and Knudsen, 2009)
Data engineering flag (*)		Only altimeter land flag based on 2 x 2 degrees mask
Applied ref. frame biases (cm)		From global analysis of differences with Topex reference frame: ENVISAT = 44.8, Jason-1 = 8.3, Jason-2 = -1.8

of 0.25 degrees. The correction for the one second altimeter data is included in the RADS database.

In the monthly comparison method the multi-mission altimeter data sets have been merged in monthly grids by a Gaussian weighted average method with grid spacing of 0.20, half-weight of 10 and search radius of 150 km. The nearest grid point to the tide gauge station location has been selected for the comparison (dots in Fig. F-10-1). In the daily comparison method the nearest altimeter point along-track has been considered (diamond in Fig. F-10-1). The differences between the results obtained in the two approaches are investigated in Section 3.

2.2 Tide gauge data

The tide gauge data have been made available from the Permanent Service for Mean Sea Level (PSMSL, - <http://www.pol.ac.uk/psmsl/>, Woodworth and Player, 2003) and from the APAT-ISPRA databases (<http://www.idromare.com>). The first provides monthly data, the second hourly data. Additional time-series have been made available by local institutions for Trieste (Department of Geosciences of the University of Trieste), Venezia and Marina di Ravenna (Zerbini, Raicich private communication). Fig. F-10-1 shows the location of thirteen tide gauge stations. For consistency with the satellite altimetry data processing described in the previous sub-session, we have applied the DAC correction to the tide gauge data to account for the effect of pressure and wind on the sea level. The DAC correction has been derived from the gridded data distributed by AVISO described in the previous section using the nearest grid point to the tide gauge station. In Trieste the DAC and the inverse barometer correction estimated by hourly pressure data are in good agreement at lower frequency, with correlation and root mean square (RMS) differences of 0.7 and 2 cm respectively for the monthly averaged time-series.

For daily comparison of sea level records from altimetry and tide gauges the hourly tide gauge data have been reduced to daily sampling and the daily values corresponding to the altimeter observations have been selected to build the time-series. The daily sampling is obtained by a two-step filtering operation. First, the dominant diurnal and semi-diurnal tidal components are removed from the quality controlled hourly values. Secondly, a 119-point

convolution filter (Bloomfield, 1976) centred on noon is applied to remove the remaining high-frequency energy and to prevent aliasing.

The seasonal variation is a large amplitude signal, which essentially depends on yearly temperature variations. To achieve more reliable trends this signal has been estimated from the sea level records. We have applied different procedures depending on data sampling. Using daily data the linear trend and the annual and semi-annual signals have been evaluated separately for the altimeter and tide gauge time-series through a least-squares procedure fitting the function:

$$m(t) = a_o + a_1 t + a_{\cos 1} \cos \omega_1 t + a_{\sin 1} \sin \omega_1 t + a_{\cos 2} \cos \omega_2 t + a_{\sin 2} \sin \omega_2 t \quad (1)$$

where a_0 , a_1 , $a_{\cos 1}$, $a_{\sin 1}$, $a_{\cos 2}$, $a_{\sin 2}$, are the parameters to be determined, and ω_1 , ω_2 are the yearly and half-yearly angular frequency respectively. The linear trend is given by the parameter a_1 and its uncertainty is equal to the standard error of the coefficient estimate. We assume that the residuals have zero mean and Gaussian distribution (Parker, 1994). We compute the linear trend $a_{t_{al-tg}}$ of the sea level difference between altimeter and tide gauges as difference of the linear trends:

$$a_{t_{al-tg}} = a_{t_{al}} - a_{t_{tg}} \quad (2)$$

where $a_{t_{al}}$ is the altimetric trend and $a_{t_{tg}}$ is the tide gauge trend. When analysing the monthly time-series, the seasonal component is first evaluated by computing the mean variability for each month in the interval of analysis and then removed from the monthly values to obtain de-seasoned monthly values. To obtain the linear trend of the difference between altimeter and tide gauge records we consider two alternative methods. In one method, the trends are first estimated from the de-seasoned sea level time-series and then their difference is computed, in the other method the trend of the de-seasoned difference altimeter minus tide-gauge is computed. Linear regression is used to estimate the linear trend and its standard error σ . We further assess the trend significance by applying the t-test to the ratio between the estimated trend and its standard error. As shown in Santer et al. (2000) and Maul and Martin (1993) classical tests of trend significance may underestimate the standard errors if the detrended time series are not statistically independent. Accounting for the temporal autocorrelation of the detrended time series, we compute an effective sample size n^1 based on the lag-1 autocorrelation coefficient r^1 (see also eq. 6 in Santer et al., 2000):

$$n^1 = n \frac{1 - r^1}{1 + r^1} \quad (3)$$

where n is the number of monthly time samples. By using the effective sample size n^1 one obtains a bigger standard error for the trend:

$$\sigma^1 = \sigma F^1 = \sigma \sqrt{\frac{1 - r^1}{1 + r^1}} \quad (4)$$

where F^1 is the inflation factor. This procedure does not alter the value of the trends, but leads to an increase of the estimated error by about 40% for de-seasoned time-series (Fenoglio-Marc et al., 2004).

The steric sea level variability has been estimated from temperature and salinity values of the Ishii climatology (Ishii and Kimoto, 2009) and of the Mediterranean Forecasting System

ocean circulation (MFSTEP) (Tonani et al., 2008). The steric sea level is computed from Equation (5), as the vertical integration of the specific volume $1/\rho$ between the two surfaces of constant pressure p_1 and p_2 :

$$h(p_1, p_2) = \frac{1}{g} \int_{p_1}^{p_2} \frac{1}{\rho} dp_1 \quad (5)$$

where ρ is the density and g the gravity acceleration. The specific volume is computed from the gridded temperature and salinity in-situ data using the formulas of state for sea water (Gill, 1982). We integrate between each two levels using the mean of the specific volume anomaly of the two levels. Integration is made down to the lowest available depth. We derive grids of steric sea level with one degree spacing and monthly temporal sampling.

We perform a Principal Component Analysis (PCA) of both altimetry and tide gauge data to quantify the spatio-temporal sea level variations in the Adriatic Sea as well as reveal regional differences between the Adriatic and the rest of the Mediterranean Sea. This is an efficient way of analysing the dominant patterns of variability, which expands the signal in terms of the basin functions that concentrate most of the variance into a small number of components, called Empirical Orthogonal Functions (EOF) (Preisendorfer, 1988). We apply a significance test based on a Monte Carlo technique to find the number k of components corresponding to a signal above the noise level. Independent sequences of Gaussian variables are generated and the eigenvalues of the correlation matrix are computed, the procedure is repeated 100 times. The normalized eigenvalue statistics (percentage of variance explained) corresponding to real and random data are compared. The rule N (Overland and Preisendorfer, 1982) is applied, that consists in considering significant the principal components having eigenvalues greater than the value 95 in the sequence. The input data are normalized to standardized anomalies by dividing each point time-series by its standard deviation and the output spatial vectors are normalized to the maximum value for each mode.

3. Results

We have first analysed the quality of the hourly data to identify outliers and spurious change in the reference level of the data before computing monthly and daily values. A 3- test is used to detect the outliers. All hourly data of the APAT-ISPRA dataset present a jump in the time-series in summer 1998 due to the change of the tide gauge instrument (APAT personal communication), therefore the five stations of Ancona, Ortona, Vieste, Bari, Otranto (squares in Fig. F-10-1 cannot be used over the complete interval without estimation of the vertical displacement of the reference point. This datum shift, estimated in Fenoglio-Marc et al. (2004) using the Topex-Poseidon data, is almost zero in Ancona and about 800 mm in Otranto and Bari. Fig. F-10-2 shows the de-seasoned monthly time-series at the thirteen stations, the last five (i-m) have the datum shift in summer 1998.

We have defined selection criteria to be applied to monthly records, based on the length of the time-series, on the length of the gaps and on the correlation with nearby stations. The criteria are as following: the data should be available over 90% of the selected time-interval, gaps should be shorter than two years and correlation with nearby stations in a radius of 200 Kilometers should be higher than 0.7. The tide gauge stations with monthly data fulfilling the above selection criteria in 1993-2008 are eight (triangle in Fig. F-10-1, stations a-h in Fig. F-10-2 and include seven stations with monthly data from the PSMSL database (Rovinj,

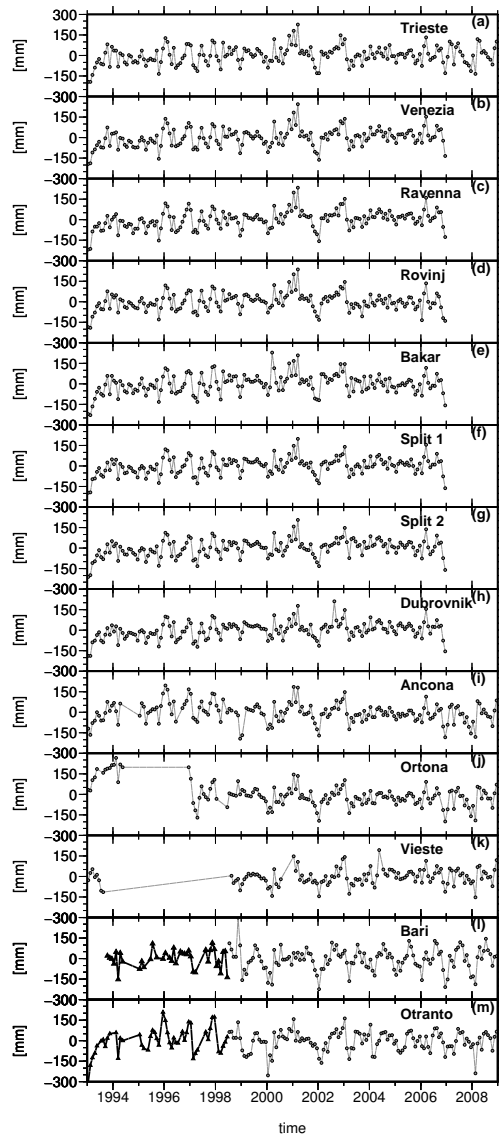


Figure F-10-2: Sea level time-series at tide gauge stations in the Adriatic Sea. The seasonal component and the mean has been removed. The first eight stations from the top (a-h) have been selected for the analysis. The other stations (i-m) present a vertical jump in summer 1998 and are not further analysed. In Bari and Otranto the data have been divided in two time-series before (black) and after the discontinuity, for representation purpose

Bakar, Split Harbour, Split Marjana, Dubrovnik, Trieste, Venezia) as well as stations with hourly data from local institutions (Trieste, Venezia, Marina di Ravenna). The correlation between the de-seasoned sea level time-series of the eight stations (a-h) is higher than 0.9 over 1993-2008.

We investigate the differences between the monthly and daily comparison methods in Trieste. The monthly and daily time-series are shown in Fig. F-10-3. The grid and the along-track altimeter points are in this example located respectively at 75 Km and 110 Km from the tide gauge station and are 30 Km apart. Correlation and RMS differences are 0.65 and 65 mm for monthly comparison, 0.57 and 112 mm for daily comparison. The differences arise from the

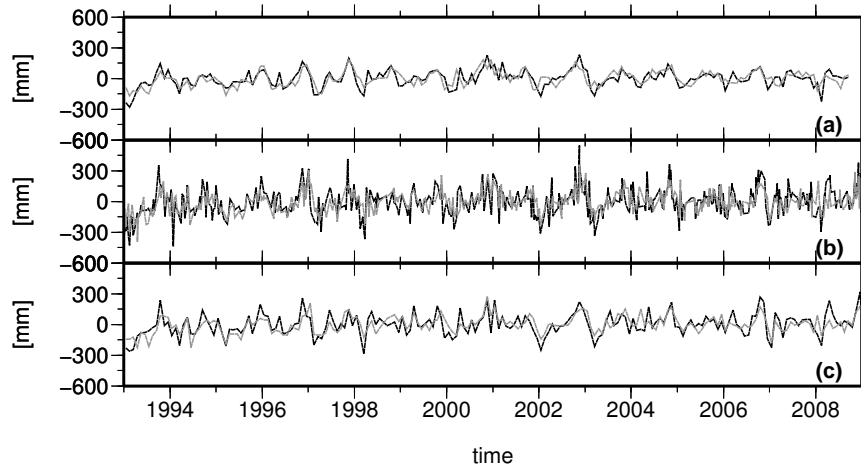


Figure F-10-3: Time-series of altimetry (grey) and tide gauge (black) data in Trieste: monthly (a), daily (b) and monthly averages of daily (c). The mean of the time-series has been removed

different time sampling: monthly averages of daily time-series used in daily comparison (Fig. F-10-3.c) give results (0.69 and 77 mm) similar to the monthly comparison (Fig. F-10-3.a). The correlation of monthly and monthly averages of daily time-series is 0.8 for tide gauge data and 0.6 for altimeter data. Here the lower correlation found for altimetry arise from the different way of building the monthly and daily altimeter time-series. The correlation is still significant and allows us to conclude that sea level time-series extracted from gridded and along-track altimeter data are comparable. The two methods give also comparable results for the trend, as shown below.

3.1 Long-term difference between altimetry and tide gauge sea level

At a given location P , the geocentric vertical land motion is the difference between the rates of the geocentric sea level change and of the sea level change relative to the Earth crust \dot{s} .

$$\dot{u}(P) = \dot{j}(P) - \dot{s}(P) \quad (6)$$

In our application the sea level change derived from tide gauge and the altimeter is not measured at the same location P . The distance between the two locations depends on the type of comparison defined in Section 2 (monthly or daily comparison), and is at least several kilometers. We apply the monthly comparison method to the eight selected locations. The altimeter and tide gauge monthly time-series, corrected for DAC and with the seasonal signal still included, have correlation of about 0.67 and standard deviation of the differences between 50 and 80 mm. The distance between the tide gauge and the co-located altimeter point is between 13 Km in Rovinj and 79 Km in Venezia. At each tide gauge we first compute the monthly differences "altimeter minus tide gauges" time-series by subtracting the tide gauge de-seasoned time-series from the altimeter de-seasoned time-series, then we estimate the trend of the resulting time-series (second procedure described in Section 2 for monthly comparison). Tab. F-10-2 shows the results for the eight selected tide gauge stations. The sea level trends estimated independently from altimetry and tide gauge are positive, the correlation between monthly records is about 0.67 with standard deviation of the differences between 50 and 80 mm. The trends of the difference of the time-series are smaller than 1.5 mm/yr at most locations and have errors of similar magnitude. They are small compared to other regional studies (Ray et al. 2010, Fenoglio-Marc et al. 2004, Kuo et al., 2004). The t-test applied

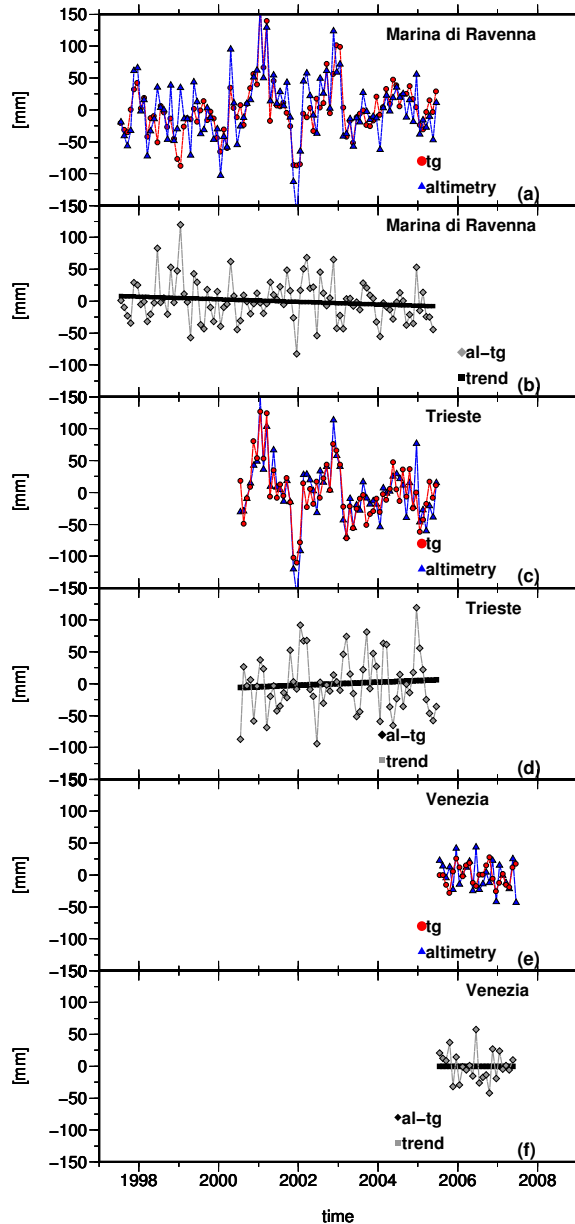


Figure F-10-4: Altimeter and tide gauge time-series with seasonal signal removed (a, c, e), their difference with trend (b, d, f) at Ravenna, Trieste and Venezia during the time-interval of GPS measurements

to the ratio of those trends to their errors leads to values above 1.3 (threshold of statistical significance for the 90% significance level) only at the stations of Rovinj (3.0 ± 1.2 mm/yr) and Marina di Ravenna (-1.5 ± 1.1 mm/yr). Trends are statistically significant at the 75% level of confidence (threshold is 0.68) in Trieste, Bakar and Split. Interpreting these trends as vertical motion, we finally found uplift in the eastern Adriatic (Rovinj, Trieste, Bakar), subsidence in Marina di Ravenna and not significant vertical motion (below the 75% confidence level) at the other stations. In Trieste the trend is 1.3 ± 1.2 from monthly comparison and 1.0 ± 1.8 mm/yr from daily comparison, it is below the 75% confidence level in this second case.

We have compared the estimated vertical motions to GPS trends at a few stations. A strong land subsidence of 10.2 ± 0.15 mm/yr has been derived in Marina di Ravenna by continuous GPS measurements over nine years from 1996 to 2005 (Wöppelmann et al., 2006)

Table F-10-2: Comparison of tide gauges (tg) and co-located altimetry (al) monthly sea level records in 1993-2008. Given are : distance between altimeter and tide gauge (column 2), standard deviation of the differences (column 3), correlation (column 4), trend of altimetric and tide gauge records (columns 5-6), trend of the differences (column 7), annual amplitude and phase of sea level at the tide gauge (columns 8-9)

Station	al-tg dist (km)	al-tg std (mm)	al-tg corr	al trend (mm/yr)	tg trend	al-tg trend	tg ampl. mm	tg phase deg
Trieste	75	86	0.67	5.9 ± 1.3	4.1 ± 1.6	1.3 ± 1.2	59.8 ± 2.2	266 ± 2
Venezia	79	76	0.66	5.9 ± 1.4	5.6 ± 1.6	-0.2 ± 1.3	60.4 ± 2.2	272 ± 2
Ravenna	46	84	0.68	5.6 ± 1.4	6.5 ± 1.5	-1.5 ± 1.1	62.2 ± 2.2	278 ± 2
Rovinj	13	77	0.65	5.9 ± 1.3	2.6 ± 1.5	3.0 ± 1.2	58.2 ± 2.2	276 ± 2
Bakar	87	81	0.67	5.9 ± 1.3	4.2 ± 1.6	1.2 ± 1.1	49.0 ± 2.2	285 ± 2
Split Harbour	29	48	0.68	5.0 ± 1.0	5.2 ± 1.4	-0.2 ± 1.1	48.2 ± 2.2	295 ± 3
Split Marjana	31	52	0.67	5.0 ± 1.0	5.9 ± 1.4	-0.9 ± 1.1	45.3 ± 2.2	296 ± 3
Dubrovnik	20	53	0.66	5.8 ± 1.0	5.4 ± 1.3	-0.1 ± 1.1	50.2 ± 2.2	292 ± 3

and a smaller negative trend has been found more recently over 1997.-2005.5 (Zerbini, personal communication). Measurements from GPS are also available over intervals shorter than five years at Trieste (2000.5-2005.5) and Venezia (2005.5-2007.5) (Zerbini, personal communication). Fig. F-10-4 shows, for the time-interval of the GPS observations, the de-seasoned monthly sea level measured from altimetry and tide gauge data at the three stations. The errors of the trends are here bigger than in Tab. F-10-2 due to the shorter time intervals. The trends are -1.6 ± 1.9 mm/yr in Marina di Ravenna, 2.4 ± 4.0 mm/yr in Trieste and 2.7 ± 4.1 in Venezia and agree in sign with the GPS rates. Only the trend in Marina di Ravenna is statistically significant at 75% confidence level and is significantly smaller than the GPS derived rate.

3.2 Temporal and spatial characteristics of sea level change

The mean seasonal sea level cycle parameters computed for the monthly records of the eight tide gauges are given in Tab. F-10-2. The annual sea level amplitude varies between 45 and 62 mm in agreement with Marcos and Tsimplis (2007). The annual cycle peaks between late September in the north and late October at the southern stations. On average, the mean seasonal cycle accounts for 60% of the total variance of monthly sea level records. The annual amplitude of sea level from altimetry ranges between 70 mm in the north and 40 mm in the south of the Adriatic Sea; the annual cycle peaks in Autumn, later than in the rest of the Mediterranean Sea (Fig. F-10-5).

The average over the Adriatic Sea of the altimetry-based sea level has been low-pass filtered by computing a running average over twelve months (Fig. F-10-6). Its trend over 1993-2008 indicates a rise of sea level of 3.2 ± 0.3 mm/yr. The rate is not uniform and two distinct periods, before and after year 2001, are identified. The trend is positive (9 ± 0.5 mm/yr) between 1993 and 2000 and negative (-2.5 ± 0.5 mm/yr) between 2001 and 2008. A composite tide gauge record has been computed by averaging the monthly eight tide gauge records. In 1993-2006 all eight stations have contributed to compute the composite tide gauge record, while in 2006-2008 only the station of Trieste could be used (see Fig. F-10-2). Finally the composite tide gauge record was low-pass filtered like the altimetric basin average. Correlation and RMS differences of the two filtered time-series are 0.84 and 12 mm, confirming the high coherence of coastal and offshore sea level variability in the Adriatic at

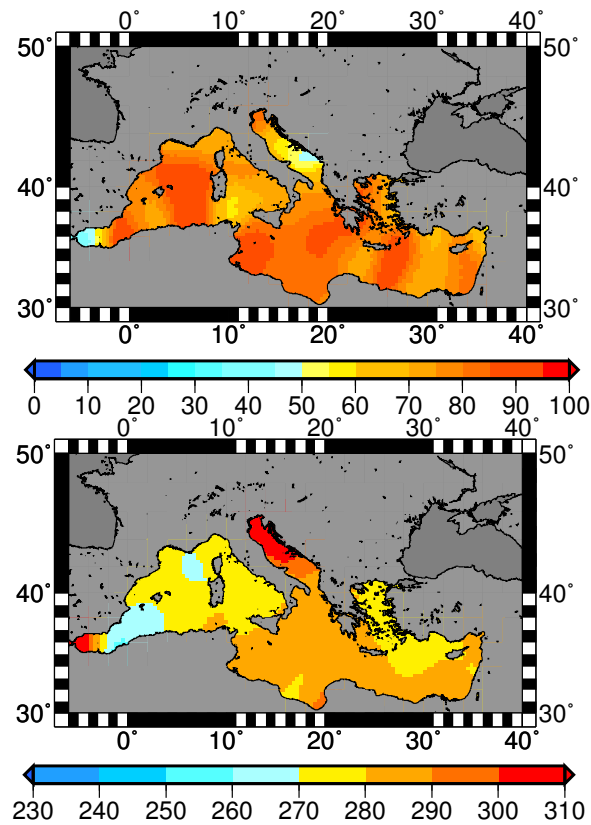


Figure F-10-5: Annual amplitude (mm) (left) and annual phase (right) of sea level from Jason-1 altimetry

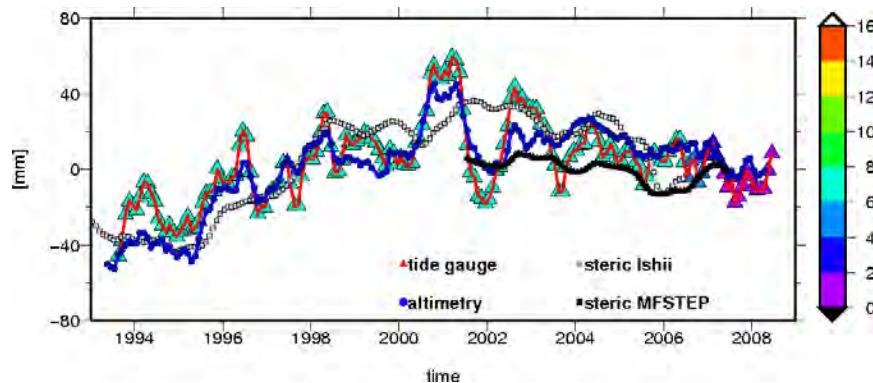


Figure F-10-6: Basin average of sea level in Adriatic Sea from altimetry (circle) and from tide gauges (triangle). Color bars indicates the number of tide gauge stations used at each time step. A maximum of eight tide gauge stations (triangles in Fig. F-10-6) are used. Basin average of the steric component of sea level from the Ishii database (grey) and from the MFSTEP model (black) are also drawn. A moving average has been applied to the monthly de-seasoned data.

interannual time scales. In 1993-2008 the linear rate of the low-pass filtered composite tide gauge record (1.9 ± 0.3 mm/yr) is lower than the linear rate of the corresponding altimeter basin average. As for the altimetric basin average, the trend is positive before 2001 (7.6 ± 0.5 mm/yr) and negative afterwards (-3.7 ± 0.8 mm/yr). Our results agree with the common mode of the tide gauge sea level found by Buble et al. (2010) after 1993, although their trends of absolute and relative sea level are different as they refer to a longer time interval.

The high correlation between coastal and offshore sea level variability is typical for the Adriatic Sea and partly due to the high number of tide gauges available. Other sub-basins

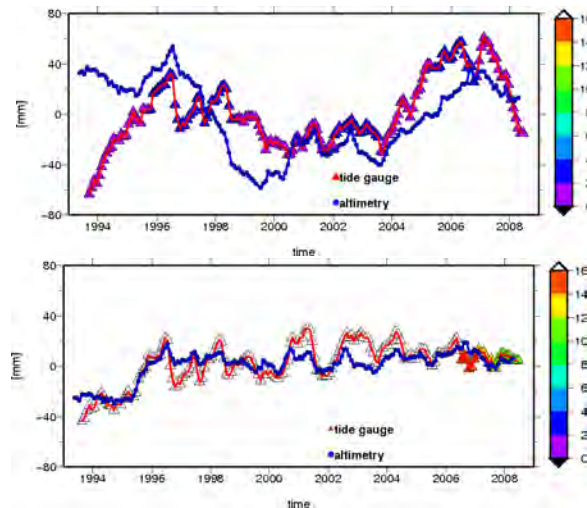


Figure F-10-7: Basin average in Ionian Sea (top) and in Mediterranean Sea (bottom) of sea level from altimetry (circle) and tide gauges (triangle). Maximum number of tide gauge stations used is two and nineteen respectively, color bars indicates the number at each time step. A moving average has been applied to monthly de-seasoned data.

of the Mediterranean Sea show a lower agreement between offshore and in-situ interannual variability. In the Ionian Sea only the two tide gauges of Valletta (Malta) and Katakolon (Greece) have been available (Fig. F-10-7). The tide gauge records are in this case less representative for the sea level of the sub-basin, being correlation and RMS differences of the low-pass filtered basin averages 0.4 and 31 mm respectively. The amplitude of the interannual signal (160 mm) in Ionian and in Adriatic Sea are comparable, their trends have opposite sign, with negative sign between 1996 and 2000 and positive sign after year 2001 in the Ionian Sea. In the Mediterranean Sea we have used sixteen tide gauge stations, which are available over most part of the interval 1993-2006. Nine of them (Malaga, Barcelona, Marseille, Toulon, La Valletta, Khalkis, Khios, Leros, Hadera and Ceuta) have been considered in addition to those used for the Adriatic (eight) and the Ionian Seas (two) (Fig. F-10-8). The tide-gauge- and the altimetry-based basin averages have good correlation and small RMS differences (0.85 and 9 mm). The amplitude of the interannual signal (80 mm) is smaller than in the two previous analysed sub-basins. The time-series show a step increase between 1994 and 1996 and a lower interannual variability after 1996 (Fig. F-10-7).

In the Adriatic Sea the sea level is highly correlated to the steric component of sea level computed from the temperature and salinity of the Ishii database (Ishii and Kimoto, 2009). The low-pass filtered basin averages have correlation and RMS differences of 0.86 and 15 mm. The linear trend of the steric sea level basin average is positive before 2001 (8.1 ± 0.4 mm/yr) and negative after 2001 (-5.1 ± 0.5 mm/yr). The MFSTEP model, available after year 2000, gives a smaller negative trend in the interval 2001-2008 (-2.2 ± 0.3 mm/yr) (Fig. F-10-7).

The rates of the geocentric sea level have been evaluated at each grid point of the altimeter grids. Over the interval 1993-2008 the trends are statistically significant at the 90% level of significance in most of the basin, with negative rates only in the Ionian Sea. The linear rates have opposite signs in the central and eastern Mediterranean Sea over the intervals 1993-2006 and 2002-2008, corresponding to the Topex/Poseidon and Jason-1 missions (Fig. F-10-8). The first interval is characterized by positive rates in Adriatic and Eastern Mediterranean and by negative rates in the Ionian Sea, the rates being of opposite sign in the second time-interval. The significance of the trends is lower over the sub-intervals, due to the shorter time span.

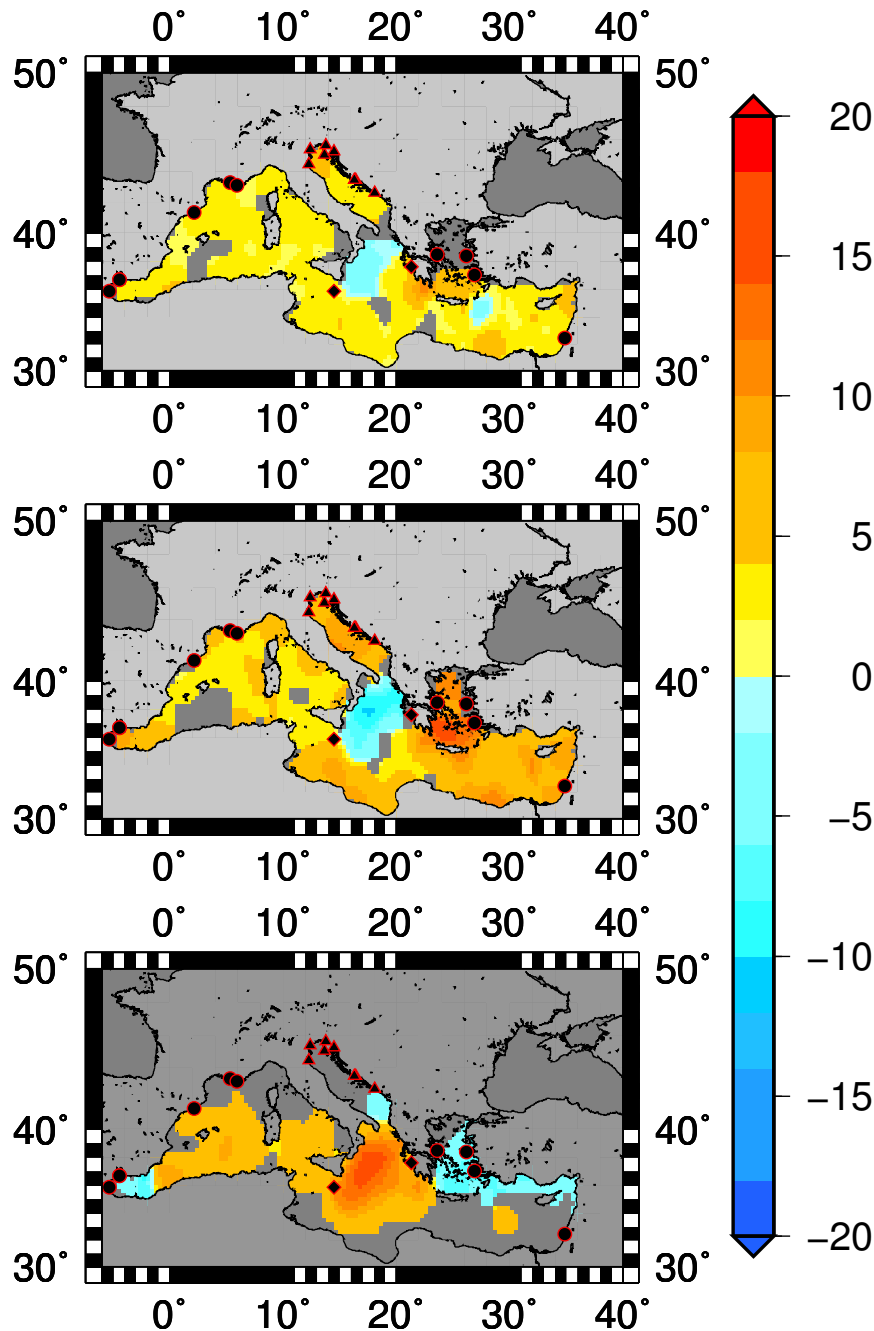


Figure F-10-8: Sea level trends (mm/yr) in Mediterranean Sea from multi-satellite altimetry in 1993-2008 (top), from Topex/Poseidon in 1993-2006 (center) and from Jason-1 in 2002-2008 (bottom). Only trends significant at least at the 90% significance level are represented. The tide gauge stations used to compute the basin averages in the Adriatic Sea (triangle), in the Ionian Sea (diamond) and in the Mediterranean Sea (all) are indicated.

The PCA decomposition of the altimeter grids covering the complete Mediterranean Sea shows regional differences between the Adriatic Sea and the rest of the Mediterranean Sea. The first four modes are statistically significant and explain together about 80% of the variance of sea level. The spatial and temporal components are shown in Fig. F-10-9. The first mode accounts for 70.3% of the variability and primarily represents the annual cycle. The second mode (5.3% of the variance) corresponds to the sea level rise in 1993-2001 in the Adriatic and

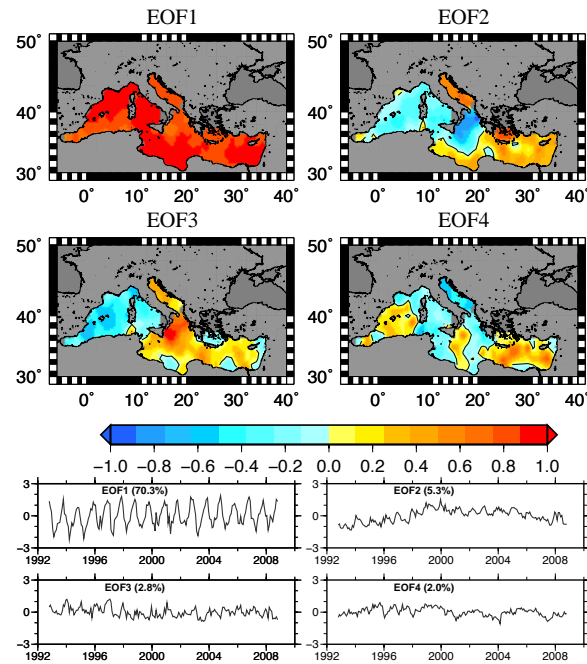


Figure F-10-9: Dominant spatial patterns (top) and temporal coefficients (bottom) of sea level variability in Mediterranean Sea from altimetric standardized monthly grids. The cumulative percentage of variance is given for each EOF component

the Eastern Mediterranean, and to the simultaneous sea level drop in the Ionian Sea. The third mode (2.8%) represents the variability in the Ionian Sea, the fourth mode (2.0%) the sea level rise in the Eastern Mediterranean Sea after year 2000 and the simultaneous decrease in the Adriatic Sea.

The first four modes of the PCA of sea level in the Adriatic Sea represent together about 98% of the variance, the first mode corresponds to an homogeneous signal (84.8% of the variance) that includes both annual and interannual components. The other modes represent local signals of higher temporal variability: the second mode (6.6% of the variance) corresponds to the variability localized in the central part of the sub-basin, the third mode (5.5%) shows a seesaw between the northern and southern Adriatic Sea. Fig. F-10-10 shows the four dominant modes, all satisfy the N rule. The PCA decomposition of the eight tide gauge monthly records shows similar dominant patterns, with the first mode corresponding to the common signal that explain 81% of the total variance.

4. Discussion and conclusions

With a combined analysis of altimetry and tide gauge data in the interval 1993-2008 we have investigated the absolute sea level rise and crustal motion in the Adriatic Sea. We have used the different characteristics of the two data types, namely their different reference and the different time and spatial sampling, to derive relevant information. Merging multi-mission altimeter data we have increased the length and the spatial and temporal resolution of the altimeter data and obtained co-located altimeter data much closer to the tide gauge stations. Applying the different definition of the sea level measured by altimeter and tide gauges, we have attempted to estimate the vertical crustal (land) motion at the tide gauge station.

The trends of the sea level differences between the altimeter and the tide gauges time-series at near locations are small compared to their uncertainties and therefore not all are

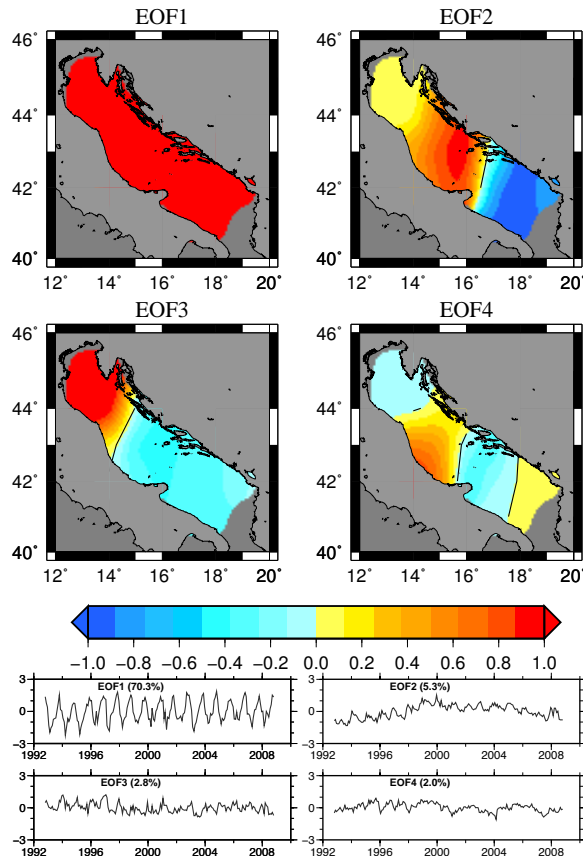


Figure F-10-10: Dominant spatial patterns (top) and temporal coefficients (bottom) of sea level variability in the Adriatic Sea from altimetric standardized monthly grids. The cumulative percentage of variance is given for each EOF component

statistically significant. A statistically significant land movement (90% confidence level) is detected in 1993-2008 only at Rovinj (3.0 ± 1.2 mm/yr) and Marina di Ravenna (-1.5 ± 1.1 mm/yr). A 75% confidence level is found in Trieste (1.5 ± 1.1 mm/yr) and Bakar (1.2 ± 1.1 mm/yr). Continuous GPS-measurements in Marina di Ravenna give a higher land subsidence rate than the rate obtained from the altimetry and tide gauge differences. The difference can arise from very local characteristics of anthropogenic origin, from the spatial distance between the locations corresponding to the altimetry and tide gauge measurements and from residual errors in the corrections applied.

The values we found for the crustal rates are in agreement with estimations made by geologic methods. Antonioli et al. (2009) compare relative sea-level change during the late Holocene, derived from geologic and archeological markers, with sea-level curves predicted from two post-glacial rebound- models (Lambeck et al. 2004, Stocchi and Spada 2009). In the North-Eastern Adriatic most of the measurements points indicate subsidence using both isostatic models as reference, the average of all points being -0.51 and -0.29 mm/yr respectively from the two models. However, in a few cores drilled in the Gulf of Trieste the tectonic subsidence reaches lower values, or even weak uplift, like in our results. This area of relative stability or weak uplift could result from the active growth of an NW-SE trending structural high recently detected across the Gulf of Trieste using high resolution seismic profiling (Busetti et al., 2007). Finally, Furlani et al. (2010) obtain tectonic rates between -1.99 mm/yr and 1.01 mm/yr near Trieste, using a multidisciplinary approach, that consists in comparing predicted curves with published data and new ^{14}C dating and geomorphological/archaeological/sedimentological observations. It is however not obvious that our estima-

tion and the estimation made by geologic methods should be equal, as the time constants used in the averaging process are very different: 16 years for the instrumental records and 1-100 kys for the geologic estimates. In a seismic zone the short term rates can be very different from the long term rates, because the instantaneous rates depend on the phase of the seismic cycle (e.g. Meade and Hager, 2004). Moreover, the geologic site usually does not coincide with the tide gauge, so local effects can provoke differences in vertical movement rates, especially in the presence of faults and changes in the compactness of the coastal rocks or sediment cover.

We have shown that both the absolute (altimetry-derived) and the relative (tide-gauge derived) sea level changes are spatially homogeneous in the region and indicate a sea level rise over 1993-2008. When averaged over the Adriatic they have both a positive trend, which is higher for the absolute (3.2 ± 0.3 mm/yr) than for the relative (1.9 ± 0.3 mm/yr) estimation. The rates are positive before 2001 and negative after 2001 and are contaminated by the inter-annual variability. At basin scale in the Adriatic Sea the linear-term of sea level change is strongly correlated to the linear-term in the steric component of sea level, suggesting that sea level changes in the Adriatic are governed by sea temperature and salinity changes. The variability in the Adriatic is coherent and strongly correlated to the eastern Mediterranean and anti-correlated with the Ionian Sea. Our results agree with Buble et al. 2010, that found over the common interval 1993-2008 similar dominant modes of sea level variability from tide gauges. These authors have considered a longer time-interval and therefore their trends of absolute and relative sea level are not comparable with ours. The crustal rates are of the same order of magnitude.

We recognize that the spatial and temporal differences between altimetry and tide gauge measurements cannot be ignored. With multi-mission altimetry data the coverage is greatly improved, however the distance between the locations of the altimeter and tide gauge observations is still several Kilometres, because of the geometry of the ground-tracks and of land-water interference caused by the radiometer and radar footprints. The differential sea level rates are correctly interpreted as crustal movement if the rates are measured at the same location or if they are spatially homogeneous. If the wavelengths of the sea level rates are of a few tens of km, then this supposition is granted, because the distance between the stations and the satellite location is of this magnitude. Also the application of specific models or empirical corrections, as ocean tide and atmospheric pressure effects can effect the results. The altimeter error budget in coastal regions remains therefore an important topic of research and discussion. In general, the comparison of altimeter and coastal tide gauge measurements needs to be thoroughly examined, in view of the growing importance of satellite altimeter measurements as a means of monitoring sea level rise and of the recent improvement of shallow-water satellite altimetry (Vignudelli et al., 2010).

Acknowledgments

We acknowledge ISPRA-APAT and PSMSL for the tide gauge data, ESA, NASA/CNES and TU-Delft for the altimetry data and RADS Database. We thank Prof. Stravisi for the tide gauge data of Trieste, Prof. S. Zerbini and Dr. F. Raicich for the tide gauge data of Marina di Ravenna, Venezia and Trieste, the GPS rates and for discussion. Comments by two anonymous reviewers helped to improve the manuscript. This research was supported by the Deutsche Forschungsgemeinschaft (DFG BE-1277, FE-354) and has benefited from funding provided by the Italian Presidenza del Consiglio dei Ministri - Dipartimento della Protezione Civile (DPC). Scientific papers funded by DPC do not represent its official opinion and policies

Bibliography

- Ablain, M., A. Cazenave, G. Valladeau, S. Guinehut (2009). A new assessment of the error budget of global mean sea level rate estimated by satellite altimetry over 1993-2008, *Ocean Sci.*, 5, 193-201. Andersen O. B. and P. Knudsen (2009). DNSCO8 mean sea surface and mean dynamic topography models, *J. Geophys. Res.*, 114, C11001, doi:10.1029/2008JC005179.
- Antonoli F., L. Ferranti, A. Fontana, A.M. Amorosi, A. Bondesan, C. Braitenberg, A. Dutton, F.G. Fontolan, S. Furlani, K. Lambeck, G. Mastronuzzi, C. Monaco, G. Spada, P. Stocchi, (2009). Holocene relative sea-level changes and vertical movements along the Italian and Istrian coastlines, *Quaternary International*, doi:10.1016/j.quaint.2008.11.008
- Beckley, B.D., F. G. Lemoine, S. B. Luthcke, R. D. Ray, N. P. Zelensky (2007). A reassessment of global rise and regional mean sea level trends from Topex and Jason-1 altimetry based on revised reference frame and orbits, *Geophys. Res. Lett.*, 34, L14608, doi:10.1029/2007GL030002.
- Bindoff N., J. Willebrand , V. Artale, A. Cazenave, J. Gregory, S. Gulev, K. Hanawa, C. Le QuÃ©rÃ©, S. Levitus, Y. Nojiri, C.K. Shum, L. Talley, A. Unnikrishnan, (2007). Observations: oceanic climate and sea level. In: *Climate change 2007: The physical Science Basis. Contribution of Working Group I to the Fourth Assessment report of the Intergovernmental Panel on Climate Change* [Solomon S., D. Qin, M. Manning, Z. Chen, M. Marquis, K.B. Averyt, M. Tignor and H.L. Miller (eds.)]. Cambridge University Press, Cambridge, UK, and New York, USA., pp 385-428.
- Blewitt, G, Z. Altamimi, J.L. Davis, R.S. Gross, C. Kuo, F. Lemoine, A.W. Moore, R. Neilan, H. Plag, M. Rothacher, C. Shum, M. Sideris, T. Schöne, P. Tregoning, S. Zerbini (2010) Geodetic observations and global reference frame contributions to understanding sea level rise and variability. In: Church J, Woodworth PL, Aarup T, Wilson S (eds) *Understanding sea level Rise and variability*. Wiley-Blackwell, London, pp 256-284.
- Bloomfield, P., 1976. *Fourier Analysis of Time Series: An Introduction*. New York: John Wiley and Sons. pp. 129-137.
- Buble G., R.A. Bennett and S. Hreinsdottir (2010). Tide gauge and GPS measurements of crustal motion and sea level rise along the eastern margin of Adria, *J. of Geophys. Res.* , 115, B02404, doi:10.1029/2008JB006155.
- Braitenberg C., P. Mariani, L. Tunini, B. Grillo, I. Nagy (2010) Vertical crustal movements from differential tide gauge observations and satellite altimetry in southern Italy, *Journal of Geodynamics* doi:10.1016/j.jog.2010.09.003.
- Busetti, M., E. Gordini, L. Baradello, A. Cova, A. Caburlotto, M. Deponte, D. Nieto, I. Tomini, (2007). The morphological and seismic stratigraphic characterization of the Grado and Marano lagoon (northern Adriatic). In: *Convegno Nazionale GeoItalia 2007, Rimini 12-14 sett. 2007*, 2, 487-S50.
- Carbognin L, P. Teatini, A. Tomasin, T. Luigi (2009). Global change and relative sea level rise at Venice: what impact in term of flooding; *Climate Dynamics* Springer Berlin / Heidelberg Earth and Environmental Science 1039- 104735610.1007/s00382-009-0617-5
- Carrère L. and F. Lyard (2003). Modelling the barotropic response to the global ocean to atmospheric wind and pressure forcing with observations, *Geophys. Res. Lett.*, 30, 8-1
- Cazenave, A., K. Dominh, F. Ponchaut, L. Soudarin, J. F. Cretaux, and C. Le Provost. (1999): Sea level changes from TOPEX-Poseidon altimetry and tide gauges, and vertical crustal motions from DORIS, *Geophys. Res. Lett.*, 26(14), 2077-2080
- Cazenave, A., C. Cabanes, K. Dominh and S. Mangiarotti (2001). Recent sea level change in the Mediterranean Searevealed by TOPEX-Poseidon satellite altimetry, *Geophys. Res. Lett.*, 28(8), 1607-1610
- Church J., N.J. White, T. Arrup, W.S. Wilson, P.L. Woodworth, C.M. Domingues, J. R. Hunter, K. Lambeck (2008). Understanding global sea levels: past, present and future, *Sustain Sci.* 3:9-22, doi:/10.1007/s11625-008-0042-4
- Chelton, D.B., J.C. Ries, B.J. Haines, L.L. Fu, P. Callahan, 2001: Satellite Altimetry, in *Satellite altimetry and Earth sciences*, ed. L.L. Fu and A. Cazanave, Academic Press, NY, pp. 57-64.

- Domingues C.M., J. Church, N.J. White, P.J. Gleckler, S.E. Wijffels, P.M. Barker and J.R. Dunn (2008). Improved estimates of upper-ocean warming and multi-decadal sea level rise, *Nature Letters*, 453, doi:10.1038
- Dong X., P. Woodworth, P. Moore, R. Bingley, (2002). Absolute calibration of the Topex/Poseidon altimeters using UK Tide gauges, GPS and Precise Local Geoid-differences, *Mar. Geod.* 25, 189-204.
- Douglas B.C. (2001). Sea level change in the era of the recording tide gauge, in *Sea Level Rise, history and consequences*, International Geophysics Series Volume 75, Academic Press
- Fenoglio-Marc L. (2001). Analysis and representation of regional sea level variability from altimetry and atmospheric data, *Geoph. J. Int.* 145, Issue 1, pp. 1-18
- Fenoglio-Marc L. (2002). Long-term sea level change in the Mediterranean Sea from multi-satellite altimetry and tide gauges, *Physics and Chemistry of the Earth*, 27, pp. 1419-1431
- Fenoglio-Marc L., E. Groten and C. Dietz, (2004). Vertical Land Motion in the Mediterranean Sea from altimetry and tide gauge stations, *Marine Geodesy*. 27, 3-4, 683-701.
- Fenoglio-Marc L. and E. Tel (2010). Coastal and global sea level change, *J. of Geodynamics*, doi:10.1016/j.jog.2009.13.003.
- Furlani, S., S. Biolchi, F. Cucchi, F. Antonioli, M. Busetti, R. Melis, (2010). Tectonic effects on Late Holocene sea level changes in the Gulf of Trieste (NE Adriatic Sea, Italy), *Quaternary International*, doi:10.1016/j.quaint.2010.06.012.
- Gill A.E. (1982). *Atmosphere and Ocean Dynamics*, International Geophysics Series , Academic Press, pp. 662
- Holgate, S. J. (2007). On the decadal rates of sea level change during the twentieth century, *Geophys. Res. Lett.*, 34, L01602, doi:10.1029/2006GL028492
- Ishii M. and M. Kimoto (2009) Re-evaluation of Historical Ocean Heat Content Variations with Time-Varying XBT and MBT Depth Bias Corrections, *J. of Oceanography*, 65, 287-299
- ISPRA (2009). Istituto superiore per la Protezione e la Ricerca Ambientale, <http://www.apat.gov.it/site/it-IT>
- Klein M. and M. Lichter (2008). Statistical analysis of recent Mediterranean Sea level data, *Geomorphology*, doi:10.1016/j.geomorph.2007.06.024
- Kuo C.Y., C.K. Shum , A. Braun and J.X. Mitrovica, (2004). Vertical crustal motion determined by satellite altimetry and tide gauge data in Fennoscandia, *Geophys. Res. Lett.* 31 (1), 10.1029/2003GL019106, L01608.
- Lambeck and Johnston (1995) Land subsidence and sea-level change: contribution from the melting of the last great ice sheets and isostatic adjustment of the Earth, in *Land Subsidence*, edited by F.B.J. Barends, F.J.J. Brouwer and F.H. Schroder, pp. 3-18, Taylor and Francis, London
- Lambeck, K., Antonioli, F., Purcell, A., Silenzi, S., 2004. Sea level change along the Italian coast for the past 10,000 yrs. *Quat. Sc. Rev.*, 23, 1567-1598.
- Lionello P., R. Mufato and A. Tomasin (2005). Sensitivity of free and forced oscillations of the Adriatic Sea to sea level rise. *Climate Research*, Vol. 29:23-39, 2005
- Marcos M. and M. N. Tsimplis (2007). Variations of the seasonal sea level cycle in southern Europe, *J. Geophys. Res.*, 112, C12011, doi:10.1029/2006JC004049
- Marcos M. and M. N. Tsimplis (2008). Coastal sea level trends in Southern Europe, *Geophys. J. Int.*, 175, 70-82, doi:10.1111/j.1365-246X.2008.03892.x
- Maul, G.A. and D. M. Martin (1993). Sea level rise at key west, Florida, 1846-1992: Americans longest Instrument record?, *Geophys. Res. Lett.*, 20, 1955-1958.
- Meade B.J. and B.H. Hager, (2004). Viscoelastic deformation for a clustered earthquake cycle, *Geophys. Res. Lett.*, Vol. 31, L10610, doi:10.1029/2004GL019643, 2004

- Mitchum, G. T., 2000: An Improved Calibration of Satellite Altimetric Heights Using Tide Gauge Sea Levels with Adjustment for Land Motion, *Marine Geodesy*, 23(3), 145-166
- Naeije M., Scharroo R., Doornbos E. and E. Schrama (2008). Global altimetry sea-level service: Glass, NUSP-2 report GO 52320 DEO, NIVR/DEOS, Netherlands
- Nerem R.S. and Mitchum G.T. (2002) Estimates of vertical crustal motion derived from differences of Topex/Toseidon and sea level measurement. *Geophys. Res. Lett.*, 29, 1934, 2002.
- Orlic and M. Pasarić (2000). Sea-level changes and crustal movements recorded along the east Adriatic coast, *Nuovo Cimento Della Societa Italiana Di Fisica C-Geophysics And Space Physics*, 23, 351-364.
- Overland J.R. and R.W. Preisendorfer (1982). A significant test for principal components applied to cyclone climatology. *Mon. Weather Rev.* 110, 1, 1-4
- Parker, R. L. (1994). *Geophysical Inverse Theory*, 386 pp., Princeton University Press, Princeton, USA
- Pascual A., M. Marcos and Damia Gomis (2008). Comparing the sea level response to pressure and wind forcing of two barotropic models: validation with tide gauge and altimetry data, *J. of Geophys. Res.* doi:10.1029/2007JC004459
- Pirazzoli, P.A., 1991. Possible defenses against a sea-level rise in the Venice area, Italy. *Journal of Coastal Research* 7, 231-248.
- Pirazzoli P. and A. Tomasin, 2008. Sea-level and surges in the Adriatic Sea: recent trends and possible near-future scenarios, *Atti dell'Istituto Veneto di Scienze, Lettere ed Arti*, Tomo CLXVI
- Prandi, P., A. Cazenave, and M. Becker (2009). Is coastal mean sea level rising faster than the global mean? A comparison between tide gauges and satellite altimetry over 1993-2007, *Geophys. Res. Lett.*, doi:10.1029/2008GL036564.
- Preisendorfer, R.W. (1988) *Principal Component Analysis in Meteorology and Oceanography*, Developments in Atmospheric Science, N. 17, Elsevier, Amsterdam. Raicich F.(2007). A Study of the early Trieste sea level data. *J. of Coastal Research*, 23(4), 1067-1073
- Ray R.D., Beckley B.D. and Lemoine F.G. (2010) Vertical crustal motion derived from satellite altimetry and tide gauges and comparison with DORIS measurements, *Advances in Space Research* 45, 1510-1522
- Santer, B. D., T. M. L. Wigley, J. S. Boyle, D. J. Gaffen, J. J. Hnilo, D. Nychka, D. E. Parker, and K. E. Taylor (2000), Statistical significance of trends and trend differences in layer-average atmospheric temperature time series, *J. Geophys. Res.*, 105(D6), 7337-S7356, doi:10.1029/1999JD901105.
- Stocchi P. and G. Spada (2009) Influence of glacial isostatic adjustment upon current sea level variation in the Mediterranean Sea, *Tectonophysics*, 474, 55-68
- Tiezzi, E. and N. Marchettini, (1997). Venezia e il problema delle acque alte. Il rischio di danno al patrimonio urbano a causa della crescita relativa del livello del mare. *Quaderni Trimestrali Consorzio Venezia Nuova* 5/2, 23-45.
- Tonani M., N. Pinardi, S. Dobricic, I. Pujol and C. Fratianni (2008). A high-resolution free-surface model of the Mediterranean Sea, *Ocean Sci.*, 4, 1-14, 2008
- Tosi, P. Teatini, L. Carbognin, and G. Brancolini (2009). Using high resolution data to reveal depth-dependent mechanisms that drive land subsidence: The Venice coast, Italy (2009) *Tectonophysics*, Volume 474, Issues 1-2, TOPO-EUROPE: The Geoscience of coupled Deep Earth-surface processes, 271-284, DOI: 10.1016/j.tecto.2009.02.026.
- Trisirisatayawong I., Naeije M., Simons W. and Fenoglio-Marc L. (2011). Sea level change in the Gulf of Thailand from GPS-corrected tide gauge data and multi-satellite altimetry, *Global and Planetary Change*, accepted
- Tushingham A.M. and W.R. Peltier (1989) ICE-3G: A new global model of late Pleistocene deglaciation based upon geophysical predictions of post glacial relative sea level change, *J. Geoph. Res.* 96, 4497-4523
- Vignudelli S., A. Kostianov, P. Cipollini and J. Benveniste (Eds.) 2011, *Coastal Altimetry*, Springer Verlag, doi:10.1007/978-3-642-12796-0

- Vigo I., D. Garcia and B.F. Chao (2005). Change of sea level trend in the Mediterranean and Black Seas, *J. of Marine Research*, 63, 185-1100
- Wöppelmann G., S. Zerbini and M. Marcos (2006). Tide gauges and Geodesy: a secular synergy illustrated by three present-day case, *C.R. Geoscience*, doi:10.1016/j.crte.2006.07.006
- Woodworth, C., 2003. Some comments on the long sea level records from the northern Mediterranean. *Journal of Coastal Research* 19, 212-S217.
- Woodworth, P. and R. Player, (2003): The Permanent Service for Mean Sea Level: An update to the 21st century. *J. Coastal Res.*, 19(2), 287-285
- Zerbini, S., B. Richter, F. Rocca, T. van Dam, and F. Matonti (2007). A Combination of Space and Terrestrial Geodetic Techniques to Monitor Land Subsidence: Case Study, the South Eastern Po Plain, Italy, *J. Geophys. Res.*, 112, B05401, doi:10.1029/2006JB004338.

7.6 Sea level change and vertical land motion in the Indonesian region

F-11: Fenoglio-Marc L., T. Schöne , J. Illigner , M. Becker , P. Manurug, Khafid, Sea Level Change and Vertical Motion from Satellite Altimetry, Tide Gauges and GPS in the Indonesian Region, *Marine Geodesy*, 35:sup1, 137-150T, 2012.

Abstract

We investigate the sea level rise in Indonesia during the period 1993-2011 using satellite altimetry and tide gauge data. Satellite altimetry indicates a positive sea level rise with mean of 4 mm/yr, which is higher than the global averaged mean sea level rise. At four tide-gauge stations the difference of the sea level trends from tide gauge and co-located satellite altimetry is greater than 3 mm/yr. Land subsidence is found in Jakarta, Surabaya and Benoa. At Enggano and Tanjung Lesung the vertical rates correspond with GPS-derived rates between 2007-2009 indicating land subsidence at the first station.

Keywords: sea level, altimetry, tide gauge, vertical land motion

1. Introduction

Indonesia consists of thousands of islands with large populations inhabiting the low-elevation coastal areas. The global sea level rise (SLR) in response to ocean warming and ice melting (Nicholls and Cazenave, 2010) has here important impacts, such as beach erosion, inundation of land, increasing salination of coastal aquifers, increasing flood and storm damage as well as the loss of coastal ecosystem.

Previous studied in the western tropical Pacific Ocean and in the nearby regions have shown that inter-annual changes in sea level are associated with the El-Niño Southern Oscillation (ENSO) (Merrifield et al., 1999). Sea level trend patterns observed through the 17-yr long altimetry observations are mainly of thermal origin (Lombard et al., 2005), the trends being driven by surface wind stress (Merrifield 2011). The climate-related sea level rise may be reinforced by land subsidence due to natural, e.g. tectonics and volcanism, and anthropogenic, e.g. ground water extraction, causes.

Altimeter satellites have directly measured SLR since 1992, whereas the tide gauge-based sea level trend account for land vertical movements. The difference between the sea level trends measured by altimetry and tide gauge is therefore a measure of the vertical land motion, if it is assumed that the sea level signals are truly common. The use of combined satellite altimeter and tide gauge data offers a valid approach for determining vertical motion at tide gauges sites (Ray et al., 2010; Nerem and Mitchum, 2002; Fenoglio-Marc et al., 2004, 2011; Trisirisatayawong et al., 2010).

Since Indonesia is an active seismic region, large vertical movement rates and displacements and consequently large differences between the sea level change estimated from altimetry and from tide gauge records are to be expected. The Sumatra-Andaman earthquake in December 2004 changed the crustal motion pattern in the region. The vertical direction ground displacements in the near field show a region of co-seismic uplift near the Sumatra trench and a region of subsidence further away from it. Evidence of 1.5 m co-seismic uplift near the epicenter and of subsidence along the coast of Sumatra have been reported (Sieh, 2005; Subarya et al., 2006). The 2007 Bengkulu earthquake also caused significant vertical

displacements of up to 0.8 m in a wider area off Sumatra measured directly with GPS and confirmed by modeling (Borrero et al., 2009).

This paper aims to clarify the following issues, (1) the main characteristics of sea level change in the Indonesian region and (2) the long-term difference between eustatic sea level observed by altimetry and sea level rise relative to land observed by tide gauge records. It is organized as follows: overall data and methodology are described in Section 2; results pertaining to inter-annual sea level variability and linear trends of sea level from both altimetry and tide gauge data and their differences are presented in Section 3; the conclusions are provided in Section 4.

2. Methodology and data

2.1 Tide gauge data

The Indonesian tide gauge station network consists of approximately 120 tide gauge stations maintained by the Coordinating Agency for Surveys and Mapping (BAKOSURTANAL). A subset is shown in Fig. F-11-1. Approximately 10 of these stations are donated by NOAA, supported by the Intergovernmental Oceanographic Commission (IOC) and installed by the University Hawaii Seal Level Centre (UHSLC). One-minute data is available at the IOC real-time monitoring facility at <http://www.ioc-sealevelmonitoring.org/>.

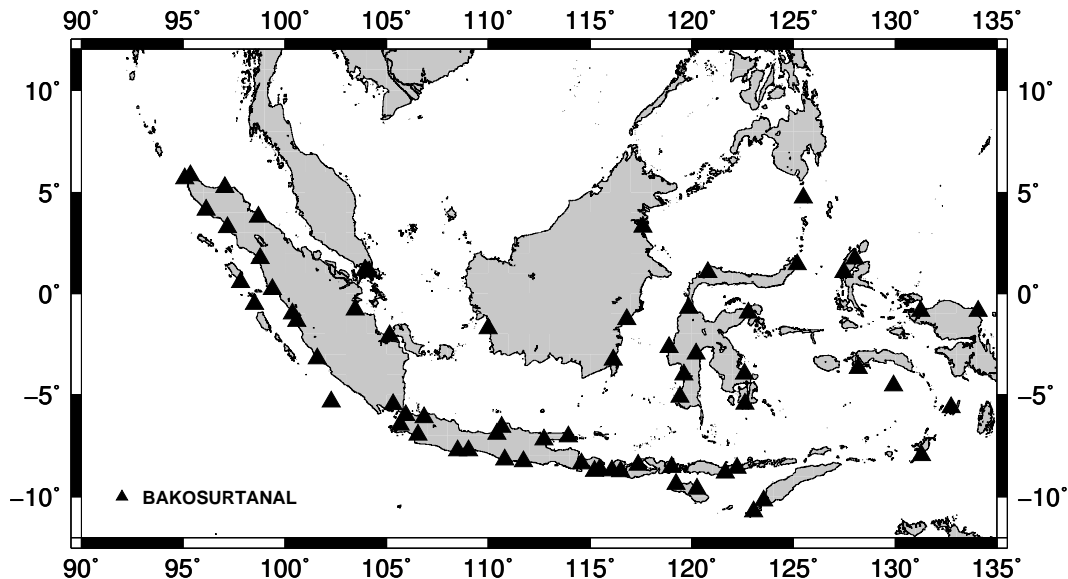


Figure F-11-1: Subset of the BAKOSURTANAL tide gauge network

Within the German Indonesian Tsunami Early Warning System (GITEWS) project and as a contribution to the Indonesian Tsunami Early Warning System (InaTEWS), 10 GPS-controlled tide gauges have been installed at sites on the islands of Sumatra, Java, Sumba, and Rote facing the Indian Ocean (Schöne et al., 2011). The purpose of GITEWS is to follow the best practice of the Global Sea Level Observing System (GLOSS) (UNESCO, 2006) and to provide near real-time information for tsunami warnings and monitoring of long-term sea level changes. The GPS-controlled stations allow a continuous monitoring of both sea level (with automated alert in case of rapid sea level change) and of the horizontal and vertical movements of the tide gauge station. Most stations have several sensors: radar (RA), pressure

sensor (PR), and shaft encoder measuring sea level in a stilling well (ENC). The longest GPS records begin in the year 2007 and the corresponding sea level tide gauge data are available via the IOC. Due to the distance between the GPS-antenna and the tide gauge at the stations of Enggano (GANO) and Teluk Dalam (TDAL) further leveling has been necessary. The calibration of the tide-gauge measurements and the referencing between the GNSS benchmark and the tide gauge zero is still in progress.

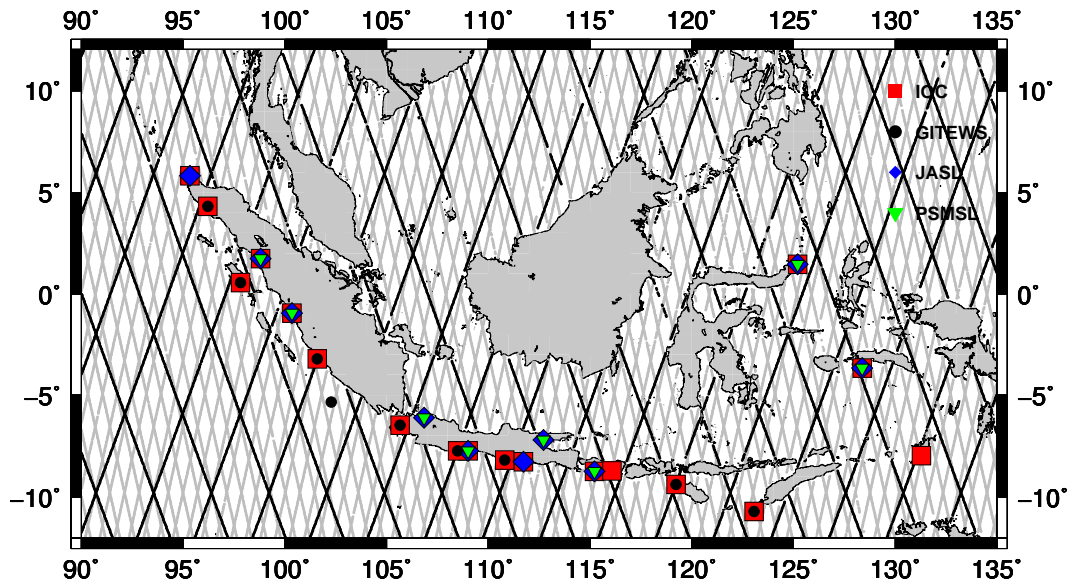


Figure F-11-2: Tide gauge stations of the IOC (square), JASL (diamond), PSMSL (inverse triangle) and GITEWS (circle) with data available during the period 1993-2011. Altimetry-tracks are from the Jason/Topex (black) and from Envisat/ERS missions (grey).

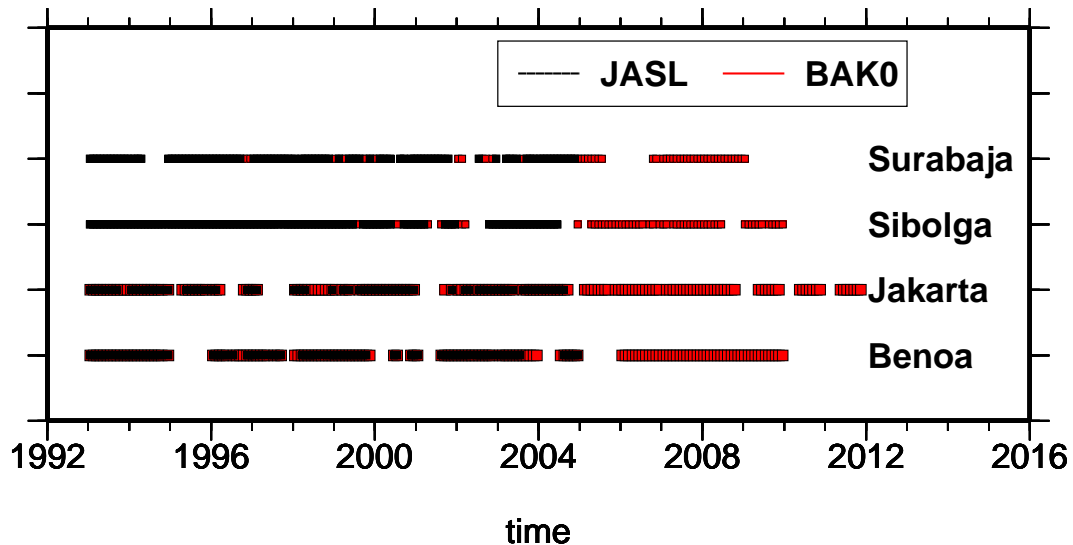


Figure F-11-3: Time availability of the data extracted from the JASL (black) and BAKOSURTANAL (red) databases for the four tide gauge stations (triangles in Fig. F-11-4).

For the previous decades a sub-set of tide gauge sea level data has been made available by the Joint Archive for Sea Level (JASL) which is a collaborative arrangement between the National Oceanographic Data Center (NODC), the World Data Center for Oceanography Silver Spring (WDC-SS), and the University of Hawaii Sea Level Center (UHSLC)

(<http://ilikai.soest.hawaii.edu/uhsic/rqds.html> providing hourly, daily and monthly data) and by the Permanent Service for Mean Sea Level (PSMSL) (<http://www.psmsl.org/> providing monthly data). The JASL database contains two more stations (Sabang and Prigi) than the PSMSL database.

Fig. F-11-2 provides the location of IOC (10) and GITEWS (9 out of 10) stations, as well as the sub-set of stations belonging to the JASL and PSMSL databases (10 and 8) with data available from 1993-2011. All stations belong to the IOC real time network or to the GLOSS network.

Monthly means of sea level height have been computed from the JASL hourly data by averaging the data collected over a period of a month. Monthly data gaps are smaller in the JASL than in the PSMSL dataset. Stations having in 1993-2003 a completeness index (CI) larger than 70% have been selected (Nurmaulia et al., 2010). The CI denotes the percent of monthly tide gauge data available in a given time interval. The four stations fulfilling this condition are Benoa, Jakarta, Sibolga, and Surabaya (triangles in Fig. F-11-4). Finally, the JASL data has been used with the gaps filled by using hourly data provided by the local organization BAKOSURTANAL. The data are available during 1993-2011 for the station of Jakarta and during 1993-2009 for the other three stations. See Fig. F-11-3 for the data coverage.

2.2 Altimetry data

The Radar Altimeter Database System (RADS) (Naeije et al, 2008) provided multi-mission altimetry data which was collected between 1993-2011, which included data from the ERS-1, -2 (1993-1996, 1995-2009), Envisat (2002-2011), Topex/Poseidon (1993-2005), Jason-1, -2 (2002-2011, 2008-2011) missions. The spatial coverage of the data is shown in Fig. F-11-2. Two types of comparisons were performed, called monthly and daily comparison methods (see also Fenoglio-Marc et al., 2011). In the first method, multi-mission gridded altimeter data are compared to monthly tide gauge records. In the second method, along-track altimeter data are compared to tide gauge records at the point of nearest approach. Both comparison methods require the same corrections to be applied to the altimeter data to compute sea level height anomalies above a reference surface. Standard geophysical corrections and the reference frame offsets have been applied to altimetry. The pole tide correction is not applied for consistency with the tide gauge records. Environmental (wet and dry tropospheric, ionospheric, sea state bias) and geophysical corrections (solid earth, ocean and load tides) have been applied. To retain more data near the coast, the wet tropospheric correction derived from the European Centre for Medium-range Weather Forecasts (ECMWF) model was chosen and most of the conservative flags were ignored, thus allowing the inclusion of data closer to land.

Both altimetry and tide gauge data have been corrected for ocean tides using the GOT4.7 ocean tide model and for the oceanic response to atmospheric pressure forcing using the Dynamic Atmospheric Corrections (DAC). The DAC corrections are produced by CLS Space Oceanography Division using the Mog2D model from Legos (Carrère and Lyard, 2003) and distributed by Aviso, with support from CNES (<http://www.aviso.oceanobs.com/>) with a temporal resolution of 6 hours and a spatial resolution of 0.25° . The correction for the one-second altimeter data is included in the RADS database.

Monthly grids of the merged multi-mission data have been produced with spacing of 0.2 degrees using a Gaussian weighted average method with half-weight equal to 1 degree and search radius of 150 km. For each tide gauge station a co-located altimeter time-series has been

selected corresponding to the nearest point in the multi-mission altimeter grid. At each grid point the linear trend and the annual and semi-annual signals have been evaluated separately for the altimeter and tide gauge time-series through a least-squares procedure fitting the function:

$$m(t) = b + ct + a_{11} \cos \omega_1 t + a_{12} \sin \omega_1 t + a_{21} \cos \omega_2 t + a_{22} \sin \omega_2 t \quad (\text{F-11-1})$$

where b , c , a_{i1} , a_{i2} , $i=1,2$, are the parameters to be determined, and ω_i and are the yearly and half-yearly angular frequency, respectively. The linear trend is given by the parameter c and its uncertainty σ is equal to the standard error of the coefficient estimate; with the assumption that the residuals have zero mean and Gaussian distribution (Parker, 1994). We perform a Principal Component Analysis (PCA) (Preisendorfer, 1988) of the residuals to quantify the spatio-temporal sea level variations at inter-annual and decadal time scales and we apply a significance test based on a Monte Carlo technique to find the components corresponding to a signal above the noise level (Overland and Preisendorfer, 1982). The input data to the PCA are first normalized to standardized anomalies by dividing each point time-series by its standard deviation and the output spatial vectors are normalized to the maximum value for each mode (Fenoglio-Marc et al., 2011).

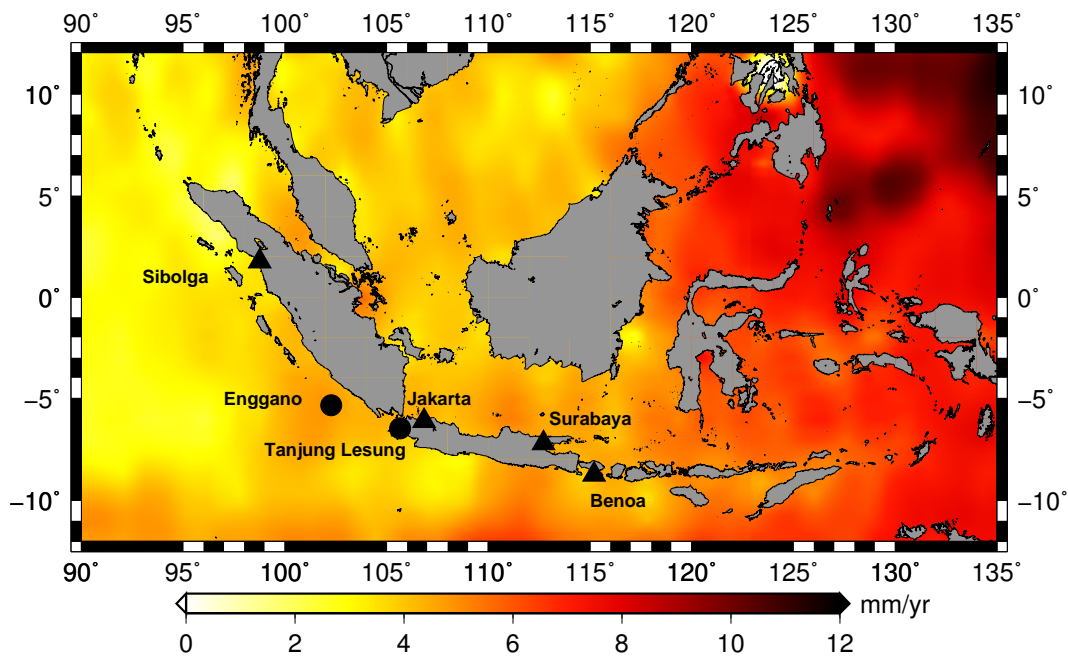


Figure F-11-4: Maps of sea level trends in the period 1993-2011 derived from satellite altimetry

Linear regression is also used to estimate the trend and its standard error of the differences between sea level as measured by the altimeter and by the tide gauge instruments. Both sea level time-series have been previously corrected for their annual and semi-annual components to account for differences in the amplitude of the seasonal components (see Fenoglio-Marc et al., 2011). We finally compute an effective sample size n^1 based on the lag-1 autocorrelation coefficient r_1 (see also Eq. 6 in Santer et al., 2000) ($n^1 = n \frac{1-r_1}{1+r_1}$) to account for the temporal autocorrelation of the de-trended time-series, where n is the number of monthly time samples. By using the effective sample size n^1 one obtains a bigger error for the trend:

$$\sigma^1 = \sigma F_l \quad (\text{F-11-2})$$

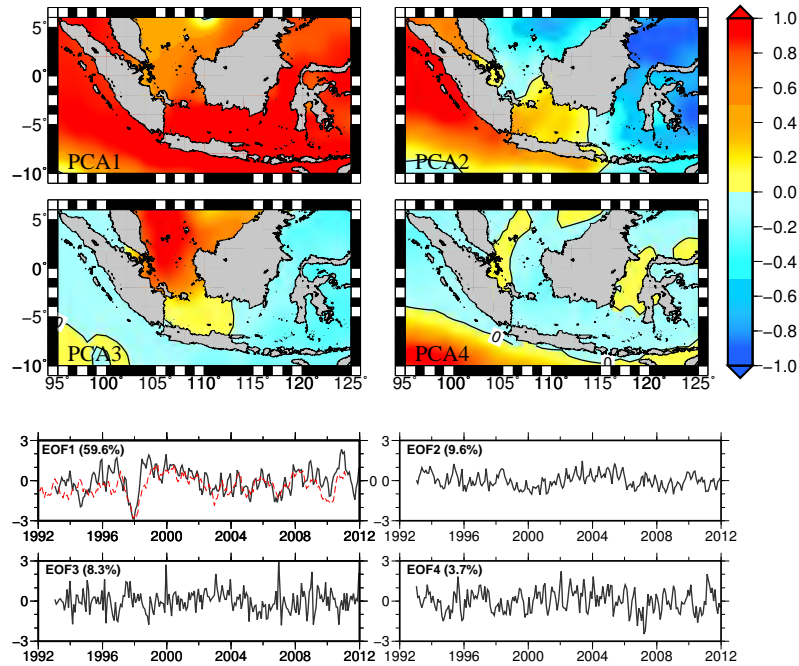


Figure F-11-5: First four spatial patterns (top) and temporal coefficients (bottom) obtained from the PCA decomposition of the inter-annual and decadal sea level variability in the period 1993-2011 (trend, annual and semi-annual components have been removed). The inverted Global-SST ENSO index is superimposed to the first PCA temporal component (dashed line).

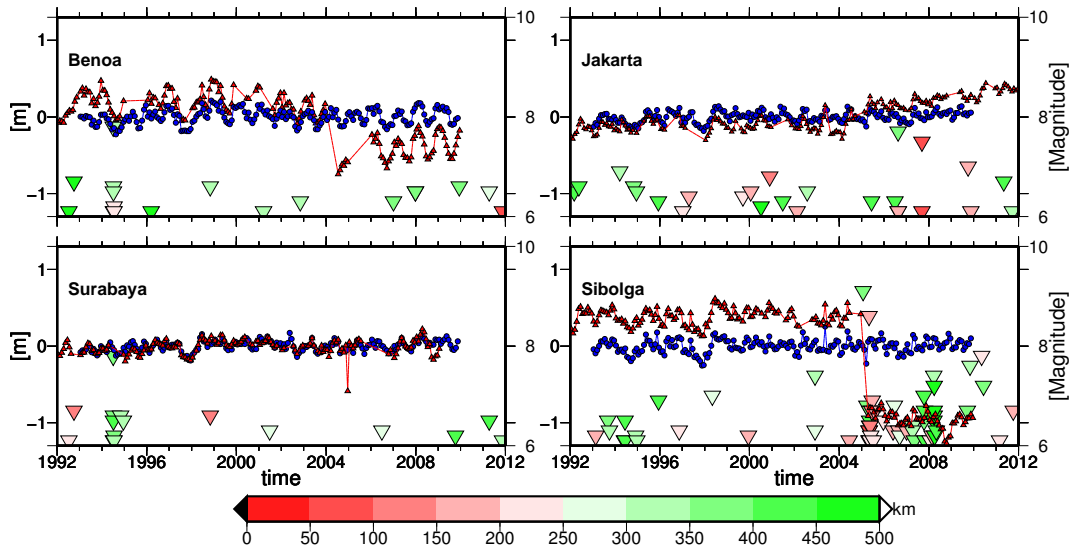


Figure F-11-6: Anomalies of monthly sea level from tide gauge (triangle) and from co-located altimetry (circle) data. Inverted triangles indicate earthquakes of magnitude higher than 6 in a radius of 500 Kilometers from the station.

where F_l is the inflation factor and the standard error of the trend. This procedure does not alter the value of the trends, but leads to an increase of the estimated error by approximately 40% for de-seasoned time-series (Fenoglio-Marc et al., 2004, 2011). The trend significance is further assessed by applying the t-test to the ratio between the estimated trend and its standard error. The jumps in tide gauge time-series are corrected by adding :

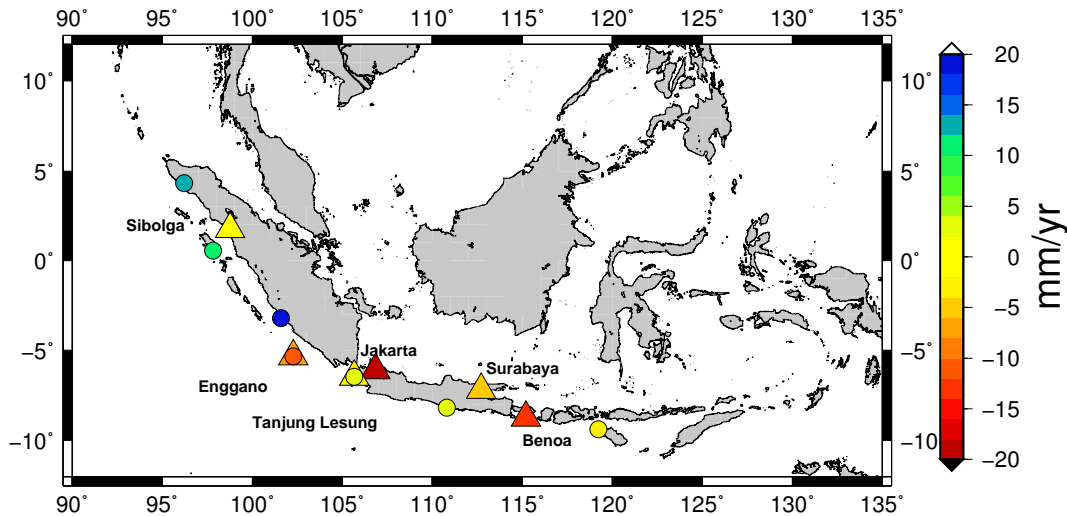


Figure F-11-7: Land vertical motion from altimetry minus tide gauge (triangle) and from GPS (circle).

$$\text{corr}_{tg} = -(h_{tg}(t_2) - h_{tg}(t_1)) + (h_{al}(t_2) - h_{al}(t_1)) \quad (\text{F-11-3})$$

to the tide gauge time-series after the discontinuity, where t_1 and t_2 are the extremes of the interval of discontinuity and h_{tg} , h_{al} are the de-seasoned monthly values. The seasonal component is first evaluated by computing the mean variability for each month in the interval of analysis, which is then removed from the monthly values to obtain de-seasoned monthly values.

3. Results

3.1 Sea level from altimetry and tide gauge stations

In the period 1993-2011 the altimetric trends are positive throughout the Indonesian region. Fig. F-11-4 shows a map of the altimeter sea level trends. The highest trends are found in the Pacific Ocean (up to 12 mm/yr, in agreement with Becker et al. (2011)): trends are lower in the shallow marginal Indonesian basins (between 4 and 8 mm/yr) and in the Indian Ocean (lower than 4 mm/yr). Trends taken between 1993-2009 are of 2-4 mm/yr at the co-located altimeter time-series in Benoa, Jakarta, Sibolga and Surabaya (Tab. F-11-1, column 3).

The strong signature of the El-Niño Southern Oscillation (ENSO), a forcing mode of the coupled Atmosphere-Ocean system, dominates the inter-annual variability. Its signature is characteristic for the sea level in the entire Indonesian region, as shown by the PCA decomposition of the de-seasoned and de-trended sea level time-series. The first four modes are statistically significant and explain together 81% of the variance of sea level during 1993-2011 in the selected region ($95 \leq \text{lon} \leq 125$, $-10 \leq \text{lat} \leq 6$). The first mode, that accounts approximately for 60% of the total variance, corresponds to an oscillation in phase of the entire basin (see Fig. F-11-5 (top)). Its temporal pattern (Fig. F-11-5 (bottom)) has a correlation 0.62 with the inverted Global-SST ENSO index, which captures the low-frequency frequencies of the ENSO phenomenon (<http://jisao.washington.edu/data/globalstsenso/>). The second mode (9.6% of the variance) corresponds to a sea level variability out of phase in the eastern and

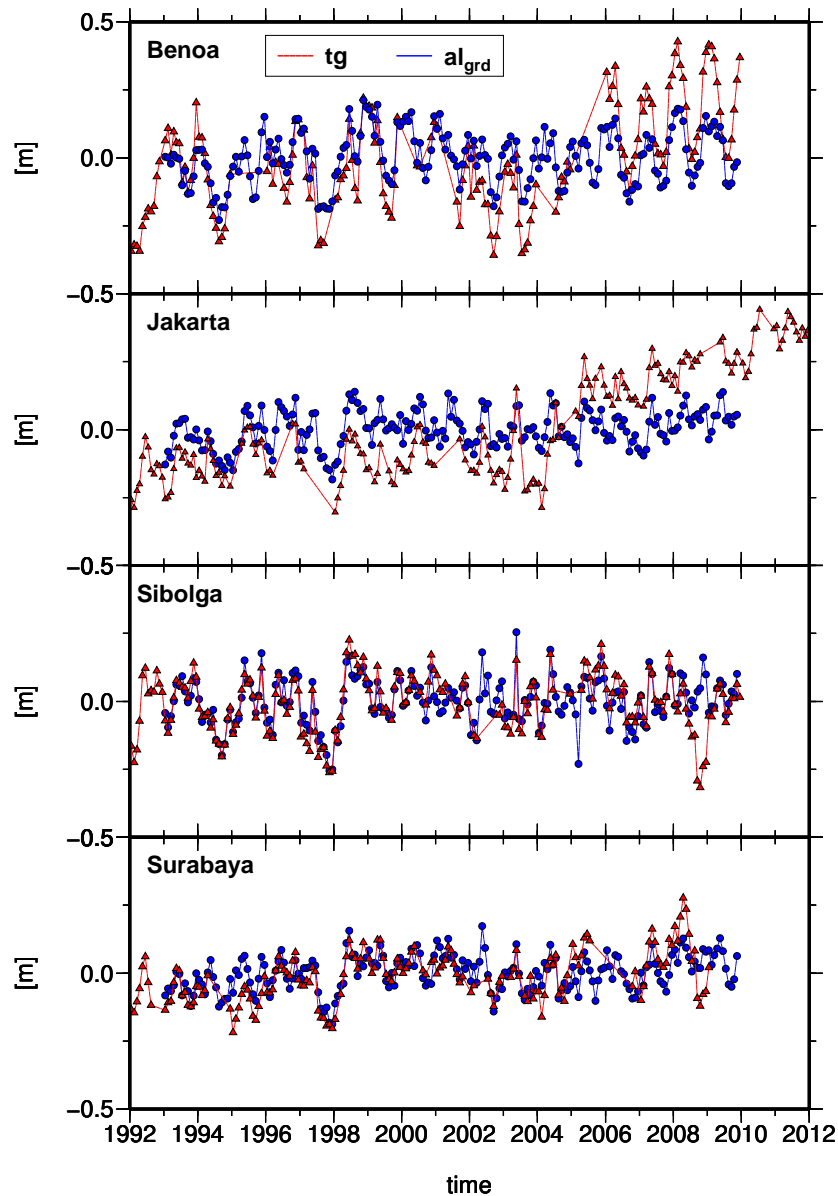


Figure F-11-8: Anomalies of monthly sea level in Fig. F-11-6, here corrected for jumps in the records using Eq. F-11-3

western regions. The third and fourth modes (8.3% and 3.7% of the total variance) represent a sub-regional variability in the internal seas and in the open Indian ocean. The co-located altimeter time-series in Bena, Jakarta, Sibolga and Surabaya have comparable inter-annual variability, differences appear at annual and higher frequencies (Fig. F-11-8).

The tide gauge sea level records present discontinuities and jumps. By using the earthquake catalogue of the National Earthquake Information Center (NEIC) (<http://earthquake.usgs.gov/regional/neic>) the relationship between these discontinuities and earthquake events has been investigated. The number of earthquakes of magnitude 6 and higher, occurring in a radius of 500 Kilometers around each station (Fig. F-11-6) have been considered and it appears that tide gauge records are affected by seismic events. Earthquakes of high magnitude are more frequent in Sibolga and Jakarta than at the other two stations. The time-series of Sibolga and Surabaya have a discontinuity in correspondence to

Table F-11-1: Comparison during the period 1993-2009 of monthly tide gauge- and co-located altimeter sea level times series. The co-located point is the nearest grid of the altimeter grid. Given are: trends of the monthly tide gauge- (b_t , column 7), altimeter- (b_a , column 8), altimeter minus tide gauge (b_{at} , column 9) sea level difference time-series, distance between tide gauge and co-located altimeter point (d , column 3), correlation of monthly time-series (r_{at} , column 4), root mean square of their difference (RMSD) and completeness index (CI) of the time-series

Station	CI (%)	d (km)	RMSD (mm)	r_{at}	$b_a \pm \sigma_a$ (mm/yr)	$b_t \pm \sigma_t$ (mm/yr)	$b_{at} \pm \sigma_{at}$ (mm/yr)
Benoa	94	6.7	124	0.68	3.2 ± 1.1	14.8 ± 2.0	-11.9 ± 1.4
Jakarta	94	14.4	146	0.48	3.8 ± 1.0	23.1 ± 1.5	-19.7 ± 1.6
Sibolga	94	25.2	73	0.70	2.4 ± 1.2	0.6 ± 1.3	1.9 ± 1.3
Surabaya	89	8.9	66	0.65	3.8 ± 1.0	8.8 ± 1.2	-5.3 ± 1.0

Table F-11-2: Vertical land motion derived from monthly differences of co-located altimetry and tide gauge sea level time-series (2008-2010) and GPS/GITEWS vertical rates at the same cGPS@TG stations (as in Tab. F-11-3). Given are: altimeter minus tide gauge (b_{at}) sea level difference time-series, distance between tide gauge and co-located altimeter point (d), correlation of monthly time-series (r_{at}), root mean square of their difference (RMSD) and completeness index (CI) of the time-series

Station	CI (%)	d (km)	RMSD (mm)	r_{at}	$b_{at} \pm \sigma_{at}$ (mm/yr)	$b_{GPS} \pm \sigma_{GPS}$ (mm/yr)
Enggano	99	20	29	0.95	-7.2 ± 2.4	-11.1 ± 0.5
Tanjung Lesung	99	22	30	0.97	-3.9 ± 4.6	2.2 ± 0.5

Table F-11-3: GPS vertical rates at the GITEWS GPS stations in 2007-2009

Station	North (mm/yr)	East (mm/yr)	Up (mm/yr)
Meulaboh (MEUL)	-34.5 ± 1.4	-15.5 ± 1.5	13.9 ± 4.1
Enggano (GANO)	8.1 ± 0.2	20.9 ± 0.2	-11.1 ± 0.5
Sadeng (SADE)	-7.6 ± 0.2	28.9 ± 0.2	3.6 ± 0.6
Seblat (SEBL)	-34.3 ± 0.9	-20.5 ± 0.8	19.2 ± 1.7
Teluk Dalam (TDAL)	1.5 ± 0.2	5.2 ± 0.2	10.1 ± 0.4
Tanjung Lesung (TJLS)	-5.5 ± 0.2	25.8 ± 0.2	2.2 ± 0.5
Waikelo (WAIK)	16.7 ± 0.2	31.1 ± 0.2	-2.9 ± 0.6

the Sumatra-Andaman earthquake in December 2004. The time-series of Sibolga has a jump of about one meter occurs after the discontinuity. However, land uplift at that station, as indicated by the lowering sea level, could not occur as the earthquake caused a subsidence along the coast of Sumatra (Subarya et al., 2006). The jump is possibly caused by a change in the zero level of the tide gauge. Also the discontinuity of the Benoa time-series end of 2003 suggests different reference levels used by UHSLC and by BAKOSURTANAL. We use Eq. F-11-3 to correct the sea level time-series of the Benoa, Sibolga and Surabaya tide gauge stations. The corrected monthly time-series and the co-located altimeter time-series (Fig. F-11-8), have been evaluated over the complete period between 1993-2009 to derive the rates of land vertical movement at the corresponding location (shown in Fig. F-11-7). Tab. F-11-3 summarizes the results. The best agreement between altimetry and tide gauge sea level time-series is found at Sibolga (correlation 0.70, Root Mean Square of the differences (RMSD) 73 mm for monthly time-series) and at Surabaya (correlation 0.65 and RMSD 73 mm), whereas

the lowest agreement occurs in Jakarta (correlation 0.48 and RMSD 146 mm). In Sibolga both time-series have low trends (0.6 ± 1.3 mm/yr and 2.4 ± 1.2 mm/yr respectively), the trend of the de-seasonalized altimetric- minus tide gauge time-series (called AL-TG rate) is not statistically significant at the 95% level of confidence (1.9 ± 1.3 mm/yr). At the other three stations a subsidence, significant at the 95% level, is detected. In Surabaya the tide gauge sea level trend (8.8 ± 1.2) is twice the altimetric trend (3.8 ± 1.0 mm/yr), the AL-TG rate is -5.3 ± 1.0 . The subsidence detected in Jakarta (-19.7 ± 1.6 mm/yr) is a known feature at that location (e.g., Abidin et al., 2001). Subsidence is also found in Benoa (-11.9 ± 1.4 mm/yr). In Benoa and in Jakarta the trend of the tide-gauge derived sea level is four and five times larger than the altimetric sea level trend. The AL-TG rates derived in this study are shown in Fig. F-11-7. They are generally larger than those reported in other regional studies (Fenoglio-Marc et al., 2004, 2011).

3.2 Vertical land motion from GPS

For all GITEWS stations vertical trends in 2007-2009 are available from GPS time-series (C. Subarya, personal communication) and can be compared to those values derived from altimetry and tide gauge data.

In Enggano the vertical land subsidence detected from the monthly comparison of altimeter and tide gauge data, i.e. the AL-TG rate, is -7.2 ± 2.4 mm/yr (Tab. F-11-2). This value is in agreement with the GPS-derived rate of -11.1 ± 0.5 mm/yr. In Tanjung Lesung the AL-TG rate is not significant (-3.9 ± 4.6 mm/yr) and also the GPS-derived rate (2.2 ± 0.5 mm/yr) does not indicate a high vertical land movement. At both stations the agreement between altimeter and tide gauge time-series (correlation higher than 0.93 and RMSD smaller than 30 mm for monthly time-series) is higher than for the four stations evaluated in Section 3.1 (Tab. F-11-2, Fig. F-11-9.a,c).

As both stations are closely located to a descending Envisat track, the daily comparison of tide gauge and along-track satellite altimetry data is here particularly suitable. Fig. F-11-9.b shows sea level anomalies and their differences for an Envisat along-track point located 20 Kilometers far from the Enggano, for cycles from 64 to 93, before that a change in the ground-track pattern occurs. The resulting correlation (0.95), standard deviation (44 mm) and linear trend of the difference between the altimeter and the tide gauge sea level time-series (-8.0 ± 4.3 mm/yr) are comparable with the results corresponding to the gridded altimeter data. This result further confirms that gridded and along-track altimetric data give similar sea level trends and variability when a comparable pre-processing is applied (see also Fenoglio-Marc et al., 2011).

Tab. F-11-3 provides GPS rates for additional GITEWS stations which have been computed taking into account the gaps due to the earthquakes. The vertical rates are smaller for stations located in Java (local uplift of 3.6 ± 0.6 mm/yr in Sadeng) than for stations in Sumatra (uplift of 10.1 ± 0.4 mm/yr in Teluk Dalam, 13.9 ± 4.1 mm/yr in Meulaboh, 19.2 ± 1.7 mm/yr in Seblat). In Fig. F-11-7 the GPS-derived rates (circle) and the AL-TG rates (triangle) are compared.

4. Conclusions

This study confirms that the sea level variability in the Indonesian region is closely linked to the ENSO mode of variability and spatially highly homogeneous at inter-annual and decadal

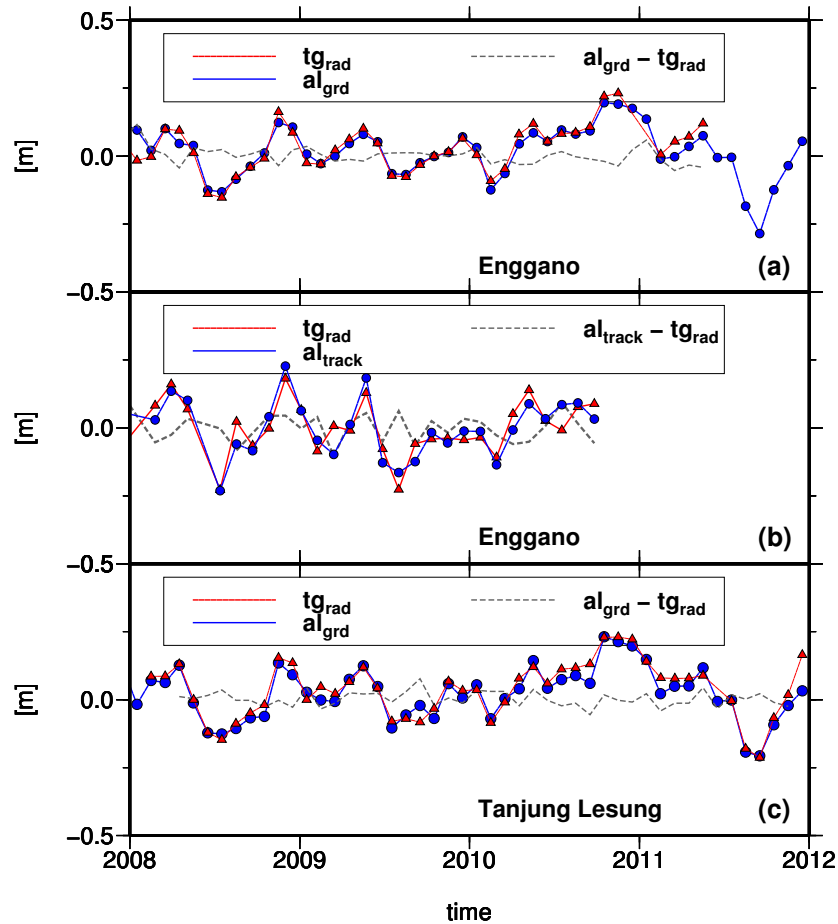


Figure F-11-9: Anomalies of sea level from altimetry (circle) and tide gauge (triangle) data and their difference (dashed line) at the GITEWS stations of Enggano (a,b) and Tanjung Lesung (c). For Enggano results are shown from both gridded monthly (a) and along-track daily analysis (b).

scales. The rates of absolute eustatic sea level rise derived from satellite altimetry through 19-yr long precise altimeter observations are in mean higher than the global mean rate of 3.3 ± 0.4 mm/yr (Nicholls and Cazenave, 2010). Sea level trends taken between 1993-2011 are of 2-4 mm/yr near selected tide gauge stations.

We have determined the vertical crustal motion at a given tide gauge location by differencing the tide gauge sea level time-series with an equivalent time-series derived from satellite altimetry and by computing the trend of the differences. This method, that assumes that both instruments measure an identical ocean signal, represents an interesting alternative to the use of collocated GPS at the tide gauge stations, when GPS is not available. We have detected the subsidence in Jakarta, in agreement with Abidin et al. (2001), and in three other tide gauge stations. The land vertical rates correspond in two stations to GPS-derived rates derived over only a few years, which should be confirmed by longer time-series.

We conclude that in Indonesia the climate-related sea level trend is reinforced by vertical land movements of a similar or even larger magnitude and that its impact on coastal areas should be seriously considered.

The proper modeling of the vertical movements is the key to sea level change studies relative to the Earth crust. In Indonesia the determination of sea level change rate from tidal data is complicated due to the co-seismic displacements of the 2004 Sumatra Andaman and

the following earthquakes, which added vertical shifts, that are still not accurately known, into tidal data from all the stations in the region. Other smaller jumps may be related to the local geodynamic activities. The instability in the reference level of the tidal records makes it difficult to use tide gauge data for sea level change studies, therefore altimetry data are today the most promising database to estimate sea level rise around Indonesia and need to be combined with tide gauges and co-located GPS measurements in regional geodynamic studies.

Acknowledgments

We acknowledge the provision of the altimetry databases by ESA and JPL/CNES, AVISO and RADS, the National Coordinating Agency for Surveys and Mapping (BAKOSURTANAL), Indonesia, and the University of Hawaii for the provision of tide gauge data. This study was partly carried out in the frame of the project COSELE funded by the Deutsche Forschungsgemeinschaft (DFG). We acknowledge the contribution of Sella Nurmaulia for the preparation of some of the tide gauge data used in this analysis.

References

- Abidin, H., R. Djaja, D. Darmawan D., S. Hadi, A. Akbar, H. Rajiyowiryo, Y. Sudibyo, I. Meilano, M. A. Kasuma, J. Kahar, and C. Subarya. 2001. Land Subsidence of Jakarta (Indonesia) and its Geodetic Monitoring, *Natural Hazards*, 23, 365-387
- Becker, M., B. Meyssignac, C. Letetrel, W. Llovel, A. Cazenave, A., and T. Delcroix. 2011. Sea level variations at tropical Pacific islands since 1950, *Global and Planetary Change*, <http://dx.doi.org/10.1016/j.gloplacha.2011.09.004>.
- Borrero, J. C, R. Weiss, E.A. Okal, R. Hidayat, Suranto, D. Arcas, and V. V. Titov. 2009. The tsunami of 2007 September 12, Bengkulu province, Sumatra, Indonesia: post-tsunami field survey and numerical modelling, *Geophysical Journal International*, 178, 1, 180-194, doi:10.1111/j.1365-246X.2008.04058.x.
- Carrère, L., and F. Lyard. 2003. Modeling the barotropic response of the global ocean to atmospheric wind and pressure forcing - comparisons with observations, *Geophys. Res. Lett.*, 30, 1275, doi:10.1029/2002GL016473.
- Fenoglio-Marc, L., E. Groten, and C. Dietz. 2004. Vertical Land Motion in the Mediterranean Sea from altimetry and tide gauge stations, *Marine Geodesy* 27 (3-4), 683-701.
- Fenoglio-Marc, L., C. Braitenberg, and L. Tunini. 2011. Sea level variability and trends in the Adriatic Sea in 1993-2008 from tide gauges and satellite altimetry, *Physics and Chemistry of the Earth*, doi:10.1016/j.pce.2011.05.014.
- Lombard, A., A. Cazenave, P.Y. Le Traon, and M. Ishii, 2005. Contribution of thermal expansion to recent-day sea-level change revisited, *Global Planet. Change*, 47, 1-16, 2005
- Merrifield, M. A. , B. Kilonsky and Shikuko Nakahara 1999. Interannual sea level changes in the Tropical Pacific associated with ENSO. *Geophys. Res. Lett.*, 26, 21, 3317-3320
- Merrifield, M. A. and M. E. Maltrud 2011. Regional sea level trends due to a Pacific trade wind intensification, *Geophys. Res. Lett.*, 38, L21605, doi:10.1029/2011GL049576.
- Naeije, M., R. Scharroo, E. Doornbos, and E. Schrama. 2008. GLobal Altimetry Sea-level Service: GLASS, Final Report. NIVR/DEOS publ., NUSP-2 report GO 52320 DEO.
- Nerem, R. S. and G. T. Mitchum. 2002. Estimates of vertical crustal motion derived from differences of TOPEX/POSEIDON and tide gauge sea level measurements, 29, 1934, doi:10.1029/2002GL015037.
- Nicholls, R. J. and A. Cazenave. 2010. Sea-level rise and its impact on coastal zones. *Science* 328, 1517.

- Nurmaulia, S., L. Fenoglio-Marc, and M. Becker. 2010. Long-term sea level change from satellite altimetry and tide gauges in the Indonesian region, in Proceedings ESA Living Planet Symposium, SP-686.
- Overland J.R. and R.W. Preisendorfer (1982). A significant test for principal components applied to cyclone climatology. *Mon. Weather Rev.* 110, 1, 1-4
- Parker, R. L. 1994. *Geophysical Inverse Theory*, 386 pp., Princeton University Press, Princeton, USA.
- Preisendorfer, R.W. (1988) *Principal Component Analysis in Meteorology and Oceanography*, Developments in Atmospheric Science, N. 17, Elsevier, Amsterdam
- Ray, R.D., B. D. Beckley, and F. G. Lemoine. 2010. Vertical crustal motion derived from satellite altimetry and tide gauges and comparison with DORIS measurements, *Adv. In Space Res.* 45, 1510-1522.
- Santer, B. D., T. M. L. Wigley, J. S. Boyle, D. J. Gaffen, J. J. Hnilo, D. Nychka, D. E. Parker, and K. E. Taylor. 2000. Statistical significance of trends and trend differences in layer-average atmospheric temperature time-series, *J. Geophys. Res.*, 105(D6), 73377-7356, doi:10.1029/1999JD901105.
- Schöne, T., J. Illigner, P. Manurung, C. Subarya, J. Khafid, C. Zech, and R. Galas. 2011. GPS-Controlled tide gauges in Indonesia - a German contribution to Indonesia's Tsunami Early Warning System, *Nat. Hazards Earth Syst. Sci.* 11, 731-740.
- Sieh, K. 2005. What happened and what next? *Nature* 434, 571-572.
- Subarya, C., M. Chlieh, L. Prawirodirdjo, J.-P. Avouac, Y. Bock, K. Sieh, A. J. Meltzner, D. H. Natawidjaja, and R. McCaffrey. 2006. Plate-boundary deformation associated with the great Sumatra-Andaman earthquake, 440, doi:10.1038/nature04522.
- Trisirisatayawong, I., M. Naeije, W. Simons, and L. Fenoglio-Marc. 2011. Sea level change in the Gulf of Thailand from GPS-corrected tide gauge data and multi-satellite altimetry, *Global and Planetary Change* 76, 137-151.
- UNESCO. 2006. *Manual on Sea-level Measurements and Interpretation, Volume IV: An update to 2006*, in: IOC Manuals and Guides No. 14, Intergovernmental Oceanographic Commission of UNESCO, Paris, France, JCOMM Technical Report No. 31, WMO/TD. No. 1339.

Chapter 8

Attribution of sea level rise

8.1 Mass variation in the Mediterranean Sea

F-12: Fenoglio-Marc L., J. Kusche, M. Becker, M., Mass variation in the Mediterranean Sea from GRACE and its validation by altimetry, steric and hydrology fields, *Geoph. Res. Lett.*, 33, L19606, 2006.

Abstract The seasonal seawater mass variation in the Mediterranean Sea is estimated between April 2002 and July 2004 from GRACE and altimetry data and from hydrologic and oceanographic models. A smoothed spatial averaging kernel is applied to each field, in order to obtain comparable basin averages. The GRACE seawater mass corrected for the leakage of continental hydrology and the filtered steric-corrected altimeter sea level have similar annual amplitude and phase. To restore the magnitude of the GRACE-derived water mass signal we apply a scaling factor to the smoothed annual amplitude. The estimated scaled mass signal has an annual amplitude of 52 ± 17 mm peaking in November. We combine the seawater mass variation with the Mediterranean freshwater deficit and obtain a net flow at the Strait of Gibraltar with annual amplitude of 60 ± 25 mm/month (0.06 Sv) and maximum in September.

1. Introduction

The ocean mass variation is addressed at global scale independently by using steric-corrected satellite altimetry or GRACE observations (Chambers et al., 2004). Low-pass filters, in form of spatial averaging kernels, are typically applied to GRACE spherical harmonic (SH) coefficients to minimise both the effects of GRACE measurement errors and the contamination from surrounding signals (Wahr et al., 1998, Swenson et al. 2002a). The choice of an effective smoothing radius is critical and the smoothing significantly affects the magnitude of the signal (Chen et al. 2005, Velicogna and Wahr 2006). The region considered here is the Mediterranean Sea, a semi-closed basin of medium size (2.5 million m^2). The annual amplitude of the basin averaged sea level is 7-8 cm (Ayoub et al., 1998) and the steric part of sea level variability represents at seasonal scales about 50% of the sea level change (Bouzinac et al., 2003; Garcia-Lafuente et al., 2004, Vignudelli et al., 2003). The mass change (loss) due to the Mediterranean freshwater deficit (MWD) is compensated by the net inflow from the Black Sea (B) and from the Atlantic Ocean (G) (Boukthir and Barnier, 2000; Mariotti et al., 2002). This last quantity is difficult to measure, estimations based on water mass budget, steric-corrected sea level and direct measurements give annual amplitudes of 0.04-0.08 Sv peaking in September (Garcia-Lafuente et al. 2002, Bryden et al. 1994).

We assess the ability of GRACE to recover the ocean mass variation in the Mediterranean Sea from April 2002 to July 2004. We first discuss the computation of water mass basin average time-series in semi-closed seas and compare the two calculations (corrected GRACE and steric-corrected altimetry) when applying a smoothed spatial averaging kernel to each data field. The magnitude of the GRACE-derived water mass signal is then restored and used together with the Mediterranean water budget to estimate the net flow through the Strait of Gibraltar.

2. Data and processing

2.1 GRACE mass variation

Twenty near-monthly level-2 CSR GRACE gravity field solutions between April 2002 and July 2004 are used. Tidal effects, including ocean tide, solid Earth and solid pole tide as well as non-tidal atmospheric and oceanic effects have been removed in the pre-processing (Bettadpur, 2003). We expand the gravity solution to spherical degree and order 90 and smooth it using an isotropic Gaussian filter to construct spatial averages and down-weight the poorly known short-wavelength SH coefficients (Wahr et al., 1998). The filtered basin average time-series of water thickness is computed as in Swenson and Wahr (2002b, eq. 13)

$$\Delta\tilde{\sigma}_m(t) = \frac{2\pi a\rho_E}{3} \sum_{l=0}^{l_{\max}} \frac{2l+1}{1+k_l} W_l \times \sum_{m=0}^l \{\vartheta_{lm}^c \Delta C_{lm}^{\text{grace}}(t) + \vartheta_{lm}^s \Delta S_{lm}^{\text{grace}}(t)\} \quad (\text{F-12-1})$$

with ϑ_{lm}^c and ϑ_{lm}^s being the SH coefficients corresponding to the basin function $\vartheta(\theta, \lambda)$ that describes the shape of the Mediterranean Sea (1 inside, 0 outside the basin), W_l the Legendre coefficients of the Gaussian filter function, $\Delta C_{lm}^{\text{grace}}$, $\Delta S_{lm}^{\text{grace}}$ the change in the GRACE Stokes coefficients with respect to the long-term solution, a the radius of the Earth, ρ_E the average density of the solid Earth, k_l the load Love numbers representing the effects of the Earth's response to surface load. We select for the filter an averaging radius of 400 km based on formal error propagation from the CSR calibrated error statistics to ensure that the filtered basin average is not worse than 2 cm for year 2003. The truncation to degree 90 is not critical, as the filter of 400 km retains only 0.001% of the signal at degree 90. With a radius of 1000 km the formal error of GRACE is lower, but the aliasing mass signal from outside the basin is larger.

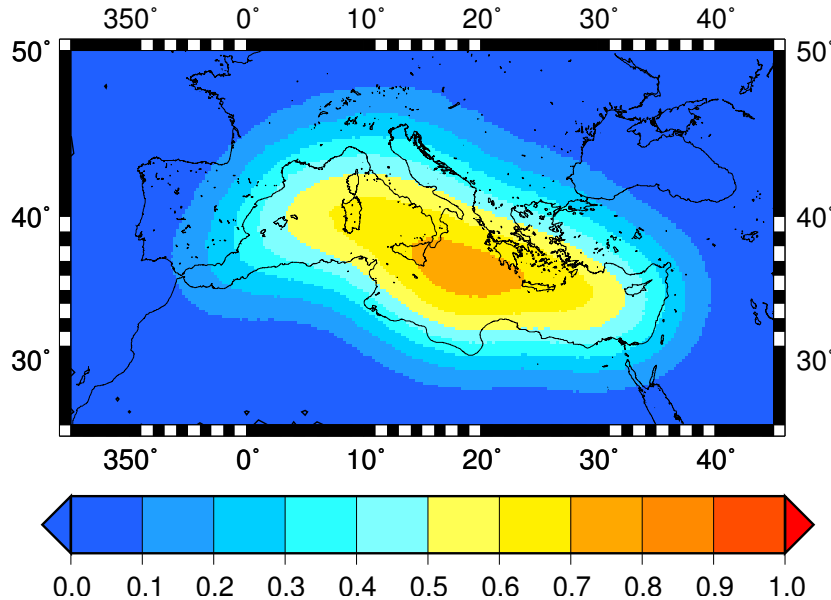


Figure F-12-1: Gaussian averaging kernel used for seawater mass variation estimation in the Mediterranean Sea

2.2 Sea level heights and steric contribution

We estimate sea level anomalies (a) using Jason-1 and Envisat altimeter from the Radar Altimeter Database System (RADS) (Naeije et al., 2002). We apply the radiometric wet tropospheric correction, the ionospheric correction from the dual frequency altimeter, solid earth tide, ocean, pole and load tide corrections and the standard inverse-barometer (IB) correction. This last correction, that is not accurate in semi-closed basin, is not necessarily consistent with the de-aliasing corrections used in the GRACE pre-processing, that are based on the response of a barotropic ocean model. The Root-Mean-Square (RMS) of the differences between the filtered basin averages of the IB and of the GRACE ocean de-aliasing corrections is however small (6 mm). The Ocean Pole Tide (OPT) correction, which is not applied in the GRACE data pre-processing, is also not applied to the altimeter data. The steric contribution to sea level variation (s) is estimated from the global ocean models ECCO/JPL (<http://ecco.jpl.nasa.gov>) and from the local model Mediterranean Forecasting System (MFSTEP) (<http://www.bo.ingv.it/mfstep>). Global and local climatologies, the World Ocean Atlas 2001 (WOA01) (<http://www.nodc.noaa.gov/OC5/WOA01>) and Medar/Medatlas (<http://www.ifremer.fr/medar>), are used for comparison.

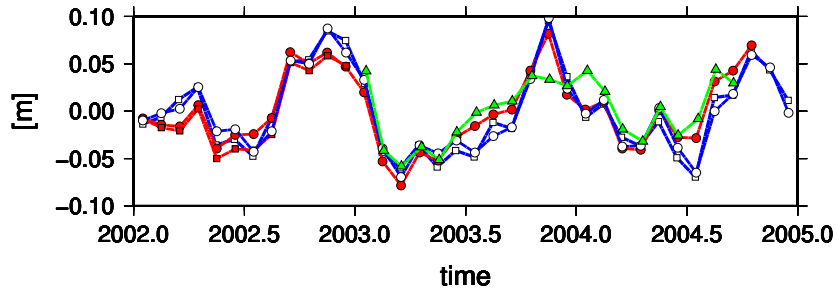


Figure F-12-2: Seawater mass anomalies in the Mediterranean Sea from Jason-1 sea level corrected for the steric contribution from ECCO/JPL ocean model (thick solid red), MFSTEP model (thin solid red), WOA01 global climatology (thick solid blue), Medar/Medatlas climatology (dashed blue). Envisat sea level corrected for the steric contribution from the ECCO/JPL ocean model is also shown (dashed red)

2.3 Continental hydrology and hydrologic cycle

Continental water storage is estimated from the Climate Prediction Center (CPC) model (Fan and van den Dool, 2004) and from the Land Dynamics Model (LaD)/Euphrates (Milly and Shmakin, 2002). Grids and unfiltered basin averages of Evaporation (E) minus Precipitation (P) (E-P) are computed from the NCEP/NCAR reanalysis daily averages of precipitation rate and surface latent heat flux and from the ERA40 ECMWF re-analysis. Climatologies of P-E, river runoff and Black Sea net flow are considered (Boukthir and Barnier 2000, Mariotti et al. 2002).

2.4 Times-series for water change comparison

We construct, in a rectangular region including the Mediterranean Sea, one degree monthly grids of steric-corrected sea level ($a-s$) (with zeros on land) and of continental water storage (h) (with zeros on sea). We compute the corresponding filtered basin average time-series $\overline{a-s}$ and \overline{h} by convolution of the grids in the spatial domain with the averaging kernel $\overline{W}(\theta, \lambda)$

created by convolving the basin function $\vartheta(\theta, \lambda)$ with a Gaussian filter as in Swenson et al. (2002a, eq. 26 and 29):

$$\Delta\tilde{\sigma}_m(t) = \frac{1}{\int_{\Omega} \overline{W}(\theta, \lambda) d\Omega} \int_{\Omega} \Delta\sigma(\theta, \lambda, t) \overline{W}(\theta, \lambda) d\Omega \quad (\text{F-12-2})$$

Fig. F-12-1 shows the Gaussian averaging kernel applied. The smoothing in spatial domain is preferred for regional application with gridded data, to avoid the computation of SH coefficients. Eqs. 1 and 2 are numerically equivalent, as shown by the good agreement of the filtered basin averages of the LAD model (RMS difference 6 mm and correlation 0.98). The filtered basin averages of steric-corrected altimetry and of GRACE water thickness are comparable only after application of additional corrections. These are (1) the monthly averages of the non-tidal barotropic oceanic contribution, which were modeled in the data processing and (2) the land hydrology, that leaks into the GRACE estimate of water mass. The first signal needs to be restored, while the second needs to be removed. We add back the monthly average of the non-tidal oceanic contribution used by the project, after correction for the effect of the atmosphere on land that is evaluated in a grid on land and smoothed in the spatial domain. To eliminate the leakage of land hydrology in the seawater mass estimated by GRACE, we subtract the filtered continental hydrology time-series \tilde{h} from the GRACE filtered basin average time-series. To be consistent with satellite altimetry measurements we include degree 1-2 of the geopotential in the estimation. As GRACE does not recover degree 1 and the degree 2 terms show anomalous large variability, we compute the filtered basin average mass variation from satellite laser ranging (SLR) degree 1 (Chen et al. 1999) and degree 2 (Cheng et al. 2002, Cheng and Tapley 2004). The SLR coefficients include the effect of the atmosphere on land, that is removed as before using the NCEP SH coefficients.

As the smoothing reduces the amplitude of the signal, we derive a scaling factor by comparing the filtered and unfiltered steric-corrected anomalies and we use it to restore the magnitude of the GRACE-derived seawater mass variation. This derivation differs from the one used in Velicogna and Wahr (2006) in that it takes the actual signal from independent information into account. The Gibraltar net flow is finally estimated from:

$$G = (E - P - R - B) + \frac{dM}{dt} \quad (\text{F-12-3})$$

with $\frac{dM}{dt}$ the seawater mass change from GRACE (scaled and corrected for the leakage).

3. Results

Monthly error estimates σ are computed as average of the RMS differences of the basin averages corresponding to various data and models and from error propagation with uncorrelated components (Tab. F-12-AUX3 in the auxiliary material).

We have fit an annual sinusoid to the basin averages computing amplitude and phase, along with their errors, for seawater mass variation and Gibraltar net flow (Tabs. F-12-1, F-12-2) and for the other fields (Tabs. F-12-AUX1 and F-12-AUX2). We consider an alternative error estimate for the annual amplitude derived from error propagation ($\frac{2}{\sqrt{N}}\sigma$, with σ from Tab. F-12-AUX3 and N equal to 20).

The unfiltered basin average of both Jason-1 and Envisat sea level has an annual amplitude of 83 mm peaking in October, the monthly error estimate is 8 mm. The basin average of the steric anomalies from the ECCO/JPL model has annual amplitude of 43 mm peaking

in September, the monthly error estimate is 13 mm. The models gives the smallest amplitudes, differences in amplitudes and phase are ≤ 10 mm and 20° . The basin average of the steric-corrected sea level anomalies evaluated from Jason-1 altimetry and steric ECCO/JPL contribution (Fig. F-12-2) has an annual amplitude of 45 ± 4 mm peaking in early November (Tab. F-12-1), the monthly error estimate is 15 mm (Tab. F-12-AUX3).

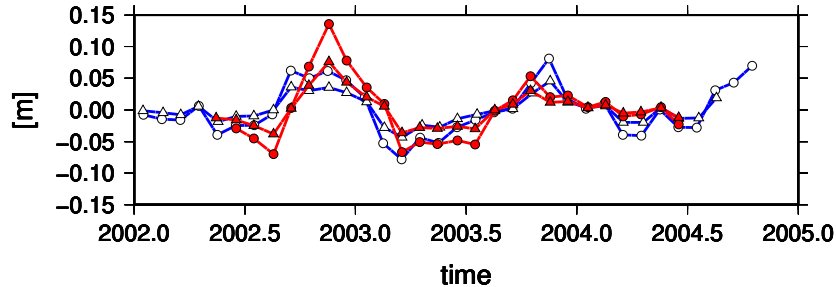


Figure F-12-3: Seawater mass anomalies from steric-corrected altimetry (Jason1-ECCO/JPL) (solid blue) and from scaled hydrology-corrected GRACE field and SLR degrees 1-2 (c2) (solid red) and their corresponding filtered curves (dashed blue and dashed red)

We compute GRACE estimates of water thickness for four cases involving various treatment of low-degree harmonics: (c1) omission of degrees 1-2, (c2) omission of degree 1 and use of degree 2 annual coefficients from Cheng et al.(2002), (c3) degree 1 from SLR (Chen et al. 1999) and degree 2 SLR annual coefficients as before, (c4) degree 1 and C20 annual coefficients obtained performing an annual fit in 2002-2004 of the SLR time-series from Cheng and Tapley (2004) and the other degree-2 coefficients from GRACE. The two different C20 annual coefficients cause small departures in the resulting basin averages (RMS difference 0.6 mm and correlation 0.67). The RMS difference between the results is ≤ 20 mm for c1-3. The smallest annual amplitude corresponds to c1 (40 mm) and is amplified by a factor 1.1 in c2, 1.4 in c3 and 1.7 in c4 (Tab. F-12-AUX1).

The minimum phase delay relative to the steric-corrected altimetry corresponds to c2 (68 days).

The filtered basin average of the continental LAD hydrology has an annual amplitude of 29 mm peaking in November and monthly error estimate of 11 mm. The leakage error is corrected by subtracting the filtered basin average of continental hydrology \tilde{h} from the filtered basin average of GRACE. The estimate given by c2 corrected using the LaD model ($\widetilde{GRACEc2} - \widetilde{LAD}$) has the best agreement in RMS (18 mm) with the filtered steric-corrected altimetry (Fig. F-12-AUX1). Its annual amplitude is 28 mm peaking in November and its phase delay relative to the steric-corrected altimetry is 25 days (Tab. F-12-1).

The filtering reduces the amplitude of the steric-corrected altimetry by a factor 0.56, while the phase remains unchanged. We restore the original magnitude of the water mass signal by multiplying the filtered basin average by the scaling factor $1/0.56$. An estimate of the error made in the filtering and scaling steps is the RMS difference (19 mm) between unfiltered and filtered-scaled steric-corrected altimetry. Monthly errors from error propagation are 39 mm for the scaled GRACE-derived seawater mass. The annual amplitude is 52 ± 11 mm and peaks in November (Tab. F-12-1), its error from error propagation is 17 mm. The two seawater mass estimates, the hydrology-corrected GRACE and the steric-corrected altimetry, have correlation 0.74 and RMS difference 32 mm (Fig. F-12-3).

The monthly error of mass change derived from error propagation ($\sqrt{2}\sigma$ with σ the monthly error estimate of mass) is bigger (21 mm/month, Tab. F-12-AUX6) than the er-

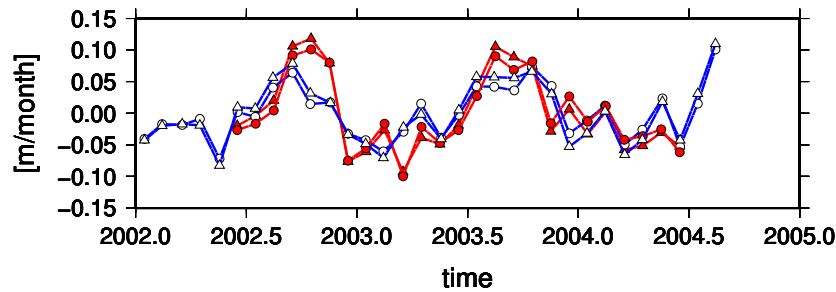


Figure F-12-4: Gibraltar net flow anomalies derived from steric-corrected altimetry (blue) and from hydrology-corrected Grace (red) accounting for Mediterranean water deficit (E-P-R) and Black Sea inflow with E-P from ECMWF (dashed) and from NCEP (solid).

ror computed as average of the RMS differences in Tab. F-12-AUX5 (11 mm/month). The monthly error of the Gibraltar net flow obtained from error propagation is 56 mm/month and 24 mm/month respectively when computed from GRACE and from steric-corrected altimetry mass variation. The Gibraltar net flow from GRACE and NCEP data has an annual amplitude of 60 ± 16 mm/month peaking in September, error from error propagation is 25 mm/month. The net flow derived from the steric-corrected altimetry has smaller values (39 ± 7 mm/month and error from error propagation of 10 mm/month) (Tab. F-12-2, Fig. F-12-4). With ECMWF data the values are bigger, the differences in amplitudes and phase are ≤ 10 mm and 9° . The two estimations of the Gibraltar net flow, from hydrology-corrected GRACE and steric-corrected altimetry, have correlation 0.71 and RMS difference 39 mm/month.

4. Conclusions

We have assessed the ability of GRACE to recover the seasonal seawater mass variation in semi-closed basins of the dimension of the Mediterranean Sea. We apply a smoothed spatial averaging kernel in order to obtain comparable basin averaged monthly time-series. The smoothing is done in the spectral domain for the GRACE SH fields and in the spatial domain for the regional gridded data to avoid their SH expansion.

Additional corrections to GRACE data, that are not applied in the global analysis, are needed in basins: (1) the correction for the leakage of hydrology due to the smoothing and to the basin shape and (2) the scaling of the amplitude because of the higher smoothing radius. The best agreement between hydrology-corrected GRACE and filtered steric-corrected altimetry, is found when using SLR degree-2 annual coefficients and LaD hydrology, the largest departure when GRACE degree-2 terms are included. We scale the seawater mass variation by the ratio of the annual amplitudes of filtered and unfiltered steric-corrected altimetry. The agreement in amplitude and phase between the scaled hydrology-corrected GRACE and the steric-corrected altimetry mass variations is within 7 mm and 26° . We conclude that GRACE is able to detect water mass variations in the Mediterranean Sea with an error budget of 39 mm for the monthly values and an annual amplitude of 52 ± 17 mm peaking in November, while values from steric-corrected altimetry are slightly smaller (monthly error budget of 15 mm, annual amplitude of 45 ± 7 mm peaking in October). The Gibraltar net flow obtained from the GRACE-derived seawater mass change has an annual amplitude of 60 ± 25 mm/month peaking in September. Results agree with values derived from the steric-corrected altimetry (annual amplitude of 39 ± 10 mm/month) and with previous estimations.

We have shown that GRACE alone cannot observe the seawater mass variation in the Mediterranean Sea without knowledge of other data. At present GRACE does not yet improve our knowledge of mass variation as the combined uncertainties of the corrections and of the GRACE fields are larger than the uncertainty of the steric-corrected altimetry. However, the improved ocean de-aliasing fields and low-degree coefficients from GRACE/SLR combinations and joint GRACE/GPS inversion (Kusche and Schrama, 2005) are expected to improve these estimates. In further investigations optimal methods for selecting the smoothing radius and for restoring the magnitude of the signal from the filtered results have to be carefully addressed. This will eventually allow to validate the steric correction applied to altimetry, that, based on cruise data, could be less accurate than expected.

Table F-12-1: Annual amplitude and phase of seawater mass variation from monthly steric-corrected altimetry ($a-s$) and from hydrology-corrected GRACE.

Field	Amplitude (mm)	Phase (deg)
$a - s$ (J1-ECCO/JPL)	45 ± 4	301 ± 5
$\widetilde{a - s}$ (J1-ECCO/JPL)	24 ± 3	301 ± 6
$\widetilde{GRACEc2 - LAD}$	28 ± 6	327 ± 13
scaled ($\widetilde{GRAc2 - LAD}$)	52 ± 11	327 ± 12

Table F-12-2: Annual amplitude and phase of the Gibraltar net flow.

Field	Amplitude (mm/month)	Phase (deg)
G (J1-ECCO/JPL, NCEP)	39 ± 7	255 ± 9
G (J1-ECCO/JPL, ECMWF)	52 ± 7	247 ± 7
G (scaled ($\widetilde{GRACEc2 - LAD}$), NCEP)	60 ± 16	269 ± 15
G (scaled ($\widetilde{GRACEc2 - LAD}$), ECMWF)	71 ± 16	260 ± 13

4. Acknowledgments

We acknowledge E.Schrama for the NCEP SH coefficients, the Mercator Project for the ECMWF data and N.Pinardi for the MFSTEP model. We thank S.Nerem, S.Vignudelli, O.Andersen and an anonymous referee for discussion and helpful reviews. This work was supported by DFG (FE534, GEPRIS/204078).

5. Auxiliary material

We present five tables and one figure as auxiliary material. Table F-12-AUX1 gives the annual amplitude and phase and their error estimates of additional fields used in the computation of the basin average seawater mass variation (Tab. F-12-2). Annual amplitude and phase and their error estimates of additional fields used in the computation of the Gibraltar net flow are found in Tab. F-12-AUX2. Tab. F-12-AUX3 gives the monthly and the annual amplitude error estimates for the basin average seawater mass variation and for the fields used in its computation. Tab. F-12-AUX6 gives the monthly and the annual amplitude error estimates for the Gibraltar net flow and for the fields used in its computation. Tab. F-12-AUX5 gives the root-mean-squares difference between the basin average time-series of seawater mass variation derived from the steric-corrected altimeter corresponding to different estimates of the

steric contribution. It also gives the root-mean-squares difference between the corresponding basin average seawater mass monthly changes. Fig. F-12-AUX1 gives the filtered basin average anomalies of seawater mass from steric corrected altimetry and from hydrology-corrected GRACE with different choices of degrees 1-2.

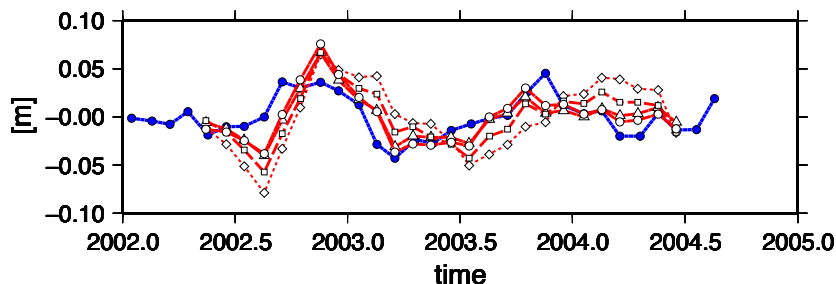


Figure F-12-AUX1: Filtered basin average anomalies of seawater mass from steric-corrected altimetry (Jason1 - ECCO/JPL) (solid circles) and from hydrology-corrected GRACE with different choices of degrees 1-2: c1 (open triangles), c2 (open circles), c3 (open squares), c4 (open diamonds)

Table F-12-AUX1: : Annual amplitude and phase of sea level (a), steric sea level (s), filtered continental hydrology (\tilde{h}), GRACE water thickness \widetilde{Gwt} filtered hydrology-corrected GRACE ($\widetilde{Gwt} - \tilde{h}$) in period April 2002-July 2004. Errors are from least square fit and based on monthly error estimates. Filtered fields : *field*.

Field	Amplitude	Phase (mm)	Data Source (deg)
a	83 ± 2	284 ± 2	Jason-1 altimetry
a	83 ± 3	285 ± 4	Envisat altimetry
s	43 ± 4	262 ± 5	ECCO/JPL
s	53 ± 4	244 ± 4	WOA01
s	55 ± 4	251 ± 4	Medar/Medatlas
s	46 ± 6	251 ± 8	MFSTEP
\tilde{h}	29 ± 3	69 ± 6	CPC
\tilde{h}	29 ± 3	43 ± 6	LAD
\widetilde{Gwt}	40 ± 7	20 ± 8	GRACE c1
\widetilde{Gwt}	43 ± 7	8 ± 7	GRACE c2
\widetilde{Gwt}	57 ± 7	28 ± 6	GRACE c3
\widetilde{Gwt}	72 ± 7	36 ± 5	GRACE c4
$\widetilde{Gwt} - \tilde{h}$	21 ± 6	337 ± 17	GRACE c1, LAD
$\widetilde{Gwt} - \tilde{h}$	35 ± 6	331 ± 10	GRACE c1, CPC
$\widetilde{Gwt} - \tilde{h}$	30 ± 6	9 ± 12	GRACE c3, LAD

6. References

- Ayoub N., P.Y. Le Traon, P.De Mey (1998). A description of the Mediterranean surface variable circulation from combined ERS-1 and TP data, *J. of Mar. Sys.*, 18, 3-40
- Bettadpur S.(2003). Level-2 gravity field product user handbook, GRACE 327-734, CSR Publ. GR-03-01, 17 pp., Univ. of Tex. at Austin, Austin

Table F-12-AUX2: : Annual amplitude and phase of evaporation minus precipitation (mm/month)

Field	Amplitude (mm/month)	Phase (deg)	Data Source
E - P	16 +/- 4	281 +/- 13	NCEP
E - P	27 +/- 4	38 +/- 2	ECMWF
E - P	30 +/- 3	292 +/- 5	Mariotti et al. 2004
E - P	21 +/- 1	282 +/- 3	Boukthir and Barnier 2002

Table F-12-AUX3: : Monthly error σ_{mon} and annual amplitude error σ_{Aan} (mm) of sea level (a), steric contribution (s), filtered GRACE (\widetilde{GRACE}_{c2}), LAD filtered hydrology (\tilde{h}), filtered hydrology corrected GRACE ($\widetilde{GRACE}_{c2} - \tilde{h}$), water mass variation from steric-corrected altimetry.

	σ_{mon} (mm)	method	σ_{Aan} (EP) (mm)
a (sea level)	8	average RMS	4
s (steric)	13	average RMS	6
\widetilde{GRACE}_{c2}	20	Error propagation	9
\tilde{h}	11	average RMS	5
$\widetilde{GRACE}_{c2} - \tilde{h}$	22	Error Propagation	10
Water mass from GRACE	39	Error Propagation	17
Water mass from a-s	15	Error Propagation	7

Table F-12-AUX4: : Monthly error σ_{mon} and annual amplitude error σ_{Aan} (mm) of E-P, rate of mass change from steric-corrected altimetry (a-s) and from re-scaled hydrology corrected GRACE ($\widetilde{GRACE}_{c2} - \tilde{h}$)

	σ_{mon} (mm/month)	method	σ_{Aan} (mm/month)
E - P	12	RMS	5
d(a-s)/dt	21	EP	9
d(scaled ($\widetilde{GRACE}_{c2} - \tilde{h}$))/dt	55	EP	25
Gibraltar net flow from a-s	24	EP	11
Gibraltar net flow from scaled ($\widetilde{GRACE}_{c2} - \tilde{h}$)	56	EP	25

Boukthir M. and B. Barnier (2000). Seasonal and inter-annual variations in the surface freshwater flux in the Mediterranean Sea from the ECMWF re-analysis project, *J. of Mar. Sys.*, 24, 343–354

Bouzinac C., J. Font, J. Johannessen (2003). Annual cycles of sea level and sea surface temperature in the western Mediterranean Sea, *J. of Geophys. Res.*, 108, C3, 3059, doi:10.1029/2002JC001365

Bryden H.L., J. Candela, T.H. Kinder (1994). Exchange through the Strait of Gibraltar, *Progress in Oceanography*, 33, 201-248.

Chambers D., R.S. Nerem, J. Wahr (2004). Preliminary observations of global ocean mass variation with GRACE, *Geoph. Res. Lett.*, 31 L13310, doi:10.1029/2004GL020461

Table F-12-AUX5: : Root-mean-square (RMS) difference (mm) between monthly basin averages of steric-corrected altimetry corresponding to steric contribution estimated from different models and databases.

	J1- ECCO/JPL	J1-MFSTEP	J1-WOA01	J1-MEDAR
J1 - ECCO/JPL	0	10 (4)	16 (15)	15 (12)
J1 - MFSTEP	10 (4)	0	18 (14)	17 (12)
J1 - WOA01	16 (15)	18 (14)	0	8 (11)
J1 - MEDAR	15 (12)	17 (12)	8 (11)	0

Table F-12-AUX6: **A**: Root-Mean Square difference (mm) between filtered basin averages of water mass derived by GRACE for various low-degree selections (c1-4).

	GRACE c1	GRACE c2	GRACE c3	GRACE c4
GRACE c1	0	6	13	26
GRACE c2	6	0	16	30
GRACE c3	13	16	0	15
GRACE c4	26	30	15	0

Chen J.L., C.R. Wilson, R.J. Eanes and R.S. Nerem (1999). Geophysical interpretation of observed geocenter variations *J. of Geophys. Res.*, 104, B2, 2683-2690

Chen J.L., C.R. Wilson, J.S. Famiglietti, M. Rodell (2005). Spatial sensitivity of the Gravity Recovery and Climate Experiment (GRACE) time-variable gravity observations, *J. Geophys. Res.*, 110, B08408, doi:10.1029/2004JB003536

Cheng M., B. Gunter, J.C. Ries, D.P. Chambers, B.D. Tapley (2002). Temporal variation in the Earth's gravity field from SLR and CHAMP GPS data, *Gravity and Geoid 2002*, I.N. Tziavos (Ed.), pp. 424-431

Cheng M. and B.D. Tapley (2004). Variations in the Earth's oblateness during the past 28 years, *J. of Geophys. Res.*, doi:10.1029/2004JB003028

Fan Y. and H. van der Dool (2004). Climate Prediction Center global monthly soil moisture data set at resolution for 1948 to present *J. Geophys. Res.*, 109, D10102, doi:10.1029/2003JD004345

Garcia-Lafuente J., J. del Rio, E. Alvarez Fanjul, D. Gomis and J. Delgado (2004). Some aspects of the seasonal sea level variations around Spain, *J. of Geophys. Res.*, 109, C09008, doi:10.1029/2003JC002070

Garcia-Lafuente J., J. Delgado, J. M. Vergas, M. Vergas, F. Plaza, T. Sarhan (2002). Low-frequency variability of the exchanged flows throught the Strait of gibraltar during CANIGO, *Deep-Sea Research, II*, 49, 4051-4067

Kusche J. and E. Schrama (2005). Surface mass redistribution inversion from global GPS deformation and Gravity Recovery and Climate Experiment (GRACE) gravity data, *J. of Geophys. Res.*, 110, B09409, doi:10.1029/2004JB003556

Mariotti A., M.V. Struglia, N. Zeng and K.-M. Lau (2002). The hydrological Cycle in the Mediterranean Region and Implication for the water budget of the Mediterranean Sea, *J. of Climate*, 15, 1674-1690.

- Milly P.C.D. and A.B. Shmakin (2002). Global modeling of land water and energy balances, Part I: The Land Dynamics (LaD) Model, *J. Hydrometeorol.*, 3, 283–299.
- Swenson S. and J. Wahr (2002a). Methods of inferring regional surface-mass anomalies from Gravity Recovery and Climate Experiment (GRACE) measurements of time-variable gravity, *J. Geophys. Res.*, 107 (B9), 2193, doi: 1029/2000JB000576
- Swenson S. and J. Wahr (2002b). Estimated effects of the vertical structure of the atmospheric mass on the time-variable geoid, *J. Geophys. Res.*, 107 (B9), 2194, doi: 1029/2000JB000024
- Wahr J., M. Molenaar and F. Bryan (1998). Time variability of the Earth's Gravity field : Hydrological and oceanic effects and their possible detection using Grace, *J. Geophys. Res.*, 103, B12, 30205–30230
- Vignudelli S., P. Cipollini, F. Reseghetti, G. Fusco, G.P. Gasparini and G.M.R. Manzella (2003). Comparison between XBT and T/P satellite altimetry in the Ligurian-Tyrrhenian Sea, *Ann. Geophys.*, 21, 123-135
- Velicogna I. and J. Wahr (2006). Measurements of Time-Varying Gravity show mass loss in Antarctica, 10.1126/science.1123785

8.2 Mass variation in the Mediterranean and Black Seas

F-13: Fenoglio-Marc L., M. Becker, R. Rietbroeck, J. Kusche, S. Grayek and E. Stanev, Water mass variation in Mediterranean and Black Sea, *J. of Geodynamics*, 59-60, 168-182, 2012. <http://dx.doi.org/10.1016/j.jog.2012.04.001>

Abstract

The mass-induced sea level variability and the net mass transport between Mediterranean Sea and Black Sea are derived for the interval between August 2002 and July 2008 from satellite-based observations and from model data. We construct in each basin two time series representing the basin mean mass signal in terms of equivalent water height. The first series is obtained from steric-corrected altimetry while the other is deduced from GRACE data corrected for the contamination by continental hydrology. The series show a good agreement in terms of annual and inter-annual signals, which is in line with earlier works, although different model corrections influence the consistency in terms of seasonal signal and trend.

In the Mediterranean Sea, we obtain the best agreement using a steric correction from the regional oceanographic model MFSTEP and a continental hydrological leakage correction derived from the global continental hydrological model WaterGAP2. The inter-annual time series show a correlation of 0.85 and a root mean square difference (RMS) of 15 mm. The two estimates have similar accuracy and their annual amplitude and phase agree within 3 mm and 23 days respectively. The GRACE-derived mass-induced sea level variability yields an annual amplitude of 27 ± 5 mm peaking in December and a trend of 5.3 ± 1.9 mm/yr, which deviates within 3 mm/yr from the altimetry-derived estimate.

In the Black Sea, the series are less consistent, with lower accuracy of the GRACE-derived estimate, but still show a promising agreement considering the smaller size of the basin. The best agreement is realized choosing the corrections from WaterGAP2 and from the regional oceanographic model NEMO. The inter-annual time series have a correlation and RMS differences of 0.68 and 55 mm, their annual amplitude and phase agree within 4 mm and 6 days respectively. The GRACE-derived seawater mass signal has an annual amplitude of 32 ± 4 mm peaking in April. On inter-annual time scales, the mass-induced sea level variability is stronger than in the Mediterranean Sea, with an increase from 2003 to 2005 followed by a decrease from 2006 to 2008.

Based on mass conservation, the mass-induced sea level variations, river runoff and precipitation minus evaporation are combined to derive the strait flows between the basins and with the Atlantic Ocean. At the Gibraltar strait, the net inflow varies annually with an amplitude of $52 \pm 10 \times 10^{-3}$ Sv peaking end of September ($1 \text{ Sv} = 10^6 \text{ m}^3 \text{ s}^{-1}$). The inflow through the Bosphorus strait displays an annual amplitude of $13 \pm 3 \times 10^{-3}$ Sv peaking in the middle of March. Additionally, an increase of the Gibraltar net inflow ($3.4 \pm 0.8 \times 10^{-3}$ Sv/yr) is detected.

1. Introduction

Being an almost closed sub-system, the Mediterranean-Black Sea region provides an interesting setting to study regional mass transports and redistribution.

The two semi-enclosed seas and the Atlantic Ocean are connected by the Bosphorus Strait and by the Gibraltar Strait respectively. Considering its size, the Mediterranean Sea is five times larger than the Black Sea ($2.5 \times 10^{12} \text{ m}^2$ versus $0.42 \times 10^{12} \text{ m}^2$). The Mediterranean

Sea can be classified as a lagoon-type basin, whereas the Black Sea is an estuarine-type basin. Although the region is densely populated, many components of the water cycle are still poorly quantified. For example, for the river-runoff R and the strait flows of Gibraltar (FG) and Bosphorus (FB) only climatological estimates are available (Mariotti et al., 2002, Grayek 2009).

Starting from 2002, the Gravity Recovery and Climate Experiment (GRACE) mission has been providing observations of water mass change, by measuring small variations of the Earth's gravity field that predominantly originate from mass redistributions in the Earth's system (Tapley et al. 2004). Generally, in order to cope with increasing noise and artefacts present in the high resolution components of the GRACE models, the GRACE models are smoothed by convolution with a kernel of gradually decreasing power. Isotropic (Wahr et al., 1998) and non-isotropic (Han et al., 2005) smoothing as well as empirical de-correlation (Swenson and Wahr, 2006) and regularization (Kusche 2007, Kusche et al., 2009) have been applied. The smoothing procedure reduces the correlated noise at the cost of signal attenuation and a decreased spatial resolution.

For basin averages, these side effects depend on (1) the type of the signal, (2) the smoothing applied and (3) the dimension and shape of the region (Klees et al., 2007, Kusche 2007). In regional studies on small ocean basins, filtering causes significant leakage of terrestrial hydrology in the oceanic mass estimated from GRACE, as the land signal is typically much larger. Retrieval of GRACE derived ocean mass variations in small ocean basins presents additional difficulties, as the dimension of the regions are small compared to the resolution of filtered GRACE estimates (Chambers, 2006). Furthermore, the oceanic background models used for de-aliasing the measurements have marginal performance in semi-enclosed basins, which increases the noise in the estimated GRACE residuals (Flechtner 2007a, 2007b).

Alternatively, steric-corrected altimetry also observes water mass changes. The satellite radar altimetry provides total (steric plus non-steric) sea level heights with an accuracy close to 3 cm (Beckley et al., 2007). In order to correct the total sea level for its steric component, this last is derived from either observed or modelled temperature and salinity. Several studies have compared steric corrected altimetry with estimates from GRACE at both global (Chambers 2006, Leuliette and Miller 2009, Willis et al. 2008) and regional scales (Swenson and Wahr 2007, Fenoglio et al., 2006, 2007, Garcia et al. 2006, 2010, Calafat et al. 2010) and have shown that the two methods yield mass change estimates which are consistent at both seasonal and inter-annual time-scales. This paper is an extension of our previous analysis in the Mediterranean Sea (Fenoglio et al. 2006, 2007) to a larger region including the Black Sea.

The main objectives of this paper are to assess in semi-enclosed basins the ability of GRACE to recover (1) the seawater mass variations at both seasonal and inter-annual time-scales and (2) the total water budget and its various components. The effect of filtering the basin averages as well as the magnitude and consistency of the corrections applied are investigated.

2. Methodology

2.1 GRACE gravimetry

We use global GRACE gravity field monthly solutions (GSM) provided by the GeoForschungsZentrum (GFZ) (level-2 products, release 4) between August 2002 and July 2008, which contain atmosphere- and ocean-corrected gravity field solutions expressed in Stokes coefficients from degree 2 to degree 120. Since we consider the complete oceanographic signal, we restore the background models, subtracted at an earlier stage during the GRACE processing. We restore here the signal over the ocean areas using the GRACE GAD product, which contains monthly averaged values of the Ocean Model for Circulation and Tides (OMCT) and of the atmospheric model of the European Centre for the Medium Range Weather Forecasts (ECMWF) (Flechtner, 2007). To enable a comparison with altimetry, we subtract the oceanic averages of the atmospheric pressure, according to [Willis *et al.*, 2008a]. This ensures that the atmospheric contribution in GRACE is consistent with the inverse barometer (IB) correction which is applied to altimetry.

The GRACE J_2 coefficient is less accurate than the estimates from satellite laser ranging (SLR) (Cheng, 2004). Additionally, GRACE does not observe geocenter variation, which is reflected in the degree 1 coefficients. We therefore replace the J_2 coefficient with one obtained from SLR (Cheng and Tapley 2004) and apply a correction accounting for the annual and semi-annual geocenter motion derived from a joint GRACE, GPS and Ocean Bottom Pressure (OBP) loading inversion (Rietbroek *et al.*, 2009, 2012). This latter correction, expressed in equivalent water heights, accounts in our region for up to 20 mm.

The error structure of the GRACE solutions is characterized by an increase in errors for coefficients of higher degrees. Furthermore, due to the observation geometry, strong non-physical north-south features are present in the standard solutions (Kusche *et al.* 2009). We therefore apply a post-processing/smoothing to the GRACE fields. We calculate from GRACE a smoothed basin average \tilde{S}_{rsl}^g in terms of equivalent water heights as follows (Swenson and Wahr, 2002):

$$\tilde{S}_{rsl}^g(t) = A_{\tilde{g}} \frac{a\rho_e}{3\rho_w\vartheta_{00}} \sum_{l=1}^{lmax} \sum_{m=0}^l \frac{2l+1}{1+k_l} \{ \tilde{\vartheta}_{lm}^C \Delta C_{lm}^G(t) + \tilde{\vartheta}_{lm}^S \Delta S_{lm}^G(t) \} \quad (\text{F-13-1})$$

where the 4π -normalized coefficients, $\Delta C_{lm}^G, \Delta S_{lm}^G$, are residual Stokes coefficients, which have the background models (the GAD products) restored and the degree 1 and J_2 coefficients corrected as described above. The post-processed basin averages (relative to the ocean bottom), $\tilde{S}_{rsl}^g(t)$, are the result of a convolution of these Stokes coefficients with the filtered basin coefficients, $\tilde{\vartheta}_{lm}$. The symbol k_l denotes the load Love number and incorporates the change in gravity of the solid Earth induced by the surface load. The mean densities of water and the solid Earth are denoted by ρ_w and ρ_e respectively, and a is the mean radius of the Earth. The smoothing and truncation generally causes the true signal to be attenuated. This can be (partly) compensated by applying an a posteriori scaling factor $A_{\tilde{g}}$. The calculation of this factor requires knowledge of both the shape and size of the basin, of the applied smoothing and an hypothesis about the actual signal of interest. Practical values for $A_{\tilde{g}}$ are provided in Tab. F-13-1.

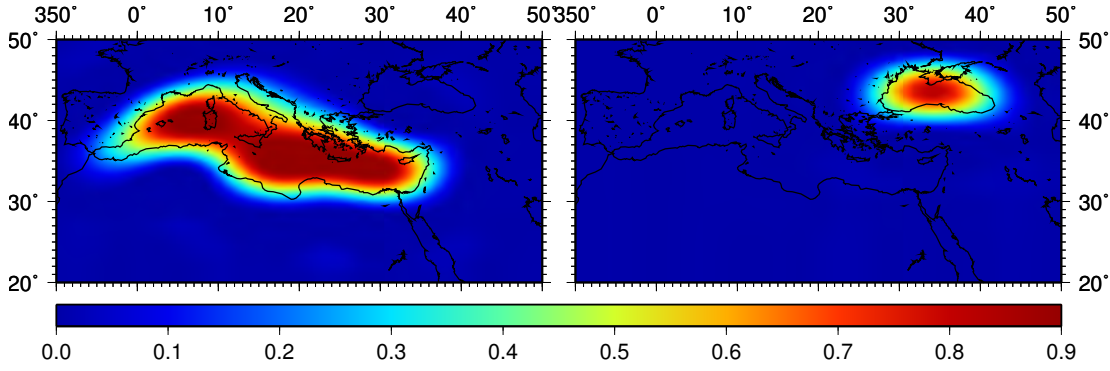


Figure F-13-1: Anisotropically filtered DDK3 basin kernels of the Mediterranean and Black Sea Sea of Azov is included

A comparison of GRACE- and altimetry-based mass-induced sea level requires to correct \tilde{S}_{rsl}^g for the load-induced ocean floor deformation, $\Delta\bar{u}$, as follows: $\tilde{S}^g = \tilde{S}_{rsl}^g + \Delta\bar{u}$. The correction $\Delta\bar{u}$ is necessary since the altimeter orbits are given in a mean frame (i.e. realized by observations corrected for a certain time span) which does not dynamically change with the induced loading. The loading effect is deduced from the monthly GRACE geopotential coefficients and the load Love number h_l (Farrell, 1972) as follows:

$$\Delta\bar{u}(t) = A_{\tilde{v}} \frac{a}{\vartheta_{00}} \sum_{l=1}^{lmax} \sum_{m=0}^l \frac{h_l}{1+k_l} \{ \tilde{v}_{lm}^C \Delta C_{lm}^{G*}(t) + \tilde{v}_{lm}^S \Delta S_{lm}^{G*}(t) \} \quad (\text{F-13-2})$$

Differently from the coefficients ΔC_{lm}^G , ΔS_{lm}^G in Eq. (F-13-1), the residual Stokes coefficients ΔC_{lm}^{G*} , ΔS_{lm}^{G*} include the background models restored over land (using the GRACE-GAC product). The GAC product contains, as the GAD product, monthly averaged values of the oceanic model OMCT and of the atmospheric model ECMWF. The main difference between the GAC and GAD products is that GAD does not include the atmosphere on land while GAC does, therefore in contrast to Eq. (F-13-1) we have restored here also the atmosphere over land. This ensures that the complete global load, including the continental atmosphere, is used in calculating the ocean floor deformation. Another difference between the GAC and the GAD products is in the way how the atmosphere is treated, as GAD contains surface pressure only while GAC contains vertically integrated atmospheric mass variation (Flechtner 2007a, 2007b). The latter difference is however not relevant, since the total load-induced ocean floor deformation, expressed in equivalent water heights, has an amplitude smaller than 8 millimeters in both basins and is therefore small compared to the GRACE-based mass variations (Tabs. F-13-3, F-13-4).

2.2 Spectral Filter

We may write the de-correlation filter in matrix notation as:

$$\tilde{\mathbf{x}} = \mathbf{W}\mathbf{x} \quad (\text{F-13-3})$$

with:

$$\mathbf{W} = (\mathbf{E}^{-1} + \alpha\mathbf{S}^{-1})^{-1}\mathbf{E}^{-1}$$

where vectors \mathbf{x} and $\tilde{\mathbf{x}}$ contain the stacked Stokes coefficients of the unfiltered and filtered field respectively, \mathbf{E} is an approximate block diagonal GRACE error covariance matrix (up

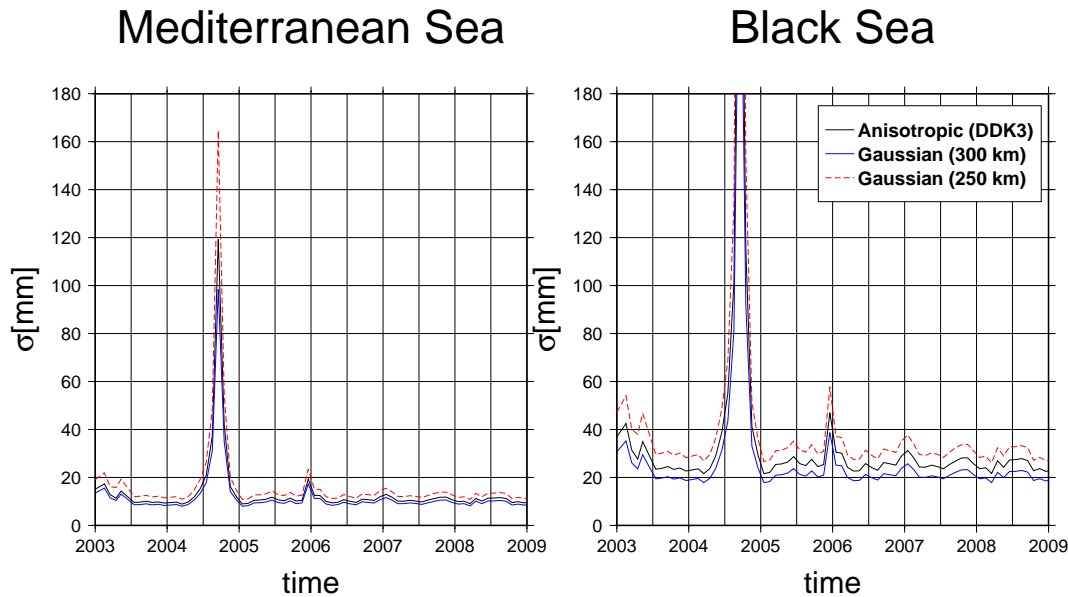


Figure F-13-2: Estimated error of GRACE monthly basin averages derived from GRACE calibrated errors. Peak errors during 2004 will in practice be smaller (but biased) since those solutions are replaced by the constrained solutions.

to degree and order 100) and \mathbf{S} a diagonal degree dependent signal covariance. The degree of smoothing is controlled by the parameter α . We use the anisotropic filter DDK3, with a degree of smoothing comparable to that of a Gaussian filter with a 300 km halfwidth (Kusche et al. 2009). The matrix \mathbf{W} of the DDK3 filter is almost symmetric. Strictly speaking however, we must apply the transpose of \mathbf{W} to the basin ϑ in order to obtain mathematically correct basin averages from equation F-13-1. The resulting patterns of the smoothed basins kernel functions are shown in Fig. F-13-1.

The sea basin averaged time series have differences in the order of a few centimeters with respect to their Gaussian equivalents. The error of the monthly basin averages obtained using the DDK3 anisotropic filter and the Gaussian filters of half-width 300km and 250km is derived from the GRACE calibrated errors and shown in Fig. F-13-2. A large peak occurred in the second half of 2004 (most notably September 2004), when GRACE was in a near-repeat orbit causing large spatial gaps in the groundtrack pattern. For those months with decreased accuracy we use the constrained solutions, as provided by GFZ.

The filtering causes a reduction in the signal, which may be compensated by multiplying the filtered basin average values with a scale factor. The factor A_{ϑ} may be derived assuming a uniform signal distribution and computing the ratio of filtered and unfiltered field (Velicogna and Wahr 2006, Swenson and Wahr 2007). Alternatively, A_{ϑ} is estimated as the average of the ratio of monthly unfiltered and filtered steric-corrected altimetric sea level averaged over the basin ($\frac{\overline{S_{mass}^{a-s}}}{\overline{S_{mass}^{s-s}}}$) (Fenoglio-Marc, 2006). The basin averages have been calculated in the spatial domain using the basin kernels from Fig. F-13-1. Both methods provide comparable factors (see Tab. F-13-1), although they assume a different hypothesis for the signal. The damping is most pronounced in the Black Sea due to its smaller area. The weakest damping corresponds to the simple truncation and depends on the chosen maximum degree. With the anisotropic filter DDK3 the factors are 1.39 and 1.4 in Mediterranean Sea and 1.62 and 1.7 in the Black Sea. Since the second method uses a more advanced hypothesis for the signal, we use the

Table F-13-1: Scaling factors derived from smoothed and unsmoothed basin kernels up to a maximum degree (truncation at degree 50, 70, 100 (d50, d70, d100)) and from direct comparison of unfiltered and filtered mass change from steric-corrected altimetry ($\frac{S_{mass}^{a-s}}{S_{mass}^{a-s}}$)

	Mediterranean Sea				Black Sea			
	d100	d70	d50	$(\frac{S_{mass}^{a-s}}{S_{mass}^{a-s}})$	d100	d70	d50	$(\frac{S_{mass}^{a-s}}{S_{mass}^{a-s}})$
unfiltered	1.17	1.25	1.31	1.7	1.19	1.3	1.47	1.0
Gauss R300	1.61	1.61	1.61	1.5	2.22	2.22	2.22	1.9
DDK3	1.39	1.39	1.39	1.4	1.62	1.62	1.62	1.7

corresponding factors, 1.4 and 1.7 for the Mediterranean and Black Sea in the remainder of the paper.

2.3 Hydrological Leakage

The post-processing filter causes, in addition to the damping effect, also the leakage of mass signal from land in the seawater mass estimate. To correct for this effect, we estimate, according to Eq. (F-13-1) the smoothed basin averaged continental hydrological leakage \tilde{S}_{hyd}^h using various hydrological models. We consider three global hydrological models: the WaterGAP2 Global Hydrology Model (WG2), (Döell et al. 2003), the Land Dynamics (LAD) Fraser model (Milly and Shmakin, 2002) and the Community Land Model of the Global Land Data Assimilation System (GLDAS-CLM, Rodell et al., 2004). All monthly maps have been converted into sets of Stokes coefficients up to degree and order 100.

The hydrological leakage correction \tilde{S}_{hyd}^h is subtracted from the GIA-corrected (see Section 3.4) filtered GRACE-based mass variations \tilde{S}^g to obtain the hydrology-corrected smoothed GRACE solution \tilde{S}_{mass}^{g-h} ($\tilde{S}_{mass}^{g-h} = \tilde{S}^g - \tilde{S}_{hyd}^h$). From a theoretical point of view, the correction is equivalent to subtracting the hydrological contribution directly from the GRACE coefficients before applying further post-processing.

3.4 Glacial Isostatic Adjustment

The Earth's surface is still viscously responding because of the surface unloading from melting of the late-Pleistocene ice sheets (e.g. Peltier 2004). This phenomenon (referred to as Glacial Isostatic Adjustment (GIA)), depends upon the viscoelastic properties of the Earth. On the time scales of this study, GIA appears in GRACE data as a secular trend in the gravity field and will affect the estimates of ocean mass changes.

Using the open source program SELEN (Spada and Stocchi, 2007), the GIA correction has been calculated for a population of nine GIA models characterized by different viscosity profiles. The nine models have been obtained by perturbing the viscosity of the Earth model VM2 (Peltier, 2004) by $\pm 0.2 \times 10^{21}$ Pa.s in the upper mantle and $\pm 2 \times 10^{21}$ Pa.s in the lower mantle. In all these experiments, the chronology of the ice sheets is unchanged. The GIA models provide the time-variations in coefficients from degree 2 to 128. For each model, we have computed the basin-averaged GIA rate expressed in equivalent water height. The procedure is consistent with the post-processing method applied to

the GRACE data. Finally, the GIA correction is estimated by taking the mean of the values obtained from the population and we adopt the standard deviation of the results as an estimate for its error. In terms of equivalent water height, we obtain a GIA rate of -2.7 ± 0.9 mmyr in the Mediterranean, and of -2.5 ± 1.0 mmyr in the Black Sea. Even considering the errors, the values are generally larger than those reported by (Paulson et al., 2007), whose model yield -1.64 mm/yr for the Mediterranean and -1.1 mm/yr for the Black Sea for a 300 km Gaussian smoothing. Investigating the cause of the difference lies outside the scope of this paper. Nevertheless, the discrepancy indicates that GIA errors, when expressed in equivalent water height, may be larger than reported by (Paulson et al., 2007) (20% of the signal) and of the same order of magnitude of the signal itself. The GIA correction is removed from the smoothed GRACE-based mass estimation \hat{S}_{mass}^g . The GRACE-based mass-induced sea level basin average \hat{S}_{mass}^{g-h} is then obtained after subtraction of the continental hydrological leakage correction \tilde{S}_{hyd}^h from \hat{S}_{mass}^g and after rescaling.

Since altimetry measures the geometrical surface height, we correct the altimetry-based sea level by removing the GIA component in terms of geoid changes. This correction is evaluated in SELEN accounting for both mass conservation and the variation of the geoid, from the same coefficients used above for GRACE. The resulting GIA geoid rate correction, expressed in basin averaged trends, is -0.34 ± 0.1 mm/yr in the Mediterranean Sea and -0.3 ± 0.1 mm/yr in the Black Sea.

2.5 Altimetric Sea Level

We estimate the sea level variability from Jason-1 and Envisat altimeter data S_{tot} using the Radar Altimeter Database System (RADS) database, which provides an harmonized, validated and cross-calibrated set of altimeter data (Naeije et al., 2008). We apply the conventional geophysical corrections (tides, wet and dry tropospheric correction, ionospheric correction, sea state bias) selecting the GOT4.7 ocean tide model, the radiometer wet tropospheric correction, the dry tropospheric correction from the ECMWF model, the dual-frequency ionosphere correction and the CLS sea state correction. On short time scales (< 30 days) the sea level response to surface pressure variations is far from an inverse barometer (LeTraon and Gauzelin 1997, Ducet et al. 1999). We therefore account for the ocean response to atmospheric wind and pressure forcing (atmospheric loading on the sea surface) by applying the Dynamic Atmospheric Correction (DAC). This consists at low frequencies of the Inverse Barometer (IB) response and at high frequencies of the sea surface response simulated by the barotropic model MOG2D-G (Carrere and Lyard 2003). Monthly equidistant grids with resolution of 0.25×0.25 degrees are then constructed from the merged data. Since the altimetry measurements include the change in geoid height due to GIA (see Section 3.2), we remove this contribution from the basin averages. For comparison, we use the basin-averaged sea level derived from the merged gridded delayed time products (Delayed Time Map of Sea Level Anomaly (DT-MSLA)) produced by SSALTO/DUACS and distributed by AVISO (<http://www.aviso.oceanobs.com>).

2.6 Steric component of sea level

We estimate the steric sea level variability S_{ster} in the Mediterranean Sea from the temperature and salinity fields of the regional Mediterranean Forecasting System ocean circulation model (MFSTEP) (Tonani et al. 2008). This is a coupled monitoring and modelling system with enhancements in coastal regions that produces daily analyses and

10-day forecasts of currents and temperature and salinity fields at approximately 6.5 km spatial resolution. It is locally refined in four sub-regional areas with a resolution up to 3 km and in four shelf areas with a resolution of 1.5 km.

We have also computed steric heights using temperature and salinity from (1) the global ocean model ECCO/JPL kf080 (Fukumori et al. 2005), and (2) from the global Ishii gridded climatologies, which are derived from hydrographic observations through objective analysis for the interval 1945–2006 (Ishii and Kimoto, 2009). Temperature and salinity error fields of the MEDAR climatology, available for the interval 1948–2002, have additionally been used to infer uncertainty estimates of the steric components (Rixen et al. 2005).

In the Black Sea, we have estimated the steric sea level variability from the temperature and salinity fields of a regional ocean general circulation model (Grayek et al. 2009) based on Nucleus for European Modelling of the Ocean (Foujols et al. 2000), hereafter called NEMO. In horizontal direction the model uses an Arakawa C grid with a resolution of approximately 10 km (Stanev et al. 2003, 2004). The vertical grid uses hard-wired hyperbolic tangent stretching function with 31 levels. Horizontal boundaries are closed for Kerch Strait and open for the Bosphorus Strait. The model’s initial conditions include vertical climatic profiles of temperature and salinity, the model forcing includes wind stress, air temperature and humidity constructed from atmospheric analysis data. Complete surface momentum and buoyancy forcing uses bulk aerodynamic formulae and simulated sea surface temperature (SST). River runoff R_B and Bosphorus FB exchange flow are also included. Altimeter data are assimilated in the model using the general concept of (Cooper 1996). Basin mean sea level and hydrological forcing are combined to consistently close the water balance based on (Peneva et al. 2001). For comparison, we have also computed the seasonal steric sea level component from the World Ocean Atlas 2005 (WOA05) (<http://www.nodc.noaa.gov>) global climatology. The ECCO model and the Ishii database are not available in the Black Sea.

2.7 Precipitation, Evaporation and River Runoff

Oceanic evaporation and precipitation are challenging quantities to derive, as neither of them is directly observed. We have estimated basin means of monthly precipitation (P) from ECMWF precipitation data (temporal resolution 6 hours and spatial resolution 0.25°).

Basin means of monthly evaporation (E) have been estimated from ECMWF atmospheric data and simulated sea surface temperatures following the bulk formula from (Stanev et al. 2003):

$$E = C_h |V| \times [e_{sat}(T_s) - r e_{sat}(T_a)] \frac{0.622}{p_a} \quad (\text{F-13-4})$$

where C_h is the drag coefficient (1.1×10^{-3}), V is the wind speed at 10 meters, r is the relative humidity at 2 meters and p_a atmospheric pressure at the sea surface. $e_{sat}(T_a)$ and $e_{sat}(T_s)$ are saturation vapour pressure at air temperature T_a , all derived from the ECMWF database, and sea surface temperature T_s simulated by the ocean models MFSTEP in the Mediterranean Sea and NEMO in the Black Sea.

For comparison, we have used alternative estimates of evaporation and precipitation from ERA-Interim and DFS4 (DRAKKAR Forcing Set 4), an improved ERA40-based atmospheric

forcing dataset (Brodeau et al., 2010). We have also considered evaporation from the air-sea fluxes dataset OAFflux (<http://oafux.who.edu>), which objectively synthesizes surface meteorology obtained from satellite products and model reanalyses and precipitation from the Global Precipitation Climatology Project (GPCP, <http://www.gewex.org>).

The river runoff in the Mediterranean Sea, R_M , and in Black Sea, R_B , are obtained from the WaterGAP2 hydrology model. The river runoff R_B is alternatively estimated from a linear reconstruction based on yearly ECMWF precipitation over the ocean and from a seasonal climatology of river runoff according to (Grayek et al. 2009). The linear reconstruction uses statistical rules of correlation between observed river runoff and precipitation data (Stanev and Peneva 2002). The seasonal river runoff characteristics derived from the climatology are superimposed to the yearly estimation. Error estimates of the river runoff show that the reconstructed annual signal reflects most of the variability with an RMS error of 23% of the total variance.

2.8 Seasonal and Inter-Annual Variability

To examine the seasonal and long-term variability of the basin averages we have estimated annual, semi-annual and a linear trend component through a least-squares fit of the function :

$$m(t) = a_o + a_1 t + A_a \cos(\omega_a t - \phi_a) + A_{sa} \cos(\omega_{sa} t - \phi_{sa}) \quad (\text{F-13-5})$$

where a_o and a_1 are the parameters describing a bias and the linear component and A_i , ω_i , ϕ_i are amplitude, frequency and phase of the annual ($i = a$) and semiannual ($i = sa$) signals. To examine the inter-annual variability of a time series we have removed the seasonal component of the above least squares fit from the monthly values.

2.9 Sea level Budget and Strait flows

Since the total basin-wide sea level change S_{tot} is composed of a steric and of a mass part:

$$S_{tot} = S_{ster} + S_{mass} \quad (\text{F-13-6})$$

we may use filtered altimetric sea level (\tilde{S}_{tot}^a), steric sea level (\tilde{S}_{ster}^s), mass change from GRACE (\tilde{S}^g) and hydrological leakage from modelling (\tilde{S}_{hyd}^h), as well as their unfiltered (S_{tot}^a , S_{ster}^s) and filtered and rescaled equivalents (\hat{S}^g , \hat{S}_{hyd}^h), to close the mean sea level (MSL) budget in a semi-closed basin:

$$\tilde{S}_{tot}^a = \tilde{S}_{ster}^s + (\tilde{S}^g - \tilde{S}_{hyd}^h) \quad (\text{F-13-7})$$

Since we have independent estimates for each component of Eq. F-13-7, we may derive either an inferred or direct estimate for S_{tot} , S_{ster} and S_{mass} . The availability of all terms of Eq. F-13-7 allows us to investigate whether the sea level budget in Eq. F-13-6 is closed observationally, i.e. if the right and left side of the equation agree within the error estimates of each term (Willis et al 2008).

We compute the mass net flow from the Black Sea into the Mediterranean through the Bosphorus Strait, FB , using the water budget equation :

$$FB = -(E - P)_B + R_B - A_B(\dot{S}_{mass})_B \quad (\text{F-13-8})$$

with R river runoff, $E - P$ evaporation minus precipitation, \dot{S}_{mass} the rate of change of the mass-induced sea level and A the surface area of the sea (see also Grayek et al. 2009). Similarly, the net flow in the Atlantic through the Gibraltar strait, FG , may be estimated using the water budget equation for the Mediterranean basin:

$$FG = (E - P)_M - R_M - FB + A_M(\dot{S}_{mass})_M \quad (\text{F-13-9})$$

where the subscript M points to the Mediterranean equivalents of E , P , A and \dot{S}_{mass} .

For a basin with surface A , a uniform change of $1 \frac{mm}{mon}$ is equivalent to a net flow of $0.38 \times 10^{-15} A$ Sv ($1 \text{ Sv} = 10^6 m^3 s^{-1}$). This implies that $1 \frac{mm}{mon}$ is equivalent to a net flow of 0.96×10^{-3} Sv in the Mediterranean Sea and of 0.16×10^{-3} Sv in the Black Sea. The water budget equations in Eq. F-13-8, F-13-9 can be written in terms of uniform basin changes (units are $\frac{mm}{mon}$) as :

$$(\dot{S}_{FB})_B = -(\dot{S}_{E-P})_B + (\dot{S}_R)_B - (\dot{S}_{mass})_B \quad (\text{F-13-10})$$

$$(\dot{S}_{FG})_M = (\dot{S}_{E-P})_M - (\dot{S}_R)_M - (\dot{S}_{FB})_M + (\dot{S}_{mass})_M \quad (\text{F-13-11})$$

where each component of Eq. F-13-8, F-13-9 has been divided by the surface area of the sea, \dot{S}_{FG} , \dot{S}_{E-P} , \dot{S}_R , \dot{S}_{FB} , \dot{S}_{mass} indicate the uniform basin changes for each basin.

3. Results

3.1 Error estimation in terms of the Basin Averages

Estimated errors of the monthly values and annual amplitudes are tabulated in Tab. F-13-7 for various measured and inferred quantities: total sea level (S_{tot}), steric sea level (S_{ster}), hydrological leakage (S_{hyd}), mass-induced sea level (S_{mass}) and its rate of change \dot{S}_{mass} , river runoff (R), $E - P$ and strait flows in terms of uniform basin changes. The errors are based on either error propagation of the various components which flow into the estimated quantity, or they are based on the RMS difference between several models and/or data sets. The latter method, reflects the spread of the datasets, but unknown systematic errors may remain.

Monthly error estimates of the DDK3-filtered GRACE basin average (\tilde{S}^g) have been discussed in Section 2.2. The errors are estimated to be around 11 mm in the Mediterranean Sea and 25 mm in the Black Sea. The error in total altimetric sea level S_{tot}^a , is found to be 10 mm for the Mediterranean Sea and 30 mm for the Black Sea.

The error in the steric component, as measured by the oceanographic models (S_{ster}^s), is found to be 20 mm in the Mediterranean Sea. An RMS-based error of 13 mm has been derived from the temperature and salinity fields of both the MFSTEP and ECCO ocean models and of the Ishii hydrographic database, this latter reaches only a maximum depth of 600m. This shallow-water ocean error is lower than the yearly uncertainty of the steric component inferred from the temperature and salinity error fields derived from the MEDAR database climatology, which is below 15 mm in the 0-600 m layer and is mainly dominated by halosteric uncertainties (Rixen personal communication). In (Fenoglio et al. 2013). In order to account for the uncertainty of the deeper layers, we adopt a total error of 20 mm for the steric component arising from the complete water column.

Table F-13-2: Comparison of mass-induced sea level from GRACE, \hat{S}_{mass}^{g-h} , with the altimetry-derived estimate, S_{mass}^{a-s} , for a variety of hydrological and steric corrections. The table shows the agreement of the series in terms of correlation and RMS difference of the monthly and the inter-annual series, denoted by the subscript mon and ia respectively. In addition, the difference of the (semi-) annual amplitudes and phases are provided. The interval of analysis is from August 2002 to July 2008. Ishii and LAD/Fraser are only available from August 2002 to July 2006 (corresponding fields are denoted by an *).

s	h	$corr_{mon}$	RMS_{mon} (mm)	ΔA (mm)	$\Delta\varphi_A$ (days)	ΔA_{SA} (mm)	$\Delta\varphi_{SA}$ (days)	$corr_{ia}$	RMS_{ia} (mm)
MFSTEP	WG2	0.86	37	3	23	6	4	0.85	15
ECCO	WG2	0.78	67	3	30	7	4	0.84	13
Ishii*	WG2	0.75	41	3	32	3	7	0.69	21
MFSTEP	GLDAS	0.66	32	14	41	0	4	0.66	21
MFSTEP	LAD*	0.91	25	1	14	1	6	0.89	12
NEMO	WG2	0.71	120	3	9	12	16	0.68	55
NEMO	GLDAS	0.69	66	20	31	6	4	0.64	60
NEMO	LAD*	0.51	81	12	69	13	123	0.50	59

In the Black Sea, following (Calafat et al. 2010), an error of 17 mm is used for the basin mean of the steric sea level simulated by NEMO. For comparison, the steric basin averages (S_{ster}^s) in the Black Sea from the NEMO model and the WOA05 climatology yield an error estimate of 14.6 mm. We have further validated the steric component derived from the NEMO model using ARGO temperature and salinity profiles available from the Global Data Assembly Centers (GDACs), however, the profiles are rather sparse and cover only the inner basin. Model simulations indicate that thermo-steric heights are dominating the basin-wide steric heights (Grayek et al. 2009). In contrast, halo-steric heights are almost negligible in terms of basin averages (< 0.5 cm) and show a pronounced spatial variability. The error for the basin averaged steric sea level is based on a few sparse profiles and is most likely realistic for thermo-steric component only. We therefore neglect the halo-steric component in the Black Sea.

For the continental hydrological leakage correction (\hat{S}_{hyd}^h), we have estimated an error of 17 mm in the Mediterranean Sea and of 29 mm in the Black Sea. These estimates are based on the inter-comparison of the output from the WaterGAP2, GLDAS-CLM and LAD hydrology models. A monthly error of 30 mm/mon, in the Mediterranean Sea, is considered for the surface water flux \dot{S}_{E-P} . This value has been derived from the mean of the root mean squares (RMS) differences between the $E - P$ used in this study (e.g. computed from ECMWF and regional model data, see Section 2.7) and the $E - P$ given by two other databases, the ERA-Interim and the DFS4 databases. The RMS differences are 28 mm/mon and 33 mm/mon respectively. Similarly, in the Black Sea the monthly error of 21 mm/mon is derived as mean of the RMS differences between the $E - P$ computed from ECMWF and regional model data (Section 2.7) and the $E - P$ given by the two other databases (18 mm/mon and 24 mm/mon respectively).

Based on the RMS difference between the reconstructed runoff and the runoff output of the WaterGAP2 model, the river runoff contribution to sea level (\dot{S}_R) has an error of 24mm/mon in the Black Sea. In the Mediterranean Sea, we assume a monthly error of 9 mm/mon, computed from the standard deviation of the runoff output of the WaterGAP2 model (an observed estimate was unfortunately not available).

Table F-13-3: Mediterranean Sea: Annual (A) and semi-annual (SA) amplitude and phase and trend for various sea level components. The component type is indicated by the subscript ($_{tot}$: total sea level, $_{ster}$: steric sea level, $_{mass}$: mass-induced sea level $_{hyd}$: hydrological leakage). Filtered fields, which have been scaled to account for signal attenuation, are denoted by a hat. The superscript, indicate the used datasets (a : altimetry, s : steric modelling, g : GRACE, h : hydrological modelling), which are in some cases augmented with the model name/dataset. The interval of analysis is from August 2002 to July 2008. Ishii and LAD/Fraser are available only from August 2002 to July 2006 (the corresponding fields are denoted by an *).

Field	A	A	SA	SA	Trend ($\frac{mm}{yr}$)
	Amp (mm)	Phase (days)	Amp (mm)	Phase (days)	
S_{tot}^{aJ1}	70±2	278±4	13±1	121±1	0.8±1.3
$S_{tot}^{g-h+s} = \hat{S}_{mass}^{g-h} + S_{ster}^s$	64±5	282±1	19±3	121±1	-4.0±2.9
S_{hyd}^{hWG2}	27±3	44±6	2±3	34±3	-1.0±0.6
S_{hyd}^{*hLaD}	32±4	41±8	2±4	35±4	-1.0±0.6
S_{hyd}^{hGLDAS}	10±4	53±6	0.3±4	172±4	-0.7±0.6
$S_{hyd}^{g-a+s} = \hat{S}^g - S_{tot}^{aJ1} + S_{ster}^{sMFSTEP}$	34±4	47±7	1±5	1±5	-8.7±2.1
\hat{S}^g	46±4	16±3	15±5	125±5	2.1±2.5
$S_{ster}^{sMFSTEP}$	58±4	258±4	0.4±4	86±4	-10.1±0.6
S_{ster}^{sECCO}	48±4	258±2	0.8±4	141±4	-3.1±0.4
$S_{ster}^{*sIshii}$	57±4	259±2	2±4	12±4	-5.8±0.4
$S_{ster}^{a-g+h} = S_{tot}^{aJ1} - \hat{S}_{mass}^{g-hWG2}$	66±4	255±3	6±3	31±3	-5.3±1.1
$S_{ster}^{a-g+h} = S_{tot}^{aJ1} - \hat{S}_{mass}^{g-hGLDAS}$	80±4	249±3	1±3	34±3	-3.1±1.2
$S_{ster}^{*a-g+h} = S_{tot}^{aJ1} - \hat{S}_{mass}^{g-hLaD}$	66±4	257±3	2±3	75±3	-10.4±1.2
$S_{mass}^{a-s} = S_{tot}^{aJ1} - S_{ster}^{sECCO}$	30±5	312±5	12±3	119±3	2.9±1.6
$S_{mass}^{a-s} = S_{tot}^{aJ1} - S_{ster}^{sMFSTEP}$	24±5	329±6	13±3	119±3	8.3±1.6
$S_{mass}^{*a-s} = S_{tot}^{aJ1} - S_{ster}^{sMFSTEP}$	25±5	327±6	14±3	118±3	19.2±1.6
$S_{mass}^{a-s} = S_{tot}^{aJ1} - S_{ster}^{*sIshii}$	30±5	316±5	16±5	116±5	6.8±1.8
$\hat{S}_{mass}^{g-h} = \hat{S}_{mass}^{g-hWG2}$	27±5	352±9	19±5	123±5	5.3±1.9
$\hat{S}_{mass}^{g-h} = \hat{S}_{mass}^{g-hGLDAS}$	38±6	5±6	13±5	123±5	2.8±1.9
$\hat{S}_{mass}^{*g-h} = \hat{S}_{mass}^{g-hLaD}$	25±6	343±6	15±5	124±5	14.9±2.9

Table F-13-4: As in Tab. F-13-3 but for the Black Sea.

Field	A	A	SA	SA	Trend ($\frac{mm}{yr}$)
	Amp (mm)	Phase (days)	Amp (mm)	Phase (days)	
S_{tot}^{aJ1}	23±4	171±5	28±4	155±3	-4.3±1.9
$S_{tot}^{g-h+s} = \hat{S}_{mass}^{g-h} + S_{ster}^s$	32±7	184±5	41±5	148±1	-11.2±4.9
S_{hyd}^{hWG2}	68±7	58±6	10±5	50±5	-0.3±0.6
S_{hyd}^{*hWLaD}	106±10	58±8	8±4	73±4	1.3±0.6
S_{hyd}^{hGLDAS}	40±5	60±6	2.3±4	70±4	-3.2±0.6
$S_{hyd}^{g-a+s} = \hat{S}^g - S_{tot}^{aJ1} + S_{ster}^{sNEMO}$	74±4	53±7	22±5	111±5	-2.5±1.1
\hat{S}^g	97±10	72±3	38±5	150±5	-19.4±2.5
S_{ster}^{sNEMO}	35±4	241±4	3.5±4	38±4	-0.3±0.6
S_{ster}^{sWOA05}	29±4	238±2	0.8±4	41±4	
$S_{ster}^{a-g+h} = S_{tot}^{aJ1} - \hat{S}_{mass}^{g-hWG2}$	40±4	235±3	19±3	32±3	0.2±1.1
$S_{ster}^{a-g+h} = S_{tot}^{aJ1} - \hat{S}_{mass}^{g-hGLDAS}$	57±4	245±3	13±3	12±3	-6.3±1.2
$S_{mass}^{a-s} = S_{tot}^{aJ1} - S_{ster}^{sNEMO}$	32±5	111±10	33±3	163±10	-12.2±5.6
$S_{mass}^{*a-s} = S_{tot}^{aJ1} - S_{ster}^{sECCO}$	34±5	118±10	26±3	166±10	11.2±5.6
$\hat{S}_{mass}^{g-h} = \hat{S}_{mass}^{g-hWG2}$	35±5	102±10	45±4	147±10	-12.2±1.9
$\hat{S}_{mass}^{g-h} = \hat{S}_{mass}^{g-hGLDAS}$	52±6	89±10	36±5	151±5	-8.8±1.9
$\hat{S}_{mass}^{*g-h} = \hat{S}_{mass}^{g-hLaD}$	44±6	180±10	46±5	30±5	30±1.9

3.2 Seawater mass estimates from corrected altimetry and GRACE

3.2.1 Mediterranean Sea

We first compare the mass-induced sea level derived from altimetry, S_{mass}^{a-s} , and the one derived from GRACE data, \hat{S}_{mass}^{g-s} , and select the most suitable steric and hydrology models.

In the Mediterranean Sea, the best agreement at seasonal and inter-annual scales between the basin averages is found with steric and hydrological leakage corrections derived from the regional ocean model MFSTEP in combination with the global hydrological model WaterGAP2 respectively (Tab. F-13-2). Correlation and RMS differences are 0.86 and 37 mm for monthly time series, are 0.85 and 15 mm for inter-annual components. The LAD/Fraser model yields a slightly higher agreement (correlation and RMS differences are 0.91 and 25mm for monthly time series, and 0.89 and 12mm for the inter-annual components) but is available only until the end 2006 and, for this reason, will not be used here.

The mass-induced sea level from GRACE has an annual amplitude of 27 ± 5 mm peaking around 18th December (Tab. F-13-3). Compared to the altimetry-derived S_{mass}^{a-s} (annual amplitude of 24 ± 3 mm peaking around 24th November) it is consistent within 3 mm and 23 days in terms of the annual amplitude and phase (Tab. F-13-2). When we apply the continental hydrological leakage correction from GLDAS-CLM to GRACE, the agreement between the series is reduced (for all available choices of the steric correction).

Fig. F-13-3 (top) graphically shows annual amplitudes and phases of the observed and inferred parameters (mass, steric- and continental hydrological leakage correction), for a variety of hydrological models (WaterGAP2, LAD, GLDAS) and steric corrections (MFSTEP, ECCO, Ishii). From the possible combinations, the mass estimates corresponding

to MFSTEP and WaterGAP2 corrections have the best agreement over the complete interval. Better agreement may have been obtained by either increasing the amplitude of the steric correction to 66 ± 4 mm, or by increasing the amplitude of the leakage of continental hydrology to 34 ± 4 mm (empty markers in Fig. F-13-3) while keeping the other correction fixed.

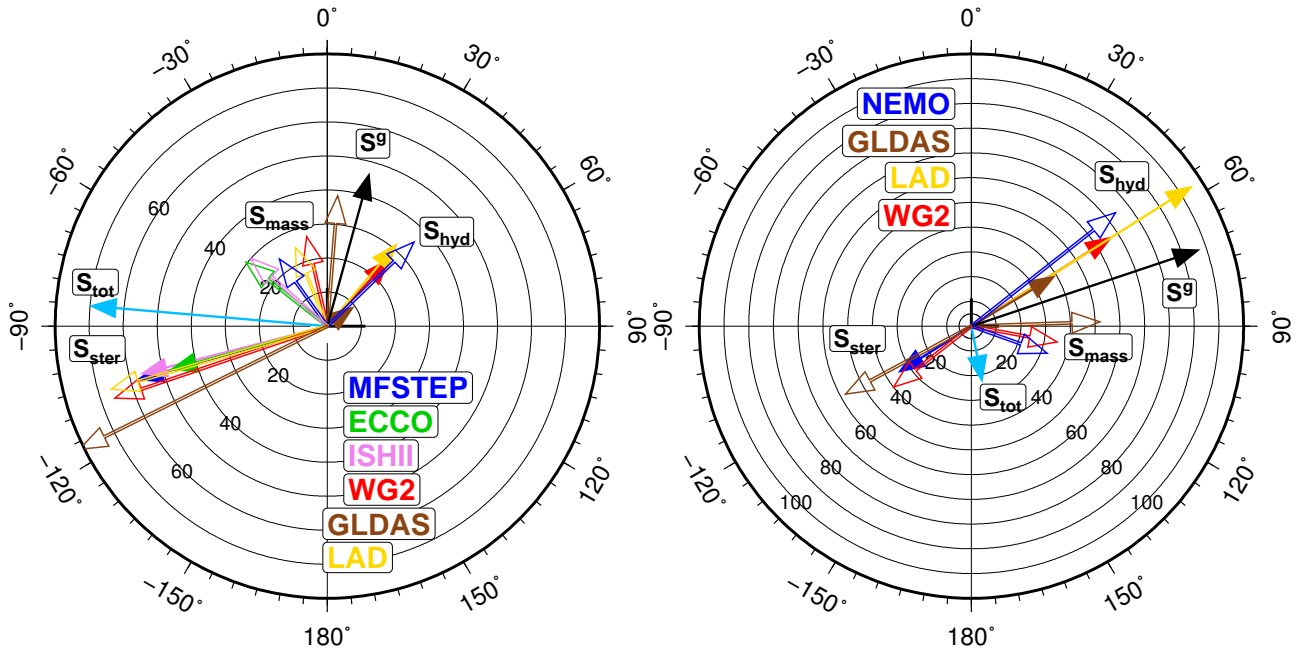


Figure F-13-3: Annual amplitude and phase in Mediterranean Sea (top) and in Black Sea (bottom) of mass-induced sea level change (S_{mass}) and of observed and inferred estimates of steric correction (S_{ster}) and continental hydrological leakage (S_{hyd}) for selected land hydrology and ocean models. The parameters derived from GRACE- and altimetric sea level observations (S^g and S_{tot}) are kept fixed. Three land hydrology models are used in each basins. Three ocean models in the Mediterranean Sea and one in the Black Sea are used. Full/empty markers indicate observed/inferred quantities.

We note that all selections of the steric and continental hydrological leakage corrections suggest a significant increase of oceanic mass. The altimetry-based and the GRACE-based mass estimates almost agree within the error bounds of the altimetry-derived mass estimate (Fig. F-13-4.a). The discrepancy between the two estimates is most visible in the trend. The trend of the selected hydrology-corrected GRACE solution is 5.3 ± 1.9 mm/yr, while the trend of the altimetry-derived mass deviates by 3 mm/yr, which is larger than the calculated error bar (Tab. F-13-3).

Using the MFSTEP steric correction and the WaterGAP2 hydrological correction, we compare, for each component entering the MSL budget (S_{ster} , S_{mass} , S_{hyd} , S_{tot} , Eq. F-13-7), the direct estimate given by the observations and the inferred one from the other components (Fig. F-13-4.b-e, and Tab. F-13-3). The observational estimate of each term are shown as black lines and their error bounds are in light gray. The dark gray lines represent inferred estimates of each term, computed by adding or subtracting the other three, as in Eq. F-13-7.

The total sea level as observed from altimetry (S_{tot}^a) is shown in Fig. F-13-4.b. The dominant seasonal signal displays an amplitude of 70 ± 2 mm and a phase of 278 ± 4 days] (peak around 4th October). The trend is not significant (0.8 ± 1.3 mm/yr). Its inferred estimate is

obtained by the addition of the steric component to the GRACE-based mass-induced sea level. The seasonal and inter-annual fluctuations of the inferred estimate are similar to those of the observational estimates. The amplitude of the seasonal cycle is slightly lower for the inferred estimate and does not agree within the expected observational error bounds. The primary difference appears to be in the trend, which is -4.0 ± 2.9 mm/yr for the inferred estimate and therefore 4.8mm/yr smaller than the trend of the altimeter, it is outside of the error bounds of the altimeter-based observations.

The steric component (S_{ster}^s) is given in Fig. F-13-4.c. Its inferred estimate is obtained by the subtraction of the GRACE-derived mass from the altimetry derived sea level (S_{tot}^a). Both the direct estimates, derived from MFSTEP, ECCO and Ishii, and the inferred estimate have an annual amplitude peaking in September (see Tab. F-13-3). The agreement in phase is remarkably good (peak on 17 or 18 September for the direct observations and between 5 and 13 September for the inferred estimates). The amplitude varies between 58 ± 4 mm (MFSTEP) and 48 ± 4 mm (ECCO), while the inferred estimate has a larger amplitude that depends on the hydrological model used (66 ± 4 with WaterGAP2 and 80 ± 4 with GLDAS). All estimates of steric sea level have significant negative trends, with the highest value for MFSTEP (-10.1 ± 0.6 mm/yr (MFSTEP), -3.1 ± 0.4 mm/yr (ECCO), -5.8 ± 0.4 mm/yr (Ishii)). The trends of the inferred estimates are -5.3 ± 1.1 mm/yr with WaterGAP2 and -3.1 ± 1.2 mm/yr with GLDAS.

The inferred estimate of continental hydrological leakage, $S_{hyd}^{g-(a-s)}$, is obtained by subtraction of the mass-induced sea level derived from altimetry from the rescaled GRACE basin average (Fig.F-13-4.d). All direct and inferred estimates have a dominant annual signal with amplitude peaking in February-March and agreement in phase within 12 days. The annual amplitude ranges from 10 ± 4 mm (GLDAS) to 32 ± 4 mm (LAD) and is 27 ± 3 mm for WaterGAP2. The inferred continental hydrological leakage (using the steric MFSTEP correction) has an annual amplitude larger than all direct estimates (34 ± 4 mm). Its phase agrees well with WaterGAP2 and is within the errors for all estimates. All trends are negative, with the highest value corresponding to the inferred estimate (-8.7 ± 2.1]mmyr) and lower values for direct estimates (-1.0 ± 0.6 mmyr for WaterGAP2, -0.7 ± 0.6 mmyr for GLDAS-CLM -1.0 ± 0.6 mmyr for LAD).

The total mass observed by GRACE, \hat{S}^g , is shown in Fig. F-13-4.e. Both the direct estimates derived from GRACE and the inferred estimate, obtained by subtraction of S_{mass}^{a-s} from the smoothed and rescaled continental hydrological leakage correction \hat{S}_{hyd}^h , have a strong annual signal. The amplitude of the GRACE direct observation is 46 ± 4 mm and peaks in January. Applying the continental hydrological leakage correction to GRACE reduces the strength of its seasonal signal: the annual amplitude is smaller and its maximum, initially in January, is shifted forward by about one month. Similarly, the removal of the steric signal from the altimetric sea level, causes a reduction of the amplitude of the altimeter sea level and its maximum, initially in October, is delayed by about one month (Fig. F-13-4.a).

Fig. F-13-5 depicts the inter-annual mass change. All choices of the hydrology model give similar results for the inter-annual mass-induced sea level derived from altimetry, S_{mass}^{a-s} and from GRACE, \hat{S}_{mass}^{g-h} , with correlation higher than 0.66 and RMS of the differences smaller than 21 mm (see Tab. F-13-2).

From the above discussion we find that the interval 2002-2008 has been characterized by a positive trend in the mass-induced sea level S_{mass} (5.3 ± 1.9 mm/yr from \hat{S}_{mass}^{g-h}) and by a negative trend in the steric sea level S_{ster} (e.g. -5.3 ± 1.1 mm/yr for S_{ster}^{a-g+h}). In contrast, the trend in the observed total sea level S_{tot} was not significant (0.8 ± 1.3 mm/yr).

Fig. F-13-6 shows for an extended interval, the 1993-2008 period, the total basin-wide sea level together with its two components (steric and mass component). Additionally, the steric component has been split up in a thermo-steric and halo-steric part. During the complete interval 1993-2008, the total sea level has a positive trend of 2.0 ± 1.2 mm/yr. The trend was higher during the sub-interval 1993-2002 (3.9 ± 2.5 mm/yr) compared to the following years, and not significant over the period 2002-2006 (-0.6 ± 0.8 mm/yr). Both the Ishii and the Medar databases indicate an increase of the steric component in 1993-2000, a feature which is missing in the ECCO model. Beginning in the year 2000, we see a better agreement in the steric components derived from various sources, namely a decrease in the sub-interval 2000-2005 and an increase afterwards are common features for both the Ishii and the Medar hydrographic databases as well as for the ECCO and MFSTEP ocean models (Fig. F-13-6.c).

The mass-induced sea level S_{mass}^{a-s} derived from steric-corrected altimetry using the ECCO model increases in 1994-1996 and shows a similar increase in 2002-2006 (Fig. F-13-6.b). The same behaviour is obtained from the Ishii data neglecting their halo-steric component. We conclude that, as the accuracy of the halo-steric component is low (Ishii personal communication), its inclusion has to be considered with care (Ishii et Kimoto, 2009).

All sources indicate a relative minimum in water-mass anomaly in 2000-2002. In summary, the rise in sea level observed by satellite altimetry in the 1990's appears to arise from both thermal expansion and mass addition. In the following decade (2000-2010) the increase in mass has been compensated by the decrease in steric sea level and for this reason the rise of sea level has been less pronounced.

3.2.2 Black Sea

The regional model NEMO is the only model available in the Black Sea to compute the steric correction. To select the most suitable hydrology model, we have first compared the altimetry-derived S_{mass}^{a-s} with the \hat{S}_{mass}^{g-h} obtained from GRACE using several hydrological corrections. As shown in Fig. F-13-3, the best agreement at seasonal and inter-annual scales between the two estimates of oceanic mass is obtained by using the correction from WaterGAP2. Correlation and RMS differences are 0.71 and 120 mm respectively, and 0.68 and 55 mm for the inter-annual monthly values (Tab. F-13-2). The annual component remains the dominant signal in the steric and continental hydrological leakage corrections, but in S_{tot} , and S_{mass} also the semi-annual signals become important (Tab. F-13-4).

The GRACE-derived mass-induced sea level, \hat{S}_{mass}^{g-h} shows an annual signal of 35 ± 5 mm amplitude peaking around 11th April and a semi-annual signal 45 ± 4 mm amplitude peaking in May (Tab. F-13-4). Their consistency with the altimetry-derived mass-induced sea level S_{mass}^{a-s} (annual signal of 32 ± 5 mm amplitude peaking around 20th April) is within 3 mm and 9 days for annual amplitude and phase but lower for semi-annual amplitudes (within 12 mm and 16 days). Compared to the hydrological correction from WaterGAP2, the correlation and

RMS differences of the monthly values are worsened when we use GLDAS-CLM (0.69 and 66mm for monthly time series, and 0.64 and 60mm for inter-annual time series). Differences between annual and semi-annual amplitudes and phases are also larger (20 mm, 22 days and 3 mm, 12 days respectively, Tab. F-13-2).

Similar to the left part of Fig.F-13-4, the right part of Fig. F-13-4.a-e shows, for the Black Sea, the direct and the inferred estimates for each component of the basin MSL budget equation (Eq. F-13-7). The agreement of the mass induced sea level is weaker compared to the time series in the Mediterranean Sea.

The total sea level, S_{tot}^a , as observed from satellite altimetry, is shown in Fig. F-13-4.b. Annual and semi-annual signals are smaller than in the Mediterranean Sea (with amplitudes 23 ± 4 mm and 28 ± 4 mm), the annual signal peaks in June.

Both the steric component derived from NEMO, S_{ster}^s , and the inferred estimate, S_{ster}^{a-g+h} , have an annual amplitude peaking end of August (Fig. F-13-4.c, Tab. F-13-4). The agreement in phase is remarkably good, although the NEMO estimate is much smoother compared to the inferred estimate. The annual amplitude is 35 ± 4 mm for NEMO and 29 ± 4 mm for the mean seasonal climatology. The amplitude of the inferred estimates is 40 ± 5 mm and therefore larger than the NEMO model value. The estimated trends (-0.3 ± 0.6 mm/yr, 0.2 ± 1.1 mm/yr) are not significant (Tab. F-13-4).

The direct estimate of the continental hydrological leakage derived from WaterGAP2, LAD, GLDAS and the inferred estimate, $S_{hyd}^{g-(a-s)}$, all show an annual amplitude peaking in February (Fig. F-13-4.d). The dominant signal is annual, with an amplitude ranging from 40 ± 4 mm for GLDAS to 106 ± 10 mm for LAD, while WaterGap2 yields 68 ± 7 mm. The agreement in phase is within 10 days. Significantly different trends have been found for the different models (-3.2 ± 0.6 mm/yr for GLDAS-CLM, -0.3 ± 0.6 mm/yr for WaterGAP, 1.3 ± 0.6 mm/yr for LAD)(Tab. F-13-4) .

The total mass-induced sea level, \hat{S}^g , observed by GRACE is shown in Fig. F-13-4.e. Both the direct estimates derived from GRACE and the inferred estimate, obtained by subtraction of the altimetry-derived mass-induced sea level from the rescaled continental hydrological leakage have a strong annual signal. The amplitude of the GRACE direct observation is 97 ± 10 mm and peaks in March. Similar to the Mediterranean, the removal of the leakage signal reduces the annual amplitude of the GRACE time series and delays its maximum, from March to the end of April (peak around 29th April, Fig. F-13-4.a). Considering the long-term behavior, the interval 2002-2008 is characterized by an inter-annual signal corresponding to a mass increase in 2003-2005 and mass decrease in 2006-2008. Fig. F-13-5 shows that results are similar for all choices of the hydrology model. The correlation with the altimetry-derived estimate is larger than 0.5 and the RMS of the differences is smaller than 60 mm (Tab. F-13-2).

Table F-13-5: Annual (A) and semi-annual (SA) amplitude and phase and the trend of water fluxes of the Mediterranean Sea. The time interval is August 2002 - July 2008. The Bosphorus and the Gibraltar strait flows, expressed in the rate of change of an uniform layer in the Mediterranean Sea are indicated by the subscripts $_{FB}$ and $_{FG}$ respectively.

	A Amp ($\frac{mm}{mon}$)	A Phase (days)	SA Amp ($\frac{mm}{mon}$)	SA Phase (days)	Trend ($(\frac{mm}{mon})/year$)
\dot{S}_{mass}^{a-s}	13±7	252±16	13±7	92±10	0.8±0.3
\dot{S}_{mass}^{g-h}	16±5	271±16	18±8	94±10	1.5±0.3
\dot{S}_{E-P}	19±7	266±16	17±7	9±10	2.5±0.3
\dot{S}_R	12±4	5±22	5±4	117±10	0.5±0.3
\dot{S}_{FB}^{a-s}	16±4	91±6	6±5	130±5	-0.8±0.4
\dot{S}_{FB}^{g-h}	13±4	80±5	9±5	117±10	-0.1±0.4
\dot{S}_{FG}^{a-s} (from \dot{S}_{FB}^{a-s})	53±10	264±5	19±8	31±10	2.2±0.8
\dot{S}_{FG}^{a-s} (from \dot{S}_{FB}^{g-h})	51±11	261±5	42±5	27±7	2.1±0.8
\dot{S}_{FG}^{g-h} (from \dot{S}_{FB}^{a-s})	55±11	274±5	19±8	48±8	3.6±0.8
\dot{S}_{FG}^{g-h} (from \dot{S}_{FB}^{g-h})	52±11	271±5	21±5	41±8	3.4±0.8

Table F-13-6: As in Tab. F-13-5, but for the Black Sea. All values are expressed as the rate of change of an uniform layer in the Black Sea.

	A Amp ($\frac{mm}{mon}$)	A Phase (days)	SA Amp ($\frac{mm}{mon}$)	SA Phase (days)	Trend ($(\frac{mm}{mon})/year$)
\dot{S}_{mass}^{a-s}	16±2	32±16	34±2	133±10	-0.1±0.3
\dot{S}_{mass}^{g-h}	11±7	44±16	41±7	113±10	3.8±0.3
\dot{S}_{E-P}	40±5	264±16	7±5	17±8	2.1±0.3
\dot{S}_R	22±6	116±12	7±6	140±10	-0.9±0.3
\dot{S}_{FB}^{a-s}	94±14	91±6	34±10	130±10	-2.0±0.8
\dot{S}_{FB}^{g-h}	81±18	80±5	58±10	117±10	-0.1±0.9

3.3 Mass fluxes and Strait flows

Using a simple numerical two point differentiation, we can estimate the water mass change per month \dot{S}_{mass} , from either steric corrected altimetry or hydrology-corrected GRACE data, where the latter method is independent from oceanographic modelling. In the Mediterranean Sea, the GRACE-derived \dot{S}_{mass}^{g-h} shows an annual signal with amplitude 16 ± 5 mm/mon ($16\pm5 \cdot 10^{-3}$ Sv) peaking around the 27th September (Fig.F-13-7.d and Table F-13-5). In the Black Sea, \dot{S}_{mass}^{g-h} has maximum amplitude in March with a strong semi-annual component, in addition to the annual component (Fig. F-13-8.d and Tab. F-13-6).

Figs. F-13-7.a, F-13-8.a show that evaporation exceeds precipitation in both basins. The annual amplitudes of $E - P$, in terms of uniform layer of water in the basins, are ± 5 mm/mon ($19\pm 5 \cdot 10^{-3}$ Sv) for the Mediterranean and 40 ± 5 mm/mon ($6\pm 1 \cdot 10^{-3}$ Sv) for the Black Sea and peak at the same time (around the 20th September)(Tabs. F-13-5 and F-13-6). In the Mediterranean Sea, our estimate of $E - P$ has a bias compared to the DFS4 and ERA-Interim results, whereas it has no bias compared to the OAFLUX-GPCP derived quantities. In the Black Sea the agreement is very good for all estimates (Figs. F-13-7.b, F-13-8.b). River runoff is the smallest component in the Mediterranean Sea, while it is

Table F-13-7: Monthly errors σ_m (mm) and propagated errors of annual amplitude σ_A ($\frac{2}{\sqrt{N}}\sigma_m$) ($mm, \frac{mm}{mon}$) in Mediterranean (left) and Black Sea (right), for the time interval from August 2002 to July 2008 (N=72). The estimate is obtained from the root mean square of differences (RMS) or from error propagation (EP).

	Med Sea			Black Sea		
	σ_m	σ_A	Method	σ_m	σ_A	Method
S_{tot}^a	10	2	RMS	30	8	RMS
$S_{tot}^{g-h+s} = \hat{S}_{mass}^{g-h} + S_{ster}^s$	30	7	EP	54	13	EP
S_{hyd}^h	17	5	RMS	29	8	RMS
$S_{hyd}^{g-a+s} = \hat{S}^g - S_{tot}^a + S_{ster}^s$	27	6	EP	54	13	EP
S_{ster}^s	20	5	RMS	17	4	RMS
$S_{ster}^{a-g+h} = S_{tot}^a - \hat{S}_{mass}^{g-h}$	24	6	EP	27	10	EP
S^g	15	4	EP	42	10	EP
S_{mass}^{a-s}	22	5	EP	35	8	EP
S_{mass}^{g-h}	23	6	EP	51	12	EP
S_{mass}^{a-s}	31	7	EP	49	12	EP
S_{mass}^{g-h}	33	8	EP	72	17	EP
\dot{S}_{E-P}	30	7	RMS	20	5	RMS
\dot{S}_R	9	2	RMS	24	6	RMS
\dot{S}_{FB}^{a-s}	10	2	EP	58	14	EP
\dot{S}_{FB}^{g-h}	13	3	EP	78	18	EP
\dot{S}_{FG}^{a-s} (from \dot{S}_{FB}^{a-s})	44	10	EP			
\dot{S}_{FG}^{g-h} (from \dot{S}_{FB}^{g-h})	45	11	EP			

comparable to $E - P$ in the Black Sea (Figs. F-13-7.c, F-13-8.c). Consequently, the freshwater budget $E - P - R$ displays mostly positive values in the Mediterranean Sea (deficit) and alternating values in the Black Sea.

Figure F-13-9 (bottom) shows the net mass outflow FB through the Bosphorus Strait computed from Eq.F-13-8. The seasonal cycle of the GRACE-derived estimate \dot{S}_{FB}^{g-h} (contributes to a layer change of 83 ± 18 mm/mon ($13 \pm 3 \times 10^{-3}$ Sv) peaking around the 28th March (Fig. F-13-8). FB has a larger annual amplitude than the river runoff R_B and vertical surface water flux $(E - P)_B$ (Table F-13-6, see also (Stanev et al. 2000)).

In the Mediterranean Sea, the vertical surface water flux $(E - P)_M$ contributes at seasonal scales to a layer change \dot{S}_{E-P} of 19 ± 2 mm/mon peaking middle of September, which is larger than the net mass flow through the Bosphorus Strait FB and the river runoff R_M (Table F-13-5).

Fig. F-13-9 (top) shows the Gibraltar flux computed from Eq. F-13-9. Its annual cycle peaks in the middle of September, in phase with the annual component of $(E - P)_M$. The contribution of $(E - P)_M$ to FG is dominant, while contributions from R_{Med} and FB are smaller. All estimations of FG using all combinations of mass change estimation from hydrology-corrected GRACE and from steric-corrected altimetry yield a mass flow FG with an annual amplitude of about 54 ± 10 mm/mon ($52 \pm 10 \times 10^{-3}$ Sv) peaking in September-October (Tab. F-13-5). Trends are positive for both the $E - P$ ($2.4 \pm 0.3 \times 10^{-3}$ Sv/yr) and the FG GRACE-derived estimates ($3.4 \pm 0.8 \times 10^{-3}$ Sv/yr).

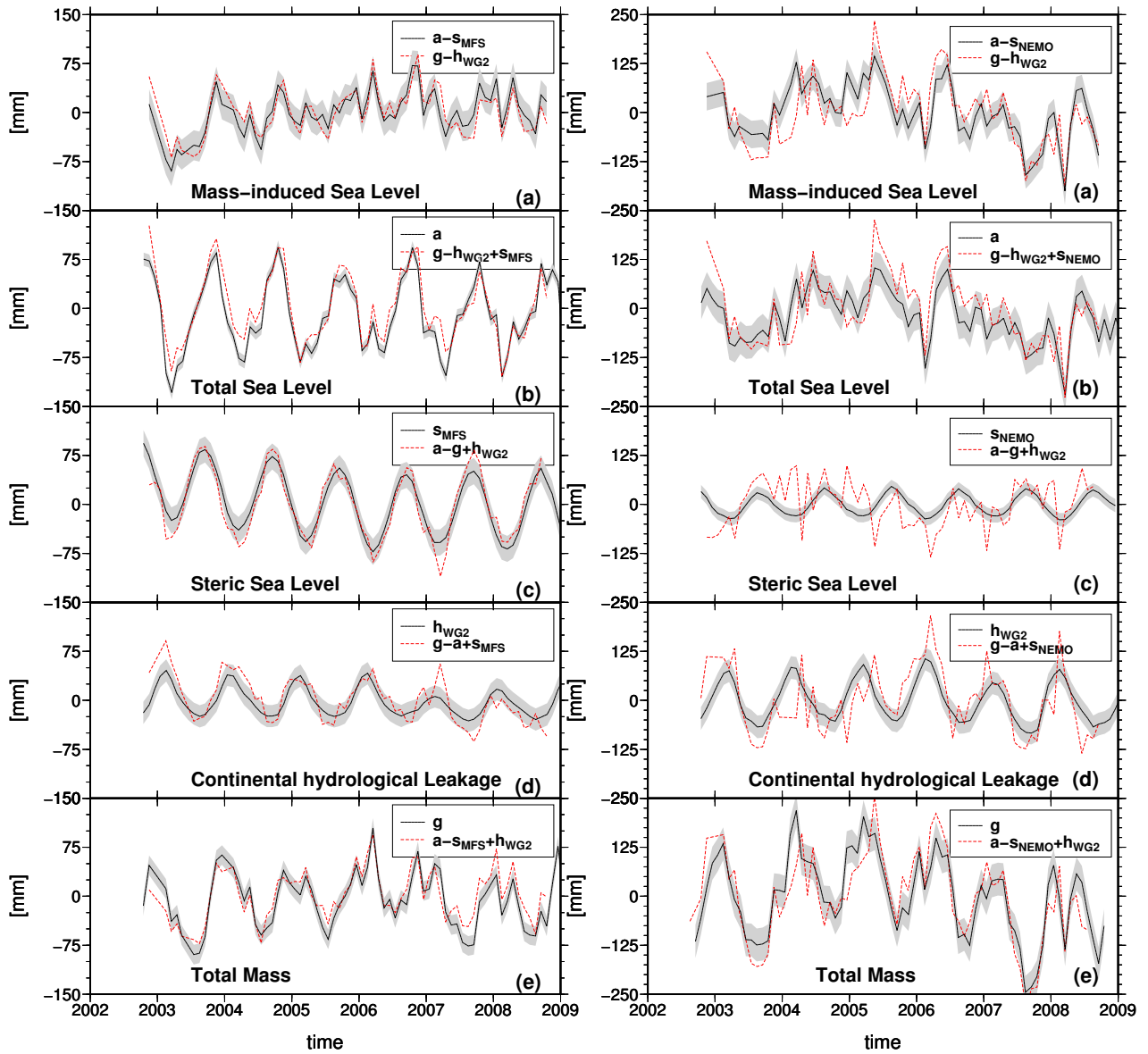


Figure F-13-4: Mediterranean Sea (left) and Black Sea (right): Basin average of water mass variation expressed in equivalent water height (a), total sea level (b) and its steric component (c), continental hydrological leakage correction (d) and mass change including hydrological leakage (e). In (a): water mass change is from steric-corrected altimetry (black) and from hydrology-corrected GRACE gravity solutions (gray), where g is the rescaled mass change computed as GRACE-load+GAD-GIA as described in Section 2.1. In b-e: observed (b,e) and modeled (c,d) quantities are black, while inferred estimates, computed by adding or subtracting the other three observational/ modeled estimates as in Eq. F-13-7, are gray. Error bounds correspond to the RMS differences, unknown systematic

In Section 3.1 we have discussed the monthly errors adopted in this study. The monthly error of the combined mass-induced sea level S_{mass} and of the strait flow FB and FG , estimated above, have been derived from uncorrelated error propagation of each components. We find that in the Mediterranean Sea monthly basin averages of GRACE- and altimetry-derived S_{mass} have comparable accuracy (23 and 22 mm). In the Black Sea, \hat{S}_{mass}^{g-h} has a lower accuracy (51 mm) compared to the altimetry-derived S_{mass}^{a-s} (35 mm) (Tab. F-13-7). Consequently, our GRACE-derived estimate of the Bosphorus strait flow FB yields a lower accuracy (78 mm/month, with a contribution of 72 mm/month from \hat{S}_{mass}^{g-h}) compared to

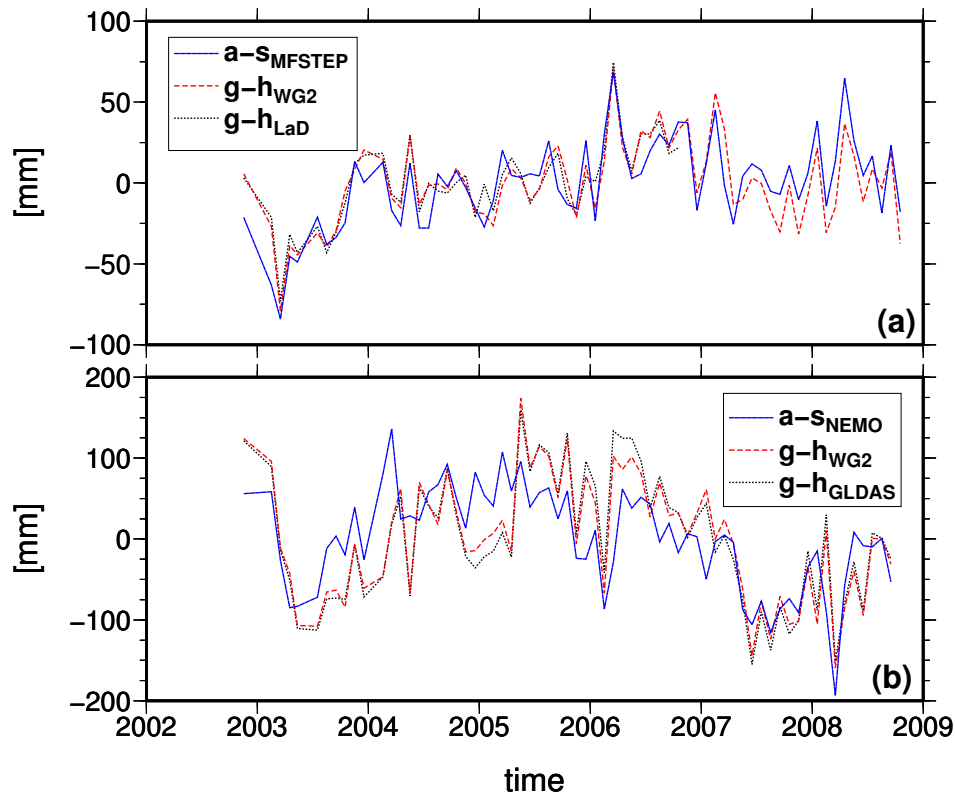


Figure F-13-5: Inter-annual basin average in Mediterranean Sea (a) and in Black Sea (b) of the mass-induced sea level (annual cycle removed) from filtered steric-corrected altimetry (black) and from hydrology-corrected GRACE (grey). Steric corrections come from MFSTEP in (a) and from NEMO in (b), continental hydrological leakage corrections come from WaterGAP2 (line) and LAD (dots) in (a) and from WaterGAP2 (line) and GLDAS (dots) in (b).

the altimetry-derived FB (58mm/month). The accuracy of the Gibraltar strait flow FG (47mm/month) is almost independent of the computed Bosphorus flow, as its effect is small in the overall estimate. In contrast, the uncertainties of the Mediterranean $E - P$ (30mm/month) and \dot{S}_{mass}^{g-h} (33 mm/month) propagate most strongly into the uncertainty of the strait flow at Gibraltar.

Conclusions and Discussion

We have here investigated the mass-induced sea level S_{mass} in the Mediterranean and Black Sea basins over an interval of six years, from August 2002 to July 2008, at both seasonal and inter-annual time scales, and therefore extended the analysis in Fenoglio et al. 2006, 2007. We have in addition studied here the closure of the water budget in both basins deriving from the water budget the strait flows both at Gibraltar and through the Bosphorus.

The comparison has required a variety of auxiliary data. We have used continental hydrological models to estimate the leakage correction to the GRACE observations and oceanographic models and data to derive the steric correction to the altimetric sea level observations. The closure of the water budget additionally requires evaporation, precipitation and river runoff estimates.

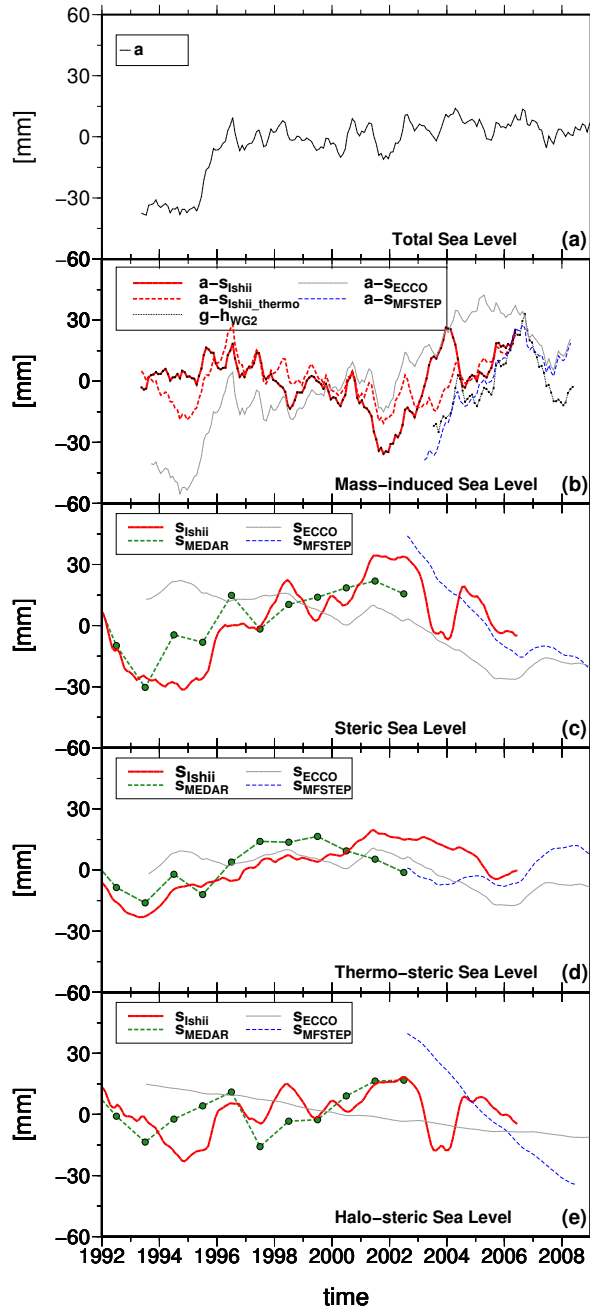


Figure F-13-6: Basin averages in the Mediterranean Sea of (a) total sea level from multi-mission satellite altimetry, (b) mass-induced sea level from GRACE (dots) and from steric-corrected altimetry with steric correction from various sources (MFSTEP (thin full line), ECCO (gray line), Ishii climatology v6.7 (thick full line) and thermo-steric-only Ishii climatology v6.7 (thick dashed line)), (c) steric, (d) halo-steric and (e) thermo-steric components of sea level with notation as above. A moving average of 12 months has been applied to the monthly values. Annual values from MEDAR are also shown in c-e (thick dashed line).

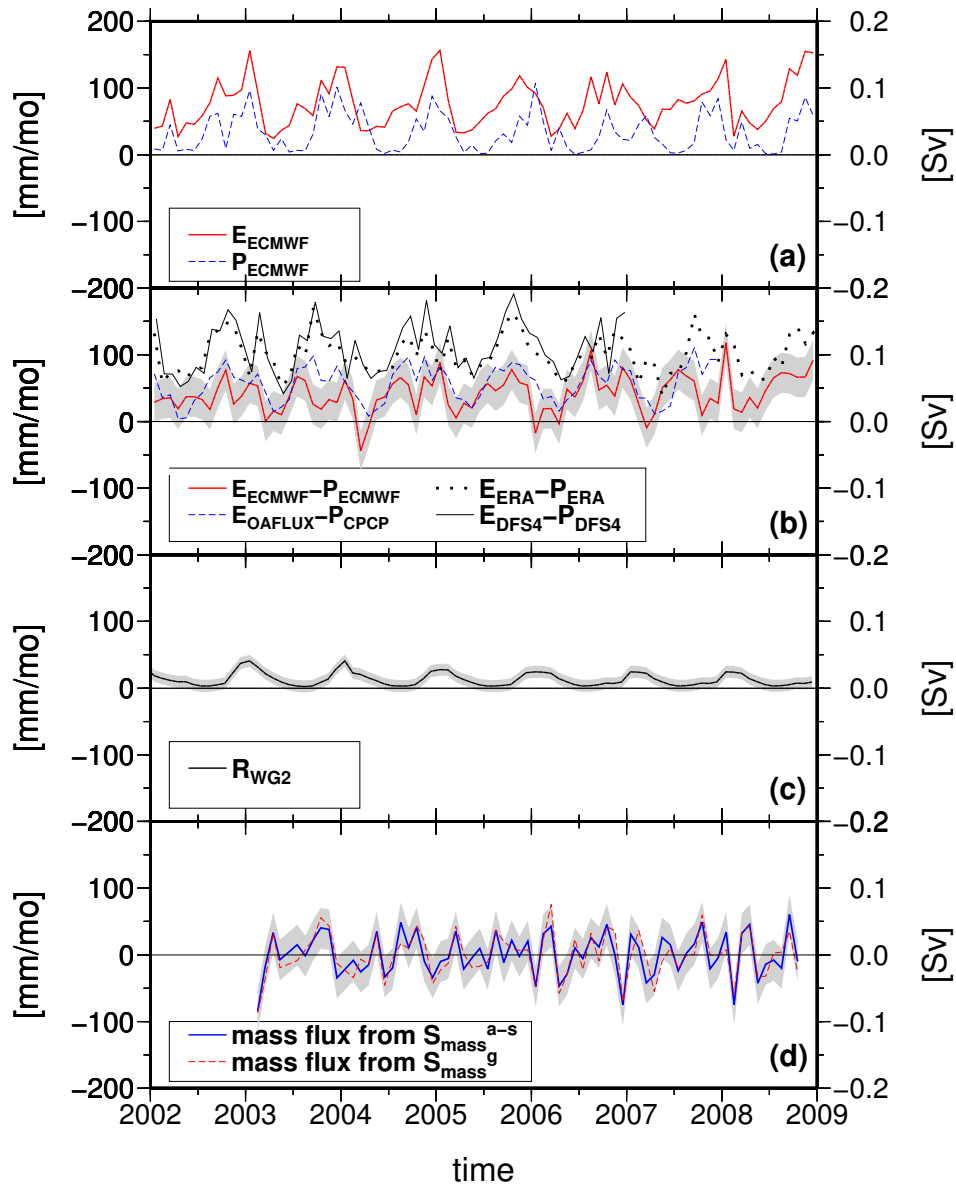


Figure F-13-7: Mediterranean water mass fluxes (as uniform basin changes and volume flow): (a) Evaporation (black) and Precipitation (grey), (b) Precipitation minus Evaporation, (c) river runoff, (d) total mass flux derived from GRACE (\hat{S}_{mass}^{g-h} , gray) and from altimetry (\hat{S}_{mass}^{a-s} , black). In (b) $E-P$ is from ECMWF (solid line), OAFLUX-CPCP (black dots), ERA (gray dots) and DFS4 (black dashed line). Error bounds correspond to RMS differences, unknown systematic errors may remain (see Tab. F-13-7).

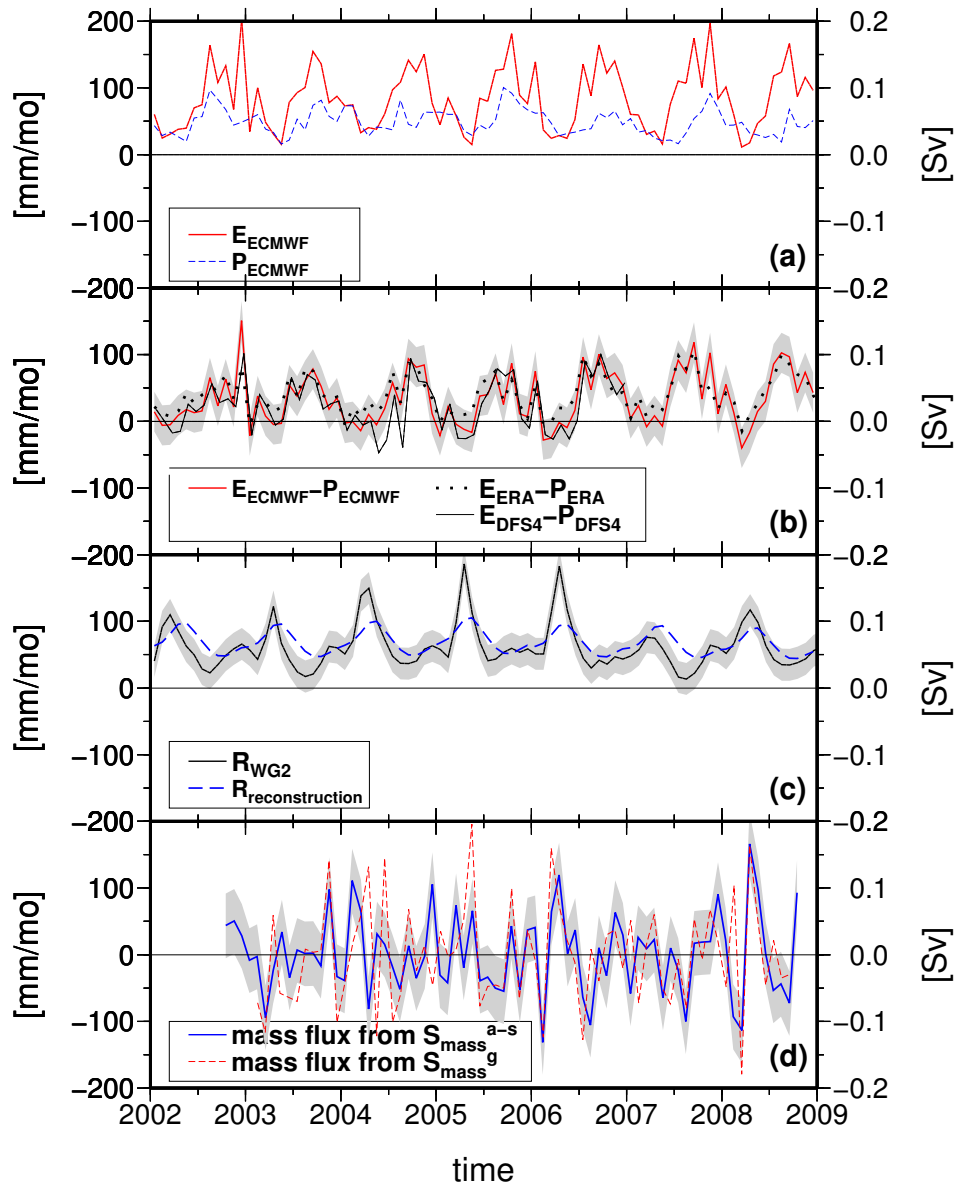


Figure F-13-8: As in Figure F-13-7, but for the Black Sea mass fluxes. In (b) $E - P$ is from ECMWF (full line), ERA (grey dots) and DFS4 (dark dashed line). In (d) the series depict \dot{S}_{mass}^{g-h} and \dot{S}_{mass}^{a-s} . Error bounds (light gray) correspond to RMS differences, unknown systematic errors may remain (see Tab. F-13-7).

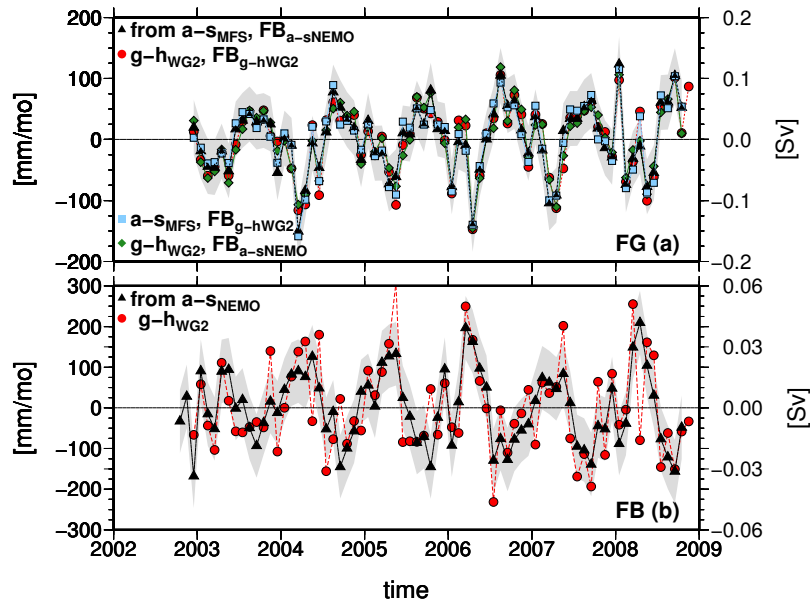


Figure F-13-9: Monthly estimates of the strait flow anomalies at Gibraltar, FG , (a) and at the Bosphorus strait, FB , (b) both as uniform layer changes in the Mediterranean Sea and in the Black Sea (mm/mo) and as volume transport (Sv). FB is derived from both GRACE-based (circle) and altimetry-based mass variation estimates (triangle). FG is derived from both GRACE-based/only (diamond) and altimetry-based/only (triangle) mass estimates in both basins and from mixed GRACE-based and altimetry-based estimates (circle and square). Error bounds (light gray) correspond to the altimetry-based/only estimates (Table F-13-7).

First we have analyzed the consistency between the basin mean of S_{mass} derived from GRACE and altimetry data and selected the most suitable steric and continental hydrological leakage corrections. We noticed that the corrections yielding the best agreement at seasonal scales (i.e. smallest difference in annual amplitude and phase, smallest standard deviation of the differences and highest correlation) are, in the Mediterranean Sea, those derived from the WaterGAP2 hydrological model and from the MFSTEP regional ocean model and, in the Black Sea, those derived from WaterGAP2 and from the NEMO regional ocean model.

In the Mediterranean Sea, the agreement in annual phase is not perfect, and our work suggests that the annual signal in either the steric correction and/or the hydrological correction is underestimated. A single hydrology model (CPC, Fan and Van der Doll, 2004) and one steric database (Ishii and Kimoto, 2009) were considered by Calafat (Calafat et al., 2010), who found both estimations of annual ocean mass peaking in October. Similarly, Garcia et al., 2010 used only one hydrology model (GLDAS) but a variety of ocean models and ocean data. These authors give an estimation of annual ocean mass peaking in January and report on the best agreement with GLDAS realized by an ideal steric component with large amplitude (77 mm). They further identify the Mercator model as the best existing model (steric correction with amplitude 68 mm).

We have shown here that, while for each hydrologic model chosen a "best" steric correction exist, the errors are most likely to arise from the combination of both corrections. Using the "best" existing corrections identified, in the Mediterranean Sea the GRACE- and altimetry-based mass-induced sea level basin averages (\hat{S}_{mass}^{g-h} and S_{mass}^{a-s}) agree within 3 mm and 23 days in annual amplitude and phase, both series peak in December. Correlation and RMS

difference are 0.86 and 37 mm for the monthly time series and 0.85 and 15 mm for the inter-annual time series. The best agreement with WaterGAP2 is realized by an ideal steric sea level component with larger annual amplitude (66 mm) than the MFSTEP correction (amplitude 58 mm). The accuracy of \hat{S}_{mass}^{g-h} and S_{mass}^{a-s} is comparable, 23 and 22 mm respectively, and the time-series agree within the error bounds. There is an excellent agreement both at seasonal and inter-annual time scales.

In the Black Sea, using the 'best' correction identified, the estimated $\hat{S}_{mass}^{g-h}, S_{mass}^{a-s}$ are less consistent than in Mediterranean Sea and do not always agree within the error bounds of the altimetry-derived mass estimate. The consistency at seasonal scales is within 4 mm and 6 days for seasonal amplitude and phase, the time series peak in April. Correlation and RMS differences are 0.68 and 55mm for monthly time series and 0.71 and 65mm for the inter-annual time series. The accuracy is lower for the monthly basin averaged \hat{S}_{mass}^{g-h} derived from GRACE (52 mm) than for the altimetry-derived S_{mass}^{a-s} (39 mm). Considering the small size of the Black Sea in relation to the GRACE spatial resolution, and despite the large magnitude of the hydrological correction, this is a promising agreement.

Also new in this paper is the analysis of the trends in S_{mass} , which depend on the choice of the GIA correction and of the steric and continental hydrological leakage corrections. We have estimated an error of 0.9mm/yr for the GIA correction in terms of equivalent water height, based on different choices of parameters for the GIA model as well as on a comparison with published results.

Nevertheless, we have identified the steric component as the main source of the uncertainty in the trend of the altimetry-derived S_{mass}^{a-s} in the Mediterranean Sea. Differences in the trends of the steric correction derived from the ocean models are up to 5mm/yr (2.9 ± 1.6 mm/yr using ECCO and 8.3 ± 1.6 mm/yr with MFSTEP). Additionally, the choice of the continental hydrological leakage correction affects the trend of the GRACE-derived \hat{S}_{mass}^{g-h} , with differences up to 3mm/yr when using different hydrological models. Trends are 2.8 ± 1.9 mm/yr when using GLDAS versus 5.3 ± 1.9 mm/yr when using WaterGap2. The trend of the GRACE-derived steric sea, S_{ster}^{a-g+h} is -5.3 ± 1.1 mm/yr, which lies between the trends of the steric sea level basin averages corresponding to the ECCO and MFSTEP models. The analysis over longer time periods suggests that significant inter-annual variations occur in both mass-induced and steric sea level components. We have identified in the 90's a period of rise in total sea level of the Mediterranean Sea, caused by a rise of both components. In the subsequent decade the situation changed, as the increase in mass was compensated by a decrease in steric sea level, resulting in a more or less constant total sea level rise.

In the Black Sea, the inter-annual variability of S_{mass} is stronger than the Mediterranean Sea, with an increase in 2003-2005 followed by a decrease in 2006-2008. The annual signal has amplitude of 32 ± 5 mm peaking in April.

The Bosphorus net flow derived from GRACE yields an annual amplitude of $13 \pm 4 \times 10^{-3}$ Sv in terms of volume transport peaking end of March (81 ± 18 mm/mon in terms of uniform layer change in the Black Sea and 13 ± 4 mm/mon in terms of uniform layer change in the Mediterranean Sea). The GRACE-based and the altimetry-based Bosphorus net flow agree within the error bounds of the altimetry-based estimate. The accuracy of \hat{S}_{FB}^{g-h} is lower than the accuracy of \hat{S}_{FB}^{a-s} , due to the lower accuracy of the GRACE-based mass estimate in the Black Sea.

The Gibraltar Strait flow derived from GRACE has an annual amplitude of $52 \pm 11 \times 10^{-3}$ Sv in terms of volume transport peaking in September-October (52 ± 11 mmmon in terms of uniform layer in the Mediterranean Sea). This amplitude agree with values reported by other authors ([*Garcia et al.*, 2006, 2010]) and is slightly smaller than the result derived from current meter measurements (*Garcia-Lafuente et al.* 2002), 78 mm/mon peaking in September). Also in this case, the GRACE-based and the altimetry-based net flow agree within the error bounds of the altimetry-based estimate. Here, however, the accuracy of the Gibraltar Strait flow is virtually independent of the mass change used in computing the Bosphorus net flux, as the effect of this strait flow is small in the estimate of the Gibraltar net flux. Moreover, both the GRACE-based Gibraltar Strait flow and the altimetry-based Gibraltar net flow have comparable accuracy, due to the comparable accuracy of the GRACE- and altimetry-derived mass estimate in the Mediterranean Sea.

We conclude that, although resolution and accuracy of the mass-induced sea level estimate have been improved by using the latest GRACE models and the improved filtering methods, results are still dependent on the accuracy of the auxiliary data and models used to compute the corrections. The cross validation performed in this study is a viable tool to asses those errors and improve them in future studies.

An improved regional hydrology model, incorporating anthropogenic water use models, is currently under development ([*Aus der Beek et al.*, 2012]). This model is expected to give valuable insights in the hydrology of the complete watershed region draining in the Black Sea and Mediterranean Sea. At the same time, it is expected to provide the river runoff forcing for the ocean models and to supply continental hydrological leakage corrections for GRACE.

Acknowledgments

The authors acknowledge G. Spada for the GIA corrections, A. Güntner for the Water-GAP2 data, B. Barnier and R. Dussin for support on DFS4 and ERA-Interim airflux data, M. Rixen and A. Shaw for helpfull discussions on the MEDAR/Medatlas data. Comments by W. Bosch and by two anonymous reviewers helped to improve the manuscript. This study has been performed within the STREMP project funded by the Deutsche Forschungsgemeinschaft (SPP1257, FE-534/3-2).

References

- Aus der Beek, T., Menzel, L., Grayek, S., Rietbroek, R., Fenoglio-Marc, L., Becker, M., Kusche, J., Stanev, E., 2012. Modelling the water resources of the Black and Mediterranean Sea river basins and their impact on regional mass changes. *Journal of Geodynamics* 59-60, 157-167.
- Beckley, B.D., Lemoine, F.G., Luthcke, S.B., Ray, R.D., Zelensky, N.P., 2007. A reassessment of global and regional mean sea level trends form TOPEX and Jason-1 altimetry based on revised reference frame and orbits. *Geophysical Research Letters*, 34.
- Brodeau, L., Barnier, B., Treguier, A.M., Penduff, T., Gulev, S., 2010. An ERA40-based atmospheric forcing for global ocean circulation models. *Ocean Modelling* 31, 88-104.

- Calafat, F., Marcos, M., Gomis, D., 2010. Mass contribution to Mediterranean Sea level variability for the period 1948-2000. *Global and Planetary Change* 73 (3-4), 193-201, <http://dx.doi.org/10.1016/j.gloplacha.2010.06.002>.
- Carrere, L., Lyard, F., 2003. Modeling the barotropic response of the global ocean to atmospheric wind and pressure forcing comparisons with observations. *Geophysical Research Letters* 30, 1-8.
- Chambers, D.P., 2006. Observing seasonal steric sea level variations with GRACE and satellite altimetry. *Journal of Geophysical Research* 111, 3010.
- Cheng, M., Tapley, B., 2004. Variations in the Earth's oblateness during the past 28 years. *Journal of Geophysical Research* 109, B09402.
- Cooper, M.K.H., 1996. Altimetric assimilation with water property conservation. *Journal of Geophysical Research* 101 (C1), 1059-1077.
- Döll, P., Kaspar, F., Lehner, B., 2003. A global hydrological model for deriving water availability indicators: model tuning and validation. *Journal of Hydrology* 207, 105-134.
- Ducet, N., Le Traon, P., Gauzelin, P., 1999. Response of the Black Sea mean level to atmospheric pressure and wind forcing. *Journal of Marine Systems* 22, 311-327.
- Fan, Y., van der Dool, H., 2004. Climate prediction center global monthly soil moisture data set at 0.5 degree resolution for 1948 to present. *Journal of Geophysical Research* 109, <http://dx.doi.org/10.1029/2003JD004345>.
- Farrell, W.E., 1972. Deformation of the earth by surface loads. *Reviews of Geophysics and Space Physics* 10, 761.
- Fenoglio-Marc, L., Kusche, J., Becker, M., 2006. Mass variation in the Mediterranean Sea from GRACE and its validation by altimetry, steric and hydrologic fields. *Geophysical Research Letters* 33, L19606, <http://dx.doi.org/10.1029/2006GL026851>.
- Fenoglio-Marc, L., 2007. Comment on "On the steric and mass-induced contributions to the annual sea level variations in the Mediterranean Sea" by David Garc a et al. *Journal of Geophysical Research* 112, C12018, <http://dx.doi.org/10.1029/2007JC004196>.
- Flechtner, F., 2007a. AOD1B Product Description Document for Product Release 01 to 04. GRACE 327-750, GR-GFZ-AOD-0001.
- Flechtner, F., 2007b. GFZ level-2 processing standards document for level-2 product release 0004. GRACE 327-743, Rev. 1.0.
- Foujols, M., Levy, M., Aumont, O., Madec, G., 2000. OPA 8.1 Tracer Model reference manual. Note du Pole de modelisation. Technical Report. Institut Pierre-Simon Laplace (IPSL), France, 45 pp.
- Fukumori, I., Menemenlis, D., Lee, T., 2005. A near-uniform basin-wide sea level fluctuation of the Mediterranean Sea, *Journal of Physical Oceanography* 37, 338-358, <http://dx.doi.org/10.1175/JPO3016.1>.
- Garcia, D., Chao, B., Boy, J.P., 2010. Steric and mass-induced sea level variations in the Mediterranean Sea revisited. *Journal of Geophysical Research* 115, C12016.
- Garcia, D., Chao, B., Del Rio, J., Vigo, I., Garcia-Lafuente, J., 2006. On the Steric and Mass Induced Contributions to the Annual Sea Level Variations in the Mediterranean Sea. *Journal of Geophysical Research* 111, C09030, <http://dx.doi.org/10.1029/2005JC002956>.
- Garcia Lafuente, J.G., Delgado, J., Vergas, M., Plaza, F., Sarhan, T., 2002. Low frequency variability of the exchanged flows through the strait of Gibraltar during CANIGO. *Deep Sea Research* 49, 4051-4067.

- Grayek, S., Stanev, E.V., Kandilarov, R., 2010. On the response of Black Sea level to external forcing: altimeter data and numerical modelling. *Ocean Dynamics* 60, 123-140.
- Han, S.C.S., Jekeli, C., Kuo, C., Wilson, C., Seo, K., 2005. Non-isotropic filtering of GRACE temporal gravity for geophysical signal enhancement. *Geophysical Journal International* 163, 18-25.
- Ishii, M., Kimoto, M., 2009. Reevaluation of historical ocean heat content variations with time-varying XBT and MBT depth bias corrections. *Journal of Oceanography* 65, 299-587.
- Klees, R., Zapreeva, E., Winsemius, H., Savenije, H., 2007. The bias in GRACE estimates of continental storage variations. *Hydrology and Earth System Sciences* 11, 1227-1241.
- Kusche, J., 2007. Approximate decorrelation and non-isotropic smoothing of timevariable GRACE-type gravity field models. *Journal of Geodesy* 81, 733-749.
- Kusche, J., Schmidt, R., Petrovic, S., Rietbroek, R., 2009. Decorrelated GRACE timevariable GRACE Gravity Solutions for Science at GFZ and their validation using an Hydrological model. *Journal of Geodesy*, 83.
- Le Traon, P., Gauzelin, P., 1997. Response of the Mediterranean mean sea level to atmospheric pressure forcing. *Journal of Geophysical Research* 102, 973-984.
- Leuliette, E.W., Miller, L., 2009. Closing the sea level budget with altimetry, Argo and GRACE. *Geophysical Research Letters* 36, L04608, <http://dx.doi.org/10.1029/2008GL036010>.
- Mariotti, A., Struglia, M., Zeng, N., Lau, K., 2002. The Hydrological cycle in the Mediterranean region and implications for the water budget of the Mediterranean Sea. *Journal of Climate* 15, 1674-1690.
- Milly, P., Shmakin, A., 2002. Global modeling of land water and energy balances. Part I: The land dynamics (LaD) model. *Journal of Hydrometeorology* 3 (3), 283-299.
- Naeije, M., Scharroo, R., Doornbos, E., Schrama, E., 2008. Global altimetry sea-level service: glass. NUSP-2 report GO 52320 DEO. NIVR/DEOS, Netherlands.
- Paulson, A., Zhong, S., Wahr, J., 2007. Inference of mantle viscosity from GRACE and relative sea level data. *Geophysical Journal International* 171, 497-508.
- Peltier, W., 2004. Global glacial isostasy and the surface of the ice-age Earth: the ICE- 5G (VM2) Model and GRACE. *Annual Review of Earth and Planetary Sciences* 32, 111.
- Peneva, E., Stanev, E., Belokopytov, V., Le Traon, P.Y., 2001. Water transport in the Bosphorus straits estimated from hydro-meteorological and altimeter data: seasonal to decadal variability. *Journal of Marine Systems* 31, 21-33.
- Rietbroek, R., Brunnabend, S., Dahle, C., Kusche, J., Flechtner, F., Schröter, J., Timmermann, R., 2009. Changes in total ocean mass derived from GRACE, GPS, and ocean modeling with weekly resolution. *Journal of Geophysical Research* 114, C11004.
- Rietbroek, R., Fritsche, M., Brunnabend, S.E., Daras, I., Kusche, J., Schröter, J., Flechtner, F., Dietrich, R., 2012. Global surface mass from a new combination of GRACE, modelled OBP and reprocessed GPS data. *Journal of Geodynamics* 59-60, 64-71.
- Rixen, M., Beckers, J., Levitus, S., Antonov, J., Boyer, T., Maillard, C., Fichaut, M., Baloupos, E., Iona, S., Dooley, H., Garcia, M., Manca, B., Giorgetti, A., Manzella, G., Mikhailov, N., Pinardi, N., Zavatarelli, M., 2005. The Western Mediterranean deep water: a proxy for climate change. *Geophysical Research Letters* 32, L12608, 2949-2952.
- Rodell, M., Famiglietti, J., Chen, J., Seneviratne, S., Viterbo, P., Holl, S., Wilson, C.R., 2004. Basin scale estimates of evapotranspiration using GRACE and other observations. *Geophysical Research Letters* 31 (L20504), <http://dx.doi.org/10.1029/2004GL020873>.

- Spada, G., Stocchi, P., 2007. SELEN: a Fortran 90 Program for solving the sea-level equation. *Computer and Geosciences* 33, 538-562.
- Stanev, E., Bowman, M.J., Peneva, E.L., Staneva, J., 2003. Control of Black Sea intermediate water mass formation by dynamics and topography: comparison of numerical simulations, surveys and satellite data. *Journal of Marine Systems* 61, 59-99.
- Stanev, E., Le Traon, P., Peneva, E., 2000. Sea level variations and their dependency on meteorological and hydrological forcing: analysis of altimeter and surface data for the Black Sea. *Journal of Geophysical Research* 105, 17, 203-17,216.
- Stanev, E., Peneva, E., 2002. Regional sea level response to global climatic change: Black Sea examples. *Global and Planetary Change* 32, 33-47.
- Stanev, E., Staneva, J., Bullister, J.L., Murray, J.W., 2004. Ventilation of the Black Sea pycnocline: parameterization of convection, numerical simulations and validations against observed chlorofluorocarbon data. *Deep Sea Research* 51 (12), 2137-2169.
- Swenson, S., Wahr, J., 2002. Methods for inferring regional surface-mass anomalies from Gravity Recovery and Climate Experiment (GRACE) measurements of timevariable gravity. *Journal of Geophysical Research* 107, 1-3.
- Swenson, S., Wahr, J., 2006. Post-processing removal of correlated errors in GRACE data. *Geophysical Research Letters* 33, L08402.
- Swenson, S., Wahr, J., 2007. Multi-sensor analysis of water storage variations of the Caspian Sea. *Geophysical Research Letters* 34, L1640.
- Tapley, B.D., Bettadpur, S., Ries, J.C., Thompson, P.F., Watkins, M.M., 2004. GRACE measurements of mass variability in the earth system. *Science* 305, 503-506.
- Tonani, M., Pinardi, N., Dobricic, S., Pujol, I., Fratianni, C., 2008. A high-resolution free-surface model of the Mediterranean Sea. *Ocean Science* 4, 1-14.
- Velicogna, I., Wahr, J., 2006. Measurements of time-variable gravity show mass loss in Antarctica. *Science Express* 311 (5768), 1754-1756, doi:10.1126/science.1123785.
- Wahr, J., Molenaar, M., Bryan, F., 1998. Time variability of the Earth's gravity field: hydrological and oceanic effects and their possible detection using GRACE. *Journal of Geophysical Research* 103, 30205-30230.
- Willis, J.K., Chambers, D., Nerem, R., 2008. Assessing the globally averaged sea level budget on seasonal to interannual timescales. *Journal of Geophysical Research* 113, C06015, <http://dx.doi.org/10.1029/2007JC004517>

8.3 Decadal variability of the net water flux at the Mediterranean Gibraltar strait

F-14: Fenoglio-Marc L., A. Mariotti, G. Sannino, B. Meyssignac, A. Carillo, M.V. Struglia, Decadal variability of the net water flux at the Mediterranean Gibraltar Strait , *Global and Planetary Change* 100, 1-10, 2013.

Abstract

Long-term variability of the net water flux into the Mediterranean Sea at the Gibraltar Strait over the period 1960-2009 is explored based on an approach combining multiple observational datasets and results from a regional climate model simulation. The approach includes deriving Gibraltar net inflow from the application of the Mediterranean Sea water budget equation using observationally based estimates of mass variation, evaporation, precipitation and simulated river discharge and Bosphorus Strait water fluxes. This derivation is compared with results from a simulation using the PROTHEUS regional ocean-atmosphere coupled model considering both individual water cycle terms and overall Gibraltar water flux. Results from both methodologies point to an increase in net water flux at Gibraltar over the period 1970-2009 (0.8 +/- 0.2 mm/mo per year based on the observational approach). Simulated Gibraltar net water flux shows decadal variability during 1960-2009 including a net Gibraltar water flux decrease during 1960-1970 before the 1970-2009 increase. Decadal variations in net evaporation at the sea-surface, such as the increase during 1970-2009, appear to drive the changes in net inflow at Gibraltar, while river runoff and net inflow at the Bosphorus Strait have a modulating effect. Mediterranean Sea mass changes are seen to be relatively small compared to water mass fluxes at the sea surface and do not show a long-term trend over 1970-2009. The Atlantic Multi-decadal Oscillation (AMO) and the North Atlantic Oscillation (NAO) are relevant indirect influences on net water flux at Gibraltar via the influence they bear on regional evaporation, precipitation and runoff

1. Introduction

As the Mediterranean Sea is a semi-enclosed basin, connected with the open Atlantic Ocean only at the Gibraltar Strait, the fluxes of water and salt through this Strait bear a major influence on the state of the Sea with impacts on the mass, salt and energy budgets. A net water inflow at Gibraltar (G) results from incoming fresh and cool Atlantic water and outflowing warm and salty Mediterranean water. Climatologically, net inflow of water at Gibraltar primarily balances the vertical loss of water at the sea-surface (water fluxes through the Bosphorus Strait (B) and river discharge (R) also contribute to balance the surface water loss; e.g. Mariotti et al., 2002). Recent research has shown that decadal changes in net Mediterranean Sea evaporation have characterized the 1958-2006 period, with an overall increase in net evaporation resulting in a substantial increase in sea-surface water loss (Mariotti, 2010; Criado-Aldeanueva et al., 2010). An open question is whether this increased water loss has induced increases in the net water inflow at Gibraltar or whether there have been changes in Mediterranean Sea water mass. In fact, while the Mediterranean thermohaline circulation is sustained by the atmospheric forcing, its intensity is controlled by the narrow and shallow Strait of Gibraltar via hydraulic control processes (Sannino et al. 2007, 2009). While measurements of the Mediterranean water outflow through Gibraltar have been collected over short time periods (Sanchez-Roman et al. 2009, Soto-Navarro et al. 2010), there are no long-term direct measurements of net water fluxes. Model simulations have been utilized to improve

the understanding of the processes that regulate water fluxes at Gibraltar, with very high-resolution models now able to represent much of the complexity characterizing the dynamics of the Strait and simulate realistic Gibraltar flows (Sannino et al. 2009, Sanchez-Garrido et al. 2011). It is interesting to note that a common assumption in state-of-art Mediterranean Sea models used for these studies is the equilibrium condition which forces the net flow at Gibraltar to strictly compensate the freshwater lost at the sea-surface (e.g. Tonani et al., 2008). Here we stress that such an assumption has still not been verified by specific observations. Nowadays, changes in Mediterranean Sea mass are directly measured by the satellite gravimetric mission GRACE. These measurements, available over the interval 2002-2010, are usually expressed in terms of changes in equivalent water thickness, i.e. water mass changes per surface area (with 1 mm water column corresponding to 1 kg/m^2 if a density of 1 gr/cm^3 is assumed). Mediterranean Sea water mass change values may also be derived from sea level change, provided the steric component of the sea level change can be estimated. In this case the water mass change is directly expressed as water thickness (volume). Recent studies have compared indirect estimates of Mediterranean Sea water mass derived from sea-level by way of steric-corrected satellite altimetry with those based on GRACE satellite mass retrievals. Results indicate a good agreement and a Mediterranean Sea mass increase during the last decade (Calafat et al., 2010; Fenoglio-Marc et al., 2012). Mediterranean sea level variability has been shown to be affected by the variability of the North Atlantic Oscillation (NAO; Hurrell et al., 2003) mainly through the impact of atmospheric sea-level pressure changes (Tsimplis and Josey, 2001). Despite these results collectively suggest long-term variations in Mediterranean Sea mass and sea-level, and large-scale atmospheric influences, to our knowledge how long-term changes in fresh water fluxes may have affected Gibraltar water fluxes is yet to be explored. The level of accuracy of the satellite-based measurements calls for a re-examination of many conventional approximations often taken for granted (Greatbatch and Lu, 2001). The goal of this work is to study the decadal variations in net water flux at the Strait of Gibraltar over the period 1960-2009 based on a combined observational-modelling approach and to indirectly explore the correctness of the equilibrium condition assumption made in state-of-art models. First, Gibraltar water flux is derived indirectly from the water budget equation based on observational estimates of Mediterranean Sea mass changes (from steric-corrected sea-level estimates and GRACE mass retrievals), regional precipitation and evaporation. Next, an independent estimate of the Gibraltar water flux is obtained from a numerical simulation by a regional ocean-atmosphere climate model. Lastly, potentially important factors regulating long-term Gibraltar flux changes are discussed. The paper is organized as follows: overall data and methodology is described in Section 2; results pertaining Mediterranean Sea mass and Gibraltar water flux variability are presented in Section 3; conclusions are in Section 4.

2. Methodology and Data

The net water inflow through Gibraltar (G), may be estimated on the basis of the water budget equation for the Mediterranean Sea:

$$G = E - (P + R + B) + \frac{dM}{dt} \quad (\text{F-14-1})$$

with E being sea-surface evaporation, P precipitation over the sea; R river discharge into the sea from the Mediterranean catchment; B net water influx from the Black Sea at the Bosphorus Strait; $\frac{dM}{dt}$ the rate of Mediterranean Sea water mass (M) change (see also Fenoglio-Marc et al. 2012, Grayek et al., 2010). (Note that changes in Mediterranean Sea

Table F-14-1: List of data. For the seven fields used in this study : temperature (T), salinity (S), sea level (S_{tot}), mass-induced sea level (S_{mass}), evaporation (E), precipitation (P), sea level pressure (SLP) the name of the database together with its time interval, spatial and temporal resolutions are given. For the T and S fields the maximum depth and the number of levels are given in addition.

Database Name	Field	Time Interval	Resolution (deg)	Depth (m)	Levels	Time Sampling
Medar/Medatlas	T, S	1945-2002	0.2 x 0.2	4000	25	yr
Ishii v6.7	T, S	1945-2006	1 x 1	700	16	30 ys
MFSTEP/ICBM	T, S	2000-2009	1x1	3850	31	30 ys
GRACE	S_{mass}	2002-2009	300 km			30 days
altimetry	S_{tot}	1993-2009	0.5 x 0.5			30days
MBMED11	S_{tot}	1970-2009	0.5 x 0.5			30 days
Protheus	E	1958-2001	30 km			30 days
OAFUX	E	1958-2009	1x1			30 days
Protheus	P	1958-2001	30 km			30 days
GPCP	P	1979-2009	2.5 x 2.5			30 days
REOFS	P	1960-2009	5 x 5			30 days
HadSLP	SLP	1960-2009	5 x 5			30 days

mass due to salinity changes are not accounted for in this water budget equation). As all quantities in Eq. F-14-1 represent a volume variation, they can be expressed as basin-uniform sea level change in units of mm/mo. We apply Eq. F-14-1 to derive G based on observational estimates of $\frac{dM}{dt}$, E and P. $\frac{dM}{dt}$ may be derived as the difference of water mass-induced sea level averaged over the sea (S_{mass}) at two following time-steps (Fenoglio-Marc et al. (2007)), as well as estimated from GRACE gravity solutions. In contrast, the independent results from the model simulation are based on the model assumption, so it is interesting to see how these results compare with the observational estimate of G and whether they can contribute to a qualitative description of long-term variability in Gibraltar water fluxes. All the quantities in Eq. F-14-1 are estimated indirectly (as explained in the following) and it is clearly a challenge to define long-term changes and uncertainties of any of these quantities, let alone the resulting G estimate. Nevertheless, we attempt to estimate errors of annual mass-induced sea level S_{mass} and derived quantities, namely $\frac{dM}{dt}$ and G. These errors estimates are based on either the root mean square (RMS) difference between the various datasets available for a given quantity, or on error propagation considering the various components contributing to a given estimated quantity (see Tab.F-14-1 for a summary of data used in this study; Tables F-14-2 to F-14-5 for associated error estimates). The first method reflects the spread of the datasets, but unknown systematic errors may remain. We account for the temporal autocorrelation of a time series, by using its effective sample size based on the lag-1 autocorrelation coefficient (Santer et al. 2000). The correlation between time-series and its double-sided significance are evaluated. Linear regression is used to estimate the linear trend and its error. We further assess the trend significance by applying the t-test to the ratio between the estimated trend and its error (Fenoglio-Marc et al. 2011). In the error propagation we consider the components to be uncorrelated (Fenoglio-Marc et al., 2006, 2012).

2.1 Mediterranean Sea Water Mass derivation

During August 2002-December 2009, Mediterranean water mass-induced sea level (S_{mass}) may be estimated directly from satellite-based gravity observations retrieved by the GRACE satellite mission (S_{mass}^g hereafter; Flechtner, 2007; Fenoglio-Marc et al, 2006). Note that since GRACE measures gravity, a priori mass changes detected by GRACE include both the effect

Table F-14-2: Correlation (Corr), root mean square difference (RMSD), number of samples (N) and level of significance of correlation (Significance) of annual time-series in common interval (Time Interval). Units are mm for sea-level (S) quantities and mm/mo for precipitation/evaporation rates and rate of mass change dM/dt. For sea level the component type is indicated by the subscript (tot: total sea level; ster: steric sea level; thermo-ster: thermo-steric sea level; halo-ster: halo-steric sea level; mass: mass induced sea level). The superscript indicates the dataset used (e.g. alti: altimetric sea level; reco: reconstructed sea level etc; see text). For precipitation and evaporation the datasets used are indicated by the subscript.

		Corr	RMSD	N	Time Interval	Significance
S_{tot}^{alti}	S_{tot}^{reco}	0.98	4.0	13	1993-2002	99
S_{tot}^{reco}	$S_{tot}^{recoalti}$	0.95	9.0	13	1993-2002	99
S_{ster}^{shii}	S_{ster}^{medar}	0.57	12.0	57	1945-2002	99
$S_{thermo-ster}^{shii}$	$S_{thermo-ster}^{medar}$	0.82	5.1	57	1945-2002	99
$S_{halo-ster}^{shii}$	$S_{halo-ster}^{medar}$	0.36	12.0	57	1945-2002	99
$S_{mass}^{reco-shii}$	$S_{mass}^{reco-medar}$	0.80	15.0	33	1970-2002	99
$dM/dt^{reco-shii}$	$dM/dt^{reco-medar}$	0.71	1.4	32	1970-2002	99
P_{gpcp}	P_{reofs}	0.41	4.9	23	1979-2001	95
$E_{oaf flux} - P_{gpcp}$	$E_{oaf flux} - P_{reofs}$	0.67	5.0	23	1979-2001	99

Table F-14-3: Correlation (Corr), root mean square difference (RMSD), number of samples (N) and level of significance of correlation (Significance) of observed and simulated annual time-series in 1979-2001 (n=23)

Simulated	Observed	Corr	RMSD (mm/mo)	Significance %
$E_{protheus}$	$E_{oaf flux}$	0.50	4.2	99
$P_{protheus}$	P_{gpcp}	0.78	2.8	99
$P_{protheus}$	P_{reofs}	0.15	5.8	50
$E_{protheus} - P_{protheus}$	$E_{oaf flux} - P_{gpcp}$	0.63	6.2	99
$E_{protheus} - P_{protheus}$	$E_{oaf flux} - P_{reofs}$	0.46	5.6	95
$G_{protheus}$	$E_{oaf flux} - P_{gpcp} + dM/dt$	0.44	7.0	95
$G_{protheus}$	$E_{oaf flux} - P_{reofs} + dM/dt$	0.59	5.6	99
$G_{protheus}$	$E_{oaf flux} - P_{reofs} + dM/dt - R - B$	0.66	6.0	99

of water and salt changes. Over the longer 1970-2009 period, S_{mass} may be also estimated indirectly from Eq. F-14-2, by correcting the total sea level (S_{tot}) for its steric component (S_{ster}) so as to account only for water mass induced sea-level (S_{mass}):

$$S_{mass} = S_{tot} - S_{ster} \quad (\text{F-14-2})$$

During 1993-2009, S_{tot} is evaluated from satellite altimetry data (S_{tot}^{alti}). For this derivation we have used along-track data of the Topex/Poseidon, Jason-1, Jason-2 and Envisat altimetry missions from the RADS database (Naeije et al., 2008) and applied the conventional geophysical corrections accounting for the ocean response to atmospheric wind and pressure forcing (atmospheric loading on the sea surface) via the Dynamic Atmospheric Correction (DAC). Grids of 0.5 degrees have been computed and used to evaluate the sea level basin average. Prior to the altimetry era, starting from 1970 S_{tot} is derived based on a reconstruction developed by Meyssignac et al. (2011) (hereafter MBMED11). Comparing the MBMED11 basin averaged reconstruction (S_{tot}^{reco}) with a reconstruction based on satellite altimetry ($S_{tot}^{recoalti}$;

Table F-14-4: Annual errors of basin averages. Methods are RMS difference (RMSD) and error propagation (EP) in (mm) or (mm/mo) as indicated in Tab. F-14-2. Bold values have been selected to provide the final error estimate for G from EP

	Annual Error	Source
S_{tot}^{salti}	3	RMSD of S_{tot}^{salti}
S_{tot}^{sreco}	6	EP, Meyssignac et al. 2011
S_{tot}	4	RMSD of S_{tot}^{salti} and S_{tot}^{sreco} (Tab. F-14-2)
	6	selected for EP
S_{ster}	12	RMSD of S_{ster}
	15-25	EP
	15	selected for EP
$S_{mass}^{salti-ster}$	12	EP of S_{tot}^{salti} and S_{ster}
$S_{mass}^{sreco-ster}$	16	EP of S_{tot}^{sreco} and S_{ster}
S_{mass}	15	RMSD using various S_{ster} (Tab. F-14-2)
S_{mass}^g	7	EP of GRACE
	16	selected for EP
$dM/dt^{reco-ster}$	23	EP of $S_{mass}^{reco-ster}$
	1.5	RMS diff. of solutions (Tab. F-14-2)
dM/dt^g	10	EP of S_{mass}^g
	23	selected for EP
E	4.2-4.8	Yu et al., 2008
	4	RMSD of E datasets (Tab. F-14-2)
	5	selected for EP
P	9-12	Adler et al., 2012
	6	RMSD of P datasets (Tab. F-14-2)
	10	selected for EP
E-P	11 i	EP
	6	RMSD of E-P datasets (Tab. F-14-2, F-14-3)
	11	selected for EP
R	2	STD of R
B	2	STD of B
G	25	EP including all components
	11	EP of E-P, neglect R, B, dM/dt
	7	RMSD of results

Meyssignac et al. 2011) one finds a good agreement with a correlation 0.95 and RMS differences 9 mm (see Tab. F-14-2). The advantage of the MBMED11 reconstruction, compared to an alternative one by Calafat and Gomis (2009), is the use of the long-term sea level patterns deduced from a 33-year long run of the ARPERA-forced NEMOMED8 ocean model (Sevault et al., 2009) instead of a 13-year long altimetry record as in Calafat and Gomis (2009), which enables to better capture Mediterranean sea level decadal variability of specific interest to our study (Meyssignac et al. 2011). We compute the steric component of sea level S_{ster} , taking into account both the effects of temperature ($S_{thermo-ster}$) and salinity ($S_{halo-ster}$). Temperature and salinity fields are obtained from two gridded climatologies: the regional Medar/Medatlas (Rixen et al. 2005; available yearly 1970-2002) and the global Ishii (Ishii and Kimoto 2009; available monthly 1970-2006); and also from the MFSTEP oceanographic model (Tonani et al., 2008; 2002-2009). We integrate from the surface down to the maximum depth with available data (see Tab. F-14-4). It is noted that models routinely provide potential temperature (Fofonoff, 1977), while climatologies give in-situ temperature; this is accounted for in our analysis concerning the estimation of steric heights.

Table F-14-5: Standard deviation (STD), trend and its significance of observed and simulated water cycle parameters in 1979-2001.

	STD (mm/mo)	Trend (mm/mo)/yr	Significance %
$E_{protheus}$	3.3	0.03 ± 0.08	-
$P_{protheus}$	4.1	-0.13 ± 0.13	75
$R_{protheus}$	2.0	-0.10 ± 0.06	90
$B_{protheus}$	2.2	-0.00 ± 0.06	-
$G_{protheus}$	7.9	0.34 ± 0.22	90
$(E - P)_{protheus}$	5.7	0.15 ± 0.14	75
$(R + B)_{protheus}$	3.4	-0.10 ± 0.11	75
$(E - P - R - B)_{protheus}$	8.5	0.25 ± 0.20	75
$E_{oaf flux}$	6.9	0.43 ± 0.09	99
P_{gpcp}	4.0	-0.31 ± 0.13	99
$E_{oaf flux} - P_{gpcp}$	8.2	0.74 ± 0.13	99
$E_{oaf flux} - P_{gpcp} - (R + B)_{protheus}$	6.9	0.84 ± 0.20	99
dM/dt	1.6	-0.09 ± 0.13	99
$E_{oaf flux} - P_{gpcp} - (R + B)_{protheus} + dM/dt$	9.1	0.74 ± 0.23	99
$E_{oaf flux} - P_{gpcp} + dM/dt$	8.4	0.66 ± 0.14	99

Table F-14-6: Correlation and significance of climatic index with variables in 1970-2006. For sea level the component type is indicated by the subscript (tot: total sea level; ster: steric sea level; thermo-ster: thermo-steric sea level; halo-ster: halo-steric sea level; mass: mass induced sea level)

Climatic Index	Field	Correlation	Significance %
NAO_{DJFM}	dM/dt	0.64	99
NAO_{DJFM}	SLP (HadSLP)	0.81	99
NAO_{DJFM}	P_{reofs}	-0.70	99
NAO_{DJFM}	$R_{protheus}$	-0.77	99
AMO	Eoaf flux	0.9	99

We compute annual basin means of S_{ster} , S_{tot} , and their difference S_{mass} to derive its rate of change $\frac{dM}{dt}$. The overlap between the GRACE-based mass estimate S_{mass}^g and the indirect sea-level-based mass derivations (two separate ones from altimetry and reconstruction) over the common 2002-2009 period allows a comparison of the various methods as a mean to gain a sense of the uncertainties associated to the mass estimates (see Tab. F-14-3 for comparisons; Calafat et al. 2010, Fenoglio-Marc et al., 2012). It is worth noticing that over the common period, the GRACE mass change estimate (including both water and salt mass changes) is found to be largely similar to the indirect sea-level based derivation which only includes the effect of water mass changes in virtue of the steric correction (see Section 3.1). This suggests that, at least for this period, mass changes measured by GRACE were mostly water induced.

2.2 Observational Evaporation and Precipitation data

Both oceanic evaporation and precipitation are challenging quantities to derive, as neither is directly observed. Mariotti (2010) provides a recent intercomparison of estimates for the Mediterranean Sea from various datasets and methodologies over the period since the late-

1950s and allows qualitative insights into the uncertainties associated with Mediterranean Sea E and P estimates. In this study, we choose to use selected estimates of E and P among those analyzed by Mariotti (2010) rather than explore the full range of estimates available, while keeping in mind the range of uncertainties highlighted by the Mariotti (2010) study. For evaporation over the period 1958-2006, we use the derivation from the air-sea fluxes dataset OAFLUX, which objectively synthesizes surface meteorology obtained from satellite products (including SSM/I, Quick Scatterometer (QuikSCAT), Advanced Very High Resolution Radiometer (AVHRR), Tropical Rainfall Measuring Mission (TRMM)) and model NCEP re-analyses (Yu et al. 2008). For precipitation over 1979-2006, we consider data from the Global Precipitation Climatology Project (GPCP; Adler et al. 2003). Back in time, for the period 1960-2006 we use a reconstruction of oceanic precipitation (REOFS hereafter; Smith et al., 2008), which aims at capturing the large-scale features of global precipitation. Estimated OAFLUX evaporation error for the Mediterranean Sea is 4.2-4.8 mm/mo (5-6 Wm^2 or more conservatively 5-8 Wm^2 ; Yu et al., 2008). Estimated GPCP precipitation error is 9-12 mm/mon for GPCP (0.3-0.4 mm/d; Adler et al, 2012). No error estimate is available for REOFS (see Tab. F-14-4 for intercomparison of error estimates).

2.3 Climate Model Simulation

We consider results from a regional ocean-atmosphere coupled model simulation with the PROTHEUS system (Artale et al, 2010). The PROTHEUS system includes the RegCM3 atmospheric regional model (Pal, 2007) and the MED-MITgcm ocean model (Sannino et al., 2009b, Marshall, 1997), that are coupled through the OASIS3 coupler (Valcke and Redler, 2006). It is a hydrostatic ocean model that uses the Boussinesq approximation (volume-conserving condition) (Song and Hou, 2006). As the volume of water in the model domain is conserved by model construction the volume of water lost from the Mediterranean basin is balanced by means of a positive flux of water over the Atlantic box (see Carillo et al. 2012 for a complete validation of the ocean model). The experiment considered here is a simulation of climate variability in the European-Mediterranean domain over the period 1958-2001 at a spatial resolution of 30 km for the atmospheric component and $1/8^\circ \times 1/8^\circ$ for the oceanic model. The model includes the Interactive River Scheme (IRIS) that computes river discharge from runoff (Dell'Aquila et al., 2011). The oceanic and the atmospheric models exchange coupling fields (SST, wind stress components and total heat and salt fluxes) every 6 hours. Surface natural boundary conditions are used for the oceanic model which treats P+R-E as a real fresh water flux. The ocean component is initialized with MEDATLAS II data (MEDAR-Group, 2002), then a 40 year spin-up is performed using a 3D relaxation of temperature and salinity to the climatological values. ERA40 re-analyses (Uppala et al., 2005) are used as atmospheric lateral boundary conditions. The two-way exchange through the Strait of Gibraltar is achieved by means of 3D relaxation of salinity and temperature toward the climatological monthly Levitus data (Levitus, 1982), in a box composed by 30 grid points located west of Gibraltar. The PROTHEUS net water flux at Gibraltar is computed as the volume transport through a latitudinal section, derived as difference of the two-way exchange given in Fig. F-14-AUX3.

Since observational estimates of R and B times series for the period 1970-2009 are not available, we consider R, B values from the PROTHEUS simulation as observational surrogates, to be used in the water budget equation (Eq. 1) to derive G, together with data from observational datasets. However the modeled terms are roughly an order of magnitude smaller than E (Mariotti et al., 2002), hence are second order factors in the estimation of G. Because of the different assumptions in the simulated G versus the indirectly observationally derived

G, comparing the two allows to both corroborate independently derived G estimates and also explore whether the model condition is indeed a realistic assumption.

2.4 Climatic indices

We consider various climatic indices to explore the role of large-scale climate phenomena on long-term G variability as it relates to other water cycle changes. Specifically, the December-March (DJFM) station-based NAO index calculated as the normalized pressure difference between Gibraltar and South West Iceland [Jones et al., 1997]; and the annual AMO index available from NOAA/OAR Physical Science Division calculated as the de-trended area-weighted average of North Atlantic (0° to 70° N) Sea Surface Temperature (SST) (available since 1856) [Enfield et al., 2001]. To compare with the NAO index, we consider DJFM means of Mediterranean mean P, R and $\frac{dM}{dt}$, and compute six-years running means to focus on long-term variability. In this analysis, we also include monthly mean sea-level pressure from the HadSLP2 dataset (SLP), combining land and marine pressure observations [Allan and Ansell, 2006]. In the comparison with the AMO index, we consider six-year running means of annual values. Annual mean anomalies are relative to the period 1979-2001, as this is the common period of availability for all data used.

3. Results

3.1 Mediterranean Sea Mass variability

Figure F-14-1 shows anomalies of annual mean basin-averaged sea-level in 1970-2009, as derived from the altimeter measurements (S_{tot}^{alti}) and the sea-level reconstruction (S_{tot}^{reco}). Over the 1970-2005 period, reconstructed sea-level displays both interannual and decadal variations with relative minima observed around 1975 and 1994. The monthly error associated with the reconstructed basin-averaged sea-level estimated by a bootstrap method (Efron and Tibshirani, 1993) is about 20 mm and significant at the 95% level (see Meyssignac et al. 2011 for more details). The corresponding annual mean error is 6 mm. The annual mean error of the altimetric basin-averaged sea level is 3 mm based on a RMS difference between data sets (Tab. F-14-4, see also Fenoglio-Marc et al., 2012). Overall, there is very good consistency for basin averaged sea-level between the altimeter estimates and the reconstructed estimates, which reinforces confidence in the sea-level reconstruction for the earlier period. Over the common interval 1993-2005, yearly mean sea-level estimates from the reconstruction and from the altimeter observations are in good agreement with a 0.98 correlation and 4 mm RMS difference (Tabs. F-14-2, F-14-4). We finally assume a value of 6 mm for the error of the combined sea level S_{tot} , to account for the lower accuracy of the reconstruction before the altimeter era (Tab. F-14-4). The overall trend of the combined sea level S_{tot} over 1970-2009 is 1.9 ± 0.2 mm/yr.

Figure F-14-2 shows the annual basin average anomalies of the steric component (S_{ster}) derived from the Medar/Medatlas and from the Ishii gridded climatologies. Over the common interval 1945-2002 correlation and RMS difference between the two derivations are 0.57 and 12 mm, with correlation significant at the 99% level (Tab. F-14-2). The RMS difference mainly arises from the difference in halo-steric components, which are still significantly correlated at the 99% level (correlation and RMS difference of 0.36 and 12 mm, respectively). The thermo-steric components (Sthermo-ster) are more similar (correlation and RMS difference are 0.81 and 5 mm respectively). These differences can be partly attributed to the different depths

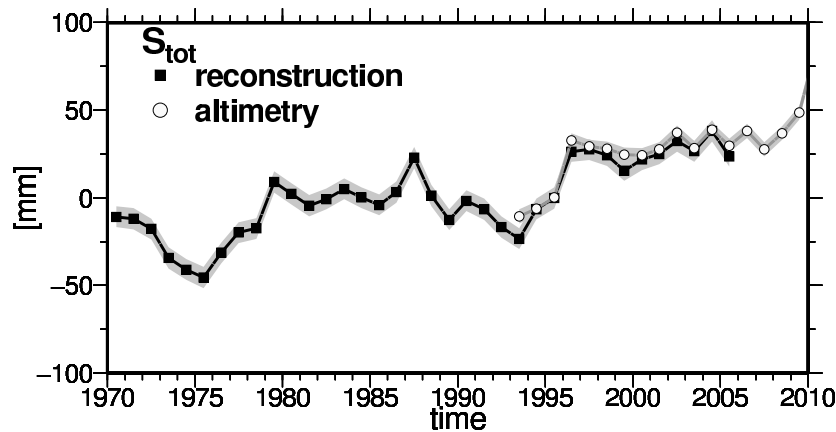


Figure F-14-1: Yearly mean sea level anomaly in the Mediterranean Sea over the period 1970-2009 derived from multi-satellite altimetry (circle) and from MBMED11 reconstruction (square) with error bounds corresponding both to the RMS difference of input data (gray shadow).

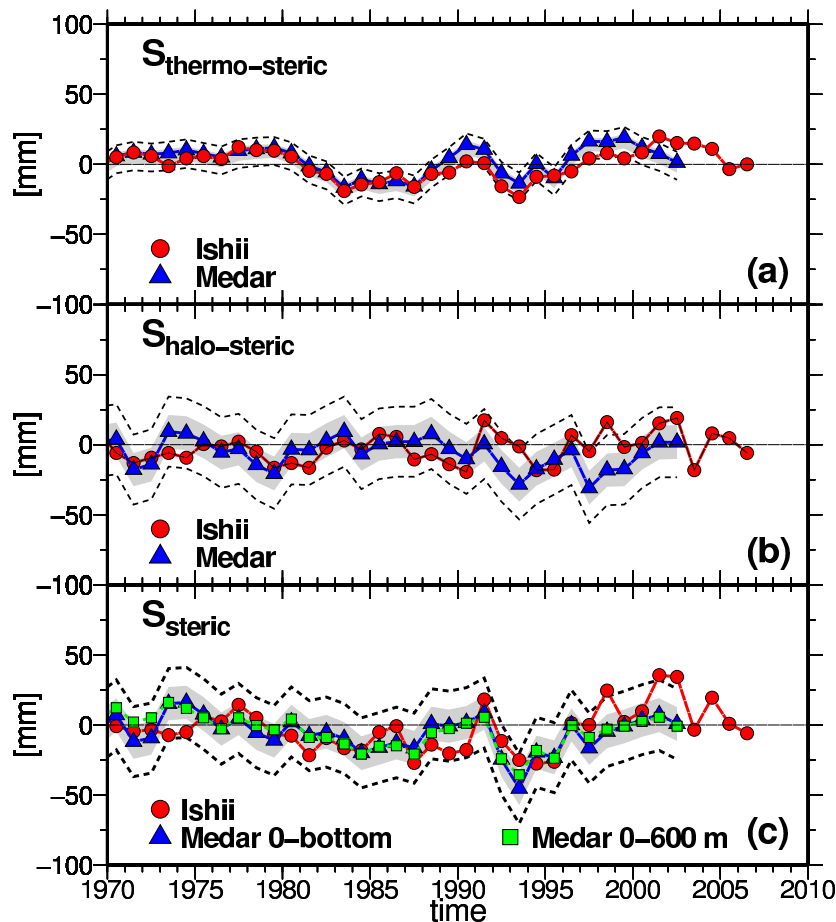


Figure F-14-2: Yearly mean thermo-steric (a), halo-steric (b), total steric (c) sea level anomalies in the Mediterranean Sea over the period 1970-2006 from Ishii version 6.7 (circle) and Medar/Medatlas integrated until 4000 meter depth (triangle). In c) Medar/Medatlas integrated until 600 (square) is shown in addition. Error bounds computed from Medar/ Medatlas (dashed line) and corresponding both to the RMS difference of input data (gray shadow) are given.

covered by the Ishii and Medar/Medatlas datasets (maximum depths available are 700 m and

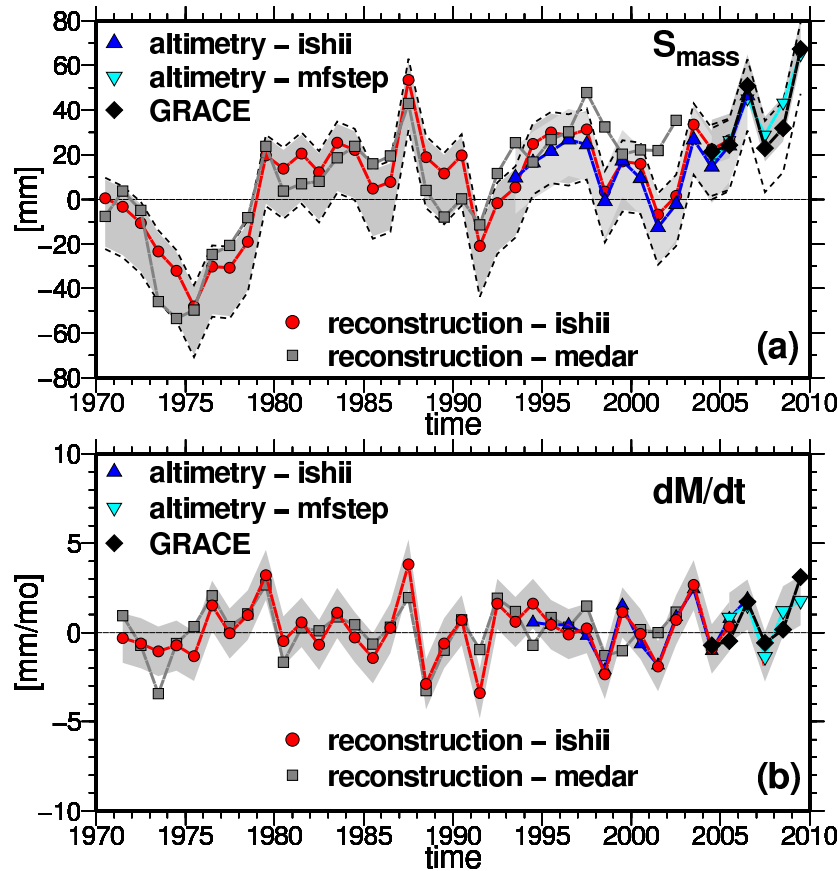


Figure F-14-3: Yearly mass-induced sea level anomaly in Mediterranean Sea (a) and its time derivative (b) over the period 1970-2009. Shown are estimates based on the steric-corrected sea-level reconstruction using two different steric corrections (squares for Medar/ Medatlas and circles for Ishii), on the steric-corrected sea-level altimetry using two different steric corrections (inverted triangles from MFSTEP and triangles from Ishii) and on GRACE-based mass retrievals (diamonds). Bounds in (a) correspond both to error propagation of components (dashed line) and to RMS difference of solutions derived from input data in Figs. F-14-1 and F-14-2 (gray shadow). In (b) only bounds corresponding to RMS of solutions are shown.

4000 m respectively) and partly attributed to the different values of temperature and salinity in the databases. As results do not change significantly when integrating Medar/Medatlas to 600 m only (see Fig. F-14-2) we may conclude that this second reason holds. The RMS-based error of 12 mm derived above is our first estimate of the error of the steric component (Tab. F-14-4). Another estimate is obtained from the grid of statistical errors associated to each Medar/Medatlas grid (Rixen et al, 2005). The error of the basin average of temperature (T) and salinity (S) for different intervals in depths has been computed from the grid of statistical errors. The error associated with the specific volume has been evaluated as :

$$\epsilon(\alpha) = \left| \frac{\partial \alpha(S, T, P)}{\partial S} \right| \epsilon(S) + \left| \frac{\partial \alpha(S, T, P)}{\partial T} \right| \epsilon(T) \quad (\text{F-14-3})$$

where $\epsilon(T)$ and $\epsilon(S)$ are the objective analysis errors associated to T and S and are function of time and space. A Monte-Carlo approach is used to perturb $\epsilon(T)$ and $\epsilon(S)$ so as to obtain the associated specific volume anomaly. The gridded temperature and salinity fields were perturbed within the range of its associated temperature and/or salinity uncertainty so as to infer total, thermo and halosteric uncertainty; 100 members were sufficient to make the

algorithm converge. Steric anomalies were directly confronted to the unperturbed reference. Figure F-14-AUX1 (additional material) shows basin averages of temperature and salinity data averaged over different intervals of depths together with the corresponding uncertainty. Being the variability range of temperature and salinity higher at the surface than at depth, and despite the lower amount of data at deeper levels, the uncertainty of the data decreases with depth. The uncertainties of the basin averages is between 0.1 and 0.2 °C in the first 150 m and lower than 0.1 °C below 150 m. Uncertainties are higher at both ends of the 1945-2002 period due to the lower amount of observations available to the objective analysis. The volume uncertainty derived from a Monte Carlo perturbation of temperature and/or salinity for year 1995 (3-year running window) is illustrated in Fig. F-14-AUX3. The steric uncertainty contributions are mainly located in deep ocean basins, as uncertainties are then integrated over larger depths. The halo-steric uncertainties dominate and reach 10 mm in the top 600 m and 15-25 mm in the complete water column (Tab. F-14-4). This is mainly due to the scarcity of salinity data in the (eastern) Mediterranean. Results for other years in the 1960-1995 period are qualitatively similar. In summary, results suggest that the total steric anomaly uncertainties are lower than 25 mm for the whole water column. The uncertainty is lower near to the surface and is less than 5 mm for the 0-150 m layer, less than 10 mm for the 150-600 m layer and less than 15 mm for the 600-4000 m layer. It is however well known that theoretical errors provided by the objective analysis techniques usually underestimates actual errors, therefore errors could be higher. We observe that the error estimated for Medar/Medatlas is larger than the error derived for RMS difference of data. We finally assume a value of 15 mm for the error of the combined steric sea level S_{ster} (Tab. F-14-4). The two different estimates of the steric component are quite consistent (Fig. F-14-2, c). They show a tendency for the steric component to decrease from 1970 until the mid-1990s and increase thereafter (considering Ishii data, trends are -1.02 ± 0.34 mm/yr during 1970-1990 and 1.19 ± 0.8 mm/yr during 1990-2006).

As described in previous section, the steric component of basin-averaged sea level (as shown in Fig. F-14-1) is used in combination with basin-averaged sea-level estimates (as shown in Fig. F-14-1) to derive basin-averaged Mediterranean water mass variations S_{mass} . Figure F-14-3 shows annual mean basin-average Mediterranean Sea water mass anomalies over the period 1970-2009 based on the multiple sea-level and steric components estimates described above. Overall the various estimates depict a quite consistent behavior during the periods for which the data overlap both on interannual and longer timescales. Specifically, the correlation and RMS differences between the mass derivations considering the two different steric corrections of the sea-level reconstruction are 0.8 and 15 mm, respectively, with correlation statistically significant at the 99% confidence level (Tab. F-14-2). Nevertheless there are differences among these estimates, highest differences are found in mid-1970s and early 1990s, which are however within the error bars based on Fig. F-14-2. Mass estimates from the Ishii steric-corrected sea-level reconstruction and the Ishii steric-corrected altimetry values are in particularly good agreement during 1993-2006. Similarly there is very good agreement between the mass estimates from the MFSTEP steric-corrected altimetry and the direct mass retrievals from GRACE for the most recent period (Fig. F-14-3). As previously mentioned, the agreement between GRACE and the steric-corrected reconstructions during the period of overlap suggests that the mass changes measured by GRACE are primarily water mass induced. Relative minima occur in the mid-1970s, the early 1990s and early in the 2000s. Over the long-term, considering the period since 1970s, Mediterranean Sea water mass is seen to increase (this is consistent with Calafat et al., 2010). The trend over the period 1970-2006 is 0.88 ± 0.33 mm/yr based on the reconstruction corrected for the Ishii steric component. Considering the extended time series (1970-2009), that combines the reconstruction- and the

GRACE-based S_{mass} , the trend is 1.1 ± 0.3 mm/yr. The estimate of the annual error of the mass-induced sea-level S_{mass} , derived by error propagation from the errors of S_{tot} and S_{ster} is 16 mm (dashed line in Fig. F-14-3.a), in very good agreement with the above obtained RMS difference-based error of 15 mm (shaded bounds in Fig. F-14-3.a). The annual error of GRACE-derived mass-induced sea-level S_{mass} is smaller (7 mm, see also Fenoglio-Marc et al., 2012). We finally assume a value of 16 mm for the annual error of the combined mass-induced sea-level S_{mass} over 1970-2009 (Tab. F-14-4).

Finally, the annual mean water mass change $\frac{dM}{dt}$ (the term that actually enters Eq. F-14-1) is derived over 1970-2009 as the difference of the combined mass-induced sea level S_{mass} at two following time steps. The timeseries shows interannual $\frac{dM}{dt}$ values of up to 3 - 4 mm/mo, its standard deviation is 1.8 mm (1.6 mm in 1979-2001, see Tab. F-14-5). The overall $\frac{dM}{dt}$ mean is 0.14 mm/mo as there is an overall mass increase over the period of consideration. However there is no significant $\frac{dM}{dt}$ trend over the period of consideration (trend value for the $\frac{dM}{dt}$ based on mass estimates from the reconstruction and Ishii steric correction is 0.018 ± 0.024 mm/mo per year). It is interesting to note that $\frac{dM}{dt}$ is small, as it is indeed often assumed to be according to the equilibrium condition; hence based on the water budget equation (Eq. F-14-1) we find a first order compensation between G and other terms of Mediterranean Sea water cycle, primarily E and P (another common assumption). We obtain for $\frac{dM}{dt}$ an annual error of 23 mm, from error propagation of S_{mass} . The annual error of the GRACE-based mass-induced sea-level $\frac{dM}{dt}$ is smaller (10 mm). Also the RMS difference of the various estimates of $\frac{dM}{dt}$ derived from various sea-level and steric data is significantly smaller (1.5 mm) (Tab. F-14-4). The standard deviation of $\frac{dM}{dt}$ is 1.6 mm and therefore much smaller than that its error.

3.2. Gibraltar water flux variability

Next, remaining Mediterranean Sea water cycle terms are considered in order to close the water budget (Eq. F-14-1) and derive G variability over the period 1960-2010 (see Fig. F-14-4; see Tables Tables F-14-2 and F-14-3 for correlation and RMS difference of the yearly time-series and Table F-14-5 for a comparison of observed and simulated trends over the period). Both observational and PROTHEUS-simulated estimated annual mean anomalies relative to the period 1979-2001 are considered for comparison (as available). Note that the PROTHEUS simulation is forced at the atmospheric boundaries by ERA40 reanalyses, independent from the observational estimates presented here. Mediterranean Sea averaged evaporation from OAFUX data shows an initial decrease 1960 to the mid-1970s, followed by an increase up until the most recent period (trend over 1979-2001 is 0.43 ± 0.09 mm/mo per year; see Mariotti 2010 for more discussion on decadal variability of Mediterranean Sea evaporation). PROTHEUS-simulated evaporation shows a similar decadal variability over the whole period, with basically no increase during 1979-2001 (Fig. F-14-4.a) GPCP precipitation shows a negative trend over the period 1979-2001 (-0.31 ± 0.13 mm/mo per year), similarly to the PROTHEUS-simulated one except the latter is smaller and weakly significant (Fig. F-14-4.b). EOF reconstruction also shows a precipitation decrease during 1979-2001 that is similar to GPCP but in the context of a long-term decrease during the period since 1960 (see also Mariotti, 2010). Correlation and RMS difference of the GPCP and EOF precipitation yearly values are 0.4 and 4.9 mm/mo respectively, correlation is significant at the 95% level (Tab. F-14-2). The correlation of simulated and observed evaporation and precipitation quantities are all significant, except for precipitation from REOFS (Tab. F-14-3). Their RMS differences are 4 mm/mo for evaporation and 6 mm/mo for precipitation (Tab. F-14-3); we adopt these

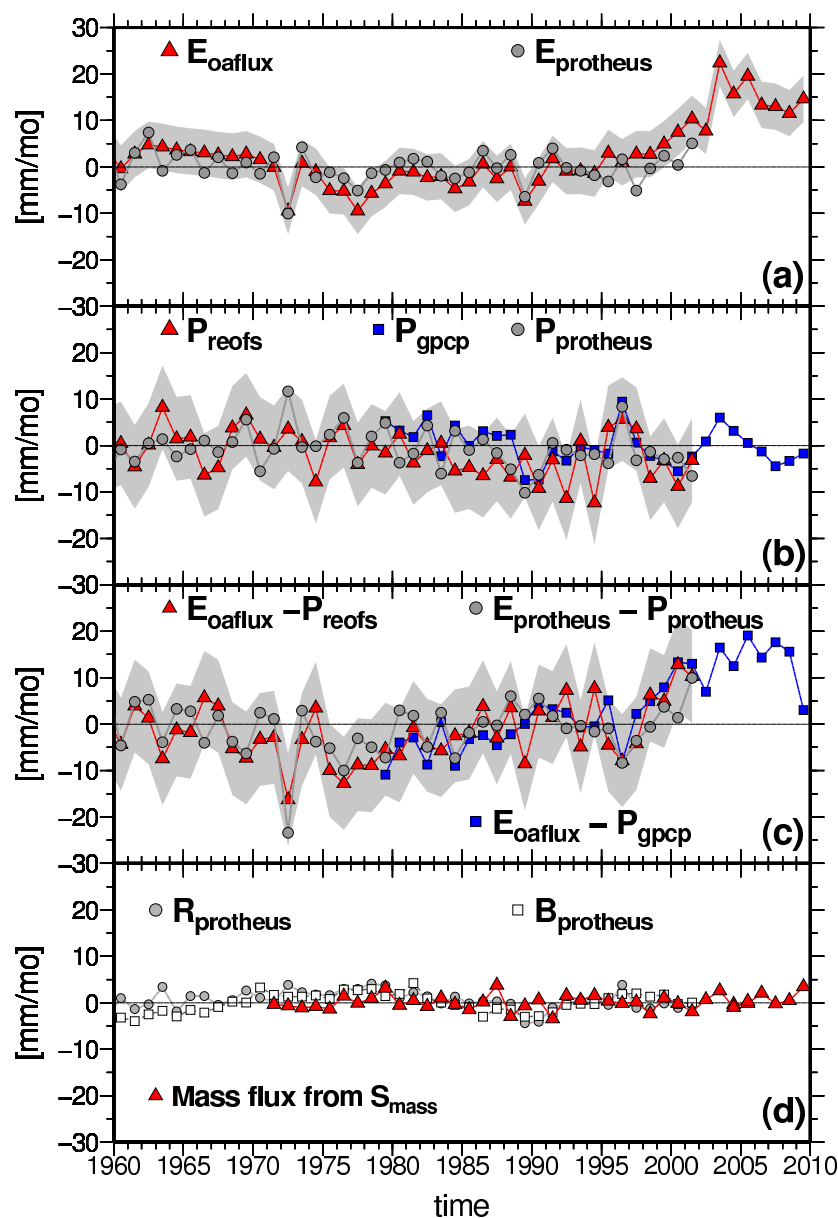


Figure F-14-4: Yearly anomalies of Mediterranean Sea water cycle components in water budget equation (Eq. F-14-1) during 1960-2009 relative to the period 1979-2001. From top to bottom: Evaporation (a), Precipitation (b), E-P (c), Bosphorus water flux, river discharge and time derivative of mass-induced sea level (Fig. F-14-3.b) (d) from model simulations (gray) and observations. Legend specifies data source. Error bounds in (a-b-c) correspond to the RMS difference of data input from databases (gray shadow).

values as the RMS-based errors for the two quantities (see Tab. F-14-4). We finally assume an error of 5 mm/mo and 10 mm/mo for the two quantities, thus error propagation gives a result of 11 mm/mo for E-P.

Based on the observational estimates, the combination of the evaporation increase seen in OAFLEX data and precipitation decrease seen in GPCP gives a significant increase in net evaporation (E - P) over the period 1979-2001 (Fig. F-14-4.c). Observationally derived trend over 1979-2001 is 0.74 ± 0.13 mm/mo per year. Simulated net evaporation trend is also seen to be positive, albeit weakly significant. The GPCP/OAFLEX E-P estimates indicate that

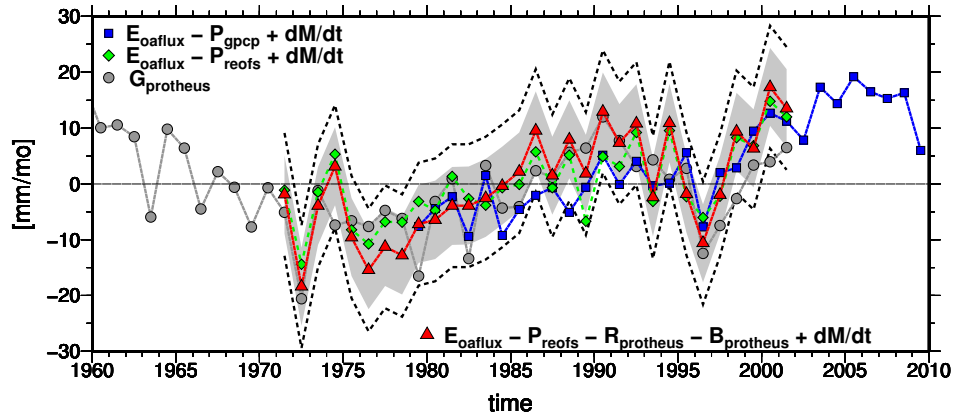


Figure F-14-5: Estimates of Gibraltar water flux anomalies during the period 1960-2010 (reference period is 1979-2001). Shown are yearly values from the PROTHEUS model simulation (circle) and from the water budget equation using observational estimates of E, P, dM/dt and simulated R and B (triangle), and similar estimates neglecting R+B (square, diamond). E is from OAFLUX, P is from the REOFS and from GPCP, dM/dt is from the steric corrected sea-level reconstruction using Ishii data. Error bounds correspond to the annual uncertainties given for E, P in Tab. F-14-4. Bounds correspond both to error propagation of components including only E, P (black dashed line) and to RMS difference of solutions including all components in Fig. F-14-4 (gray shadow).

the increase has been continuing up until the recent period (trend over 1979-2009 is 0.79 ± 0.1 mm/mo per year). Error propagation gives a result of 11 mm/mo for E-P (Tab. F-14-4), while the RMS-based error computed from various datasets is lower than 6.2 mm/mo (Tabs. F-14-2, F-14-3).

Since observational river discharge and Bosphorus water flux anomalies are not available for the period of investigation, we consider the simulated quantities as a surrogate (in any case, as previously discussed these are second order terms in Eq. F-14-1). Simulated river discharge shows a significant negative trend over 1979-2001 (-0.1 ± 0.06 mm/mo per year; Tab. F-14-5), consistent with simulated precipitation behavior. Simulated water flux at the Bosphorus Strait does not indicate a significant trend. Relying on a single run of a single model we cannot attribute an error bar to such estimate, however this fact does not impair our results, as the river runoff is, together with the Bosphorus the smallest term in Eq. F-14-1 and does not exceed the 20 (Fig. F-14-4.d), as the standard deviation of $\frac{dM}{dt}$ is 1.6 mm/mo (Tab. F-14-5) and therefore smaller than for all the other components in Eq. F-14-1.

Combining observational E and P estimates with simulated R and B, we obtain estimates of the overall mean fresh water budget anomalies that have characterized the Mediterranean Sea over 1979-2001. Interannual anomalies are of the order of 5-10 mm/mo with a linear trend over 1979-2001 of 0.84 ± 0.20 mm/mo per year (this trend value is based on GPCP precipitation, OAFLUX evaporation and simulated R and B), that is a linear increase of about 19 mm/mo in total over this period. The corresponding simulated fresh water budget quantity also shows an increase, however trend value is smaller than observed (0.25 ± 0.20 mm/mo per year or about 6 mm/mo in total over this period). Error propagation gives an error of 11 mm/mo for E-P-R-B, if we neglect the errors of R and B. If we assume for R and B an error equal to their standard deviation (2 mm/mo, Tab. F-14-4), the resulting error is not significantly different.

Finally, we combine the fresh water budget changes discussed above with mass changes $\frac{dM}{dt}$ as derived in the previous section to depict Gibraltar water flux (G) variability during 1960-

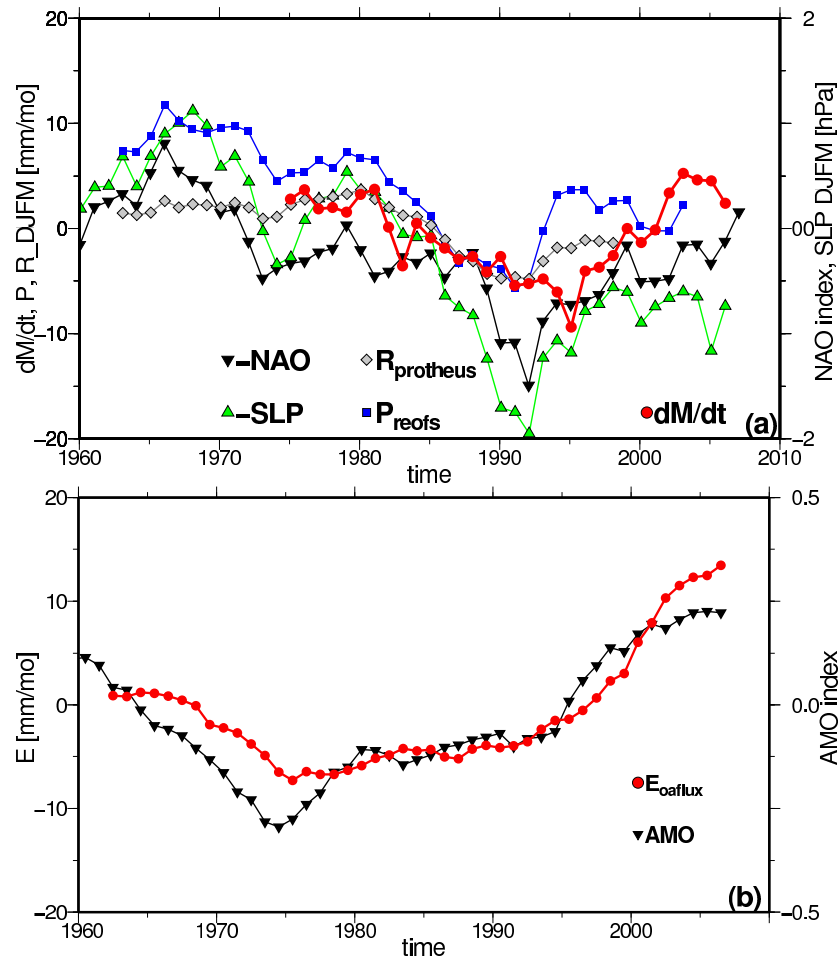


Figure F-14-6: Influence of large-scale climate modes on Mediterranean water mass budget components. DJFM yearly values of NAO index and anomalies of P, R sea level pressure, dM/dt (note: the signs of the NAO and SLP are reversed) (top panel) and yearly values of the AMO index and of OAFLEX evaporation anomalies (bottom panel). For all, a six-year running mean is shown to focus on long-term anomalies.

2009 based on the application of the water budget equation (Equ. F-14-1) (see Fig. F-14-5). All G estimates, whether combining observational and PROTHEUS-simulated terms or derived purely from the PROTHEUS simulation, show an overall increase in the net water flux at Gibraltar since the mid-1970s. It is worth underlying that a priori the observationally derived G and the PROTHEUS simulated G could be quite different, because of the assumptions built-in the model, in primis the equilibrium condition assumption. The best agreement with the model is obtained when all components of Eq. F-14-1 are included (correlation and RMS difference are 0.66 and 6 mm, see Tab. F-14-3); neglecting R and B, the correlation drops to 0.59, with significance level still 99%. If one neglects R and B, and derives G purely based on observations (using estimated $\frac{dM}{dt}$, OAFLEX evaporation and precipitation from either GPCP or REOFs), one still finds an increase in G since the mid-1970s that is consistent with the PROTHEUS simulated G estimate. Based on the combined observational/modeling approach we find for G a linear trend over the period 1979-2001 of 0.74 ± 0.23 mm/mo per year (see Tab. F-14-5), that is a linear increase of about 16 mm/mo over this period. The linear trend is even higher (0.80 ± 0.21 mm/mo per year) when the recent years are included (period 1970-2009) even neglecting the contribution of R and B. Simulated G values give similar qualitative results, however with a 50

The accuracy of the Gibraltar Strait flow is almost independent from the accuracy of the rate of change of mass in the basin, river runoff and the Bosphorus strait flow, as their magnitude is small when compared to the effect of evaporation and precipitation on the resulting Gibraltar net flux. The error estimate of G , derived by error propagation from each component in Tab. F-14-4, is 25 mm. This value is 3 times larger than the RMS difference (7 mm) of the various solutions obtained for G from the available data and models. For a realistic error estimate only the errors in E and P are considered and give an error of 11 mm/mo for the Gibraltar Strait flow.

3.3 Large-scale influences

In order to gain some insights on the mechanisms driving the long-term Gibraltar water flux changes described above, we explore the relationship with major large-scale climate phenomena known to have had significant influence on decadal climate variability over the Mediterranean region (Mariotti and Dell'Aquila, 2012). Fig. F-14-6.a shows the DJFM means of the NAO index (NAODJFM) and Mediterranean mean P , R and sea level pressure (SLP), with a 6-year moving average applied (see Tab. F-14-6 for correlation values among the various time-series). Consistently with previous studies, the NAO shows a significant negative correlation with regional precipitation (-0.70 based on REOFS). In addition we also find a significant negative correlation with regionally averaged simulated river-discharge (-0.77; as also shown by Struglia et al. (2004), based on observational river discharge). All correlations are significant at the 99% level. Observed NAO variability during 1960-2009, with a well-known long-term increase during the 1960s to the early 1990s (Hurrell, 1995), has resulted in a precipitation and river discharge decrease during winter with an overall effect on annual means of these water cycle quantities. This in turn has contributed to increase the Mediterranean Sea fresh water budget ($E-P-R$) and related water fluxes at Gibraltar based on results from this work.

Previous studies have suggested the NAO also impacts Mediterranean sea-level owing to the inverse barometer effect (IB) (e.g. as described by Tsimplis and Josey, 2001). However in our study the altimeter data have been corrected for direct atmospheric effects including the IB and the PROTHEUS model does not simulate the effect of pressure. Therefore the effects of the NAO through local pressure have been removed and should not impact estimated mass changes and Gibraltar fluxes. However, for DJFM, we find an anti-correlation between the NAO index and regionally averaged sea level pressure SLP (-0.81) and also a significant anti-correlation between the NAO and Mediterranean rate of mass change $\frac{dM}{dt}$ (-0.64). These results suggests that the NAO may affect the mass component of sea level S_{mass} through mechanisms associated to redistribution of water, other than the atmospheric pressure changes. Those mechanisms could be associated to winds near the Gibraltar strait (Menemenlis et al., 2007) and to ocean circulation. However, these hypotheses need to be substantiated by targeted process studies.

Recent studies have shown a significant connection between Mediterranean Sea SST and the AMO, as well a connection between regional surface air temperature and the AMO particularly during the summer season (Mariotti and Dell'Aquila, 2012; Marullo et al., 2011). Because of the impact temperature can have on the humidity gradient and sea surface evaporation, we investigate the linkage between the AMO and Mediterranean Sea evaporation variability. Fig. F-14-6.b, shows 6-years running means of OAFLUX annual Mediterranean Sea evaporation anomalies together with those of the AMO index. We find significant positive correlation between evaporation and the AMO (0.9) which is consistent with the thermody-

namical linkage hypothesized above. Again, this speculated connection needs to be investigated by further studies using different evaporation datasets and in-depth analyses of the thermodynamic changes associated with AMO variability in the Mediterranean. If confirmed, our study suggests that the impact of AMO variability on Mediterranean Sea is not only confined to Mediterranean SST (as also suggested by Mariotti and Dell'Aquila 2012) but also affects the sea more broadly with evaporation-driven changes in Gibraltar water fluxes.

4. Conclusions

We have explored the long-term variability of net water flux into the Mediterranean Sea at the Gibraltar Strait over the period 1960-2009 based on an approach combining multiple observational datasets and results from a regional climate model simulation. The approach includes deriving Gibraltar water fluxes from the application of the full Mediterranean Sea water budget equation using observationally based estimates of mass variation (from GRACE satellite and indirect derivations from steric-corrected sea level changes from altimetry and a sea-level reconstruction), evaporation, precipitation and simulated river discharge and Bosphorus Strait water fluxes. This derivation is compared with results from a simulation using the PROTHEUS regional ocean-atmosphere coupled model considering both individual water cycle terms and overall Gibraltar water flux. Based on observational estimates of Mediterranean Sea mass, we find that its changes are relatively small compared to water fluxes at the sea surface and with no long-term trend over 1970-2009. Hence, the equilibrium condition assumption, common to many Mediterranean Sea models is indeed a reasonable one. As a result, decadal variations in net evaporation (E-P) at the sea-surface drive changes in net inflow at Gibraltar as dictated by the water budget equation, while changes in river runoff and net inflow at the Bosphorus Strait have a secondary modulating effect. Estimates from this approach have been compared to the PROTHEUS simulated Gibraltar Strait water fluxes over the period 1960-2001. Results from both methodologies point to an increase in net water flux at Gibraltar over the period 1970-2009 (0.8 ± 0.2 mm/mo per year based on the observational approach) primarily resulting from an increase in evaporation and a decrease in precipitation during this period. Above mentioned G increase over 1970-2009 is in the context of broader decadal including a net Gibraltar water flux decrease during 1960-1970 before the 1970-2009 increase, as found in both observations and the model simulation. The accuracy of the Gibraltar Strait flow is virtually independent from the accuracy in the rate of change of mass in the basin, river runoff and Bosphorus strait flow, as their effect on the resulting Gibraltar net flux is small compared to the effect of evaporation and precipitation. Uncertainties associated with variations of evaporation and precipitation, underlying the observational derivation of Gibraltar fluxes, are particularly hard to quantify when dealing with decadal timescales. By means of data intercomparison, Mariotti (2010) showed that although differences exist in the amplitude of the evaporation increase from the mid-1990 to late 2010s, this increase is a robust feature of all analyzed datasets; similarly precipitation decrease from the mid-1970 to the mid-1990s is also a robust feature seen in various observational datasets. Hence, the increase in Gibraltar water fluxes over this period we derive based on observational datasets is also likely to be a robust feature although the exact amplitude of the increase needs to be further investigated. An additional boost in confidence in the results for G, is given by the fact that the PROTHEUS system independently simulates decadal G variability that is qualitatively similar to that derived from observations. A priori, because of the model built-in assumptions (in primis the equilibrium condition assumption), the observational and model G derivations could have significantly differed. A posteriori we find that they do not because, as we find in our observational analysis, the equilibrium assumption is indeed a reasonable one.

Our investigation points to an important role for large-scale climate variability, specifically the Atlantic Multi-decadal Oscillation (AMO) and the North Atlantic Oscillation (NAO) climate modes, in driving observed Gibraltar fluxes which needs to be further investigated. These climate modes appear to influence net water flux at Gibraltar indirectly via the influence they bear on regional evaporation, precipitation and runoff.

5. Acknowledgments

We thank L. Li and an anonymous reviewer for their comments that helped to significantly improve our manuscript. This study was partly carried out in the frame of the projects STREMP funded by the DFG/SPP1257 and TOPO-EUROPE funded by the EU. The PROTHEUS model simulation has been performed as part the CIRCE Integrated Project, funded under the European Commission Sixth Framework Program. The authors acknowledge M. Tsimplis and A. Shaw for helpful discussion providing the Medar/Medatlas data.

6. Auxiliary material

The first three figures of the auxiliary material have been discussed in the paper. Fig. F-14-AUX1 shows the long-term basin average of temperature and salinity of the Medar/Medatlas database and the corresponding uncertainty for selected depth intervals. Fig. F-14-AUX2, gives the uncertainty for the steric, thermo-steric and halo-steric sea level derived from the Monte Carlo analysis. Finally the transport at the Gibraltar Strait as evaluated from the Protheus model is represented in Fig. F-14-AUX3.

From the one dimensional analysis we have seen that the decadal sea level change in the Mediterranean Sea is driven by mass change, while the steric change contribution is less important. Similar conclusions follow from the two dimensional analysis based on Canonical Correlation analysis (PCA-CCA). For the first three modes of PCA-CCA the correlation between the temporal components of sea level and mass change is larger than 0.9. The first three modes represent together about 95% of the total variability. The highest correlation is obtained in the Eastern Mediterranean (1st mode) (Fig. F-14-AUX4). Also the PCA of each single field has temporal and spatial components which are similar for sea level and mass change (Figs. F-14-AUX5, F-14-AUX6). The first mode represents an oscillation in phase of the all basin with temporal component similar to the basin averaged variability in Fig. F-14-1 and F-14-3). Finally the PCA of the steric sea level component is given in Fig. F-14-AUX7.

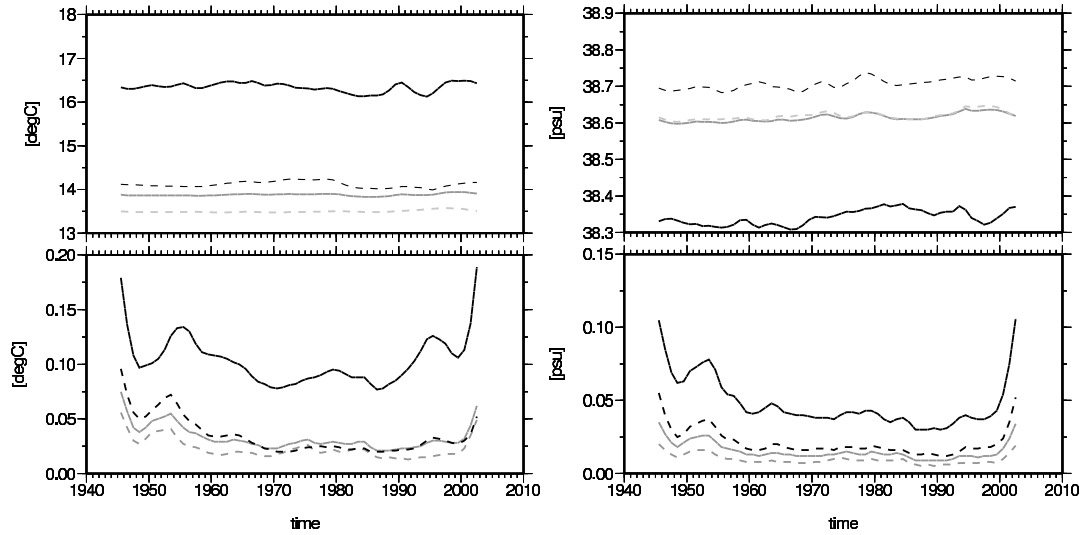


Figure F-14-AUX1: Long-term basin average over various depth intervals for sea water temperature (left) and salinity (right) from the Medar/Medatlas gridded database (top) and corresponding uncertainty (bottom) for various depth-intervals: surface-150m depth (black solid line), 150-600m (black dashed line), 600m-bottom (grey dashed line), full water column (grey solid line)

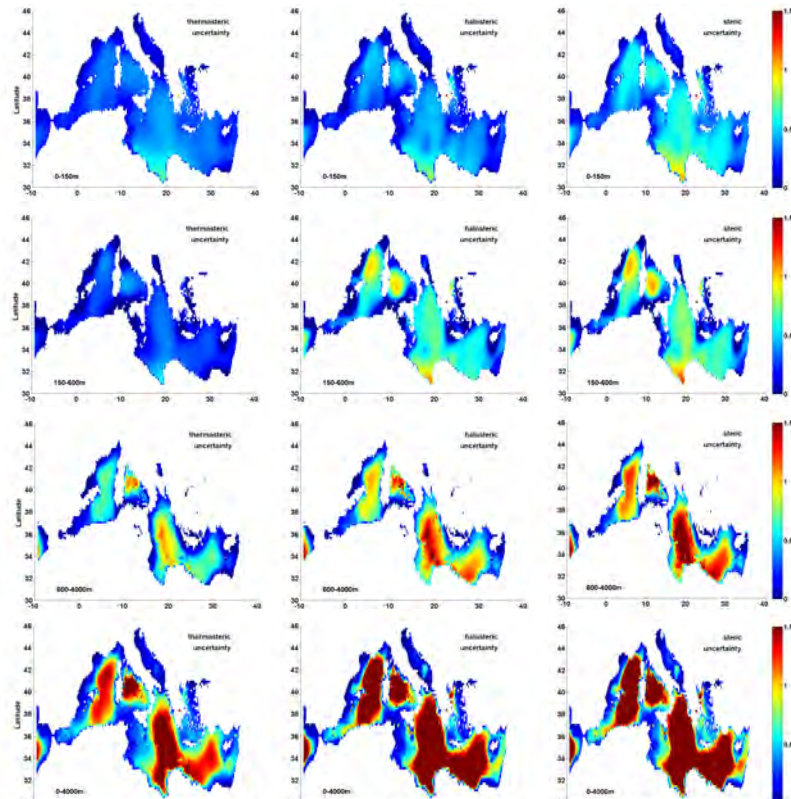


Figure F-14-AUX2: Uncertainty (cm) derived from Monte Carlo analysis of year 1995, 3-year running window for thermo-steric (left), halo-steric (middle) and steric (right) over various depth intervals. Rows from top to bottom correspond to 0-150m, 150-600m, 600-4000m and the whole water column 0-4000m.

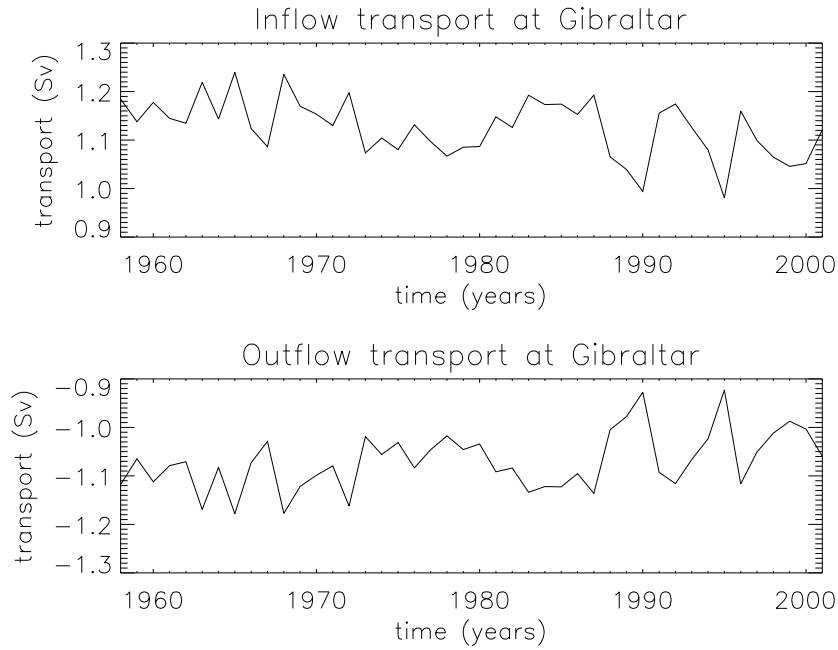


Figure F-14-AUX3: Inflow (top) and outflow (bottom) transport a Gibraltar evaluated from the Protheus model

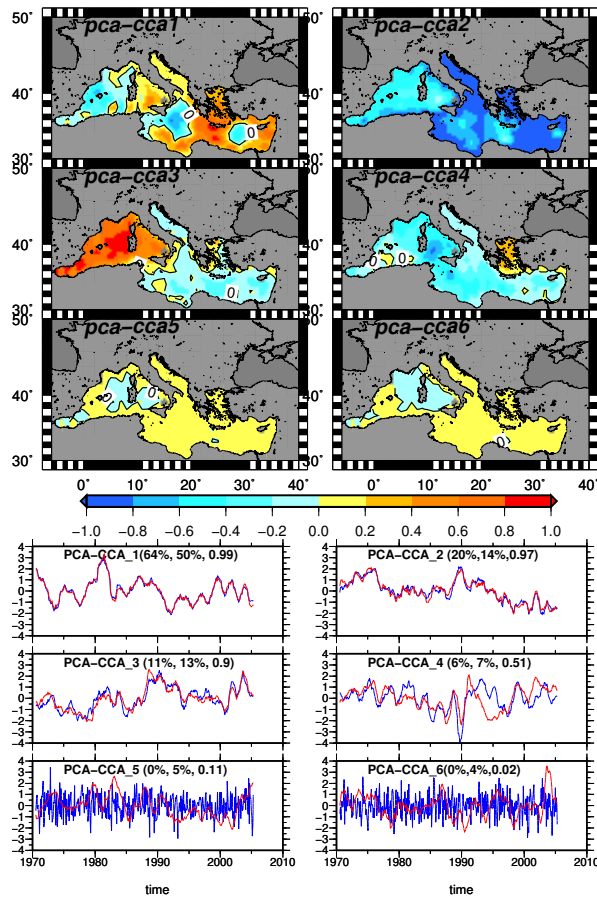


Figure F-14-AUX4: Dominant spatial patterns and temporal coefficients of the Canonical Correlation Analysis of sea level and mass change at interannual scales

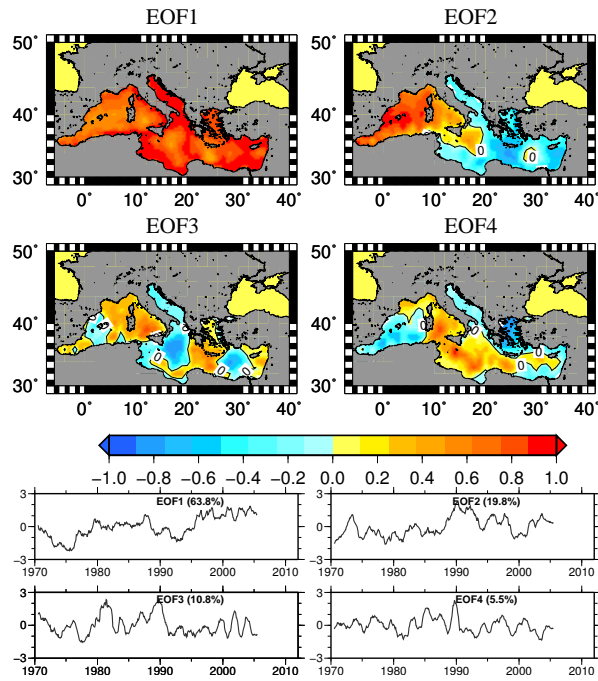


Figure F-14-AUX5: Dominant PCA spatial patterns and temporal coefficients of sea level variability at interannual scales

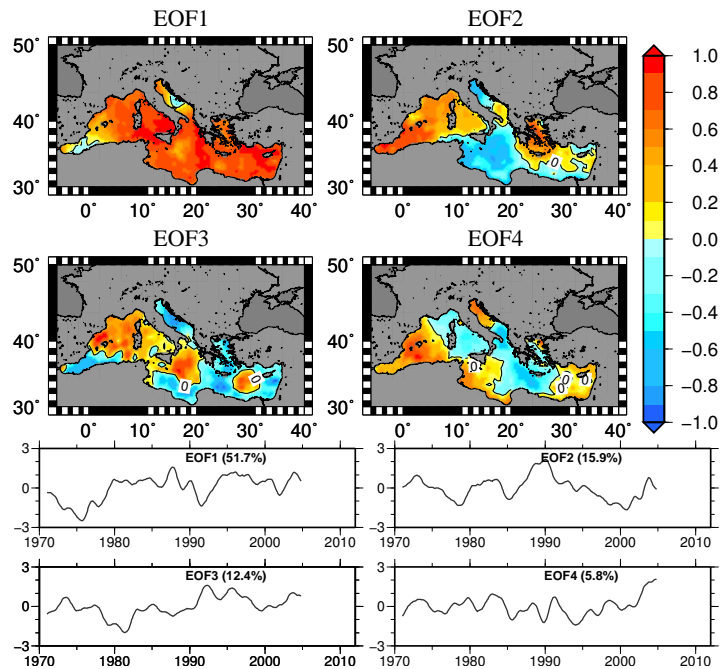


Figure F-14-AUX6: Dominant PCA spatial patterns and temporal coefficients of mass variability at interannual scales

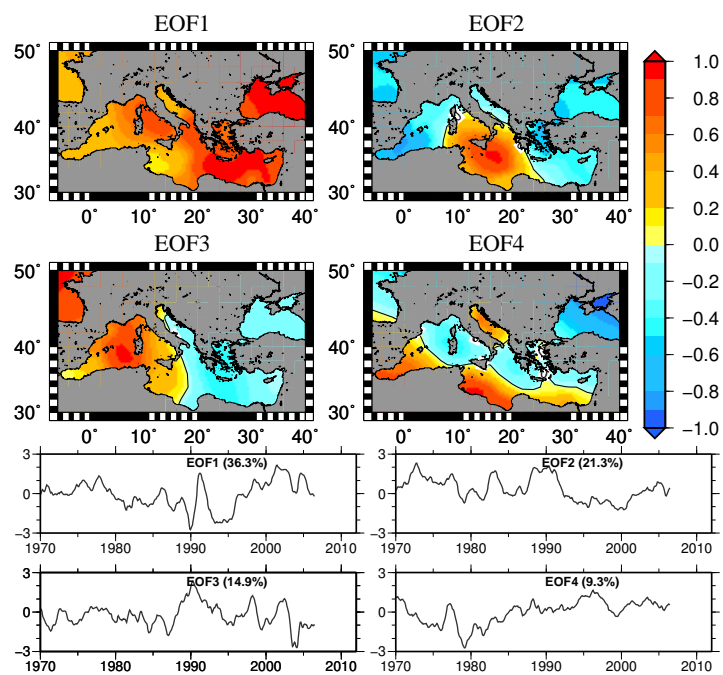


Figure F-14-AUX7: Dominant PCA spatial patterns and temporal coefficients of the steric component at interannual scales

7. References

- Allan, R., and T. Ansell, 2006. A new globally complete monthly historical gridded mean sea level pressure dataset (HadSLP2): 1850-2004 *J. of Climate*, 19(22), 5816-5842.
- Adler, R. F. and Coauthors, 2003. The version-2 Global Precipitation Climatology Project (GPCP) monthly precipitation analysis (1979-present). *J. Hydrometeorol.*, 4, 1147-1167.
- Adler, Robert F., Guojun Gu, George J. Huffman, 2012. Estimating Climatological Bias Errors for the Global Precipitation Climatology Project (GPCP). *J. Appl. Meteor. Climatol.*, 51, 84-99. doi: <http://dx.doi.org/10.1175/JAMC-D-11-052.1>
- Artale, V. and Coauthors, 2010. An atmosphere-ocean regional climate model for the mediterranean area: assessment of a present climate simulation. *Clim.Dyn.* 35, 721-740.
- Calafat F. and D. Gomis, 2009. Reconstruction of Mediterranean sea level fields for the period 1945-2000, *Global and Planetary Change*, 66, 225-234, doi:10.1016/j.gloplacha.2008.12.015
- Calafat F.M., M. Marcos and D. Gomis, 2010. Mass contribution to Mediterranean Sea level variability for the period 1948-2000, *Global and Planetary Change*, 73, 193-201, doi:10.1016/j.gloplacha.2010.06.002
- Calafat, F. M., G. Jordá , M. Marcos, and D. Gomis, 2011. Comparison of Mediterranean sea level variability as given by three baroclinic models, *J. Geophys. Res.*, VOL 117, C02009, doi:10.1029/2011JC007277.
- Carillo A., G. Sannino, V. Artale, P. M. Ruti, S. Calmanti, A. Dell'Aquila, 2012. Steric sea level rise over the Mediterranean Sea: present climate and scenario simulations, *Climate Dynamics*, doi :10.1007/s00382-012-1369-1
- Criado-Aldeanueva F., X. Soto-Navarro and J. Garcia-Lafuente, 2010. Seasonal and interannual variability of surface heat and freshwater fluxes in the Mediterranean Sea: budgets and exchange through the Strait of Gibraltar *Int. J. Climatol.* doi: 10.1002/joc.2268
- Dell'Aquila A., S. Calmanti, P. Ruti, M.V. Struglia, G. Pisacane, A. Carillo, G. Sannino, Impacts of long term fluctuations of the seasonal cycle in an A1B scenario over the Euro-Mediterranean area using a regional earth system model, submitted to *Climate Research*, 2011
- Enfield, D. B., et al., 2001. The Atlantic Multidecadal Oscillation and its relationship to rainfall and river flows in the continental U.S., *Geophys. Res. Lett.*, 28, 2077-2080. Fenoglio-Marc L., J. Kusche, and M. Becker, 2006. Mass variation in the Mediterranean Sea from GRACE and its validation by altimetry, steric and hydrologic fields, *Geophys. Res. Lett.*, 33, L19606, doi:10.1029/2006GL026851.
- Fenoglio-Marc L., J. Kusche, M. Becker and I. Fukumori, 2007. Comments on "On the steric and mass-induced contributions to the annual sea level variations in the Mediterranean Sea" by D. Garcia et al., *J. of Geophysical Res.*, Vol. 112, C12018,doi:10.1029/2007JC004196
- Fenoglio-Marc L. C. Braitenberg and L. Tunini, 2011. Sea level variability and trends in the Adriatic Sea in 1993-2008 from tide gauges and satellite altimetry, *Physics and Chemistry of the Earth*, doi:10.1016/j.pce.2011.05.014
- Fenoglio-Marc L., R. Rietbroek, S. Grayek, M. Becker, J. Kusche, E. Stanev, 2012. Water mass variation in the Mediterranean and Black Sea, *J. of Geodynamics.* doi:10.1016/j.jog.2012.04.001
- Flechtner F. (2007) GFZ level-2 processing standards documents for level-2 product release 4, GRACE 327-743, Rev. 1.0
- Fofonoff, 1977. Computation of potential temperature of sea water for an arbitrary reference pressure, *Deep Sea Res.*, 24, 489-491
- Grayek S., E. Stanev, R. Kandilarov, 2010. On the response of Black Sea to external forcing: altimeter data and numerical modelling, *Ocean Dynamics*, 60: 123-140
- Greatbatch R.J. and Lu, Y., 2001. Relaxing the Boussinesq Approximation in Ocean Circulation Models, *J. of Atmospheric and Oceanic Technology*, 1911-1923.
- Hurrell, J. W. 1995. Decadal trends in the North-Atlantic Oscillation Regional temperatures and precipitation, *Science*, 269(5224), 676-679.

- Hurrell, J. W., et al., 2003. The North Atlantic Oscillation: Climate Significance and Environmental Impact, 279.
- Ishii M., M. Kimoto, 2009. Reevaluation of Historical Ocean Heat Content Variations with Time-Varying XBT and MBT Depth Bias Corrections, *J. of Oceanography*, Vol. 65, 287-299
- Jones, P. D., et al., 1997. Extension to the North Atlantic Oscillation using early instrumental pressure observations from Gibraltar and south-west Iceland, *Int. J. Climatol.*, 17(13), 1433-1450.
- Levitus, S., 1982. Climatological Atlas of the World Ocean. NOAA Professional Paper 13, U.S. Government Printing Office, Washington D.C., 173pp.
- Mariotti, A., M.V. Struglia, N. Zeng, K.M. Lau, 2002. The Hydrological Cycle in the Mediterranean Region and Implications for the Water Budget of the Mediterranean Sea, *Journal of Climate*, 15, 1674-1690
- Mariotti, A., 2010. Recent Changes in the Mediterranean Water Cycle: A Pathway toward Long-Term Regional Hydroclimatic Change? (2010), *J. of Climate*, 23
- Mariotti, A. and A. Dell'Aquila, 2012. Decadal climate variability in the Mediterranean region : roles of large scale forcing and regional processes, *Clim Dyn*, doi:10.1007/s00382-011-1056-7
- Marshall, J., A. Adcroft, C. Hill, L. Perelman, C. Heisey, 1997. A finite volume, incompressible Navier Stokes model for, studies of the ocean on parallel computers. *J. Geophys. Res.* 102 (C3), 5753-5766
- Marullo S., V. Artale, R. Santoleri, 2011: The SST multidecadal variability in the Atlantic-Mediterranean region and its relation to AMO. *J. Climate*, 24, 4385-4401. doi: 10.1175/2011JCLI3884.1
- MEDAR Group, 2002. Medatlas/2002 database. Mediterranean and Black Sea database of temperature salinity and bio-chemical parameters. Climatological atlas. IFREMER Edition.
- Menemenlis D., J. Fukumori, T. Lee, 2007: Atlantic to Mediterranean Sea level difference driven by winds near Gibraltar Strait, *J. Phys. Oceanogr.*, 37, 359-376
- Meyssignac B., F. M. Calafat, S. Somot, V. Rupolo, P. Stocchi, W. Llovel, A. Cazenave, 2011. Two-dimensional reconstruction of the Mediterranean sea level over 1970 - 2006 from tide gauge data and regional ocean circulation model outputs. *Global and Planetary Change*
- Naeije M., R. Scharroo, E. Doornbos and E. Schrama, 2008. Global altimetry sea-level service: Glass, NUSP-2 report GO 52320 DEO, NIVR/DEOS, Netherlands
- Pal, J.S., F. Giorgi, X. Bi, N. Elguindi, F. Solmon, X. Gao, S. Rauscher, R. Francisco, A. Zakey, J. Winter, M. Ashfaq, F. Syed, J. Bell, N. Duffenbaugh, J. Karmacharya, A. Konar, D. Martinez, R. da Rocha, L. Sloan, A. Steiner, 2007. Regional climate modeling for the developing world: the ICTP RegCM3 and RegCM3. *Bull. Am. Meteorol. Soc.* 88, 1395-1409.
- Rixen M., J.M. Beckers, S. Levitus, J. Antonov, T. Boyer, C. Maillard, M. Fichaut, E. Baloupos, S. Iona, H. Dooley, M.-J. Garcia, B. Manca, A. Giorgetti, G. Manzella, N. Mikhailov, N. Pinardi and M. Zavatarelli, 2005. The Western Mediterranean Deep Water: a proxy for climate change, *Geophys. Res. Lett.*, 32, L12608, doi:10.1029/2005GL022702, 2949-2952
- Sanchez-Roman A., G. Sannino, J. Garcia-Lafuente, A. Carillo and F. Criado-Aldeanueva, 2009. Transport estimates at the western section of the Strait of Gibraltar: A combined experimental and numerical modeling study, *J. of Geophys. Res.* 114, C06002, doi:10.1029/2008JC005023.
- Sanchez-Garrido J.C., G. Sannino, L. Liberti, J. Garcia-Lafuente and L. Pratt, Numerical Modelling of Three-Dimensional Stratified Tidal Flow Over Camarinal Sill, Strait of Gibraltar, *J. Geophys. Research*, 2011 in press.
- Sannino G., L. Pratt and A. Carillo, 2009. Hydraulic criticality of the exchange flow through the Strait of Gibraltar, *J. of Physical Oceanography*, Vol 39, 11, 2779-2799. doi:10.1175/2009JPO4075.1
- Sannino, G., M. Herrmann, A. Carillo, V. Rupolo, V. Ruggiero, V. Artale, P. Heimbach, 2009b. An eddy-permitting model of the Mediterranean sea with a two-way grid refinement at the strait of Gibraltar. *Ocean Modelling* 30 (1), 56-72.

- Sannino, G., A. Carillo, and V. Artale, 2007. Three Player view of transports and hydraulics in the Strait of Gibraltar: A three dimensional model study, *J. Geophys. Res.*, 112, C03010, doi:10.1029/2006JC003717
- Santer, B. D., T. M. L. Wigley, J. S. Boyle, D. J. Gaffen, J. J. Hnilo, D. Nychka, D. E. Parker, and K. E. Taylor, 2000. Statistical significance of trends and trend differences in layer-average atmospheric temperature time series, *J. Geophys. Res.*, 105(D6), 7337-7356, doi:10.1029/1999JD901105.
- Sevault, F., S. Somot, J. Beuvier, 2009. A regional version of the NEMO ocean engine on the Mediterranean sea: NEMOMED8 users guide. Note de centre N 107, CNRM, Toulouse, France.
- Smith, T. M., M. R. P. Sapiano, and P. A. Arkin, 2008. Historical reconstruction of monthly oceanic precipitation (1900-2006). *Atmospheres*, 113, D17115, doi:10.1029/2008JD009851.
- Soto-Navarro, J., F. Criado-Aldeanueva, J. Garcia-Lafuente, and A. Sanchez-Roman, 2010. Estimation of the Atlantic inflow through the Strait of Gibraltar from climatological and in situ data, *J. Geophys. Res.*, 115, C10023, doi:10.1029/2010JC006302
- Song, T. and Hou, T., 2006. Parametric vertical coordinate formulation for multiscale Boussinesq, and non-Boussinesq ocean modeling, *Ocean Modelling* 11, 298-332.
- Struglia M.V., A. Mariotti, A. Filograsso, 2004. River Discharge into the Mediterranean Sea: Climatology and Aspects of the Observed Variability, *Journ. of Clim.* 17, pp. 4740-4751
- Tonani, M., N. Pinardi, S. Dobricic, I. Pujol, C. Fratianni, 2008. A high-resolution free-surface model of the Mediterranean Sea. *Ocean Sci.*, 4, 1-14, 1-14.
- Tsimplis M. and S. Josey, 2001. Forcing of the Mediterranean Sea by atmospheric oscillations over the North Atlantic, *Geophysical Research Letters*, 2001, 28, 803-806,5
- Uppala, S. M., Kellberg, P. W., Simmons, A. J., Andrae, U., Bechtold, V. D. C., Fiorino, M., Gibson, J. K., Haseler, J., Hernandez, A., Kelly, G. A., Li, X., Onogi, K., Saarinen, S., Sokka, N., Allan, R. P., Andersson, E., Arpe, K., Balmaseda, M. A., Beljaars, A. C. M., Berg, L. V. D., Bidlot, J., Bormann, N., Caires, S., Chevallier, F., Dethof, A., Dragosavac, M., Fisher, M., Fuentes, M., Hagemann, S., Hólm, E., Hoskins, B. J., Isaksen, I., Janssen, P. A. E. M., Jenne, R., McNally, A. P., Mahfouf, J.-F., Morcrette, J.-J., Rayner, N. A., Saunders, R. W., Simon, P., Sterl, A., Trenberth, K. E., Untch, A., Vasiljevic, D., Viterbo, P. and Woollen, J., 2005. The ERA-40 re-analysis. *Q.J.R. Meteorol. Soc.*, 131: 2961-3012. doi: 10.1256/qj.04.176
- Valcke S and R. Redler (2006) OASIS3 User guide. PRISM support initiative report no 4, 60 pp
- Yu L., X. Jin and R. A. Weller, 2008. Multidecade global flux datasets from the Objectively Analyzed Air-Sea Fluxes (OAFlux) Project: Latent and sensible heat fluxes, ocean evaporation, and related surface meteorological variables. Woods Hole Oceanographic Institution OAFlux Project Tech. Rep. OA-2008-01, 64 pp

Appendix A

Glossary

Table A1: Glossary

ALT-TG	Altimetry minus Tide gauge sea level
AMO	Atlantic Multidecadal Oscillation
AORCM	atmosphere-ocean regional climate model
APA	Air Pressure Anomaly
APAT	Agenzia per la Protezione dell'Ambiente e Servizi Tecnici
AR5	Fifth Assessment Report
AVISO	Archiving, Validation and Interpretation of Satellite Oceanographic data
AVHRR	Advanced Very High Resolution Radiometer
AWAC	Acoustic Wave and Current Profiler
BAKOSURTANAL	National Coordinating Agency for Survey and Mapping, Indonesia
BfG	Bundesanstalt für Gewässerkunde
BKG	Bundesamt für Kartografie und Geodäsie
BMBF	Bundesministerium für Forschung
BSH	Bundesamt für Seeschifffahrt und Hydrografie
BSHcmod	BSH circulation model
CCA	Canonical Correlation Analysis
CCI	Climate Change Initiative Program
CERSAT	Centre ERS d'Archivage et de Traitement - French ERS Processing and Archiving Facility
CHAMP	Challenging Mini-Satellite Payload for Geo-scientific Research and Applications program
CI	Completeness Index of the time series
CGSL	Coastal Global Sea Level
CGSLA	Coastal Global Sea Level from Altimetry, distance from coast < 150 Km
CGSLAT	Coastal Global Sea Level from Altimetry at selected TG locations
CGSLT	Coastal Global Sea Level at tide gauge locations
CLS	Collecte Localisation Satellites
CNES	Centre National d'Etudes Spatiales
CO ₂	Carbonic Dioxide
CODAR	Coastal Ocean Dynamics Applications Radar for measuring sea surface current
COASTALT	COASTal Altimetry Project
COSELE	COactal SEa LEvel
CRYOSAT-2	CRYOsphere SATellite 2010-
CSCF	Cumulative Squared Covariance Fraction
CTOH	Center for Topographic studies of the Ocean and Hydrosphere
CVF	Cumulative Variance Fraction
DAAD	German Academic Exchange Service
DAC	Dynamical Atmospheric Correction
DD	Delay-doppler
DEOS	Delft Institute for Earth-Oriented Space Research
DFG	German Research Foundation
DGFI	Deutsches Geodätisches Forschungsinstitut
DOF	Degree Of Freedom
DORIS	Doppler Orbitography und Radiopositioning
DWD	Deutscher Wetterdienst
DXO	Dual Crossover
ECMWF	European Centre for Medium-range Weather Forecasts
ECCO	Estimating the Circulation and Climate of the Ocean
ECV	Essential Climate Variables
EDOF	Effective Degree Of Freedom
EMB	Elektromagnetic Bias
ENSO	EL Nino Southern Oscillation
ENVISAT	European Space Agency Environmental Satellite 2002-2012
EPN	European Permanent Network
ERS-1	European Remote Sensing satellite 1, 1991-2000
ERS-2	European Remote Sensing satellite 2, 1995-2011
ESA	European Space Agency
EU	European Union
EUMETSAT	European Organisation for Exploitation of Meteorological Satellites
EVRF	European Vertical Reference Frame
ESEAS-RI	European Sea Level Service Research Infrastructure
ETRS89	European Terrestrial Reference System 1989
EUREF	IAG Reference Frame Sub-Commission for Europe

Table A1: Glossary

FBR	Full Bit Rate
FFT	Fast Fourier Transform
FINO	ForschungsInsel Nord- und Ostsee (FINO-1, FINO-2 und FINO-3)
FoV	Field of View
GCOS	Global Climate Observing System
GDACS	Global Data Assembly Centers
GEBCO	General Bathymetry Chart of the Ocean
GDR	Geophysical Data Records
GIM	Global Ionosphere Maps
GNSS	Global Navigation Satellite System
GPCP	Global Precipitation Climatology Project
GREF	Geodetic Reference Frame Network
GRS80	Geodetic Reference System 1980
GDR	Geophysical Data Records
GEO2TECDI	GEOdetic Earth Observation Technologies for Thailand
GEOSAT	GEOdetic SATellite 1985-1990
GFO	Geosat Follow-On 1998-2008
GGOS	Global Geodetic Observing System
GLDAS	Global Land Data Assimilation System
GIA	Geophysical Post Glacial Rebound
GITEWS	German Indonesian Tsunami Early Warning System
GMES	Global Monitoring for Environment and Security
GNSS	Global Navigation Satellite System
GPS	Global Positioning System
GRACE	Gravity Recovery and Climate Experiment
GSLA	Global averaged Sea Level from Altimetry
HY-2A	National Satellite Ocean Application Service, NSOAS P.R. China, 2011-
IAU	International Astronomical Union
IB	Inverse Barometer
ICA	Independent Component Analysis
IERS	International Earth Rotation and Reference Systems Service
IGS	International GNSS Service
IRI2007	International Reference Ionosphere
ITRF2005	International Terrestrial Reference Frame 2005
IERS	International Earth Rotation and Reference Systems Service
IFREMER	Institut Francais de Recherche et d'Exploitation de la MER
IGS	International GNSS Service
IMP	Improvement Percentage
INSAR	Interferometric Synthetic Aperture Radar
IPCC	Intergovernmental Panel on Climate Change
JASL	Joint Archive for Sea Level
JASON-1, -2	Joint Altimetry Satellite Oceanography Network -1 2001-2013, -2 2008-
JASON-CS	JASON Continuity of Service
L1b	Level 1 b
LAD	Land Dynamics
LEGOS	Laboratoire d' Etudes en Géophysique et Océanographie Spatiales
LRM	Low Resolution Mode
LSM	Land Surface Model (land) or Local Wave Model (sea)
GMSL	Global Mean sea Level
GOCE	Gravity field and steady-state ocean circulation explorer
GSLA	Global Sea Level from Altimetry
ME	Mean Error
MAE	Mean Absolute Error
MED	Mediterranean Sea
MEDCLIVAR	Mediterranean CLImate VARIability and Predictability
MFSTEP	Mediterranean Forecasting System Ocean Circulation Model
MLE3	Maximum Likelihood Estimator to solve for 3 parameters
MOG2D	barotropic 2D Gravity Waves model
MSL	Mean Sea Level
MWD	Mediterranean Freshwater Deficit
MWR	Microwave radiometer

Table A1: Glossary

NAO	North Atlantic Oscillation
NASA	National Aeronautics and Space Administration
NCAR	National Center for Atmospheric Research
NCEP	National Centers for Environmental Prediction
NEIC	National Earthquake Information Center
NEMO	Nucleus for European Modelling of the Ocean
NOAA	National Oceanic and Atmospheric Administration
NODC	National Oceanographic Data Center
NP	Normal Point
NRT	Near Real Time
OAFLEX	Objectively Analysed air-sea FLUXes for the Global Oceans
OCOG	OCenter Of Gravity retracker
PCA	Principal Component Analysis
PCA-CCA	Canonical Correlation in Principal Component Analysis basis
PPCA-CCA	Predicted Canonical Correlation in Principal Component Analysis basis
PDO	Pacific Decadal Oscillation
PODAAC	Physical Oceanography Distributed Active
PLRM	Pseudo Low Resolution (Pulse Limited) Mode
PROTHEUS	atmosphere-ocean regional climate model (AORCM) for the Mediterranean Sea
PSMSL	Permanent Service for Mean Sea Level
RADS	Radar Altimeter Database System
RECOSETO	REgional COastal SEa level change and sea surface TOpography
R-GDR	Retracked Geophysical Data Records for Topex/Poseidon
RMS, RMSE	Root Mean Square, Root Mean Square Error
SAMOSA	SAR Altimetry MOde Studies and Applications
SAR	Synthetic Aperture Radar
SELEN	SEa LLevel equatioN
SMOS	Soil Moisture and Ocean Salinity
SGDR	Sensor GDR
SH	Spherical Harmonics
SLR	Satellite Laser Ranging
SLV	Sea Level Variability
SO, SOI	El Nino Southern Oscillation, El Nino Southern Oscillation index
SONEL	Système d'Observation du Niveau des Eaux Littorales
SRAL	Synthetic Aperture Radar Altimeter on Sentinel-3
SSB	Sea State Bias
SSDT	Sea Surface Dynamic Topography
SSH	Sea Surface Height
SST	Sea Surface Topography
STA	Sea Temperature Anomaly
SVD	Singular Value Decomposition
SWH	Significant Wave Height
SWOT	Surface Water Ocean Topography
T/P	Topex/Poseidon (Ocean Topography Experiment) 1992-2005
TG	Tide Gauge
UNFCCC	United Nations Framework Convention on Climate Change
UHSLC	University of Hawaii Sea Level Center
U10	Wind Speed at 10 m height above sea level
VLBI	Very Long Baseline Interferometry
VLM	Vertical Land Motion
WDC-SS	World Data Center for Oceanography Silver Spring
WOA01	World Ocean Atlas 2001
WSA	Wind Speed Anomaly
WSV	Wasser- und Schifffahrtsverwaltung des Bundes
TIGA	GPS Tide Gauge Benchmark Monitoring
UELN	United European Levelling Network
VLBI	Very Large Base Interferometry
WaterGAP	Water Global Assessment and Prognosis
WSA	Wasser- und Schifffahrtsamt
WSV	Wasser- und Schifffahrtsverwaltung des Bundes
WAM	Wave model
WW3	Wave Watch III model

Bibliography

- Abdalla, S., P. A. E. M. Janssen, and J.-R. Bidlot, Altimeter Near Real Time Wind and Wave Products: Random Error Estimation, *Marine Geodesy*, 34, 393–406, doi:http://dx.doi.org/10.1080/01490419.2011.585113, 2011.
- Ablain, M., A. Cazenave, G. Valladeau, and S. Guinehut, A new assessment of the error budget of global mean sea level rate estimated by satellite altimetry over 1993–2008, *Ocean Sci.*, 5, 193–201., 2009.
- Amarouche, L., P. Thibaut, O. Z. Zanife, J.-P. Dumont, P. Vincent, and N. Steunou, Improving the Jason-1 Ground Retracking to Better Account for Attitude Effects, *Marine Geodesy*, 27(1-2), 171–197, doi:10.1080/01490410490465210, 2004.
- Aus der Beek, T., L. Menzel, L. Fenoglio-Marc, S. Grayek, R. Rietbroeck, M. Becker, J. Kusche, and E. Stanev, Modelling water resources of the Black and Mediterranean Sea river basins and their impacts on regional mass changes, *J. of Geodynamics*, doi:10.1016/j.jog.2011.11.011, 2012.
- Becker, M., B. Meyssignac, C. Leletrel, W. Llovel, A. Cazenave, and T. Delcroix, Sea level variations at tropical Pacific islands since 1950, *Global and Planetary Change*, 80-81, 85–98, doi:10.1016/j.gloplacha2011.09.004, 2012.
- Beckley, B. D., F. Lemoine, S. Luthcke, R. D. Ray, and Z. N.P., A reassessment of global and regional mean sea level trends from topex and jason-1 altimetry based on revised reference frame and orbits, *Geophys. Res. Lett.*, G 34, L14608, doi:10.1029/2007GL030002, 2007.
- Bindoff, N., J. Willebrand, V. Artale, A. Cazenave, J. Gregory, S. Gulev, K. Hanawa, C. Le Quere, S. Levitus, Y. Nojiri, C. Shum, L. Talley, and A. Unnikrishnan, *Climate change 2007: The physical Science Basis. Contribution of Working Group I to the Fourth Assessment report of the Intergovernmental Panel on Climate Change*, chap. Observations: oceanic climate and sea level., pp. 385–428., Cambridge University Press, Cambridge, UK, and New York, USA., 2007.
- Bouffard, J., L. Roblou, F. Birol, A. Pascual, L. Fenoglio-Marc, C. Cancet, R. Morrow, and Y. Ménard, *Coastal altimetry*, chap. Assessment of improved coastal altimetry strategies over the north western Mediterranean Sea, Springer Verlag, doi:10.1007/978-3-642-12796-0, 2011.
- Brown, G. S., The Average Impulse Response of a Rough Surface and Its Applications, *IEEE Transactions on Antennas and Propagation*, 25 n.1, 67–74, 1977.
- Buchhaupt, C., Entwicklung einer Toolbox in Matlab für Retracking and Validierung von pulse-limited und SAR Altimeterdaten im Küstenbereich, Binnengewässern und über Eisschilden, *Bachelor Thesis*, pp. 1–54, 2013.

- Buchhaupt, C., L. Fenoglio, M. Becker, and C. Prigent, Water level change in the Mekong Area , Poster, Living Symposium Edinburgh, ESA, 2013.
- Caballero, I., J. Gomez-Enri, S. Vignudelli, G. D. Quartly, C. P. Gommenginger, P. Cipollini, P. G. Challenor, and J. Benveniste, Validation of high Spatial resolution Wave Data from Envisat RA-2 Altimeter in the Gulf of Cadiz , *IEEE Geoscience and Remote Sensing Letters*, 2013.
- Calafat, F., and D. Gomis, Reconstruction of Mediterranean sea level fields for the period 1945-2000, *Global and Planetary Change*, 66, 225–234, doi:10.1016/j.gloplacha.2008.12.015, 2009.
- Cazenave, A., and W. Llovel, Contemporary sea level rise, *Annu. Rev. Mar. Sci.*, 2, 145–173, doi:10.1146/annurev-marine-120308-081105, 2010.
- Cazenave, A., and S. Nerem, Present-day sea level change, Observations and causes, *Rev. of Geophys.*, 42, doi:10.1029/2003RG000139, 2004.
- Cazenave, A., O. Henry, S. Munier, T. Delcroix, A. L. Gordon, B. Meyssignac, W. Llovel, H. Palanisamy, and M. Becker, Estimating enso influence on the global mean sea level, 1993-2010, *Marine Geodesy*, 35(sup1), 82–97, doi:10.1080/01490419.2012.718209, 2012.
- Chelton, D. B., E. J. Walsh, and J. L. McArthur, Pulse Compression and Sea Level Tracking in Satellite Altimetry, *Journal of Atmospheric and Oceanic Technology*, 6, 407–438, 1989.
- Church, D., and N. White, Sea-level rise from the late 19th to the early 21st century, *Survey in Geophysics*, doi:10.1007/s10712-011-9119-1, 2011.
- Church, J., and N. White, A 20th century acceleration in global sea-level rise, *Geoph. Res. Lett.*, L01602, doi:10.1029/2005GL024826, 2006.
- Church, J., N. White, L. Konikow, C. Domingues, J. G. Cogley, E. Rignot, J. Gregory, M. van den Broeke, A. Monaghan, and I. Velicogna, Revisiting the earth's sea level and energy budgets from 1961 to 2008, *Geoph. Res. Lett.*, 38, doi:10.1029/2011GL048794, 2011.
- Church, J., P. Clarke, A. Cazenave, J. Gregory, S. Jevrejeva, A. Levermann, M. Merrifield, G. Milne, R. Nerem, P. Nunn, A. Payne, W. Pfeffer, D. Stammer, and A. Unnikrishnan, *Sea level, Chapter 13 of the V Assessment Report of the Intergovernmental Panel on Climate Change (IPCC)*, Working Group I, The Physical Science Basis, Cambridge University Press, 2013.
- Church, J. A., N. J. White, T. Aarup, W. S. Wilson, P. L. Woodworth, C. M. Domingues, J. R. Hunter, and K. Lambeck, Understanding global sea levels: Past, present and future, *Sustain Sci*, 3, 9–22, 2008.
- CLS, Radar Altimetry Tutorial , <http://www.altimetry.info>, 2013.
- Döll, P., F. Kaspar, and B. Lehner, A global hydrological model for deriving water availability indicators: model tuning and validation, *J. of Hydrology*, 207, 105–134., 2003.
- Domingues, C., J. Church, N. White, P. Gleckler, S. Wijffels, P. Barker, and J. Dunn, Improved estimates of upper-ocean warming and multi-decadal sea level rise, *Nature Letters*, 453, doi:10.1038, 2008.

- Dorandeu, J., M. Ablain, Y. Faugere, F. Mertz, B. Soussi, and P. Vincent, Jason global statisti-cal evaluation and performance assessment : Calibration and cross-calibration re-sults,, *Marine Geodesy*, 27(t (2004). J), 345–372, 2004.
- Douglas, B., *Sea level change in the era of the recording tide gauge*, *International Geophysics Series*, vol. 75, AGU, 2001.
- Dufau, C., C. Martin-Puig, and L. Moreno, *User Requirements in the Coastal Ocean for Ocean Altimetry in book Coastal altimetry*, Springer Verlag, doi:10.1007/978-3-642-12796-0_3, 2011.
- Fenoglio-Marc, L., and E. Groten, Time varying mean sea level, in *Handbook of Geomathematics*, vol. 1, edited by W. Freedden, M. Z. Nashed, and T. Sonar, pp. 353–370, Springer Verlag, Berlin, 2010.
- Fenoglio-Marc, L., E. Tel, M. J. Garcia, and N. Kjær, Inter-annual to de-cadal sea level change in the south-western Europe from satellite altimetry and in-situ measurements, *Gravity, Geoid and Space Missions, International Association of Geodesy Symposia, Springer*, 129, 242–247, 2005.
- Fenoglio-Marc, L., J. Kusche, M. Becker, and I. Fukumori, Comment on "On the steric and mass-induced contributions to the annual sea level variations in the Mediterranean Sea" by David García et al., *Journal of Geophysical Research*, 112, C12,018, doi:10.1029/2007JC004196, 2007.
- Fenoglio-Marc, L., R. Rietbroek, S. Grayek, M. Becker, J. Kusche, and E. Stanev, Water mass variation in the Mediterranean and Black Sea, *J. of Geodynamics*, doi:10.1016/j.jog.2012.04.001, 2012.
- Fenoglio-Marc, L., S. Dinardo, R. Scharroo, A. Roland, B. Lucas, R. Weiss, M. Detour Sikiric, M. Becker, and J. Benveniste, A Validation Exercise for CryoSat-2 in SAR Mode in the German Bight Area, 2013a.
- Fenoglio-Marc, L., A. Mariotti, G. Sannino, B. Meyssignac, A. Carillo, and M. Struglia, Decadal variability of the net water flux at the Mediterranean Gibraltar Strait, *Global and Planetary Change*, 100, 1–10, 2013b.
- Fenoglio-Marc, L., S. Dinardo, R. Scharroo, B. Lucas, A. Roland, M. Dutour, M. Becker, J. Benveniste, and R. Weiss, The German Bight: a validation of CryoSat-2 altimeter data in SAR mode , *J. of Advanced Space Research*, doi:http://dx.doi.org/10.1016/j.asr.2015.02.014, 2015.
- Garcia, D., B. F. Chao, J. Del Rio, I. Vigo, and J. Garcia-Lafuente, On the steric and mass-induced contributions to the annual sea level variations in the mediterranean sea, *Journal of Geophysical Research: Oceans*, 111(C9), n/a–n/a, doi:10.1029/2005JC002956, 2006.
- Garcia, D., B. Chao, and J.-P. Boy, Steric and mass-induced sea level variations in the Mediter-ranean Sea revisited, *J. Geophys. Res.*, 115, C12016, doi:10.1029/2009JC005928., 2010.
- Gomez-Enri, J., S. Vignudelli, G. D. Quartly, C. Gommenginger, P. Cipollini, P. G. Challenor, and J. Benveniste, Modeling Envisat RA-2 Waveforms in the Coastal Zone: Case Study of Calm Water Contamination, *IEEE Geoscience and Remote Sensing Letters*, 7 n.3, 474–478, 2010.

- Gomis, D., M. Tsimplis, M. Marcos, L. Fenoglio-Marc, B. Perez, F. Raicich, I. Vilibic, G. Wopelmann, and S. Monserrat, *The Climate of the Mediterranean Region from past to future*, P. Lionello (eds), chap. Mediterranean Sea Level Variability and trends, Elsevier, 2012.
- Gommenginger, C., P. Thibaut, L. Fenoglio-Marc, D. X., J. Gomez-Enri, and G. Y., *Coastal altimetry*, chap. Retracking altimeter waveforms near the coasts, Springer Verlag, doi:10.1007/978-3-642-12796-0, 2011.
- Halimi, A., C. Mailhes, J.-Y. Tourneret, and P. Thibaut, A new Model for Peaky Altimetric Waveforms, *IEEE, IGARSS*, pp. 2825–2828, 2011.
- Halimi, A., C. Mailhes, J.-Y. Tourneret, P. Thibaut, and F. Boy, Parameter Estimation for Peaky Altimetric Waveforms, *IEEE TRANSACTIONS ON GEOSCIENCE AND REMOTE SENSING*, 51, 3, 1568–1577, doi:10.1109/TGRS.2012.2205697, 2013.
- Henry, O., P. Prandi, W. Llovel, A. Cazenave, S. Jevrejeva, D. Stammer, B. Meyssignac, and N. Koldunov, Tide gauge based sea level variations since 1950 along the Norwegian and Russian coasts of the Arctic Ocean: contribution of the steric and mass components, *J. of Geophysical Research*, 117, C09,023, doi:10.1029/2011JC007706, 2012.
- Holgate, S., and P. Woodworth, Evidence for enhanced coastal sea level rise during the 1990s, *Geophys. Res. Lett.*, 31(L07305), doi:10.1029/2004GL019,626, 2004.
- Holgate, S., and P. Woodworth, On the decadal rates of sea level change during the twentieth century, *Geophys. Res. Lett.*, 34(L01602), doi:10.1029/2006GL028,492, 2007.
- Hwang, C., Analysis of some systematic errors affecting altimeter-derived sea surface gradients with application to geoid determination over Taiwan, *J. of Geodesy*, 71, 113–130, 1997.
- Idris, N. H., and X. Deng, The retracking technique on multi-peak and quasi-specular waveforms for jason-1 and jason-2 missions near the coast, *Marine Geodesy*, 35(sup1), 217–237, doi:10.1080/01490419.2012.718679, 2012.
- Jevrejeva, S., A. Grinsted, J. C. Moore, and S. Holgate, Nonlinear trends and Multiyear cycles in sea level records, *Journal of Geophysical Research*, 111, 11, doi:10.1029/2005JC003229, 2006.
- Kohl, A., and D. Stammer, Decadal Sea Level Changes in the 50-Year GECCO Ocean Synthesis, *J. Climate*, 21, 1876–1890, doi: http://dx.doi.org/10.1175/2007JCLI2081.1, 2008.
- Kusche, J., W. Bosch, and M. Becker, Vermessung des globalen Wandels aus dem Weltraum: Meeresspiegel und Klima , *ZFV*, 1, 2013.
- Le Traon, P., and P. Gauzelin, Response of the Mediterranean mean sea level to atmospheric pressure forcing, *Journal of Geophysical Research*, 102(C1), 973–984, 1997.
- Leuliette, E., and R. M. Nerem, Calibration of Topex/Poseidon and Jason altimeter data to construct a continuous record of mean sea level changelosing the sea level rise budget with altimetry, Argo, and GRACE, *Mar. Geod.*, 23, 23, doi:10.1080/01490410490465193, 2004.
- Levitus, S., J. I. Antonov, T. Boyler, and C. Stephens, Warming of the World Ocean, *Science*, 287, 2225–2229, 2000.
- Lombard, A., Les variations actuelles du niveau de la mer: observations et causes, *PhD thesis, University of Toulouse*, 2005.

- Lombard, A., A. Cazenave, L. T. P.Y., and M. Ishii, Contribution of thermal expansion to present-day sea-level change revised, *Global and Planetary Change*, 47, 11–16, 2005.
- Masters, D., R. S. Nerem, C. Choe, E. Leuliette, B. Beckley, N. White, and M. Ablain, Comparison of global mean sea level time series from topex/poseidon, jason-1, and jason-2, *Marine Geodesy*, 35(sup1), 20–41, doi:10.1080/01490419.2012.717862, 2012.
- Meyssignac, B., F. Calafat, S. Somot, V. Rupolo, P. Stocchi, W. Llovel, and A. Cazenave, Two-dimensional reconstruction of the mediterranean sea level over 1970-2006 from tide gage data and regional ocean circulation model outputs, *Global and Planetary Change*, 77, 49–61, doi:http://dx.doi.org/10.1016/j.gloplacha.2011.03.002, 2011.
- Meyssignac, B., D. Salas y Melia, M. Becker, W. Llovel, and A. Cazenave, Tropical pacific spatial trend patterns in observed sea level: internal variability and/or anthropogenic signature?, *Climate of the Past*, 8, 787 – 802, doi:10.5194/cp-8-787-2012, 2012a.
- Meyssignac, M., B., M. Becker, W. Llovel, and A. Cazenave, An Assessment of Two-Dimensional Past Sea Level Reconstructions Over 1950-2009 Based on Tide-Gauge Data and Different Input Sea Level Grids, *Surveys in Geophysics*, 2012b.
- Mitchum, G., An improved calibration of satellite altimetric heights using tide gauge sea levels with adjustment for land motion, *Marine Geodesy*, 23, 145–166, 2000.
- Moore, J., S. Jevrejeva, and A. Grinsted, The historical global sea-level budget, *Annals of Glaciology*, 52959, 2011.
- Nicholls, R. J., and A. Cazenave, Sea-level rise and its impact on coastal zones, *Science*, 328(5985), 1517–1520, doi:10.1126/science.1185782, 2010.
- Passaro, M., P. Cipollini, S. Vignudelli, G. D. Quartly, and H. M. Snaith, Ales: A multi-mission adaptive subwaveform retracker for coastal and open ocean altimetry, *Remote Sensing of Environment*, 145(0), 173 – 189, doi:http://dx.doi.org/10.1016/j.rse.2014.02.008, 2014.
- Passaro, M., L. Fenoglio-Marc, and P. Cipollini, Validation of significant wave height from improved satellite altimetry in the german bight, *Geoscience and Remote Sensing, IEEE Transactions on*, 53(4), 2146–2156, doi:10.1109/TGRS.2014.2356331, 2015.
- Pinardi, N., and E. Masetti, Variability of the large scale general circulation of the Mediterranean Sea from observations and modelling: a review, *Palaeo*, 7(158), 153–174, 2000.
- Prandi, P., A. Cazenave, and M. Becker, Is coastal mean sea level rising faster than the global mean? A comparison between tide gauges and satellite altimetry over 1993-2007, *Geophys. Res. Letters*, p. 19, 2008.
- Prigent, C., P. F., F. Aires, W. Rossow, and E. Matthews, Global inundation dynamics inferred from multiple satellite observations, 1993-2000, *J. Geophys. Res.*, 112, doi:10.1029/2006JD007847, 2007.
- Ray, C., C. Martin-Puig, M. Clarizia, C. Ruffini, D. S., C. Gommenginger, and J. Benveniste, Sar altimeter backscattered waveform model, *IEEE Transactions on Geoscience and remote sensing*, 53, 2, doi:10.1109/TGRS.2014.2330423, 2015.
- Rietbroek, R., S. Brunnabend, J. Kusche, and . Schroeter, Resolving sea level contributions by identifying fingerprints in time-variable gravity and altimetry , *J. of Geodynamics*, doi: 10.1016/j.jog.2011.06.007, 2012.

- Roesler, C. J., W. J. Emery, and S. Y. Kim, Evaluating the use of high-frequency radar coastal currents to correct satellite altimetry, *Journal of Geophysical Research: Oceans*, *118*(7), 3240–3259, doi:10.1002/jgrc.20220, 2013.
- Scharroo, R., and L. Fenoglio, Cyclone Xaver seen by SARAL/AltiKa, <http://www.eumetsat.int/website/home/Images/ImageLibrary/DAT2087062.html>, 2013.
- Scharroo, R., J. Lillibridge, W. W.H.F. Smith, and E. Schrama, Cross-Calibration and Long-Term Monitoring of the Microwave Radiometer of ERS, Topex, GFO, Jason and Envisat, *Marine Geodesy*, *27*, 279–297, 2004.
- Solomon, S., D. Qin, M. Manning, Z. Chen, M. Marquis, K. Averyt, M. Tignor, and H. Miller, *Climate change 2007: The physical Science Basis. Contribution of Working Group I to the Fourth Assessment report of the Intergovernmental Panel on Climate Change*, Cambridge University Press, Cambridge, UK, and New York, USA., 2007.
- Stammer, D., A. Cazenave, R. M. Ponte, and M. E. Tamisiea, Causes for contemporary regional sea level changes, *Annual Review of Marine Science*, *5*(1), 21–46, doi:10.1146/annurev-marine-121211-172406, PMID: 22809188, 2013.
- Thibaut, P., J. C. Poisson, E. Bronner, and N. Picot, Relative Performance of the MLE3 and MLE4 Retracking Algorithms on Jason-2 Altimeter Waveforms, *Marine Geodesy*, *33*(sup1), 317–335, doi:10.1080/01490419.2010.491033, 2010.
- Timmermann, A., S. McGregor, and F. Jin, Wind effects on past and future regional sea level trends in the southern Indo-Pacific, *J. Climate*, *23*, 4429–4443, doi: <http://dx.doi.org/10.1175/2010JCLI3519.1>, 2010.
- Trisirisatayawong, I., M. Naeije, W. Simons, and L. Fenoglio-Marc, Sea level change in the Gulf of Thailand from GPS-corrected tide gauge data and multi-satellite altimetry, *Global and Planetary Change*, *76*, 137–151, doi:10.1016/j.gloplacha.2010.12.010, 2011.
- Tsimplis, F., M.N.AND Raicich, L. Fenoglio-Marc, A. Shaw, M. Marcos, S. Somot, and A. Bergamasco, Recent developments in understanding sea level rise at the adriatic coasts, *Physics and Chemistry of the Earth*, doi:<http://dx.doi.org/10.1016/j.pce.2009.11.007>, 2011, 2011.
- Tsimplis, M., A. Shaw, A. Pascual, M. Marcos, M. Pasarić, and L. Fenoglio-Marc, *Remote Sensing of the European Sea*, chap. Can we reconstruct the 20th century sea level variability in the Mediterranean Sea on the basis of recent altimetric measurements?, Springer Science, doi:http://dx.doi.org/10.1007/978-3-642-01546-5_12, 2007.
- Tsimplis, M., M. Calafat, M. Marcos, G. Jorda, D. Gomis, L. Fenoglio-Marc, S. M.V., and S. Josey, The effect of the NAO on Mediterranean Sea level and on mass changes, *J. of Geophys. Res.*, *118*, 994–952, doi:10.1002/jgrc.20078, 2013.
- Weiss, R., Erfassung und Beschreibung der Meeresoberfläche im Bereich der Deutschen Buch, Master's thesis, Technische Univesität Darmstadt, 2013.
- White, N., A. Church, and J. Gregory, Coastal and global averaged sea level rise for 1950 to 2000, *Geophys. Res. Lett.*, *32*(L01601), doi:10.1029/2004GL021,391, 2004.
- Willis, J. K., D. Chambers, and R. Nerem, Assessing the globally averaged sea level budgt on seasonal to interannual timescales, *J. Geophys. Res.*, *113*, C06015, doi:10.1029/2007JC004517, 2008a.

- Willis, J. K., D. P. Chambers, and R. S. Nerem, Assessing the globally averaged sea level budget on seasonal to interannual timescales, *Journal of Geophysical Research*, 113, 2008b.
- Wingham, D. J., L. Phalippou, C. Mavrocordatos, and D. Wallis, The Mean Echo and Echo Cross Product From a Beamforming Interferometric Altimeter and Their Application to Elevation Measurement, *IEEE Transactions on Geoscience and Remote Sensing*, 42(10), 2305–2323, doi:10.1109/TGRS.2004.834352, 2004.
- Wingham, D. J., C. R. Francis, S. Baker, C. Bouzinac, D. Brockley, R. Cullen, P. de Chateau-Thierry, S. W. S.W. Laxon, U. Mallow, C. Mavrocordatos, L. Phalippou, G. Ratier, L. Rey, F. Rostan, P. Viau, and D. W. Wallis, CryoSat: A mission to determine the fluctuations in Earth's land and marine ice fields, *Advances in Space Research*, 37, 841–871, doi:10.1016/j.asr.2005.07.027, 2006.

Acknowledgements

This habilitation thesis has been written during my time as postdoctoral researcher in the field of Physical Geodesy and Satellite Geodesy at the Technischen Universität Darmstadt. I acknowledge Prof. Dr.-Ing. Matthias Becker for his support and open mindedness to new ideas, which gave me the chance to shape my research topic. I am grateful to Prof. Dr.-Ing. Erwin Groten for his interest in my work and to Prof. Dr.-Ing. Andreas Eichhorn for his contribution as reviewer.

A particular thanks goes to Dr. Anny Cazenave and Prof. Dr.-Ing. Jürgen Kusche for their collaboration over the last years, for the challenging suggestions, fruitful discussions and finally for appraising this manuscript.

Further on, I am grateful to the many colleagues of geodesy and near disciplines met within the various projects. The challenging atmosphere in workshops and summer schools greatly helped to better understand our Earth and its complex behaviour and to realize how important inter-disciplinarity is. Thanks also to all colleagues of the sea level and altimetry scientific communities.

Working with students and colleagues at our Institute has been quite enjoyable, thanks for their collaboration.

The Deutsche Forschungsgemeinschaft (DFG) has funded most of my post-doc research, first with an habilitanden fellowship and then with four projects. The European Union (EU) and the European Space Agency (ESA) funded two other projects. I am grateful for these supports, which made this research possible.

Finally I thank my family for all the support, encouragement and interest they demonstrated in different ways during the years.

Luciana Fenoglio-Marc

Darmstadt, February 2015